Functional heterogeneity of CPVT-mutant human cardiac ryanodine receptors: evaluation of the influence of S2031 and S2808 phosphorylation sites

Shanna Hamilton

A thesis submitted for the degree of Doctor of Philosophy

November 2017

School of Medicine,

Cardiff University

ACKNOWLEDGEMENTS

First and foremost, to Lowri Thomas; your intelligence, resilience and humility have always inspired me. Thank you for everything.

To Alan Williams; I am very grateful and privileged to work in your laboratory – I have enjoyed (nearly) every minute. Thank you for your continuous support.

Thanks to Chloe Ormonde for being a wonderful and much-needed friend; to David Edwards for being my favourite source of procrastination and laughter; to Chris George for helpful guidance and a timely confidence boost; to Saptarshi Mukherjee, Bevan Cumbes and Mark Bannister for your friendship and help with my work. Thanks to all for making the AJW laboratory a place of reassurance during some eventful periods. I wish you all the best for your future endeavours and hope to remain your colleague and friend for years to come.

To the British Heart Foundation for funding this Ph.D. studentship, a fruitful visit to an international conference and much of the research in our laboratory.

Finally, to my husband Joshua, for putting up with me during this period.

SUMMARY

Human cardiac ryanodine receptors (hRyR2) are calcium (Ca^{2+}) release channels central to excitation-contraction coupling. Mutations in hRyR2 are linked to catecholaminergic polymorphic ventricular tachycardia (CPVT), a genetic disorder characterized by arrhythmia, occurring under adrenergic drive. Recent studies suggest gain-of-function mutant channels may undergo different mechanisms of dysfunction, with some showing altered Ca^{2+} release under basal conditions and others requiring an additional trigger (possibly in the form of β-adrenergic phosphorylation). This study evaluated whether mutants from different domains of hRyR2 (S2246L and N4104K) were functionally heterogeneous in a cellular setting and whether this was related to phosphorylation status.

Cells (human embryonic kidney 293) expressing N4104K-hRyR2 displayed smaller, faster Ca^{2+} release events than those expressing the wild type (WT), while those of cells expressing S2246L-hRyR2 were similar to WT. However, a lower proportion of S2246L cells showed any kind of Ca^{2+} release functionality compared to those expressing WT or N4104K, reinforcing that these mutations cause different types of dysfunction. Assessment of phosphorylation status using site-specific antibodies for protein kinase A (PKA) target sites S2808 and S2031 showed that mutant phosphorylation levels were different to each other and to that of the WT, indicating a possible role of phosphorylation in this. Activation of PKA-mediated phosphorylation in cells using a cyclic AMP analogue resulted in changes to the kinetics of spontaneous Ca^{2+} release via WT hRyR2, but did not significantly affect that of mutants. Genetic phosphorylation at either PKA site (S2808D and S2031D) altered the Ca^{2+} release of mutants as well as WT hRyR2, but this was found to be due to changes in expression of sarco-endoplasmic reticulum Ca^{2+}-ATPase (SERCa) pump, which also contributes to Ca^{2+} homeostasis.

These findings reinforce the concept that phosphorylation is linked to dysfunction and contributes to our understanding of hRyR2 mutation in arrhythmia, highlighting that ‘gain-of-function’ does not necessarily equate to dysfunction via the same mechanism.

CONTENTS

LIST OF FIGURES AND TABLES

CHAPTER 1: General Introduction

Figures

CHAPTER 2: Materials and Methods

Figures

Tables

CHAPTER 3: Investigating the functional heterogeneity of CPVT hRyR2 mutants using Ca^{2+} imaging

Figures

Tables

CHAPTER 4: The influence of phosphorylation at the S2808 and S2031 sites on WT and CPVT mutant function

Figures

Tables

CHAPTER 6: General Discussion

Figures

APPENDIX

Figures

ABBREVIATIONS

($^{+/+}$)	Homozygous mutation in a mouse model
($^{+/-}$)	Heterozygous mutation in a mouse model
2D	Two dimensional
3D	Three dimensional
AC	Adenylyl cyclase
ACh	Acetylcholine
ADP	Adenosine diphosphate
AF	Atrial fibrillation
AM	Acetoxymethyl
ANOVA	Analysis of variance
AOBS	Acousto-optical beam splitter
AP	Action potential
ApoCaM	Ca^{2+}-free state of calmodulin
ARVC/D	Arrhythmogenic right ventricular cardiomyopathy/dysplasia
ATP	Adenosine triphosphate
β-AR	β-adrenergic receptor|
BCA	Bicinchoninic acid
BLAST	Basic local alignment search tool
Bsol	Bridging solenoid
Ca^{2+}	Calcium ion
CaCam	Calcium-calmodulin
CaM	Calmodulin
CaMKII	Calcium-calmodulin-dependent protein kinase II
cAMP	Cyclic adenosine monophosphate
CCD	Central core disease
CCM	Calcium-dependent cardiomyopathy
cDMEM	Complete Dulbecco's modified eagle's medium, with 10 % FCS and 2 % PSG
CICR	Calcium-induced calcium release
CPVT	Catecholaminergic polymorphic ventricular tachycardia
CPVT1	CPVT caused by mutations in RyR2
CPVT2	CPVT caused by mutations in CSQ2
Cryo-EM	Cryo-electron microscopy
CSQ	Calsequestrin
CSQ1	Calsequestrin isoform type 1, skeletal
CSQ2	Calsequestrin isoform type 2, cardiac

CTD	C-terminal domain
CV	Coefficient of variance
DAD	Delayed afterdepolarization
DcAMP	Dioctanoyl-cAMP
dmd	Duchenne muscular dystrophy
DMEM	Dulbecco's modified eagle's medium (also referred to as minimal DMEM, mDMEM)
DMSO	Dimethyl sulfoxide
DTT	Dithiothreitol
EAD	Early afterdepolarization
EC	Excitation-contraction
ECL	Enhanced chemiluminescence
eGFP	Enhanced green fluorescent protein
EGTA	Ethylene glycol tetra acetic acid
eNOS	Endothelial nitric oxide synthase
Epac	Exchange factor directly activated by cAMP proteins
Epac1	Epac protein type 1
Epac2	Epac protein type 2
ER	Endoplasmic reticulum
F	Peak signal intensity
F_0	Basal signal intensity
FBS	Fetal bovine serum
FKBP	FK506 binding protein
FKBP12	FKBP protein of molecular weight 12 kDa, also known as calstabin
FKPB12.6	FKBP protein of molecular weight 12.6 kDa, also known as calstabin2
F.U.	Fluorescence units
Gi	Inhibitory G protein
Gs	Stimulatory G protein
GFP	Green fluorescence protein
HEDTA	Hydroxyethyl ethylene diamine tri acetic acid
HEK293	Human embryonic kidney cells 293
HF	Heart failure
HPLC	High pressure liquid chromatography
HRP	Horseradish peroxidase
hRyR2	Human cardiac ryanodine receptor
IF	Immunofluorescence
IP_3R	Inositol triphosphate receptor

iPSC-CMs	Induced pluripotent stem cell cardiomyocytes
JSol	Junctional solenoid
JUN	Junctin
K^+	Potassium ion
KI	Knock in
KO	Knock out
KRH	Krebs Ringer Heinslet buffer
LB	Luria Bertani broth
LTCC	L-type calcium channel, also known as dihydropyridine channel
mAKAP	Muscle A-kinase anchoring protein
MS	Mass spectrometry
Mg^{2+}	Magnesium ion
MH	Malignant hyperthermia
MI	Myocardial infarct
M_2R	Muscarinic receptor type 2
M_3R	Muscarinic receptor type 3
MW	Molecular weight
Na^+	Sodium ion
NADPH	Nicotinamide adenine dinucleotide phosphate
NCX	Sodium-calcium exchanger
NK	N4104K RyR2 (sometimes eGFP-hRyR2)
NK08	N4104K-S2808D eGFP-hRyR2
NK31	N4104K-S2031D eGFP-hRyR2
NO	Nitric oxide
NOS	Nitric oxide synthase
NTA	Nitrilotriacetic acid
NTD	N-terminal domains
PBS	Phosphate buffered saline
PCR	Polymerase chain reaction
P domain	Phosphorylation domain
PKA	Protein kinase A
PKAr	Regulatory subunit of protein kinase A
PKC	Protein kinase C
PKG	Protein kinase G
PLB	Phospholamban
PLM	Phospholemman
P_o	Open probability

PP	Protein phosphatase
PP1	Protein phosphatase 1
PP2A	Protein phosphatase 2A
PP2B	Protein phosphatase 2B, also known as calcineurin
PSG	Penicillin-Streptomycin-Glutamine
PVDF	Polyvinylidene fluoride
pVSD	Pseudo voltage-sensor domain
ROI	Region of interest
ROS	Reactive oxygen species
RNS	Reactive nitrogen species
RyR	Ryanodine receptor
RyR1	Ryanodine receptor isoform 1, skeletal
RyR2	Ryanodine receptor isoform 2, cardiac
RyR3	Ryanodine receptor isoform 3
S2808	Serine-2808
S2808A	Serine-2808 replaced by Alanine
S2808D	Serine-2808 replaced by Aspartic Acid
S2811	Serine-2811
S2814	Serine-2814
S2814A	Serine-2814 replaced by Alanine
S2814D	Serine-2814 replaced by Aspartic Acid
S2031	Serine-2031
S2031A	Serine-2031 replaced by Alanine
S2031D	Serine-2031 replaced by Aspartic Acid
S2797	Serine-2797
SALVO	Synchrony-Amplitude-Length-Variability of Oscillation software
SCLP	Shell core linker peptide
SDS	Sodium dodecyl sulfate
SDS-PAGE	polyacrylamide gel electrophoresis
SE	Standard error
SEM	Standard error of the mean
SERCa	Sarco/endoplasmic reticulum calcium-ATPase
SERCa1a	Skeletal isoform of SERCa
SERCa2a	Cardiac isoform of SERCa
SF	Selectivity filter
SL	S2246L RyR2 (sometimes S2246L eGFP-hRyR2)
SL08	S2246L-S2808D eGFP-hRyR2

SL31	S2246L-S2031D eGFP-hRyR2
SOC	Super optimal broth with catabolite repression
SOICR	Store overload-induced calcium release
SPRY	Domain named from SPIa and RYanodine receptor
SR	Sarcoplasmic reticulum
T2810	Threonine-2810
T2876	Threonine-2876
TAC	Transverse aortic constriction
TAE	Tris, acetic acid and EDTA buffer
TBS	Tris buffered saline
TBS-T	Tris buffered saline with Tween 20
TEMED	Tetramethylethylenediamine
TM	Transmembrane
TMx2	Transmembrane helices (two)
TnC	Troponin C
TnI	Troponin I
TRDN	Triadin
TT	T tubules
VF	Ventricular fibrillation
VT	Ventricular tachycardia
v/w	Volume by weight
v/v	Volume by volume
WT	Wild type (sometimes WT eGFP hRyR2)
WT08	WT-S2808D eGFP hRyR2
WT31	WT-S2031D eGFP hRyR2
w/v	Weight by volume

Chapter 1

General Introduction

1.1 Calcium signalling

1.1.1 Versatility of Ca^{2+} signalling

Calcium (Ca^{2+}) is a ubiquitous secondary messenger responsible for controlling many cellular processes, including gene expression, energy metabolism, cell proliferation, fertilization and muscle contraction (Berridge et al. 2000). Increasing intracellular Ca^{2+} levels from resting levels of ~100 nM to ~1 mM activates a cell for many of these processes. While this action is relatively simple, control of this process via a network of Ca^{2+} signalling components allows for enormous versatility, whereby components can be mixed and matched to create a range of spatial and temporal Ca^{2+} signals (Berridge et al. 2000). Berridge et al. (2000) describe how this Ca^{2+} signalling network can be split into four functional units; *Ca^{2+}-mobilizing signals*, triggered by a stimulus; *ON mechanisms*, activated by the former, that feed Ca^{2+} into the cytoplasm; *messenger signals*, where Ca^{2+} functions to stimulate many Ca^{2+}-sensitive processes; and *OFF mechanisms*, composed of pumps and exchangers that remove Ca^{2+} from the cytoplasm to restore a cell to a resting state.

An elevation of intracellular Ca^{2+} concentration is achieved during *on* reactions, whereby stimuli cause the entry of external Ca^{2+} and the release of internal Ca^{2+} from intracellular stores, the endoplasmic/sarcoplasmic reticulum (ER/SR) (Berridge et al. 2003). *Off* reactions terminate a cellular event and return intracellular Ca^{2+} concentrations to resting levels by extruding Ca^{2+} from the cell by exchangers and pumps. Ca^{2+} homeostasis is therefore dependent on fluxes of multiple Ca^{2+} channels and handling proteins during these *off* and *on* reactions.

1.1.2 Compartmentalization of Ca^{2+} signalling

Versatility of Ca^{2+} signalling is achieved by variation of the localization, amplitude and duration of a signal. Propagation and termination of these events is dependent on cytoplasmic buffering, Ca^{2+} extrusion and internal store uptake by proteins and organelles within the cell. Ca^{2+} must therefore enter the cell near the target protein, or pass through the cell as a propagating signal (Berridge et al. 2000). Internal stores are held within the ER or equivalent organelle in muscle cells, the SR. The Ca^{2+} release from intracellular SR stores through ryanodine receptors (RyR) in a cardiomyocyte is an example of signal compartmentalization.

Activation of a single RyR channel is termed a "nanoscopic Ca^{2+} release event" or "Ca^{2+} quark", resulting in a small increase in localized cytoplasmic Ca^{2+} levels (~30 nM) that spreads no more than ~2 μm in the cell and last ~200 msec (Niggli and Shirokova 2007; Lipp and Niggli 1996). Activation of several neighbouring RyR channels in a cluster produces a Ca^{2+} release event termed a 'Ca^{2+} spark', the first discovered subcellular Ca^{2+} signal (H. Cheng et al. 1994). Up to 20 RyR channels may open during each Ca^{2+} spark, resulting in a greater increase in localized Ca^{2+} levels (~100-300 nM) that spreads up to ~6 μm, lasting ~500 msec (Niggli and Shirokova 2007). If many Ca^{2+} sparks occur in RyR clusters close together, this can result in the generation of a propagating 'Ca^{2+} wave' that spreads throughout the cell (H. Cheng et al. 1994). The amplitude of the whole-cell Ca^{2+} transient is therefore regulated by recruiting Ca^{2+} sparks, which then sum up to shape the cellular Ca^{2+} transient (Collier et al. 1999; Inoue and Bridge 2003).

1.2 Calcium signalling in the heart

1.2.1 Structure of cardiac muscle and the mechanism of contraction

The wall of the heart, the myocardium, predominantly consists of cardiomyocytes which are critical for muscle contraction (see **Figure 1.1**). A ventricular myocyte is typically rod like in shape, with a diameter 10-20 μm and a length of 50-100 μm. These cells are connected in a longitudinal direction and connect at intercalated discs. This gives cardiac muscle a characteristic striated patterning. (Shimada *et al.*, 2004).

The outside layer of the cardiomyocyte is bounded by a lipid bilayer containing various ion channels that allow transport in and out of the cell and is termed the sarcolemma. Invaginations of the sarcolemma form transverse tubule structures (t-tubules, TT) that protrude into the cell. These invaginations mean that L-type Ca^{2+} channels (LTCC) and cardiac RyR channels (RyR2), present on the intracellular SR, are in close proximity. TTs are 100-300 nm in diameter and occur every 1.8 μm along the axis of every cell in a highly-ordered fashion, forming a branched and interconnected network (L.-S. Song et al. 2005). These 'calcium release units' formed at the junctional contact between TTs and the SR are critical for Ca^{2+} signalling (Franzini-Armstrong et al. 1998; Hong and Shaw 2016).

Cardiomyocytes contain myofilaments, proteins that form the contractile apparatus (see **Figure 1.1**). An organized array of myofilament fibres makes up the sarcomere, comprised of titin filaments and repeating units of thick and thin filaments. Thin filaments consist of regulatory proteins tropomyosin and the troponin complex (troponin T, I and C), while thick filaments are composed of myosin and accessory proteins (Gautel and Djinović-Carugo 2016). Cardiomyocyte contraction involves the interaction of these filaments and proteins.

In diastole, a cardiomyocyte is relaxed, with tropomyosin wrapped around the actin filament, preventing interaction with the myosin filament. In systole, elevated levels of cytoplasmic Ca^{2+} causes a conformational switch in troponin C (TnC), exposing an active site between actin and myosin. Hydrolysis of adenosine triphosphate (ATP) by ATPase on myosin (which is no longer inhibited by troponin I, TnI) induces cross bridge formation between myosin heads and active sites on actin. This interaction causes the myosin head to 'pull' itself along the actin filament. Adenosine diphosphate (ADP) is released from myosin heads, which then binds to a new ATP molecule, releasing the actin filament. The cycle can then repeat, with myosin travelling along the actin molecules, progressively shortening the muscle sarcomere

while cytosolic Ca^{2+} concentrations remain high enough to inhibit TnI and there is enough ATP present for cross bridge formation. Extrusion of Ca^{2+} from the cardiomyocyte dissociates Ca^{2+} from TnC, TnI is no longer inhibited and myocytes return to their original conformation – myocyte relaxation occurs (Gautel and Djinović-Carugo 2016).

The process linking action potential and cycling of Ca^{2+} throughout the cell to generate cardiomyocyte contraction and relaxation in this manner is termed excitation-contraction (EC) coupling (Bers 2002a).

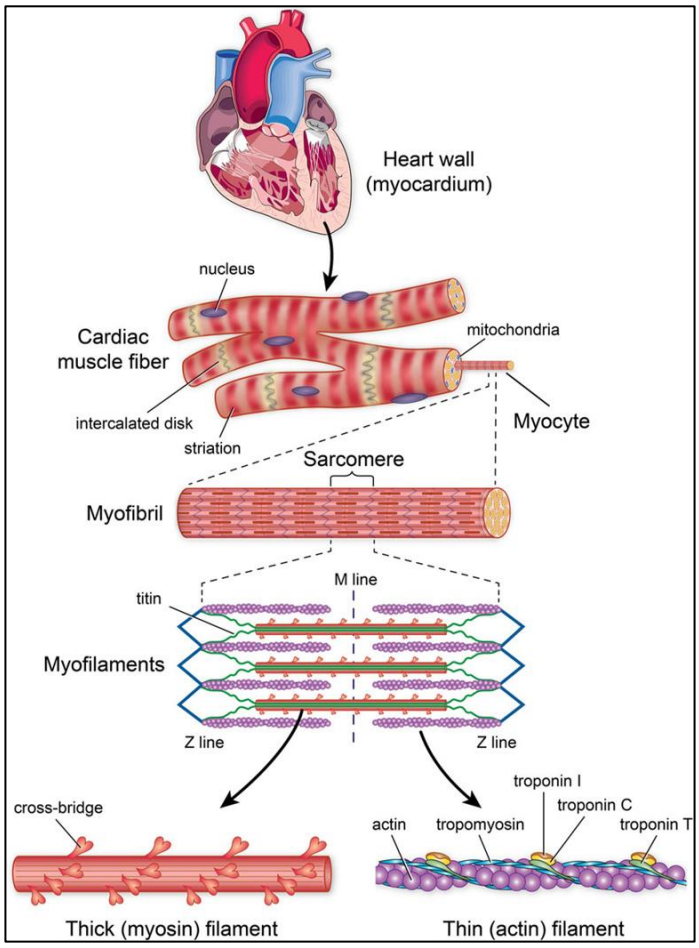

Figure 1.1 Cardiac muscle structure. Cardiac myocytes form muscle fibres that are separated by intercalated disks, which allow for signal transduction across the muscle. Each myocyte consists of sarcomere structures; repeating thin (actin) and thick (myosin) filaments.
Figure taken from Golob et al. (2014).

1.2.2 The cardiac action potential

Excitability in the heart is generated by a delicate balance of polarizing and depolarizing ionic currents, mediated by channels and transporter proteins that move positively or negatively charged ions to enter or leave the cell. The electrical origin of cardiac contraction is called cardiac action potential (AP). There are four distinct phases of ventricular cardiac AP (**Figure 1.2**), outlined below (Bers 2008; Marbán 2002; Bers 2002b):

Phase 4 – This phase represents a cardiomyocyte under diastolic (resting) conditions, at a resting membrane potential (E_m) of -85 mV. This is maintained by the K^+ gradient across the membrane.

Phase 0 – Voltage-dependent activation of fast inward Na^+ currents results in a rapid depolarization, a sharp increase in membrane potential, to +40 mV.

Phase 1 – After depolarization, the inward Na^+ current is inactivated. Efflux of K^+ and Cl^- ions from the cell causes slight repolarization, a downward shift in membrane potential.

Phase 2 – A balance between efflux of K^+ ions through delayed rectifier K^+ channels and influx of Ca^{2+} through LTCCs causes a plateau in membrane potential.

Phase 3 – Inward Ca^{2+} current stops as there is RyR2-mediated Ca^{2+} release from the SR, Ca^{2+} reuptake into the SR via cardiac sarcoplasmic reticulum Ca^{2+} ATPase (SERCa2a) and K^+ ions continue to be extruded by outward K^+ channels. This removes positive charge from the cell, which continues until a resting potential of -85 mV is once again reached. During this period the cell is refractory to any further activation, until the rapid depolarization and increase in membrane potential in *Phase 0*. The whole AP event lasts ~300 msec.

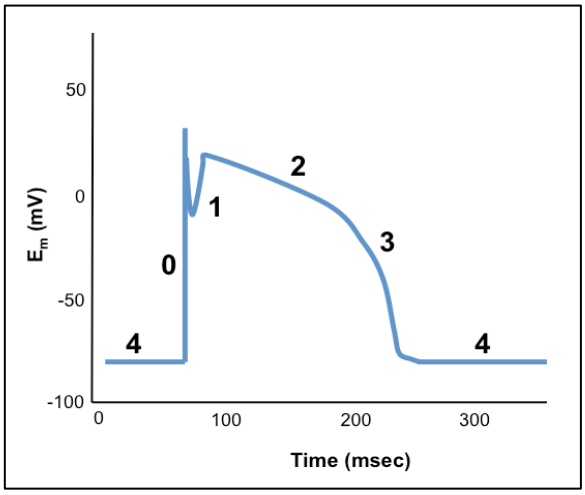

Figure 1.2 The cardiac action potential. Distinct phases are numbered and discussed further in Section 1.2.2. Adapted from Marban (2002).

1.2.3 Excitation-contraction coupling

In normal ventricular EC coupling, in response to inward Na^+ current during AP, depolarization of the sarcolemma activates voltage-gated LTCCs in TTs. Ca^{2+} influx into the cytoplasm via LTCCs subsequently induces massive Ca^{2+} release from clusters of RyR2 channels on the sarcoplasmic reticulum (SR) (Bers 2008). There is also a small amount of Ca^{2+} release from the SR via inositol 1,4,5-trisphosphate receptors (IP_3R). This is a mechanism termed Ca^{2+}-induced Ca^{2+} release (CICR) and the close physical association of sarcolemmal LTCCs and junctional SR membrane RyR2 channels (~15 nm) is necessary for optimal CICR and efficient EC coupling (Fabiato 1985b; Bers 2002b; Hong and Shaw 2016). CICR is also highly sensitive to both the speed and amplitude of the Ca^{2+} trigger (Fabiato 1985a; Fabiato 1985b). The global increase in intracellular Ca^{2+} levels activates contractile machinery and leads to muscle contraction. For relaxation to occur, there must be a decrease in intracellular Ca^{2+} levels. Ca^{2+} is extruded from the cell via Na^+/Ca^{2+} exchanger (NXC) and plasmalemmal ATPase, while Ca^{2+} is returned to mitochondria by a/the mitochondrial Ca^{2+} uniporter, and sequestered to the SR via SERCa2a (Bers 2002b). SERCa2a activity is modulated by phospholamban (PLB), whose inhibitory association to SERCa2a is relieved by phosphorylation. **Figure 1.3** outlines EC coupling within a ventricular cardiomyocyte.

The events that occur in EC coupling are tightly regulated to ensure a Ca^{2+} flux balance, whereby during the steady state, the amount of Ca^{2+} entering the cell is equal to that which is removed from the cell (Negretti et al. 1995; Eisner et al. 1998). In response to imbalances between Ca^{2+} influx and efflux, Ca^{2+} transient amplitude changes. The amplitude of a Ca^{2+} transient is controlled by both Ca^{2+} current and SR Ca^{2+} content. Increased Ca^{2+} current through activated LTCCs will increase the number of RyR2 channels that open, thus (albeit briefly) increasing the Ca^{2+} current through RyR2. This explains the observation of an increased amplitude of systolic Ca^{2+} transient amplitude in cardiomyocytes upon the addition of submicromolar levels of caffeine, concentrations which enhance the opening of RyR2 (O'Neill et al. 1990; Trafford et al. 2000). This increase in Ca^{2+} transient is brief however, as to restore a Ca^{2+} flux balance, the SR Ca^{2+} content decreases until a new steady state is achieved, thus Ca^{2+} transient amplitude declines. The amplitude of a Ca^{2+} transient is therefore a steep function of SR Ca^{2+} content (Bassani et al. 1987; Trafford et al. 1997). The content of the SR is determined by balance of Ca^{2+} uptake into SR by SERCa and efflux through RyR2 (Eisner et al. 2017). This therefore depends of biophysical properties of these proteins as well as the concentration of Ca^{2+} in the cytoplasm.

Although SR content is tightly controlled, Ca^{2+} will leak out of the SR through RyR2s due to stochastic channel openings and some spark activity (Bridge 1986; Sitsapesan and Williams 1994; Zima et al. 2010). Decreased SR Ca^{2+} content and decreased Ca^{2+} transient amplitude occurs because of Ca^{2+} leak, even in a physiological setting, but is compensated for by fine tuning of the flux balance to restore a steady state. However, increased Ca^{2+} leak can be arrhythmogenic, as a result of intracellular Ca^{2+} waves. Waves occur when Ca^{2+} spark frequency in flux through RyR2 increases, activating other RyR2 channel clusters in a propagating and untimely manner (Cheng H. et al. 1996). This can activate NCX, driving an arrhythmogenic inward depolarization (Ferrier et al. 1973). This is discussed further in **Section 1.6**.

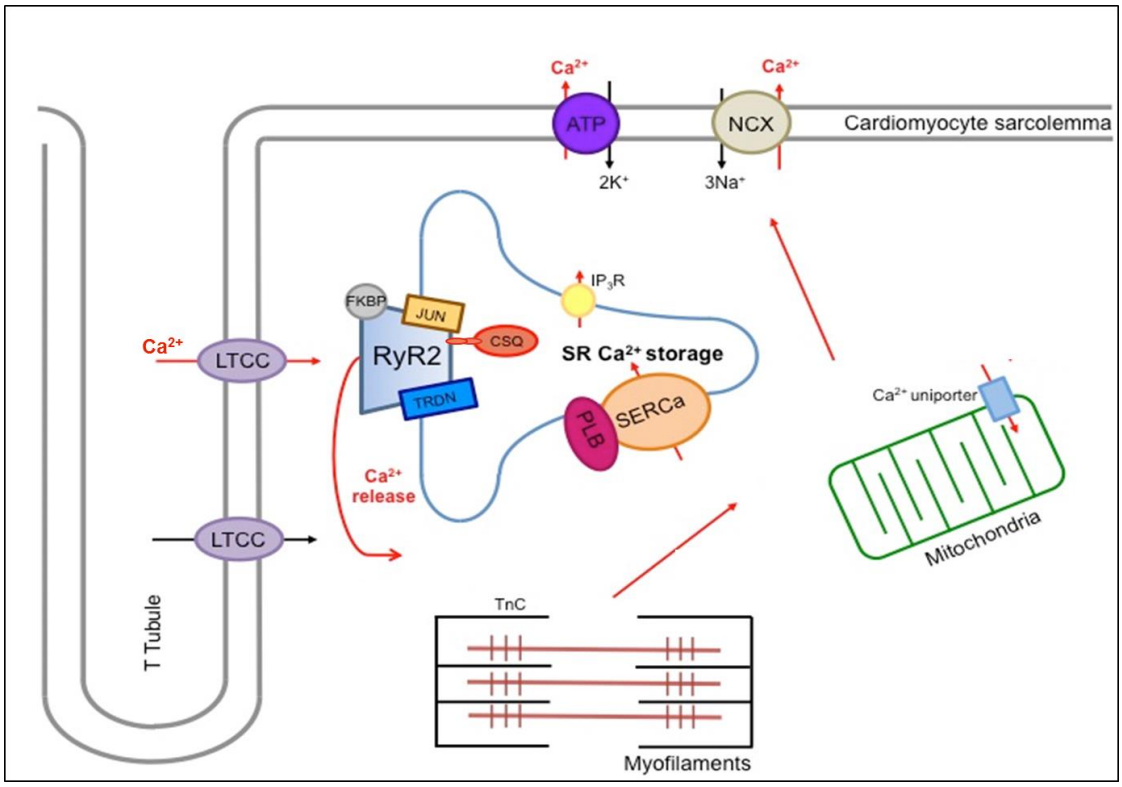

Figure 1.3 Excitation-contraction coupling within a ventricular cardiomyocyte. Illustrated are the major proteins involved in EC coupling. Depolarization of the ventricular cardiomyocyte initiates Ca^{2+} influx through LTCCs, triggering Ca^{2+} release from the SR store through RyR2 channels. There is also Ca^{2+} release via inositol 1,4,5-trisphosphate receptors (IP_3R). An overall increase in cytosolic Ca^{2+} level initiates the contraction of myofilaments. During relaxation, there is Ca^{2+} reuptake via SERCa (SERCa2a) back into the SR (modulated by PLB), as well as Ca^{2+} uptake into mitochondria via uniporters and removal of Ca^{2+} from the cell via NCX. Associated proteins of RyR2 include FK-506 binding protein 12.6 (FKBP), junctin (JUN), triadin (TRDN) and calsequestrin (CSQ2). These proteins are discussed in **Section 1.3.4.** Figure adapted from Bers (2002).

1.2.4 The β-adrenergic pathway

The force and rate of the heartbeat increases to pump more blood around the body in response to increased metabolic demand and there are many mechanisms to regulate this, both intrinsic and extrinsic to the heart. In situations of physical and emotional stress, the 'fight or flight response' is critical to maintain Ca^{2+} homeostasis (Marx, Reiken, et al. 2001; Marks et al. 2002). Stimulation of β-adrenergic receptors by catecholamines such as adrenaline (epinephrine) leads to increased production of secondary messenger cyclic AMP (cAMP, see **Figure 1.4**). When intracellular levels of cAMP rise, cells that generate AP to trigger cardiac contraction (sinoatrial node cells) depolarize faster. This leads to an increase in chronotropy (an acceleration in heart rate).

Increased levels of cAMP also activate protein kinase A (PKA) that phosphorylates many proteins involved in EC coupling, upregulating their activity (Reiken et al. 2003; Bers 2002b). PKA-mediated phosphorylation of LTCCs increases Ca^{2+} influx into the cell, whereas that of RyR2 and IP3R increases Ca^{2+} release from the SR. This increased concentration of cytosolic Ca^{2+} results in a positive inotropic effect i.e. with more Ca^{2+} ions being available to bind to the contractile machinery, increasing actin-myosin cross bridge formation and therefore contractile force (as described in **Section 1.2.1**).

Phospholemman (PLM) is also phosphorylated, relieving its inhibitory effect on plasmalemmal Na^+/K^+ ATPase (ATP in Figure **1.4**), therefore increasing Na^+ extrusion and K^+ influx (Q. Song et al. 2011; Tulloch et al. 2011). Enhanced Ca2+ efflux therefore upregulates lusitropic effects (faster relaxation). PKA-mediated phosphorylation of NCX is suggested to increase NCX activity, although this is disputed (Reppel et al. 2007; Bers et al. 2006). Overall, these actions result in increased cardiac output (G. D. Thomas 2011; Bers 2008; Bers 2001).

The roles of Ca^{2+}/Calmodulin-dependent protein kinase II (CaMKII) and exchange factor directly activated by cAMP (Epac) in this process are discussed in **Section 1.4**.

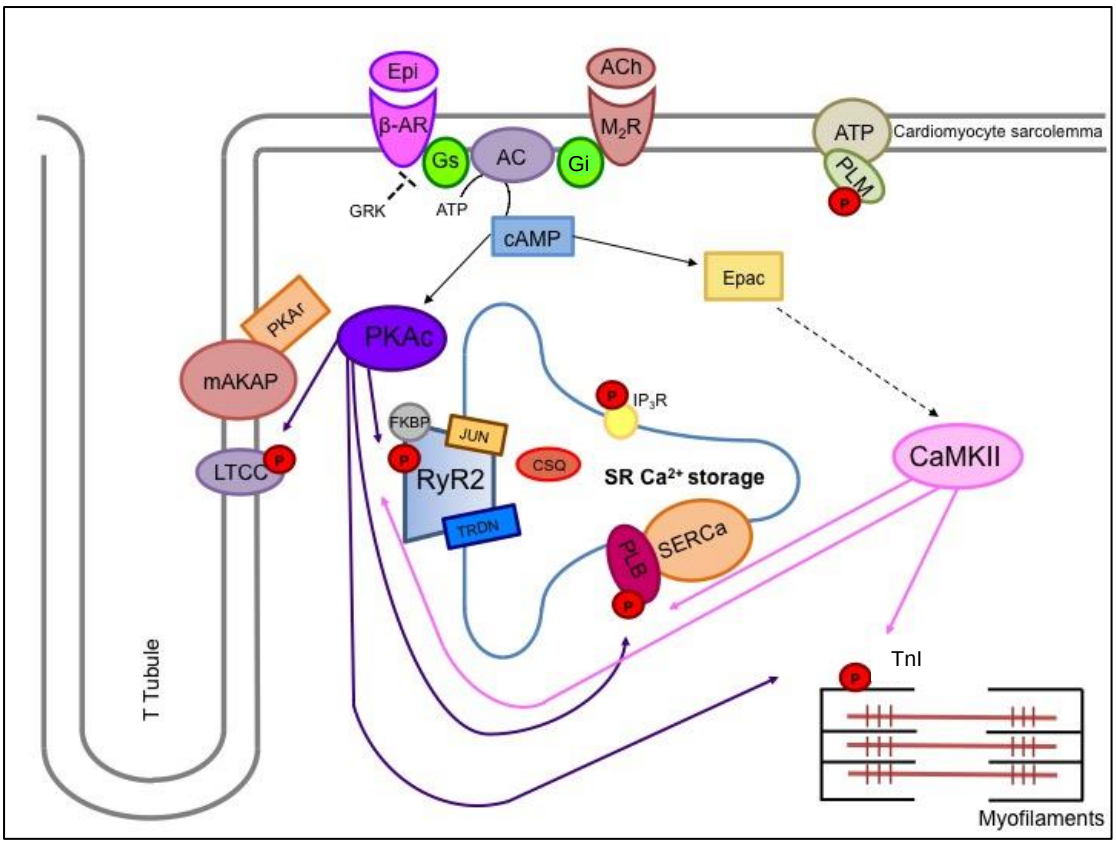

Figure 1.4 β-adrenergic stimulation and phosphorylation of EC coupling proteins. Sympathetic beta-adrenergic receptor (β-AR) activation by catecholamines such as adrenaline (Epi) triggers downstream signalling cascades leading to increased inotropy and lusitropy in EC coupling. Stimulatory G protein (Gs) activates adenylate cyclase (AC) to produce the secondary messenger cAMP from ATP. This in turn stimulates the catalytic unit of PKA (PKAc) and Epac. PKAr, the regulatory subunit, is anchored to the sarcolemma by muscle anchoring protein kinase A (mAKAP, (Newlon et al. 1999; L. J. Huang et al. 1997; Scott and McCartney 1994)). When PKAc is dissociated from PKAr by cAMP, it phosphorylates proteins LTCC, RyR2, IP_3R, TnC and PLB. The stimulation of Epac is thought to activate CaMKII, which also leads to phosphorylation of proteins RyR2, PLB and TnC. Proteins which feature in this figure that are not mentioned here are discussed in more detail in **Section 1.4.** Also indicated on the diagram are proteins activated by parasympathetic stimulation, the muscarinic receptor (M_2R). Stimulation via acetylcholine (ACh) and activation of inhibitory G protein (Gi) decreases inotropic and lusitropic effects. Adapted from Bers (2002) Ruiz-Hurtado et al. (2013) and Pereira et al. (2007).

1.3 RyR2 as an ion channel

RyR channels are the largest ion channels known, functional as a ~2.2 MDa homotetramer consisting of four 565 kDa subunits (Tunwell et al. 1996). They reside on the ER/SR as Ca^{2+} release channels and are so named after their interaction with alkaloid ryanodine, extracted from the *Ryania speciosa* plant (Jenden and Fairhurst 1969; Pessah et al. 1986). Although ryanodine was first isolated as an insecticide, paralytic action on both skeletal and cardiac muscle was quickly evident (Fabiato 1985a; Sutko and Kenyon 1983; Nayler et al. 1970; Fairhurst 1973; Elison and Jenden 1967). The alkaloid was shown to inhibit Ca^{2+} release from the SR by binding to a high molecular weight protein present in the membrane (Fabiato 1985a; Sutko and Kenyon 1983; Cannell and Vaughan 1985). This protein was subsequently purified and revealed as a homotetrameric ion channel (Inui et al. 1987; Holmberg and Williams 1989; Lai et al. 1988; Campbell et al. 1987; Tunwell et al. 1996; Hymel et al. 1988; Sitsapesan and Williams 1994a; Pessah et al. 1986).

RyR channels are expressed in many cell types in a variety of tissues, but are at highest density in striated muscle (Fill and Copello 2002). Molecular cloning studies have identified three different mammalian isoforms, encoded by three different genes found on different chromosomes (Zorzato et al. 1990; Marks et al. 1989; Takeshima et al. 1989). RyR1 is predominately expressed in skeletal muscle (Otsu et al. 1990; Zorzato et al. 1990; Ogawa 1994); RyR2 predominately in cardiac muscle, although also in the brain (Lai et al. 1988; Tunwell et al. 1996; Sorrentino and Volpe 1993; Otsu et al. 1990); and RyR3 more ubiquitously throughout the body, including the brain, diaphragm and smooth muscle tissue (Sutko 1991; Froemming et al. 2000; Nakai et al. 1990). At the amino acid level, these isoforms share ~70% homology (Nakai et al. 1990; Hakamata et al. 1992). While each isoform is tissue specific, similar characteristics include that they function as a poorly selective Ca^{2+} channels with high conductance, regulated by Ca^{2+}, magnesium (Mg^{2+}), ATP and caffeine (Fill and Copello 2002).

1.3.1 Structure of RyR

The structure of solubilized RyR channels can be assessed by three-dimensional (3D) reconstruction techniques whereby electron microscopy images of the protein at different angles are merged (Y. Cheng et al. 2015; Frank 2009). In combination with cryo-electron microscopy (cryo-EM) the specimen can be imaged without staining and under frozen-hydrated conditions, allowing access to the structure of the protein fully hydrated within physiological buffer (Skiniotis and Southworth 2015; Samsó 2016).

Three single particle cryo-EM studies have recently described the architecture of the closed state of rabbit RyR1, with a near-atomic model described for ~70 % of the channel at a resolution of 3.8 Å (Efremov et al. 2014; Zalk et al. 2014; Yan et al. 2014). The open state structure has been resolved to ~4 Å (Georges et al. 2016; Wei et al. 2016). The elucidation of RyR2 channels in this manner is hindered by difficulties in isolating large quantities of purified functional channels from cardiac muscle, but with ~70 % sequence homology between isoforms, much can be gleaned from the structure of RyR1 (Z. Liu et al. 2001; Nakai et al. 1990; Hakamata et al. 1992).

Originally described as 'foot-like structures' observed at the junction between cisternae of the SR and the TT network, RyR channels have a mushroom-shaped architecture with a large N-terminal domain that protrudes into the cytosol (Franzini-Armstrong et al. 1998). The C-terminal domain of the protein consists of a pore-forming region and ~6 transmembrane (TM) helices. Regulatory proteins that associate to the channel make the structure overall a large macromolecular complex (see **Section 1.3.4,** (Yano et al. 2009)).

RyR1 can be divided into a 'cytosolic shell', consisting of the N-terminal domains through to the end of the bridging solenoid for each subunit, and a 'channel and activation core' from the C-terminal remainders, including the core solenoid and associations with cytosolic extensions from the tetrameric pore ((Georges et al. 2016), see **Figure 1.5 A**).

The cytosolic shell has a flat square prism shape formed by multiple domains of each of the four identical subunits. N-terminal domains A, B and C (NTD-A, -B and -C)
SPRY domains are protein-protein interaction molecules that consist of a β-sandwich of two β-sheets, named after their discovery in sp1A kinase and RyR channels (D'Cruz et al. 2013; Efremov et al. 2014; Ponting et al. 1997). There are three SPRY domains per RyR1 subunit (SPRY1, 2 and 3); SPRY 1 protrudes into the cytoplasmic assembly and forms part of the binding site for FKBP12 (see **Section 1.4.1.5**), SPRY2 interacts with subunits of LTCCs

(although the equivalent peptide of RyR2 does not), and SPRY3 sits on the surface of RyR1 facing TTs (Yuchi et al. 2015; Ponting et al. 1997; Leong and MacLennan 1998; Samsó 2016). RyR repeats 1&2 (also referred to as P1) is a sequence that continues from the SPRY cluster, with two β-sheets forming an L-shaped attachment (Yuchi et al. 2015).

Following RyR repeats is the junctional solenoid (JSol, also known as the Handle domain) and the bridging solenoid (BSol, also known as HD1 and HD2). JSol is formed by 16 α-helices and contains the binding sites for FKBP12 and CaM, while BSol forms an extended α-solenoid that includes a crevice and a 200 Å-long ribbon that loops out and connects JSol to SPRY2 of the neighbouring subunit (Georges et al. 2016). Both JSol and SPRY1 bind FKBP12.6. The flexibility and architecture of these domains confer elasticity to the structure and are likely to have a role in long range allosteric communication (Samsó 2016). They also lie close to the phosphorylation P domain, predicted at residues 2735-2938 (Yuchi et al. 2013). The analogous region in RyR2 contains phosphorylation sites Serine 2808 and Serine 2814.

The channel and activation core are linked to the cytosolic shell by a shell-core linker peptide (SCLP) that contains CaM and JSol binding sites. The core solenoid (CSol, or central domain) is the only cytoplasmic domain that interacts with the transmembrane domain, and is thought to regulate conformational changes necessary to control channel opening and closing (Georges et al. 2016; Yan et al. 2014). This domain contains two EF hands that are suggested to confer Ca^{2+}-sensing ability to the channel by a large conformational change upon binding Ca^{2+} in the pore of the protein (Y. Chen et al. 2014). It also contains a ‘thumb and forefinger’ domain (TaF) and two auxiliary transmembrane domains (TMx2) that are located between pVSD and pore domains of adjacent protomers (Georges et al. 2016).

The secondary structure of the pore is predicted to have six helical transmembrane regions per subunit (S1-S6, see **Figure 1.5 B**), which collectively form the pseudo voltage sensor domain (pVSD (Georges et al. 2016; Yan et al. 2014)). pVSD is named as such as RyR does not exhibit voltage dependence but this fold is characteristic of voltage-gated ion channels. The fold is formed by the sequences in between S2 and S3 transmembrane regions and links to the C-terminal domain (CTD), four of which contact each other in the closed state of the channel, forming the ‘cytoplasmic restriction’ (Samsó et al. 2009). CTD resides close to S1-S4 regions and forms a ‘column-like’ structure with CSol. A luminal hairpin loop between S5 and the pore helix projects into the lumen of the SR and resides above the selectivity filter, and together with S6 transmembrane region forms the channel

pore. The selectivity filter (SF) and S6, rich in aspartic and glutamic acid residues, form a long pathway of ~90 Å for ion conduction that allows Ca^{2+} transport across the SR membrane (Yan et al. 2014).

Channel gating is thought to involve global conformational changes in both the cytosolic shell and channel and activation core, including bending of the S6 transmembrane segment (Georges et al. 2016). Subsequent pore dilation, displacement and deformation of the S4-S5 linker leads to conformational changes in the pVSD allowing for Ca^{2+} ion transport.

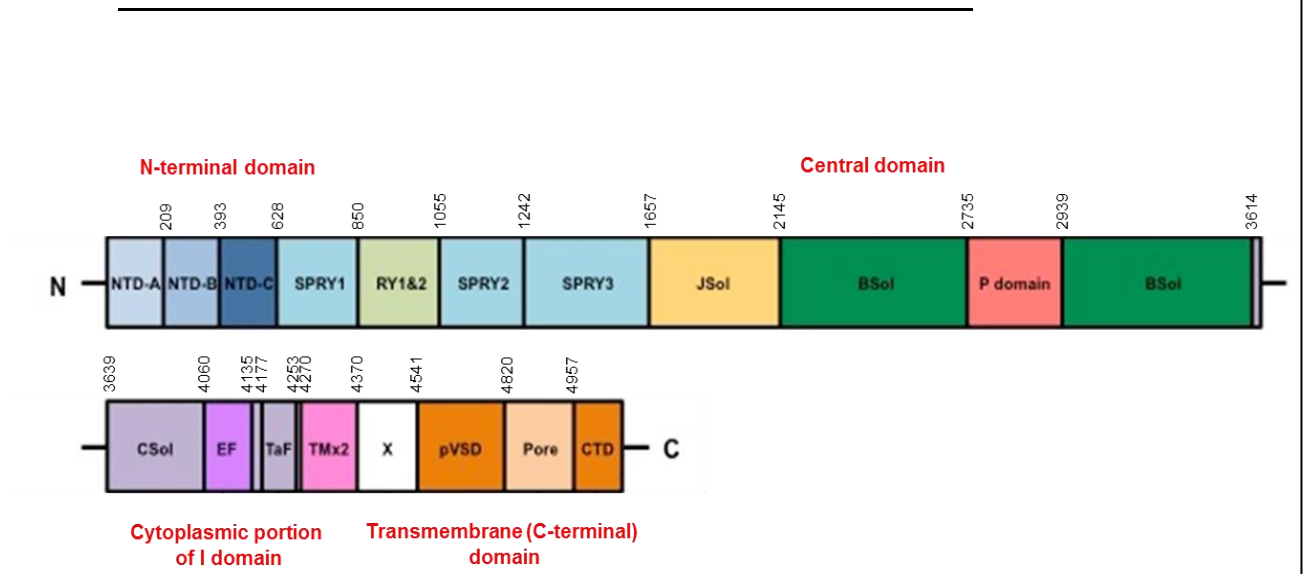

Domain symbol	Identification	Residue Span
Cytosolic shell		1-3613
NTD-A	N-terminal A domain	1-208
NTD-B	N-terminal B domain	209-392
NTD-C	N-terminal C domain	393-627
SPRY1	SP1a/RyR domain 1	628-849
RY1&2	RyR repeats 1 and 2	850-1054
SPRY2	SP1a/RyR domain 2	1055-1241
SPRY3	SP1a/RyR domain 3	1242-1656
JSol	Junctional solenoid	1657-2144
BSol	Bridging solenoid	2145-3613
P domain	Phosphorylation domain	2735-2938
Channel and Activation core		3614-5037
SCLP	Shell-core linker peptide, CaM and JSol binding sites (from BSol to part way through CSol)	3614-3666
CSol	Core solenoid	3639-4174
EF	EF-hand pair	4060-4134
TaF	Thumb and forefingers domain	4177-4253
TMx2	Auxiliary transmembrane helices	4270-4369
X	Unknown due to lack of EM density, predicted as a number of EF-hand domains	4252-4540
pVSD	Pseudo voltage sensor domain	4541-4819
Pore	Channel pore domain	4820-4956
CTD	C-terminal domain	4957-5037

Figure 1.5 An Illustration of the structure of RyR channels. Schematic displaying the domains with residue spans of RyR1. Image and table modified from des Georges et al. (2016).

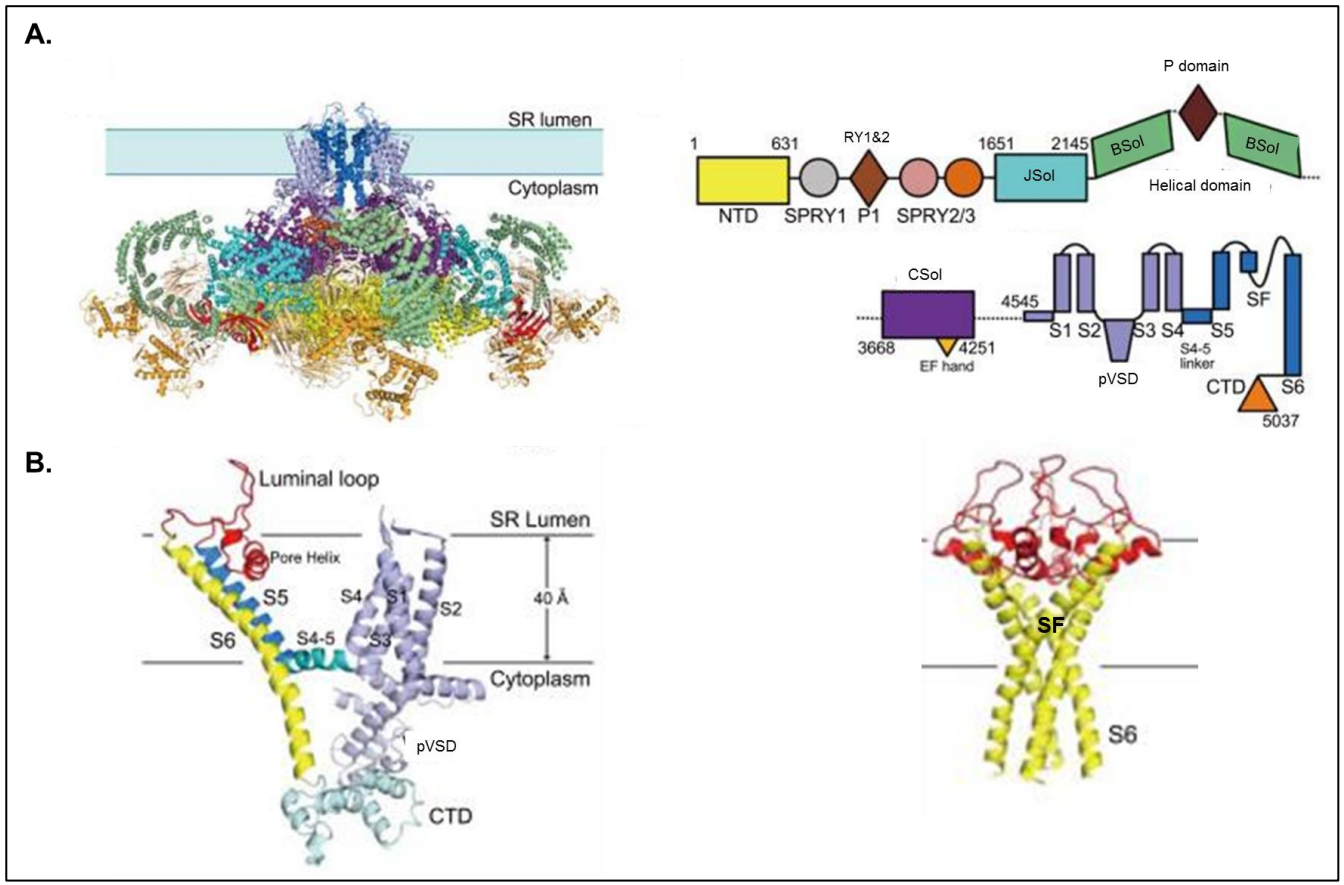

Figure 1.5 B Illustrations of the structure of RyR channels. *A.* Illustration of the RyR1 channel, domain organization and it's positioning in the SR lumen (left). The domains are colour-coded per the labelled schematic (right). *B.* Transmembrane regions (S1-S6), pore helix, luminal loops etc. are shown in one RyR1 protomer (left). Also shown is the ion-conducting pathway of the channel, predicted to consist of a selectivity filter (SF) and S6 segments (right). Image modified from Yan et al. (2015).

1.3.2 RyR2 organization and coupled channel gating

RyR2 channels do not normally act independently of one another. Activation of other RyR2 channels within a cluster is a critical component of CICR. RyR2 channels in cardiac muscle therefore are suggested to form regular arrays within the native environment (see **Figure 1.6**) - two dimensional (2D) crystals often described as a 'checkerboard' (Franzini-Armstrong 2016; Cabra et al. 2016; Franzini-Armstrong et al. 1998; Ferguson et al. 1984). Adjacent RyR2 channels within a cluster can be as close as 30nm apart, allowing Ca^{2+} released by one RyR2 channel to travel and activate neighbouring channels (Kunitomo and Terentyev 2011). Coordinated Ca^{2+} release through RyR2 channels within a cluster constitutes a Ca^{2+} spark (H. Cheng et al. 1994). During pathological conditions of aberrant Ca^{2+} release, Ca^{2+} sparks ignite neighbouring clusters by a fire-diffuse-fire mechanism, triggering regenerative CICR-driven Ca^{2+} waves that are proarrhythmic (Bovo et al. 2011; Kunitomo and Terentyev 2011).

This supports the notion that allosteric movements of one RyR2 channel can be transmitted mechanically to neighbouring channels. In single channel studies of both RyR1 and RyR2, it has been observed that RyR2s can undergo 'coupled gating', whereby two or more channels open simultaneously (Mojzisova 2002; J. Gaburjakova and M. Gaburjakova 2016; Porta et al. 2012; Marx et al. 1998; J. Gaburjakova and M. Gaburjakova 2014; Marx, Gaburjakova, et al. 2001). The Marks group proposed that a coupled interaction of RyR2 channels is mediated by FKBP12.6 and that dissociation from RyR2 disrupts gating, without causing a physical uncoupling (Marx et al. 1998; Marx, Gaburjakova, et al. 2001). However, the role of FKBP12.6 dissociation on RyR2 channel function remains heavily debated (see **Section 1.4.2.1**).

In single channel studies, where authors report to observe coupled RyR2 channels, there is a change in the kinetics of channel gating (J. Gaburjakova and M. Gaburjakova 2014; Porta et al. 2012; J. Gaburjakova and M. Gaburjakova 2008; J. Gaburjakova and M. Gaburjakova 2010). Where channels are coupled they exhibit much longer closed times and less openings, as well as much longer open times under activating conditions. Coupled gating of individual RyR2 channels recruited into a functional complex is suggested to ensure the correlation of Ca^{2+} fluxes during Ca^{2+} release.

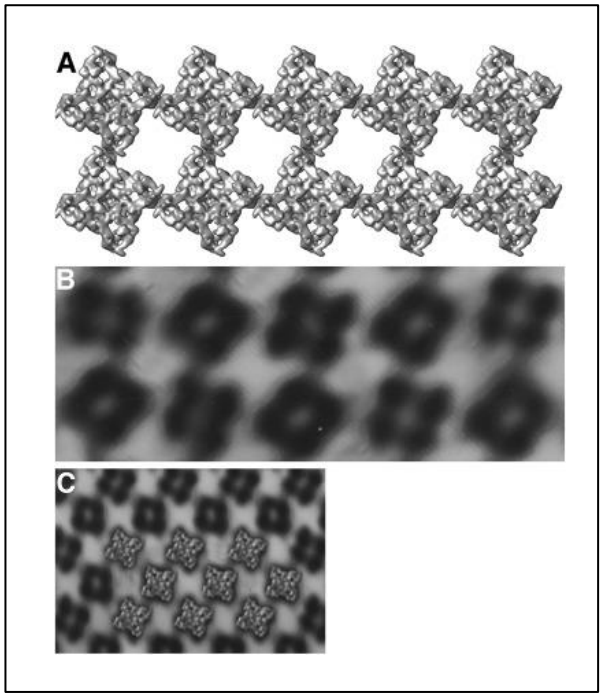

Figure 1.6 Illustration of possible RyR arrays. *A.* The checkerboard array of RyR1 in skeletal muscle is well established. *B.* A filtered and two-dimensional reconstructed image from the RyR array of scorpion tail muscle shows two alternate orientations of RyRs. *C.* Profiles of RyR2 oriented as predicted by the "oblique interaction" whereby two partially overlapped RyR2s form an angle of 12 º, fit well over the scorpion array, suggesting this may be a possible disposition of RyR2 in cardiac muscle. Image modified from Cabra et al. (2016) and Franzini-Armstrong (2016).

1.3.3 Regulation by endogenous modulators

A variety of physiological ligands can modulate RyR2 activity, with Ca^{2+} by far the most important effector of channel function. There remains debate as to the specific contributions of cytosolic and luminal Ca^{2+} to channel activation and the termination of CICR by RyR2 channels during EC coupling. However, four Ca^{2+}-sensing/binding sites per RyR2 monomer have been proposed by Laver (2007, **Figure 1.7**). Contribution of each of these sites and related physiological ligands is discussed below.

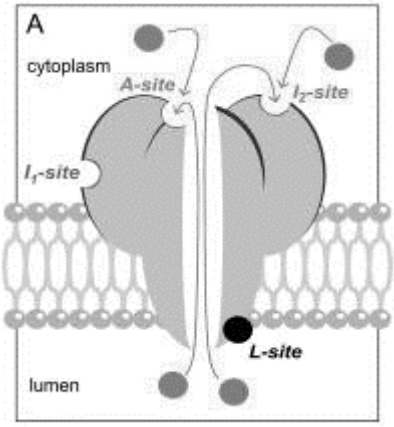

Site	Proposed effect	Ligand	Dissociation constant
A-site	Cytoplasmic activation	Ca^{2+}	1-10 µM
I_1-site	Cytoplasmic inhibition	Ca^{2+} and Mg^{2+}	10 mM
I_2-site	Cytoplasmic inactivation	Ca^{2+}	1 µM
L-site	Luminal activation	Ca^{2+}	60 µM

Figure 1.7 Schematic of location of proposed RyR2 binding sites. Image from Laver (2007). Exact locations of these binding sites remain to be identified.

1.3.3.1 RyR2 activation by cytosolic and luminal Ca^{2+}

Single channel analysis of RyR2 from explanted hearts of patients with end-stage heart failure (HF) revealed that raising the cytosolic Ca^{2+} concentration from 1 to 100 µM, when luminal Ca^{2+} concentration was maintained at 67 mM, increased the number of channel opening events significantly (Holmberg and Williams 1989). Cytosolic Ca^{2+} also increases the number of opening events of RyR2 channels isolated from healthy human hearts (that were not required for transplant) and of WT recombinant human RyR2 (Mukherjee et al.

2012; Walweel et al. 2014). In the work of Mukherjee et al. (2012), the greatest increase in recombinant hRyR2 open probability (P_o) was observed at cytoplasmic Ca^{2+} concentrations between 100 nM -1 µM at 5 nM luminal Ca^{2+} concentration, while increases in concentration about 10 µM caused P_o to reach saturation.

Luminal Ca^{2+} has been implicated in regulating RyR2 channel function since the early works of Fabiato (Fabiato 1985a; Fabiato 1985b) and demonstration of luminal regulation of single RyR channels in the early 1990s {Sitsapesan:1994vs, Sitsapesan:1995tw}. As spontaneous Ca^{2+} release and waves occurs when SR Ca^{2+} content reaches a critical threshold (Venetucci et al. 2008), it would logically follow that luminal Ca^{2+} concentration is causative of this release event. The *feed-through hypothesis* proposes that luminal Ca^{2+} can activate the channel by flowing through the open channel and activating cytosolic activation sites, (Tripathy and Meissner 1996)(L. Xu and Meissner 1998). However, single channels have been shown to activate under conditions where luminal-to-cytosolic Ca^{2+} flux is prevented (Gyorke 1998; Ching et al. 2000). Ca^{2+} release also increases in a nonlinear fashion with increased SR Ca^{2+} content (Shannon et al. 2000), suggesting the process is regulated by more than one mechanism (Rovetti et al. 2010). In the *luminal-triggered feed through mechanism*, luminal Ca^{2+} is thought to be sensed by a luminal Ca^{2+} activation site (*L-site*, **Figure 1.7**), which is distinct from the cytosolic *A-site* (Laver 2007), but the identity of this site remains to be defined (Priori and S. R. W. Chen 2011). This luminal activation has also been suggested as CSQ2-dependent (Terentyev 2008), the accessory protein acting as a luminal Ca^{2+} sensor, exerting an inhibitory effect on RyR2 (see **Section 1.3.4.1**).

1.3.3.2 Termination of CICR by cytosolic and luminal Ca^{2+}

CICR by nature is a positive feedback mechanism, whereby the increase of cytosolic Ca^{2+} concentrations lead to RyR2 Ca^{2+} release from intracellular stores. In turn this increases cytosolic Ca^{2+}, so should be a self-regenerating and inherently unstable process (Fill and Copello 2002; Kunitomo and Terentyev 2011). However, this is not observed in cardiomyocytes and regulation by either cytosolic Ca^{2+}, luminal Ca^{2+}, both or other RyR2 channel modulators must be key to terminating SR Ca^{2+} release. Several mechanisms have been proposed that involve RyR2 Ca^{2+} binding sites (Zima et al. 2014; Stern and H. Cheng 2004).

Fabiato originally proposed that an increase in intracellular cytosolic Ca^{2+} levels during CICR stops RyR2 Ca^{2+} release via binding of Ca^{2+} to cytosolic low affinity sites, suggested by Laver (2007) as the *I_1-site* (**Figure 1.7**) on the channel at concentrations of 1-10 mM.

Evidence has accumulated that inactivation of RyR2 by cytosolic Ca^{2+} plays a limited role in the termination of CICR, with single channel experiments showing no evidence of Ca^{2+}-dependence at these low Ca^{2+} concentrations (Percival et al. 1994; 1995).

It was demonstrated that RyR2 responds to change in luminal Ca^{2+} concentration within the SR, and this luminal-Ca^{2+} dependent deactivation has been proposed as an underlying cause of the termination of Ca^{2+} sparks (Terentyev, Kubalova, et al. 2008; Gyorke 1998; Brochet et al. 2005; Sitsapesan and Williams 1994b; Zima et al. 2008). This is supported by further evidence that Ca^{2+} sparks cease when the SR Ca^{2+} concentration falls to a critical threshold level (Terentyev, Kubalova, et al. 2008; Brochet et al. 2005; Zima et al. 2008). Termination in this instance may occur by two different mechanisms. Firstly, the depletion Ca^{2+} from the SR may drive unbinding of Ca^{2+} from the RyR2 luminal activation site (L-site) and promote channel closing via direct regulation (Terentyev, Kubalova, et al. 2008; D. Jiang et al. 2007). Secondly, a local SR Ca^{2+} depletion could reduce the unitary current via RyR2, decreasing local intracellular Ca^{2+} levels and breaking the feedback of local CICR within a cluster (Laver et al. 2012; T. Guo et al. 2012; Sato and Bers 2011).

Adaptation was proposed by Györke and Fill, who found that the application of fast trigger Ca^{2+} signals to single RyR2 channels led to an initial burst of single-channel activity with high P_o values, which spontaneously decayed with no evidence of Ca^{2+}-dependent inactivation (Györke and Fill 1993a). On application of a second Ca^{2+} stimulus, the 'inactivated' channels were reactivated (exhibiting a short-lived Ca^{2+} transient termed the 'fast Ca^{2+} overshoot'), suggesting spontaneous decay of P_o after the initial stimulus was not due to a Ca^{2+}-dependent inactivation, but mediated by a process termed adaptation (Valdivia et al. 1995; Györke and Fill 1993a). This spurred debate, with not all groups reporting 'adaptive behaviour' and that flash photolysis application of Ca^{2+} in this experiment simply leads to deactivation following the fast Ca^{2+} overshoot (Lamb et al. 2000; Lamb and Stephenson 1995). It has since been suggested that adaption is due to a time and Ca^{2+}-dependent shift in gating behaviour of single channels and that it is not a mutually exclusive mechanism from Ca^{2+}-dependent inactivation (Zahradník et al. 2005; Györke and Fill 1993b; Györke 1999).

Stochastic attrition refers to random spontaneous closing of an individual RyR2 channel. Stern (1992) hypothesized from mathematical modelling that this process was sufficient to terminate local Ca^{2+} release from the SR if there were <10 RyR2 channels within a cluster, but likelihood of termination in clusters of 10-30 channels was low (Stern 1992; Sham et al. 1998). However, the rate of Ca^{2+} release termination is proportional to the magnitude of the

release event (Lukyanenko and Wiesner 1998), so stochastic attrition is unlikely to play a major role in CICR (Fill and Copello 2002)

1.3.3.3 Role of ATP and Mg^{2+}

The cytosol of a cardiomyocyte contains approximately ~5 mM total ATP, with most in a Mg^{2+}-bound form (Fill and Copello 2002). Free ATP (~300 μM) binds to and activates RyR2 and has been shown to increase RyR2 P_o, but only when cytoplasmic Ca^{2+} is present (Laver 2007; Witcher et al. 1991). ATP may sensitize the channel to activation by Ca^{2+}, rather than direct activation, although earlier studies suggest that ATP can in fact have a Ca^{2+}-independent action {Kermode:1998ga}.

Mg^{2+} is a potent channel inhibitor, but its action is more complicated. Firstly, it inhibits RyR2 activity in the millimolar concentration range, most prominently at low cytoplasmic Ca^{2+} concentrations, suggestive that Mg^{2+} exhibits physiological effects during diastole (Rousseau and Meissner 1989; Rousseau et al. 1987; Holmberg and Williams 1989). This action is likely by competition with Ca^{2+} at the non-specific Ca^{2+} inhibition I_1-site (**Figure 1.7**, (Laver 2007)). Secondly, Mg^{2+} has been shown to increase RyR2 activation at higher cytoplasmic Ca^{2+} concentrations (~10-100 μM) in one instance and may compete with luminal Ca^{2+} at the luminal activation L-site (Laver 2007; Chugun et al. 2006).

1.3.4 Accessory and associated proteins

Accessory and associated proteins of the macromolecular RyR2 complex are illustrated in **Figure 1.8** and are described below.

The termination of SR Ca^{2+} release through RyR2 remains incompletely understood, yet it appears to involve luminal Ca^{2+} regulation of channel activity (Terentyev et al. 2002; Radwański et al. 2012). A luminal Ca^{2+} sensor is formed within the RyR2 quaternary complex (see **Figure 1.8**), consisting of cardiac calsequestrin (CSQ2) and SR membrane proteins triadin and junctin (G. Liu and Pessah 1994; W. Guo and Campbell 1995; L. Zhang et al. 1997). The presence of all these accessory proteins is thought to be required for CSQ2 to regulate RyR2 activity in response to changes in luminal Ca^{2+} concentrations (Gyorke *et al.*, 2004; Gyorke *et al.*, 2009). Luminal Ca^{2+} has been shown to directly affect RyR2, and indirectly affect the channel through CSQ2, a Ca^{2+} buffering protein that traps Ca^{2+} within the SR store (Terentyev 2008; Wenqian Chen et al. 2014; Beard et al. 2009; M. Gaburjakova et al. 2012). CSQ2 exists as organized aggregates; monomers and dimers at low concentrations and polymers at high concentrations of luminal Ca^{2+} (E. Kim et al. 2007; Beard et al. 2005). The C-terminal of CSQ2 is negatively charged which allows high capacity binding of Ca^{2+} ions, ensuring Ca^{2+} is available at the pore of the RyR2 channel, ready for Ca^{2+} release during CICR (E. Kim et al. 2007). Functional association of RyR2 and CSQ2 has been well established, but only recently has a direct interaction been shown to exist (Handhle et al. 2016).

Junctin (JUN), a 26 kDa anchoring protein component of the luminal Ca^{2+} sensor, is a non-catalytic splice variant encoded by the aspartate-β-hydroxylase (*Asph*) gene (Dulhunty et al. 2009; Dulhunty et al. 2012). Junctin contains binding sites for both CSQ2 and RyR2 in a long luminal C-terminal domain containing several charged sequence repeats known as 'KEKE' motifs (L. R. Jones et al. 1995; Altschafl et al. 2011; Y. M. Kobayashi et al. 2000). JUN is suggested to act as a direct regulator of RyR2 activity, or transduce signals from CSQ2 to the channel in a Ca^{2+}-dependent manner, or both (Beard et al. 2009; Hester et al. 2004)). Interaction between the cytoplasmic domain of JUN and the cytoplasmic, not luminal domain of RyR2 has been evidenced, with binding enhancing RyR2 channel activity (L. Li et al. 2015). Knockout of the protein (KO) or knockdown in mouse models leads to an enhancement of Ca^{2+} release, suggestive that JUN or JUN-CSQ2 inhibit RyR2 at low concentrations of luminal Ca^{2+}, anchoring and positioning CSQ2 near the channel (L. Zhang et al. 1997; Fan et al. 2008; Hester et al. 2004).

Triadin (TRDN) can exist as three different isoforms produced by alternative splicing of the single *TRDN* gene (Marty 2014; Thevenon et al. 2003). Trisk 32 (32 kDa, also known as TRDN1) is the major cardiac isoform (Y. M. Kobayashi and L. R. Jones 1999). Much like JUN, TRDN is thought to anchor CSQ2 in the vicinity of RyR2, facilitating Ca^{2+} release indirectly by permitting CSQ2 to buffer luminal Ca^{2+} near the Ca^{2+} release site of RyR2 (L. Zhang et al. 1997; Y. M. Kobayashi et al. 2000). While functional studies have shown that TRDN itself is able to inhibit the activity of the RyR calcium channel *in vitro (*studies in RyR1), *in vivo* investigations suggest this RyR2 regulation is only via interaction with CSQ2 (Terentyev et al. 2007; Ohkura et al. 1998; Kučerová et al. 2012).

Calmodulin (CaM) is a 16.7kDa Ca^{2+} binding protein that directly associates with and regulates RyR2 channels, as well as other proteins and ion channels (Samsó and Wagenknecht 2001; Bers 2004). Structurally it consists of two pairs of Ca^{2+} binding EF hand domains separated by a flexible peptide linker, and binds to one site on each RyR2 monomer (Fruen et al. 2000). After binding to Ca^{2+}, CaM undergoes a conformational change and is known as Ca^{2+}-calmodulin or CaCaM, while the Ca^{2+}-free state is known as apoCaM (Samsó and Wagenknecht 2001; Chin and Means 2000). CaM is predicted to regulate RyR2 channel activity in both states. It has been proposed to inhibit RyR2 opening at the single channel level (S. L. Hamilton et al. 2001; Tripathy et al. 1995) and prevention of CaM binding to RyR2 in a knock-in mouse model harbouring a central domain CPVT mutation resulted in an arrhythmogenic phenotype (Xu *et al.*, 2010), suggestive that CaM has a critical role in regulating RyR2 function. CaM is also critical in regulating the activity of CaMKII, a protein kinase involved in RyR2 phosphorylation (see **Section 1.4.1**). CaM binding to RyR2 has also been suggested as required for the activity of the drug dantrolene (Nishimura et al. 2015; Oo et al. 2015). See Section **1.7.4** for further discussion.

Sharing structural features with CaM, sorcin is also an EF hand-containing Ca^{2+} binding protein of 22 kDa which directly interacts with RyR2 channels (Farrell and Antaramian 2003; Meyers et al. 1998; Bers 2004; Balshaw et al. 2002). The precise role of sorcin is yet to be established, but it has been shown to bind to Ca^{2+} with high affinity and is thought to cause RyR2 inhibition in a similar way to CaM (Farrell and Antaramian 2003; Zamparelli et al. 2000; Lokuta et al. 1997). S100A (also known as S100A1) is another EF hand-containing protein predicted to regulate RyR2 activity, reported to increase the likelihood of RyR2 opening (Prosser et al. 2011). It has also been shown to interact with CaMKII, inhibiting kinase activity, while CaMKII has been shown to phosphorylate sorcin, suggesting a joint regulatory effect on RyR2 channels (Anthony et al. 2007). Recent work suggests that CaM

and S100A can concurrently bind to RyR2 and modulate its activity, but this does not involve direct competition at the RyR2 CaM binding site (Rebbeck et al. 2016).

FK506 binding proteins are accessory proteins of RyR2 found in the macromolecular complex, also implicated in phosphorylation of the channel. They are described as immunophilins, based on their interactions with immunosuppressant drugs FK506 and rapamycin (Timerman et al. 1996; Zissimopoulos and Lai 2004). Two FKBP isoforms are detected in the cardiomyocyte, FKBP12 (or calstabin) and FKBP12.6 (or calstabin2), named as such by molecular weight (12 vs. 12.6 kDa). FKBP12.6 however has ~600-1000 fold increased affinity for RyR2 and it has been shown to directly interact with the cytoplasmic assembly of the protein (T. Guo et al. 2010; Timerman et al. 1996). There is a single FKBP12.6 binding site on each RyR2 monomer and therefore RyR2 associates with FKBP12.6 in a 1:4 stoichiometry (Jeyakumar et al. 2001; Timerman et al. 1996).

FKBP12 does not alter Ca^{2+} spark frequency of RyR2 as opposed to FKBP12.6 (T. Guo et al. 2010), or modulate recombinant RyR2 in heterologous expression systems (Goonasekera et al. 2005; George, SORATHIA, et al. 2003), indicating that FKBP12 may be functionally irrelevant to the channel. FKBP12 was shown as the predominant isoform in cardiac SR of many mammals and it has been reasoned that FKBP12 may undergo post-translational modifications that induce structural changes so that is resembles FKBP12.6 and confers the high-affinity binding observed with FKBP12.6 (Zissimopoulos et al. 2012).

FKBP12.6 interaction with RyR2 has been proposed to stabilize the channel, preventing spontaneous Ca^{2+} release and SR Ca^{2+} leak observed in disease states (Marx et al. 2000; George, SORATHIA, et al. 2003; Wehrens et al. 2005; Yano et al. 2003; Prestle et al. 2001). In other studies, treatment of WT single channels treated with drugs that suppress the FKBP12.6:RyR2 interaction (rapamycin and FK506) has significant effect of RyR2 channel function (Barg et al. 1997; Timerman et al. 1996). Overexpression of FKBP12.6 in mice resulted in reduced Ca^{2+} spark frequency, and enhanced cardiac output and contractility (Prestle et al. 2001; F. Huang et al. 2006; Gellen et al. 2008). More recent studies indicate in fact that RyR2-FKBP12.6 association is less than stoichiometric with ~40 % of available RyR2 sites occupied in mouse, pig and rabbit heart, suggesting FKBP12.6 saturation is not critical for channel function (Zissimopoulos et al. 2012). It has been hypothesized that the association of FKBP12.6 and RyR2 is dependent on the phosphorylation state of the channel (Wehrens 2003; Marx et al. 2000; Marx, Reiken, et al. 2001). This is discussed further in **Section 1.4**.

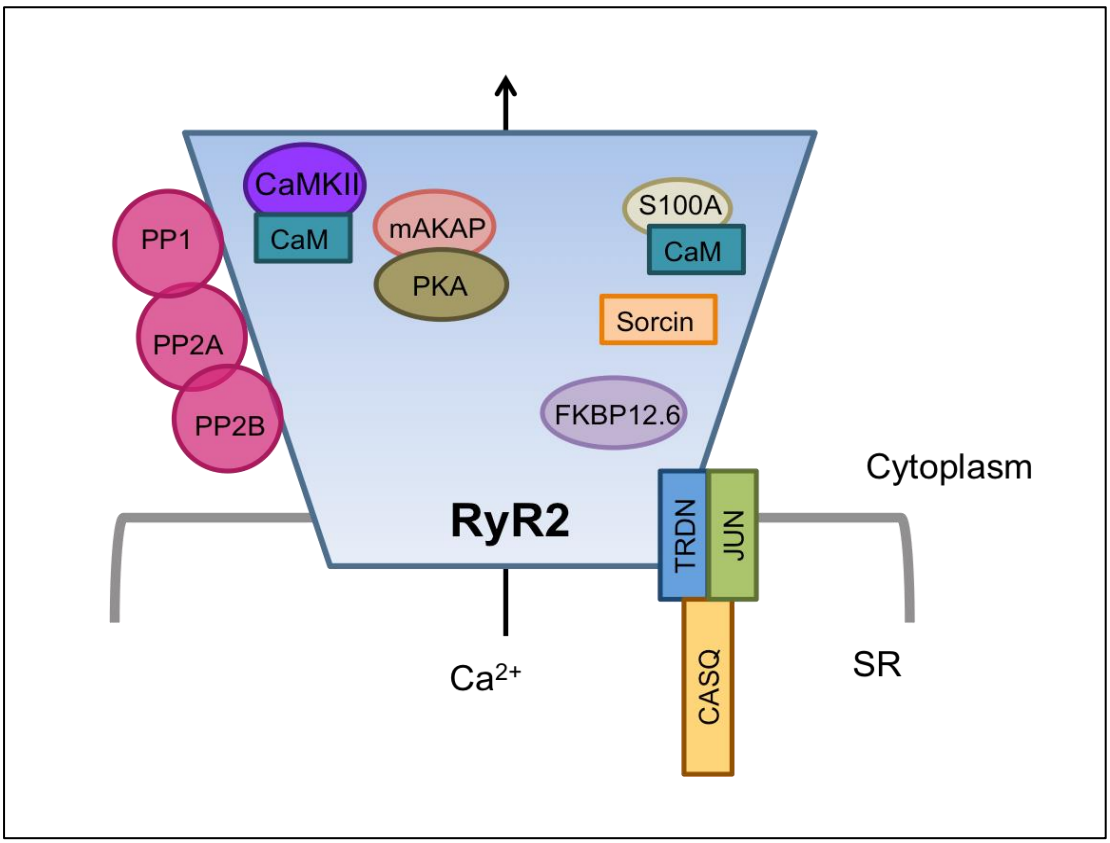

Figure 1.8 Schematic representation of accessory and associated proteins in the RyR2 macromolecular complex. Diagram of the RyR2 complex. The left-hand side illustrates components involved in phosphorylation of RyR2, while the right-hand side illustrates accessory proteins. Tetramers may contain more than one interaction for each protein and proteins may not be constitutively bound to RyR2; this can be dependent on physiological conditions (discussed further in **Section 1.3.4.**). Adapted from Terentyev and Hamilton (2016).

1.4 Phosphorylation as a posttranslational modification

Phosphorylation is well established in many cellular processes as a regulatory mechanism, not just limited to cardiac function. In β-adrenergic stimulation, as part of the 'fight-or-flight' response, several EC coupling proteins are targets for phosphorylation by protein kinases, leading to the upregulation of ion channel activity, increased chronotropy and inotropy required in response to increased metabolic demand of the body (Marx et al. 2000; Eschenhagen 2010; Bers 2002a). **Section 1.2.4** outlines the pathway in more detail.

RyR2 is also a target of protein kinases during β-adrenergic stimulation. The importance of RyR2 phosphorylation in channel activity and regulation was first highlighted in 1984, before channel [^{3}H] ryanodine binding properties were first investigated by Pessah (Pessah et al. 1985), and the ryanodine receptor was simply referred to as 'high molecular weight junctional SR proteins' (Seiler et al. 1984). These proteins were found to not only bind CaM, but act as a substrate for endogenous CaMKII and exogenously added cAMP-dependent protein kinase; a dual phosphorylation mechanism thought to play a role in mediating Ca^{2+} flux at the SR junction. For the 30 years since, phosphorylation has remained a highly investigated and deeply contentious area of cardiac Ca^{2+} signalling and RyR2 research, as to the exact mechanism and functional consequence of such posttranslational modifications.

Figure 1.4 in **Section 1.2.4** highlights the kinases and phosphorylation target proteins involved in the β-adrenergic stimulation signalling pathway, as well as accessory and adaptor proteins that are discussed in more detail in subsequent sections.

1.4.1 Effects of protein kinases on RyR2

Early works of Takasago et al. showed that RyR2 could be phosphorylated by many exogenous serine/threonine kinases including PKA, PKG, PKC and CaMKII (Takasago et al. 1989; Takasago et al. 1991). The role of various kinases involved in RyR2 phosphorylation is discussed below.

1.4.1.1 Role of PKA

PKA was one of the first protein kinases to be discovered and structurally consists of two subunits: regulatory (PKAr) and catalytic (PKAc) (D. A. Walsh et al. 1968). Regulatory subunits act as major receptors for secondary messenger cAMP, a product of β-adrenergic stimulation. In the inactive form, regulatory subunits sequester catalytic subunits in a heterotetrameric holoenzyme. After activation of the β-adrenergic receptor, activatory ligand cAMP binds to the PKA regulatory subunit and leads to dissociation of catalytic subunits from the holoenzyme, which are then free to phosphorylate EC coupling proteins within the cardiomyocyte (see **Figure 1.4**). Overall, the major physiological role of PKA phosphorylation includes increasing Ca^{2+} influx via LTCCs, as well as increasing SR Ca^{2+} content via PLB phosphorylation, subsequently enhancing SERCa activity (Reuter et al. 1974; Tada et al. 1975; Eisner et al. 2017). This underlies the positive inotropic, chronotropic and lucitropic effects observed in β-adrenergic stimulation (described in **Section 1.2.4**).

As the effector kinase in the classical β-adrenergic stimulation pathway, PKA-mediated phosphorylation of RyR2 has been studied extensively in both health and disease, yet whether and how it alters channel gating remains contentious. This is discussed further in **Section 1.4.2.1** and **1.4.2.2**.

1.4.1.2 Role of CaMKII

CaMKII is a serine-threonine specific protein kinase critical for many processes in the cardiomyocyte, including EC coupling, chronotropic control of LTCCs and the uptake and release of SR Ca^{2+} via phosphorylation of PLB and RyR2 (Marx and Marks 2013; Kushnir et al. 2010). Unlike PKA, CaMKII is not activated by a neurohormonal pathway, but is activated by Ca^{2+}-bound CaM. CaMKII monomers contain three subunits: one catalytic, one regulatory and an associating subunit that assembles the holoenzyme (Z.-W. Wang 2008; Rosenberg et al. 2006). Under basal conditions, catalytic subunits are restrained by regulatory subunits. When intracellular Ca^{2+} concentration is elevated, regulatory subunits bind to CaM,

generating a conformational shift that release catalytic subunits for subsequent substrate binding and phosphorylation (Gaertner et al. 2004; Rostas and Dunkley 1992). In a physiological setting, CaMKII targets critical ion channels important for cell excitability to regulate and maintaining cardiac function (Mohler et al. 2014). This includes voltage-gated Na^{2+} channels, LTTCs and repolarizing potassium channels. CaMKII also alters SR Ca^{2+} release and reuptake via phosphorylation of RyR2 and PLB, altering the activity of SERCa. The signalling molecule has a broad range of targets including transcription factors MEF2 and CREB and is implicated in transcriptional activation of hypertrophy (Mattiazzi et al. 2015).

The role of CaMKII as a major regulator of RyR2 function in disease is strongly supported (Luo and Anderson 2013; Cutler et al. 2012; Pereira et al. 2007; T. Guo et al. 2006; Fischer et al. 2013). Studies have provided evidence that chronic CaMKII activity leads to cardiac arrhythmia and HF (Anderson et al. 2011; Ling et al. 2009). Patients and animals with HF display increased levels of CaMKII expression (Hagemann et al. 2001; Hoch et al. 1999), with overexpression of a CaMKII inhibitor, AC3-I, delaying development of HF in mice (R. Zhang et al. 2005). There is some agreement of research groups that CaMKII (as opposed to PKA) increases SR Ca^{2+} leak (Ai 2005; Jerald Curran et al. 2007; Bers 2012), but this is not universal (Wehrens et al. 2006; D. Yang et al. 2007). This is discussed further in **Sections 1.4.2.1** and **1.4.2.3**.

1.4.1.3 Role of PKC and PKG

Most studies to date have only focused on the role of CaMKII and PKA, but it is likely that other serine and threonine kinases can also phosphorylate the protein (Ather et al. 2012; Dobrev 2014). Protein kinase C (PKC) and protein kinase G (PKG) were originally implicated in RyR2 phosphorylation by Takasago et al. (1991), who suggested that these kinases phosphorylated the same fragmented phosphopeptide as CaMKII i.e. possibly the same site(s).

PKC phosphorylation of RyR2 has been reported to increase [^{3}H] ryanodine binding, suggesting an increase in the P_o of PKC-treated channels (Takasago et al. 1991), while Carter et al ((Carter et al. 2011)) suggested that endogenous PKC phosphorylation leads to RyR2 becoming 'uncoupled' from the influence of cytosolic Ca^{2+}, where lowering Ca^{2+} concentrations to sub-activating levels no longer closes the channels PKCα activated by β-adrenergic receptors, phosphorylates many other EC coupling proteins including LTCCs, troponin and large number of other substrates (Kooij et al. 2013; L. Yang et al. 2004;

Malhotra et al. 2010; Sumandea 2003; Hidalgo et al. 2009), including those included in pathways that lead to β-adrenergic receptor desensitization (Malhotra et al. 2010). Moreover, PKCα-overexpression studies suggest a role for this kinase in cardiac remodelling (Kooij et al. 2013; L. Yang et al. 2004; Malhotra et al. 2010; Sumandea 2003; Hidalgo et al. 2009).

PKG is associated with parasympathetic stimulation via the muscarinic receptor 2 (M_2R), the predominant isoform of muscarinic receptor in cardiac muscle (Hulme 1990; Dhein et al. 2001). M_2R is coupled to an inhibitory G protein (Gi) that inhibits adenylate cyclase and PKA (see **Figure 1.4**). However, this also causes nitric oxide-dependent stimulation of PKG (Harvey and Belevych 2003; Massion 2003) and subsequent phosphorylation of EC coupling proteins, including RyR2.. In a recent publication from the Györke group, parasympathetic stimulation is shown to initiate a novel mode of EC coupling that enhances the efficiency of SR Ca^{2+} store utilization (Ho et al. 2016). This involves reciprocal changes in phosphorylation of RyR2 at S2808 and S2814, which increases systolic release at low SR Ca^{2+} content while preventing Ca^{2+} leak. Activation of PKG via M_2R is suggested to mediate phosphorylation at S2808, while decreased activation of CaMKII by another muscarinic receptor, M_3R, led to dephosphorylation at S2814 in WT mouse and canine ventricular myocytes. The overall observed effect of these phosphorylation changes in RyR2 included an increase in systolic Ca^{2+} release at a low SR Ca^{2+} content, yet a reduction in Ca^{2+} leak.

1.4.1.4 Role of Epac

Exchange factor directly activated by cAMP proteins, known as Epac, is also implicated in kinase activity and the phosphorylation of RyR2. Epac is involved in the formation of gap junctions in cardiomyocytes, necessary for ions to transverse and coordinate cardiac contractions (Somekawa 2005). Traditionally, cAMP was thought to influence contractility and relaxation processes in the heart via PKA. However, accumulating evidence suggests that both isoforms Epac1 and Epac2 are also targets of cAMP in the cardiomyocyte and play important roles in the function of the heart in both physiological and pathological conditions (Fujita et al. 2016; Hothi et al. 2008). β-adrenergic stimulation is suggested to activate Epac2, inducing SR Ca^{2+} leak via CaMKII phosphorylation of a specific RyR2 site, S2814 (Pereira et al. 2013).

PKA and Epac are both expressed in all tissues, so any increase in intracellular cAMP levels will activate both pathways. cAMP signalling is therefore more complex than initially believed and the classical PKA activation pathway during β-adrenergic stimulation may involve

crosstalk between Epac and PKA. Whether the two intracellular cAMP receptors act independently, synergistically, or oppose each other in regulating a specific cellular function remains to be fully elucidated (X. Cheng et al. 2008; Bers 2007; Ruiz-Hurtado et al. 2012).

1.4.2 Potential phosphorylation sites of RyR2

The RyR2 homotetramer contains 46 serine/threonine sites per subunit that can potentially be phosphorylated (www.phosphosite.org, (Terentyev and S. Hamilton 2016). To date, five serine phosphorylation sites have been investigated in RyR2, located at amino acid positions 2808 (S2808), 2811 (S2811), 2814 (S2814), 2031 (S2031) and 2797 (S2797) in the human RyR2 (hRyR2) sequence (Witcher *et al.*, 1991; Wehrens *et al.*, 2004; Xiao *et al.*, 2005; Huke & Bers, 2008), although S2808, S2031 and S2814 are the main sites which have been studied.. Most of these sites as well as additional residues have been detected as phosphorylated in animal models (Huttlin et al. 2010; Brill et al. 2009) and are discussed below. Phosphorylation site nomenclature throughout this thesis follows positioning in the hRyR2 sequence.

The phosphorylation domain (P domain in **Figure 1.5 A and B,** circled domain 6 in **Figure 1.9** below) is predicted at residues 2735-2938 in RyR1 (Yuchi et al. 2013). The analogous region in RyR2 contains phosphorylation sites S2808 and S2814. This region (corresponding to the domain named RyR3&4 in **Figure 1.5**) was solved at atomic resolution by crystallography (Yuchi et al. 2013). It was initially docked to a corner of the structure (where the orange RyR1&2 domain resides in **Figure 1.9,** labelled 10) but in view of the sequence path in higher resolution cryo-EM structures, it has been reassigned (Yuchi et al. 2015)and lies close to both JSol and SPRY1 (that bind FKBP12.6) in the 3D structure of RyR (Georges et al. 2016; Samsó 2016; Yan et al. 2014).

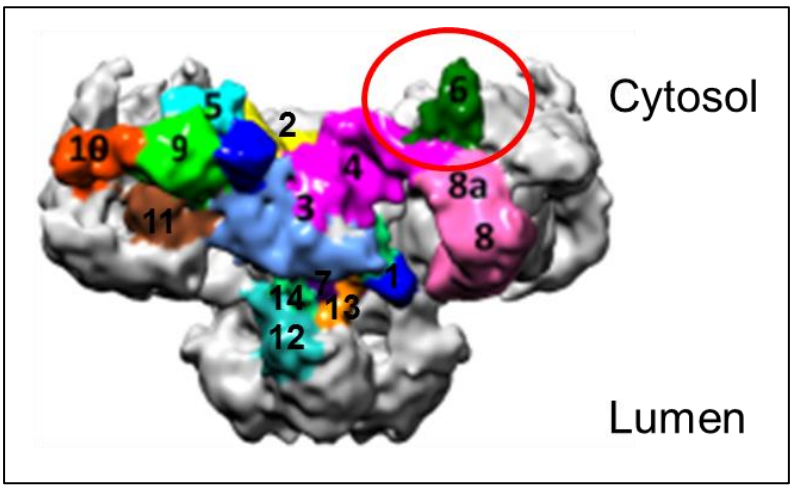

Figure 1.9 The RyR phosphorylation domain location in the 3D channel structure. A side view of the RyR channel, with domains labelled numerically as follows; 1. EF hand, 2. NTD, 3. JSol, 4. BSol, 5. SPRY3, 6. P domain, 7. CTD, 8(a). BSol, 9. SPRY1, 10. RyR1&2, 11. SPRY2, 12. pVSD, 13. U motif, 14. CSol. See **Figure 1.5** for description and residue spans of these domains. Modified from Samso (2016).

1.4.2.1 S2808

The serine at residue 2808 was the first phosphorylation site to be identified in RyR2 (Witcher et al. 1991). In a landmark publication in 2000, the Marks group proposed that the action of PKA at the S2808 site alone was responsible for dysfunction and arrhythmia observed in HF (Marx et al. 2000). In failing hearts where circulating catecholamines are markedly increased, activation of the β-adrenergic signalling pathway generates increased cAMP levels and activates PKA. The stoichiometry of back-phosphorylation (see **Section 4.1.2.1**) of RyR2 channels from isolated failing hearts was 0.7 ± 0.3 moles of phosphate transferred per mole of failing channel, in comparison 3.1 ± 0.1 moles of phosphate transferred per mole of non-failing channel. Authors proposed that RyR2-S2808 is 'hyperphosphorylated' in this scenario, a term used to describe this four-fold increase in PKA phosphorylation of RyR2 observed in failing hearts from dogs and humans. Three of the four PKA sites in the tetrameric channel were phosphorylated *in vivo*, in comparison to one phosphorylated PKA site in RyR2 isolated from non-failing hearts. This hyperphosphorylation was suggested to cause FKBP12.6 dissociation from RyR2, which directly enhances SR Ca^{2+} leak and store depletion, contributing to systolic dysfunction in HF (see **Figure 1.10**). The model was later extended, with down-regulation of phosphatases in HF suggested to lead to this PKA-dependent hyperphosphorylation and that diastolic SR Ca^{2+} leak also contributes to triggered activity (Bellinger et al. 2008; Wei Chen et al. 2011; Shan et al. 2012; Lehnart et al. 2008; Shan, Betzenhauser, et al. 2010; Shan, Kushnir, Betzenhauser, Reiken, J. Li, Lehnart, Lindegger, Mongillo, Mohler and Marks 2010b).

The Marks group found that phosphoablation (replacing serine with alanine, preventing phosphorylation at this site) at S2808 severely limits the β-adrenergic response and increases RyR2 P_o in post-myocardial infarct (MI) hearts (Wehrens et al. 2006; Shan, Kushnir, Betzenhauser, Reiken, J. Li, Lehnart, Lindegger, Mongillo, Mohler and Marks 2010a). These data supported the idea that RyR2 phosphorylation at a single residue was responsible for normal effects on cardiac contractility and for observed defects in HF.

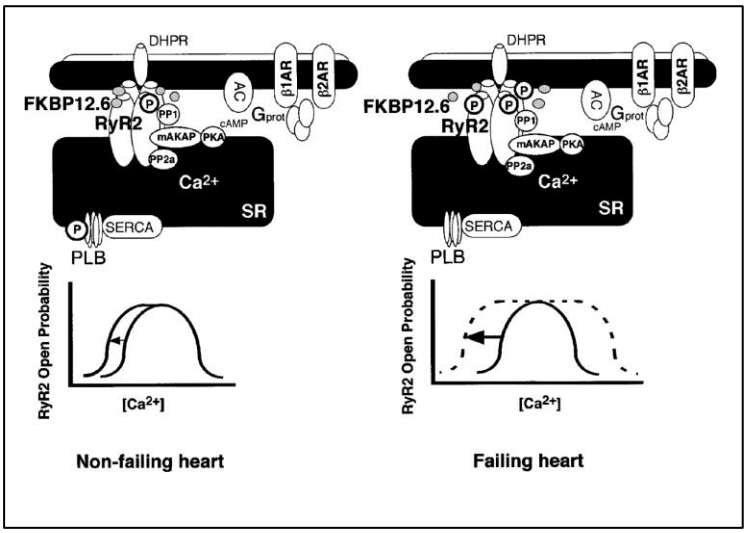

Figure 1.10 The Marks original model of the effects of PKA phosphorylation of RyR2 in the heart. In the nonfailing heart (left panel) β-agonists bind to receptors (β1 and β2 AR) coupled to G-proteins (Gprot), which in turn activate adenylyl cyclase (AC), raising cAMP levels and activating PKA. PKA phosphorylation of RyR2 induces dissociation of one FKBP12.6 from the channel, shifting the Ca^{2+} dependence for activation to the left, increasing the sensitivity of the RyR2 to activation by Ca^{2+} influx via DHPR (LTCC) and increasing RyR2 channel P_o. The result is increased SR Ca^{2+} release and cardiac contractility. The tetrameric RyR2 channel is part of a macromolecular signalling complex (components discussed in **Section 1.3.4**). Ca^{2+} reuptake into the SR occurs via the SERCA and PLB. In failing hearts (right panel), PKA hyperphosphorylation of RyR2 may contribute to the blunted response to β-agonists observed in failing heart muscle because the channels cannot be further PKA phosphorylated. RyR2 channels in failing hearts exhibit a shift in the Ca^{2+}-dependence for activation such that they are activated at resting levels of cytosolic Ca^{2+}. Figure and legend from Marx et al. (2002).

Although Marks has consistently published data from his laboratory that defends this hypothesis, the relevance of PKA phosphorylation at this site and indeed as a mechanism for dysfunction has been highly disputed since. Many prominent research groups in the field have been unable to replicate or confirm many aspects of the hypothesis (B. Xiao et al. 2006; Benkusky et al. 2007; Eschenhagen 2010; George 2007b). In newer findings from Wehrens (previous co-author of Marks papers) and Dobrev, modifications were made to the original hypothesis (referred to here on as the Wehrens-Marks hypothesis) to suggest that hyperphosphorylation at S2808 is only evident in selective forms of HF, and that the role of phosphorylation of another site, S2814, is the main cause of Ca^{2+} leak that leads to arrhythmia and exacerbates other forms of HF (Chen-Izu et al. 2007). Authors have suggested that S2808 genetic ablation in mice protects against ischemic HF but has no prominent role in nonischemic HF. This does not fit well with the original Marks hypothesis, which was based on S2808 hyperphosphorylation observed in tachypacing-induced heart failing dogs, a nonischemic model of HF. Wehrens and colleagues have also found no evidence of S2808-RyR2 hyperphosphorylation in any form of human HF (Respress et al. 2012), although treatment of patients with β-blockers before death may have normalized this phosphorylation state (Ai 2005; Jerald Curran et al. 2007; Houser 2014). In hypertrophied hearts from human biopsy, a condition that precedes HF, no increase in S2808 phosphorylation is observed either, although phosphorylation at another phosphorylation site, S2814, is increased by 300 % (Fischer et al. 2013b).

Using the same strategy as Marks, introducing a missense mutation to mimic dephosphorylation, Houser and Valdivia have also created an S2808A knock in (KI) mouse, although not from the same mouse line (Benkusky et al. 2007). Interestingly, results differ to that of the Marks group, with no distinguishable differences from WT mice in respect to response to β-adrenergic stimulation, channel gating or dysfunction following MI (H. Zhang et al. 2012; MacDonnell et al. 2008). There have been calls for S2808A KI mouse models to be freely shared between groups to address the stark differences in experimental results, but this has yet to take place (Dobrev and Wehrens 2014; Bers 2012; 2012).

Many groups find that the basal phosphorylation status of S2808 is already substantial (at least 50 % of PKA sites phosphorylated), which would therefore limit the potential increase at this site (Huke and Bers 2008; Rodriguez et al. 2003; B. Xiao et al. 2005; Currie et al. 2004; Benkusky et al. 2007). RyR2 isolated from non-failing sheep hearts was shown to be phosphorylated to 75% of maximum at the S2808 residue. Some groups have failed to detect any increase in S2808 phosphorylation in HF models. However, this may well depend on the animal species (publications include RyR2 from mouse, rat, canine) or specific

phospho-antibodies used (publications include commercial and 'in house' antibodies' (Fischer, Herting, Tirilomis, Renner, Neef, Toischer, Ellenberger, Förster, Schmitto, Gummert, Schöndube, Hasenfuss, Maier and Sossalla 2013a; Huke and Bers 2008; Carter et al. 2011; Terentyev, Rees, W. Li, Cooper, Jindal, Peng, Lu, Terentyeva, Odening, Daley, Bist, Choi, Karma and Koren 2014a; Carter et al. 2006; R. Liu et al. 2015; Cooper et al. 2013; Belevych, Sansom, et al. 2011). Carter et al. suggested that channels are S2808-phosphorylated up to 75 % of maximum, calculated by Western blotting, comparing against a maximally phosphorylated sample (Carter et al. 2006).

When a critical protein involved in EC coupling has been eliminated or altered, adaptive remodelling of other Ca^{2+} regulatory proteins has been shown to occur (Pott et al. 2006; Brittsan et al. 2003). In a conditional NCX-deficient mouse with a reduction of Ca^{2+} efflux capacity, LTCC expression is significantly reduced, adapting to reduce the Ca^{2+} influx, helping to preserve basal function (Pott et al. 2006). In studies of RyR2 phosphorylation, Western blot analysis revealed that ablation of S2808 is accompanied by marked increase in phosphorylation of S2031 and S2814 in the presence of isoproterenol (Iso) suggestive of adaptive remodelling. This important finding highlights possible redundancy in these sites, a likelihood which is almost always overlooked as the phosphorylation status of all three serines is usually not reported in any one study (Terentyev and S. Hamilton 2016; Benkusky et al. 2007). Houser and Valdivia however report no alterations in adrenergic regulation of Ca^{2+} current, myocyte Ca^{2+} transients and contractions, EC coupling, or *in vitro/in vivo* S2808A-RyR2 mouse cardiac function and suggest there were no adaptions in this model because there is no role for S2808 phosphorylation in cardiac contractility (H. Zhang et al. 2012; MacDonnell et al. 2008).

The role of S2808 phosphorylation and FKBP12.6 in the dysfunction of RyR2 activity also remains hotly disputed. In the Marks hypothesis, the protein was originally suggested to stabilize RyR2 channel gating, preventing long-lasting subconductance states and diastolic SR Ca^{2+} leak (Marx et al. 2000). Depletion of FKBP12.6 has been implicated in an aberrant increase in cytosolic Ca^{2+} concentration as a result of SR leak and has been associated with HF, cardiomyopathy and fatal cardiac arrhythmias (Marx et al. 2000; Wehrens et al. 2006; Fauconnier et al. 2010; Wehrens 2003; Kushnir et al. 2010). Expression of FKBP12.6 has been reported as reduced in both HF and cardiomyopathy as well as a decreased ratio of the protein to RyR2, which would indicate dissociation in these instances (Hu et al. 2009; Y.-S. Cheng et al. 2011; Y. Zhang et al. 2008).
However, this hypothesis has limited support from other research groups (Barg et al. 1997; Timerman et al. 1996; T. Guo et al. 2010; Zissimopoulos and Lai 2004; B. Xiao 2004; T. Guo

et al. 2006; Stange et al. 2003; Mukherjee et al. 2012). S2808D KI mice with genetically phosphorylated channels have been shown to exhibit normal FKBP12.6 binding (Shan, Kushnir, Betzenhauser, Reiken, J. Li, Lehnart, Lindegger, Mongillo, Mohler and Marks 2010a). In a FKBP12.6 knockout mouse model, the absence of the protein did not alter the incidence of spontaneous Ca^{2+} release or single RyR2 activity in comparison to WT mice (B. Xiao et al. 2007). The location of the S2808 phosphorylation site is 105-120 Å away from the FKBP12.6 binding site in RyR2, making direct involvement of S2808 phosphorylation in FKBP12.6 binding unlikely (Meng et al. 2007). More recent studies suggest that other posttranslational modifications, such as oxidation and S-nitrosylation, combined with phosphorylation of RyR2 are required to dissociate FKBP12.6 from RyR2, increasing channel P_o (Shan, Betzenhauser, et al. 2010; Fauconnier et al. 2010). FKBP12.6:RyR2 association has also been implicated in arrhythmia caused by mutations in RyR2. This is discussed in **Section 1.4.1.5** and **1.7.3.1.**

There remains disagreement on whether PKA-dependent RyR2 phosphorylation alters function in general – if not, this would render the PKA phosphorylation level at S2808 functionally irrelevant with respect to diastolic Ca^{2+} release. Early work using single channels isolated from the RyR2-S2808A mouse in lipid bilayers suggested that ablation of this site led to a significantly reduced P_o in comparison to WT after the application of PKA (Wehrens et al. 2006). While Marks and Chen groups both report no changes in S2808A activity at basal conditions, Xiao and colleagues reported no change in channel activity after treatment with PKA (B. Xiao et al. 2007). Also, in direct conflict with the Marks-Wehrens hypothesis, Shannon and Bers find that CaMKII and not PKA is responsible for Ca^{2+} leak from the SR, suggesting that PKA phosphorylation of the S2808 site is not critical in RyR2 channel dysfunction {Ai:2005ct, Curran:2007de}.

1.4.2.2 S2031

In work of the Chen group in 2005, two-dimensional phosphopeptide mapping (see **Section 4.1.2.2**) revealed two major PKA phosphopeptides in RyR2, one of which corresponded to the already established S2808 (B. Xiao et al. 2005). The other was identified as a novel phosphorylation site, S2031. Using phospho-specific antibodies, this novel site was shown to be phosphorylated in Iso-stimulated rat cardiomyocytes, but not in unstimulated cells. S2031 was phosphorylated by PKA and not CaMKII and ablation of the site did not alter FKBP12.6-RyR2 interactions, nor the Ca^{2+} dependence of [^{3}H] ryanodine binding. Chen also argued that levels of phosphorylation at S2808 were similar in both failing and non-failing

canine hearts and therefore that S2031 was in fact the major PKA phosphorylation site in RyR2 (B. Xiao et al. 2005).

Basal phosphorylation at this site is consistently reported as very low (Huke and Bers 2007; Cooper et al. 2013; Belevych, Sansom, et al. 2011). The Chen group demonstrated that recombinant RyR2 S2031A single channels behave similar to WT, which would fit with these consistent findings (B. Xiao et al. 2007). On exposure to PKA, S2031A channels displayed a reduced sensitivity to luminal Ca^{2+} in comparison to WT, or the fully phosphorylated counterpart (S2031D). However, work of the Marks group, also using recombinant RyR2, showed a PKA-mediated increase in the P_o of S2031A channels similar to that of WT, while S2031D channels (fully phosphorylated) displayed only a small change in activity upon phosphorylation , challenging the PKA-mediated functional relevance of the S2031 site (Wehrens et al. 2006). Data from the Györke laboratory suggests that S2031 can also be phosphorylated by CaMKII (Belevych, Sansom, et al. 2011), suggestive that other kinases may confer effects on RyR2 channel function by phosphorylation at this site, or sites in close proximity.

1.4.2.3 S2814

S2814 was originally identified by the Marks group as a CaMKII specific site (Wehrens, Lehnart, Reiken and Marks 2004). Introducing mutations into human recombinant RyR2, the group showed that S2808A could still be phosphorylated by CaMKII, yet S2814A could not, indicating this was the unique CaMKII phosphorylation site on recombinant RyR2. The basal level of phosphorylation at the S2814 site increases in the presence of phosphatase inhibitors and the β-adrenergic agonist Iso, and significantly decreases in the presence of phosphatases or the Ca^{2+} chelator EGTA (Belevych, Terentyev, et al. 2011; Huke and Bers 2008; Huke and Bers 2007; Terentyev, Rees, W. Li, Cooper, Jindal, Peng, Lu, Terentyeva, Odening, Daley, Bist, Choi, Karma and Koren 2014b; Cooper et al. 2013). Increases in S2814 basal phosphorylation of up to 300 % at this site have been reported in HF when normalized to RyR2 protein expression in Western blot experiments (Fischer et al. 2014).

In myocytes isolated from a S2814A KI mouse model, there were no obvious changes in SR Ca^{2+} release in comparison to WT, yet the fully phosphorylated mimic counterpart S2814D exhibited enhanced SR Ca^{2+} leak and a reduced SR Ca^{2+} content (van Oort, McCauley, Dixit, Pereira, Yang, Respress, Wang, De Almeida, Skapura, Anderson, Bers and Wehrens 2010b). An important finding in genetic ablation of the site is that S2814A KI mice showed delayed development of HF after transverse aortic constriction (TAC), were protected

against ischemia-reperfusion induced arrhythmia and displayed reduced Ca^{2+} homeostasis abnormalities that precede ventricular arrhythmia when crossed with a mouse model of Duchenne muscular dystrophy, *dmd* (Respress et al. 2012; Ather et al. 2013). The induction of atrial fibrillation in FKBP12.6 knockout mice was also prevented by the introduction of S2814A (N. Li et al. 2012).

It is difficult to discern how sites in RyR2 could be exclusively phosphorylated by a certain kinase, given their close proximity in the phosphorylation 'hotspot' in RyR2. It has been shown that S2808A channels can be fully activated by CaMKII, and S2814A channels by PKA (Wehrens et al. 2006; Wehrens, Lehnart, Reiken and Marks 2004; N. Li et al. 2014). This indicates that genetic ablation of one site does not prevent phosphorylation of others in this region from altering RyR2 channel function (2012). Wehrens and Valdivia more recently suggest that PKA and CaMKII do not affect heart rate by a unique target site that governs SR Ca^{2+} release or uptake, including S2808 or S2814 (Wu et al. 2016). Genetic ablation of these sites in mice failed to affect heart rate responses *in vivo* to adrenergic agonists and authors argue that RyR2 phosphorylation sites do not control heart rate individually and that additional sites may also contribute.

In recent work of Wehrens and Bers, WT and S2814D KI mouse cardiomyocytes under acute CaMKII activation displayed increased SR Ca^{2+} leak, with a reduced CaM-RyR2 binding affinity and a pathological shift in RyR2 conformation (detected using a structural peptide DPc10, discussed in more depth in **Section 1.7.3.2**) in comparison to S2814A KI myocytes (Uchinoumi et al. 2016). These same effects were observed in rabbits with pressure/volume-overload induced ventricular fibrillation (VF). Treatment of permeabilized S2814D myocytes with excess CaM or dantrolene shifts the pathological conformation back to normal, restoring CaM affinity, decreasing SR Ca^{2+} leak and preventing triggered arrhythmias. The authors propose that multiple pathways converge to increase Ca^{2+} leak in pathological conditions (Uchinoumi et al. 2016), including; increased CaMKII activity; RyR2 structural unzipping between N-terminal and central domains (discussed in **Section 1.7.3.2**); oxidation (see **Section 1.5**); and reduced CaM binding to RyR2 (Oda 2005; Oda et al. 2015; Ai 2005; X. Xu et al. 2010; Uchinoumi et al. 2010). These RyR2 modifications are thought to cause a 'common pathological conformation state', the shift to which is promoted by CaMKII phosphorylation at S2814 (Uchinoumi et al. 2016). The role of CaM in RyR2 channel activity adds another layer of complexity to elucidating the effects of phosphorylation.

1.4.2.4 Other investigated phosphorylation sites

Mass spectrometry of the RyR2 protein has revealed additional phosphorylation sites, including S2811, S2797, threonine 2876 (T2876) and possibly threonine 2810 (T2810) (Yuchi et al. 2012; Huttlin et al. 2010).

The S2811 site is another phosphorylatable residue found within the 'phosphorylation hotspot' (Yuchi et al. 2012) and forms part of the CaMKII phosphorylation consensus ^{2805}RRISQTSQVSV^{2815} (underlined). It has been reported as phosphorylated *in vitro* by both CaMKII and PKA and in mice stimulated by β-adrenergic agonists (Yuchi et al. 2012; Huttlin et al. 2010). As S2808 and S2814 are well established phosphorylation sites in RyR2, it is suggested nearby residues S2797, T2810 and S2811 that are within or near the same segment are also accessible to protein kinases for phosphorylation. T2876 does not reside in the phosphorylation linker loop and was not detected *in vivo* by Yuchi et al. (2012) so was therefore suggested as inaccessible in full length RyR2 and a possible artefact of experimental conditions.

It remains unclear whether the S2811 site, as well as others in close proximity, contribute to the effects of CaMKII and PKA phosphorylation (Camors 2014). There are also concerns that phosphorylation at this site may distort the signal of phospho-specific antibodies pS2808 and pS2814 as they are in very close proximity, therefore making it difficult to clarify the specificity of kinases for certain residues and the functional relevance of phosphorylation at a single site (Huke and Bers 2008; Camors 2014).

1.4.3 Effects of serine/threonine phosphatases on RyR2

While RyR2 function is thought to be upregulated by the action of protein kinases and phosphorylation in β-adrenergic stimulation, control is restored by the reverse action of protein phosphatases, which dephosphorylate the channel and other EC coupling proteins in the cardiomyocyte. The degree of phosphorylation of sites in RyR2 and channel activity therefore depends on a fine balance between the multiple kinases and phosphatases present. Several protein phosphatases (PP) are present in the macromolecular complex and associate with RyR2 through adaptor proteins and regulatory subunits (**Figure 1.11**). Serine/threonine phosphatases in the complex include PP1, PP2A and PP2B, also known as calcineurin (Weber et al. 2015). These phosphatases are estimated responsible for 90% of phosphatase activity in the heart (Cohen and Cohen 1989; MacDougall et al. 1991). The structure of these enzymes allows specific subcellular targeting and substrate affinity, where a complex combination of regulatory and catalytic subunits provides a mechanism for precise control of activity (Heijman et al. 2013).

PP1 consists of catalytic and regulatory subunits in a dimer structure. This phosphatase is not freely available within the cardiomyocyte, but instead there is competition of over 200 regulatory subunits to form a complex with a catalytic subunit, as a holoenzyme (Herzig and Neumann 2000; Ceulemans and Bollen 2004; Heroes et al. 2013). The >200 PP1 regulatory subunits can be classified by their activity into two groups: those that regulate PP1 activity, or those that target PP1 to specific substrates such as myosin or the plasma membrane (Cohen 2002; Heroes et al. 2013; Heijman et al. 2013). PP2A structure is more complex, being coded for by at least 17 distinct genes with large sequence diversity (T. A. Jones et al. 1993). It exists as a trimer with catalytic, regulatory and additional structural scaffolding subunits. Regulatory subunits can be grouped into four families as opposed to two, and some of these have different splice variants and multiple isoforms. B56α of the PP2A-B family is one of the most studied isoforms, which is indicated in the RyR2 macromolecular complex (**Figure 1.11**). PP2B also exists as a dimer, with calmodulin-binding catalytic and regulatory subunits. The enzyme can also be modulated by interacting proteins, including mAKAP or Cain, a PP2B inhibitor (Wolska 2009; H. W. Lim and Molkentin 1999; Y. Wang et al. 2014; Heineke and Ritter 2012).

Work of the Marks group showed that PP1 and PP2A are scaffolded to the RyR2 macromolecular complex by leucine-isoleucine zipper motifs of their regulatory subunits (PP1 by subunit spinophilin, PP2A by subunit PR130) (Marx, Reiken, et al. 2001; Marks et

al. 2002). PP2A has also been shown to scaffold to mAKAP via regulatory subunit B56δ and B56α (Dodge-Kafka et al. 2010; Belevych, Sansom, et al. 2011). Posttranslational modifications of catalytic and regulatory subunits can also occur, adding further control of local phosphatase activity (DeGrande et al. 2013; Heijman et al. 2012; Dodge-Kafka et al. 2010; Lei et al. 2015; El-Armouche et al. 2003). For example, phosphorylation at Serine 566 in PP2A catalytic subunits causes destabilization of interaction with the regulatory subunit, reducing phosphatase activity (DeGrande et al. 2013; Dodge-Kafka et al. 2010; J. Chen et al. 1992). PP2A phosphorylation also modulates PDE4D3, the phosphodiesterase anchored on the mAKAP scaffold within the RyR2 complex (Lei et al. 2015). Specificity of phosphatases for RyR2 phosphorylation sites remains to be elucidated. PP1 has been demonstrated to dephosphorylate S2808 and S2814, while PP2A dephosphorylated S2814 only (Huke and Bers 2008). Work of the Györke laboratory in experiments of PP2A suppression, through translational inhibition with muscle-specific microRNAs 1 and 133, showed control of phosphorylation by this phosphatase at S2814 and S2031 of RyR2, not S2808 (Terentyev et al. 2009; Belevych, Sansom, et al. 2011).

Evidence is growing that RyR2 activity is modulated by the action of both kinases and phosphatases. Phosphorylation at S2808, S2814 and S2031 to maximal levels is associated with increased RyR2 P_o and subsequent treatment with PP1 reduces this activity in several studies (Carter et al. 2006; Carter et al. 2011). Interestingly in single channel experiments, dephosphorylation of RyR2 at S2808 by PP1 also increases P_o (Carter et al. 2006; Terentyev et al. 2003). Carter et al. have shown that this activity is not associated with changes in sensitivity to cytosolic Ca^{2+}, instead stemming from shortening of the closed states of the channel (Carter et al. 2011; Carter et al. 2006).

Györke and colleagues utilized their mouse model of Ca^{2+}-dependent cardiomyopathy (CCM), with CSQ2 KO and SERCa1a overexpression, to examine the potential role of S2808 phosphorylation in the development of the disease (Ho et al. 2014; Kalyanasundaram 2013). SERCa1a functionally substitutes SERCa2a in cardiac muscle in this model, and overexpression prevents depletion of the SR Ca^{2+} store. By cross-breeding with RyR2 S2808A mice, Györke et. al (2014) found that the application of PP1 to permeabilized triple mutant mouse cardiomyocytes produced a transient increase in Ca^{2+} spark frequency at unchanged SR Ca^{2+} content (Ho et al. 2014). Consistent with previous reports, RyR2 was found to be highly phosphorylated (75 % of available phosphorylation sites in a tetramer) at S2808 in WT and double mutant hearts, while S2808A mutation rendered triple mutant mouse hearts either partially or non-phosphorylatable. Given the high basal phosphorylation level, it was suggested that dephosphorylation rather than further phosphorylation leads to

exacerbated CCM and abnormal Ca^{2+} cycling in triple mutant mouse by enhancing RyR2 activity. In another study with WT rat cardiomyocytes, catalytic subunits of PP1 and PP2A resulted in a dramatic increase in leak and a rapid depletion of SR Ca^{2+} stores, suggestive that this leak is due to the change in RyR2 function when dephosphorylated (Terentyev et al. 2003). These data also implicate dephosphorylation in increasing RyR2 channel activity

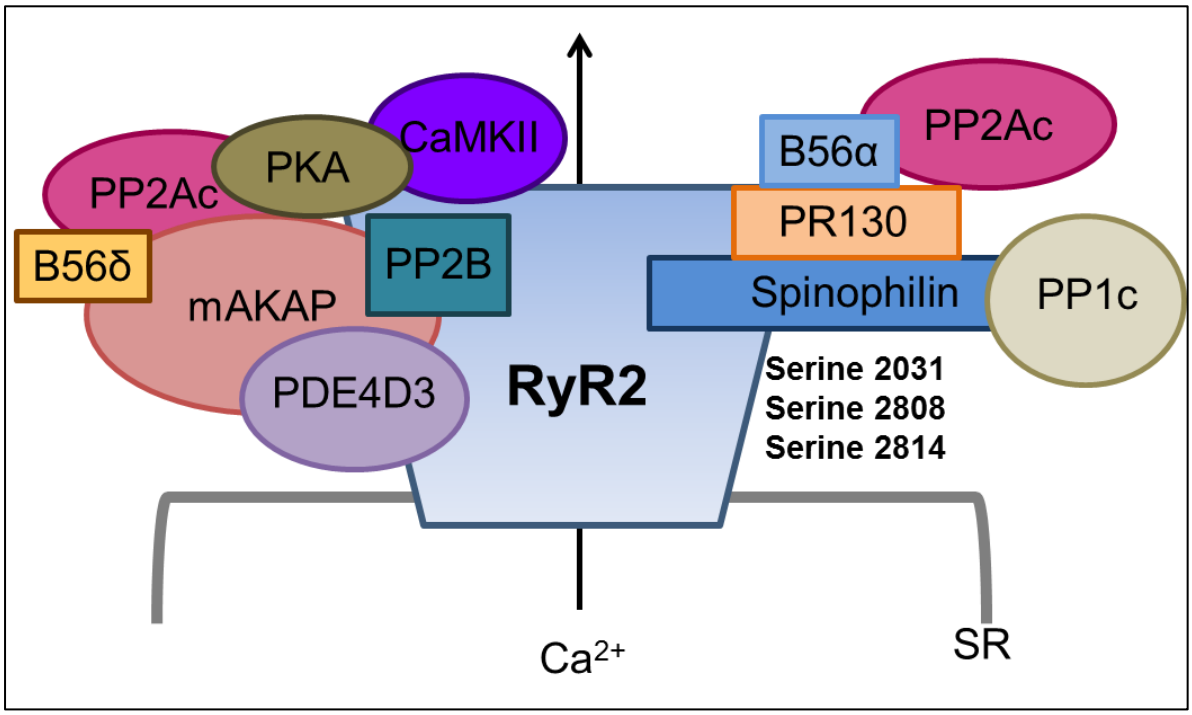

Figure 1.11 The RyR2 macromolecular complex with associated accessory proteins that influence its phosphorylation status. The action of protein kinases CaMKII and PKA on RyR2 phosphorylation sites S2031, S2808 and S2814 are opposed by protein phosphatases PP1, PP2A and PP2B. PP1c and PP2Ac are directed to the complex via their regulatory subunits, spinophilin and PR130 and B56α respectively. In addition, PP2A scaffolds to the complex via B56δ and mAKAP, which is anchoring PP2B, PKA and PDE4D. Image from Terentyev and Hamilton (2016).

1.4.4 Theoretical models of phosphorylation

1.4.4.1 Mark's hypothesis of phosphorylation causing Ca^{2+} leak via dissociation of FKBP12.6

The original Marks hypothesis, published made in 2000, postulated that PKA phosphorylation regulates FKBP12.6 binding to RyR2, an accessory protein thought to stabilise the closed state of channel (Marx et al. 2000). According to this theory, FKBP12.6 dissociation as a result of PKA hyperphosphorylation at the S2808 is thought to increase the Ca^{2+} sensitivity and P_o of single RyR2 channels, with long-lasting subconductance states. This increase in channel activity led to decreased SR Ca^{2+} content, diastolic Ca^{2+} waves and arrhythmia in HF (see **Figure 1.10**). The PKA/RyR2-S2808/FKBP12.6 mediated Ca^{2+} leak mechanism has been extended as a critical pathway in genetic arrhythmias, seizures, and even skeletal muscle fatigue (Shan et al. 2010; Lehnart et al. 2008; Shan et al. 2008). However, numerous reports fail to reproduce critical aspects of the Marks hypothesis, including hyperphosphorylation of RyR2 at S2808 in HF and any major role of PKA in the phosphorylation of the channel (Y. Li et al. 2002; Ai 2005; Jerald Curran et al. 2007; M. T. Jiang et al. 2002; Stange et al. 2003; B. Xiao et al. 2007; B. Xiao et al. 2005; George 2007b; Timerman et al. 1996). **Figure 1.12** grades the strength of support for key aspects of Marks' hypothesis.

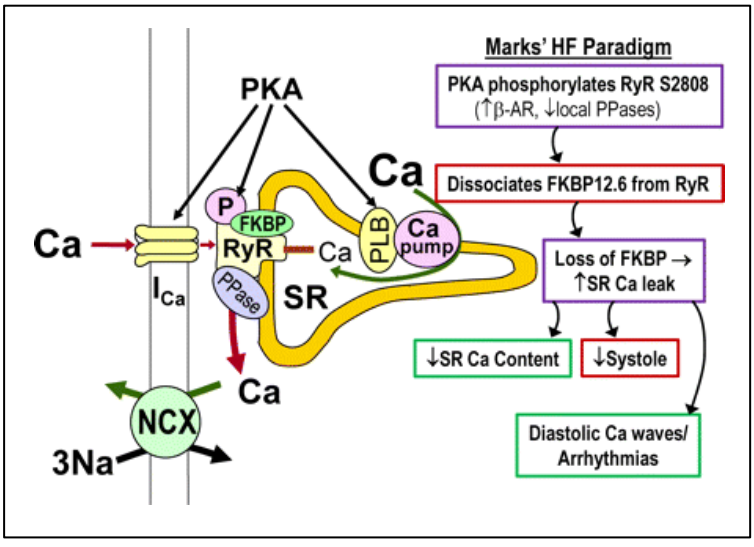

Figure 1.12 Schematic of the steps in Marks' working hypothesis of RyR alteration in HF, graded by strength of support. P is phosphorylation, PLB is phospholamban, PPase is phosphatase, NCX is Na/Ca exchange. Box colour indicates strength of support (**green**=strong, **purple**=equivocal, **red**=weak). Figure and legend taken from Bers (2012).

The contribution of SR Ca^{2+} leak through RyR2 to dysfunction in HF remains unclear. Work of Eisner, Trafford and Venetucci shows that changes in RyR2 Ca^{2+} sensitivity have only transient effects on systolic function due to an 'autoregulation' mechanism (Sankaranarayanan et al. 2016; Venetucci et al. 2008; Eisner et al. 2009). The first beat of an isolated cardiomyocyte with higher Ca^{2+} sensitivity has a greater Ca^{2+} release, which in turn drives Ca^{2+} extrusion from the cell via NCX – an initial fast phase of Ca^{2+} transient decay. SR Ca^{2+} uptake then progressively decreases, with a new steady state achieved at a lower SR Ca^{2+} content with higher Ca^{2+} release, but where Ca^{2+} influx and efflux are rebalanced so that the Ca^{2+} transient is unaltered. However, as diastolic SR Ca^{2+} leak increases (for example due to increased β-adrenergic stimulation) the initial rapid phase of Ca^{2+} transient decay disappears, and a second slow phase of decay occurs, where even at low SR Ca^{2+} content, leak is large enough to oppose the increased action of SERCa. To summarize, mild or moderate SR Ca^{2+} leak through RyR2 will not reduce Ca^{2+} transient amplitude, while severe Ca^{2+} leak reduces the Ca^{2+} transient amplitude and slows the rate of decay (Sankaranarayanan et al. 2016).

1.4.4.2 Experimental differences due to different models and methods

Potential reasons for such divergent results when investigating the Marks hypothesis include the variety of animal and experiment models, reagents and data analysis methods used by different research groups (Eschenhagen 2010; Dobrev 2014). However, in the instance of the Valdivia-Houser S2808A KI mouse, reasons for such differences are not so easily explained. Using the same strategy and similar experimental procedures as the Marks group, S2808A KI mice are functionally indistinguishable to WT, in terms of response to β-adrenergic stimulation, RyR2 channel activity and cardiac dysfunction post-MI (H. Zhang et al. 2012; MacDonnell et al. 2008; Benkusky et al. 2007). Marks and colleagues, with the same mouse (albeit from a different line), had previously found completely the opposite, where genetic ablation of the S2808 site severely limits such responses (Wehrens et al. 2006; Shan et al. 2010a). The only area of agreement in all studies with S2808A KI mice is that it has no basal phenotype, with contractility both *in vitro* and *in vivo* the same as WT (H. Zhang et al. 2012; Shaen et al. 2010a, Wehrens et al. 2006; MacDonnell et al. 2008; Benkusky et al. 2007; Shan et al. 2010b). While mouse models are not shared between research groups, reasons for differences remain unexplained.

1.4.4.3 Consideration of other RyR2 phosphorylation sites and the action of phosphatases

It also remains that the Mark's model disregards the functional relevance of the S2031 phosphorylation site as well as other potential sites. In an updated model, Wehrens offered an explanation that reconciles the roles of both S2808 and S2814 RyR2 phosphorylation (Respress et al. 2014). The group suggest that PKA exclusively phosphorylates S2808 and dissociates FKBP12.6, leading to increased RyR2 channel activity, while CaMKII almost exclusively phosphorylates S2814, has no effect on FKBP12.6 and still increases RyR2 channel activity. This was based on observations of S2814A KI mice, where preventing phosphorylation at this site protected against nonischemic HF but not ischemic HF.

Doubt has also been cast on the clean targeting of phosphorylation sites described by Respress et al. (2012), with suggestions this is oversimplified (2012). Structural data reveals that S2808 and S2814 form part of a larger phosphorylation hotspot in RyR2, in a flexible linker loop that protrudes on the RyR2 surface (Yuchi et al. 2012; Yuchi et al. 2013). This would suggest that the whole phosphorylation hotspot could be accessed by several kinases. Valdivia suggests that phosphorylation sites within this hotspot may provide 'functional redundancy', whereby phosphorylation of one site may lead to the same downstream effects of another due to such tight clustering (2012). Sequential addition of phosphate groups to the hotspot could lead to a graded response of RyR2 to multiple kinases, which could aid in explaining the variable response to phosphorylation observed by investigators.

Findings imply that altered RyR phosphorylation and function can also be due to changes in local phosphatase activity, as evidenced in both acquired and inherited cardiac conditions (DeGrande et al. 2013; Gupta et al. 2003; Wijnker et al. 2011; Neumann et al. 1997; Belevych, Sansom, et al. 2011). For example, decreased expression of PP2A catalytic subunits B56α and B56δ in a canine model of HF was accompanied by excessive RyR2 phosphorylation at S2031 and S2814 and increased RyR2-mediated diastolic Ca^{2+} leak (Niggli et al. 2012; Belevych, Terentyev, et al. 2011; Wijnker et al. 2011; Belevych, Sansom, et al. 2011). Marx et al. (2000) showed that a significant decrease in levels of PP1 and PP2A associated with the RyR2 macromolecular complex in failing human and canine hearts, even with the rise of cellular levels of PP1. Along with the evidence that dephosphorylation can also increase RyR2 channel activity (Carter et al. 2011), this suggests that both maximum phosphorylation and incomplete dephosphorylation of RyR2 results in increased activity of the channel (Terentyev and S. Hamilton 2016). This hypothesis may aid in the reconciliation

of contradicting results from different research groups, where any observed effects of kinases or phosphatases depend on initial RyR2 phosphorylation levels at multiple sites, which may vary due to experimental method.

The Marks group have evidenced PKA RyR2 hyperphosphorylation in models of human, mouse and rat heart failure (Marx et al. 2000; Reiken et al. 2001; Antos et al. 2001; Reiken et al. 2003). Inconsistencies described by other groups have been attributed to the activity of phosphatases during experimental procedures such as cardiomyocyte isolation and the importance of phosphatase inhibitors suggested as paramount (Reiken et al. 2003). It also remains that other posttranslational modifications, such as oxidation, can alter RyR2 channel function (Gonzalez et al. 2007; J. Sun et al. 2008).

1.5 Other posttranslational modifications

1.5.1 Oxidation by reactive oxygen species

There are many sources of reactive oxygen and reactive nitrogen species (ROS/RNS) that can alter the intracellular redox potential. Sources of ROS within the cardiomyocyte include sarcolemmal nicotinamide adenine dinucleotide phosphate (NADPH) oxidase, xanthine oxidase and the mitochondrial electron transport chain (Niggli et al. 2012). At low concentrations, ROS can serve as intracellular messengers, but at higher concentrations can lead to oxidative stress and subsequent redox modifications of EC coupling proteins with cysteine residues, including RyR2. Early works of the Williams laboratory demonstrated effects of ROS on RyR2 P_o {Boraso:1994fx, Holmberg:1991vx}. Oxidative conditions increase RyR2 P_o and in cardiomyocytes leads to a rapid increase in Ca^{2+} sparks, suggestive that the functional consequence of moderate oxidative stress is an immediate enhancement of SR Ca^{2+} release (Eager et al. 1997; Marengo et al. 1998; L. Xu et al. 1998; Salama et al. 2001). Increased ROS generation and subsequent oxidation and irreversible activation of RyR2 has been linked to many cardiovascular conditions, as well as diabetes (Bidasee et al. 2003; Terentyev, Belevych, et al. 2008; Y. M. Kim et al. 2005; C. Jung et al. 2007; Kyrychenko et al. 2012). There are reports of xanthine oxidase (a source of ROS) upregulation in several models of HF and abnormal SR Ca^{2+} release in myocytes from infarcted and failing heart associated with an increase in RyR2 oxidation (Cappola et al. 2001; Gonzalez et al. 2010; Terentyev, Belevych, et al. 2008; Belevych et al. 2009).

1.5.2 Nitrosylation

The major source of RNS in the cardiomyocyte is nitric oxide synthase (NOS) in either endothelial or neuronal form (eNOS or nNOS). This enzyme modifies RyR2 channels by the addition of nitric oxide (NO) groups to thiol moieties on cysteine residues in a process termed *S*-nitrosylation (Niggli et al. 2012; G. Lim et al. 2007). NOS and xanthine oxidase have been shown to physically interact in the left ventricles of mouse hearts and NO has an inhibitory effect on ROS production by xanthine oxidase (Khan et al. 2004). NOS has also been shown to move from the SR to the sarcolemma in failing hearts, potentially removing the cardioprotective effect of xanthine oxidase inhibition in this instance (Hare and Stamler 2005). Both constitutive isoforms of NOS have been shown to co-immunoprecipitate with RyR2 (Bendall et al. 2004). Evidence suggests that NO may regulate RyR2 channel P_o in both a PKA activity- and concentration-dependent manner (Fauconnier et al. 2010; Petroff et al. 2001). The interaction of RyR2 modifications resulting from both ROS and RNS remains to be fully elucidated, but it has been suggested that a precise balance of the two species within the cell is important, with disequilibrium leading to abnormal channel behaviour (Niggli et al. 2012; G. Lim et al. 2007).

1.5.3 Glutathionylation

During oxidative stress, free thiols of RyR2 can be oxidized to form sulfenic, sulfinic or sulfonic acid products (Giles and Jacob 2002). Reduced glutathione, a highly abundant antioxidant, usually attenuates ROS production by scavenging free radicals. It can also readily react with sulfenic acids to form reversible *S*-glutathionylation of RyR2 and protein-glutathione-mixed dilsulfide products, thought to have a protective role during cellular oxidative changes (Zima and Mazurek 2016; Townsend 2008). In the cardiomyocyte, the ratio of oxidized and reduced glutathione is therefore an important indicator of redox state. During normal physiological conditions, cytosolic glutathione is mostly reduced. During oxidative stress, the ratio can increase significantly, as well as the total amount of protein-glutathione-mixed dulsulfides (Tang et al. 2011; Werns et al. 1992; Ceconi et al. 1988). An increase in these compounds has been implicated as a critical signalling mechanism that is causative in cardiovascular disease (Zima and Mazurek 2016).

1.5.4 Crosstalk between redox modifications and phosphorylation

Posttranslational modifications of RyR2 are unlikely to be entirely mutually exclusive, yet causal links between them and alterations of RyR2 function are yet to be established. Competition between NOS/NO-dependent S-nitrosylation and ROS-dependent thiol oxidation has recently been observed, with both suggested to increase Ca^{2+} leak through RyR2 channels (Gonzalez et al. 2007; J. Sun et al. 2008). The Marks group suggested that oxidation reduces the affinity of RyR2 for FKBP12.6 and sensitizes the channel for PKA phosphorylation at S2808, a cooperative mechanism that increases Ca^{2+} leak (Shan, Betzenhauser, et al. 2010; Shan, Kushnir, Betzenhauser, Reiken, J. Li, Lehnart, Lindegger, Mongillo, Mohler and Marks 2010a). Under non-oxidizing conditions, PKA may not destabilize FKBP12.6 binding, therefore offering an explanation as to why others did not observe this phenomenon (see **Section 1.4**). Interestingly, genetic inhibition of RyR2 phosphorylation at S2808 or S2814 phosphorylation sites reduced RyR2 oxidation in mice with Duchenne muscular dystrophy (*dmd* mice) exhibiting progressive cardiac deterioration, suggesting a potential interaction between pathways (Kyrychenko et al. 2012; Q. Wang et al. 2015). Redox conditions can also easily differ between laboratories, protocols and reagents, so different redox states of RyR2 channels in question may account for some published controversies on the role of phosphorylation on RyR2 channel function (Eschenhagen 2010).

1.6 Dysregulation of RyR and disease

1.6.1 Diseases linked to RyR1

Dysfunction of both RyR1 and RyR2 isoforms has been linked to life-threatening conditions (MacLennan and Zvaritch 2011). Associated diseases of mutant RyR1 include malignant hyperthermia (MH) and central core disease (CCD). MH is triggered by volatile anaesthetics or by muscle relaxants, while CCD is characterized by progressive muscle weakness and cores (inactive tissue) within muscle fibres (Fujii et al. 1991; Quane et al. 1993; Mulley et al. 1993; Gillard et al. 1991; Jungbluth et al. 2005). Many of the associated mutations cluster in regions highly conserved between species and isoforms in distinct disease 'hotspots', with diseases of RyR1 and RyR2 found in the N-terminal region (~1-600 residues), a central region (~2100-2500 residues), and a C-terminal region (~3900 residues to end) (Van Petegem 2012). This suggests functional importance of these regions within RyR isoforms (George 2007a; Laitinen et al. 2001; Postma 2005).

1.6.2 Diseases linked to RyR2

Finely tuned cardiomyocyte Ca^{2+} signalling is critical to normal cardiac function and given the central role of RyR2 in this process, any perturbations of SR Ca^{2+} release through RyR2 channels is implicated in many cardiovascular diseases. Decreased SR Ca^{2+} load occurs as a result of 'leaky' destabilized RyR2 channels in pathophysiology (Marx et al. 2000). This Ca^{2+} leak can result in a decreased Ca^{2+} transient amplitude and potentially drive inward Ca^{2+} currents through NCX, causing premature AP, early and delayed after depolarizations (EADs and DADs, see **Section 1.7.1**). A downregulation of NCX or upregulation of SERCa2a can contribute to this phenomenon, as observed in HF (Bers 2006). An increase of SR Ca^{2+} content may also perturb Ca^{2+} homeostasis, as it can increase the sensitivity of RyR2 to activation and lead to increased Ca^{2+} sparks, subsequently causing EADs and DADs (Carnes 2008; Bers 2008). Cardiac pathologies involving altered Ca^{2+} handling via RyR2 are discussed below.

1.6.2.1 Heart failure and triggered arrhythmia

HF is characterized by a progressive deterioration of cardiac function, with the heart unable to pump sufficient amounts of blood to support the metabolic need of body tissues. Prevalence is alarmingly high, with ~900,000 people in the UK affected, causing and

complicating ~5% of all emergency hospitalizations (Bhatnagar et al. 2016). HF is the final common pathway for many cardiovascular conditions, including ischemic heart disease, hypertension and genetic abnormalities. The in-hospital mortality rate for those patients admitted with acute HF is ~10%, with premature death occurring from haemodynamic collapse due to poor cardiac pump function, or from lethal arrhythmias (Bhatnagar et al. 2016; Henkel et al. 2009).

Characteristics vary depending on the stage of condition, but the failing heart is usually pumping against excessive systemic pressures and is dilated, requiring the diseased heart to generate an increased systolic wall stress. Cardiomyocytes generate greater forces to eject normal or often reduced output. HF is generally acknowledged as a disease state in which normal β-adrenergic stimulation is disrupted and with receptors downregulated and responsiveness to elevated circulating catecholamines severely attenuated (Fischer et al. 2012). Patients are dependent on this hyperadrenergic state to maintain cardiac output under normal conditions (Houser and Margulies 2003). Myocytes in the failing heart also structurally and functionally remodel in response to increased metabolic demand. There are changes in the expression and phosphorylation state of many EC coupling proteins underlying contractile dysfunction in HF, including LTCCs, SERCa2a, NCX and RyR2 (Houser and Margulies 2003; X. Chen et al. 2002; Dipla et al. 1999; Houser et al. 2001; Piacentino 2003; Gaughan et al. 1999).

Major alterations in the Ca^{2+} handling of a failing ventricular cardiomyocyte are caused by downregulation of SERCa and upregulation of NCX function, thereby increasing Ca^{2+} efflux and reducing SR Ca^{2+} content (Bers et al. 2006). As Ca^{2+} transient amplitudes are smaller due to a reduced SR content, there may be less Ca^{2+}-dependent inactivation of LTCCs, thus a greater integrated Ca^{2+} influx into the cell. In HF, SR Ca^{2+} content is also depressed by enhanced Ca^{2+} leak, implicating enhanced RyR2 activity (Eisner et al. 2017).

Enhanced RyR2 activity is implicated in multiple forms of HF, including compensated early stages of the disease where Ca^{2+} transient amplitude remains unaltered (Sossalla et al. 2010; Jerry Curran et al. 2010; Belevych, Terentyev, et al. 2011). As discussed in **Section 1.4**, phosphorylation of RyR2 has been intensely investigated as a means of altering channel function, especially in terms of pathophysiological changes in Ca^{2+} handling during HF. The leading cause of death in patients with HF is cardiac arrhythmia, namely ventricular tachycardia and fibrillation (Orn and Dickstein 2002). Increased RyR2 activity can lead to different patterns of Ca^{2+} handling including self-propagating waves and triggered activity arising from EADS and DADs, events that can lead to ventricular tachycardia (VT)

(Venetucci et al. 2008; Monsuez et al. 1995; Janse 2004; Belevych, Terentyev, et al. 2011; Xie and Weiss 2009; Pogwizd 2004; Keurs and Boyden 2007).

Atrial fibrillation (AF) is another common form of human arrhythmia, usually attributed to an increased substrate for reentry due to tissue fibrosis and altered EC coupling protein expression. RyR2 dysfunction is thought to underlie triggered ectopic activity in AF (Hove-Madsen et al. 2004; Vest et al. 2005; Heijman et al. 2016). The activities of phosphatases PP1 and PP2 are increased in AF, and although this increased activity is expected to dephosphorylate EC coupling proteins, RyR2 phosphorylation levels are also increased (El-Armouche 2006; Greiser et al. 2009). It has been proposed that uneven distribution of phosphatases between subcellular compartments with decreased activity in the RyR2 microdomain contributes to this increased RyR2 phosphorylation (El-Armouche 2006). Alternatively, enhanced activity of CaMKII may outweigh phosphatase activity, leading to increased RyR2 phosphorylation and ultimately an increase in channel activity that contributes to AF (Chelu et al. 2009).

1.6.2.2 Arrhythmogenic right ventricular cardiomyopathy

Arrhythmogenic right ventricular cardiomyopathy (ARVC), also known as arrhythmogenic right ventricular dysplasia (ARVD) is an inherited condition, distinguished by ventricular arrhythmia and right ventricular degeneration (Marcus et al. 2010; Marcus et al. 1982). The disease is autosomal dominant in nature and there are more than 10 causative genes linked to the condition (Ohno 2016; Ruder et al. 1985). ARVC2 is linked to mutations of RyR2, with mutation carriers in the first identified ARVC family showing exercise-induced polymorphic ventricular tachycardia much like another disease, catecholaminergic polymorphic ventricular tachycardia (CPVT) (Rampazzo et al. 1995). However, instead of having a structurally normal heart, ARVC2 patients presented with fibro-fatty replacement of cells in the right ventricular myocardium, thereby distinguishing the condition from CPVT. Four RyR2 mutations (R176Q, L433P, N2386I and T2504M) from three ARVC families were identified, although later suggestions were made that families were presenting with a variant of CPVT (Ohno 2016; Tiso et al. 2001). In a KI mouse model of R176Q (heterozygous for the mutation, $^{+/-}$), mice exhibited normal resting phenotype but with β-adrenergic stimulated premature ventricular beats (Kannankeril et al. 2006). No fatty-fibrous tissue was found in R176Q mouse hearts, suggestive that this mutation in fact causes CPVT.

1.7 Catecholaminergic polymorphic ventricular tachycardia

1.7.1 Pathophysiology

Catecholaminergic polymorphic ventricular tachycardia (CPVT) is an inherited arrhythmogenic disease associated with sudden cardiac death (Priori et al. 2001). It causes syncopal episodes following stress or exercise with symptoms often beginning in childhood, although later onset has been reported. These symptoms only usually occur during β-adrenergic stimulation, implicitly linking upregulation of EC coupling proteins by phosphorylation in disease pathogenesis. It is characterized by delayed after depolarizations (DADs, see **Figure 1.13**) and polymorphic or bidirectional VT, but in contrast to ARVC, this is in the absence of any structural alterations to the heart. Both forms of VT can degenerate into VF and sudden cardiac death which is often the first manifestation of the condition (Swan, Piippo, Viitasalo, Heikkilä, Paavonen, Kainulainen, Kere, Keto, Kontula and Toivonen 1999b; Allouis et al. 2005). Prevalence of CPVT within the population is estimated at 1:10,000, with the majority of patients having a family history of syncopal or arrhythmic events (Jabbari et al. 2013; Ylänen et al. 2010; Keurs and Boyden 2007). However, phenotypic manifestations of the disease are very heterogeneous, sometimes even within the same family (George 2007a).

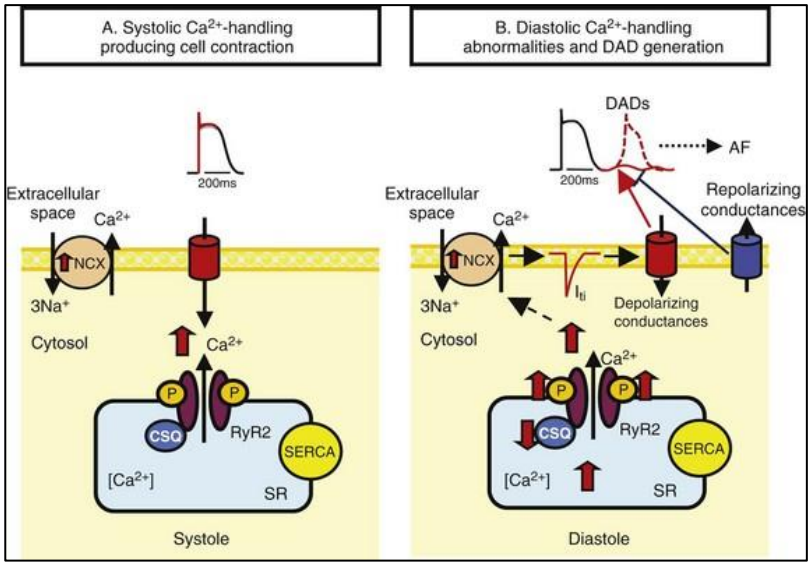

Figure 1.13 Abnormal Ca^{2+} handling in cardiomyocytes leading to delayed after depolarizations. *A.* During the plateau phase of action potential, Ca^{2+} influx occurs through LTCCs and triggers CICR, initiating cardiomyocyte contraction during systole. B. Spontaneous Ca^{2+} release through RyR2 channels increases cytosolic Ca^{2+} concentration during diastole. This is extruded from the cytosol by NCX leading to an inward depolarizing current (I_{ti}) that can cause delayed after depolarizations (DADs). Phosphorylation (P) is also implicated. Figure from Nattel et al. (2014).

1.7.2 'Hotspot' domains of RyR2 CPVT1 mutations

'Catecholamine-induced' severe ventricular arrhythmia was first identified in 1978 as a novel clinical condition (Coumel 1978). However, it wasn't until the advancement of molecular genetics that linkage studies and direct sequencing revealed mutations linked to the condition mapped to chromosome 1q42-q43 and subsequently, the human *RyR2* gene (Priori et al. 2001; Swan, Piippo, Viitasalo, Heikkilä, Paavonen, Kainulainen, Kere, Keto, Kontula and Toivonen 1999a). CPVT can be inherited in either an autosomal dominant (CPVT1) or the recessive fashion (CPVT2) (Lahat et al. 2001; Priori et al. 2001; Laitinen et al. 2001). CPVT1 is the most common form, caused by mutations in RyR2 and is caused by aberrant Ca^{2+} release from the SR through the RyR2 channel. RyR2 mutations are autosomal dominant in nature, so inheritance of a single allele is sufficient to cause the disease phenotype. While most patients with the condition have a family history of cardiac events, some have been identified as the only symptomatic family member with neither parent carrying a mutant allele, suggestive that mutations can arrive *de novo* (Postma 2005; Priori et al. 2001). CPVT2 is linked to chromosome 1p13-21 and the *CSQ2* gene (Lahat et al. 2001; Lahat et al. 2002). CSQ2 mutations are recessive, so inheritance on both alleles is required for the disease phenotype, making this form of CPVT less common (Lahat et al. 2002). CSQ2 is a Ca^{2+}-buffering protein that regulates Ca^{2+} release through RyR2 (see **Section 1.3.4**). Mutations in other accessory proteins that regulate RyR2 function have more recently been suggestive as causative of CPVT, including in CaM and TRDN (Walweel et al. 2016; Rooryck et al. 2015; Gomez 2016; M. A. Walsh et al. 2016).

hRyR2 CPVT1 mutations preferentially map to three (or four) distinct 'hotspots' or loci in the RyR2 polypeptide, with many of these mutations in regions conserved across multiple species isoforms. The fourth domain is referred to as the cytoplasmic portion of I domain and all domains (N-terminal, central, cytoplasmic portion of the I and transmembrane domain) can be visualised in **Figure 1.14** (N. L. Thomas et al. 2006; George et al. 2007). The conserved nature of these mutation-rich regions reinforces the hypothesis that mutations are associated with functional changes in the hRyR2 gene product. To date, there are over 170 CPVT1 mutations reported in the literature (www.hgmd.com, (Medeiros-Domingo et al. 2009), with approximately only ~10% of these mutations functionally characterized in some way. The RyR2 domain containing the highest number of mutations is the B-solenoid of the central domain, however the domain containing the highest density/concentration of mutations is the EF hand domain (**Figure 1.15**). Interestingly, Guo et al. (2016) found that some mutations in the EF-hand motifs or in fact entire deletion of the domain did not affect the Ca^{2+}-dependent activation of [^{3}H] ryanodine binding or the cytosolic

Ca^{2+} activation of the RyR2 channel. However, the E4071A mutation in the EF-hand binding motif (residues 4081-4127) in RyR2 altered spontaneous Ca^{2+} release in HEK293 cells, increasing the termination threshold for SOICR. Deletion of the entire domain also markedly decreased the sensitivity of single RyR2 channels to luminal activation. Authors therefore suggest that the EF hand Ca^{2+} binding domain is important for luminal Ca^{2+} activation and SOICR, but not necessarily cytosolic Ca^{2+} activation of the channel (W. Guo et al. 2016).

Whether CPVT1 mutation location and severity of clinical phenotype in patients is linked remains unclear, with some groups suggesting C-terminal domain mutations may increase the odds of non-sustained VT in patients in comparison to N-terminal domain mutations (Yamazoe and Furukawa 2016; van der Werf et al. 2012). Others point out that the clinical manifestation is highly heterogeneous and that many mutation carriers can appear completely asymptomatic of disease (Priori 2002; Tester et al. 2004; Postma 2005; Tester et al. 2006; Tiso et al. 2001; Priori et al. 2001; Aizawa et al. 2007; Laitinen et al. 2001). Mutations investigated in this thesis are found in the B solenoid and EF hand domain.

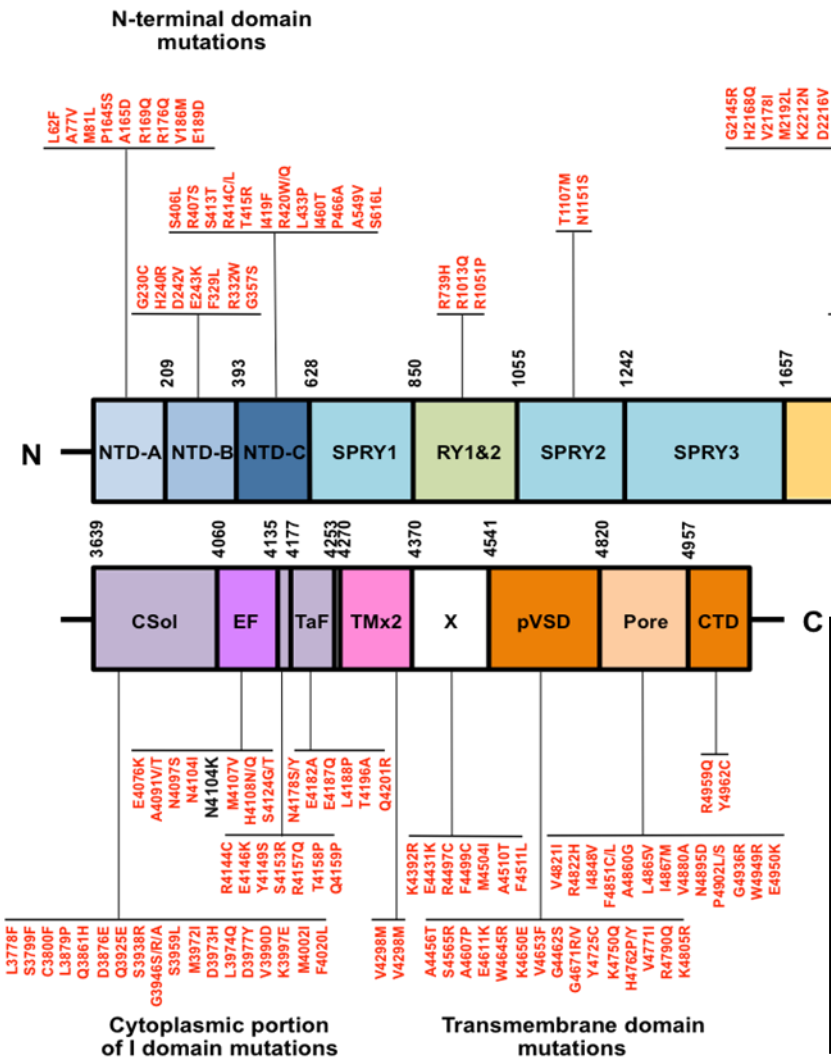

Figure 1.14 Schematic diagram to illustrate the clustering of CPVT1 mutations in functional domains of the RyR2 polypeptide. CPVT1 mutations (red text) are grouped and indicated on the diagram in each domain, with mutations in black investigated in this thesis. Domains of the polypeptide defined in the table and discussed in more detail in **Section 1.3.1.** Mutations are classified into four groups – N-terminal domain (residues 77-1724), central domain (residues 2246-2534), cytoplasmic portion of I domain (residues 3778-4201), and transmembrane domain mutations (residues 4497-4959). Figure and table adapted from des Georges *et al.* (2016).

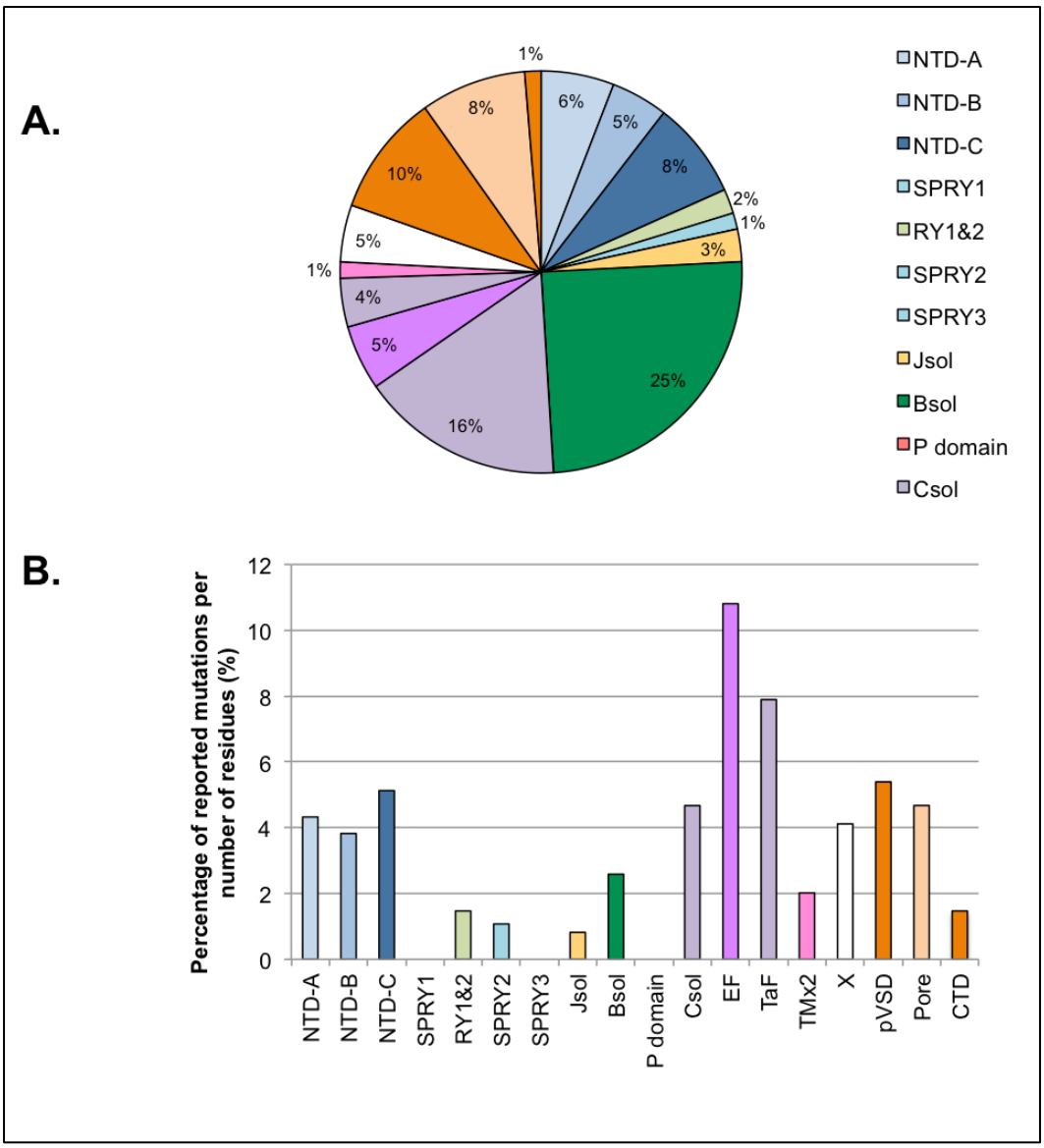

Figure 1.15 Distribution of CPVT1 mutations in the functional domains of RyR2. *A.* A pie chart of all CPVT1 mutations in **Figure 3.1**, highlighting the distribution across domains of the polypeptide. Most mutations are found in the B-solenoid domain. *B.* Graph of the percentage of reported CPVT1 mutations per number of residues. The EF hand domain has the most concentrated area of mutations. Colour-coding follows that in **Figure 1.14**.

1.7.3 Mechanisms of RyR2 dysfunction

Controlled intracellular Ca^{2+} release through RyR2 is key during EC coupling and requires precise regulation (Bers 2004; Bers 2002b) with activation of the channel by cytosolic Ca^{2+} underpinning CICR (Fabiato 1985b). However, it has long been established that spontaneous Ca^{2+} release can occur in the absence of cell depolarization (Fabiato 1992), caused by a luminal SR Ca^{2+} 'overload', when Ca^{2+} within the SR reaches a critical threshold (Lakatta 1992; Orchard et al. 1983). Such overload can be caused by a variety of conditions, including the release of catecholamines during increased metabolic demand during stress or exercise; conditions that require a higher cardiac output to deliver more blood to the body via β-adrenergic stimulation (Marx and Marks 2013; Bers 2001). The clinical manifestation of CPVT1 occurs during these periods (Priori et al. 2001) and disease-causing mutations in RyR2 are suggested to reduce the threshold for Ca^{2+} release, increasing the susceptibility for arrhythmogenesis (D. Jiang et al. 2004; Priori and S. R. W. Chen 2011; Venetucci et al. 2008). The mechanism of pathogenic RyR2 Ca^{2+} signalling has been intensely investigated (Belevych et al. 2013; Venetucci et al. 2008), but it remains to be elucidated how a single point missense mutation can have such catastrophic consequences on Ca^{2+} handling in EC coupling, regardless of its location in the RyR2 polypeptide.

With variable penetrance of RyR2 mutations, the sheer number of different mutations in different domains of the channel and reported phenotypic heterogeneity of CPVT1 patients, it is highly unlikely that these mutations result in dysfunction by a single unifying mechanism (Bauce et al. 2002; Marjamaa et al. 2009; George 2007b). Three mechanisms of RyR2 dysfunction have been proposed:

1.7.3.1 Dissociation of FKBP12.6 and RyR2 'hyperphosphorylation

The hypothesis involving FKBP12.6 dissociation from RyR2 causing channel destabilization and Ca^{2+} leak from the SR proposed by Marx et al. (2000) was extended to explain altered Ca^{2+} homeostasis in CPVT1, with mutant RyR2 channels suggested as having a reduced binding affinity for FKBP12.6. However, this has been challenged by other groups, who found unaltered FKBP12.6 association to mutant RyR2 expressed in heterologous and cardiac cell lines in comparison to WT, before or after stimulation with catecholamines (Zissimopoulos and Lai 2005; P. P. Jones et al. 2008; Tester et al. 2007; George, SORATHIA, et al. 2003; D. Jiang 2005). In KI mice with CPVT mutations (R2474S and R4497C), stress-induced DADs and arrhythmia were observed despite apparent normal FKBP12.6:RyR2 association (Fernández-Velasco et al. 2009; N. Liu et al. 2006; Uchinoumi

et al. 2010). The role of FKBP12.6 dissociation and RyR2 phosphorylation is discussed in more detail in **Section 1.4.2.1**.

1.7.3.2 Disruption of interdomain interactions

Interdomain interactions are thought to enable proper protein folding and assembly, stabilizing the closed RyR2 channel (Z. Liu et al. 2010; Yamamoto and Ikemoto 2002; George et al. 2004). Disruption of such interdomain interactions by RyR2 mutation, termed 'domain unzipping' has been suggested to weaken this stabilization and make channels more sensitive to activating Ca^{2+}, subsequently leading to an open RyR2 channel during diastole. Ikemoto and Matsuzaki postulated a model in which there are two coupled domain-domain interactions: that of the N-terminal and the central domain (**See Figure 1.16**), and that of the I-domain (residues 3722-4610) and the IP-domain (the unidentified putative partner of the I-domain (Oda 2005; Yamamoto and Ikemoto 2002; Tateishi et al. 2008; Suetomi et al. 2011; Uchinoumi et al. 2010). Each of these coupled domains forms zipped complexes. When disrupted by CPVT1 mutation in the N-terminal or central domain, this induces diastolic Ca^{2+} leak via a destabilization of the N-terminal-central domain interaction, followed by destabilization of the I-IP domain interaction. CPVT1 mutations in the I-domain however, do not disrupt interactions in the same manner; I-IP domain interactions are disrupted, but N-terminal-central domain interactions remain stable.

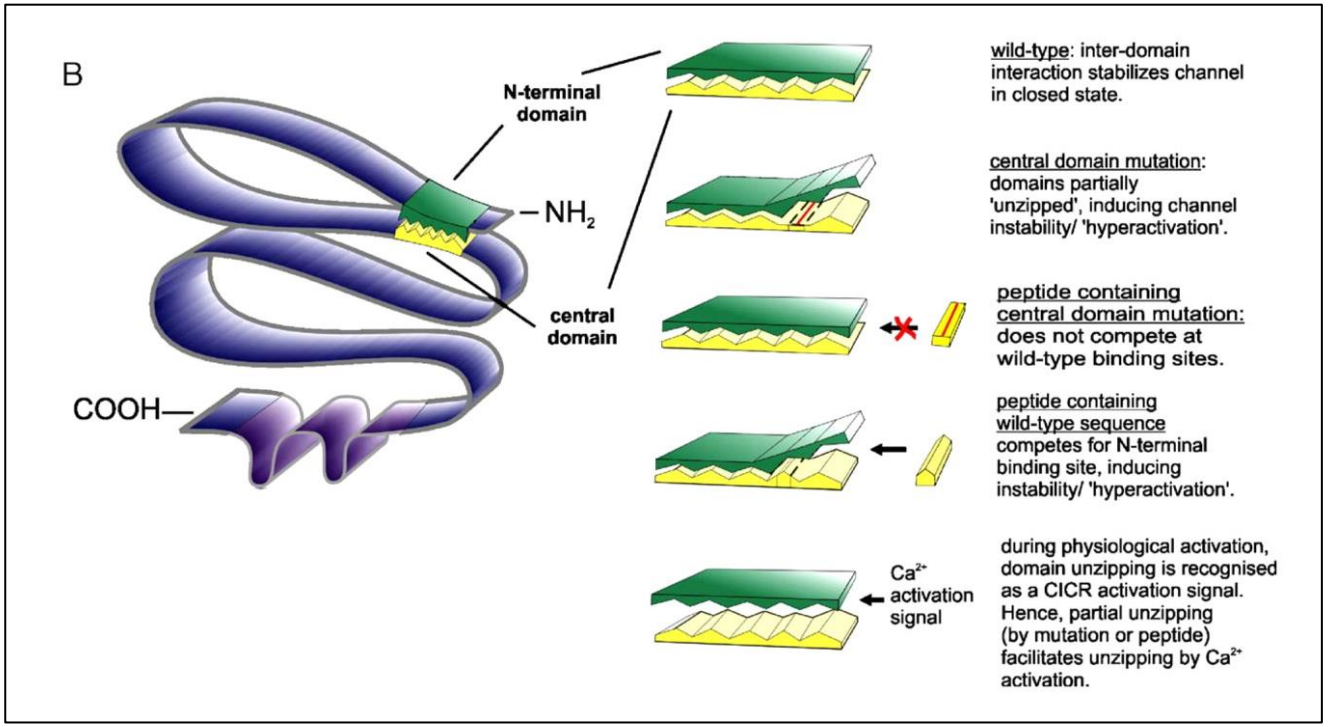

Figure 1.16 Proposed action of unzipping between N-terminal and central domains in RyR2. Postulated domain unzipping is caused by either CPVT1 mutation or a competitive interaction with domain peptides that mimic a region of the polypeptide. Figure adapted from Yang et al. (2006).

DPc10 is a short synthetic peptide that is homologous to the central domain of RyR2, spanning residues 2460-2495 (Oda et al. 2005). This was used to mimic the effect of CPVT1-linked RyR2 mutations, with the authors reporting that the peptide destabilized interactions between the N-terminal and central domains of RyR2 (YANG et al. 2006; Oda et al. 2005; Z. Liu et al. 2010). Reversal of the unzipped state to a normal zipped state by the drug K201 (see **Section 1.7.4**) was reported by Oda et al. (2005), whereby the drug is proposed to stabilize the closed state of the channel by enhancing FKBP12.6 binding. In isolated WT rat cardiomyocytes, inserting the R2474S mutation into the peptide abolished the effects of DPc10 (Yang et al. 2006). Authors suggest that this mutation in the peptide will not interfere with interdomain interactions as does the WT peptide and that this particular residue is important in maintaining a stabilized RyR2 channel.

Abnormally strong intradomain interactions are also implicated in dysfunction caused by altered interaction within the central domain. Synthetic peptide DP2446, corresponding to residues 2232-2266 in the central domain, binds to residues 1741-2270 within the same domain. Introduction of the CPVT1-linked mutation S2246L into DP2446 causes what is described as an abnormally tight interaction between DP2446 and the K201-binding domain (residues 2114-2149), with an increased affinity of peptide binding observed by fluorescence quench assay (Suetomi et al. 2011). Authors suggest that this tight interaction opens the Ca^{2+} channel and their dissociation closes the channel. The abnormally tight intradomain interaction caused by the S2246L mutation was proposed to explain increased Ca^{2+} spark frequency observed in isolated cardiomyocytes of S2246L ($^{+/-}$) KI mice.

Peptides that are homologous to the N-terminal (DP163-195) and C-terminal (DP4090-4123) domains of CPVT1 have also been utilized, mimicking CPVT mutations R176Q and N4104K respectively (Z. Liu et al. 2010; Tateishi et al. 2008). While addition of either peptide to isolated WT canine cardiomyocytes induced domain unzipping, increasing Ca^{2+} spark frequency and SR Ca^{2+} leak, treatment with K201 suppressed these effects induced by DP163-195 only. This is suggestive that K201 zipping occurs within only certain domains. Authors propose that mutations in the C-terminal region of RyR2 can also induce spontaneous Ca^{2+} leak, but not through communication with the N-terminal and central domain interaction, but by disruption of other domain interactions that are yet to be identified.

In the latest 3D structure of RyR (see **Section 1.3.1**), the conduction pathway of the channel is formed by membrane regions of the four S6 inner helices, with the intracellular gate located in the S6 helix bundle crossing region (Yan et al. 2014). The cytoplasmic region of

the S6 helix appears to interact with the U motif of the central domain (Bai et al. 2016; Yan et al. 2014). The U motif is formed from the carboxyl-terminal sequences of the central domain that form a U-shaped subdomain. It consists of a β-hairpin, an α-helix hairpin at the carboxyl-terminus, and an intervening short α-helix (Yan et al. 2014). In the most recent work of the Chen group, authors hypothesized that interactions between the U motif of the central domain and the S6 cytoplasmic region was involved in channel stabilization (B. Sun et al. 2016). Mutating each residue in the S6 cytoplasmic region, authors found that mutating residues either side of the S6 helix that faces the U motif increased RyR2 channel activity. Within this region, the V4880A RyR2 mutation not only increased arrhythmogenic spontaneous Ca^{2+} release when expressed in a heterologous cell system but increased activity of the single channels in near zero concentrations of activating Ca^{2+}. It was therefore proposed that mutations in this region may disrupt interactions between the S6 helix and the U motif of the central domain, destabilizing the closed channel state, increasing basal activity and the propensity for spontaneous Ca^{2+} release (B. Sun et al. 2016).

1.7.3.3 Altered RyR2 Ca^{2+} sensitivity and 'store overload-induced Ca^{2+} release'

CPVT1-linked RyR2 mutations have been suggested to cause altered sensitivity to activation by Ca^{2+}. Introduction of the DPc10 peptide to mimic central domain mutation of RyR2 induced disruption, causing sustained SR Ca^{2+} leak by lowering the threshold for cytoplasmic Ca^{2+} activation (YANG et al. 2006). The Chen group have recently investigated mutations of the cytoplasmic portion of the I domain (referred to by authors as central domain mutations between residues 3778-4201(P. Li and S. R. Chen 2001; Z. Xiao et al. 2016)). Eight disease-associated RyR2 mutations in this domain appeared to enhance cytosolic Ca^{2+}-dependent activation of single channels. Authors therefore suggested that this domain is important in the cytosolic Ca^{2+} activation of RyR2 and that any alterations of this activation and sensitivity to cytosolic Ca^{2+} may enhance susceptibility to arrhythmia. Complicating matters, the RyR2 mutations G230C and K4750Q have been demonstrated to exhibit increased sensitivity to both cytosolic and luminal Ca^{2+} activation in single channel experiments(Y. Liu et al. 2013; Uehara et al. 2017).

As many CPVT1-linked RyR2 mutants also appear to exhibit similar cytosolic Ca^{2+} sensitivity in single channel experiments (Tester et al. 2007; Marjamaa et al. 2009; D. Jiang 2005), another hypothesis is that the major functional consequence of mutation is enhanced luminal Ca^{2+} sensitivity, with a lowered critical threshold for Ca^{2+} release from the SR (P. P. Jones et al. 2008; D. Jiang et al. 2007; D. Jiang et al. 2004; D. Jiang 2005). 'Store overload-induced Ca^{2+} release' (SOICR, see **Figure 1.17**) was a term first used to describe spontaneous Ca^{2+}

release by Chen's group in 2004 (D. Jiang et al. 2004). This term was chosen based on its occurrence being dependent on the SR Ca^{2+} store with a critical threshold level for Ca^{2+} release. The group examined a number of CPVT1 mutant (mouse) RyR2 channels recombinantly expressed in HEK293 cells and found they showed an increased propensity for oscillation i.e. more transfected cells displayed Ca^{2+} oscillations compared to WT transfected cells and at lower extracellular Ca^{2+} concentrations. Authors looked at the kinetic parameter of frequency of spontaneous Ca^{2+} oscillations, and found this was enhanced in mutant transfected cells, as well as a decrease in the ER Ca^{2+} store (measured by caffeine-induced Ca^{2+} release). This observation was accompanied by an increased single channel P_o in response to luminal Ca^{2+} compared to WT RyR2 channels, but unaltered [^{3}H]-ryanodine binding in response to activating Ca^{2+}, thought to reflect an equivalent sensitivity to cytosolic Ca^{2+} concentrations (D. Jiang 2005; D. Jiang et al. 2004). SOICR of CPVT mutations has also been investigated in HL-1 cardiomyocytes and enhanced spontaneous Ca^{2+} release was also observed, thought to reflect sensitivity to luminal Ca^{2+} of CPVT1 mutations compared to WT (D. Jiang 2005).

Authors suggested these mutations therefore enhance the propensity for SOICR in HEK293 cells, as well as increase the sensitivity to activation by luminal Ca^{2+} (which would therefore suggest that the critical threshold for Ca^{2+} release is decreased), increasing susceptibility to DADs and triggered activity (D. Jiang et al. 2004; D. Jiang 2005). As mentioned previously, during pathological conditions of aberrant Ca^{2+} release, Ca^{2+} sparks ignite neighbouring clusters by a fire-diffuse-fire mechanism, triggering regenerative CICR-driven Ca^{2+} waves that are proarrhythmic (Bovo et al. 2011; Kunitomo and Terentyev 2011).

The term SOICR is somewhat a misnomer, referring to a lowered threshold and not necessarily an actual store 'overload'. The resting level of SR free Ca^{2+} may have also adapted to such a reduced threshold via autoregulation (Eisner 1998), therefore under resting conditions a modest reduction should not elicit pathogenic Ca^{2+} signalling during normal EC coupling, explaining how enhanced SOICR occurs despite the observed reduction in ER Ca^{2+} content. Subsequent experiments with a luminal sensitive indicator protein D1ER, which allowed more direct monitoring of Ca^{2+} within the store, also determined that the V4653F RyR2 mutant expressing cells had a reduced threshold for SOICR (Palmer et al. 2004; P. P. Jones et al. 2008).

Although enhanced propensity for SOICR and sensitivity to luminal Ca^{2+} likely plays an important role in the dysfunction of some RyR2 mutants, it is unlikely to be the sole mechanism of channel dysfunction in CPVT1 (Uchinoumi et al. 2010; Laver et al. 2007; Meli

et al. 2011). Increased sensitivity to cytosolic Ca^{2+}-dependent activation via dissociation of FKBP12.6 (Lehnart et al. 2004; Meli et al. 2011; Wehrens et al. 2003; Lehnart et al. 2008) as well as the induction of defective inter-domain conformational changes have also been implicated as mechanisms of RyR2 dysfunction in CPVT (Uchinoumi et al. 2010; Laver et al. 2007).

The persistence of so many candidate mechanisms of RyR2 dysfunction in CPVT1 may indicate more convolution than a general one-fits-all model.

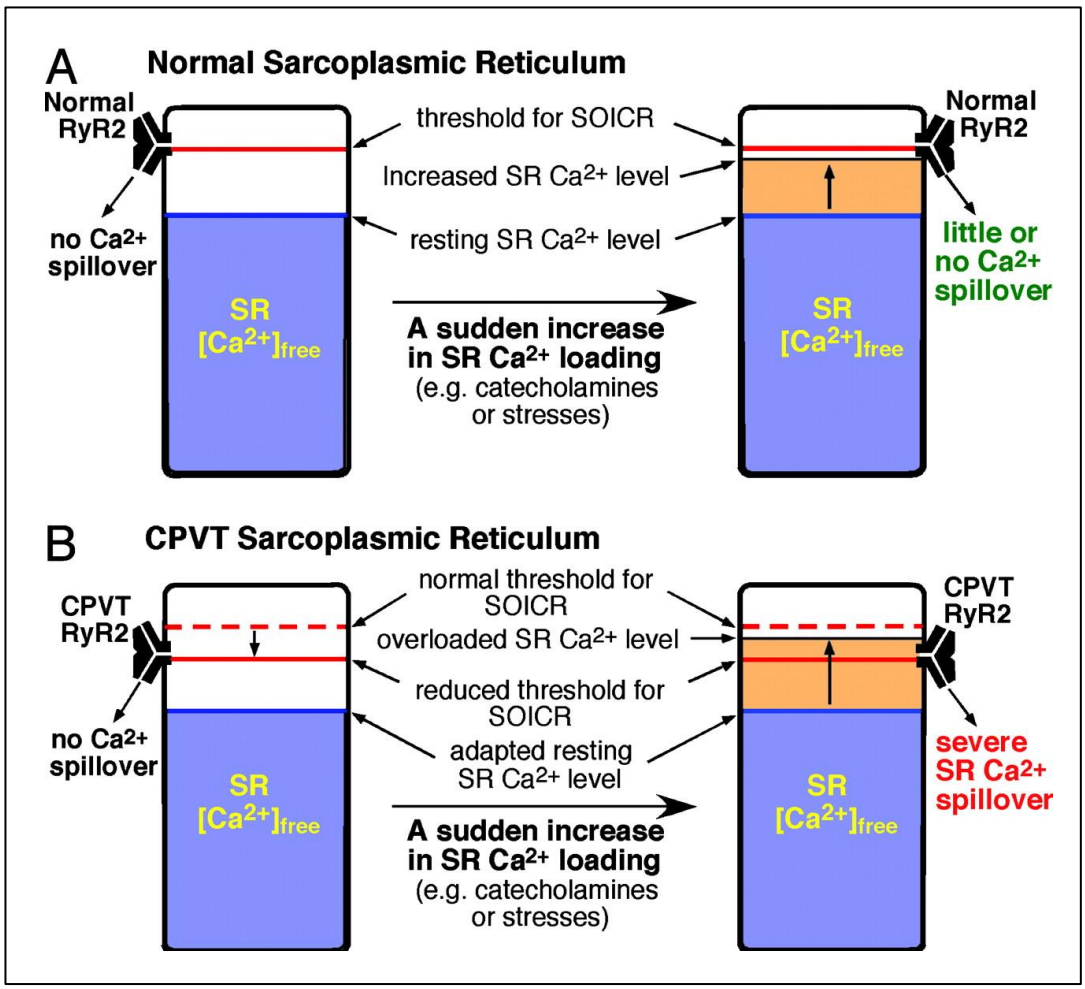

Figure 1.17 'SOICR': a proposed mechanism for CPVT1 associated with RyR2 mutations. Chen's group proposes that the relationship between the threshold for store overload-induced Ca^{2+} release (SOICR) and the SR-free Ca^{2+} level in normal (A) and CPVT1 SR (B) is altered. Resting states are shown on the left, stimulated states on the right. The threshold for SOICR is depicted by the red line and is reduced in the CPVT1 SR as a consequence of RyR2 mutations. The blue area depicts the level of free SR Ca^{2+}. An increase in free SR Ca^{2+} by stimulation via catecholamines or stress is shown by the yellow area. When free Ca^{2+} reaches the SOICR threshold, SOICR occurs leading to a large Ca^{2+} spill over. This can then generate DADs and triggered arrhythmia. Figure from D. Jiang et al. (2004).

1.7.4 Current treatment

Untreated, CPVT has a high rate of mortality, with 30 % of individuals of classic phenotype dying before the age of 40 (Priori 2002; Hayashi et al. 2009). Since the condition was first described, β-adrenergic receptor antagonists (β-blockers) remain the cornerstone of therapy for patients to date (Priori et al. 2001; Priori et al. 2013). This is to prevent the stimulatory effects of the β-adrenergic pathway. However, a significant number of patients remain symptomatic despite β-blocker therapy, or suffer severe side effects. An 8-year study of 101 patients with CPVT1 found that cardiac fatal and non-fatal effects were not sufficiently low, at 27 % and 11 % respectfully (Hayashi et al. 2009). In another cohort of 205 CPVT1 patients, 25 % of patients taking β-blockers alone experienced at least one treatment failure including syncope and/or cardiac arrest (Roston et al. 2015). The inconsistencies between patient responses could indicate that not all mutations of RyR2 result in CPVT1 by the same pathogenic mechanism, and dysfunction is not entirely dependent on β-adrenergic stimulation.

Treatment using implantable cardioverter defibrillator (ICD) is normally administered to patients unresponsive to β-blocker therapy; this is a more traumatic course of treatment that also is not always successful (Pizzale et al. 2008). In young and active patients, this necessitates routine device replacement and is associated with device malfunction and infection (Roston et al. 2015; Miyake et al. 2013). Left cardiac sympathetic denervation has been suggested as a therapeutic option before ICD implantation, as it has shown to be effective in cases of β-blocker contraindication and large multicentre studies have reported efficacy for this surgical procedure in decreasing cardiac events in CPVT (De Ferrari et al. 2015; Schwartz 2004; Schwartz et al. 1991; Moss et al. 2000). However, the technique is underutilized and there are also associated risks, including refractory transient arrhythmias and Horner syndrome, a disruption of the nerve pathway from the brain to the face (Cho 2015; Roston et al. 2015).

Verapamil is routinely used in the treatment of supraventricular tachycardia, hypertension and chest pain (Al-Zaiti and Magdic 2016; Muijsers et al. 2002). The drug has also been used to treat CPVT1, but with limited success. It is an LTCC agonist, reducing spontaneous Ca^{2+} release at high concentrations (injected intraperitoneally, at 8 μg/g of mouse body weight), although these exceeded toxicity levels (Alcalai et al. 2010). The drug has not been shown to affect disrupted RyR2 intra-domain interactions, nor prevent arrhythmia during

exercise-stress testing, but does reduce the threshold of arrhythmia occurrence in mice(Sumitomo et al. 2002; Alcalai et al. 2010; N. Liu et al. 2010).

Rycals are 1,4 benzothiazepine derivatives and include K201 (JTV-519) and S107, first reported by Kaneko et al. (1994). Many groups have reported that rycals display cardioprotective effects and anti-arrhythmic properties in mice (Loughrey et al. 2007; Wehrens, Lehnart, Reiken, Deng, et al. 2004; Lehnart et al. 2006; Yano et al. 2003; Kaneko 1994). K201 is suggested to prevent abnormal Ca^{2+} leak by stabilizing RyR2 channels and inhibiting SERCA, preventing SR Ca^{2+} overload under pathological conditions (Wehrens et al. 2005; Wehrens, Lehnart, Reiken and Marks 2004; Yano et al. 2003; Darcy et al. 2016). In three KI mouse models of CPVT1, S107 reduced diastolic SR Ca^{2+} leak in atrial myocytes and decreased burst-pacing induced AF *in vivo* (Shan et al. 2012). RyR2 from dmd mice hearts were S-nitrosylated and depleted of FKBP12.6, resulting in "leaky" RyR2 channels and a diastolic SR Ca^{2+} leak (Fauconnier et al. 2010). Marks et al. reported that in this instance, inhibiting depletion of FKBP12.6 with S107 treatment prevented arrhythmia, suggesting FKBP12.6 was necessary for the therapeutic action. However, FKBP12.6 involvement in CPVT1 remains contentious (Barg et al. 1997; J. Xiao et al. 2007; Hunt et al. 2007). K201 was not shown to alter FKBP12.6 interaction or occurrence of arrhythmic episodes in the R4496C mouse and it also abolished spontaneous Ca^{2+} release in heterologous cell lines that do not endogenously express RyR2, independent of FKBP12.6 association to the channel. SERCa2a has also been suggested as the main target of K201 rather than RyR2 (Loughrey et al. 2007). In the latest work of Copello, the group suggest that K201 is a Ca^{2+}-dependent inhibitor of SERCa2a and a partial agonist of RyR2, with the effects of K201 on RyR2 P_o in single channel experiments unaltered by adding FKBP12.6 (Darcy et al. 2016).

Dantrolene is a muscle relaxant used in patients that have malignant hyperthermia caused by mutations in RyR1. It has been shown to target a corresponding sequence of RyR1 in RyR2, improving intracellular Ca^{2+} handling in failing canine cardiomyocytes and in a mouse model of CPVT1 harbouring the R2474S mutation (S. Kobayashi et al. 2009; S. Kobayashi et al. 2010). In patient-derived induced pluripotent stem cell cardiomyocytes (iPSC-CMs) from a CPVT1 patient with RyR2 mutation S406L, dantrolene restored normal Ca^{2+} spark properties, rescuing the arrhythmogenic phenotype (C. B. Jung et al. 2012). The drug is proposed to stabilize defective intra-domain interactions in RyR2, dependent on the location of the mutation. This stabilizing effect was observed in cells expressing the central domain mutation R2474S, but had no effect on cells expressing C-terminal mutation N4104K with spontaneous Ca^{2+} release events still evident (N. Liu et al. 2010; D. Jiang et al. 2007;

Uchinoumi et al. 2010). It has recently been suggested that CaM is essential in the inhibition of RyR2 by dantrolene, whereby the drug caused inhibition of sheep RyR2 in single channel experiments (inhibition of P_o to 52 % of controls) only after the addition of 100 nM CaM (Nishimura et al. 2015; Oo et al. 2015). The mechanism by which CaM facilitates this inhibition remains unclear, although Oo et al. (2015) postulate the protein may put RyR2 into a conformation that allows dantrolene access to its RyR2 binding site {Seidel:2014kq}.

Flecainide is a Na^+ channel antagonist, approved for the suppression of VT since 1984. More recently, it was shown to be effective in preventing arrhythmia in CPVT1 patients who were not responsive to β-blockers and verapamil and is now considered an 'emerging recommendation' for patients with the condition (Priori et al. 2013; Watanabe et al. 2009). In a CPVT2 mouse model, flecainide decreased the frequency of spontaneous Ca^{2+} waves. The proposed mechanism of action was that apart from Na^{2+} channel block, flecainide also has a direct blocking effect on RyR2 (Hwang et al. 2011; Hilliard et al. 2009; Watanabe et al. 2009). This has been opposed by two independent groups including our own, who show that neither the drug nor its charged derivative is able to block physiologically relevant cation flux through RyR2 single channels (Bannister et al. 2016; N. Liu et al. 2011; Bannister et al. 2015; Sikkel et al. 2013).

It is evident that a clear understanding of the pathological mechanisms of RyR2 CPVT1 mutations is crucial to not only explain why some patients are responsive to certain therapeutic interventions while others are not, but in design of RyR2-targeting therapies in the future.

1.7.5 Evidence of functional heterogeneity

Current mechanisms and the conventional view of arrhythmogenesis in CPVT is that spontaneous Ca^{2+} release occurs via RyR2 and that hyperactive RyR2 channels are essential components of this gain-of-function scheme (Allen 2003; D. Jiang et al. 2002). Diastolic Ca^{2+} release activates an inward NCX depolarizing current and subsequently can result in arrhythmogenic activity. In other words, missense mutations in RyR2 lead to altered channel sensitivity to opening stimuli, mediating excessive Ca^{2+} release when the channel should be closed. This would be amplified during β-adrenergic stimulation, where catecholamine levels are increased to drive enhanced cardiac output.

Analysis of the R4497C mutation by heterologous expression in HEK293 cells supported this hypothesis, as [^{3}H] ryanodine binding studies revealed that the mutation showed an increased channel activity and sensitivity to pharmacological ligands, as well as more frequent spontaneous Ca^{2+} release events compared to WT-RyR2 transfected cells (D. Jiang et al. 2002). Single channel analysis showed that R4497C channels also exhibited channel openings at low cytosolic [Ca^{2+}] of less than 5 nmol/L, whereas WT single channel activity was almost completely inhibited under the same conditions. These properties were therefore expected to promote the SR Ca^{2+} leak during diastole and subsequent DADs observed in CPVT.

Findings by other groups also supported this conclusion; S2246L, R2474S, N4104K and R4497C were also identified as gain-of-function RyR2 channels, exhibiting aberrant Ca^{2+} release following channel activation compared to WT (Wehrens 2003; D. Jiang et al. 2004; George, Higgs, et al. 2003; D. Jiang et al. 2002; D. Jiang 2005). Three ARVC2 mutations linked to sudden cardiac death were characterized by Thomas et al. (2004) and also fitted the gain-of-function model of dysfunction, with an increased sensitivity to caffeine compared to WT channels. More recent studies of CPVT1 mutations in each peptide domain also identify gain-of-function as a unifying mechanism for RyR2 channel dysfunction in both HEK293 cell imaging systems and mutant mouse models (Paavola et al. 2007; Zhabyeyev et al. 2013; van Oort, McCauley, Dixit, Pereira, Yang, Respress, Wang, De Almeida, Skapura, Anderson, Bers and Wehrens 2010a).

Although numerous studies support the concept, the gain-of-function designation of CPVT1 mutations has been suggested inadequate the explain lethal arrhythmia in patients that harbour loss-of-function mutations (Zhao et al. 2015). There are over 170 CPVT1 mutations

in RyR2 currently identified, but this list is likely to grow, and therefore it may be an oversimplification to classify all these mutations based on the data of a small proportion.

The heterogeneous nature of RyR2 mutations was first proposed by Thomas et al. (2004), who investigated CPVT1 and ARVC-linked RyR2 mutations and their Ca^{2+} release properties in HEK293 cells. All mutations investigated appeared to result in an increased duration of elevated cytoplasmic Ca^{2+} levels following channel activation with caffeine, but one mutant (L433P) showed a significant decrease in sensitivity to channel activation compared to others. This challenged the notion that all RyR2 mutations linked to CPVT1, as well as sudden cardiac death in other conditions, resulted in altered RyR2 channel functionality (Gómez and Richard 2004).

Work by Chen and colleagues showed that recombinant mutant A4860G-RyR2 channels expressed in HEK293 cells displayed a dramatic depression of activity, manifesting as a loss of luminal Ca^{2+} sensitivity (D. Jiang et al. 2007). In work by Zhao et al, the same mutation was recombinantly expressed and shows drastic decreases in channel activity in both [^{3}H] ryanodine binding and single channel recordings (Zhao et al. 2015). Mice heterozygous for the mutation (RyR2-A4860G$^{+/-}$) exhibited no structural alterations in the heart with basal bradycardia, while no homozygotes were detected at birth. This is indicative of a lethal phenotype, with sympathetic stimulation of heterozygous mice also eliciting malignant arrhythmia. Interestingly, when ventricular myocytes were stimulated with Iso, the peak of Ca^{2+} release during systole was decreased, gradually filling the SR with Ca^{2+} leading to resultant ‘overload’. This scenario is thought to lead to EADs rather than DADs, whereby triggered impulses that result from sub-threshold membrane depolarizations occur during repolarization of the previous impulse, rather than when repolarization is complete (Scoote and Williams 2002). Therefore, unlike the characterization of gain-of-function mutants with spontaneous and diastolic Ca^{2+} release (D. Jiang et al. 2004), the defining feature of this loss-of-function mutation appears to be induced and systolic Ca^{2+} release.

Adding to the complexity of RyR2 mutant classification, the N terminal mutation R420Q has been identified as both loss- or gain-of-function, depending on cytosolic Ca^{2+} concentration within the cell (Domingo et al. 2015). Ventricular myocytes from mice heterozygous for the central domain mutation V2475F display not only altered sensitivity to luminal [Ca^{2+}] but also increased cytosolic Ca^{2+} activation (Loaiza et al. 2013). Spontaneous Ca^{2+} release events were also more frequent in Iso-stimulated cardiomyocytes from these mice but the SR Ca^{2+} release threshold remained unchanged in comparison to WT. Other channelopathies that

are associated with sudden cardiac death are also linked to both gain- and loss-of-function mutations in Na^+ and K^+ channels (Shirai et al. 2002; Baroudi et al. 2002).

Since most CPVT1 mutations investigated to date have been classified as gain-of-function, loss-of-function mutations are therefore not included as part of my project.

1.7.6 The broad classification of RyR2 mutations as 'gain-of-function'

Evidence has accumulated that while mutations may fall within the 'gain-of-function' classification i.e. causing enhanced Ca^{2+} release through RyR2, this may be via different mechanisms with mutations actually exhibiting functional heterogeneity.

Structural data suggest that a mutation may affect points of contact within the protein and disrupt intra-RyR interactions. Further peptide-based studies by the Ikemoto/Matsuzaki group have investigated the effects of mutations in the domains of RyR2 and add weight to the hypothesis that altered domain interactions are implicated in arrhythmogenesis (Suetomi et al. 2011; Tateishi et al. 2008). This suggests a one-fits-all mechanism of dysfunction cannot be applicable to all CPVT mutations of RyR2. Other data support functional heterogeneity; CPVT1-linked mutations N4104K and R4497C occurring within the I-domain cause RyR2 channel instability via defective intra-domain interactions, resulting in spontaneous Ca^{2+} release (George et al. 2006), however introduction of S2246L into a domain peptide representing the central domain increased the affinity of peptide binding, indicative of an abnormally tight domain-domain interaction (Suetomi et al. 2011). Both scenarios however resulted in RyR2-mediated Ca^{2+} release dysfunction, suggestive of diverse mechanisms of channel dysfunction that could be locus-dependent as opposed to a unifying mechanism.

Post-translational modifications of RyR2 may also be implicated in functional heterogeneity of CPVT1 mutant channels and Ca^{2+} release. Under conditions that stimulate stress, such as PKA phosphorylation, recombinant RyR2 mutant single channels have been shown to display a significant gain-of-function phenotype (Tester et al. 2007)**.** One mutation (R2267H, central domain) shows normal function under basal conditions but significantly increased activity after phosphorylation by PKA. A second mutation (S4565R – cytoplasmic portion of the I-domain) shows chronic 'leakiness' even under non-stressed conditions and only a slight increase in activity after phosphorylation (**Figure 1.18**).

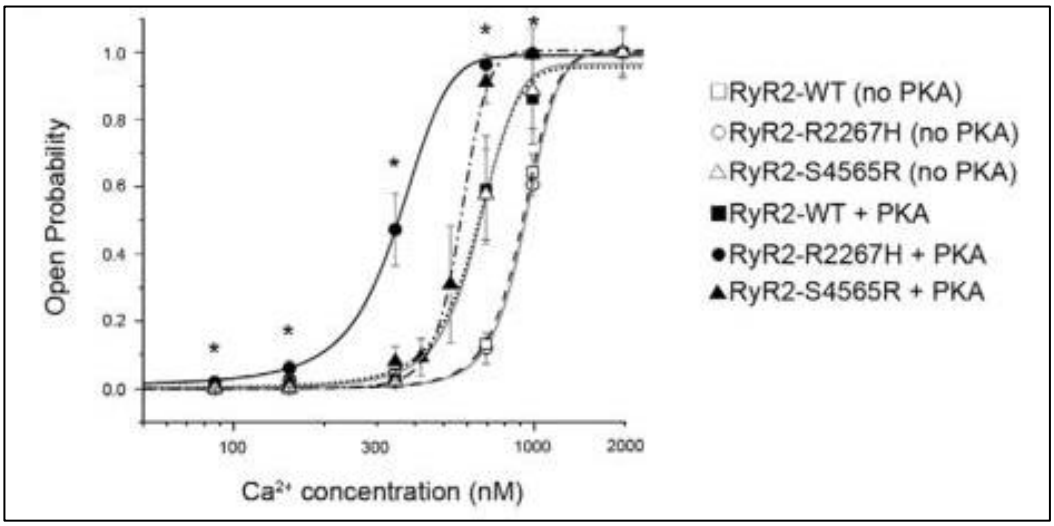

Figure 1.18 Open probability of mutant and WT RyR2 channels with and without PKA treatment reveals that phosphorylation significantly alters WT and R2267H RyR2 channel function but not S4564R. RyR2-R2267H P_o is already significantly left-shifted without PKA treatment in comparison to RyR2-WT. P_o was measured at Ca^{2+} concentrations from 90 nM to 2 μM. Each data point represents the open probability calculated as an average from several independent experiments shown as mean ±SE. Figure taken from Tester et al. (2007).

These data also support the notion that some CPVT1 mutations are dysfunctional at 'basal' conditions i.e. during rest, while others are not. CPVT1 mutations G230C, S2246L and P2328S have altered channel activity at low cytosolic levels of Ca^{2+}, but only after PKA phosphorylation (Wehrens et al. 2003; Meli et al. 2011). However, the data from Tester et al. (2007) indicate that S4565R RyR2 channels show increased sensitivity to cytosolic Ca^{2+} compared to WT without such modification (**Figure 1.18**). Interestingly, the mutation was first identified in an infant who was not under any exertion and died during sleep. Marks and colleagues also found that H29D RyR2 mutant channels also display significantly higher P_o and opening frequency compared to WT under non-stress conditions (Cheung et al. 2015). Although the mechanism for dysfunction of these channels appears at odds with the clinical phenotype of CPVT1 (arrhythmia after physical or emotional stress), authors speculated that the H29D mutation destabilized domain or protein-protein interactions, which may confer the 'leakiness' of CPVT1 channels sometimes observed in a non-PKA phosphorylated state.

Diverse mechanisms of mutant RyR2 channel dysfunction are also evident in the response of patients to pharmacological therapies. It has long been reported that there is a high rate of symptom recurrence and sudden cardiac death in CPVT1 patients and the phenotypic manifestation appears to be very heterogeneous (Priori 2002; George 2007a; Medeiros-Domingo et al. 2009). Even in patients adequately medicated with β-blockade, many require

ICDs after experiencing syncope or cardiac arrest despite receiving these treatments (Ylänen et al. 2010). For example, K201 has been shown effective in treating arrhythmogenesis observed in mice and dogs with N-terminal and central domain RyR2 mutations (Lehnart et al. 2008; Suetomi et al. 2011; Tateishi et al. 2008). However, it was not effective in treating RyR2-R4496C+/- mice with VT (N. Liu et al. 2006) and Ca^{2+} leak induced by the I-domain peptide DP4090-4123 was not inhibited by the drug in peptide-based studies (Tateishi et al. 2008). This is suggestive that K201 is less effective in correcting arrhythmogenesis caused by mutations in the I-domain, with point mutations such as N4104K seen in CPVT1 possibly inducing weakened domain interactions between the I-domain and the unidentified IP-domain, independent of interactions between N-terminal and central domains.

The varied response to frontline CPVT1 therapies could therefore suggest that RyR2 channel dysfunction may be different depending on which mutation a patient presents with. It follows that if an RyR2 mutant channel is leaky under non-stress conditions, such as H29D or S4565R, prevention of phosphorylation via β-blockade may not be sufficient to prevent arrhythmogenic activity in such patients. Investigating the mechanism of mutant RyR2 channel dysfunction could therefore enable risk stratification or personalized therapies for CPVT1 patients. Drug-binding to RyR2 channels is thought to be state-dependent, with some suggested to block the open channel such as class I antiarrhythmic propafenone (Hwang et al. 2011) and others suggested to favour binding to the closed state such as dantrolene (Paul-Pletzer et al. 2005). The open and dwell closed times of mutant channels therefore should also be considered – if a mutation exhibits longer periods of channel opening, a closed channel blocker may not be an appropriate treatment, and this may aid in explaining the discrepancies of drug efficacy reported in the literature.

1.8 Research project aims

As discussed, the broad classification of CPVT1-linked RyR2 mutations as exhibiting a 'gain-of-function' may be too simplistic, with subtleties of dysfunction being masked in previous studies, eager to establish a universal mechanism for SR Ca^{2+} leak. The mere size and complexity of RyR2, the varied response to pharmacological agents as well as the fact that domains have been assigned discrete functionality is not fully considered. The role of phosphorylation during β-adrenergic stimulation may also be implicated in mutant RyR2 channel dysfunction, when functional heterogeneity of CPVT1 mutants is observed under basal conditions. To investigate this hypothesis, the aims of this thesis therefore fall in two parts:

- Investigating in detail Ca^{2+} release kinetics and expression of two CPVT1-linked RyR2 mutants, S2246L and N4104K, within HEK293 cells. These mutations are commonly classified as 'gain-of-function'. Investigation may reveal any common perturbations of CPVT1-linked mutations or differences in Ca^{2+} handling and expression between mutant RyR channels (where the mutations in question reside in different channel domains). This investigation will validate detailed interrogation of spontaneous Ca^{2+} release events in hRyR2-transfected HEK293 cells as a method of identifying functional heterogeneous mutations.
- Assessing the functional consequences of PKA phosphorylation at the S2808 and S2031 sites on WT and mutant RyR2 channels, via a two-fold approach:
    - Basal phosphorylation levels of WT and mutant hRyR2s will be determined, as well as the response to PKA phosphorylation initiated using an analogue of cAMP.
    - The effects 'mimicked' phosphorylation at each site will be investigated by the generation of phosphomimetic RyR2 constructs and the subsequent investigation of Ca^{2+} handling and expression in HEK293 cells. This will be the first study of its kind to apply this molecular technique in the study of CPVT1-mutant RyR2 phosphorylation. In this way the effects of genetic and PKA-mediated phosphorylation can be compared in the hope of identifying the functional importance of each phosphorylation site.

Chapter 2

Materials and Methods

2.1 Working in the laboratory

2.1.1 General laboratory equipment and reagents

- *Analytical grade chemicals:* All chemicals were obtained from Fisher Scientific or Sigma-Aldrich. All reagents were dissolved in autoclaved dH_2O, stored at room temperature (unless otherwise stated).
- *pH meter:* Solution pH was measured using a Mettler Toledo FE20 pH meter (Camlab) and altered using either 100 mM HCl or 100 mM NaOH.
- *Plastics and glassware:* purchased from Greiner or Fisher Scientific. Glassware was soaked in detergent and washed before use.
- *Filter sterilisation:* solutions were filtered when necessary using a 0.22 µm Millex ® syringe filter (Millipore).

2.1.2 Health and safety

Full general health and safety training was received from the WHRI safety officers including microbiology, cell culture and centrifuge safety training prior to beginning any laboratory work. Experiments were carried out in accordance with COSSH regulations and after completion of appropriate risk assessments.

2.1.3 Computer software and data analysis

Microsoft Excel was used to plot generated numerical data. Statistical analyses were carried out using GraphPad Prism® (GraphPad Software, Inc.), with graph data expressed as mean ± standard error. Statistical analyses depended on normality of the data in question, as assessed by D'Agostino-Pearson omnibus normality test. If data distribution was normal, t tests and one way ANOVA with Bonferroni posthoc tests were applied as appropriate. If data distribution was not normal, Mann Whitney tests and Kruskal-Wallis with Dunn's posthoc tests were applied as appropriate.

2.2 Materials

Materials and methods described within this section are common to every following results chapter, as the propagation of plasmid DNA was essential for any experiments with the eGFP-hRyR2 construct. Methods pertaining to each chapter are described in detail therein.

2.2.1 The hRyR2 expression vector

The mammalian expression vector pcDNA™3 (Invitrogen) containing human RyR2 with an eGFP tag (pcDNA3-eGFP-hRyR2) was obtained from Dr Christopher George (Thomas et al. 2004; George et al. 2003). The eGFP tag is placed at the N-terminus of hRyR2, separated by a four amino acid spacer (Thr-Ser-Gly-Ser).
Vectors containing the CPVT-linked RyR2 mutations S2246L, N4104K and R4496C were also obtained from Dr Christopher George and Dr N. Lowri Thomas.

2.2.2 Transformation of bacterial cell lines

- *MAX Efficiency Stbl2 Competent Cells:* provided with SOC medium (ThermoFisher Scientific).
- *SOC medium:* 20 g/L tryptone, 5 g/L yeast extract, 0.5 g/L NaCl, 0.18 g/L KCl, 0.95 g/L $MgCl_2$, made up to 1 L with dH_2O and autoclaved. Medium was cooled to below 50 ˚C before the addition of glucose at 2 % (w/v) of total stock solution concentration.
- *Luria Bertani (LB_{AMP}) broth:* 10 g/L tryptone, 5 g/L yeast extract, 5 g/L NaCl, autoclaved. Ampicillin was added before use.
- *LB_{AMP} agar plates:* made with LB broth constituents with the addition of 15 g/L, autoclaved. Ampicillin was added before setting into 10 cm^2 sterile petri dishes.
- *Ampicillin 100 mg/ml stock:* filter sterilized, stored at -20 °C and used at a working concentration of 100 µg/mL.

2.2.3 Small-scale plasmid isolation - 'Miniprep'

- *Zyppy™ Plasmid Miniprep Kit (Zymo Research):*
    i. *7X Lysis Buffer (Blue):* containing SDS and sodium hydroxide.
    ii. *Neutralization Buffer (Yellow):* containing guanidium chloride.
    iii. *Endo-Wash Buffer:* containing guanidium chloride and propan-2-ol.
    iv. *Zyppy™ Wash Buffer (concentrate):* containing Tris(hydroxymethyl)aminomethane hydrochloride (proprietary), 192 mL of 100 % ethanol added to 48 mL buffer before use.
    v. *Zyppy™ Elution Buffer:* containing 10 mM Tris-HCl, pH 8.5 and 0.1 mM EDTA.

2.2.4 Restriction digest for verification

- *Restriction digest enzymes:* All High Fidelity (HF) restriction digest enzymes were purchased from either ThermoFisher Scientific or New England Biolabs, and used with the optimized 10x buffers provided. Enzymes were kept at -20 °C or -80 °C according to manufacturer instructions.
- *TAE, 50x stock:* 2 M Tris, 2 M glacial acetic acid, 50 mM EDTA.
- *Agarose:* high purity, added to 1x TAE at 1 % (w/v) for gels.
- *DNA loading buffer:* 50 % 1x TAE buffer, 50 % (v/v) glycerol with the addition of Orange G to achieve the appropriate detection colour.
- *UltraPure™ Ethidium bromide (Invitrogen):* 10 mg/mL stock, used at a working concentration of 0.1 µg/mL.
- *1 Kb Plus DNA Ladder (Invitrogen):* molecular weight DNA marker, spanning 100-12,000 bp.

2.2.5 Large-scale plasmid isolation - 'Maxiprep'

- *HiSpeed Plasmid Maxi Kit (Qiagen):*
    i. *Buffer P1 (resuspension buffer):* 50 mM Tris/HCl pH 8, 10 mM EDTA, 100 µg/ml RNase A.
    ii. *Buffer P2 (lysis buffer):* 200 mM NaOH, 1 % SDS (w/v).
    iii. *Buffer P3 (neutralization buffer):* 3 M potassium acetate pH 5.5.
    iv. *Buffer QBT (equilibration buffer):* 750 mM NaCl, 50 mM MOPS pH 7, 15% isopropanol (v/v), 0.15 % Triton® X-100 (v/v).
    v. *Buffer QC (wash buffer):* 1 M NaCl, 50 mM MOPS pH 7, 15 % isopropanol (v/v).
    vi. *Buffer QF (elution buffer):* 1.25 M NaCl, 50 mM Tris/HCl pH 8.5, 15% isopropanol (v/v).
    vii. *TE:* 10 mM Tris/HCl pH 8, 1 mM EDTA.

2.2.6 HEK293 cell maintenance and subculture

- *Dulbecco's Modified Eagle Medium (Life Technologies):* containing 25 mM D-glucose, 4 mM L-glutamine and 1 mM sodium pyruvate (referred to as minimal DMEM or mDMEM). This was supplemented with 10 % (v/v) heat-inactivated fetal calf serum (FCS) and 2 % (v/v) 100 µg/mL penicillin-streptomycin-glutamine (PSG) to make complete DMEM (referred to as cDMEM).
- *Sodium chloride solution (Fresenius Kabi):* supplied as a 0.9 % (w/v) solution
- *Trypsin EDTA 0.05 % (Life Technologies)*: 1x solution, with phenol red dye.
- *Freezing medium:* FCS supplemented with 10 % (v/v) dimethyl sulphoxide (DMSO).

2.2.7 Calcium phosphate transfection of HEK293 cells

- *Calcium chloride ($CaCl_2$):* purchased from Sigma-Aldrich, supplied as a 1M stock and stored at -20 °C.
- *2x Hepes Buffered Saline (HBS):* 280 mM NaCl, 10 mM NaCl, 10 mM KCl, 1.5 mM Na_2HPO_4, 10 mM glucose, 50 mM Hepes. pH was adjusted to 7.05, solution was filter sterilised and stored in aliquots at -20 °C.
- *Sodium butyrate (NaB):* 1 M stock prepared with autoclaved dH_2O. Used as a concentration of 2 mM.
- *Zeiss Fluorescence Microscope (Zeiss):* uses a Xenon light lamp source with a peak excitation of ~488 nm, and a 515 ± 30 nm band-pass filter.

2.2.8 Cell homogenate preparation

- *Hypo-osmotic lysis buffer:* 20 mM Tris, 1 mM EDTA, 1 mM NaF, 1 mM Na_3VO_4, 1 % (v/v) Triton™ X-100, adjusted to pH 7.4. 1 protease inhibitor cocktail tablet (Roche) dissolved per 25ml solution.

2.2.9 Protein assay for quantification

- *BCA™ Protein Assay Kit (ThermoFisher Scientific):*
    i. *Micro BCA Reagent A:* proprietary alkaline tartrate-carbonate buffer.
    ii. *Micro BCA Reagent B:* proprietary bicinchonic acid solution.
    iii. *Micro BCA Reagent C:* proprietary copper sulphate solution. Reagents were used in a ratio of 50 Reagent A: 48 Reagent B: 2 Reagent C.
    iv. *Albumin Standard Ampules:* 10 x 1 mL ampules containing bovine serum albumin at 2 mg/mL, in solution of 0.9 % saline and 0.05 % sodium azide. Samples were serial diluted with dH_2O.

2.2.10 SDS Polyacrylamide Gel Electrophoresis (SDS/PAGE)

- *SDS-PAGE Separating buffer:* 1.5 M Tris/HCl pH 8.8.
- *SDS-PAGE Running buffer:* 25 mM Tris, 250 mM glycine, 0.1 % (w/v) SDS.
- *Acrylamide (Biorad):* 40 % (w/v) mix solution of acrylamide/bisacrylamide, in a 37.5:1 ratio.
- *Ammonium persulphate:* a 10 % (w/v) solution, prepared fresh per use.
- *SDS-PAGE loading buffer x5:* 0.5M Tris (pH 6.8), 10 % (w/v) SDS, 25 % (v/v) β-mercaptoethanol, 10 % (v/v) glycerol, 0.5 % (w/v) bromophenol blue. Prepared and filter sterilized immediately before use.
- *Kaleidoscope Precision Plus™ Protein Prestained Standards (Biorad):* molecular weight protein ladder, with markers from 10 to 250 kD.
- *Mini-gel tank and apparatus (Biorad):* all SDS-PAGE gels were poured, and electrophoresis performed using Biorad glass plates, well combs, and tanks.

2.2.11 Transfer of protein onto PVDF membrane

- *iBLOT® Gel Transfer Device (Invitrogen):* a self-contained blotting unit for fast dry blotting of proteins.
- *iBLOT® Transfer Stack, PVDF, mini (Invitrogen):*
    i. iBLOT® Cathode Stack, Top mini: a copper electrode with cathode buffers in a gel matrix to act as an ion reservoir.
    ii. iBLOT® Anode Stack, Bottom mini: a copper electrode with anode buffers in a gel matrix, as well as an integrated preactivated PVDF membrane.
    iii. iBLOT® Disposable Sponge: a sponge placed on top of the transfer stack to absorb excess liquid and to generate even pressure across the assembly.
    iv. iBLOT® Filter paper mini: filter paper is soaked in dH_2O before placed on top of SDS-PAGE gels to protect gel integrity during blotting.

2.2.12 Western blot analysis by chemiluminescence

- *Tris-buffered saline (TBS):* 20 mM Tris, NaCl, pH corrected to 7.6 before the addition of 1 ml/L Tween 20 to make TBS-T.
- *Blocking solution:* 5 % (w/v) low-fat dried milk powder in TBS-T.
- *ab-GFP (B-2) antibody (Santa Cruz Biotechnology):* mouse monoclonal primary antibody raised against the full length green fluorescent protein of *Aequorea victoria* origin, provided at 200 µg/mL. Used at 1:1,000 dilution for Western blot analysis.
- *Wash buffer/blocking solution:* 1 % (w/v) low-fat dried milk powder in TBS-T.
- *(HRP)-conjugated anti-mouse antibody:* Used at 1:10,000 dilution for Western blot analysis.
- *Amersham ECL Prime Western Blotting Detection Reagent (GE Healthcare):*
    i. Solution A: luminol solution.
    ii. Solution B: peroxide solution.
- *G:BOX Chemi XX6 (Syngene):* a chemiluminescence imaging system.
- *GeneSys software (Syngene):* automatic control software for the G:BOX imaging system.
- *GeneTools software (Syngene):* program used for densitometric analysis of Western Blots.

2.3 Methods

2.3.1 Transformation of bacterial cell lines

hRyR2 is a large, fragile plasmid (~21kb) prone to spontaneous recombination (George et al. 2005) . As such hRyR2 transformation requires super-competent bacterial cells to propagate the plasmid. MAX Efficiency Stbl2 Competent Cells were used to propagate WT and mutant eGFP-hRyR2 plasmid DNA at a high yield. This strain of Escherichia coli (*E. coli*) is deficient of all known restriction systems, as well as recombination (*recA*-) and endonuclease (*endA*-) genes, increasing plasmid stability and quality.

For the transformation of full-length eGFP-hRyR2 plasmids, 50 µL MAX Efficiency Stbl2 cells were thawed on ice. Plasmid DNA (1 ng) was added and mixed gently. Cells were incubated on ice for 30 min before heat-shock treatment in a 42 °C water bath for 30 sec. Cells were immediately transferred to ice for 2 mins, prior to the addition of 500 µL SOC medium and incubation at 37 °C with shaking at 225 rpm for 1 hr. Cells were then plated onto LB_{AMP} agar plates at two unequal concentrations (to allow for single colony isolation) and incubated at 30 °C for ~24-28 hrs before examination for colony growth. Single colonies were picked using sterile plastic pipette tips and used to inoculate approximately 6 mL of LB_{AMP} broth. Cultures were incubated at 30 °C with shaking at 225 rpm for ~15-18 hrs.

Approximately half (3 mL) of the bacterial culture was centrifuged at 13,000 rpm for 1 min to pellet bacteria (Microfuge R, Beckman). Bacterial pellets were prepared for plasmid isolation by resuspension in 600 µL dH_2O.

LB_{AMP} broth (3 mL) was added to the remaining bacterial cultures and they were incubated at 30 °C with shaking at 225 rpm for an additional 8 hrs to allow for growth prior to large-scale culture inoculation (See **Section 2.2.5**).

2.3.2 Small-scale plasmid isolation - 'Miniprep'

Plasmid DNA was purified from bacterial cell culture using an alkaline lysis method employed by the Zyppy™ Plasmid Miniprep Kit, following manufacturer instructions. A blue coloured Lysis Buffer (100 µL) was added and the sample mixed by inverting the tube 4-6 times, with a colour change from opaque to clear blue indicating complete lysis of cell membranes and the release of cell contents. To avoid further lysis which could shear the plasmid, 350 µL cold Neutralization Buffer (yellow) was added within 2 minutes and the sample mixed thoroughly. A colour change from blue to yellow indicated complete neutralization and that a precipitate would form. Samples were centrifuged at 13,000 rpm (5417R refrigerated centrifuge, Eppendorf) for 3 min to pellet cell debris. Avoiding disturbance of the pellet, the supernatant (~900 µL) was transferred to the provided Zymo-Spin™ IIN column. The column was placed in a collection tube and centrifuged for 15 secs to allow DNA binding to the resin. Flow-through was discarded, and 200 µL of Endo-Wash Buffer was added to the column, followed by centrifugation for 30 secs to wash the plasmid DNA. Zyppy™ Wash Buffer (400 µL) was added to the column for a second wash step, and centrifuged for 1 minute. The column was then transferred to a clean 1.5 mL centrifuge tube and 30 µL of Zyppy™ Elution Buffer was applied directly to the column matrix and allowed to stand for 1 min at room temperature, before final centrifugation for 30 secs to elute the plasmid DNA. Plasmids were immediately verified by restriction digest with appropriate endonucleases with resulting fragments visualized by agarose gel electrophoresis. Verified plasmids were stored at -20 °C or -80 °C.

2.3.3 Restriction digest for verification

Restriction endonucleases were used as a diagnostic tool, producing patterns of restriction fragments from digested eGFP-hRyR2 plasmids. These could be verified by comparison to a visual digest of the full-length hRyR2 sequence, using http://tools.neb.com/NEBcutter2/. Restriction digests were performed at two 'check points' during propagation of WT and mutant eGFP-hRyR2 plasmid DNA (See **Figure 2.2**). A combination of single digests (*EcoRI*, *HindII*, *BamHI* and *BgIII* high fidelity restriction endonucleases) was used to verify full-length eGFP-hRyR2 plasmids before and after large-scale amplification. Only plasmids that yielded fragments of the correct MW were selected for propagation (See **Figure 2.1** below). Restriction digests were typically carried out with 1 µg DNA and 1-10 U of High Fidelity endonuclease (following manufacturer instructions). Reaction mixtures were prepared with 1x endonuclease buffer and made up to a total volume of 20 µL with dH_2O. Reaction mixtures were incubated at 37 °C in a waterbath for 30 minutes, before products were loaded onto an agarose gel and separated by electrophoresis. Agarose gel electrophoresis was used to separate DNA fragments according to their MW and compared against a 1 kb DNA marker to verify size. A 1 % (w/v) agarose gel was formed by the addition of agarose to 1x TAE buffer and warming in a microwave oven to dissolve. The agarose mixture was cooled to ~50 °C before the addition of ethidium bromide (EtBr) to a working concentration of 0.1 µg/mL. The mixture was then set in a Biorad Mini-Sub® cast and assembled with a well comb, according to manufacturer instructions. Each gel was placed in a Biorad tank and covered with 1x TAE buffer. Samples were prepared with 1x loading buffer (from a 2x stock) before gel loading. Electrophoresis was performed under constant voltage of 80V until the dye front had migrated approximately two thirds down the gel. This allowed for sufficient DNA fragment separation. UV transillumination was used to view resolved EtBr stained DNA fragments, via the Biorad XRS Chemidoc Imaging System®.

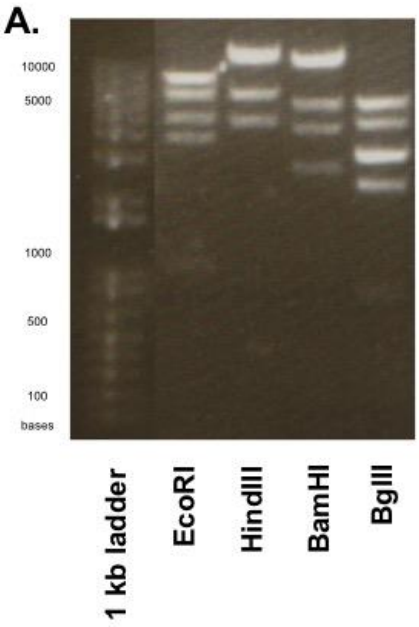

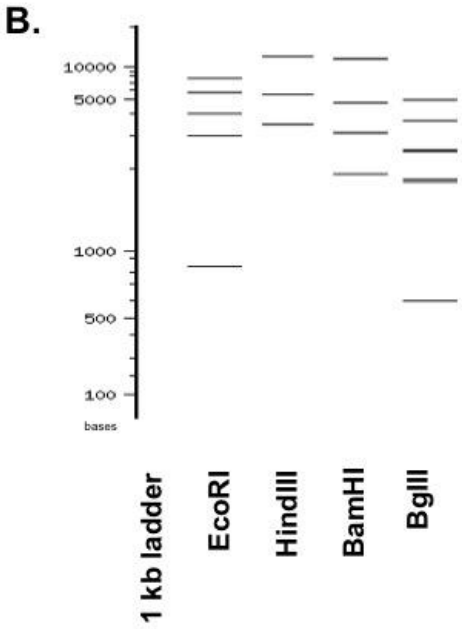

C.

Restriction Enzyme	Specificity	Length of fragment (bp)
EcoRI	GAATTC	7683 5741 3952 3015 838
HindIII	AAGCTT	11759 5700 3700
BamHI	GGATCC	10664 4971 3461 2199 34
BglII	AGATCT	5182 3805 2632, 2610, 2573 1905, 1873 649

Figure 2.1 Restriction digest for the verification of full-length eGFP-hRyR2 cDNA. *A.* WT and mutant eGFP-hRyR2 cDNA (1 µg) were digested with restriction enzymes (*EcoRI*, *HindIII*, *BamHI* and *BglII*). Products were run on a 1 % agarose gel against a 1 kb DNA ladder. The ladder lane from the same gel has been spliced across in the figure for presentation purposes. *B.* Anticipated digest pattern determined via NEBcutter, using the full-length eGFP-hRyR2 DNA sequence. *C.* Table of restriction enzyme specificity and expected fragment size.

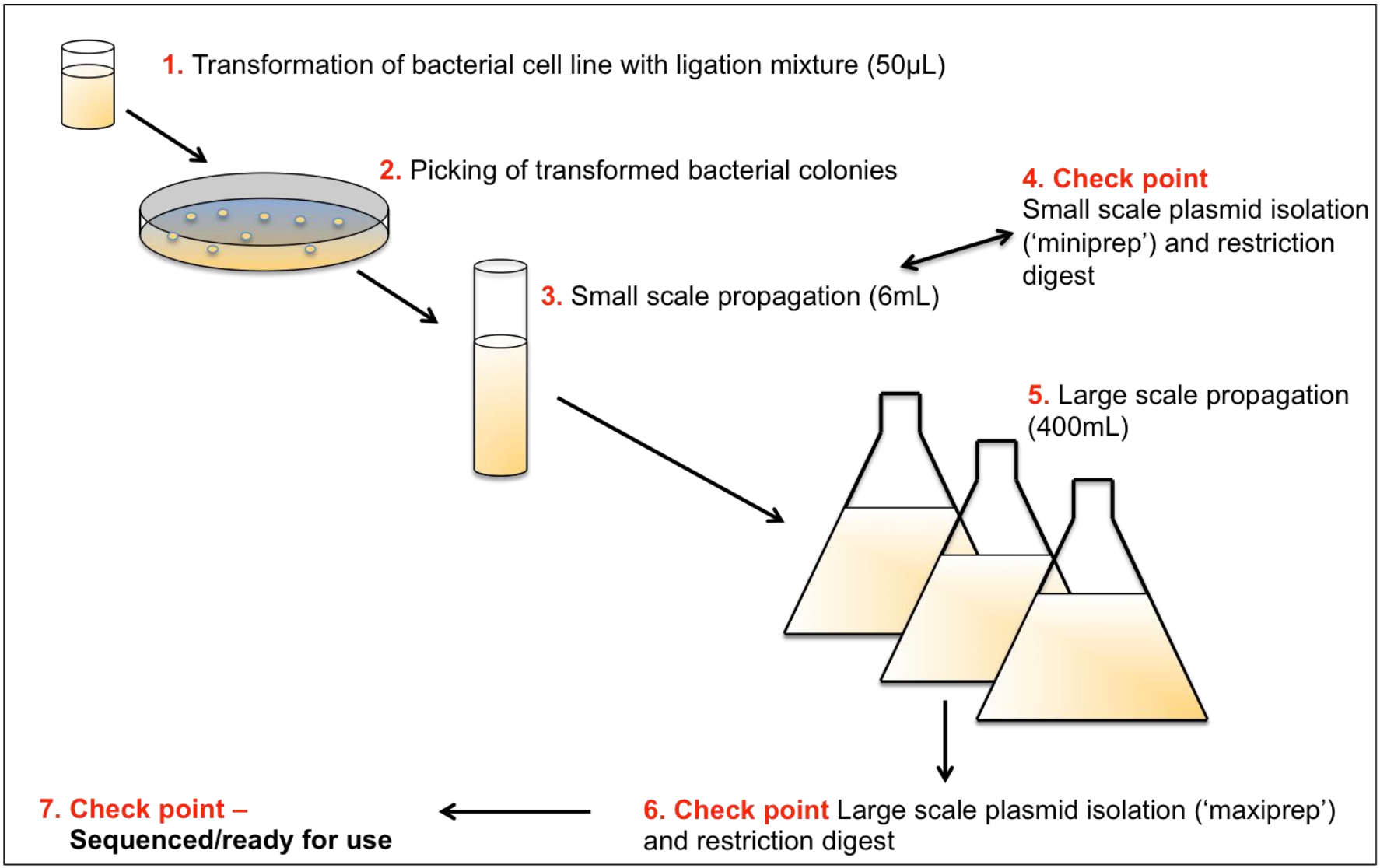

Figure 2.2 Schematic for the propagation of WT and mutant eGFP-hRyR2 plasmid DNA.

2.3.4 Large-scale plasmid isolation - 'Maxiprep'

Plasmids verified by restriction digest or sequencing (site-directed mutagenesis products) at the 'miniprep' stage were prepared for large-scale isolation. Small-scale bacterial cultures (See **Section 2.2.1 ii**) were used to inoculate 400 mL LB_{AMP} cultures at a dilution of 1:100 and grown overnight at 30˚C with shaking at 225 rpm. Bacterial suspension was then centrifuged at 6500 xg for 15 min using a JLA16.250 fixed-angle rotor (Avanti J-25, Beckman) to obtain a cell pellet.

Plasmid DNA was purified from cell pellets of bacterial culture by a modified alkaline lysis method using the HiSpeed Plasmid Maxi Kit, which is a gentle method of isolating DNA by ion-exchange and prevents shearing of such a large plasmid. Bacterial pellets were resuspended in 10 mL Buffer P1 with added RNase A and LyseBlue particles, ensuring no clumps remained. Buffer P2 (10 mL) was added, mixed thoroughly by inversion and incubated for no longer than 5 minutes at room temperature to allow for complete lysis without damaging the plasmid DNA. The mixing results in a homogenously blue coloured suspension, which should not have cell clumps or colourless regions – this would indicate incomplete lysis. Chilled Buffer P3 (10 mL) was added to the lysate, mixed immediately and thoroughly by gentle inversion. After the addition of this buffer, a white precipitate formed which contained genomic DNA, proteins and cell debris. The lysate was then transferred to a QIAfilter Cartridge and allowed to incubate at room temperature for 10 min. This stage was essential to allow precipitate to float and form a layer above the solution, preventing clogging during filtration. During this incubation, a HiSpeed Maxi Tip was equilibrated by 10 mL Buffer QBT. The cap of the QIAfilter cartridge was then removed, and a plunger inserted into the cartridge to filter the cell lysate through the equilibrated HiSpeed Tip. Cleared lysate entered the resin of the HiSpeed Tip by gravity flow. It was then washed with 60 mL Buffer QC. This medium-salt wash removed RNA, proteins, dyes and low MW impurities. DNA was then eluted with 15 mL high-salt Buffer QF, followed by the precipitation and concentration of DNA with the addition of 10 mL (0.7 volumes) isopropanol, which was mixed and incubated at room temperature for 5 min. A QIAprecipitator Maxi Module (filter) was attached to a 30 mL syringe, and eluate/isopropanol mixture plunged through into a waste bottle. Precipitated DNA was trapped in the filter as a thin layer. The DNA in the filter was then washed with 2 mL 70 % (v/v) ethanol and dried by plunging air through the syringe several times. Using a fresh 5 mL syringe, 1 mL of dH_2O was plunged through the filter using constant pressure to elute the DNA.

Plasmids were quantified using the NanoVue™ Plus (See **Section 2.2.1 v**) and verified by restriction digest with appropriate endonucleases and fragments visualized by agarose gel electrophoresis, before storage at -20 °C. Site-directed mutagenesis products were stored at -80 °C due to fragility.

2.3.5 DNA quantification

DNA concentration was determined by spectrophotometric quantification, using the NanoVue™ Plus Spectrophotometer (GE Healthcare). This equipment measures the DNA absorbance of light at a wavelength of 260 nm (A_{260}) in µg/mL, and can be programmed to account for dilution factor. Only 2 µL of DNA sample was required to obtain an accurate measurement. The ratio of A_{260}/A_{280} was also measured; giving a value that corresponds to plasmid purity. Contamination of the plasmid DNA with protein has peak absorption at A_{280}, so an increased value would lower the ratio. Values of ≥1.8 therefore indicated high purity DNA samples. DNA preparations with values below this were discarded.

2.3.6 HEK293 cell maintenance and subculture

All mammalian cell culture work took place in HEPA filtered Class II laminar flow containment hoods, in a designated laboratory. HEK293 cells were purchased from the European Collection of Authenticated Cell Cultures (ECACC). Cells were grown in T75 cm^2 culture flasks with filter caps in cDMEM. They were incubated at 37 °C, gassed with 5 % CO_2 and kept at a humidity of 98 % in a ThermoScientific HeraCELL 240i CO_2 incubator.

Routine sub-culture (passaging) was essential to maintain a healthy population of cells in a monolayer, preventing over-confluency and cell death. On reaching 80 % confluency, cells were washed with 10 mL 0.9 % (w/v) saline solution and detached from culture flasks by trypsinisation for 1 min. The action of the enzyme was inhibited by the addition of 10 mL cDMEM and dissociated cells were collected as a cell suspension.

Cell number was calculated using a Luna™ Dual Fluorescence Cell Counter (Labtech) following manufacturer instructions. After pelleting of the cells by low-speed centrifugation (1,000 xg for 3 min in an Allegra 6R centrifuge, Beckman), the cell density was adjusted by gentle resuspension in the appropriate volume of cDMEM. Typically, cells were passaged biweekly for cell maintenance.

2.3.7 Ca^{2+} imaging in HEK293 cells

While many fluorescent dyes are available with unique profiles, Fluo-3 (see **Table 2.1**) was chosen for these experiments, offering a suitable dynamic range with minimal damage to the cells, a low compartmentalization tendency and appropriate Ca^{2+} binding affinity (D. Thomas et al. 2000).

Loading is achieved with the acetoxymethyl (AM) conjugated form of the dye, which can cross the cell membrane before hydrolysis by esterases, leaving the fluorescent indicator trapped within the cell. Although Fluo-3 has a near identical excitation/emission profile to eGFP, relative changes in fluorescence in this system are entirely Ca^{2+}-dependent (N. L. Thomas et al. 2004).

Calcium Indicator	Excitation Peak	Emission Peak	Ratiometric?	Advantages	Disadvantages
Indo-1	338 nm	475 nm + 400 nm	*Yes* Free Ca^{2+} and bound Ca^{2+} emit different wavelengths	Accurate measurement of free Ca^{2+} Corrects for variable loading and dye leak	UV wavelengths can damage live cells Expensive equipment required
Fura-2	340 nm + 380 nm	510 nm			
Fluo-2	488 nm	515 nm	*No* Dependent on free Ca^{2+} and only emits one wavelength	Wavelengths are less damaging to live cells Can use multiple dyes at once	Can be dependent on other factors i.e. differential loading
Fluo-3	488 nm	525 nm			
Fluo-4	506 nm	520 nm			
Calcium Green-1	488 nm	530 nm			
Rhod-2	556 nm	576 nm			

Table 2.1 Comparison of Ca^{2+} indicator dyes used in confocal microscopy. Fluo-3 is highlighted, as this was the chosen dye for imaging experiments in this project.

2.3.7.1 Effectene transfection of HEK293 cells

HEK293 cell maintenance is described in **Section 2.3.6**. The Effectene Transfection Reagent (Qiagen, with kit containing reagent, Buffer EC and enhancer) was used to introduce eGFP-hRyR2 into HEK293 cells for calcium imaging experiments. This gentle method uses a non-liposomal lipid formation in order to achieve highly reproducible transfection efficiencies compared to the calcium phosphate method, so was deemed optimal for these experiments. Calcium phosphate transfection also leads to a higher rate of cell death, unsuitable for live cell imaging experiments.

HEK293 cells were plated onto 10 mm poly-D-lysine coated glass coverslips (Mattek Corporation) at a density of 1-2 $x10^5$ cells/plate, within 200 µL cDMEM. Cells were incubated at 37˚C at 5 % CO_2 for 24 hours before transfection.

To transfect 7 coverslips, 0.8 µg of eGFP-hRyR2 DNA was made up to a total volume of 100 µL with Buffer EC (a DNA condensation buffer), followed by the addition of 6.4 µL of enhancer. The solution was mixed by vortexing, and incubated at room temperature for 5 minutes. Effectene (20 µl) was then added to the solution and mixed thoroughly by vortexing. The solution was incubated at room temperature for 10 minutes, which allowed condensed Effectene-DNA complexes to spontaneously form. The solution was then mixed with 600 µL cDMEM and 100 µL

was added drop wise to each coverslip. Coverslips were returned to the incubator for 8 hours, before they were removed from the incubator and flooded with cDMEM to prevent cell death. Coverslips were placed back into the incubator for at least 24 hours post-transfection before any loading for calcium imaging.

2.3.7.2 Loading cells for Ca^{2+} imaging

Fluo-3 AM (50µg, AAT Bioquest) was dissolved in 15 µL DMSO containing 20 % (w/v) Pluronic® F-127 acid, resulting in a 3 mM stock of Fluo-3 AM. This was then added to mDMEM at a concentration of 10 µM. cDMEM was removed from the coverslips before the addition of a 200 µL meniscus of dye-containing mDMEM. Coverslips were incubated at 30 ˚C and 5 % CO_2 for 30 min and then flooded with mDMEM for 10 min to allow de-esterification before calcium imaging experiments took place.

2.2.7.3 Confocal microscopy for Ca^{2+} imaging

To visualize calcium-dependent fluorescence, cells loaded with Fluo-3 AM were imaged using a laser scanning confocal microscope (Leica SP5) with an x63 objective oil immersion lens and an Argon laser (See **Figure 3.3**). Excitation was initiated at 488 nm and emission detected at 525 ±25 nm by a photomultiplier tube (PMT). mDMEM was removed from a coverslip before the addition of a 200 µL Krebs-Ringer-Hepes (KRH: 9 g/L glucose, 7 g/L NaCl, 6 g/L HEPES, 0.35 g/L KCl, 0.16 g/L KH_2PO_4, 0.29 g/L $MgSO_4$, 1.3 mM $CaCl_2$, filter sterilized and pH adjusted to 7.4) meniscus for the experiment. Data were acquired at a rate of 5 frames per second, using Leica LAS AF software at 512 x 512 pixel resolution. After a field of view was identified to have oscillating cells, data were recorded for a total of 180 sec, with the addition of 10 mM caffeine (dissolved in KRH) at 150 sec to identify functional hRyR2 channels. Fluorescence intensities were measured from regions of interest (ROIs) outlining individual cells (approx. 45-47 μm^2). All cells were counted but only cells that responded to caffeine were used in Ca^{2+} oscillation analysis.

2.3.7.4 Analysis of calcium imaging data with SALVO

Calcium imaging experiments have been analysed using 'SALVO' (**S**ynchrony-**A**mplitude-**L**ength-**V**ariability of **O**scillation), a semi-automated program specifically designed to look in detail at the spatiotemporal patterns of Ca^{2+} signals. Parameters

of a Ca^{2+} oscillation (**Figure 2.3**) determined by analysis with SALVO and the method of calculation for each is detailed below:

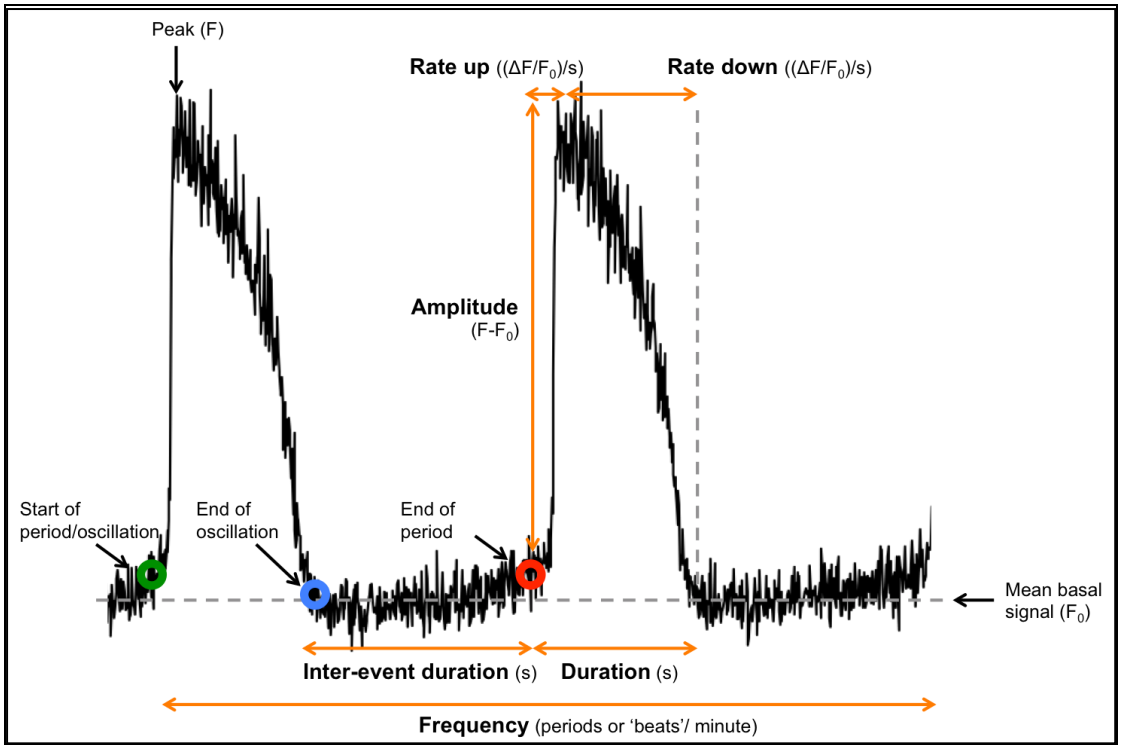

Figure 2.3 Parameters of a Ca^{2+} oscillation measured in transfected HEK293 cells:

Mean Basal Signal Intensity

Basal signal intensity (F_0) was measured by taking an average of signal intensities between each calcium release event. F_0 is highlighted by a dashed line in **Figure 2.3.**

Amplitude

The amplitude of an oscillation of Ca^{2+} release was determined by subtracting the peak signal intensity (F) from the mean basal signal intensity (F_0). The amplitude was expressed as a proportion of the basal intensity signal ($F-F_0/F_0$ or $\Delta F/F_0$). This parameter represents the fluorescence change of the Ca^{2+} indicator following RyR2 channel activation, and is linked to the Ca^{2+} ER load.

Duration

The duration of a Ca^{2+} release oscillation was determined by subtracting the time at which signal intensity begins to increase from the time the signal returned to basal intensity (F_0). Points of the start and end of an oscillation are highlighted on the diagram. Duration was measured in seconds (sec). This parameter reflects Ca^{2+} release and extrusion of Ca^{2+} from the cytosol.

Inter-event Duration

Inter-event duration is the time between two Ca^{2+} release oscillation events. This was determined by subtracting the time at which a new event occurred from the time at which the previous event ended, returning to basal signal intensity. Inter-event duration was measured in seconds (sec).

Frequency

The frequency was calculated as how many periods occurred per minute (ppm). A period is highlighted on **Figure 2.3** and includes both the Ca^{2+} release event duration and inter-event duration added together. This parameter is dependent on the Ca^{2+} load of the ER store, the sensitivity of RyR2 to cytosolic Ca^{2+} concentration, and the refractoriness of RyR2 Ca^{2+} release.

Rate up

The rate up is a calculation of the rate of initial Ca^{2+} release, expressed as a change in signal intensity per second ($(\Delta F/F_0)$/sec). The time of oscillation initiation was subtracted from the time of peak signal intensity (F), and the amplitude of the event ($\Delta F/F_0$) was divided by this time to calculate the rate at which this occurred. This can be interpreted as the rate of activation of the RyR2 population.

Rate down

The rate down is a calculation of the time taken for a spontaneous Ca^{2+} release event to decay and intensity to return to baseline (F_0). This parameter is indicative of removal of Ca^{2+} from the cytosol. It is expressed as a change in signal intensity per second ($(\Delta F/F_0)$/sec). The time at peak oscillation intensity was subtracted from the time at which the oscillation event ended, and the amplitude of the event ($\Delta F/F_0$) was divided by this time to calculate the rate at which this occurred, giving a negative value. This is a measure of the time taken for Ca^{2+} release to terminate.

Caffeine-sensitive ER Ca^{2+} load

ER Ca^{2+} load was determined by calculating the amplitude of caffeine-induced Ca^{2+} release (see **Figure 2.4**), after the addition of 10mM caffeine. The mean basal signal intensity (F_0) was subtracted from the Ca^{2+} release peak fluorescence (Fc).

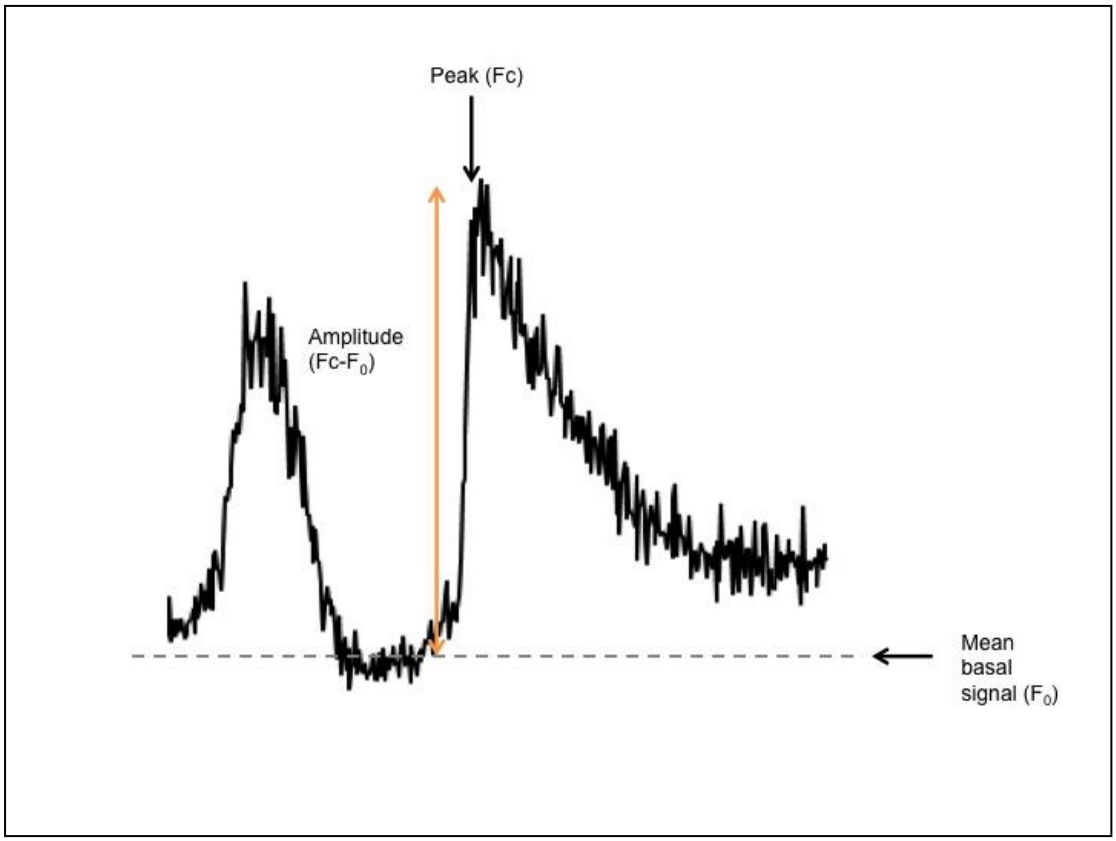

Figure 2.4 The ER Ca^{2+} load was estimated after the addition of caffeine. Mean basal signal intensity (F_0) was subtracted from the amplitude of caffeine-induced Ca^{2+} release (Fc).

2.3.8 Calcium phosphate transfection of HEK293 cells

The calcium phosphate transfection principle was used to introduce eGFP-hRyR2 DNA into HEK293 cells (for maintenance of cell cultures see **Section 3.2.1.1**). A modified precipitation method was employed, where a high DNA: cell ratio is used for optimal transfection efficiency of mammalian cells (Chen and Okayama 1987). Cells were plated onto 10 cm^2 petri dishes at a density of 1.5-2x10^6 cells/dish within 10 mL cDMEM and incubated (See **Section 2.2.2**) for 24 hr before transfection, to allow for growth to confluency of ~75 %. Plasmid DNA (12 µg/dish) was mixed with 124 mM $CaCl_2$ solution (pH 7) and dH_2O to a total volume of 500 µL to generate $CaPO_4$-DNA

complexes. The solution was added dropwise to 500 µL of warmed 2x HBS (pH 7.05) with continuous vortexing. The DNA/$CaCl_2$/HBS mix was incubated for 20 min at room temperature to allow a fine precipitate to form, essential to allow DNA to be introduced into the cells via endocytosis. The 1 mL solution per plate was then added dropwise to the confluent cell monolayer, before incubation at 37 °C at 5 % CO_2 for 24 hours. Cell media was then replaced with 10 mL of cDMEM containing 2 mM NaB for up-regulation of cell expression (Gorman et al. 1983). Cells were incubated at 37 °C at 5 % CO_2 for a further 24 hours before visualisation using a Zeiss fluorescence microscope to assess transfection efficiency, by counting the total number of cells and the total exhibiting eGFP fluorescence. Cells were harvested by trypsinisation and cell number was calculated using the Luna™ Dual Fluorescence Cell Counter, before cells were pelleted by centrifugation at 1,500 xg for 5 min (Allegra 6R centrifuge). Pellets were either stored at -80 °C or immediately lysed for cell homogenate preparation.

2.3.9 Cell homogenate preparation

After the calcium-phosphate transfection protocol, HEK293 cell pellets were immediately resuspended in hypo-osmotic buffer (50 µL per 1 $x10^6$ cells) containing 1 % (v/v) Triton-X-100 on ice. This buffer puts the cells under osmotic stress causing them to rupture. Cells were then homogenised by ejection through a 23 G needle 20-25 times before 6 cycles of freeze-thaw waterbath sonication, using liquid N_2 and a Decon F5100b sonicator (Decon Laboratories Ltd.). Centrifugation at 1,000 xg for 5 mins (Eppendorf 5741R) pelleted cell nuclei and the supernatant was removed, containing cell homogenates. Preparations were aliquoted into volumes suitable for individual experiments and snap-frozen with liquid N_2 before being stored at -80 °C.

2.3.10 Protein assay for quantification

Total protein in cell homogenate samples was quantified using a colorimetric reagent-based protein assay. The BCA™ System relies on two reactions:

- The reduction of Cu^{2+} ions from copper (II) sulphate in the BCA solution to Cu^{+} by peptide bonds of protein
- The chelation of each Cu^{+} ion to two molecules of bicinchoninic acid, forming a purple coloured complex

The amount of Cu^{2+} reduced is proportional to the amount of protein present in the solution, and the purple complex strongly absorbs light at wavelength of 560 nm. Dilutions of samples (1:100, 1:200, 1:500) were prepared as well as protein standards (0-500 µg bovine serum albumin, BSA) for the plotting of a standard curve. Each sample (100 µL) and each protein standard (in duplicate) was mixed with 100 µL BCA kit working solution, prior to incubation at 37 °C for 30 mins to allow for colour development. Absorbance readings at 560 nm were taken using a Biorad iMark™ Microplate Absorbance reader (Biorad), following manufacturer instructions.

A standard curve was plotted of absorbance vs. protein concentration (µg/mL). Sample protein concentration could then be derived from the standard curve, using the linear equation y=mx+c. (see **Figure 2.5**).

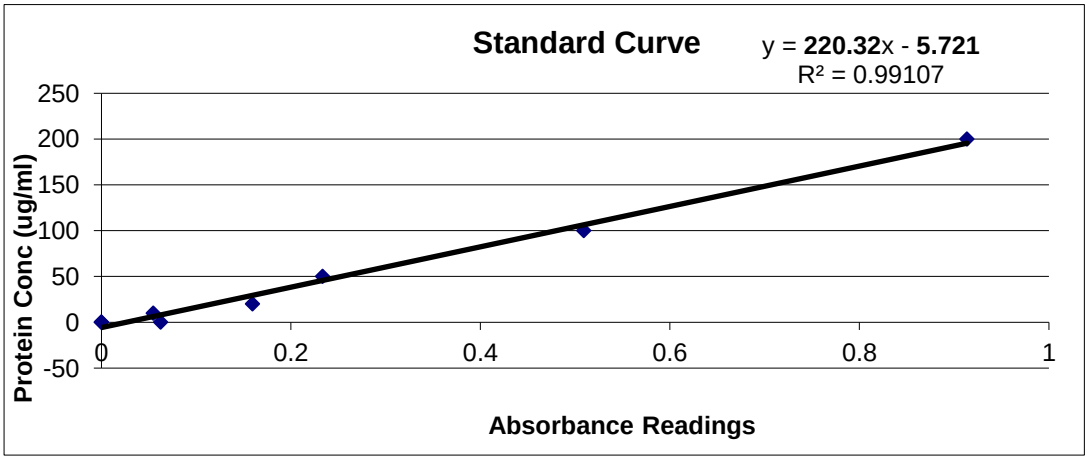

Figure 2.5: Example of a standard curve for protein assay.

2.3.11 SDS Polyacrylamide Gel Electrophoresis (SDS/PAGE)

eGFP-hRyR2 protein expression levels were assessed by SDS/PAGE (Laemmli 1970). Samples were separated using a 4 % (v/v) acrylamide gel, where RyR2 at a MW of 565 kDa can be resolved towards the top. The inert, cross-linked structure of polyacrylamide gel means larger molecules migrate slower through the pores than smaller molecules when an electric field is applied. Separating gels were prepared as in **Table 2.2**, supplemented with 1 % (w/v) agarose to strengthen and eliminate the need for an additional stacking gel. Ammonium persulphate acted as a chemical initiator and TEMED as a catalyst, causing cross-linking chain reactions between acrylamide and bisacrylamide monomers, hence these solutions were added last to the mixture. Glass plates in a Biorad gel casting system were cooled for 30 mins on ice prior to use. Gel solution was poured between pre-cooled glass plates in a Biorad gel casting system with combs inserted to form loading wells. The gel casting system was then cooled on ice for 5 minutes and then left to set for at least two hours at room temperature before use.

Reagent	**Volume (µL)**
40 % Acrylamide/Bis (37.5:1)	1,000
Separating Buffer	2,500
10 % SDS	100
dH_2O	1,345
10 % Ammonium Persulphate	50
TEMED	5
1 % (w/v) agarose	5,000
TOTAL	*10,000 µL*

Table 2.2 Separating 4 % acrylamide gel composition. Amounts of SDS/PAGE components made enough solution for 1 gel. Samples were prepared for electrophoresis by addition of SDS-PAGE x5 loading buffer and 20 min incubation at 42 °C. This denatured and linearized proteins. The 10 % (v/v) β-mercaptoethanol in the buffer also reduced the protein, dissociating aggregates that would otherwise be difficult to separate. Samples were then loaded onto the gel alongside Kaleidoscope protein MW marker. Electrophoresis was carried out at a constant current of 0.02 A until the appropriate coloured markers were resolved.

2.3.12 Transfer of protein onto PVDF membrane

Once SDS-PAGE was complete, proteins separated on acrylamide gels were transferred onto preactivated 0.2 µM polyvinylidene difluoride (PVDF) membrane using the iBLOT™ dry blotting system (Invitrogen) and specialised transfer stacks following manufacturer guidelines. The system allowed a fast electrophoretic transfer time of 13 min at 20 V. PVDF membranes were chosen because of their high protein binding capacity and mechanical strength, ideal for stripping and reprobing experiments.

2.3.13 Western blot analysis by chemiluminescence

After transfer, PVDF membranes were immediately incubated for 1 hr in 5 % (w/v) blocking solution on a rocker to prevent nonspecific antibody binding. For detection, primary antibodies were prepared in 1 % (w/v) wash buffer/blocking solution at the appropriate dilution and applied to the membranes. They were incubated for 2 hr at room temperature or overnight at 4 °C on a rocker. The HRP-conjugated secondary antibody was prepared in 1 % (w/v) wash buffer/blocking solution at the appropriate dilution. Membranes were washed three times using 1 % (w/v) wash buffer/blocking solution for 5 min on a rocker to remove unbound antibody, before the application of the secondary antibody and incubation at room temperature on a rocker for a further 1.5 hr. Membranes were then washed 5 times using TBS-T for 5 min on a rocker to remove background and remaining traces of antibody or blocking solution.

To visualise transferred protein bands, enhanced chemiluminescence reagents were used (ECL Prime, GE Healthcare) according to the manufacturer instructions. Antibodies conjugated to horseradish peroxidase catalyse the oxidation of luminol and results in light emission. Maximum light emission occurs at wavelength of 425 nm and is detected by the G:BOX Chemi XX6 (Syngene) chemiluminescence imaging system, using the GeneSys software (Syngene) and following manufacturer instructions.

Chapter 3

Investigating the functional heterogeneity of CPVT-linked hRyR2 mutants using Ca^{2+} imaging

3.1 Introduction

3.1.1 Methods of functional characterization of CPVT1 mutations

Many techniques are employed to unravel the molecular mechanisms by which both WT and CPVT1 RyR2 channels release Ca^{2+} from the SR. Unfortunately, it is difficult to interpret data and understand the definitive mechanism of dysfunction when multiple assays are employed to investigate RyR2 channel behaviour (George et al. 2005). While single channel isolation is both valuable and essential to investigate gating mechanisms and modulation by physiological ligands, it also remains that such studies are not always regarded as physiologically relevant (Bers 2014). Conversely, investigating the function of RyR2 channels within intact cell systems pose other disadvantages; while perhaps more physiological, it is difficult to delineate the exact contribution of RyR2 channels to Ca^{2+} release when there are many other modulators within the complex environment of a cell, including the contribution of the SR Ca^{2+} store. Described below are three of the major experimental methods used to investigate Ca^{2+} release events of the RyR2 channel:

3.1.1.1 Assessing RyR2 function using single channel recordings

RyR2 channels are located within the intracellular network of the SR and are more difficult to access than ion channels which span the sarcolemma; therefore conventional electrophysiological techniques such as patch-clamping are not viable (Mortensen and Smart 2007). Current through RyR2 channels therefore requires the incorporation of isolated single channels into an artificial membrane system, namely planar lipid bilayers (Favre et al. 1999; Mortensen and Smart 2007). This is the only method available to observe mechanistic information about channel gating and the effects of channel modulators in real time (Laver 2001; Williams et al. 2001) .

RyR2 channels are incorporated into bilayers either as native membrane vesicles or as purified single channels. An advantage of using native membrane vesicles is that regulatory proteins that form RyR2 macromolecular complex may remain associated with the channel in the bilayer (Tester et al. 2007; Marx et al. 2000). However, this will limit the characterization of channel function, as other ion channels (such as K^+ channels) present will contaminate current measurements. Although Ca^{2+} can be used as the current carrier to eliminate this issue, many studies use monovalent

permeant ions rather than divalent ions in order to increase the signal-to-noise ratio (Bannister et al. 2015; Mukherjee et al. 2012; Williams et al. 2001). Therefore, it will be impossible to delineate conductance of single RyR2 channels in this manner. Limitations can be overcome by the use of purified single channels, with RyR2 separated from other membrane proteins after detergent-solubilisation and isolation by density gradient centrifugation.

A dispersion of lipid in n-decane is applied over a small partition between two chambers, *cis* and *trans*, which contain suitable ionic solutions (See **Figure 3.1**), spontaneously thinning to form a bilayer (White 1986)(Laver 2001). RyR2 will then incorporate within the bilayer in a fixed orientation, allowing cytosolic and luminal sides of the protein to be defined (Sitsapesan and Williams 1994). Incorporation of channels can be detected by conductance changes in the bilayer membrane (Coronado et al. 1992). Subsequently, single channel gating and ion translocation can be monitored, as well as responses to physiological and nonphysiological ligands in a controlled environment under voltage clamp conditions (Rousseau et al. 1986; Williams et al. 2001; Favre et al. 1999; Holmberg and Williams 1989).

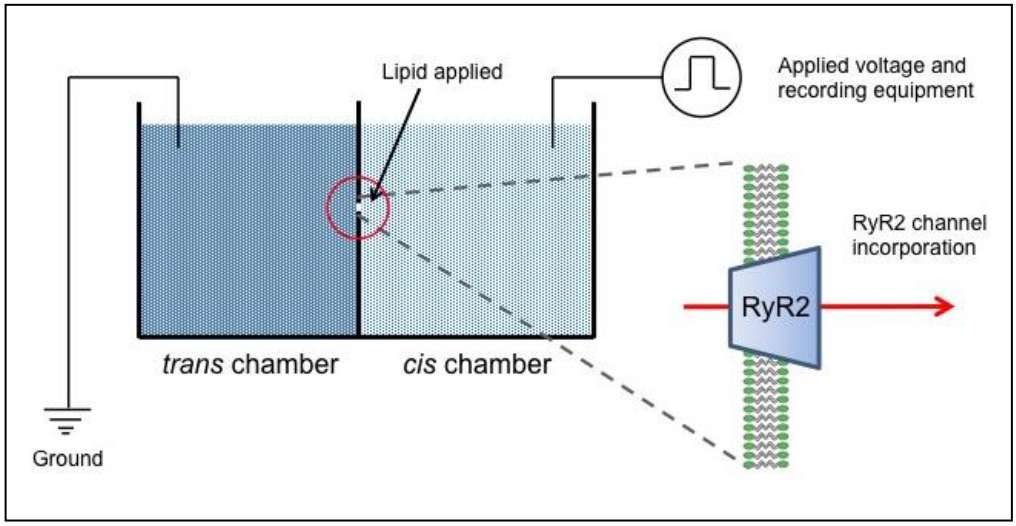

Figure 3.1 Schematic of planar lipid bilayer setup for recording single RyR2 channel currents. Lipid bilayers are formed across a small partition (~200μm in diameter) between two chambers, *trans* and *cis*, filled with controlled chemical solutions. Recombinant RyR2 channels are incorporated by the addition of purified RyR2 protein to the *cis* chamber, induced by a chemical gradient. After removal of excess RyR2 protein and perfusion of the *cis* chamber to a symmetrical solution as in the *trans* chamber, channel behaviour is monitored under voltage clamp conditions.

Isolation of single channels from the native cellular environment and experiments in this fashion however will subject the channel to non-physiological conditions, which may alter channel function (Meissner 2004). Detergent lysis may alter molecular interactions within single channels, with speculation that subconductance states identified in single channel recordings may in fact be an artefact of tetramer destabilization following detergent solubilisation (Carter et al. 2006; M. T. Jiang et al. 2002) Observed effects of solubilisation may be due to the loss of accessory proteins and therefore this *in vitro* functional characterization may not be reflective of in situ channel behaviour within a cell (George et al. 2005; Du et al. 2001; George, SORATHIA, et al. 2003; Wagenknecht and Radermacher 1997).

3.1.1.2 [^{3}H] Ryanodine binding as a surrogate marker of channel population function

Arguably one of the most important contributions to the study of RyR2 is the discovery of the plant alkaloid ryanodine (**Figure 3.2**) (Jenden and Fairhurst 1969), followed by the production of radiolabelled [^{3}H] ryanodine (Pessah et al. 1985). This led to the subsequent identification, purification, single channel analysis and cloning of RyR2 over the following twenty years (Tunwell et al. 1996; Campbell et al. 1987; Lai et al. 1989; Hymel et al. 1988; Holmberg and Williams 1989). Ryanodine binds to RyR2 with high-affinity in the open conformation only, therefore by exploiting this property, changes in [^{3}H] ryanodine binding levels can be used as an indicator of changes in RyR2 channel function (Lai and Meissner 1989; Meissner and El-Hashem 1992). Experimentally, it is a straightforward assay in which multiple conditions can be manipulated, where Ca^{2+} sensitivity of channel populations can be quantified (Viero et al. 2012). [^{3}H] ryanodine binding has been used extensively to investigate the effects of ligands on RyR2, both physiological and non-physiological (Hunt et al. 2007; Holmberg and Williams 1989).

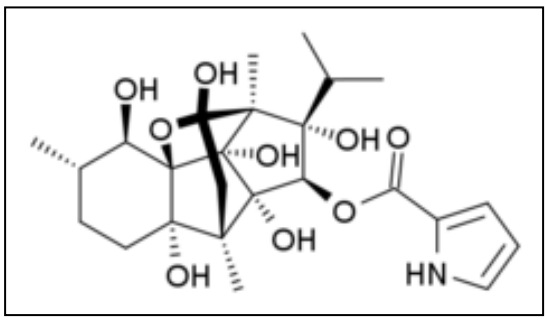

Figure 3.2 The chemical structure of ryanodine ($C_{25}H_{35}NO_9$), which binds to the RyR2 channel in the open state.

Investigating CPVT1 mutations with this assay has in some cases shown that mutant channels that exhibit increased Ca^{2+} leak also display increased sensitivity to Ca^{2+}-dependent [^{3}H] ryanodine binding (Jones et al. 2008; Fernández-Velasco et al. 2009). However, the technique can produce misleading results when mutant channels are examined – some RyR2 mutations alter the [^{3}H] ryanodine binding affinity without changing single channel gating (Gao et al. 2000; Wayne Chen et al. 2002; Zhao et al. 1999). Mutations can also cause inherent RyR2 instability, rendering some channels non-functional outside of the cellular environment; therefore it would be impossible to study with this technique (Fessenden et al. 2004).

3.1.1.3 Ca^{2+} release function of RyR2 channel populations as assessed by Ca^{2+} imaging

Although precise mechanisms of channel dysfunction cannot be elucidated without analysis in planar lipid bilayers, examination of RyR2 in intact cell systems can provide a more physiologically relevant environment for functional characterization. Utilizing Ca^{2+}-indicator fluorescent dyes that can bind to free Ca^{2+} within a cell, as well as high-powered laser scanning confocal microscopy (See **Figure 3.3** for a schematic), intracellular Ca^{2+} imaging is now a widely used technique to study RyR2 mutant channel function (N. L. Thomas et al. 2004; D. Jiang 2005; N. L. Thomas et al. 2005). Changes in fluorescence intensity indicate changes in the binding of free Ca^{2+} to the indicator and is therefore reflective of Ca^{2+} release from intracellular stores.

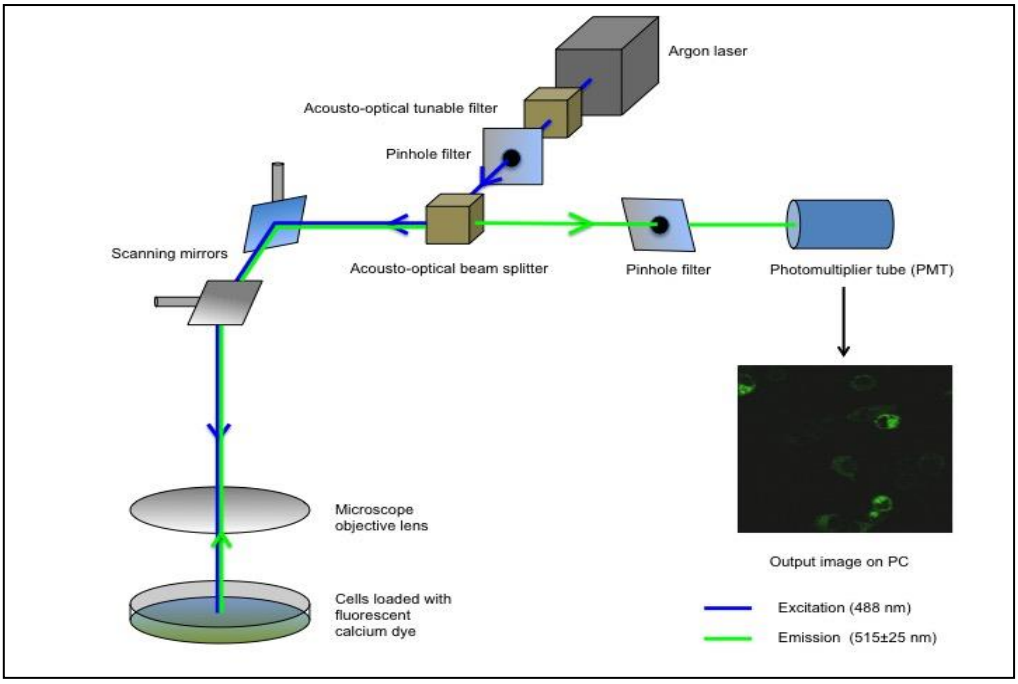

Figure 3.3 Schematic representation of Ca^{2+} imaging with a confocal microscope. Briefly, excitation light from the Argon laser passes through pinhole filters, before being directed by the acousto-optical beam splitter (AOBS) to rotating scanning mirrors. These direct excitation light to systematically scan across each point of the sample, exciting fluorescent indicators in the sample on a point-by-point basis, decreasing the effects of photo bleaching. The rotating scanning mirrors then direct emitted light from the sample towards the AOBS. Here light is 'tuned' to a particular wavelength before being filtered of light that did not originate from the sample. The photomultiplier tube then amplifies the fluorescent signal and the output is converted to a signal that reflects the magnitude of fluorescence within the sample. Figure constructed based on literature by Leica Microsystems Science Lab.

As there are many types of Ca^{2+} signal that occur during Ca^{2+} cycling of the cell, (influx, reuptake, extrusion, release from other channels), it is difficult to identify the precise contribution of RyR2 to experimental observations. Interpretation of Ca^{2+} release events is therefore dependent on the choice of cell line in which to study RyR2. There are many cell lines in which recombinant RyR2 can be expressed (see **Table 3.1**), but RyR2-deficient cell lines remain the cell system of choice, without accessory proteins or endogenous RyR isoforms to contribute to the complexity of Ca^{2+} signalling. The lack of endogenous RyR in cell lines allows for homotetrameric channel expression after transfection with RyR2 cDNA, as well as heterotetrameric channel expression after co-transfection with equal ratios of WT and mutant RyR2 cDNA (Lehnart et al. 2008; Tong, McCarthy, et al. 1999). HEK293 cells are the most widely used RyR2-deficient cell line, in both isolation of purified recombinant RyR2 channels for single channel analysis (Bannister et al. 2015; D. Jiang et al. 2004; M. T. Jiang et al. 2002; Mukherjee et al. 2012) and in the investigation of Ca^{2+} handling within the cell (D. Jiang 2005; N. L. Thomas et al. 2004; N. L. Thomas et al. 2005). Although HEK293 cells lack the accessory proteins and contractile machinery of a cardiomyocyte, they appear to produce comparable functional data to that of RyR2 isolated from native tissue (Xu and Meissner 1998; Li and Chen 2001; Du 1998; Bhat et al. 1999). Functionality of channels expressed in HEK293 cells can also be tested by caffeine-induced Ca^{2+} release (N. L. Thomas et al. 2004), with release of intracellular Ca^{2+} only from those successful transfected with RyR2.

For these reasons, HEK293 cells were chosen as an appropriate heterologous cell system for the intracellular characterization of RyR2 mutations in a living-cell based context within this project.

Cell Line	CHO	HEK293	HL-1
Species	Chinese hamster	Human	Mouse
Tissue	Ovary	Kidney, embryo	Atrial cardiomyocyte
Cell type	Epithelial	Epithelial	Myocyte
Method of engineering	Sub clone of the parental CHO line[1]	Transformed with sheared human Ad5 DNA[2]	Derived from the AT-1 mouse atrial myocyte tumour lineage[3]
Endogenous RyR	No	No	Yes
Contractile Machinery	No	No	Yes
Accessory Proteins	No	No	Yes, full set
Advantages	Can express recombinant RyR2 in homotetramers Effects of RyR2 can be separated from influences of accessory proteins	Human cell line with no endogenous RyR[4] Can express recombinant RyR2 at high levels in homotetramers Widely used to characterize RyR2 mutations, where effects of RyR2 can be separated from influences of accessory proteins	Contain all the cardiac accessory proteins and contractile machinery proteins Can maintain cardiac-specific phenotype after repeated passaging
Disadvantages	Cell line is not human Decreased cell viability with high levels of recombinant RyR2 expression	No accessory proteins or contractile machinery present	Cell line is not human Endogenous expression of RyR isoforms complicates interpretation of any recombinant RyR2 effects and recombinant RyR2 expression levels are low

Table 3.1 Cell lines used in the expression and functional characterization of RyR2 channels. HEK293 cells remain the most widely used in characterization of RyR2 mutations. References: [1] (Tjio 1958), [2] (Russell et al. 1977), [3] (Claycomb et al. 1998), [4] (Tong, McCarthy, et al. 1999),

3.1.2 Preliminary single channel data on two CPVT1 hRyR2 mutants indicating functional heterogeneity

3.1.2.1 The S2246L and N4104K hRyR2 mutations

S2246L and N4104K were two of the first CPVT1-causing mutations to be identified in the *hRYR2* gene (Priori et al. 2001) and are in different domains of the RyR2 protein (see **Figure 1.14**). The clinical phenotype of both mutations has been investigated, with functional characterization experiments performed at both the single channel level and within a heterologous cell system (D. Jiang 2005; Wehrens et al. 2003; George et al. 2006; D. Jiang et al. 2004). KI S2246L and N4104K mouse models have also been developed that exhibit the CPVT1 phenotype when challenged with β-agonists and caffeine (Suetomi et al. 2011; Nishimura et al. 2015). **Table 3.2** provides a summary of the functional characteristics of these RyR2 mutations.

	S2246L	N4104K
Base change	Serine (S) to Leucine (L)	Asparagine (N) to Lysine (K)
Location	Central domain B solenoid domain (residues 2145-3613)	Cytoplasmic portion of the I domain EF hand pair domain (4060-4134)
Patient phenotype	First identified in an 8-year-old male who presented with recurrent syncopal events induced by exercise. Normal heart structure and resting heart rhythm, with bidirectional or polymorphic VT induced on stress or exercise[1,2],	First identified in a 14-year-old male who presented with loss of consciousness during exercise. Normal heart structure and resting heart rhythm, with non-sustained bidirectional VT on stress or exercise[1,2],
Mouse phenotype	No appreciable changes in functional characteristics at rest, with epinephrine inducing VT[3].	No appreciable changes in function at rest, with caffeine plus epinephrine infusion to N4104K mice inducing VT/VF[9].
Isolated mouse cardiomyocyte phenotype	Increased SR Ca^{2+}-dependent spark frequencies in mouse cardiomyocytes, with an abnormally tight interaction in the central domain of the peptide[3].	Saponin-permeabilized mouse cardiomyocytes show increased spark frequencies in comparison to WT. Spontaneous Ca^{2+} transients were more frequently observed compared to WT after the addition of isoproterenol[9].
Single channel analysis	Recombinant mouse RyR2 channels exhibit single channel properties similar to WT and displayed functional differences only upon activation by PKA phosphorylation, with increased P_o and gating frequencies[4]. Mouse RyR2 channels display increased P_o on high luminal Ca^{2+} activation compared to WT[5].	Recombinant mouse RyR2 channels display a higher P_o on high luminal Ca^{2+} activation compared to WT, at low cytosolic Ca^{2+} concentrations[6].
[^{3}H] Ryanodine binding	No alteration of basal level of [^{3}H] ryanodine binding to RyR2 compared to WT[5].	Enhanced basal level of [^{3}H] ryanodine binding to RyR2 compared to WT[6]
Expression in heterologous cell systems (i.e. HEK293 cells)	Mouse S2246L showed increased frequency of Ca^{2+} oscillations with no effect on amplitude and a decreased ER Ca^{2+} store in HEK293 cells[5]. Recombinant human S2246L perturbed intra-RyR2 domain interactions, with augmented Ca^{2+} release in CHO and HL-1 cells[7].	Mouse N4104K showed increased frequency of Ca^{2+} oscillations and a decreased ER Ca^{2+} store in HEK293 cells[6]. Recombinant N4104K perturbed intra-RyR2 domain interactions, with augmented Ca^{2+} release in CHO and HL-1 cells[7].

Table 3.2 A summary of functional characteristics observed in S2246L and N4104K RyR2 mutations in different experimental systems. References: [1] (Priori et al. 2001), [2] (Priori 2002), [3] (Suetomi et al. 2011), [4] (Wehrens et al. 2003), [5] (D. Jiang 2005), [6] (D. Jiang et al. 2004), [7] (George et al. 2006), [8] (Tester et al. 2004), [9] (Nishimura et al. 2015)

3.1.2.2 Preliminary single channel data indicates functional heterogeneity

Plasmids encoding mutant S2246L and N4104K hRyR2s were previously constructed in our laboratory (George, Higgs, et al. 2003) and therefore available for characterization at the single channel level in a minimal environment (Mukherjee et al. 2012). Preliminary single channel data were obtained by Dr. N.L. Thomas for these mutants and provided as supporting evidence in the grant application for this project.

The literature on the functional characterization of RyR2 at the single channel level shows many inconsistencies because of the wide range of experimental conditions used by groups studying the channel in this way. Channels used for bilayer experiments have been obtained from many sources, including SR preparations from animals (Sitsapesan and Williams 1990a; Sitsapesan and Williams 1990b), membrane preparations from cells in which recombinant RyR2 channels have been expressed (Li and Chen 2001; Tester et al. 2007) or purified from either of these sources (Lindsay et al. 1994; Li and Chen 2001). Some channel preparation processes retain accessory proteins with RyR2 channels, while others do not. The inclusion of modulators such as ATP, Mg^{2+}, cytosolic and luminal Ca^{2+} can also alter the function of RyR2, as well as posttranslational modifications such as phosphorylation and oxidation (Fill and Copello 2002; Carnes 2008; Terentyev 2008) . Due to the different starting materials, permeant ions, chemical modulators and accessory proteins used within experiments, models of hRyR2 channel behaviour are therefore rarely directly comparable (Zahradník et al. 2005; Laver 2007; Mukherjee et al. 2012).

This lack of consensus regarding single channel experiments with RyR2 prompted the Williams group to study the recombinant hRyR2 in a minimal environment, away from accessory proteins and other modulatory ligands, with the sole focus of elucidating the role of cytosolic Ca^{2+} on the intrinsic mechanisms involved in modulating the open probability of the channel. They developed a mathematical model to describe purified WT recombinant hRyR2 gating kinetics in this system, suggesting the physical conformational changes that occur when the channel is activated by cytosolic [Ca^{2+}] (Mukherjee et al. 2012). The destabilization of channel closure can be measured in the model by the rate of isomerization between two closed states, with one that is long and unresponsive.

Preliminary gating data obtained under these minimal conditions by Dr N.L. Thomas for this project revealed differences between S2246L and N4104K channels. In **Figure 3.4**, N4104K RyR2 channels present an increased P_o at 1 µM cytosolic Ca^{2+} concentration in comparison to WT, whereas S2246L does not. When cytosolic Ca^{2+} concentration was buffered to nominally zero (with 1 mM EGTA, 1 mM HEDTA/NTA), surprisingly an N4104K channel showed brief open events (<200 µsec) with a P_o of 0.0007 in comparison to a P_o of zero for both S2246L and WT RyR2 channels.

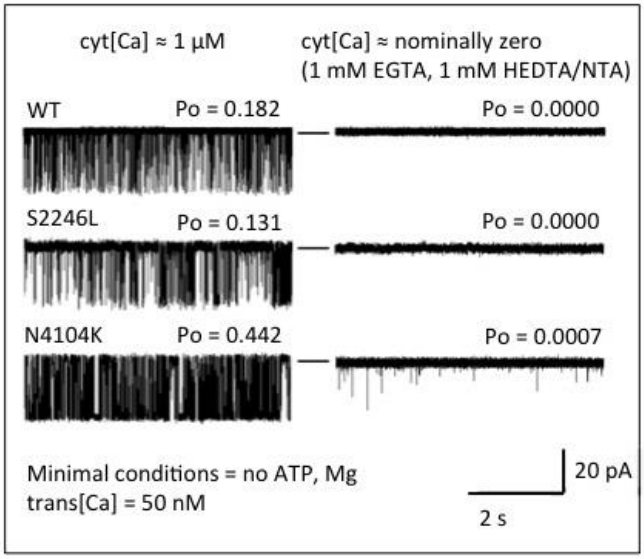

Figure 3.4 Preliminary single channel recordings show that N4104K exhibits unliganded gating events, whereas S2246L and WT hRyR2 do not. *A.* Representative single channel recordings of gating events in WT and mutant hRyR2 channels. Openings are downward from the closed level (black line). Data acquired and analysed by Dr. N.L. Thomas.

Mathematical modelling of Ca^{2+} activation data for these mutants by Dr N.L. Thomas suggests that N4104K RyR2 channels spend less time in the longer Ca^{2+} unresponsive closed state in comparison to S2246L RyR2 channels.

.

Preliminary data suggests that the pathogenic N4104K RyR2 mutation is associated with increased constitutive opening activity under nominally zero Ca^{2+} conditions, in the absence of activating ligand, demonstrating an intrinsic effect on channel gating. Constitutive activity is not evident in both mutations studied: S2246L RyR2 channels must require further stimulation (other than cytosolic Ca^{2+}) to unmask the dysfunction linked to CPVT1.

Previous work on S2246L RyR2 channels show that they activate with cytosolic Ca^{2+} in an identical way to WT, in the absence of luminal Ca^{2+} (Wehrens et al. 2003). This is somewhat reflected in the preliminary data presented here, with channel behaviour similar to WT when cytosolic [Ca^{2+}] is the only activating ligand. Jiang et al (2005) also report very low open probability of S2246L at 45 nM cytosolic/luminal Ca^{2+} concentrations, similar to WT (Po=0.0002 and 0.0004, respectively). However, this superficial analysis only considered P_o as a measure of channel function, whereas improved methods within our laboratory are more likely to resolve channel activity that may have been missed such as dwell open and closed times (Mukherjee et al. 2012).

Interestingly, unliganded channel opening analogous to that of N4104K channels displayed in this data has previously been reported in studies of another CPVT1 mutation, R4497C (D. Jiang et al. 2002). Single channels exhibited enhanced activity at nanomolar concentrations of Ca^{2+} (controlled by the addition of 0.1M EGTA) in comparison to WT, with a P_o ~10x greater (0.00013 vs. 0.0000089, respectively). This supports the hypothesis that some mutant RyR2 channels display increased basal activity in comparison to others.

Ligand-independent activity in other types of channels has been observed, induced by specific disease-causing mutations. Disease-causing mutations in the acetylcholine receptor also show increased unliganded channel activity, as well as an increase in the unliganded equilibrium constant (Purohit and Auerbach 2009; Grosman and Auerbach 2000; Milone et al. 1997). Unliganded gating has also been reported as increased in the cystic fibrosis transmembrane conductance regulator (CFTR) ATP-gated ion channels when there are gain-of-function mutations in cystolic loops of the CFTR polypeptide structure (Okeyo et al. 2013). This constitutive gating activity can therefore be used as a marker of the functional alteration of RyR2 caused by CPVT1 mutations (Mukherjee et al. 2012). The observation that N4104K hRyR2 channels favour the closed responsive state, leading to subsequent unliganded openings is suggestive that this constitutive gating is the product of intrinsic structural defects within the channel. Conversely, S2246L hRyR2 channels do not display the same gating kinetics; this highlights that RyR2 CPVT1 mutations are functionally heterogeneous, even at the single channel level in a minimal environment.

While both S2246L and N4104K mutant RyR2 channels have been characterized using several different methods and there have been few differences in function noted (see **Table 3.2**), our understanding of RyR2 dysfunction remains far from complete. While both mutations have been investigated within the heterologous HEK293 cell system, a method successful first employed by Chen's group and later others ((Seidel et al. 2014; Kong et al. 2008; N. L. Thomas et al. 2005; D. Jiang et al. 2004; D. Jiang 2005; N. L. Thomas et al. 2004)), more recent work has suggested assessment of the propensity for Ca^{2+} release alone is not a clear-cut indication of dysfunction. Loaiza et al. (2013) investigated the Ca^{2+} release of WT and heterotetrameric WT/V2475F RyR2 channels in HEK293 cells and found there was no statistical difference between the percentages of oscillating cells between groups at varying concentrations of extracellular Ca^{2+}. This was in conjunction with an abnormal response to PKA phosphorylation, as well as increased cytosolic Ca^{2+} sensitivity and altered luminal Ca^{2+} concentration regulation in other experimental assays. Most CPVT1-linked mutations that have been shown to display a decreased threshold for SOICR also display a significant decrease in mean close time (7-20 fold shorter than WT channels) (D. Jiang 2005; Kashimura et al. 2010), whereas the mutation investigated by Loaiza et al. did not show the same dramatic decrease (1.2 fold shorter than WT). This is suggestive that the threshold for SOICR does not solely determine the arrhythmogenic Ca^{2+} release in all RyR2 mutations (Loaiza et al. 2013).

A more detailed investigation of Ca^{2+} release events in RyR2-transfected HEK293 cells is therefore warranted, interrogating kinetic parameters in more detail, such as rates of release and time periods between release events. This may reveal differences undetectable by measure of propensity of release.

3.1.3 Chapter aims

There is a growing body of evidence to suggest that within the classification 'gain-of-function', mutations in RyR2 are not identical and are in fact functionally heterogeneous (Tateishi et al. 2008; Loaiza et al. 2013; George et al. 2005; Suetomi et al. 2011; N. L. Thomas et al. 2005). Based on preliminary single channel data generated in the study of a central domain mutation S2246L and a transmembrane domain mutation N4104K, it appears that this functional heterogeneity can be revealed within a minimal environment, with cytosolic Ca^{2+} concentration as the only activating ligand. S2246L channels exhibit different gating mechanisms to that of N4104K channels. Unliganded channel openings observed in N4104K indicate there may be an intrinsic structural defect within this RyR2 channel, while S2246L channels may require further stimulation to reveal dysfunction, such as phosphorylation (Tester et al. 2007).

It is therefore proposed that functional heterogeneity at the single channel level will be reflected at the cellular Ca^{2+} release level, shown by intracellular Ca^{2+} imaging in the heterologous HEK293 cell system, a well-established system used in the characterization of RyR2 mutations. This was investigated by:

- Detailed interrogation of the Ca^{2+} release events of WT, S2246L and N4104K hRyR2 within HEK293 cells via confocal microscopy. Interrogating kinetic parameters as well as the frequency and propensity for spontaneous Ca^{2+} release in this system will reveal alterations that would have been missed by these measurements alone.
- Assessing the expression levels of WT and mutant hRyR2 channels in HEK293 cells by Western blotting to determine whether any observed changes in function are attributable to changes in protein expression, of the construct or of SERCa, another Ca^{2+} handling protein within the system.
- Assessing the formation of functional hRyR2 channels and the ER Ca^{2+} load after transfection into the heterologous cell system, via caffeine-induced Ca^{2+} release.
- Determining the intracellular localization of hRyR2 within HEK293 cells with immunofluorescence to confirm any alterations in Ca^{2+} handling is not due to mislocalization of recombinant mutant hRyR2.

3.2 Materials and methods

3.2.1 Evaluating the expression of WT and mutant eGFP-hRyR2

It was important to evaluate the expression of RyR2 in transfected HEK293 cells to determine whether differences in calcium imaging between WT and mutant RyR2 transfected cells were attributable to altered protein expression.

Methods employed to express, prepare cell homogenate and Western blot for RyR2 protein are detailed in **Chapter 2**. Briefly, WT and mutant eGFP-hRyR2 DNA was transfected into HEK293 cells by the calcium phosphate method. After 48 hours post-transfection, cells were immediately first assessed for transfection efficiency before lysis and preparation as a homogenate to assess protein expression by Western blotting. After protein assay to calculate the concentration of these homogenate preparations, both 50 µg and 100 µg (normalized to WT transfection efficiency) of each construct preparation were incubated with the appropriate amount of x5 loading buffer, before loading onto an agarose-strengthened SDS-PAGE gel. Electrophoresis was carried out at constant current until the appropriate coloured markers on a ladder were resolved. Separated proteins were then transferred onto PVDF membranes, before blocking and incubation with primary antibody. This was followed by wash steps and incubation with the appropriate secondary antibody.

Antibodies used in this chapter included:

- Ab-GFP (B-2) antibody (Santa Cruz Biotechnology): mouse monoclonal primary antibody raised against the full-length green fluorescent protein of *Aequorea victoria* origin. Used at 1:1,000 dilution.
- Ab-Vinculin (ab129002, [EPR8185]) antibody (Abcam): rabbit monoclonal primary antibody raised against human vinculin. Used at 1:10,000 dilution as a loading control. Loading controls are proteins with high and ubiquitous expression and can be utilized to account for loading error across experiments – expression levels of these proteins should remain consistent. Vinculin was chosen as an appropriate loading control in this instance, as at molecular weight of ~117 kDa, this protein can still be visualised after the long period of electrophoresis required to separate hRyR2 protein.

- Ab-SERCA (1/2, clone Y/1F4) antibody (Badrilla): mouse monoclonal antibody specific to both human SERCa1a and SERCa2a. Used at 1: 2,000 dilution.
- Ab-β-tubulin (ab6046) antibody (Abcam): rabbit polyclonal antibody specific to β-tubulin. Used at 1:500 dilution as a loading control, with a molecular weight of 50 kDa.

After several wash steps to remove excess HRP-conjugated secondary antibody from the membranes, protein bands were visualized by enhanced chemiluminescence, detected by the G:BOX Chemi XX6 (Syngene) system. Densitometric analysis of visualized bands was then performed with GeneTools software (Syngene) and data then analysed with Microsoft Excel and GraphPad Prism as appropriate.

3.2.2 Immunofluorescence (IF) analysis of cells expressing eGFP-hRyR2

Immunofluorescence (IF) is a technique that uses the specificity of antibodies to their antigen to target fluorescent dyes to specific molecular targets within a cell. IF analysis was carried out to confirm correct trafficking of recombinant hRyR2 constructs to the ER and that observed functional consequences of CPVT1 mutations were not due to incorrect localization. The ER in HEK293 cells is thought to be the equivalent cellular compartment to the junctional SR of cardiac muscle (Knollmann 2010).

Cells were prepared and transfected on poly-lysine coated glass coverslips as described previously (see **Section 3.2.1.2**). Assays were started 48 hours post transfection. Cells were washed 3 times in Phosphate Buffered Saline (PBS: 137 mM NaCl, 2.7 mM KCl, 4.3 mM Na_2HPO_4, 1.4 mM KH_2PO_4, pH adjusted to 7.4, filter sterilized) and fixed with 4 % (v/v) paraformaldehyde in PBS solution for 10 minutes in the dark. Cells were then washed and rehydrated in PBS for at least 1 hour at room temperature. Coverslips were washed with dH_2O and mounted on glass slides with drops of Fluorsave (Calbiochem). To detect hRyR2 in fixed cells, permeabilization was achieved by incubation in 0.1 % (v/v) Triton X-100 detergent (Sigma Aldrich) in PBS for 30 minutes. Solution was removed and cells were washed with PBS. A blocking solution of 10% (v/v) FCS in PBS was used to prevent nonspecific immune-reactivity and was applied for 90 minutes at room temperature. Primary antibody (pAb-1093: rabbit polyclonal antiserum raised to residues 4514-4564 of RyR2, without cross reactivity to RyR1) was then applied at a 1: 1,000 dilution in PBS for 90 minutes. Coverslips were washed and fluorescent secondary antibody (Alexa Fluor 546) was applied at the appropriate dilution in PBS for a further 90 minutes. Coverslips were washed in PBS before final fixing with Fluorsave. Slides could then be stored a 4˚C until viewing with a Leica SP5 confocal microscope. To visualize eGFP fluorescence, an Argon laser was used, with excitation at 488 nm and emission 525 ±25 nm. To visualize Alexa-546 fluorescence, a Helium/Neon laser was used with excitation at 546 nm and emission at 572 ±30 nm. Images of cells were acquired with Leica AS software.

3.2.3 Ca^{2+} imaging in a heterologous cell system

HEK293 cells were chosen as the heterologous cell system for experimentation, due to their wide use in RyR2 characterization and lack of accessory proteins that may complicate data interpretation. Spontaneous Ca^{2+} release events were visualized with confocal microscopy via a fluorescent calcium-indicator Fluo 3. Further details are found in Chapter 2.

3.3 Results

3.3.1 Do S2246L and N4104K differ in their recombinant expression level compared to WT hRyR2?

Given that differing expression levels of hRyR2 cDNA within HEK293 cells will affect Ca^{2+} release, it was important to assess this prior to detailed analysis of Ca^{2+} release event kinetics. WT and mutant hRyR2 cell homogenate preparations were analysed by Western blotting at loads of 50 µg and 100 µg, normalized to WT transfection efficiency, such that expression level per hRyR2 expressing cell could be estimated. This should mean that all lanes in the blot displayed equivalent signal, if the expression level of hRyR2 per cell was equivalent for each construct. The intensity of bands at 50 µg for each preparation was low and variable across six separate experiments and it was sometimes difficult to visualize these via enhanced chemiluminescence in comparison to the equivalent 100 µg band. Choosing normalization points with low quantified intensities is suggested to result in high data coefficient of variance (CV), increasing false negatives (Degasperi et al. 2014). Consequently, expression levels were analysed only at 100 µg of loading (**Figure 3.7**), although original blots and graphs for 50 µg protein expression can be found in **Appendix III and IV**.

Expression of WT or mutant eGFP-hRyR2 was assessed using the intensity of signal given at the expected molecular weight of ~565kDa after probing using an anti-GFP antibody (see **Section 2.2.12** and **2.3.12**). This signal was corrected for loading error by normalising to the signal obtained for the endogenous, constitutively expressed cytoskeletal protein vinculin and expressed as a proportion of this signal. An average was then taken from at least three separate blots. Densitometric analysis revealed that N4104K protein expression levels were significantly higher than WT at 100 µg of loading (**Figure 3.7 B**, one way ANOVA with Bonferroni posthoc test, $p<0.005$ *, $n=6$).

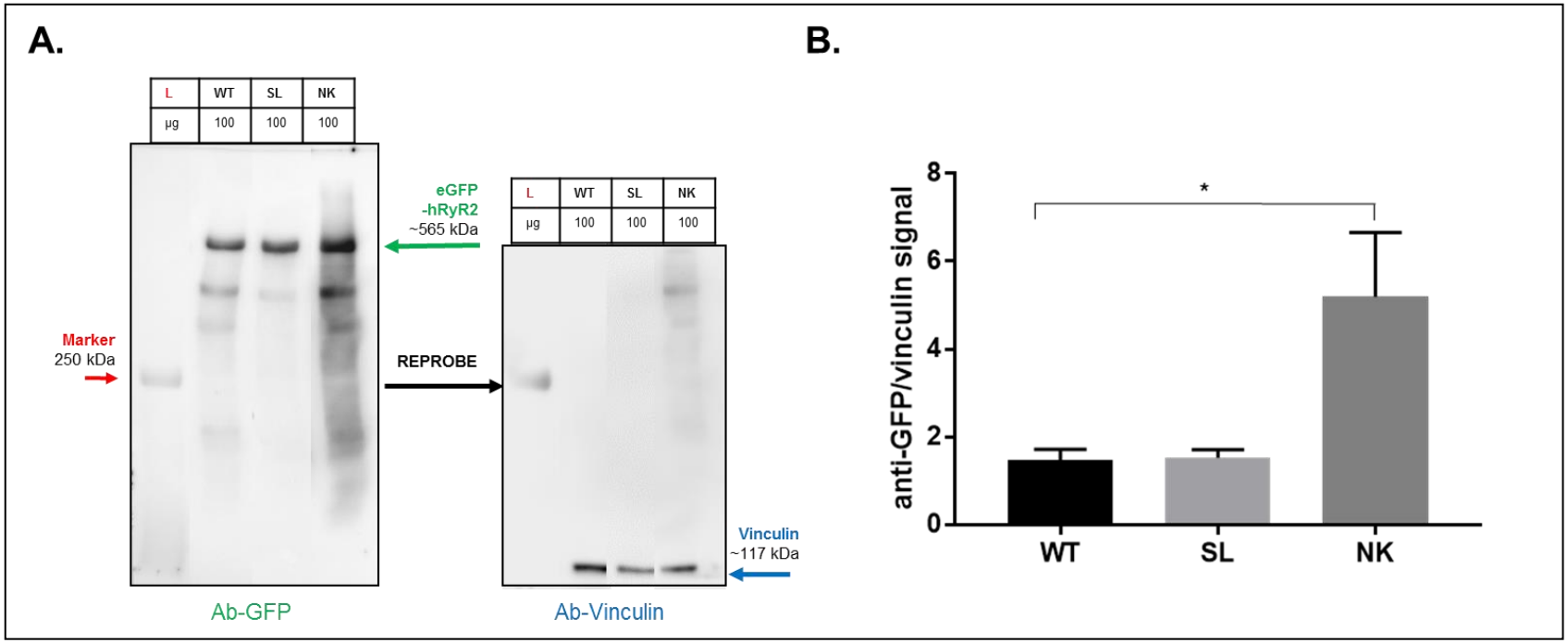

Figure 3.6 Western blot analysis of WT and mutant eGFP-hRyR2 reveals that protein expression levels are not equivalent. *A.* Representative protein bands achieved from Western blot analysis of WT, S2246L and N4104K hRyR2, detected in cell homogenate preparation. hRyR2 bands are 565 kDa in size, indicated by comparison to 250 kDa protein marker. After reprobing with vinculin antibody (right image), the blot contains some RyR2 remnant bands. L refers to ladder. Original and additional Western blots are found in **Appendix I**. *B.* Anti-GFP signal was normalized to the equivalent vinculin signal (117 kDa). Densitometric analysis of the 100 µg expression levels of WT and mutant hRyR2 preparations revealed that N4104K signals were significantly higher. Data were analysed by one way ANOVA with Bonferroni Posthoc test in GraphPad Prism, $p < 0.05$, n=6 experiments.

3.3.2 Does CPVT1 mutation alter the expression of SERCa in HEK293 cells expressing hRyR2?

Expression of SERCa was also determined for WT and mutant hRyR2 homogenate preparations by Western blotting (**Figure 3.8**) as an alteration in expression of SERCa may account for altered Ca^{2+} release kinetics observed in hRyR2-transfected HEK293 cells. This isoform of SERCa is SERCa1 not SERCa2a, as the cardiac isoform is not present in HEK293 cells (Tong, McCarthy, et al. 1999; Tong, Du, et al. 1999). In the assessment of vinculin expression as a loading control, bands were very close together (the molecular weight of SERCa and vinculin is ~109 kDa and ~117kDa, respectively, **Appendix III**) and therefore β-tubulin was chosen instead with a molecular weight of ~50 kDa. This loading control cannot be used when assessing RyR2 expression due to the required separation for this high molecular weight protein. Attempts were made to use a gradient gel to visualize hRyR2 GFP expression and β-tubulin on the same Western blot, but they were unsuccessful (**Appendix IV**). Although electrophoresis was carried out for >6 hours, no GFP expression was present while β-tubulin was successfully probed. Band separation is much more visible between SERCa and β-tubulin on the same standard blot. Densitometric analysis when SERCa expression is normalized to β-tubulin follows the same pattern as when normalized to vinculin and although more pronounced, changes of mutant SERCa expression remain non-significant when compared to WT expression (**Figure 3.8 A and B**).

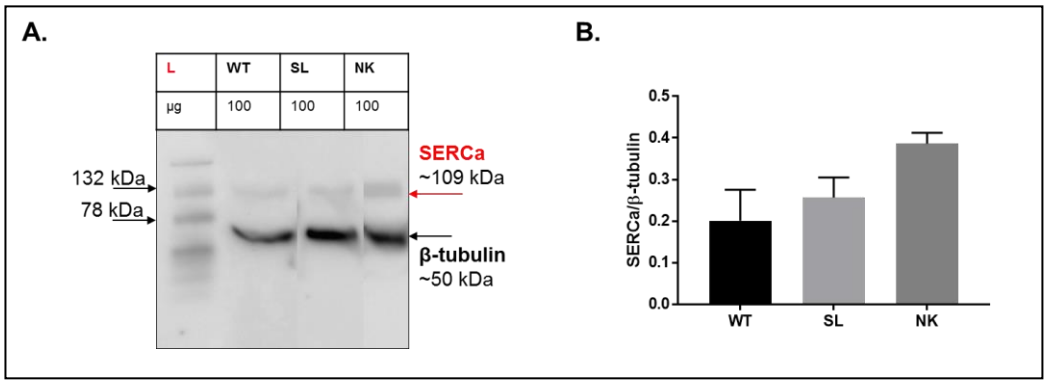

Figure 3.8 Endogenous HEK293 SERCa expression is not significantly altered after expression of mutant, as opposed to WT, eGFP-hRyR2. *A.* Representative bands of SERCa and β-tubulin protein. Bands are clearly separated. *B.*Densitometric analysis of SERCa expression normalized to β-tubulin expression, n=4 experiments, presented as mean ±SEM. No significant differences were detected in either analysis by one way ANOVA with Bonferroni posthoc in GraphPad Prism.

3.3.3 Do recombinant CPVT1-linked hRyR2 mutants undergo altered cellular trafficking or form functional release channels in a heterologous cell system?

The size and morphology of cells expressing mutant hRyR2 channels were indistinguishable from those expressing WT hRyR2, which is consistent with previous studies (Wehrens et al. 2003; N. L. Thomas et al. 2004; George, Higgs, et al. 2003).

Fluorescence colocalization analysis was used to determine whether an Alexa^{546} conjugated antibody to the C-terminus of the hRyR2 protein (pAb-1093) and the N-terminal eGFP tag were observed in the same cellular compartment, thereby suggesting that the eGFP-hRyR2 protein is fully transcribed/translated and is intact (**Figure 3.9**). The 'lace-like' reticular pattern of these fluorescent signals suggests that the cellular compartment targeted is the ER (Porter et al. 1945).

The total co-incidence between eGFP fluorescence and immunolocalization via IF labelling of recombinant RyR2 was calculated by Manders overlap coefficient using ImageJ software (MANDERS et al. 1993)(Dunn et al. 2011). This calculates two values: the colocalization of pAb-1093 pixels to eGFP pixels, (red to green) and vice versa (green to red). A value closer to 1 indicates positive cooccurrence. The two calculated values can be different – for example, all red pixels may overlap green pixels, but green pixels may appear alone in a region where no red signal is present (Adler and Parmryd 2012). High coefficient values would indicate the expression of intact, full-length recombinant hRyR2 within the ER, as pAb-1093 binds to RyR2 at residues 4455-4474 of the C terminus.

Colocalization of green to red gave coefficients between 0.8844-0.9083 and colocalization of red to green gave lower coefficients of 0.6830-0.7536, although no significant differences between colocalization of WT and mutant hRyR2 constructs were detected by one way ANOVA. This is suggestive that while some red antibody signal was identified without eGFP (i.e. that some hRyR2 channels were degraded from the N-terminus), this was comparable for WT and mutant constructs, indicating that mutation does not affect hRyR2 trafficking.

Transfected cells expressing hRyR2 were easily identified by their caffeine-induced Ca^{2+} release, with a sharp increase in Fluo-3 signal amplitude after caffeine addition

(10 mM) and no further Ca^{2+} release events. This signified the expression of functional hRyR2 channels within the HEK293 cell and is shown in **Figure 3.10 A**. This figure also demonstrates that untransfected HEK293 cells do not exhibit a caffeine-induced response (**C**), confirming the lack of functional RyR in these cells as previously reported (Tong, McCarthy, et al. 1999). The ER Ca^{2+} content, measured by determining the amplitude of the Ca^{2+} transient induced by application of caffeine (10 mM), was calculated as described in **Section 3.2.3.4,** (see **Appendix V** for scatter plot)**.**

Figure 3.11 B. shows that the ER Ca^{2+} content was not significantly altered by the expression of either mutant compared to that of WT hRyR2, suggesting that any heterogeneity in channel dysfunction did not result from a reduced Ca^{2+} store.

Calculation of the percentage of cells exhibiting eGFP fluorescence following Effectene-mediated transfection demonstrated comparable efficiencies (22-37 %) for WT and mutant RyR2 constructs, with no significant difference following statistical analysis ($p>0.05$ by Kruskal-Wallis with Dunn's posthoc) (**Figure 3.15**).

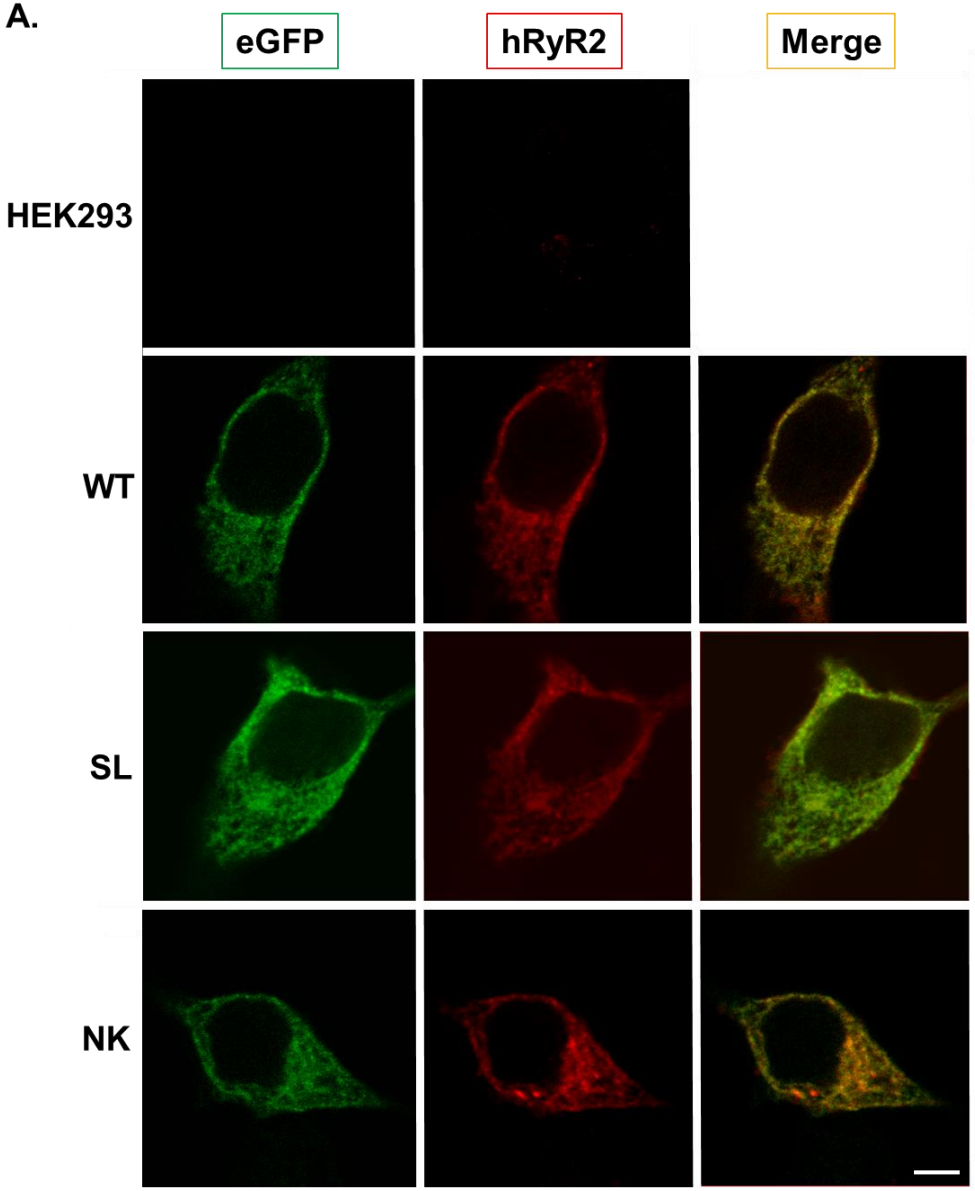

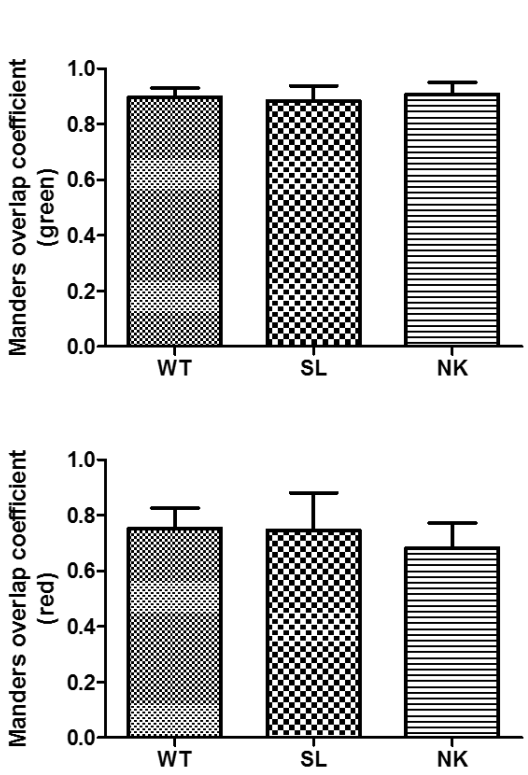

Figure 3.9 WT, S2246L and N4104K eGFP-hRyR2 constructs exhibit correct intracellular trafficking. HEK293 cells transfected with hRyR2 constructs were examined for eGFP fluorescence (ex. 488 nm, em. 525±25 nm, left images) and immunofluorescence of Alexa546 secondary antibody targeted to hRyR2 primary antibody pAb-1093 (em. 546 nm, ex. 572±30 nm, centre images). Colocalization (of green to red and red to green) was calculated by Manders overlap coefficient, with no significant differences calculated by one way ANOVA, n = 4-5 cells per construct. The scale bar represents 10 µm.

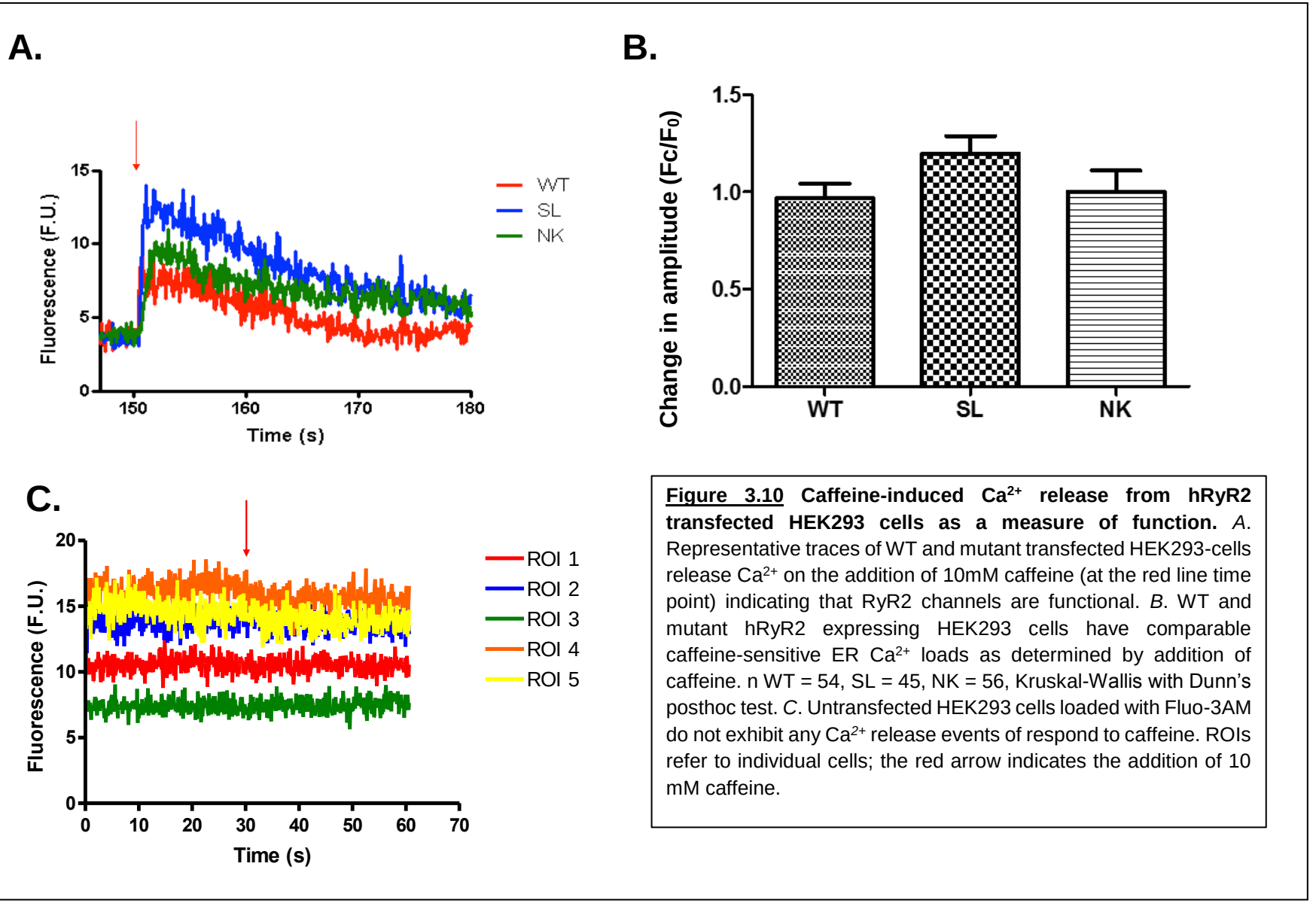

Figure 3.10 Caffeine-induced Ca^{2+} release from hRyR2 transfected HEK293 cells as a measure of function. *A*. Representative traces of WT and mutant transfected HEK293-cells release Ca^{2+} on the addition of 10mM caffeine (at the red line time point) indicating that RyR2 channels are functional. *B*. WT and mutant hRyR2 expressing HEK293 cells have comparable caffeine-sensitive ER Ca^{2+} loads as determined by addition of caffeine. n WT = 54, SL = 45, NK = 56, Kruskal-Wallis with Dunn's posthoc test. *C*. Untransfected HEK293 cells loaded with Fluo-3AM do not exhibit any Ca^{2+} release events of respond to caffeine. ROIs refer to individual cells; the red arrow indicates the addition of 10 mM caffeine.

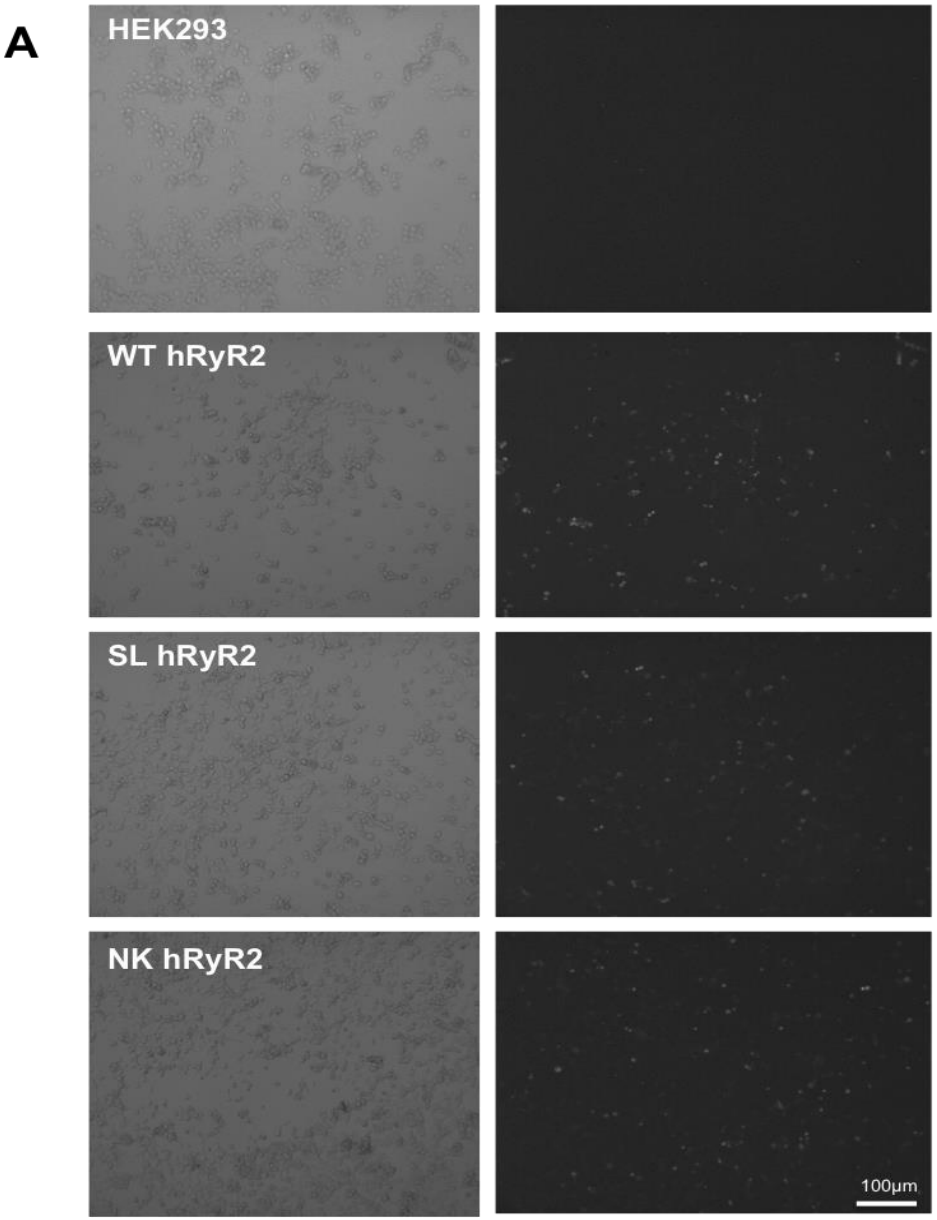

Figure 3.11 Expression of WT or mutant eGFP-hRyR2 in HEK293 cells following Effectene-mediated transfection. *A.* Bright field (left) and fluorescence (right) images of transfected cell populations. Untransfected HEK293 cells do not exhibit eGFP fluorescence. *B.* Transfection efficiencies of each hRyR2 construct using the Effectene reagent were comparable, with no statistically significant difference (Kruskal-Wallis with Dunn's posthoc, $p>0.05$). The total number of transfections for each hRyR2 construct: WT n=8, SL n=7, NK n=6. Transfection efficiency was calculated by comparing the total number of cells in the bright field of view to the total number of cells visible under fluorescence.

3.3.4 Is Ca^{2+} imaging data normally distributed?

The D'Agostino-Pearson test for normality was used by the GraphPad Prism software. This 'omnibus K2' test calculates skewness and kurtosis, calculating how far a distribution is from Gaussian normality in terms of shape and symmetry, giving a single P value from the sum of discrepancies for these values. If the given p value is less than 0.05, deviations from normal Gaussian distribution are statistically significant. (D'Agostino 2005). The following table (**Table 3.4**) shows such values for the Ca^{2+} imaging data acquired (shown in **Section 3.3.5**).

Ca^{2+} oscillation event parameters	**WT**	**S2246L**	**N4104K**
Amplitude	0.0015	0.0086	<0.0001
Duration	<0.0001	<0.0001	0.0001
Inter-event duration	<0.0001	<0.0001	<0.0001
Frequency	0.0002	0.0267	0.0113
Rate up	<0.0001	<0.0001	<0.0001
Rate down	<0.0001	<0.0001	0.0063

Table 3.4 Tests for normality of Ca^{2+} imaging data show that distribution is not normal. n WT=164, n SL=109, n NK=97. D'Agostino-Pearson test, p<0.05 is significantly different to normal Gaussian distribution, indicated with red font.

Within each parameter, all groups have data that are not normally distributed (**Table 3.4**). Although parametric tests are not very sensitive to deviations from normality, the assumption cannot be made when the set so clearly deviates from Gaussian distribution; therefore it is most appropriate to use non-parametric test equivalents when comparing groups i.e. Kruskal-Wallis tests with Dunn's posthoc, as opposed to one way ANOVA with Bonferroni correction (Lix et al. 1996; Harwell et al. 1992; Glass et al. 1972). All analysis of Ca^{2+} imaging data within this Chapter uses Kruskal-Wallis tests where appropriate. For a comparison of the statistical analysis between parametric and nonparametric tests, see **Appendix IV**.

Post-hoc power analysis tests were also conducted using G*Power*3.19.2 software (**Table 3.5**, www.gpower.hhu.de) to determine whether appropriate numbers of experiments were completed, and to confirm that where differences were determined non-significant, this was not a product of lower power. All studies were calculated using this method as highly powered. However, amplitude and inter-event duration appears lower powered compared to other parameters in analysis of S2246L HEK293 cells, even though this is above a suitable

threshold for detecting differences in the data (Beck, 2013). When considering the total number of cells observed in the experiments, as opposed to the number of oscillating cells only, post-hoc analysis shows that power increases to >99 %. It is therefore reasonable to suggest that the number of samples for each group was more than adequate for detecting differences between groups.

Ca^{2+} oscillation event parameters	**S2246L vs WT**	**N4104K vs WT**
Amplitude	80 %	99 %
Duration	>99 %	>99 %
Inter-event duration	83 %	99 %
Frequency	98 %	98 %
Rate up	>99 %	>99 %
Rate down	97 %	>99 %

Table 3.5 Posthoc power analysis of Ca^{2+} imaging data. All experimental groups have power of >80 %, calculated with G*Power*3.19.2 software (Faul et al. 2009). n WT=164, SL=109, NK=97.

3.3.5 Do mutant hRyR2 channels exhibit heterogeneity in their spontaneous Ca^{2+} release?

SOICR-events in hRyR2-transfected HEK293 cells were observed in calcium-containing external solution (KRH buffer containing 1.3 mM Ca^{2+}), which were not observed in untransfected HEK293 cells in accordance with Jiang et al (2004).

The number of cells that exhibited a response to Ca^{2+} or caffeine (black column in **Figure 3.12**) within this system was generally equivalent to the number of cells expected to respond as calculated by transfection efficiency (grey column) for both WT and N4104K hRyR2 transfected cells, suggesting that expression is closely correlated with function. However, the number of caffeine-responsive S2246L transfected cells was found to be significantly lower than anticipated by the determined S2246L transfection efficiency ($p<0.05$ by Mann Whitney U test). This was also significantly lower than the number of WT caffeine-responsive cells ($p<0.05$ by Kruskal-Wallis and Bonferroni posthoc test). Although most caffeine-sensitive cells exhibited oscillatory Ca^{2+} release events, some did not (~2%).

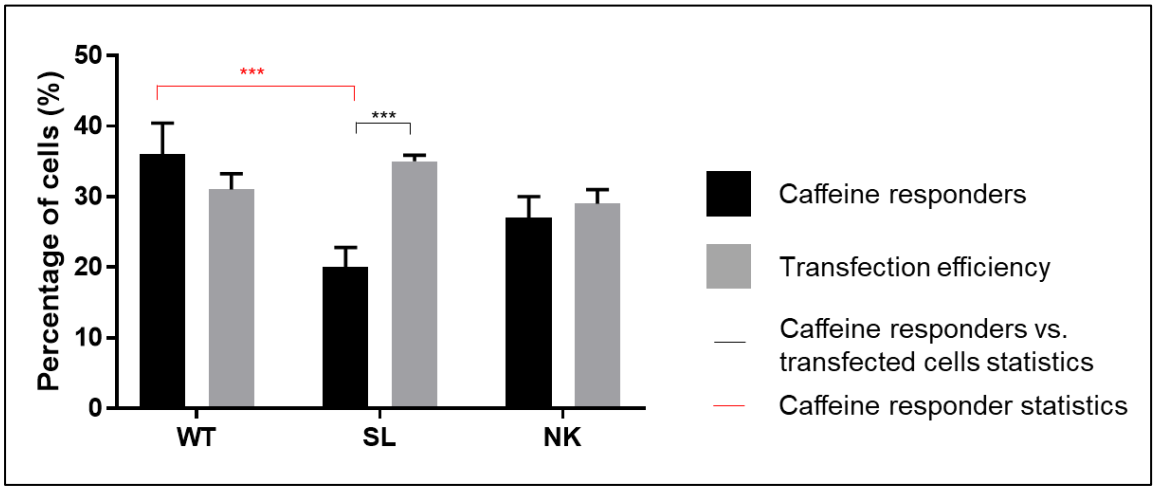

Figure 3.12 Comparison of percentage of caffeine responsive cells vs the percentage of expected responders, as calculated by transfection efficiency. Differences between the parameters was calculated by Mann Whitney in GraphPad Prism, $p<0.05$. S2246L hRyR2 transfected cells responded to calcium or caffeine significantly less than expected. Total number of cells n WT =1003, SL=1274, NK=981. Number of transfections n WT=6, SL=7, NK=4.

The propensity for SOICR events was determined and found to be significantly decreased in S2246L hRyR2 transfected cells in comparison to WT (**Figure 3.13**, $p<0.05$ by one way ANOVA with Bonferroni posthoc). Cells expressing N4104K hRyR2 were not found to have a significantly different propensity, in contrast to work by Jiang et al (2004 and 2005). Changes in propensity were not due to altered transfection efficiency, as these were comparable.

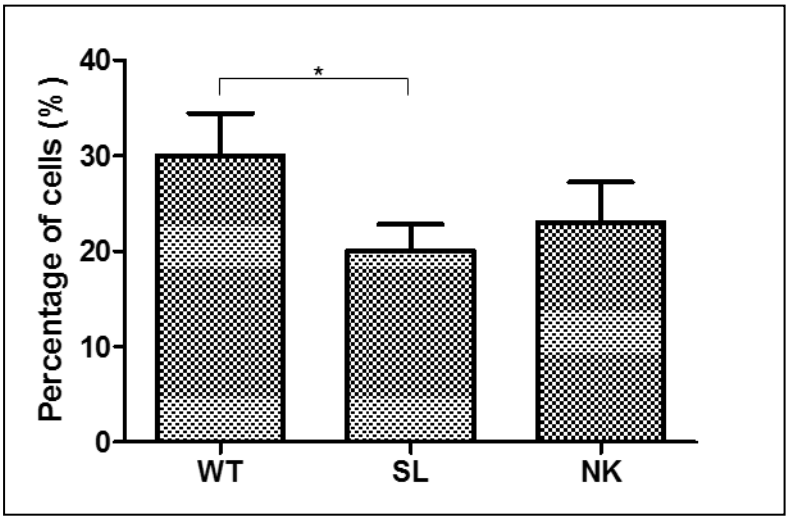

Figure 3.13 Propensity of transfected HEK293 cells for Ca^{2+} release – S2246L transfected cells have a decreased propensity. Data displayed as mean percentages ± SEM. Total number of transfections n WT=8, SL=7, NK=6. Analysis by Kruskal-Wallis with Dunn's posthoc in GraphPad Prism, $p<0.05$ is indicated on the graph by *. The propensity for calcium release was significantly decreased in HEK293 cells expressing S2246L hRyR2.

As illustrated in **Figure 3.14,** representative traces for WT and mutant-expressing HEK293 cells appear markedly different from one another, with altered Ca^{2+} handling. An in-depth analysis of Ca^{2+} oscillation events is presented as a series of bar graphs in **Figure 3.15**, with Ca^{2+} handling kinetic parameters calculated as described in **Section 3.2.3.4** with SALVO analysis software. Scatter plots showing the spread of these data can be found in **Appendix V**.

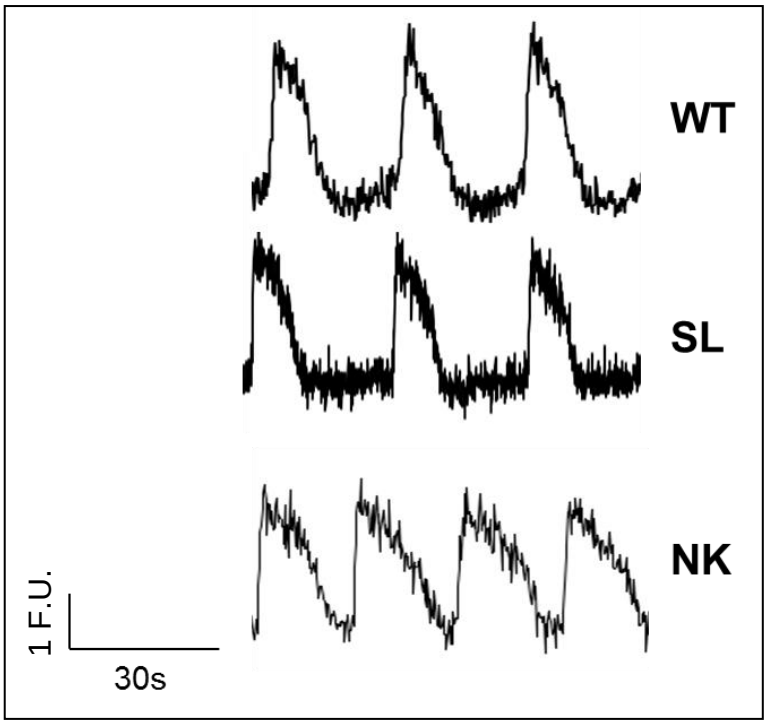

Figure 3.14 Representative traces of spontaneous Ca^{2+} release events in WT and mutant hRyR2 expressing HEK293 cells, measured by changes in Fluo-3 Ca^{2+} dye fluorescence. Representative traces indicate that there may be differences in Ca^{2+} release dynamics between mutant and WT expressing cells, with S2246L RyR2 expressing cells appearing to exhibit less frequent release events in the same period as N4104K and WT RyR2 expressing cells.

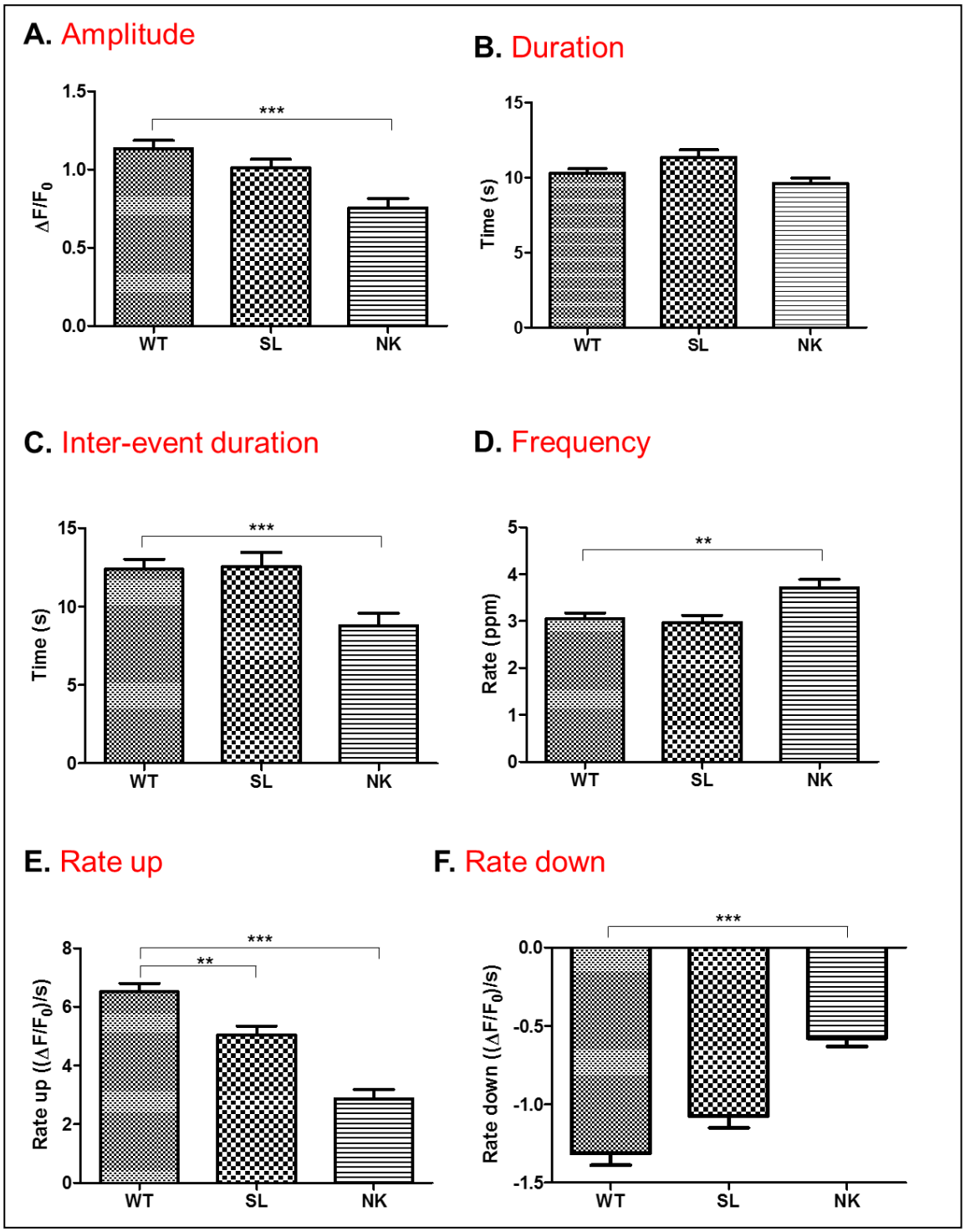

<u>Figure 3.15</u> Assessment of the spontaneous Ca^{2+} release events in HEK293 cells expressing WT or mutant hRyR2. All parameters were calculated as described in Section 3.2.1.4. n WT=164, SL=109, NK=97 cells. Data are presented as mean ± SEM, p<0.01 is denoted by **, p<0.001 by ***, as calculated by Kruskal-Wallis with Dunn's posthoc analysis with GraphPad Prism. Scatter plots of this data are found **Appendix V**.

The S2246L mutation only results in an alteration in the rate up of an oscillation in comparison to WT, which appears significantly decreased (**Figure 3.15, E**). N4104K transfected cells also have a decreased rate up, but also exhibit many other changes in comparison to WT. This includes a decreased Ca^{2+} oscillation amplitude (**Figure 3.15, A**), a decreased inter-event duration and rate down (**Figure 3.15, C** and **F** respectively), as well as an increased frequency (**Figure 3.15, D**)). **Table 3.6** summarizes the differences in calcium handling parameters between WT and mutant RyR2 transfected HEK293 cells.

Ca^{2+} oscillation event parameters	**WT**	**S2246L**	**N4104K**
Amplitude	1.133 ± 0.05	1.011 ± 0.05	0.7556 ± 0.06
Duration	10.29 ± 0.30	11.35 ± 0.50	9.611 ± 0.35
Inter-event duration	12.38 ± 0.64	12.56 ± 0.89	8.773 ± 0.81
Frequency	3.047 ± 0.13	2.975 ± 0.15	3.709 ± 0.18
Rate up	6.510 ± 0.29	5.042 ± 0.30	2.861 ± 0.33
Rate down	-1.313 ± 0.07	-1.076 ± 0.07	-0.578 ± 0.05

Table 3.6 Summary of Ca^{2+} handling parameters in transfected HEK293 cells. Mean values for calcium handling parameters of WT and mutant hRyR2-expressing HEK cells, ± SEM. Red indicates a statistically significant increase compared to the equivalent parameter in WT hRyR2-expressing HEK293 cells, whereas blue indicates a statistically significant decrease, (Kruskal-Wallis with Dunn's post hoc test, $p<0.01$).

3.4 Discussion

Loaiza et al (2013) recently demonstrated that a CPVT1 mutant (V2475F) exhibited a pronounced gain-of-function in [^{3}H] ryanodine binding and single channel assays, but displayed a similar external Ca^{2+} threshold to WT for spontaneous Ca^{2+} release. This is suggestive that the measurement of propensity and incidence of Ca^{2+} release alone is not sufficient in explaining mutant channel dysfunction. Rather than evaluating the incidence of spontaneous Ca^{2+} release as a function of extracellular Ca^{2+} concentration, the parameters of Ca^{2+} release themselves were investigated in this project. It is apparent that kinetics of Ca^{2+} release events of N4104K are significantly different (in comparison to WT) within the HEK293 cell expression system and that mutant channels appear functionally heterogeneous within this assay. Kinetics of Ca^{2+} release events of S2246L are comparable to WT, but the rate up is different by a small but significant margin. Examining the spontaneous Ca^{2+} release events of CPVT1 mutant hRyR2 channels in HEK293 cells therefore appears to be an effective technique to reveal differences in Ca^{2+} release kinetics and functional heterogeneity that has been indicated at the single channel level caused by different hRyR2 mutations.

Major chapter findings include:

- Mutant hRyR2 constructs traffic to the ER correctly but have different expression levels in HEK293 cells, which affects analysis of Ca^{2+} handling kinetics
- Assessment of Ca^{2+} release kinetic parameters of hRyR2-transfected HEK293 cells reveals functional heterogeneity of mutant hRyR2 channels
- The S2246L mutation does not appear as a ‘gain-of-function’ mutation in this heterologous cell system

3.4.1 Both mutant hRyR2 constructs traffic to the ER in HEK293 cells, but have different expression levels

Visualization of recombinant hRyR2 using eGFP fluorescence or immunofluorescent detection via anti-RyR antibodies revealed high co-incidence (**Figure 3.10**) indicating the expression of full-length hRyR2 within the ER of HEK293 cells.

In calculations of Mander's overlap coefficients, colocalization of red to green gave lower coefficients in comparison to colocalization of green to red, although no significant differences between WT and mutant hRyR2 constructs were detected by one way ANOVA. This observation of N-terminus degraded hRyR2 channels (hence isolated red antibody signal) could be contributed to the action of calpain cleavage. Calpains are Ca^{2+}-dependent cysteine proteases expressed ubiquitously in mammals and generate a characteristic ~400 kDa proteolytic fragment after cleavage at an N-terminal site (Pedrozo et al. 2010; Zissimopoulos et al. 2013). Evidence of this fragment can be observed in many Western blot experiments presented in this thesis, as a strong band below that of hRyR2 protein (see **Appendix I, VIII-XII, XX and XXV**).

Transfection efficiencies of WT and mutant hRyR2 constructs were reproducible and comparable (**Figure 3.11**). However, it was important to assess the expression of mutant hRyR2 constructs within HEK293 cells in comparison with WT via Western blotting, as this may have influenced Ca^{2+} handling. It was revealed that N4104K hRyR2 expression in HEK293 cells was significantly increased in comparison to WT (**Figure 3.7**). An altered expression level of mutant RyR2 channels in this system is in contrast to some studies (N. L. Thomas et al. 2005; Cheung et al. 2015), but is observed in others (Guo et al. 2016). Specifically, N4104K RyR2 has been previously reported to have an equivalent expression level in HEK293 cells to that of WT transfect cells (D. Jiang et al. 2004). The recombinant RyR2 construct used by Chen's group is mouse recombinant cDNA however, as opposed to a recombinant human construct as used within this project. It is very difficult to speculate as to why N4104K hRyR2 expression is increased in HEK293 cells in comparison to WT hRyR2. This could be an artefact of the heterologous expression system or the method of normalization used, or may be a direct effect of mutation on protein turnover in the cell.

3.4.2 Functionality, as measured by spontaneous Ca^{2+} oscillation and caffeine-induced Ca^{2+} release, does not tally with expression for S2246L

To confirm expression of functional hRyR2 channels after transfection, caffeine (10mM) was added at the end of every Ca^{2+} imaging experiment, resulting in a large Ca^{2+} transient, followed by no further spontaneous Ca^{2+} oscillations, indicating depletion of the store through release via functional hRyR2 channels (**Figure 3.9**). Both WT and mutant-transfected HEK293 cells release Ca^{2+} after application of caffeine, indicative of functional RyR2 channels that undergo appropriate regulation and can operate in this setting. This also confirms that the N-terminal eGFP tag of the RyR2 construct does not interfere with channel function in agreement with previous studies (Hiess et al. 2015; George, Higgs, et al. 2003; N. L. Thomas et al. 2004; Liu et al. 2005; Zhang et al. 2003).

Interestingly, there was a discrepancy between the percentage of S2246L hRyR2-transfected cells exhibiting eGFP fluorescence and the percentage of cells which displayed caffeine-induced Ca^{2+} release, whereby the latter was significantly decreased (**Figure 3.12**). This was also reflected in a decreased propensity for spontaneous Ca^{2+} release events (**Figure 3.13**). Although channels may be present in HEK293 cells with the eGFP tag, there are less functional channels. This could indicate that the S2246L mutation is fundamentally affecting channel function. Interestingly Jiang et al. (2005) reported that a greater fraction of S2246L-expressing cells displayed Ca^{2+} oscillations as compared with WT cells, with similar findings in the study of N4104K (D. Jiang et al. 2004). This is contrary to the findings presented in this chapter, where the propensity of S2246L-transfected cells to release Ca^{2+} was significantly lower than those expressing WT hRyR2 and there were less responders than anticipated for the S2246L mutant construct compared to the calculated transfection efficiency than WT. No significant change in the propensity of N4104K-transfected cells was detected, contrary to previous reports. Power calculations indicate that these findings are robust (<99% power for each parameter, see **Table 3.5**) and n numbers are higher than those in the aforementioned studies (n WT=1003, SL=1274, NK=1405 vs. Jiang 2004/2005: n WT=563, SL=unclear (described as 3-7 experiments), NK=327).

Given that a caffeine responsive is indicative of functional hRyR2 channels within a HEK293 cells and as expected, the percentage of cells that exhibit spontaneous Ca^{2+}

release events tallies closely with the percentage of cells that exhibit caffeine-induced Ca^{2+} release (**Figure 3.12** and **Figure 3.13**), caffeine-induced Ca^{2+} release can be used in future chapters as a marker of propensity.

3.4.3 Store load and SERCa expression remains unaltered after transfection of HEK293 cells with hRyR2 constructs

It was also important to explore the possibility that the expression of SERCa may have been altered in this system. SERCa cycles Ca^{2+} back into the ER in a HEK293 cell after release into the cytoplasm, so any expression changes caused by transfection of a mutant hRyR2 plasmid need to be considered. Assessment by Western blotting and densitometry, however, found no significant changes in SERCa expression for over expression of mutant vs WT hRyR2 (**Figure 3.8**). This is in line with work of Thomas et al. (2005), SERCa expression of WT and mutant hRyR2-transfected HEK293 cells was normalised to that of untransfected HEK293 cells, with no significant differences observed. Although the trend appears that in N4104K transfected cell SERCa expression is increased, this was not shown to be significant by one way ANOVA, with n =4-6. This therefore suggests that any changes in Ca^{2+} release kinetics are due to mutant hRyR2 expression alone. Caffeine-sensitive ER Ca^{2+} loads were also calculated as comparable between WT and mutant hRyR2-transfected HEK293 cells, which further suggests that SERCa levels are equivalent (see **Figure 3.6**).

In a cardiomyocyte, phosphorylation and upregulation of PLB could also be implicated in Ca^{2+} release – changes in expression or function will in turn modulate SERCa, increasing Ca^{2+} re-entry into the store. However, PLB expression has been shown not to express in HEK293 cells (Kurzydlowski 1996; Asahi et al. 2003; Toyofuku et al. 1994), therefore the expression of this protein was not investigated in this project.

Estimation of ER Ca^{2+} content, calculated by the amplitude of caffeine-induced Ca^{2+} release in transfected HEK293 cells, showed that there was no significant difference between WT and mutant hRyR2 expressing cells (**Figure 3.11**). This is in agreement with other studies of mutant RyR2 channels in this system (N. L. Thomas et al. 2004) (Loaiza et al. 2013; George et al. 2006), but not with others (D. Jiang 2005; D. Jiang et al. 2004; D. Jiang et al. 2007). Specifically, D. Jiang et al (2004) showed that

HEK293 cells expressing N4104K or two other I-domain CPVT1 mutants R4496C and N4895D had a decreased Ca^{2+} store content as compared to WT cells.

Direct and time resolved measurements of free Ca^{2+} in the SR/ER have become much more desirable since the emergence of the pathological importance of the store (Niggli 2016). The application of the RyR2 agonist caffeine as described within this chapter allows an estimate of ER Ca^{2+} by recording the amplitude of the subsequent Ca^{2+} transient. This method has been used widely (D. Jiang et al. 2007; Loaiza et al. 2013; George et al. 2006; D. Jiang 2005) but is not without limitation; it is an indirect static measurement that can be rendered inaccurate by Ca^{2+} release events occurring before caffeine application (Fernández-Velasco et al. 2009). Therefore, while the addition of caffeine at 150 sec for each experiment maintained consistency, the application would not have been at the same point in a Ca^{2+} oscillation, a time point that would have been impossible to predict. This could therefore explain the discrepancies seen between some papers in the relative store load in WT of mutant RyR2-expressing HEK293 cells. There is also evidence that HEK293 cells expressing recombinant RyR have a functionally compartmentalized ER Ca^{2+}store, which consists of a significant caffeine-insensitive component (Tong, McCarthy, et al. 1999). It would be advantageous to utilize chemical low affinity Ca^{2+} indicators (such as Fluo-5N) to quantify the changes of free Ca^{2+} in the ER directly (Kubalova et al. 2005; Brochet et al. 2005; Shannon et al. 2003), but this will not give an estimate of the total Ca^{2+} in the store, nor does this method come without drawbacks, with cytosolic indicator dye contamination and the physically small volume of the ER an issue (Fernández-Velasco et al. 2009). A genetically encoded Ca^{2+} indicator such as D1ER could also alleviate the uncertainty of ER Ca^{2+} measurements – this construct signal is ratiometric, permitting single-cell resolution without quenching and the potential to monitor Ca^{2+} simultaneously in both the ER and the cytosol when used in conjunction with another high-affinity Ca^{2+} indicator (Palmer et al. 2004).

3.4.4 Assessment of Ca^{2+} release kinetic parameters in hRyR2-transfected HEK293 cells reveals that S2246L mutants are similar to WT, while N4104K mutants are dysfunctional

HEK293 cells transfected with S2246L hRyR2 exhibited no change in frequency of spontaneous Ca^{2+} release events (**Figure 3.14 D**). This is in contrast to work with stable-inducible HEK293 cells transfected with S2246L RyR2, which displayed increased frequency and a decreased amplitude of Ca^{2+} oscillations, as well as an overall decreased ER Ca^{2+} load (D. Jiang 2005). These data challenge both the hypothesis that this mutation is 'gain-of-function' and the mechanism of dysfunction described by Jiang et al. (2004). If frequency of events was the only measure of dysfunction and this dysfunction is caused by increased luminal Ca^{2+} sensitivity, the S2246L hRyR2 mutation could not be classified as such. One would assume this mutation is barely dysfunctional if the only change recorded is that the rate up decreases in comparison to WT. Expression and function do not tally in the same way as in WT hRyR2-transfected HEK293 cells as discussed above.

Detailed interrogation of Ca^{2+} handling kinetics reveals only a decreased rate up of Ca^{2+} release. This therefore could suggest that the channel opening is at a significantly slower rate than WT, but channels must compensate for that during the release period, as inter-event duration remains unaltered. This change in kinetics could be due to altered individual channel activation, or also an altered distribution of mutant channels within the cell. Less dense clustering of S2246L-hRyR2 channels in the ER would mean less Ca^{2+} release event propagation across the population. However, increased clustering of RyR2 has previously been evidenced in spontaneously hypertensive rats with heart failure {Chen-Izu:2007hm}. Clustering of RyR2 channels in disease is discussed further in **Section 4.1.1**.

As illustrated in **Figures 3.14 and 3.15**, spontaneous Ca^{2+} release events in cells expressing N4104K hRyR2 were found to be markedly different to S2246L and WT hRyR2. Expression of this mutant led to altered kinetics of Ca^{2+} release. The rate up of Ca^{2+} release was significantly decreased, the rate down significantly decreased and the inter-event duration in turn also decreased. This explains increased frequency and the altered shape of Ca^{2+} transient in comparison to S2246L hRyR2 expressing cells. This may suggest that N4104K hRyR2 channels have difficulty shutting down, with the total duration of Ca^{2+} release remaining equivalent to WT,

similar to S2246L hRyR2 expressing cells. RyR2 channels may also be in denser clusters within the ER as expression calculated by Western blotting is significantly increased in comparison to WT. The time taken to stop CICR would therefore be decreased, meaning Ca^{2+} release events could repeat more quickly, hence the increased frequency reported here, in line with previous SOICR studies of HEK293 cells (D. Jiang et al. 2004)

It could be that the density of channel clustering is altered, or also that sensitivity to Ca^{2+} concentration (luminal, cytosolic, or both) is changed. The EF hand domain is the location of the N4104K mutation and has the highest number of CPVT1 mutations per number of residues, as highlighted in **Figure 1.5**. In a recent publication investigating the effect of mutations in the EF-hand motif or deletion of the entire domain, unaltered Ca^{2+}-dependent activation of [^{3}H] ryanodine binding and cytosolic Ca^{2+} activation in single channel experiments was reported (Guo et al. 2015). Furthermore, mutations studied appeared to raise the threshold for SOICR termination. Chen and colleagues therefore suggested that the EF-hand is not required for RyR2 activation by cytosolic Ca^{2+}, but plays an important role in luminal Ca^{2+} activation and SOICR. It is important to note however, that N4104K is outside of the domain that Chen and colleagues label as the EF hand (residues 4036-4082) and therefore may explain why, in single channel experiments in preliminary data, N4104K RyR2 channels display a fundamental gating defect, whereby the channel opens in a minimal experimental system devoid of agonist.

After RyR2 channel activation, Ca^{2+} release from the store is terminated, at least in part due to the effect of the reduced Ca^{2+} levels within the store after release (Terentyev 2008). This refractory period of Ca^{2+} signalling allows Ca^{2+} released into the cell to be sequestered back into the store, ready for release in the next cycle (Belevych et al. 2012). While one could suggest that the decreased inter-event duration in fact shows a decreased refractory period of Ca^{2+} release, it must be considered, however, that the data presented in this chapter have been obtained from resting, non-stimulated cells, in an expression system lacking endogenous accessory proteins such as CSQ2 that contribute to any refractory period.

While assessment of Ca^{2+} release kinetic parameters reveals differences in this setting, it remains that the data is difficult to interpret while we do not have data on Ca^{2+} fluxes across the membrane (Trafford et al. 2000).

3.4.5 Does functional heterogeneity in single channel recordings relate to observations in HEK293 cells?

Observations at the single channel level provided as preliminary data for this project by Dr N.L. Thomas demonstrated that in contrast to N4104K, S2246L channels did not show significantly more unliganded openings than the WT hRyR2 channels in the absence of other activatory ligands. This is in line with previous single channel analysis which found that under basal conditions, S2246L RyR2 exhibited normal single channel properties, indistinguishable from WT (Wehrens et al. 2003). This is unsurprising when CPVT1 patients do not present with symptoms at rest (Priori 2002). Interestingly, in Ca^{2+} imaging assays, S2246L hRyR2-expressing HEK293 cells in fact appeared to have unchanged frequency of spontaneous Ca^{2+} release oscillations in comparison to WT (**Figure 3.14, B**) contrary to previous reports (D. Jiang 2005). Within the HEK293 expression system, S2246L hRyR2 channels, much like in preliminary single channel data, appear to behave very similarly to WT.

Another observation from single channel data is that N4104K exhibit unliganded channel openings in the absence of activating ligand (**Figure 3.4**). This is therefore indicative of an intrinsic structural defect within the channel, which impairs the correct response to Ca^{2+}. This is somewhat reflected within HEK293 cells, as N4104K RyR2 transfected cells exhibit altered rates of Ca^{2+} release within an oscillation cycle, suggestive of channel defects in the response to cytosolic or luminal Ca^{2+} concentrations.

Both methods of functional characterization have their merits and drawbacks (see **Section 3.1**), but in conjunction with one another reveal functional heterogeneity of RyR2 CPVT1 mutations, in contrast to previous reports. There may not be a straightforward unifying mechanism of dysfunction, which therefore has consequences for therapeutic targeting of dysfunctional RyR2. This work has clearly shown investigation of RyR2 within a heterologous cell expression system can reveal dysfunction that is mirrored in single channel analysis.

3.4.6 Why doesn't S2246L appear as a gain-of-function mutation in HEK293 cells?

Within the single channel data presented in this chapter, it is impossible to distinguish dysfunction of the S2246L RyR2 channel. Without detailed interrogation of Ca^{2+} handling in HEK293 cells, it is also difficult to discern how channel function may be altered, with a frequency of spontaneous Ca^{2+} release unaltered compared to WT transfected cells, even though it is classically defined as a gain-of-function mutation. Even under more detailed interrogation of Ca^{2+} release kinetics, only the rate up of Ca^{2+} release is altered in comparison to WT. The channels appear to therefore function in a comparable way to the WT in this system. However, it also remains that Ca^{2+} release kinetics remain difficult to interpret in this system as there is no data on Ca^{2+} fluxes across the membrane (Trafford et al. 2000).

RyR2 channels also undergo posttranslational modifications within the cardiomyocyte (Niggli et al. 2013), as discussed in detail in **Section 1.4 and 1.5**. S2246L dysfunction has only been reported as apparent after treatment with PKA (Wehrens et al. 2003; Lehnart et al. 2004), which would stimulate posttranslational phosphorylation of the channel. It could therefore be reasoned that S2246L may appear as WT without PKA phosphorylation. The central domain mutation R2267H in the work of Tester et al. (2007) shows normal function under basal conditions in comparison to WT. However, phosphorylation uncovers RyR2 channel dysfunction, whereby R2267H activity is significantly increased after phosphorylation by PKA in comparison to WT channels treated in the same way. This aids in the explanation of functional heterogeneity of the two mutant RyR2 channels studied within this project. It may be that S2246L is analogous to R2267H in the work of Tester et al., requiring activation under stress conditions and channel phosphorylation before dysfunction becomes apparent. Notably, both mutations are located in the CPVT1 mutant 'hotspot' central domain of the RyR2 polypeptide. Work of the Marks group has investigated the effects of PKA on S2246L within single channel experiments, finding that phosphorylation significantly increased P_o and gating frequencies in comparison to PKA phosphorylated WT channels (Wehrens et al. 2003). These finding also support the clinical observation that patients carrying CPVT1 mutations do not present with arrhythmogenic activity unless exposed to factors associated with increased sympathetic activity.

It may also be that N4104K channel activity is analogous to that of S4565R, both mutations also located in the same domain. N4104K as evident in preliminary single channel data displays augmented Ca^{2+} release even without activatory ligand; S4565R shows enhanced channel activity at basal conditions (Tester et al. 2007). The sensitivity of these channels at basal was in fact similar to PKA-treated WT channels. In light of this, it could be hypothesized that N4104K RyR2 channels will not therefore exhibit significant functional differences after phosphorylation, whereas S2246L will, revealing the classic gain-of-function phenotype that has not been observed in HEK293 cells. Investigating the role of phosphorylation on RyR2 mutant channel function will allow not only a deeper appreciation of CPVT1 disease phenotype and mechanism, but offer an explanation for functional heterogeneity. This therefore leads on to my next results chapter, in elucidating the effects of phosphorylation of both WT and mutant RyR2 channels.

Chapter 4

The influence of phosphorylation at the S2808 and S2031 sites on WT and CPVT mutant hRyR2 function

4.1 Introduction

4.1.1 Phosphorylation of RyR2 in CPVT1

Abnormal phosphorylation of RyR2, leading to defective Ca^{2+} release has not only been implicated in the pathogenesis of HF but also in that of CPVT1. As discussed in **Section 1.8.3**, the data of Tester et al. (2007) suggest that the response of mutant RyR2 channels to phosphorylation is altered, not only in comparison to WT channels but to each other. Few published studies have investigated the functional effects of CPVT1-linked mutant RyR2 channel phosphorylation, and those few focus mostly on the more controversial S2808 site.

According to Wehrens et al. (2003), in single channel studies of S2246L, R2474S and R4497C mutant RyR2, under basal conditions (cytosolic Ca^{2+} at 150 nM) all mutant channels exhibited single channel activity indistinguishable from that of WT channels. While PKA phosphorylation increased the activity (P_o) of both WT and mutant RyR2 single channels, the P_o of mutant channels was significantly increased in comparison to WT, indicating that CPVT1 mutant channels were more sensitive to activation by PKA phosphorylation. Only upon treatment with PKA was mutant channel dysfunction apparent in this study.

In an early investigation of the effect of β-adrenergic activation in HL-1 cells expressing mutant hRyR2 (George et al. 2003), using a pan-phosphoserine antibody, authors found that endogenous RyR2, WT and mutant hRyR2 were all phosphorylated to equivalent levels in untreated cells, as well as upon β-adrenergic stimulation with isoproterenol. Importantly, while Iso activation of the β-adrenergic cascade disrupted the RyR2:FKBP12.6 interaction in both WT and mutant hRyR2-expressing HL-1 cells, this extent of dissociation was equivalent. Hyperphosphorylation of RyR2 and RyR2:FKBP12.6 dissociation was proportional to the elevation in cAMP concentration on treatment with Iso. Mutants did however exhibit a left-shifted dose response of Ca^{2+} release to Iso as well as a significant increase in the duration of Ca^{2+} release events, in comparison to cells expressing WT hRyR2. While differential phosphorylation of mutants was not evidenced in this study, it could be the case that in stimulated cells, a differential sensitivity to equivalent phosphorylation may underpin abnormal Ca^{2+} release under such conditions. This data is also suggestive that selective dissociation of FKBP12.6 from CPVT1-linked hRyR2 mutants does not occur.

Ikemoto and Matsuzaki suggest that PKA-dependent phosphorylation induces defective inter-domain interactions between N-terminal and central domains in CPVT1-mutant RyR2 channels, leading to defective Ca^{2+} release (see **Section 1.7.4.2**, (Uchinoumi et al. 2010). In R2474S $^{(+/-)}$ RyR2 KI mice, the increase in phosphorylation level of S2808 of RyR2 after the addition of cAMP was equivalent to that of WT mice under the same conditions (Xu et al. 2010). The affinity of CaM binding to mutant RyR2 was reduced in response to cAMP (1 μmol/L) compared to that for the WT, but not before treatment. In WT hearts, CaM binding to RyR2 was unchanged in response to cAMP but decreased in the presence of peptide DPc10 (which mimics central domain mutations). Addition of this peptide didn't further decrease RyR2-CaM binding in cAMP treated R2474S KI hearts. The authors suggest that PKA phosphorylation at the S2808 site induces domain unzipping in CPVT1 mutant RyR2 but not WT RyR2, reducing the binding affinity of the channel for CaM. As CaM inhibits the activity of RyR2 channels at physiological concentrations of Ca^{2+} and is essential for normal channel function, reduced binding is suggested to cause spontaneous Ca^{2+} release and lethal arrhythmia seen in CPVT1 (Oda et al. 2005; Xu et al. 2010; Uchinoumi et al. 2010).

In more recent work of the Valdivia group, V2475F CPVT1 mutant RyR2 channels display multiple mechanisms of dysfunction (Loaiza et al. 2013) including an abnormal response to PKA phosphorylation in comparison to WT recombinant mouse RyR2 channels. Treatment of WT or V2475F RyR2 channels with the PKA catalytic subunit, increased the phospho-signal at the S2808 and S2031 sites. This is the only published study to investigate changes in phosphorylation at both PKA phosphorylation sites in CPVT-related RyR2 dysfunction. In measuring the Ca^{2+}-dependence of [^{3}H] ryanodine binding, the authors found that PKA phosphorylation did not change the Ca^{2+} sensitivity of WT channel activation but did exaggerate the abnormal sensitivity of V2475F for cytosolic Ca^{2+}. These data suggest that PKA phosphorylation of V2475F RyR2 exacerbates channel dysfunction, leading to uncontrollable Ca^{2+} release.

A study of RyR2-R2474S$^{(+/-)}$ mice suggested that interval treadmill exercise training could reduce VT by decreasing CaMKII-dependent phosphorylation of RyR2 (Manotheepan et al. 2016). Isolated cardiomyocytes from exercise-trained mice showed less diastolic SR Ca^{2+} leak and decreased phosphorylation at the CaMKII-specific S2814 site, compared to those from control mice. This further suggests changes in RyR2 phosphorylation level are associated with

dysfunction of mutant RyR2 channels and is also the only investigation of the CaMKII-specific S2814 phosphorylation site in a CPVT1 mutant.

Increased clustering of RyR2 has already been evidenced in a disease setting, in tandem with increased RyR2 phosphorylation at the S2808 site {Chen-Izu:2007hm}. In work of Asghari et al. (2014), dual-tilt electron tomography was utilized to produce views of dyads in rat ventricular myocytes. Treatment with a phosphorylation cocktail (10 µmol/l cAMP, 10 µmol/l 3-isobutyl-1-methylxanthine, 10 µmol/l okadaic acid, 0.5 µmol/l calyculin A and 1 µmol/l thapsigargin) moved RyR2 tetramers into a checkerboard configuration (see **Section 1.3.2**), while a concentration of Mg^{2+} (4 mmol/L) induced a dense side by side arrangement. A checkerboard association was also associated with a significant increase in Ca^{2+} spark frequency compared to control where RyR2 arrangement was mixed (Asghari et al. 2014). Increased hRyR2 channel clustering means an enhanced 'fire-diffuse-fire' mechanism, whereby single Ca^{2+} release events can easily ignite neighbouring channels, resulting in events that are large enough to be quantifiable by fluorescence (Kunitomo and Terentyev 2011).

Others have shown that disease and increased phosphorylation in fact causes fragmentation of RyR2 clusters. Sobie et al. (2006) suggest there is a decrease in coupled gating between clustered RyR2s in response to phosphorylation in disease, as well as the existence of 'rogue', unclustered RyR2 channels which may respond differently to local Ca^{2+} concentrations. RyR2 clusters in fixed atrial myocytes from sheep with persistent AF showed ultrastructural reorganization, with increased fragmentation associated with overactive Ca^{2+} release (Macquaide et al. 2015). If phosphorylation does lead to less dense RyR2 clusters, this may destabilize tightly regulated Ca^{2+} release from the SR, while rogue channels may each contribute a fraction to an overall increased Ca^{2+} leak (Sobie et al. 2005).

In summary, although phosphorylation of RyR2 has been extensively investigated and remains controversial, studies on the effect of phosphorylation of RyR2 in CPVT are very few and the conclusions disparate and complicated by the use of different disease models and conditions. This experimental chapter will describe attempts to characterise the functional effects of cAMP mediated phosphorylation, characterised at both S2808 and S2031 PKA-specific sites, in WT, S2246L and N4104K hRyR2.

4.1.2 Investigating RyR2 phosphorylation: commonly used experimental strategies

4.1.2.1 *In vitro* kinase assays and 'back phosphorylation'

The method first used to investigate phosphorylation of cardiac proteins involved labelling the intracellular ATP pool with radioactive phosphorous-32 (^{32}P), a technique used to reveal that both PLB and troponin I are phosphorylated in response to β-adrenergic stimulation (Manning et al. 1980; England 1976; Lindemann et al. 1983). However, this method does not allow discrimination between the kinases responsible, nor between different phosphorylation reactions (Karczewski 1991).

Back-phosphorylation was employed to overcome this issue, and was first used to describe protein phosphorylation in brain tissue (Forn and Greengard 1978). Early works of RyR2 phosphorylation involved this technique (Hohenegger and Suko 1993; Witcher et al. 1991; Takasago et al. 1989; Takasago et al. 1991; Seiler et al. 1984). Utilizing the principle that the capacity to incorporate phosphate is dependent on kinases and phosphatases linked specifically to the protein in question, this assay comprises fixing of the phosphorylation state of a protein and extraction from the rest of the cell, before back-phosphorylation of the remaining phosphate capacity, with [γ-^{32}P]ATP and exogenous protein kinase (Karczewski 1991). The phosphorylation state of the protein before extraction, *in vivo*, is therefore indirectly assessed. This technique is not without limitation; it does not address the role of potential endogenous kinase activity in the assay, or reveal much information about the expression or functional state of the protein in question (Karczewski 1991). The high energy particles emitted and short half-life (~14 days) of ^{32}P also makes the technique potentially harmful in the laboratory, and safety precautions such as lead shielding are necessary to protect the body.

4.1.2.2 Phosphopeptide mapping

In this procedure, a radiolabelled protein is proteolytically digested, and the resulting phosphopeptides are separated in two dimensions on a Thin Layer Chromatography (TLC) plate. The phosphopeptides are also analysed by High Pressure Liquid Chromatography (HPLC) and mass spectrometry (MS) or peptide microsequencing. This mapping gives information about the number of phosphorylation sites present in the protein, and can also be used to find out if sites of phosphorylation on a protein change upon treatment of cells with specific compounds (Dephoure et al. 2013, Meisenhelder et al. 2008).

In work of Takasago et al. (1991), phosphopeptide mapping provided evidence that PKA, PKC and PKG predominantly phosphorylated serine resides in the same fragmented phosphopeptide, whereas CaMKII phosphorylated serine residue(s) in a different phosphopeptide. This led to the first suggestion that site-specific phosphorylation in RyR2 is dependent on different kinases.

Unfortunately, as the phosphate moiety is relatively labile, it is often released during fragmentation leading to reduced quality MS spectra (Dephoure et al. 2013) and as such, many phosphorylation sites within a protein can appear as low occupancy – i.e. a small fraction of the protein molecules appear to be phosphorylated in this experiment (Olsen et al. 2010). It may also be difficult to identify a specific site of phosphorylation, as peptides with the same sequence phosphorylated on different residues will still have identical masses (Dephoure et al. 2013).

4.1.2.3 Phospho-epitope antibodies

Phosphorylation-state specific antibodies take advantage of the sensitivity and selectivity of immunochemical methods to detect changes in phosphorylation of a protein at a particular site, with relatively simple preparation and broad application.

Few groups have successfully generated and utilized RyR2-phospho specific antibodies ‘in-house’ (Rodriguez et al. 2003; Xiao 2004; Wehrens et al. 2003) and antibodies that target both phosphorylated and dephosphorylated protein are commercially available from Badrilla Ltd, Leeds, with use cited in some recent publications (Miyazaki et al. 2012; Chakraborty et al. 2014;

Beca et al. 2012; Uchinoumi et al. 2010; Sedej et al. 2010). A study comparing the residue-specific phospho-antibodies used by different research groups demonstrated that the sensitivities of the antibodies and the results they obtained varied significantly (Huke and Bers 2008), possibly providing an explanation for the discrepancies between publications from different groups (Dobrev 2014). However, they remain an invaluable, inexpensive and popular tool for probing the effects of phosphorylation on RyR2 channel function.

4.1.2.4 Pharmacological phosphorylation

β-adrenergic agonists (e.g. Iso and epinephrine) are routinely used to activate the signalling cascade leading to the phosphorylation of RyR2. These act on the cell surface and do not permeate through cell membranes, resulting in the activation of adenylyl cyclase, increasing intracellular concentrations of cAMP and leading to subsequent phosphorylation of EC coupling proteins primarily by PKA, but also by CaMKII (**Section 1.4**). In experiments within a cellular environment, drugs that activate further down the pathway (such as adenylate cyclase) must be able to cross the cell membrane or activate other mechanisms coupled to phosphorylation of the channel.

cAMP is a downstream secondary messenger in β-adrenergic stimulation, responsible for the activation of PKA and subsequent phosphorylation of RyR2. A cell-permeable cAMP analogue was utilized by Paavola et al. (2007) to simulate sympathetic stimulation in the study of two CPVT1 RyR2 mutations, P2328S and V4653F. The authors reported that at baseline (no treatment), both WT and mutant RyR2-transfected HEK293 cells showed a low frequency of Ca^{2+} release events, in contrast to earlier reports of increased basal activity of RyR2 carrying these 'gain-of-function' mutations (Lehnart et al. 2004; Jiang et al. 2002). Treatment with 1-50 μM dioctanoyl-cAMP (DcAMP, a cell-permeable cAMP derivative that mimics the effects of exogenous cAMP but with approximately 100 times greater activity), increased the propensity of Ca^{2+} release events in RyR2-transfected cells. The authors also reported that a significantly larger number of cells transfected with P2383S or V4653F RyR2 exhibited Ca^{2+} release events on treatment with DcAMP, in comparison to WT.

Pharmacological treatment is frequently used in the study of RyR2 activity and dysfunction. However, without the addition diagnostic techniques (e.g. with phospho-epitope antibodies or phosphopeptide mapping) it isn't possible to attribute any observed changes to phosphorylation (or lack of phosphorylation) to one particular site in RyR2. It is also likely that all PKA target proteins within the assay will be phosphorylated, and as discussed in **Section 1.4**, PKA activity may also be linked to Epac and activation of CaMKII, which is also thought to have RyR2 site-specific and other targets that could be phosphorylated in this process, all of which must be considered in data interpretation.

4.1.2.5 Genetic phosphorylation

Genetic phosphorylation was first used by Marks' group in the study of the functional effects of RyR2 phosphorylation (Marx et al. 2000; Marx et al. 2001). This method exploits the fact that some non-phosphorylated amino acids appear chemically similar to phosphorylated amino acids (**Figure 4.1**).

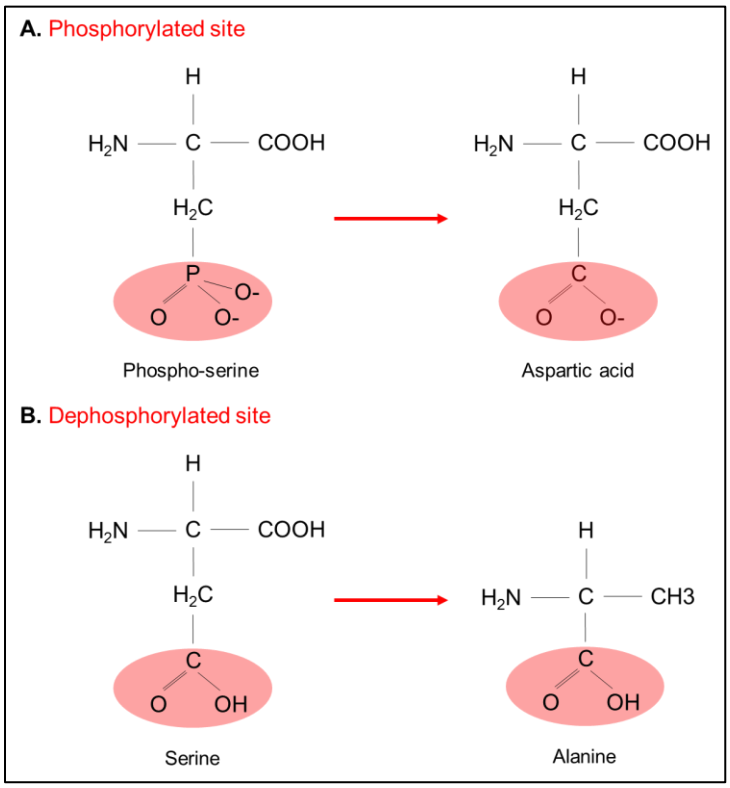

Figure 4.1 The use of phosphomimetics takes advantage of the chemical similarities between amino acids to mimic phosphorylated or dephosphorylated sites within a protein. *A.* Genetic phosphorylation involves the substitution of serine for aspartic acid, as aspartic acid is chemically similar to phosphorylated serine. *B.* Genetic phospho-ablation involves the replacement of serine by alanine, which renders the site unphosphorylatable.

By the introduction of missense mutations at phosphorylation sites, a phosphorylated amino acid could be mimicked in terms of structure and charge. When an aspartic acid replaces a serine, it is therefore a 'phosphomimetic' of serine. Genetic phospho-ablation of RyR2 refers to the replacement of serine by alanine at a particular site, amino acids that are structurally similar. Phospho-ablation is a term used to indicate that the site can no longer be phosphorylated after

this substitution, so mimics a dephosphorylated serine site. The protein is then assumed to maintain the level of activity caused by phosphorylation or dephosphorylation at this site.

Many research groups have applied this technique to the investigation of RyR2 phosphorylation, including the Meissner, Marks, Chen and Wehrens groups. Studies using phospho-ablative or mimicking mutations remain invaluable to study effects at specific phosphorylation sites (Dobrev and Wehrens 2014). The technique allows for precise control over the phosphorylation status of one site within RyR2, avoiding misinterpretation of results due to phosphorylation of other EC coupling proteins as with pharmacological phosphorylation. However, genetic phosphorylation/phospho-ablation of RyR2 (especially in KI/KO mouse models) may lead to adaptive remodelling, with increased expression of EC coupling proteins to compensate for altered RyR2 activity (Pott et al. 2006; Brittsan et al. 2003).

Further discussion on the many different phosphomimetic mouse models and recombinant cDNA studies can be found in **Chapter 5**.

4.1.3 Chapter aims

CPVT1-linked arrhythmia occurs, by definition, after acute β-adrenergic stimulation following stress or exercise. However, it remains unclear whether sympathetic stimulation is an obligatory step to elicit the abnormal Ca^{2+} release observed from mutant RyR2 channels, or simply exacerbates dysfunction (Loaiza et al. 2013). PKA is the principal effector kinase in the β-adrenergic stimulation pathway. The data of Tester et al. (2007) also indicate that diverse functional effects of different mutations may result in an equally diverse response to PKA phosphorylation (see section in CH3). It is therefore reasonable to hypothesize that PKA phosphorylation of hRyR2 channels in HEK293 cells may reveal CPVT1-linked channel dysfunction. As evidenced in the previous Chapter, S2246L-hRyR2 transfected HEK293 cells display little alteration in the kinetics of Ca^{2+} release events in comparison to WT-hRyR2 transfected cells. It follows to hypothesize that phosphorylation at PKA sites S2031 and S2808 may lead to dysfunction of S2246L RyR2 channels, but not necessarily N4104K channels, which already display dysfunction in Ca^{2+} imaging experiments (i.e. their dysfunction may not be able to be further exacerbated by phosphorylation). This investigation will attempt to provide an explanation for why functionally heterogeneous hRyR2 mutant channels result in similar arrhythmogenic outcomes.

This was investigated by:

- Western blot analysis of WT and mutant hRyR2 expression, using antibodies specific to the S2808 and S2031 phosphorylation sites, to determine basal phosphorylation levels.
- Treatment of cells expressing WT or mutant hRyR2 cells with a cell-permeable cAMP analogue (DcAMP, previously used with recombinant RyR2 in HEK293 cells (Paavola et al. 2007)) to stimulate PKA phosphorylation and subsequent Western blot analysis to detect any changes between WT and mutants in the level of phosphorylation of hRyR2 at these two sites.
- Further Western blot analysis of DcAMP treated hRyR2-transfected HEK293 cells to assess any changes in SERCa expression. This was to ensure changes in Ca^{2+} release events were most likely due to the alteration of hRyR2 phosphorylation levels, as opposed to increased Ca^{2+} efflux into the store via an increased number of SERCa pumps. HEK293 cells do not endogenously express PLB or CSQ2 (Kurzydlowski 1996; Asahi et al. 2003; Toyofuku et al. 1994), other proteins that are physiologically phosphorylated by PKA in the cardiomyocyte.

- Detailed interrogation of the Ca^{2+} release events of WT and mutant hRyR2-transfected HEK293 cells, as previous, before and after stimulation with DcAMP to identify changes after pharmacological phosphorylation, as well as determination of the ER Ca^{2+} store load and propensity for spontaneous Ca^{2+} release.

Given that PKA phosphorylation is reported as site-specific to S2808 and S2031, phosphorylation at the CaMKII site S2814 was not investigated in this project. While there is evidence of both PKA and CaMKII being endogenously expressed in HEK293 cells (Tian et al. 2002; Ashpole et al. 2012), it is not yet known whether these cells endogenously express Epac. If Epac is not present in the cell, this means there should not be crosstalk between pathways (see **Section 1.4.1.4**).

4.2 Materials and methods

4.2.1 Evaluation of hRyR2 phosphorylation levels at S2031 and S2808 using phospho-antibodies

4.2.1.1 Cell homogenate preparation

Methods to express, prepare cell homogenate and Western Blot for the eGFP-hRyR2 protein are detailed in **Chapter 2**, with minor alterations implemented for subsequent experiments. To prevent the action of phosphatases and preserve phosphorylation status of hRyR2, cells were harvested and immediately resuspended in hypo-osmotic lysis buffer containing phosphatase inhibitors (20 mM Tris, 1 mM EDTA pH 7.4, 1 mM NaF, 1 mM Na_2VO_4, 1 % Triton X 100, and 1 cOmplete™ EDTA-free protease inhibitor tablet (Roche) per 25 mL of solution). Cells were then immediately lysed by freeze-thaw sonication as described previously and prepared for Western blot analysis.

4.2.1.2 Western blotting for protein expression

The expression of eGFP-hRyR2 phosphomimetic constructs was assessed by methods described in **Section 3.2.3.** Antibodies used in this chapter included:

- Ab-GFP (B-2) antibody (Santa Cruz Biotechnology): mouse monoclonal primary antibody raised against the full-length green fluorescent protein of *Aequorea victoria* origin, provided at 200 µg/mL. Used at 1:1,000 dilution.
- Ab-Vinculin (ab129002, [EPR8185]) antibody (Abcam): rabbit monoclonal primary antibody raised against human vinculin (loading control), provided at 100 µL at 0.054 mg/mL. Used at 1:10,000 dilution.
- Ab-SERCA (1/2, clone Y/1F4) antibody (Badrilla): mouse monoclonal antibody specific to both human SERCa1 and SERCA2a (skeletal and cardiac isoforms). Used at 1:2,000 dilution.
- Ab-β-tubulin (ab6046) antibody (Abcam): rabbit polyclonal antibody specific to β-tubulin (loading control). Used at 1:500 dilution.
- Ab-pSer2808 RyR2 (A010-30AP) antibody (Badrilla): rabbit polyclonal antibody to S2808-phosphorylated RyR2, raised to amino acids 2801-2810. Used at a 1:2,000 dilution. Referred to as Ab-pS2808 in Figures.

- Ab-pSer2030 RyR2 (A010-32) antibody (Badrilla): rabbit polyclonal antibody to S2030-phosphorylated RyR2, raised to amino acids 2023-2033. Used at a 1:1,000 dilution. Referred to as Ab-pS2030 in Figures. S2030 is equivalent to the human S2031 residue in RyR2, hence the different name for the antibody.

4.2.1.3 PVDF membrane stripping for reprobing

The Western blot signal obtained when using RyR2 phospho-specific antibodies is of course dependent on the level of phosphorylation at that specific site, but is also influenced by the RyR2 expression level itself, which may vary slightly between experiments (as reflected by the range of transfection efficiencies (**Figure 3.12**) and the changes in expression between WT and mutant constructs (**Figure 3.7**). The phosphorylation level was therefore expressed as a proportion of the protein expression level.

PVDF is suitable for membrane stripping since it incurs a comparatively minimal loss of sample. It was therefore deemed appropriate to strip membranes probed for phosphorylated hRyR2. This allowed subsequent probing of membranes using the anti-GFP antibody and assessment of the S2808/S2031 hRyR2 phosphorylation level as a proportion of eGFP-hRyR2 expression.

Each blot to be stripped, was placed in a tube containing 50 mL pre-warmed stripping buffer (50 mM Tris/HCl, pH 6.8, 2 % SDS and 0.1M β-mercaptoethanol, made up with dH_2O) and incubated at 50 °C for 10 minutes in a waterbath set in a fume cupboard, before 3x 5 minute washes in excess TBS-T solution to remove any traces of β-mercaptoethanol, which would affect antibody binding. Blots were then placed in blocking solution (5 % milk in TBS-T) for at least one hour, before probing with anti-GFP antibody as outlined previously in **Chapter 2**. Optimization of stripping conditions and integrity of protein before and after the process is discussed in **Section 4.3.1 and 4.4.5.**

A sample of mouse cardiac SR preparation was acquired from Dr S. Zissimopoulos and 100 µg was loaded as a positive control for the detection of phospho-RyR2 on each blot (labelled ‘CONT’ in all Western blot figures), though it was not used for quantitative purposes. This signal should not be visible after stripping and re-probing with the anti-GFP antibody and so its subsequent absence was also used as a measure of successful blot stripping.

4.2.2 Investigating phosphorylation status after stimulation with DcAMP

4.2.2.1 Preparation of a PKA-phosphorylated control

For *in vitro* phosphorylation of cell homogenate samples, PKA (catalytic subunit from bovine heart, ≤9 units/µg, Sigma-Aldrich) was prepared in dH_2O containing dithiothreitol (DTT, 0.6 mg/mL) and left to stand for 10 minutes at room temperature, before suitable size aliquots were frozen at -80ºC, ready for use. This reducing agent prevented loss of enzyme activity and maintained reduced thiol groups.

In the presence of ATP, the catalytic subunit of PKA will transfer the terminal phosphate of ATP to serine/threonine residues in the protein sample, without the presence of cyclic AMP, which would normally be required to bind to the regulatory subunit of PKA and catalyse a reaction.

Cell homogenate protein samples (100 µg) were incubated with phosphorylation buffer (50 mM histidine, 5 mM $MgSO_4$, 1 mM EGTA, 5 mM NaF in dH_2O, pH 7) and PKA (1 U/ 2 µL) for 5 minutes in a waterbath at 37 °C (Rodriguez et al. 2003). ATP (magnesium salt, Sigma-Aldrich) was prepared immediately before use, in dH_2O at a concentration of 5 mM. A final concentration of 200 µM was added to the reaction and incubated at 37 °C for 1 minute. The reaction was then terminated by addition of the appropriate amount of SDS PAGE loading buffer, before incubation at 40 °C and loading as described in **Section 2.3.10**. An example of a typical *in vitro* phosphorylation reaction mixture is described below in **Table 4.1.**

Reagent	**Amount**
Cell homogenate preparation	100 µg
PKA	2.5 U
ATP	200 µM
PKA phosphorylation buffer	Up to 50 µL

Table 4.1 Example of an *in vitro* PKA phosphorylation reaction for Western blotting. The reaction was incubated at 37 °C in a waterbath, before the addition of SDS PAGE x5 loading buffer to terminate the reaction.

4.2.2.2 Preparation of DcAMP analogue and treatment of transfected HEK293 cells

DcAMP (Na salt, Santa Cruz Biotechnology), provided as a lyophilized 50 mg solid, was prepared at a concentration of 50 mM in DMSO as per manufacturer instructions. Stock solutions in DMSO were then made at 10 µM and 100 µM for subsequent experiments. HEK293 cells expressing WT or mutant hRyR2 were prepared (as described previously in **Section 2.3.6** and **2.3.7**) and used to assess the effects of DcAMP for 30 minutes on the phosphorylation level at the S2808 site of hRyR2. One large scale transfection was completed per hRyR2 DNA variant (i.e. 3 in total, WT, SL and NK), divided into a total of 36 dishes. These dishes were arranged into 6 groups of 6 dishes, with each group receiving a drug or control treatment (final DcAMP concentrations of 1 µM, 10 µM, 100 µM and 1 mM, DMSO carrier only negative control, and a PKA treatment positive control as described in **Section 4.2.2.1**). This allowed for the administration of each dose of DcAMP to cells from the same transfected population, in order to minimize variation in hRyR2 expression level between groups. A cell homogenate preparation of untransfected HEK293 cells was also collected as an additional negative control. The DMSO control is referred to as DMSO, the PKA control as PKA and the HEK293 control as HEK in subsequent Western blotting figures.

4.2.2.3 Assessment of DcAMP stimulated phosphorylation at S2808

Cell homogenate preparation and Western blotting were carried out as described in **Chapter 2**, with assessment of S2808 phosphorylation and eGFP-hRyR2 expression as described in **Section 4.2.1**. As cells treated with concentrations of DcAMP in DMSO were all from the same transfection (i.e. 6 dishes were treated with each concentration, with a total of 36 dishes assessed from the same transfection of each hRyR2 DNA type), it was therefore not necessary to normalize densitometric values to eGFP-hRyR2 expression, as this should be equal for each sample.

Phosphorylated hRyR2 expression was normalized to vinculin to account for loading error as described previously.

S2031 phosphorylated hRyR2 expression was not investigated at this stage due to technical issues with the pSer-2030 antibody, discussed further in **Section 4.3.2 and 4.4.**

4.2.3 Ca^{2+} imaging after stimulation with DcAMP

Although there was no obvious effect of DMSO on treated HEK293 cells in preparation for Western blot analysis, it is known that the vehicle can affect Ca^{2+} imaging experiments, given that DMSO is an osmolyte (Lang et al. 1998; Gordeliy et al. 1998; Cheng et al. 2015). While any osmotic effect would equilibrate in the cells over time, there is an acute effect which would likely be visible during Ca^{2+} imaging experiments that measure the immediate effects of drug addition on spontaneous Ca^{2+} release kinetics. Prior to these experiments, it was therefore important to test DMSO as a drug delivery vehicle.

To minimise any possible effects of the vehicle, concentrated stocks, near saturation were prepared. However, the solubility of DcAMP in DMSO was not optimal (with final concentrations of 100 µM and 1 mM requiring an additions equivalent to 1% v/v) and so another vehicle, methanol, was also tested.

HEK293 cells were transfected with hRyR2 WT and mutant constructs and prepared for Ca^{2+} imaging experiments as described previously (**Section 3.2.3**). Spontaneous Ca^{2+} release events of DcAMP treated HEK293 cells expressing WT or mutant RyR2 were recorded as in **Section 3.2.1 (**with modifications discussed below)**,** to observe any changes in cell activity or toxic effects of drug and/or vehicle. Oscillating cells were identified in a field of view and recorded for 3 minutes, before the addition of methanol, DMSO or DcAMP in either vehicle at a working concentration of 100 µM or 1 mM, within the 200 µL meniscus of KRH solution on the Mattek dish. Controls included the maximum volume used of each drug vehicle. The recording was then continued for a further 3 minutes, before the addition of caffeine and recording for a final 30 sec. Recordings were therefore for a total of 6 minutes 30 sec, with the experiment repeated for HEK293 cells transfected with either WT, S2246L or N4104K hRyR2 constructs. Data were collected and analysed as described in **Section 3.2.1.4**.

4.2.3.2 Cell viability assay

The effects of DcAMP on cell viability were assessed using a Trypan blue assay. Trypan blue is a diazo dye that stains dead cells blue – live cells do not absorb the compound through the cell membrane, so remain unstained. Cell viability after

treatment with DcAMP in DMSO was not assessed, given that this drug vehicle was inappropriate for experiments that measure the effects immediately after addition (see **Section 4.3.5**).

The Luna™ Dual Fluorescence Cell Counter (Labtech) and the dye exclusion method was utilized to assess cell viability after 30 minutes of treatment with concentrations of DcAMP dissolved in methanol. Readings were collected from three separate transfected wells per treatment and construct.

HEK293 cells were seeded in a Greiner CELLSTAR® 12-well dish (4 cm^2 surface area) at a density of 3 x 10^5 cells per well in 1 mL cDMEM. Cells were incubated at 37 °C at 5 % CO_2 for 24 hours before transfection using Effectene (Qiagen). Transfection of each well was carried out as follows: plasmid DNA (eGFP-hRyR2, 0.3 µg) was made up to a total volume of 75 µL with Buffer EC, followed by the addition of 2.4 µL of enhancer. Effectene reagent (8 µL) was then added to the solution before mixture with 300 µL cDMEM before dropwise addition to the cells. Dishes were placed back into the incubator for at least 24 hours post-transfection and expression assessed by eGFP visualisation before any treatment with drug for cell viability studies.

Media was removed from each well and replaced with either 1 mL fresh cDMEM (3 wells), 1 mL cDMEM with 2 % methanol (3 wells), cDMEM with 100 µM DcAMP in methanol (1 % of final concentration (v/v), 3 wells) or cDMEM with 1 mM DcAMP in methanol (2 % of final concentration (v/v), 3 wells). Cells were incubated at 37 °C, 5 % CO_2 for 30 minutes before harvesting by trypsinisation (**Section 2.3.7**).

Each cell suspension was mixed at a 1:1 ratio with 0.4 % trypan blue (provided in the Luna™ Dual Fluorescence Cell Counter kit, Labtech), before counting as per manufacturer instructions.

4.3 Results

4.3.1 What are the optimal conditions for use of Badrilla phospho-hRyR2 antibodies for assessment of phosphorylation levels by Western blotting?

Western blots were prepared with hRyR2-transfected HEK293 cell homogenate samples and cut in half, down the marker lane such that the same samples were on each side of this same marker (**Figure 4.2 A**). Samples on the left side of the blot were probed for eGFP-hRyR2 expression and samples on the right were probed for S2808-phosphorylated hRyR2. Clear signals were obtained with both antibodies. Blot images were overlaid using GBOX software to confirm the bands were of the same molecular weight. The right half of the blot was then stripped and reprobed (1 hour) for eGFP-hRyR2 expression (lower panel). The lack of native mouse control (CONT) present in the lower panel indicates that the strip was successful. Even under harsh membrane stripping conditions (i.e. 10 % (w/v) SDS at 50 °C), signal intensities for eGFP-hRyR2 were strong and reliable as seen previously in this laboratory (George et al. 2004; Thomas et al. 2004).

Probing samples with the pAb-S2030 proved much more difficult (**Figure 4.2 B,** see **Appendix VIII for** further blots). In contrast to results with pAb-S2808, no signal for phosphorylated hRyR2 was detected after 1 hour incubation with the antibody. Instead, overnight incubation was required. The antibody did not produce a clean signal, picking up bands at disparate molecular weights, not corresponding that of hRyR2 (see **Figure 4.2 B** centre panel). The control signal also appeared weak and in other blots, no signal was detected (**Appendix VIII**). It was difficult to assess which band corresponded to S2031-phosphorylated hRyR2 until after stripping and reprobing with the more reliable GFP antibody and comparing the molecular weights of the signals using GeneTools software. It took a total of 17 attempts to obtain n=4 of suitable blots for subsequent experiments.

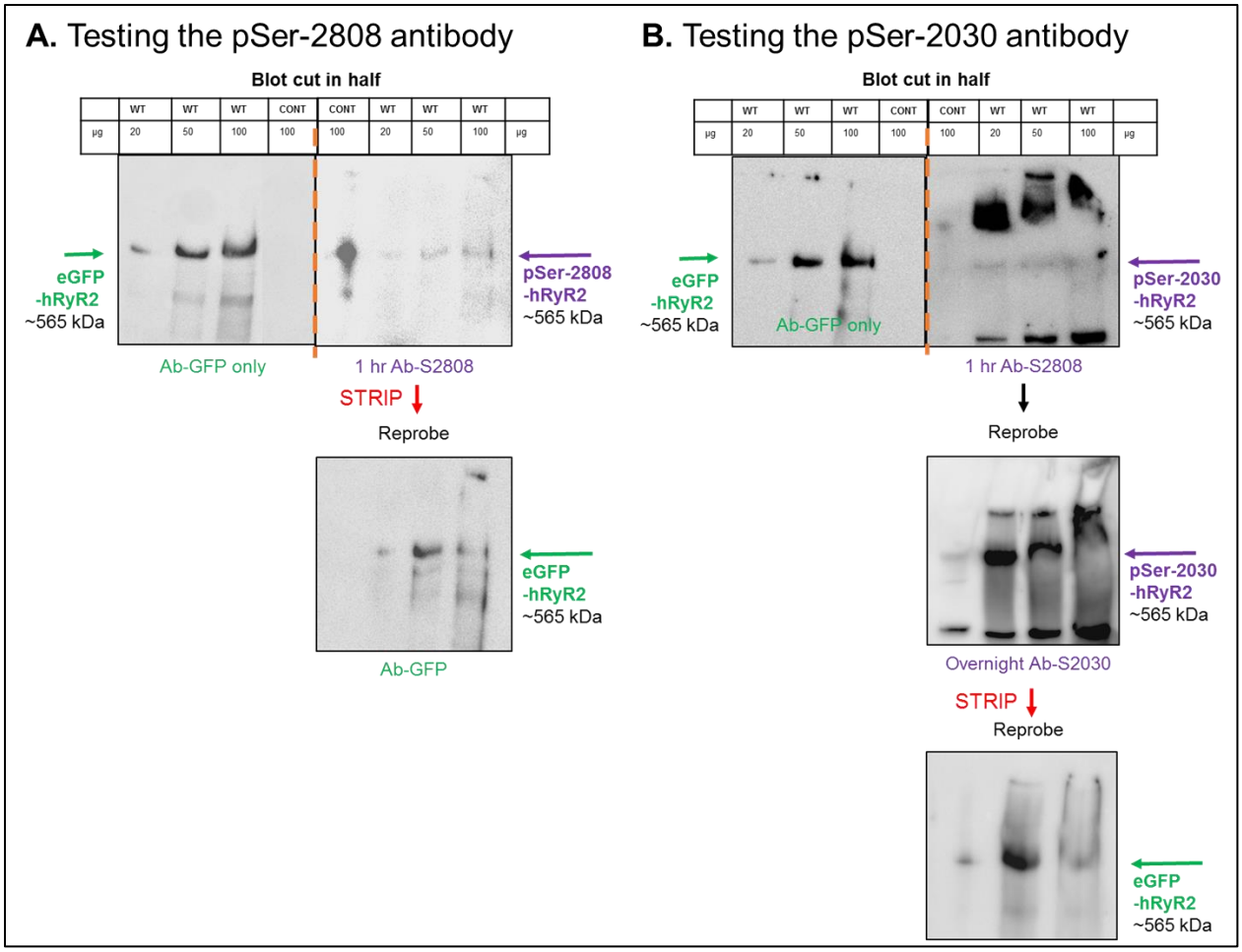

Figure 4.2 Optimization of stripping conditions for probing with phospho-RyR2 antibodies. *A.* Samples on the left side of the blot were probed for eGFP-hRyR2 expression and samples on the right were probed for S2808-phosphorylated hRyR2 (upper panel). The right half of the blot was stripped and reprobed (1 hour) for eGFP-hRyR2 expression (lower panel). *B.* A Samples on the left side of the blot were probed for eGFP-hRyR2 expression and samples on the right were probed for S2031-phosphorylated hRyR2 (upper panel). Signal for pS2031 was poor, but incubation overnight in antibody produced a better signal (centre panel) though the CONT signal appears very weak. The right half of the blot was stripped and reprobed (1 hour) for eGFP-hRyR2 expression (lower panel). For both stripped blots, the lack of native mouse control (CONT) present in the lower panels indicates that the strip was successful.

4.3.2 Does Western blot analysis with phospho-antibodies reveal differences in basal phosphorylation between mutant and WT RyR2 at S2808 and S2031?

WT and mutant hRyR2 cell homogenate preparations were analysed by Western blotting at loads of 50 µg and 100 µg. Although 50 µg loads were assessed, protein expression levels were analysed only at 100 µg of loading, for reasons discussed in **Section 3.3.1**. While original blots can be found in **Appendix I, VII** and **VIII**, blots in Figures hereafter have been spliced to show only 100 µg loads for this reason. Antibody signals that were compared to each other were only on the same blot.

Densitometric analysis was used to assess the level of phosphorylation at S2808 and S2031 sites in WT and mutant hRyR2 channels. The signal detected from cell homogenate samples by these phospho-specific antibodies was expressed as a proportion of the signal for eGFP-hRyR2 expression. This was obtained by stripping membranes and reprobing with an anti-GFP antibody. A comparison is made within the same lane but with a different antibody and so this would make the use of a loading control redundant, as even if different amounts were loaded for WT and mutant hRyR2-transfected cell homogenate samples, normalization in this instance would account for it.

Using this method of densitometric analysis, basal phosphorylation at the S2808 site of hRyR2 appears increased in both S2246L and N4104K hRyR2 cell homogenate preparations in comparison to WT (**Figure 4.3**). In fact, S2808 phosphorylation of S2246L hRyR2 appeared to be approximately 4x that of WT, significant by one way ANOVA with Bonferroni posthoc test ($p<0.01$) while N4104K S2808 phosphorylation levels appear roughly 2x that of WT, but due to variation in the dataset, the increase is not significant.

Basal phosphorylation at the S2031 site of hRyR2 appears decreased in both S2246L and N4104K hRyR2 cell homogenate preparations in comparison to WT (**Figure 4.4**). Phosphorylation levels at S2031 are ~half that of WT in S2246L-transfected cells ($p<0.05$), while levels are approximately a quarter of that of WT in N4104K-transfected cells ($p<0.01$). However, it was very difficult to obtain blots suitable for analysis when probing with pAb-S2030, (see **Section 4.3.1**). The antibody also often led to an inaccurate signal on chemiluminescence (discussed in **Section 4.4.1** and see **Appendix VIII**) and while the significant differences appear to be robust, the reliability of the antibody must therefore be considered when interpreting these

data. This antibody also does not always give a signal for the native mouse control (CONT), yet signal is seen for hRyR2-transfected homogenate samples.

For this data set, it should be kept in mind that normalization of expression levels may have influenced these results, especially where n numbers are low. Protein load of mutant hRyR2-transfected cells was first normalized based on transfection efficiency in comparison to that of WT-transfected cells (see **Section 3.3.1**). Expression level of phospho-hRyR2 and total hRyR2 was also normalized to WT hRyR2 expression level, loading control expression level, or the expression level before treatment with DcAMP. It remains that these normalizations leave room for uncertainty and potential error, especially in the case of the pSer-2030 antibody and data with N4104K.

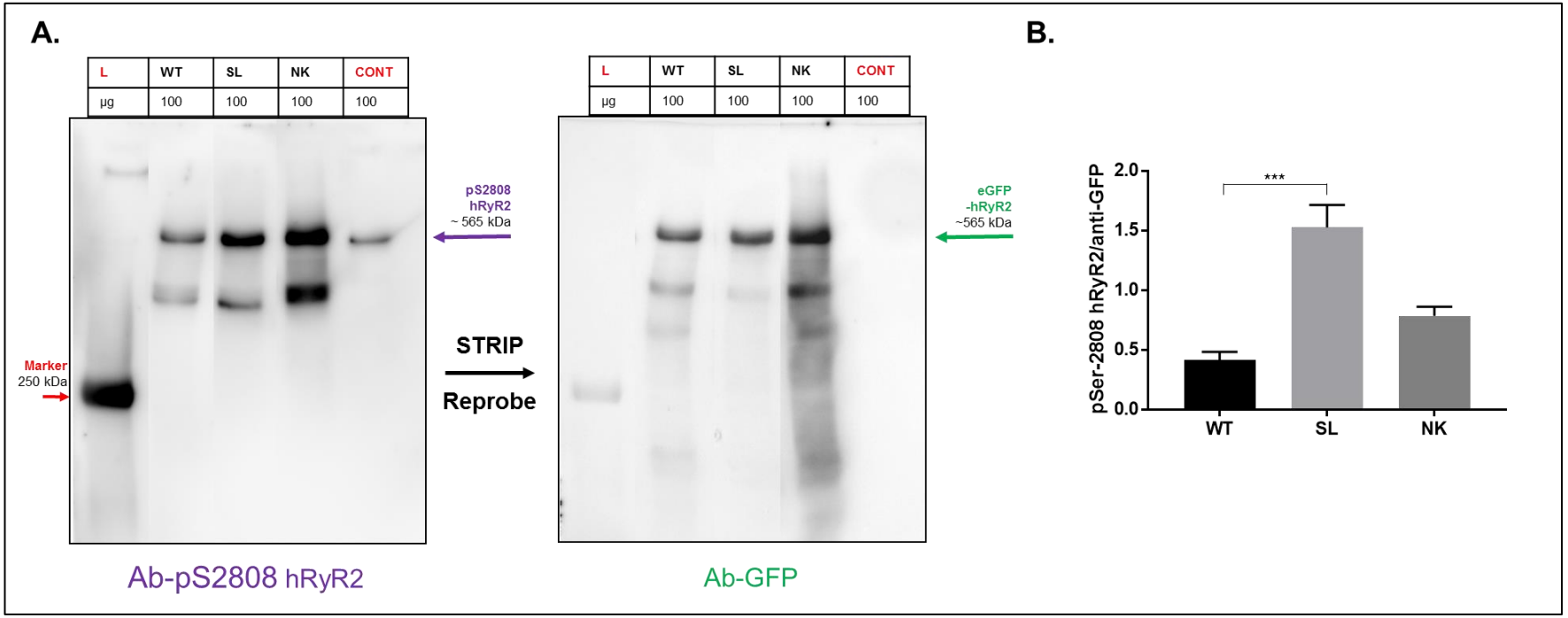

Figure 4.3 Western blot analysis of hRyR2-transfected HEK293 cells with phospho-antibodies reveals that basal phosphorylation at the S2808 is increased in S2246L. *A.* Representative protein bands achieved from Western blot analysis of 100 µg cell homogenate from HEK293 cells expressing WT, S2246L or N4104K hRyR2. Samples were first assessed for S2808-phosphorylated hRyR2 expression (left) before membrane stripping and assessment of eGFP-hRyR2 expression (right). L refers to ladder of defined MW proteins. CONT refers to 100 µg of mouse cardiac SR preparation. All original and additional Western blots are found in **Appendix VII**. *B.* Anti-pS2808 hRyR2 signal was normalized to the equivalent anti-GFP signal. Densitometric analysis revealed that S2246L signals were significantly higher than WT. Data are displayed as mean ± SEM and were analysed by one way ANOVA with Bonferroni posthoc test in GraphPad Prism, $p < 0.001$ indicated by ***, n=4 experiments.

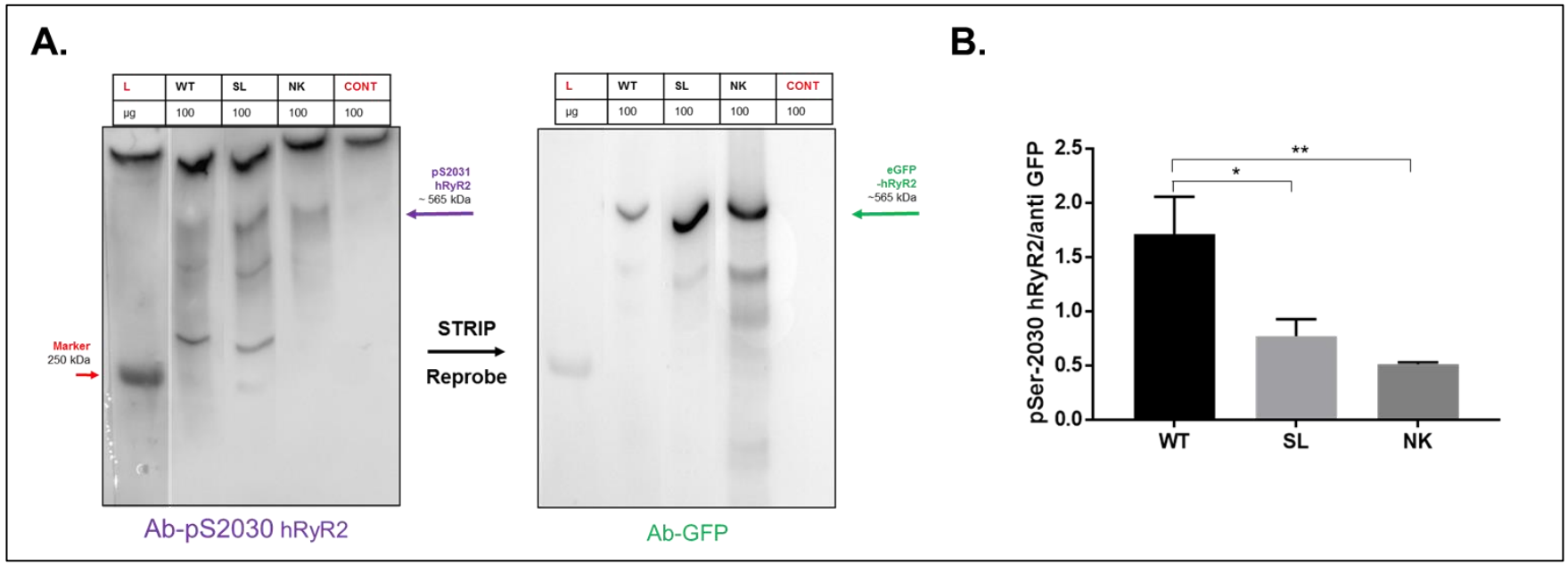

Figure 4.4 Western blot analysis of hRyR2-transfected HEK293 cells with phospho-antibodies reveals that basal phosphorylation at the S2031 site is decreased in both S2246L and N4104K. *A.* Representative protein bands achieved from Western blot analysis of 100 µg cell homogenate from HEK293 cells expressing WT, S2246L or N4104K hRyR2. Samples were first assessed for S2808-phosphorylated hRyR2 expression (left) before membrane stripping and assessment of eGFP-hRyR2 expression (right). L refers to ladder of defined MW proteins. CONT refers to 100 µg of mouse cardiac SR preparation. All original and additional Western blots are found in **Appendix VII**. *B.* Anti-pS2030 hRyR2 signal was normalized to the equivalent anti-GFP signal. Densitometric analysis revealed that S2246L and N4104K signals were significantly lower than WT. Data are displayed as mean ± SEM and were analysed by one way ANOVA with Bonferroni posthoc test in GraphPad Prism, $p < 0.001$ indicated by ***, n=4 experiments.

4.3.3 Does treatment with DcAMP affect the PKA-mediated phosphorylation level of recombinantly expressed WT and mutant hRyR2?

In this experiment, cells from one transfection each for WT, SL and NK were split into several groups of dishes and treated with different concentrations of DcAMP or vehicle (DMSO). Since each treatment/control group was from the same transfected population for each construct, all should have the same eGFP-hRyR2 expression. With this being the case phosphorylated hRyR2 signals were normalized to the vinculin loading control, eliminating the need for stripping membranes, as the two proteins of interest are of different molecular weight.

For WT hRyR2 (**Figure 4.5**), phosphorylation at the S2808 site increases as the concentration of DcAMP increases. In comparison to cells treated with DMSO alone, 100 µM cAMP, 1 mM DcAMP and PKA-treated positive control samples have significantly higher levels of S2808-phosphorylated hRyR2 as calculated by one way ANOVA with Bonferroni posthoc test, $p<0.05$.

In both S2246L and N4104K-hRyR2 transfected HEK293 cells (**Figure 4.6** and **4.7**), DcAMP treatment does not increase phosphorylation in the same manner. While it appears that 1 mM DcAMP and treatment with PKA (treatment of microsomes from the same transfection with the enzyme to achieve maximum phosphorylation, acting as a positive control) increases S2808-hRyR2 phosphorylation levels in the samples, these increases are not statistically significant.

Assessment of phosphorylation at the S2031 site of hRyR2 was not carried out due to issues encountered with the pAb-S2030 antibody, discussed in **Section 4.3.1 and 4.4.1**. There are no other commercially available antibodies that target this specific site.

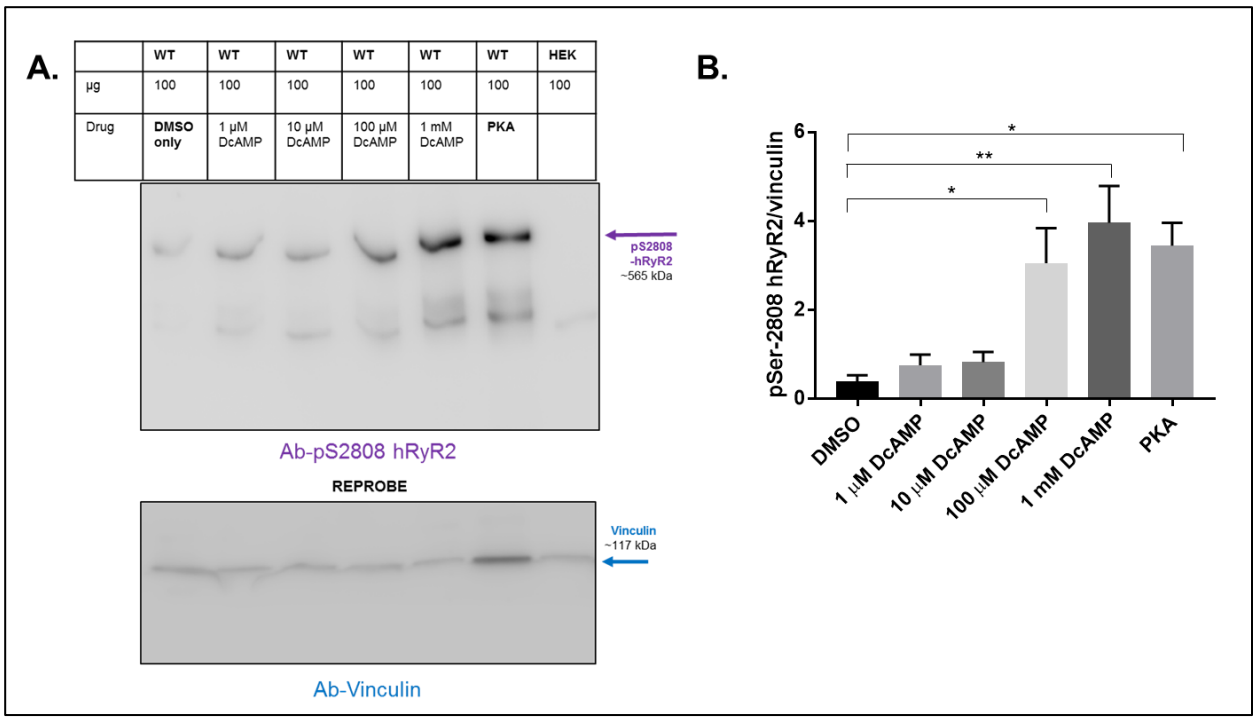

Figure 4.5 Western blot analysis of DcAMP treated WT hRyR2-transfected HEK293 cells with the S2808 phospho-antibody. *A.* Samples prepared as in **Section 4.2.2**. were assessed for S2808-phosphorylated hRyR2 expression (upper panel) and vinculin expression (lower panel). PKA refers to a PKA-treated sample, representing maximal phosphorylation. HEK refers to an untransfected HEK293 sample, as a negative-RyR2 control. All original blots can be seen in **Appendix X**. *B.* S2808-phosphorylated hRyR2 signal was normalized to that for vinculin in each lane. Densitometric analysis shows that S2808 phosphorylation increases significantly after treatment with 100 µM and 1 mM DcAMP. Data are displayed as mean ±SEM and statistical analysis was by one way ANOVA with Bonferroni posthoc in GraphPad Prism, $p<0.05$ indicated on the graph by *, $p<0.01$ by **, n=3.

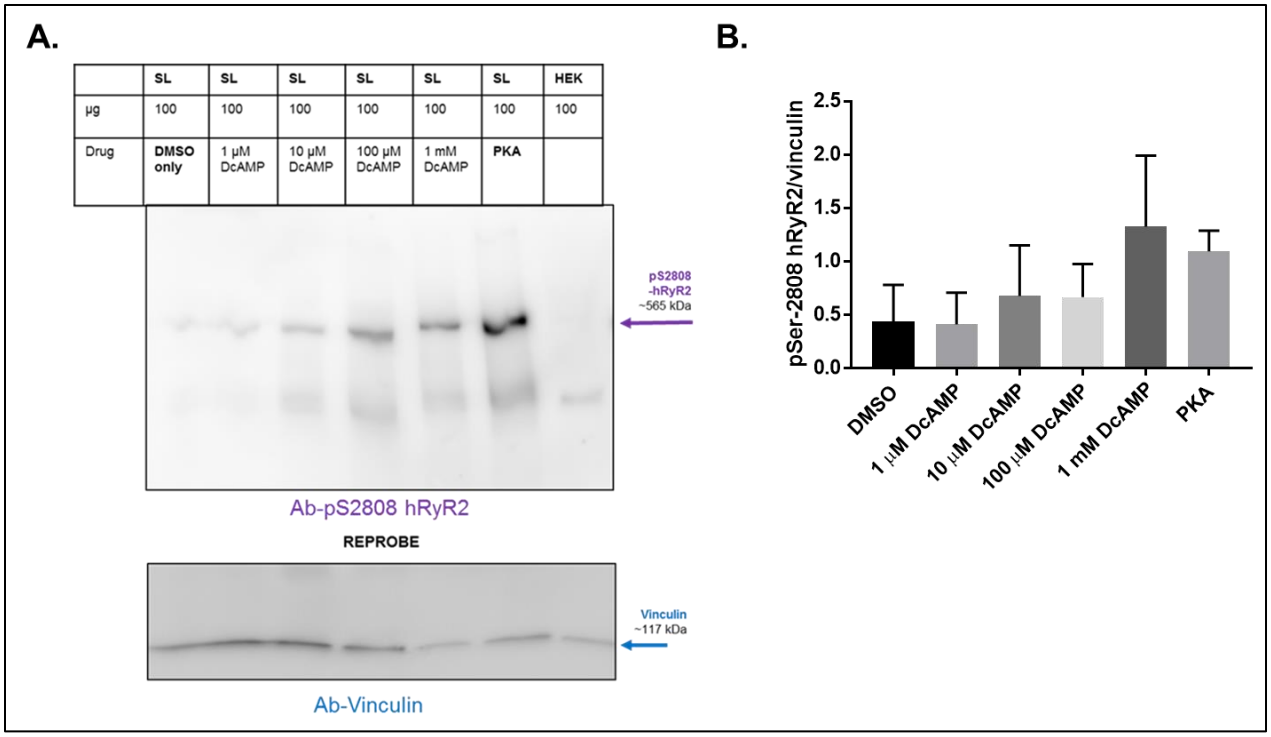

Figure 4.6 Western blot analysis of DcAMP treated S2246L hRyR2-transfected HEK293 cells with the S2808 phospho-antibody. *A.* Samples prepared as in **Section 4.2.2**. were assessed for S2808-phosphorylated hRyR2 expression (upper panel) and vinculin expression (lower panel). PKA refers to a PKA-treated sample, representing maximal phosphorylation. HEK refers to an untransfected HEK293 sample, as a negative-RyR2 control. All original blots can be seen in **Appendix XI**. *B.* S2808-phosphorylated hRyR2 signal was normalized to that for vinculin in each lane. Densitometric analysis shows that S2808 phosphorylation shows no significant differences after treatment with DcAMP 1 mM DcAMP. Data are displayed as mean ±SEM and statistical analysis was by one way ANOVA with Bonferroni posthoc in GraphPad Prism, $p<0.05$ indicated on the graph by *, $p<0.01$ by **, n=3.

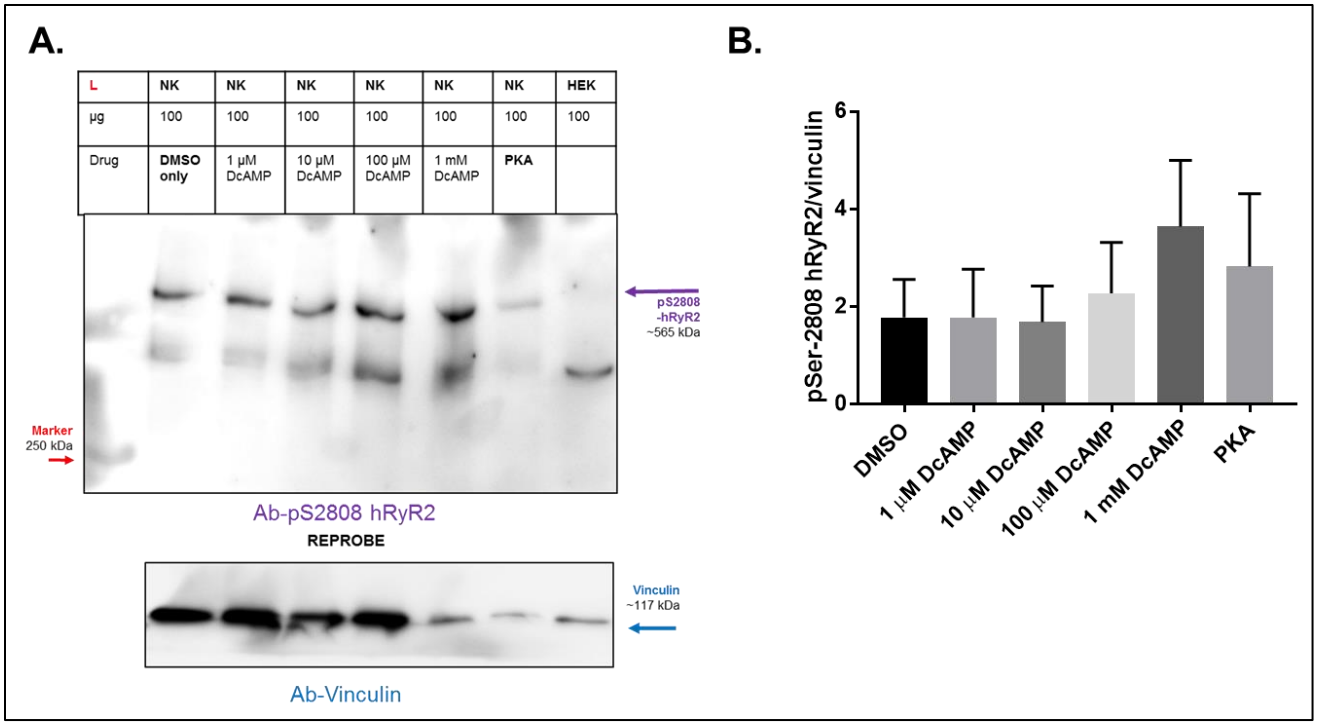

Figure 4.7 Western blot analysis of DcAMP treated N4104K hRyR2-transfected HEK293 cells with the S2808 phospho-antibody. *A.* Samples prepared as in **Section 4.2.2**. were assessed for S2808-phosphorylated hRyR2 expression (upper panel) and vinculin expression (lower panel). PKA refers to a PKA-treated sample, representing maximal phosphorylation. HEK refers to an untransfected HEK293 sample, as a negative-RyR2 control. All original blots can be seen in **Appendix X**. *B.* S2808-phosphorylated hRyR2 signal was normalized to that for vinculin in each lane. Densitometric analysis shows that S2808 phosphorylation shows so significant difference to control after treatment with DcAMP. Data are displayed as mean ±SEM and statistical analysis was by one way ANOVA with Bonferroni posthoc in GraphPad Prism, $p<0.05$ indicated on the graph by *, $p<0.01$ by **, n=3.

4.3.4 Which vehicle solvent for DcAMP is suitable for use in Ca^{2+} imaging experiments?

Dose-dependent DcAMP stimulated phosphorylation of WT and mutant hRyR2 was assessed by Western blot using phosphospecific antibodies prior to functional studies. As a result, only concentrations of agonist which changed phosphorylation (i.e. 100 µM and 1 mM, see **Section 4.3.3**) were used during Ca^{2+} imaging experiments.

Although recommended by the manufacturer of DcAMP (Santa Cruz Biotechnology) as a vehicle for drug delivery, the effects of DMSO on Ca^{2+} imaging in HEK293 cells was assessed (**Figure 4.8 A**) as the use of this solvent is known to be problematic when used in this type of experiment. In > 90 % (n =77 of 85) of oscillating hRyR2-transfected HEK293 cells, a large increase in fluorescence was recorded approximately 20 seconds after the addition of DMSO (only) at 1 % (v/v) (2 µL in a KRH meniscus of 200 µL on a Mattek dish). No further oscillations were observed in the following 30 minutes after this increase in fluorescence, suggesting that DMSO was stopping SOICR or interfering with Fluo-3 dye and was therefore unsuitable for use in Ca^{2+} imaging experiments. It was not possible to use a smaller volume of DMSO in subsequent experiments, as DcAMP was already at its limit of solubility in this solvent.

Methanol was also recommended by the manufacturers as a suitable solvent for DcAMP. The addition of methanol to a final volume equivalent to that required for the addition of 1 mM DcAMP in this solvent had no effect on Ca^{2+} release events observed in recordings of 600 sec after addition in 36/36 oscillating WT hRyR2-transfected HEK293 cells (**Figure 4.8 B**), suggesting it would be a more suitable vehicle for the delivery of DcAMP in these experiments.

Oscillating cells were recorded for 60 seconds before the addition of DcAMP (reconstituted in methanol) at final concentrations of 100 µM (**Figure 4.8 C**) or 1 mM (**Figure 4.8 D**) and recorded for a further 600 secs in the presence of the agonist. Upon treatment with 1 mM DcAMP in methanol, the spontaneous Ca^{2+} release in cells expressing WT hRyR2 remained unperturbed for ~2 min before a sudden, irreversible increase in fluorescence (examples shown in Figure 4.10 D), which was observed in ~75 % (n=64 of 88) of oscillating cells.

Oscillating cells treated with 100 µM DcAMP in methanol appeared to change the initial Ca^{2+} transient after addition (increasing amplitude and or duration, see examples in **Figure 4.8 C**), in

38/103 hRyR2-transfected oscillating cell. The increased fluorescence observed in previous treatments was also seen in 54/103 hRyR2-transfected oscillating cells, at approximately 250 seconds after addition (ROI1= 252 sec, ROI2=306 sec after addition, ROI3=no increase after addition, **Figure 4.8 C**). This therefore suggested that the DcAMP compound could be delivered to HEK293 cells in methanol, but that it was affecting Ca^{2+} release behaviour and stopping SOICR activity after longer periods of time or at a higher concentration. Spontaneous Ca^{2+} release events were subsequently recorded for 180 secs only and cells that exhibited a sharp upstroke in fluorescence were not included in analysis.

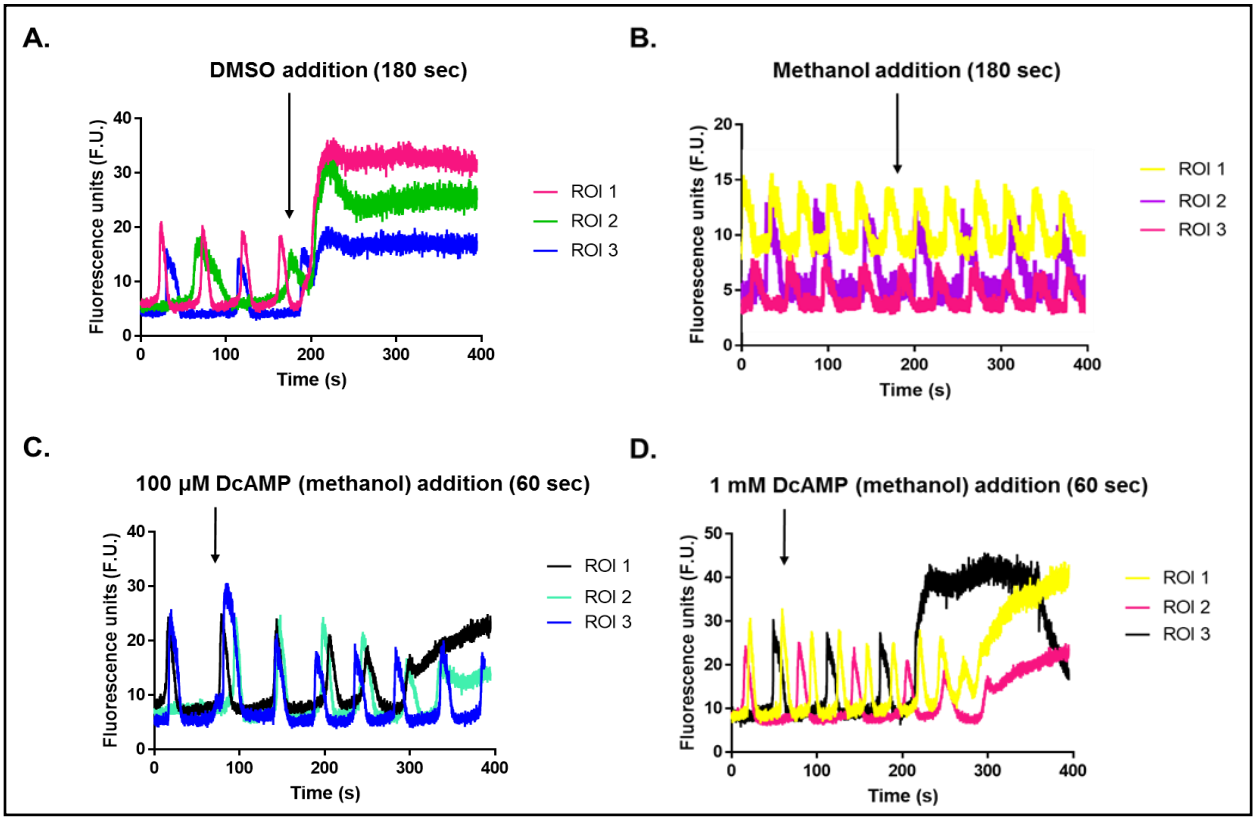

Figure 4.8 Testing of DMSO and methanol as vehicles for DcAMP drug delivery for WT hRyR2-transfected cells in Ca^{2+} imaging experiments. HEK293 cells expressing WT-hRyR2 were assessed for changes in Ca^{2+} release after the addition of DcAMP solvents/concentrations. Three coverslips were observed for each experiment *A.* Addition of 2 µL DMSO (the volume equivalent for 100 µM DcAMP) at 180 secs caused the cessation of Ca^{2+} oscillation, with an evident increase in fluorescence at ~200 secs (64 of 88 cells that oscillated). *B.* The addition of 4 µL methanol (the volume equivalent for 1 mM DcAMP) at 180 secs, caused no observable change in Ca^{2+} oscillation (36 of 36 oscillating cells). *C.* Addition of 100 µM DcAMP in methanol at 60 secs, has no effect on the presence of Ca^{2+} oscillation in most cells (37 of 46 cells) while some displayed an increase in fluorescence with no subsequent oscillations (9 of 46 cells). *D.* Addition of 1 mM DcAMP in methanol at 60 secs, results in an increase of fluorescence at ~250 secs in approximately 80 % of oscillating cells (34 of 44 cells).

A cell viability assay was used to assess whether methanol itself, or DcAMP in methanol damaged cells after an incubation period of 30 minutes (**Figure 4.9**). No significant differences in viability between untreated cells and methanol only treated cells were detected. For cells transfected with each hRyR2 construct, 1 mM DcAMP in methanol decreases the cell viability significantly after 30 minutes, to <60 % (WT=36.3 ±4.1 %, S2246L=58 ±2.5 %, N4104K=39.7 ±2.7 %). A concentration of 100 µM DcAMP in methanol only significantly decreases viability in N4104K-transfected cells, to 75.3 ±5.2 %.

Cumulatively, these data therefore suggest that the compound in methanol is damaging to cells at higher concentrations and after longer periods of incubation. A concentration of 100 µM DcAMP in methanol was decided as most appropriate to investigate in Ca^{2+} imaging experiments, with recording after treatment for three minutes only.

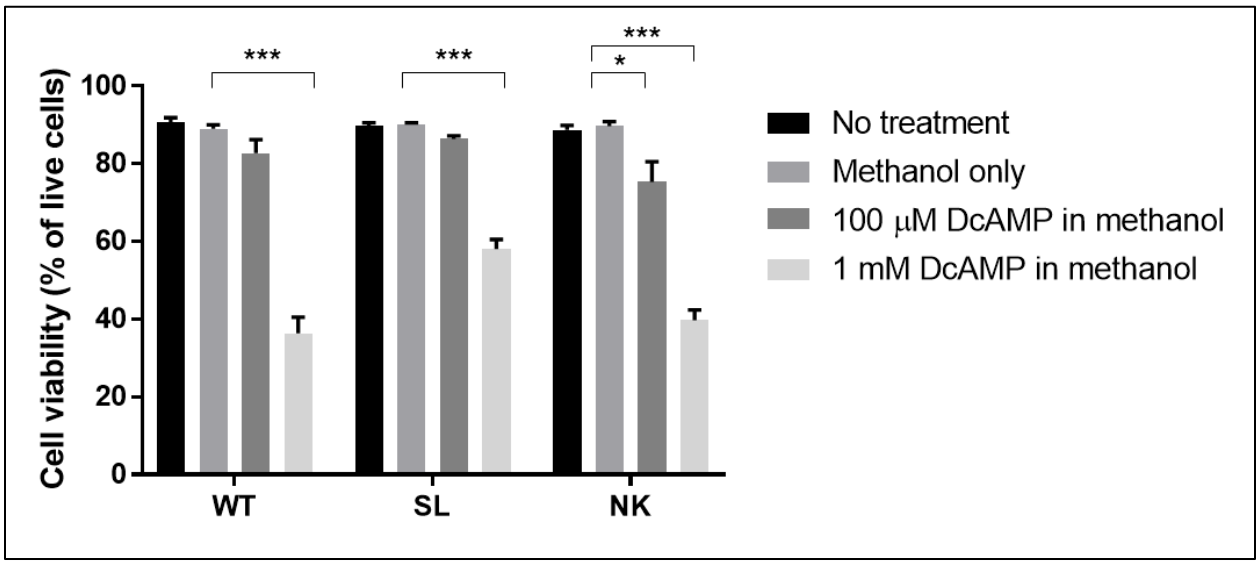

Figure 4.9 Trypan blue cell viability assay suggests minimal toxicity of 2 % v/v methanol but significant cell death with 1mM DcAMP after 30 minutes' incubation. Untreated and methanol only treated cells transfected with each hRyR2 DNA plasmid showed no differences in cell viability WT=90.7 ±1.2 vs 89.0 ±1.0 %, SL=89.6 ±0.9 vs 90 ±0.6 %, NK=88.7 ±0.9 vs 89.7 ±1.2 %). However, 1 mM cAMP in methanol decreases the cell viability significantly after 30 minutes in comparison to methanol only treatment, to <60 % (WT=36.3 ±3.5 %, S2246L=58 ±2.5 %, N4104K=39.7 ±2.7 %). A concentration of 100 µM cAMP in methanol decreases viability only in N4104K-transfected cells (75.3 ±5.2 %). Data are presented as mean ± SEM of n=3 wells per construct and treatment. Analysis was by one way ANOVA and Dunn's posthoc test (data was calculated as normal by D'Agostino Pearson's test), $p<0.05$ indicated on the graph by *, $p<0.001$ indicated by ***.

4.3.5 Is the propensity for Ca^{2+}-induced Ca^{2+} release and store load of hRyR2-transfected cells modified by the addition of DcAMP?

D'Agostino-Pearson tests for normality found that the Ca^{2+} imaging data in this chapter were not normally distributed (see **Appendix XIV**) and so were analysed using non-parametric statistical tests.

Post-hoc power analysis tests were also conducted using G*Power*3.19.2 software (www.gpower.hhu.de) to determine whether appropriate numbers of experiments were completed. In this Chapter, the results are paired i.e. any change in Ca^{2+} handling is a direct comparison of before and after treatment with DcAMP, therefore it would be inappropriate to compare treated cells to untreated cells from different experiments (other than for comparisons of ER load where this is unavoidable). All data sets (found in **Appendix XV**) were calculated as highly powered (≥80 %) and above the suitable threshold for detecting differences (Beck, 2013).

The ER Ca^{2+} content was measured by determining the amplitude of the Ca^{2+} transient induced by application of caffeine (10 mM) as described in **Section 3.2.1.5.** While the ER Ca^{2+} content of cells expressing WT or N4104K was not altered, that of cells expressing S2246L-hRyR2 was significantly decreased after treatment with 100 µM DcAMP when compared to S2246L-hRyR2 before treatment (**Figure 4.10 B**, Mann-Whitney test, $p<0.01$). However, in cells treated with DcAMP, those transfected with mutant hRyR2 (either S2246L or N4104K) both showed a significantly decreased store load when compared to the load of those transfected with WT hRyR2 (**Figure 4.10 D**, Mann-Whitney test, $p<0.01$).

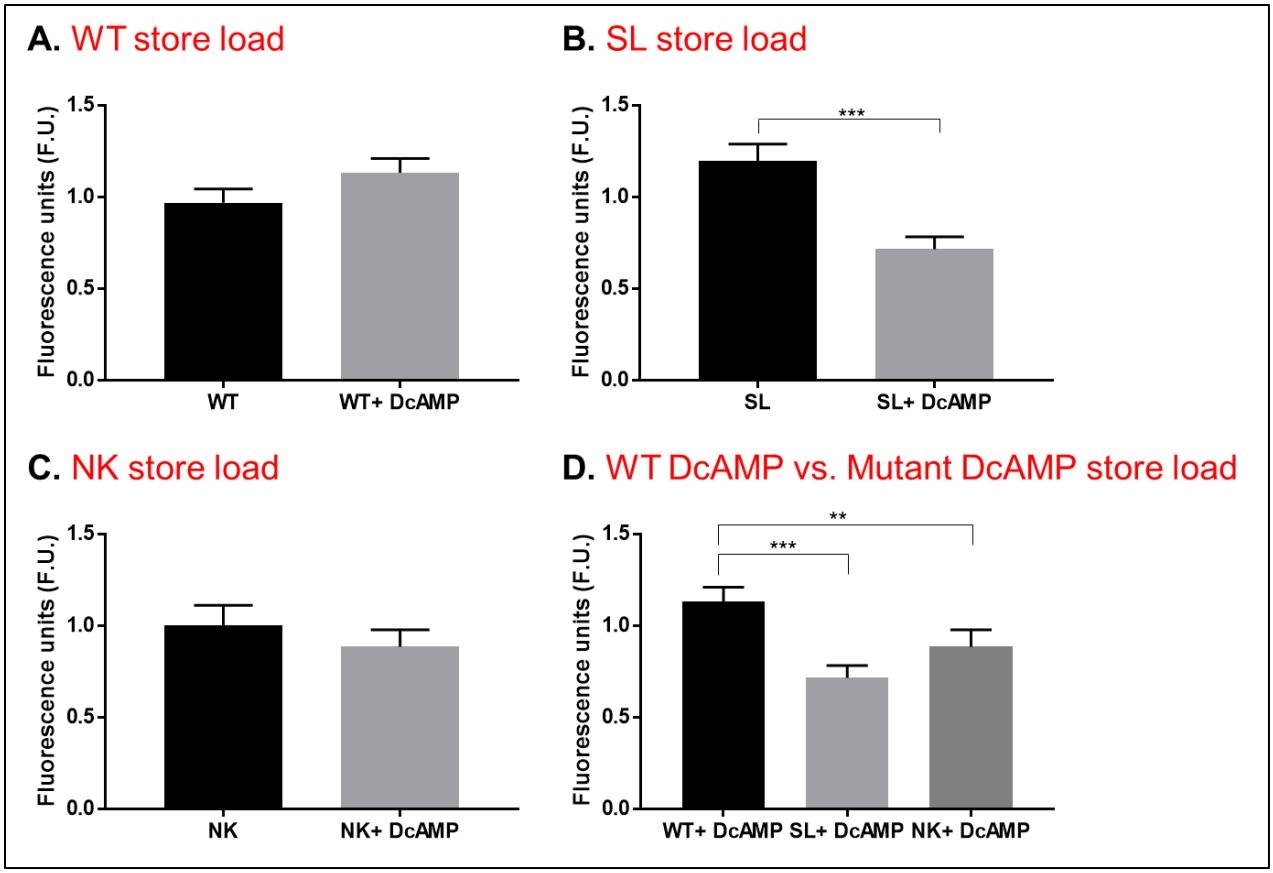

Figure 4.10 Treatment with 100 μM DcAMP decreases the ER Ca^{2+} store load in cells expressing S2246L hRyR2. DcAMP refers to the addition of 100 μM dioctanoyl-cAMP. n WT=41, WT +DcAMP =64, S2246L=43, S2246L +DcAMP =31, N4104K=25, N4104K +DcAMP=48. Statistical significance calculated by Mann-Whitney with Dunn's posthoc test, $p<0.01$ indicated by **. Scatter plots of these data are found in **Appendix XVI**.

The propensity for Ca^{2+} oscillation was calculated by dividing the number of cells that spontaneously release Ca^{2+} by the total number of cells in a field of view. This parameter was not significantly altered after treatment with 100 µM DcAMP for each variant of hRyR2 (**Figure 4.11**). Given that propensity differences between untreated WT and mutant hRyR2-transfected HEK293 cells were investigated previously (see **Figure 3.13**), data were normalized to propensity before drug additions.

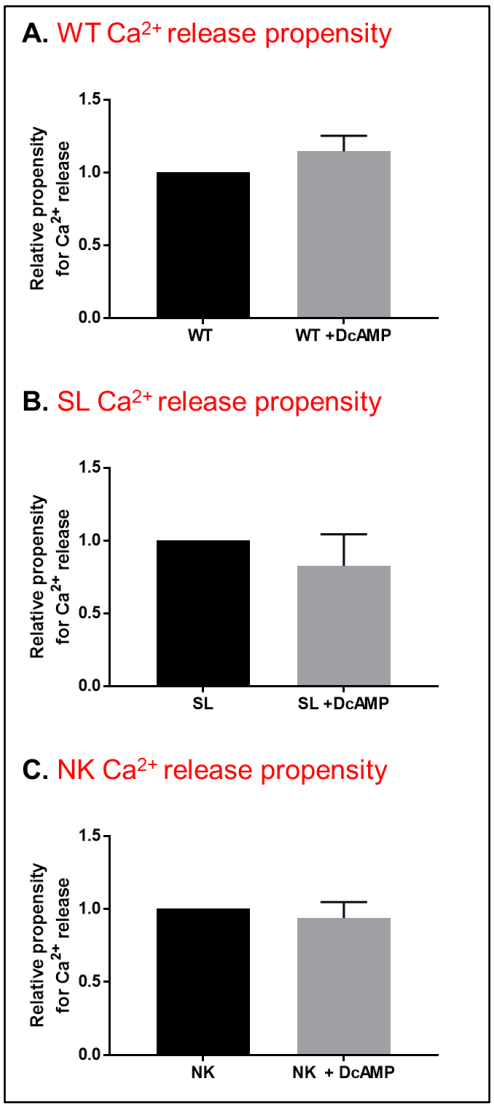

<u>Figure 4.11</u> There is no significant alteration in the propensity for Ca^{2+} release after treatment of transfected cells with 100 µM DcAMP. Data were normalized to propensity for Ca^{2+} release before treatment and displayed as mean ± SEM. Total number of cells showing Ca^{2+} oscillations WT= 110 of 609, WT+ DcAMP=117 of 609, S2246L=64 of 464, S2246L+ DcAMP=75 of 464, N4104K=43 of 424, N4104K+ DcAMP=43 of 424. Analysis by Mann-Whitney test in GraphPad prism, with no significant differences calculated between no treatment and treatment for each construct.

4.3.6 Are the kinetic parameters of Ca^{2+} release altered after treatment with DcAMP?

As in the previous Chapter, spontaneous Ca^{2+} release event kinetics were analysed with SALVO software. **Figure 4.12** shows representative traces for WT and mutant-expressing HEK293 cell, illustrating the altered Ca^{2+} handling seen on the addition of 100 µM DcAMP. Although the representative traces, appear to show a shift in baseline fluorescence after the addition of DcAMP, no significant differences were found when these data were analysed (**Figure 4.13**).

An in-depth analysis of Ca^{2+} oscillation events is presented as a series of bar graphs and dot plots in **Figure 4.14, 4.15** and **4.16**, with Ca^{2+} handling kinetic parameters calculated as described in **Section 3.2.1.4** with SALVO analysis software.

Table 4.2 summarizes the differences in calcium handling parameters between WT and mutant RyR2 transfected HEK293 cells on treatment with 100 µM DcAMP, displayed in bar graphs in **Figures 4.14, 4.15** and **4.16**. It is apparent that DcAMP treatment of WT transfected cells decreases the amplitude and rate up, as well as increases the duration and decreases the rate down of Ca^{2+} release. However, treatment of mutant-hRyR2 transfected HEK293 cells leads to fewer differences in Ca^{2+} release. Both S2246L and N4104K hRyR2-transfected HEK293 cells display decreased Ca^{2+} release amplitude and rate up, as well as a decreased rate down in response to DcAMP. For a summary table that compares all Ca^{2+} release kinetics to untreated WT-hRyR2 HEK293 kinetics, (as opposed to the untreated equivalent) see **Appendix XX**.

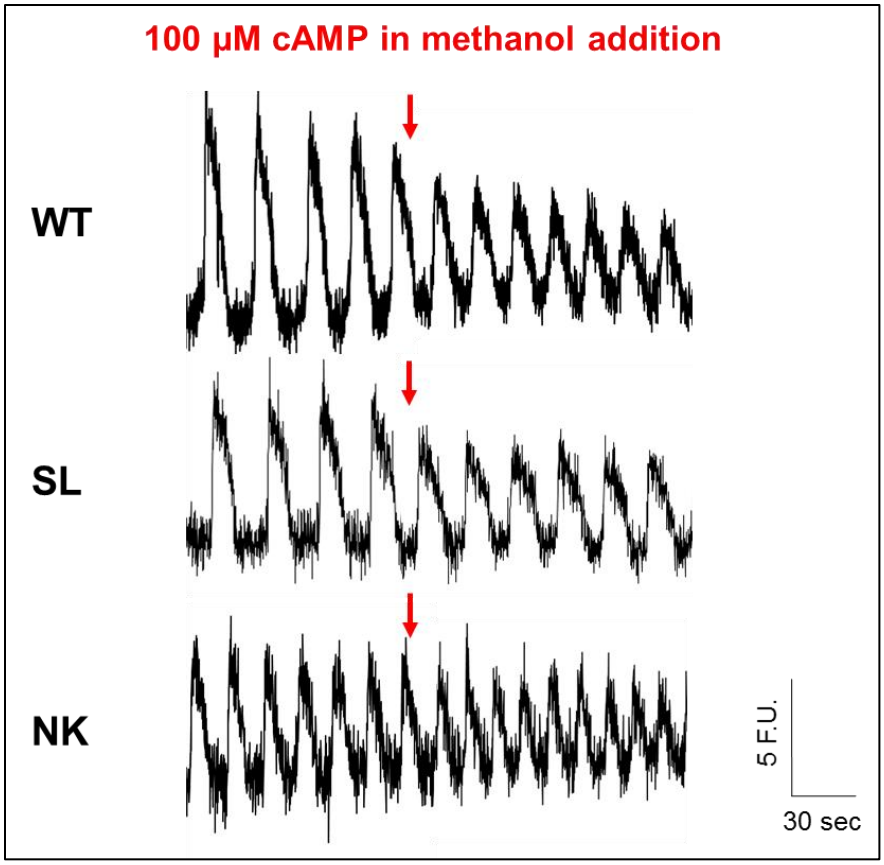

Figure 4.12 Representative fluorescence traces of hRyR2-transfected HEK293 cells, treated with 100 µM DcAMP. Red arrows indicate time of addition of DcAMP (in methanol).

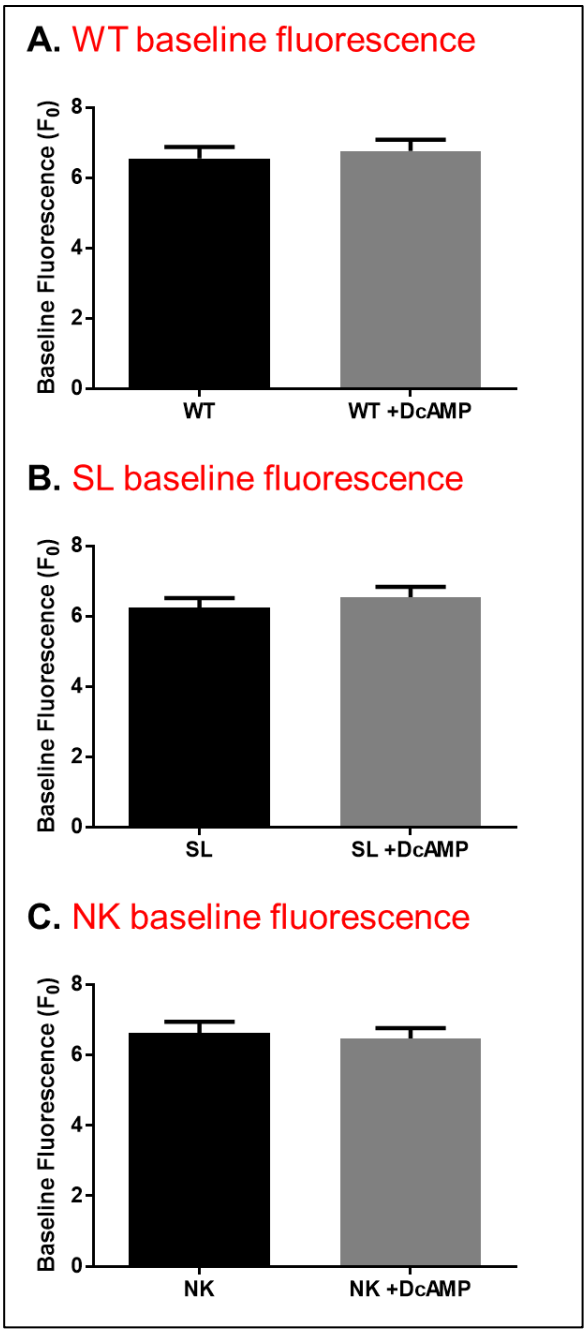

Figure 4.13 Changes in baseline fluorescence of WT and mutant hRyR2-transfected HEK293 cells are not induced by the addition of DcAMP. Baseline fluorescence (F_0) was calculated as described in **Section 3.2.1.4**. DcAMP refers to the addition of 100 μM dioctanoyl-cAMP. n WT=110, WT+ DcAMP=117, SL=64, SL+ DcAMP=75, NK=43, NK+ DcAMP=43. Data are presented as mean ± SEM, with no significant differences calculated by Mann-Whitney analysis with GraphPad Prism. Scatter plots can be found in **Appendix XIII**.

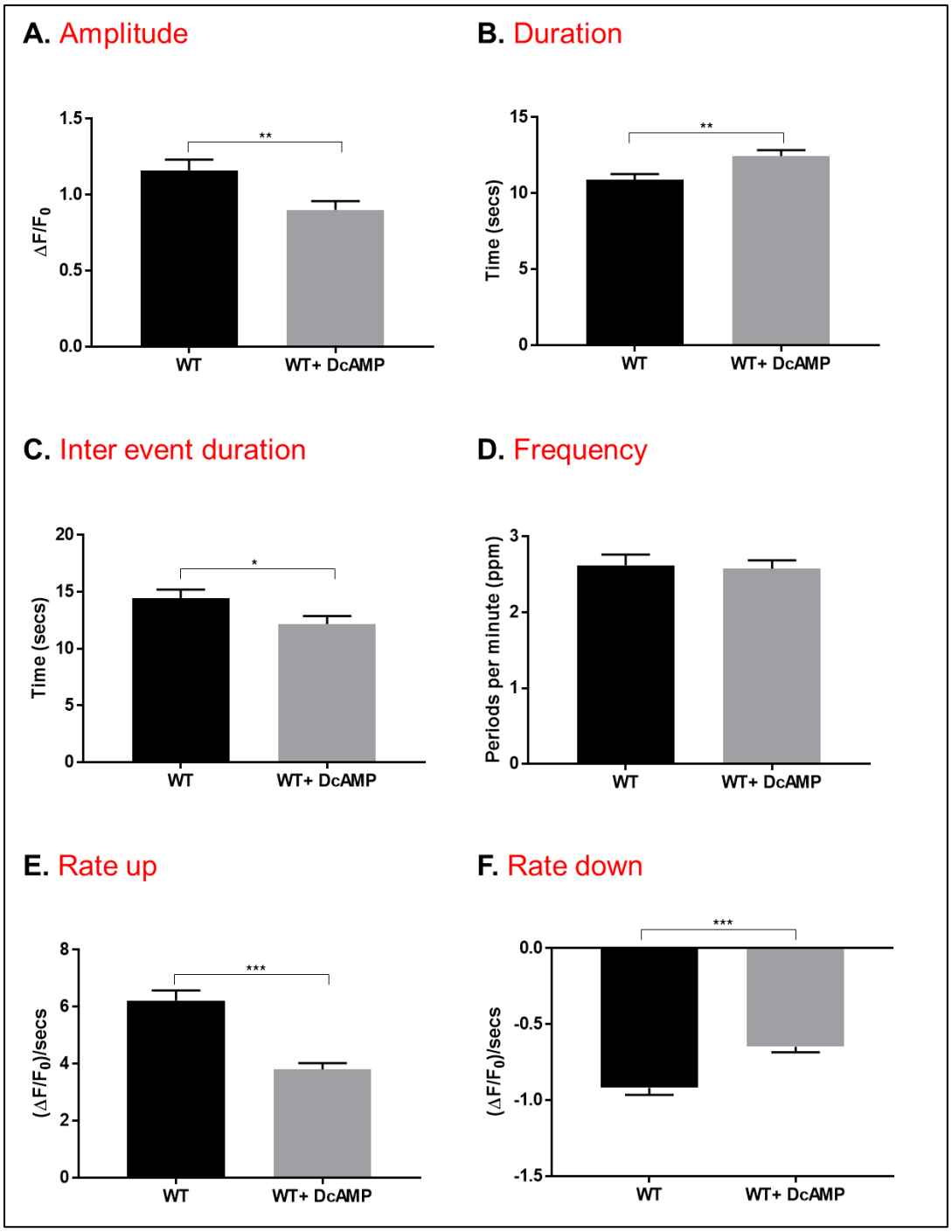

Figure 4.14 Assessment of spontaneous Ca^{2+} release events in WT hRyR2-expressing HEK293 cells before and after treatment with DcAMP. All parameters were calculated as described in **Section 3.2.1.4**. DcAMP refers to the addition of 100 μM dioctanoyl-cAMP. n WT=110, WT+ DcAMP=117. Data are presented as mean ± SEM, $p<0.05$ is denoted by *, $p<0.01$ as ** and $p<0.001$ as ***, calculated by Mann-Whitney analysis with GraphPad Prism. Scatter plots can be found in **Appendix XVII**.

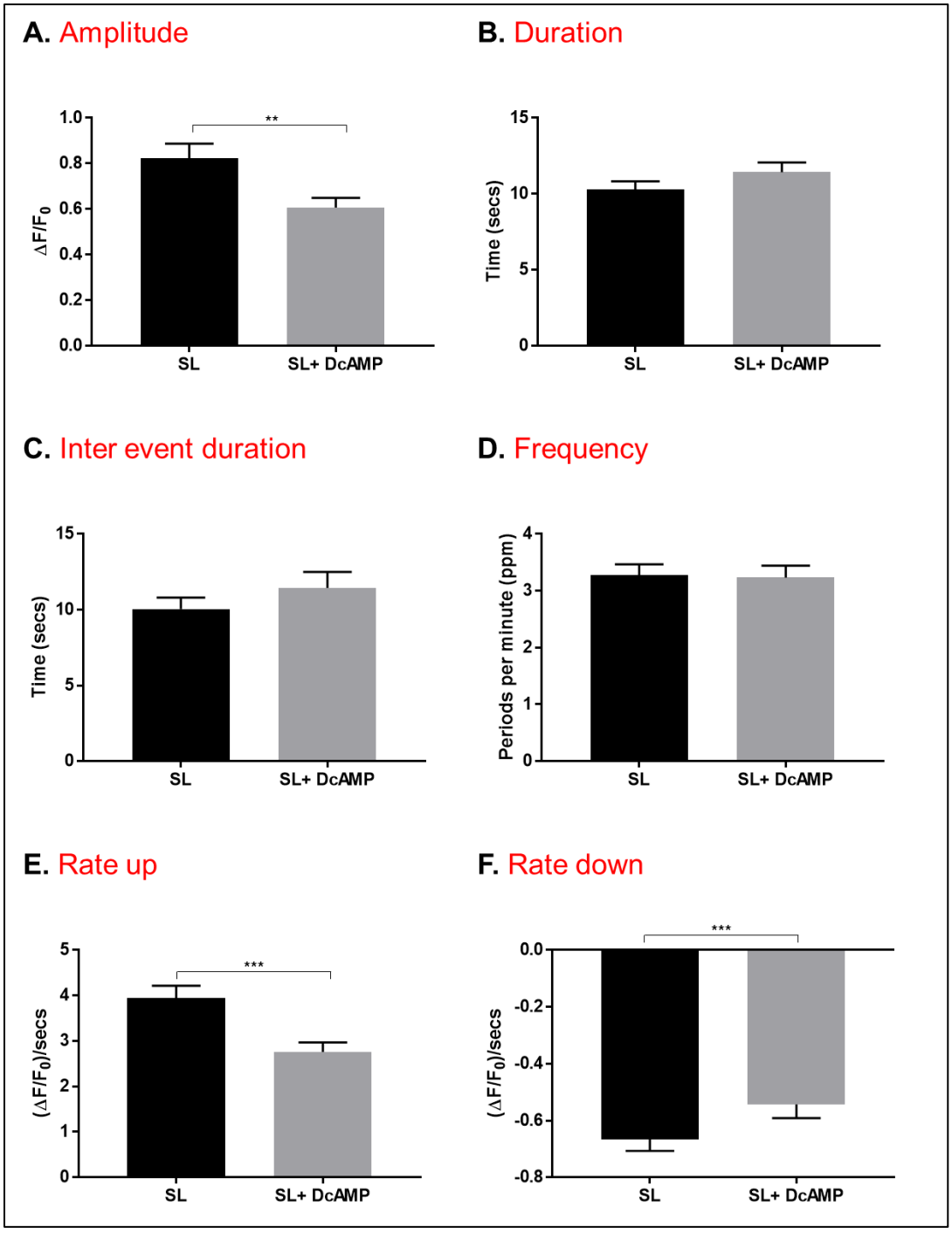

Figure 4.15 Assessment of spontaneous Ca^{2+} release events in S2246L hRyR2-expressing HEK293 cells before and after treatment with DcAMP. All parameters were calculated as described in **Section 3.2.1.4**. DcAMP refers to the addition of 100 μM dioctanoyl-cAMP. n SL=64, SL+ DcAMP=75. Data are presented as mean ± SEM, $p<0.05$ is denoted by *, $p<0.01$ as ** and $p<0.001$ as ***, calculated by Mann-Whitney analysis with GraphPad Prism. Scatter plots can be found in **Appendix XVIII**.

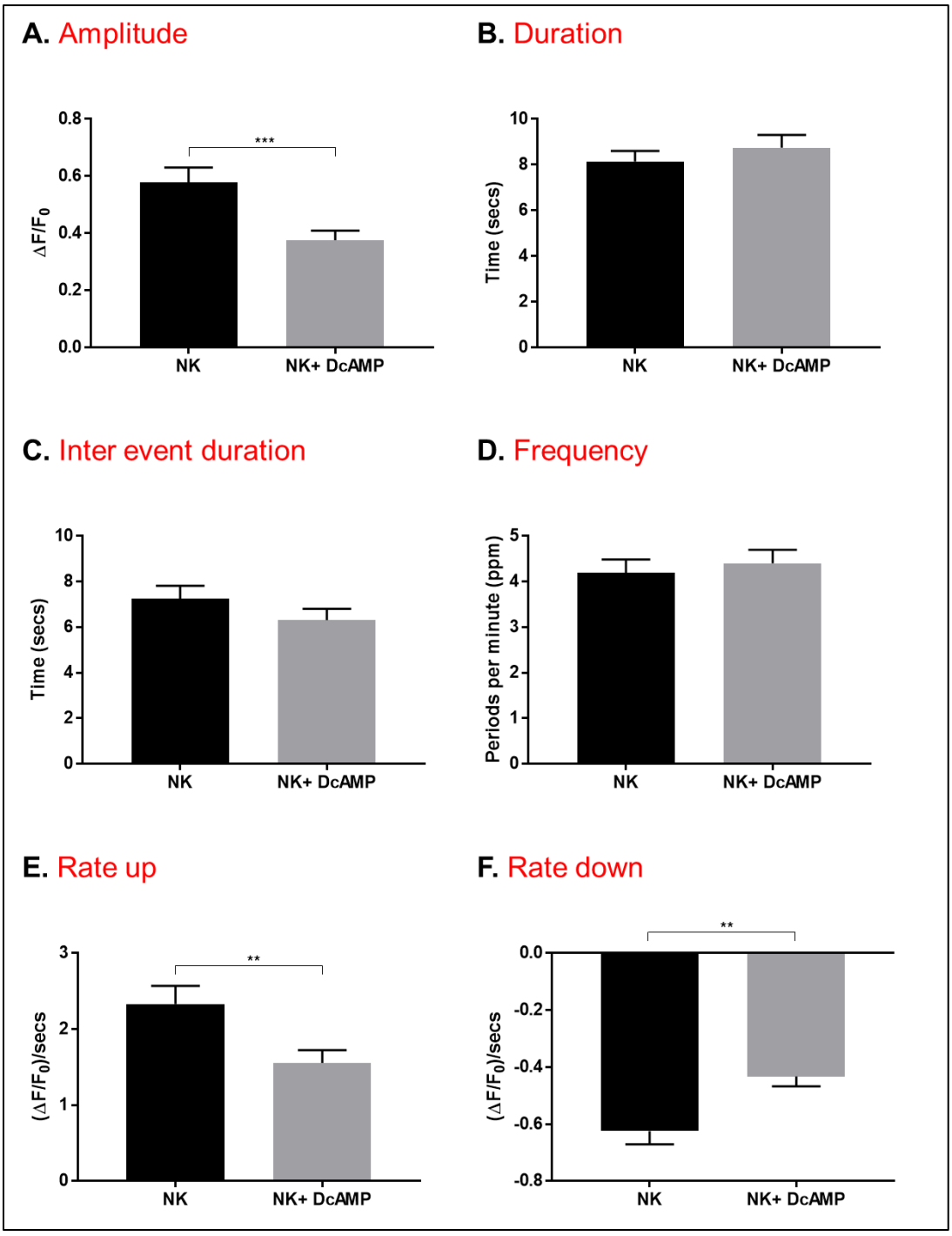

Figure 4.16 Assessment of spontaneous Ca^{2+} release events in N4104K hRyR2-expressing HEK293 cells before and after treatment with DcAMP. All parameters were calculated as described in **Section 3.2.1.4**. DcAMP refers to the addition of 100 µM dioctanoyl-cAMP. n NK=43, NK+ DcAMP=43. Data are presented as mean ± SEM, $p<0.05$ is denoted by *, $p<0.01$ as ** and $p<0.001$ as ***, calculated by Mann-Whitney analysis with GraphPad Prism. Scatter plots can be found in **Appendix XIX**.

Ca^{2+} oscillation event parameters	WT	WT+ 100 µM DcAMP	SL	SL+ 100 µM DcAMP	NK	NK+ 100 µM DcAMP
Amplitude	1.16 ± 0.07	0.901 ± 0.06	0.824 ± 0.06	0.606 ± 0.04	0.579 ± 0.05	0.376 ± 0.03
Duration	10.91 ± 0.36	12.46 ± 0.38	10.28 ± 0.55	11.44 ± 0.63	8.148 ± 0.46	8.747 ± 0.56
Inter-event duration	14.41 ± 0.80	12.18 ± 0.69	10.05 ± 0.74	11.45 ± 1.05	7.236 ± 0.59	6.309 ± 0.49
Frequency	2.622 ± 0.14	2.576 ± 0.11	3.279 ± 0.19	3.233 ± 0.21	4.193 ± 0.29	4.404 ± 0.30
Rate up	6.223 ± 0.36	3.805 ± 0.22	3.946 ± 0.27	2.762 ± 0.20	2.332 ± 0.24	1.553 ± 0.17
Rate down	-0.918 ± 0.05	-0.648 ± 0.04	-0.666 ± 0.04	-0.543 ± 0.05	-0.625 ± 0.05	-0.433 ± 0.03

Ca^{2+} oscillation event parameters	WT+ 100 µM DcAMP	SL+ 100 µM DcAMP	NK+ 100 µM DcAMP
Amplitude	0.901 ± 0.06	0.606 ± 0.04	0.376 ± 0.03
Duration	12.46 ± 0.69	11.44 ± 0.63	8.747 ± 0.56
Inter-event duration	12.18 ± 0.69	11.45 ± 1.05	6.309 ± 0.49
Frequency	2.576 ± 0.11	3.233 ± 0.21	4.404 ± 0.30
Rate up	3.805 ± 0.22	2.762 ± 0.20	1.553 ± 0.12
Rate down	-0.648 ± 0.04	-0.543 ± 0.05	-0.433 ± 0.03

Table 4.2 Summary of Ca^{2+} handling parameters in WT and mutant hRyR2-transfected HEK293 cells. Mean values for calcium handling parameters of WT and mutant hRyR2-expressing HEK cells, ± SEM. Differences are calculated compared to the equivalent parameter in hRyR2-expressing HEK293 cells before treatment i.e. data is paired. Red indicates a statistically significant increase whereas blue indicates a statistically significant decrease as calculated by Mann-Whitney or Kruskal-Wallis with Dunn's/Bonferroni post hoc test, $p<0.01$.

4.3.7 Does DcAMP treatment result in compensatory changes in the expression of SERCa?

Given the changes in ER Ca^{2+} store identified in S2246L hRyR2-transfected HEK293 cells after treatment with DcAMP, as well as changes in amplitude and rate of Ca^{2+} release upon treatment of WT and mutant hRyR2-transfected HEK293 cells, it was important to assess the expression of SERCa. Any changes in expression levels of this protein could affect the amount of Ca^{2+} sequestered into the store and available for subsequent Ca^{2+} release events. Western blots were not probed for other proteins that modify the store load (CSQ, SERCa) as they are not thought to be present in HEK293 cells (Kurzydlowski 1996; Asahi et al. 2003; Toyofuku et al. 1994).

The expression of SERCa was determined for cells expressing WT or mutant hRyR2 incubated for 30 min in the presence or absence of 1 mM DcAMP (Figure **4.17**). This concentration was chosen as it altered phosphorylation levels at S2808 in WT hRyR2 transfected cells. The signal intensity of bands was normalized to β-tubulin expression in the same lane as a loading control as described **in Section 3.3.1**. Densitometric analysis revealed no significant differences in SERCa expression of WT or mutant cell homogenate preparations after treatment with DcAMP (Figure 4.19 B, student's t test). No significant differences were seen in SERCa expression between WT and mutants before treatment (as in Chapter 3), or between WT and mutants after treatment, as calculated by one-way ANOVA. There will be further discussion of SR related proteins (including PLB and CSQ2) and their modification in these experiments in the discussion section of this chapter.

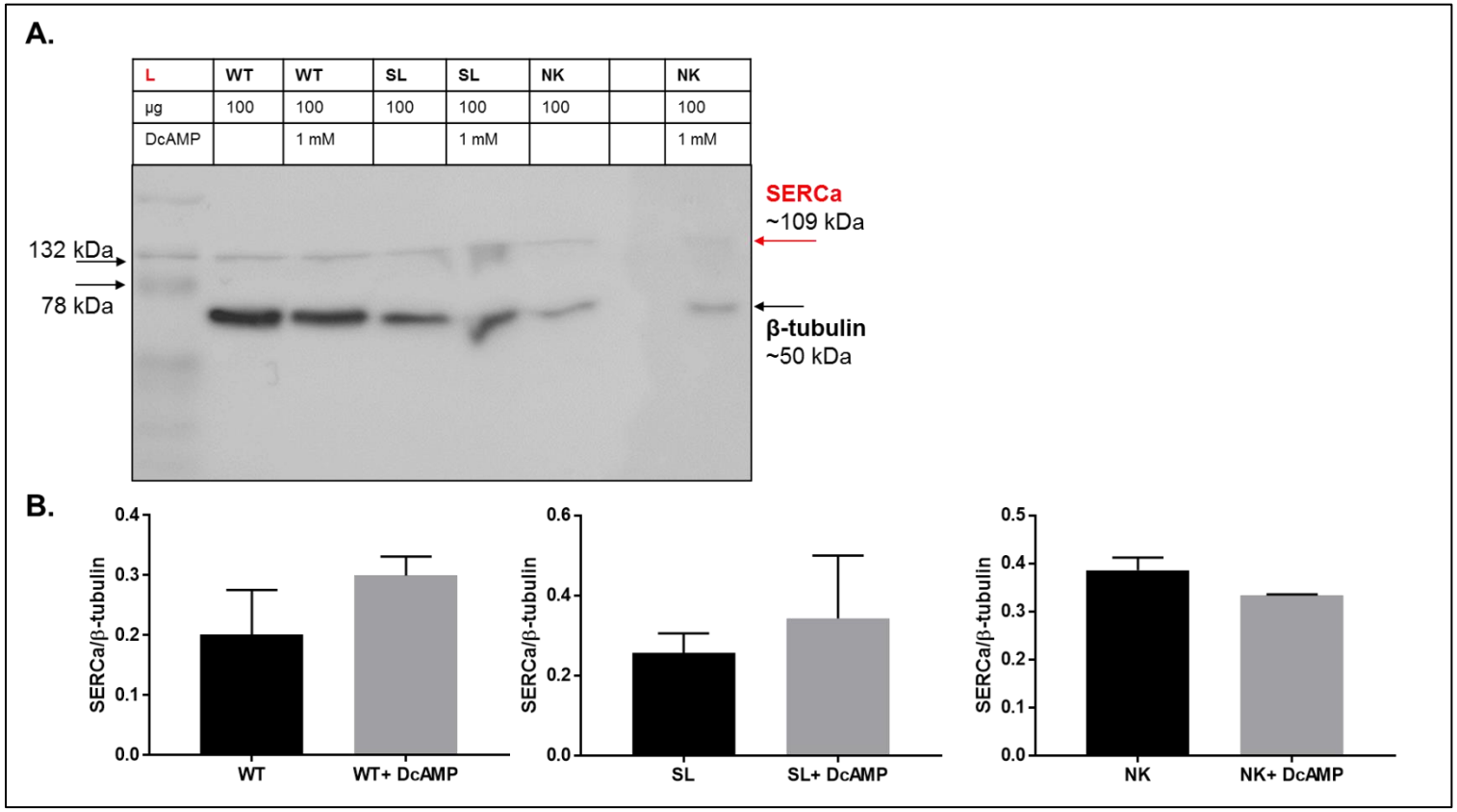

Figure 4.17 Assessment of cell homogenate from WT and mutant hRyR2-transfected HEK293 cells reveals no significant difference in SERCa expression after treatment with 1 mM DcAMP. *A.* Representative bands of SERCa and β-tubulin signal of transfected HEK293 cells treated with DMSO only, (WT, SL and NK lanes), and of cells treated with 1 mM dioctanoyl-cAMP in DMSO (+DcAMP lanes). L refers to protein ladder. Original and additional blots can be found in the Appendix *B.* Densitometric analysis of SERCa signal normalized to β-tubulin expression, n= 2-4 experiments (WT, SL and NK bands from 4 blots, +DcAMP from 2 blots). Data are displayed as mean ± SEM. No significant differences were detected before or after treatment by t test in GraphPad Prism.

4.4 Discussion

Major chapter findings include:

- Mutant hRyR2s show different basal levels of phosphorylation in comparison to WT at S2808 and S2031 sites
- DcAMP has a limited effect on the S2808 phosphorylation status of mutant hRyR2. This implies that S2808 phosphorylation plays little or no role in influencing channel function
- DcAMP may not be suitable as an analogue to elicit endogenous PKA phosphorylation of hRyR2 in Ca^{2+} imaging experiments

4.4.1 Is the Badrilla phospho-S2030 RyR2 antibody reliable?

Probing cell homogenate samples with commercially available pS2808 RyR2 antibody (Badrilla) gave strong, clear signals for phosphorylated hRyR2 protein (**Figure 4.2 A and 4.3**). The antibody appears specific and reliable, could be applied to blots at lower dilutions than the pSer-2030 antibody (1: 5,000 as opposed to 1: 1,000) and bands could be visualized after only one hour of primary antibody incubation. Probing with the pSer-2030 antibody, produced by the same manufacturer, was not so successful (**Figure 4.2 B**). PVDF membranes required at the minimum overnight incubation in primary antibody and often, no signal was detected by chemiluminescence. It took 17 separate attempts to obtain blots for n=4 (an unworkable ~24% success rate) because signal was so poor (see **Figure 4.4** and **Appendix VII**).

According to the CiteAb website (www.citeab.com) and a search of the literature, the pS2030 RyR2 antibody has only one citation (Beca et al. 2012). This is in comparison to 56 citations for the pS2808 RyR2 antibody, also produced by Badrilla. In the publication by Beca et al. (2012), antibody signal for the assessment of S2030-phosphorylated RyR2 in mouse heart lysate shows no non-specific background. This is in complete contrast to antibody signal identified by chemiluminescence in the many assessed for this Chapter. In each of these experiments, a native mouse control (although a cardiac SR preparation, rather than homogenate as in Beca et al. (2012)) was also included and in 2/4 cases no signal was exhibited under chemiluminescence for this preparation. While this control was a cardiac SR preparation, rather than a homogenate preparation as in Beca et al. (2012), the mouse species was the same. This is suggestive that the lack of signal is not because hRyR2-transfected homogenate cell samples

come from a recombinant source and that they aren't phosphorylated because of an absent kinase. Conversely, this could suggest that mouse RyR2 isn't phosphorylated at S2030, but this is highly unlikely given the body of evidence supporting phosphorylation at this site in mouse studies (Huke and Bers 2008; Xiao et al. 2006; Xiao et al. 2005; Jones et al. 2008).

Supplementary data in Beca et al. (2012) does not indicate any differences in antibody incubation, other than the use of milk in PBS as opposed to TBS-T. Manufacturers do not specify which buffer diluent is appropriate. There appears to be no indication in the literature as to why PBS-T would be advantageous over TBS-T. As well as experimental differences mentioned above, method of transfer may also account for differences, but it is not evident in the manuscript how this was achieved.

4.4.2 Mutant hRyR2s show different levels of basal phosphorylation in comparison to WT at S2808 and S2031 sites

The level of basal phosphorylation of RyR2 and therefore the scope for subsequent change in phosphorylation level has often been investigated as an indicator of the functional relevance of phosphorylation at a particular site. As with much of the research surrounding the role of phosphorylation in physiological and pathological RyR2 Ca^{2+} release, reports are often disputed. Previously, discrepancies between data of groups investigating the phosphorylation status of RyR2 have been partly attributed to the unaccounted activity of phosphatases (Reiken et al. 2003). Given that HEK293 cell lysis releases phosphatases from the cytosol that may degrade phosphorylation at specific sites of RyR2, serine/threonine phosphatase inhibitors $NaVO_4$ and NaF were included in all preparations for Western blotting.

A RyR2 channel exists as a tetramer with available phosphorylation sites on each of the four subunits (Lai et al. 1989). Some channels within a population may have none of four specific sites in a tetramer phosphorylated, while other channels may have all of the four sites phosphorylated, and other channels may have a combination of phosphorylated/unphosphorylated subunits. Therefore, basal phosphorylation signal in this Chapter is a mean for a population of RyR2 channels.

4.4.2.1 Basal phosphorylation of S2246L vs. WT hRyR2

In the assessment of S2808-hRyR2 phosphorylation, S2246L-transfected cells had a basal phosphorylation level approximately 4x that of WT-transfected cells, calculated as statistically significant (see **Figure 4.3** and **Appendix VI**).

Given that S2246L-hRyR2 transfected HEK293 cells do not appear dysfunctional under basal conditions, nor as isolated single channels in a minimal environment of no cytosolic or luminal Ca^{2+} (see **Figure 3.4**), it is interesting that they exhibit very high basal phosphorylation levels at the S2808 site in comparison to WT. These data can be interpreted in many ways. One hypothesis is that subsequent further phosphorylation at this site is irrelevant as a means of increasing RyR2 channel activity, given it is already substantially phosphorylated, equivalent to maximal phosphorylation levels achieved with PKA treatment.

The S2246L mutation is also located in close proximity to the phosphorylation domain of the channel (see **Figure 1.15**). Valdivia argues that clean targeting of RyR2 phospho-epitopes by kinases is an oversimplification of a complex mechanism of channel regulation by phosphorylation (2012). He suggests that phosphorylation of one site in the phosphorylation domain could lead to functional redundancy i.e. phosphorylation of one residue within this hotspot of different sites may be undistinguishable by the channel's gating domains. S2811 has been identified as a potential phosphorylation site in RyR2 and in particular is very close to the S2808 site (Yuchi et al. 2012; Huttlin et al. 2010). It would not be unreasonable to suggest that phosphorylation of S2808 may confer the same effects of phosphorylation at a site four amino acids downstream. Also, it may not be unreasonable to suggest that the S2246L mutation itself could confer effects or disrupt interactions of the nearby phosphorylation domain, and may account for increased baseline phosphorylation levels observed in this chapter. In a previous study of mouse S2246L RyR2, the mutation has been reported to induce an abnormally tight local subdomain interaction within the central domain involving the mutation site (Suetomi et al. 2011). This in turn induces a defective interaction between the N-terminal and central-domain and was suggested to explain the increase in cAMP-dependent spark frequency of saponin-permeabilized S2246L KI cardiomyocytes and VT observed in KI mice after exercise.

While basal phosphorylation levels are high in comparison to WT hRyR2, it also remains that very modest alterations in phosphorylation at this site within S2246L hRyR2 may be enough to elicit increased channel activity as observed in β-adrenergic stimulation. It was only upon treatment with PKA that single channels displayed an altered activity in comparison to WT in work of Wehrens et al. (2003).

In the assessment of S2031-hRyR2 phosphorylation, S2246L-transfected cells had a basal phosphorylation level approximately 0.5x that of WT-transfected cells, calculated as significantly different (see **Figure 4.4** and **Appendix VII**). While differences appear robust in this assessment of basal phosphorylation of WT and mutant hRyR2 with small errors (WT=1.712 ±0.34, S2246L=0.7708 ±0.15, N4104K=0.5117 ±0.02), the reliability of the pS2030 antibody should be taken into consideration and any interpretation based on these results made with caution. Dephosphorylation by protein phosphatases may also elicit a change in activity, given such high basal phosphorylation. This posttranslational modification has been evidenced as upregulated in many disease settings {Terentyev:2016jf}. Carter et al. (2006, 2011) have shown

that WT single channel P_o can be increased by either the action of PKA or by PP1 on the S2808 site. Perhaps dephosphorylation of S2031 could also increase mutant hRyR2 P_o.

4.4.2.2 Basal phosphorylation of N4104K vs. WT hRyR2

In contrast to S2246L, N4104K hRyR2 channels do not display a significant increase in basal S2808 phosphorylation in comparison to WT hRyR2 in HEK293 cells, yet in Ca^{2+} imaging experiments, transfected cells appear dysfunctional without further stimulation. This is suggestive that dysfunctional Ca^{2+} release in HEK293 cells by N4104K mutant hRyR2 channels is not necessarily caused by altered basal phosphorylation of hRyR2 at S2808, or that it only requires a modest change in phosphorylation level at this site to elicit a functional change. It could also point to lack of functional relevance of this site, given that channel dysfunction is observed without any significant change in phosphorylation levels. The N4104K mutation itself is located within the EF hand domain, far away from the phosphorylation (P) domain and the S2808 site (**Figure 1.16**). Dysfunction of N4104K may be caused by disrupted interdomain interactions of the C-terminal domain and an unidentified domain, as discussed in **Section 1.7.4.2** (Suetomi et al. 2011; Uchinoumi et al. 2010). Given that the phosphorylation domain is not part of these inter-domain interactions and is located within the central region of the RyR2 polypeptide, it may be that phosphorylation of these sites does not equate to alteration of function in what is already a dysfunctional channel. This hypothesis is somewhat supported by the data of Tester et al. (2007), where authors found that RyR2 channels with a mutation located in the C-terminal domain (S4546R) displayed higher Po in comparison to WT in basal conditions (in the absence of PKA), with enhanced sensitivity to cytosolic Ca^{2+}. Further phosphorylation by PKA did not further increase Po during single channel Ca^{2+} activation.

A clear finding of these data is that increased basal S2808 phosphorylation in mutant hRyR2 channels expressed in HEK293 cells does not seem to equate to Ca^{2+} release dysfunction. S2246L, a CPVT1 hRyR2 mutant that displays similar Ca^{2+} release events to WT in the absence of PKA stimulation, has a significantly higher basal phosphorylation at the S2808 site. Meanwhile, N4104K, a CPVT1 mutant that displays dysfunctional Ca^{2+} release events in the absence of PKA stimulation, does not show increased basal phosphorylation at S2808.

N4104K hRyR2 channels also displayed a decreased basal phosphorylation level at S2031, at approximately 0.25x that of WT hRyR2. N4104K hRyR2 channels are dysfunctional in a

minimal environment in single channel experiments, as well as in the Ca^{2+} imaging experiments shown in this study. It could be that lower basal phosphorylation levels at S2031 lead to mutant channel dysfunction in this instance, thereby implicating dephosphorylation in the regulation of channel activity.

Conversely, the data may suggest that the S2031 site is of little functional relevance in N4104K mutant hRyR2 channels, or in fact any hRyR2 channel. Basal phosphorylation at the S2031 site in S2246L hRyR2 is also significantly lower than WT, yet the channel appears much like WT in both single channel experiments in minimal conditions and during Ca^{2+} imaging experiments without the addition of any kinases. Work of the Marks group, also using recombinant RyR2, showed a PKA-mediated increase in the P_o of WT S2031A (not phosphorylatable) channels similar to that of WT, while untreated S2031D channels (fully phosphorylated) displayed a low Po in single channel experiments in comparison to WT channels treated with PKA {Wehrens:2006fq}. These data challenge the functional relevance of increased phosphorylation at the S2031 site and either point towards enhanced channel activity as a result of dephosphorylation (given that N4104K hRyR2 is dephosphorylated to a greater extent than WT or S2246L), or as a result of PKA phosphorylation at another site.
The methodology used to assess basal phosphorylation in this Chapter however does not identify whether these phosphorylation sites are PKA-specific and therefore direct targets during β-adrenergic stimulation, during which CPVT1 pathogenesis in patients is revealed.

4.4.3 The effects of DcAMP treatment on the phosphorylation level of WT hRyR2-transfected HEK293 cells

Both S2808 and S2031 phosphorylation sites have been implicated in enhanced RyR2 channel activity during β-adrenergic stimulation, although the functional relevance of both sites remains controversial (Marx et al. 2000; Huke and Bers 2008; Dobrev and Wehrens 2014; Bers 2012; 2012; Xiao et al. 2006). Therefore, simulating β-adrenergic stimulation by treatment of RyR2 channels with PKA may reveal enhanced or altered channel activity at either or both suggested sites.

The cAMP analogue DcAMP was chosen as a method of hRyR2 phosphorylation in this setting. DcAMP activation of endogenous PKA within a HEK293 cell and subsequent Western blot analysis of S2808 phosphorylation levels could reveal whether the S2808 site is in fact a target of PKA phosphorylation.

A control hRyR2 sample, exogenously treated with the PKA enzyme (following the protocol of Rodriguez et al. (2003)) was included in Western blot experiments to demonstrate maximum phosphorylation levels. Given cells are lysed and homogenized, PKA can access hRyR2 channels in prepared sample easily. A negative control i.e. fully dephosphorylated sample was unable to be obtained due to the methods of lysis and protein preparation used. To obtain a negative control for these experiments, cell homogenate from the same transfection would need to be treated with alkaline phosphatase. However, the lysis buffer used throughout this thesis incorporates phosphatase inhibitors, which prevent alkaline phosphatase from working.

Unfortunately, given the poor signal obtained when using the pS2030 antibody, investigation of PKA-mediated phosphorylation at the S2031 site was not investigated. Research groups consistently report that basal phosphorylation of WT at the S2031 site is low (Huke and Bers 2007; Cooper et al. 2013; Belevych et al. 2011). This may still apply to these data, as the maximally phosphorylated PKA-treated WT sample was not investigated using the pS2030 antibody in this thesis given its caveats.

Densitometric analysis shows that S2808 phosphorylation increases as DcAMP increases in this setting (**Figure 4.5**). Concentrations of 100 µM and 1 mM elicited significant increases in S2808 phosphorylation level of WT hRyR2 in comparison to DMSO (control) treatment. The

increase in phosphorylation level was ~x6 that of control sample. This WT PKA control also displays an increased hRyR2 phosphorylation level at S2808 compared to control.

Such a large increase in S2808 phosphorylation of WT hRyR2 not only signifies that PKA does in fact phosphorylate hRyR2 at this site, but that basal phosphorylation levels must be low or moderate in HEK293 cells to allow for such a change. This is in contrast to published studies, where basal phosphorylation levels of WT RyR2 isolated from sheep hearts have been reported as high as 75 % of stoichiometry (Carter et al. 2006). Many groups have reported that basal phosphorylation at the S2808 site in WT RyR2 is substantial in rat, mouse and rabbit cardiomyocytes, to at least 50 % of full stoichiometry (Huke and Bers 2008; Rodriguez et al. 2003; Xiao et al. 2005; Currie et al. 2004; Benkusky et al. 2007). Carter el al. (2006) suggest that higher levels of phosphorylation at this site 'optimizes channel control' by phosphorylation or dephosphorylation, allowing for dramatic changes in function after stimulation with PKA. This implicates the action of not only kinases but phosphatases at this site and suggests that modest alterations in basal phosphorylation levels may elicit functional change (Terentyev and Hamilton 2016; Carter et al. 2011; Carter et al. 2006). Others have argued that phosphorylation at the S2808 site is categorically not implicated in enhanced dysfunctional RyR2 channel activity observed in HF and is suggestive also that this site is not implicated in CPVT1 dysfunction (Houser 2014; Xiao et al. 2006).

As discussed previously, these experiments are most often based on RyR2 channels isolated from cardiomyocytes in comparison to HEK293 cells. It could be suggested that data presented in this thesis are more pertinent in terms of physiological RyR2 phosphorylation in human disease, given that experiments are with hRyR2 as opposed to animal RyR2. However, animals have a physiological PKA response, whereas in this instance, this response is imposed in a recombinant RyR2 channel. This finding therefore may be a result of the *in vitro* environment, as other assessments of basal phosphorylation have involved different animal models and RyR2 isolation from a cardiomyocyte, rather than a heterologous cell system that is devoid of other cardiac proteins that cycle Ca^{2+} in and out of the cell in the same manner {Bers 2008; Rodriguez et al. 2003; Xiao et al. 2005; Currie et al. 2004; Benkusky et al. 2007). The type and extent of post translational processing, including phosphorylation, is therefore likely to vary between cell types and endogenous levels of kinase may vary that could potentially phosphorylate RyR2 at this site. The level of basal phosphorylation could also be antibody dependent, given that

groups often use ‘in house’ as opposed to commercially available antibodies (Rodriguez et al. 2003; Xiao 2004; Wehrens et al. 2003; Huke and Bers 2008; Eschenhagen 2010).

It should also be noted that FKBP12.6 is not endogenous to HEK293 cells and therefore does not form a macromolecular complex with transfected hRyR2 in these cells. The contribution of FKBP12.6 also remains disputed, with some groups finding depletion from the RyR2 macromolecular complex is key to enhanced channel activity while others do not (Marx et al, 2000; Wehrens et al. 2006; Fauconnier et al. 2010; Wehrens et al. 2003; Kushnir et al; 2010; Guo et al. 2006; Shan et al. 2010). Given the evidence that suggests FKBP12.6: RyR2 interaction is irrelevant to RyR2 channel function, especially in terms of CPVT1 (George et al. 2003; Zissimopoulos et al. 2009), this was not investigated in this thesis.

4.4.4 DcAMP-mediated changes in Ca^{2+} release kinetics of WT hRyR2-transfected HEK293 cells

Western blot analysis of the effects of varying concentrations of DcAMP informed the choice of 100 µM to be used in Ca^{2+} imaging experiments, given that this was the lowest concentration to elicit a significant change in WT hRyR2 phosphorylation at the S2808 site. There was no change in the propensity of WT or mutant hRyR2-transfected HEK293 cells for Ca^{2+} release events after treatment with DcAMP (**Figure 4.11**). This was surprising given that the Chen group propose altered propensity for Ca^{2+} release as a marker of enhanced channel activity in CPVT1 mutant RyR2 channel dysfunction (Jiang et al. 2007; Jiang et al. 2010; Jiang et al. 2004; Jiang 2005), Arguably, this should not be utilized as a marker of enhanced hRyR2 channel activity in disease or conditions of stress or exercise, as discussed in **Section 3.1.2.2**.

As previously mentioned, it is difficult to interpret changes in Ca^{2+} release parameters in the absence of information of Ca^{2+} fluxes across the cell. However, treatment of WT hRyR2-transfected HEK293 cells with DcAMP did lead to measurable changes in kinetics of Ca^{2+} release. The amplitude, rate up and rate down of Ca^{2+} release events were significantly decreased. The net result of these changes is a longer duration of release (**Figure 4.14).** The decreased rate down is indicative that it takes longer for Ca^{2+} release to terminate from the PKA-phosphorylated RyR2 population. It could also be that sensitivity either to luminal Ca^{2+} concentration, cytosolic Ca^{2+} concentration or both concentrations is altered, given that the ER load for DcAMP treated WT hRyR2-transfected HEK293 cells is decreased. Luminal Ca^{2+} sensitivity of single RyR2 mouse channels has previously been reported as altered after PKA phosphorylation (Ullrich et al. 2012). In the Chen hypothesis of SOICR, authors suggest that mutations in RyR2 increase the occurrence of SOICR and the frequency of Ca^{2+} oscillation, as well as reduce the store Ca^{2+} content (Jiang et al. 2004). As SOICR is triggered by SR Ca^{2+} overload, or rather, a reduced threshold for Ca^{2+} release, it is likely that CPVT1 RyR2 mutations alter the channel sensitivity to activation by luminal Ca^{2+}. Taken together, Chen and colleagues suggested that RyR2 luminal Ca^{2+} sensitivity is a critical determinant of the threshold for SOICR and consequently for the SR Ca^{2+} content. The amplitude of Ca^{2+} release events in experiments here after treatment of cells with DcAMP also decreases, possibly indicating a small decrease in ER Ca^{2+} store due to leak that cannot be observed as spontaneous Ca^{2+} release. A decreased amplitude with longer duration and no change in frequency could suggest a change in wave

propagation or a change in Ca^{2+} buffering within the cell. However, for WT hRyR2-transfected cells, the store is not decreased after treatment with DcAMP.

It is also interesting that the changes in amplitude, rate up and rate down upon treatment of WT hRyR2-transfected HEK293 cells with DcAMP are similar to those changes in Ca^{2+} imaging experiments upon introduction of the N4104K mutation to hRyR2 in Chapter 3 (see **Figure 3.14** and **Table 3.6**). Perhaps these changes that lead to the enhanced WT hRyR2 activity during β-adrenergic stimulation lead to the dysfunctional Ca^{2+} release of N4104K hRyR2 during basal conditions in the context of CPVT1. It would not be expected that any of these observed changes are due to altered RyR2 channel clustering within a cell, as drug is only applied, and release events assessed for a very short period of time (3 min).

It is also interesting to note that no changes in the frequency of Ca^{2+} release events were observed upon treatment of hRyR2-transfected cells with DcAMP. An increased frequency of events is another hallmark of enhanced channel activity proposed by Chen and colleagues (Jiang et al. 2007; Jiang et al. 2004). PKA phosphorylation is thought to upregulate channel activity during β-adrenergic stimulation in the cardiomyocyte in response to increased metabolic demand in a physiological setting. PKA-mediated phosphorylation may increase single channel P_o by increasing the length of open time, rather than the frequency of open events (Carter et al. 2011). In HEK293 cells, a population of RyR2 channels may stay open longer rather than opening and closing more frequently. Longer Ca^{2+} release events are more likely to recruit other channels to make a more global spontaneous Ca^{2+} release event, whereas frequently opening channels will not contribute to the 'fire-diffuse-fire' mechanism and instead will represent a small, invisible Ca^{2+} leak from the ER store (Kunitomo and Terentyev 2011). In light of this it could be argued that the frequency of Ca^{2+} release events is not an adequately sensitive indicator of enhanced channel activity in hRyR2-transfected HEK293 cells.

4.4.5 DcAMP treatment has limited effect on the S2808 phosphorylation status of mutant hRyR2, compared to WT - but has similar effects on spontaneous Ca^{2+} release

In contrast, treatment of S2246L and N4104K hRyR2-transfected HEK293 with increasing concentrations of DcAMP (**Figure 4.6** and **Figure 4.7**) resulted in no further significant increase in phosphorylation at S2808 compared to basal levels. No significant differences were detected between PKA control (maximally phosphorylated) and DMSO control (basally phosphorylated) samples. This is interesting given the differences calculated in basal phosphorylation of each mutant hRyR2, with S2246L hRyR2 channels displayed higher S2808 phosphorylation level than WT hRyR2. N4104K hRyR2 does not display a significant difference in basal S2808 phosphorylation in comparison to WT hRyR2.

These data could indicate that both hRyR2 mutants have a diminished response to phosphorylation at this site, or are already substantially phosphorylated. It is logical that S2808 in S2246L hRyR2 may not be further phosphorylated by PKA given such high basal phosphorylation levels calculated previously (**Figure 4.3**). However, in the case of N4104K hRyR2 this argument does not follow. Basal phosphorylation was not calculated as significantly different to WT hRyR2 at the S2808 site. The data may therefore imply that N4104K hRyR2 channels are unable to undergo phosphorylation beyond the basal level at this site. Altered inter-domain interactions caused by the N4104K mutation may have rendered post translational modification at this site impossible due to disruption of the phosphorylation domain.

Despite not being able to significantly increase the phosphorylation of N4104K at S2808, DcAMP is reported as a highly efficient analogue of cAMP. While HEK293 cells may be devoid of cardiac Ca^{2+} cycling proteins that could be upregulated by phosphorylation mediated by either kinase (see **Section 3.4.3**), there may be other cellular targets that are activated or upregulated, given the role of cAMP in many cellular processes (Hofer and Lefkimmiatis 2007). The effectiveness of DcAMP in mediating phosphorylation is discussed further in **Section 4.4.6**.

Assessment of the phosphorylation status of the S2031 site after DcAMP treatment would have further informed the change in the nature of Ca^{2+} oscillations seen, in particular as the preliminary results collected suggested that phosphorylation at this site was significantly lower in mutants than it was for the WT under basal conditions (i.e. before stimulation with DcAMP).

However, as discussed, this was not possible due to the variable quality of results produced using this antibody (see **Section 4.4.1.**).

While treatment of mutant hRyR2-transfected cells with increased concentrations of DcAMP did not increase phosphorylation at the S2808 site, it appeared that the expression of loading control, vinculin, decreased (see **Figure 4.5-4.7**). This points to the fact that DcAMP (or its effects) may be damaging over the course of 30 mins, with less viable cells and therefore protein present for the Western blot experiments. The potential damaging effects of DMSO are discussed further in **Section 4.4.6**.

It is interesting that both S2246L and N4104K transfected cells display the same changes in Ca^{2+} release kinetics, in response to DcAMP treatment (**Figure 4.15** and **4.16** respectively). Both exhibit a decreased amplitude, a decreased rate up and an increased rate down of Ca^{2+} release. This pattern of change is also observed in WT-hRyR2 transfected cells treated with the drug (albeit additional changes are also seen, see **Table 4.2**). It could be that PKA-mediated changes in Ca^{2+} release kinetics are not due to phosphorylation at the S2808 site in mutant hRyR2, since phosphorylation at this site does not significantly increase for either mutant with DcAMP stimulation (**Figure 4.6** and **4.7**). This could implicate either PKA-mediated phosphorylation at S2031, or at other potential phosphorylation sites in hRyR2. It could also implicate another protein which may influence Ca^{2+} signalling in the cell. As discussed in **Section 4.4.3**, DcAMP may also upregulate other cellular signalling pathways which account for common changes in Ca^{2+} release kinetics that are not necessarily due to changes in RyR2 S2808 phosphorylation.

However, when you compare the Ca^{2+} release kinetics of DcAMP-treated WT hRyR2-transfected cells with treated mutant hRyR2-transfected cells, differences are evident (see **Table 4.2**). While changes caused by treatment of S2246L and N4104K-hRyR2 transfected cells follow the same pattern of changes as in treated WT, they are to a lesser extent. Treated N4104K-hRyR2 transfected cells show additional differences in Ca^{2+} release kinetics via this analysis, whereby the inter-event duration is decreased in comparison to treated WT. This suggests that the N4104K hRyR2 mutant is dysfunctional, regardless of phosphorylation status. N4104K hRyR2 also displays a dysfunctional response to pharmacological phosphorylation in this setting.

When ER Ca^{2+} store load was assessed by the addition of caffeine, S2246L hRyR2-transfected HEK293 cells displayed a significantly decreased load after the addition of DcAMP (**Figure 4.9**)**.** Considering the decreased amplitude and the decreased ER Ca^{2+} load of WT and mutant hRyR2-transfected HEK293 cells when treated with DcAMP, it was important to assess the expression of SERCa given its role of Ca^{2+} sequestration back into the ER. No significant differences were calculated in SERCa expression between WT and mutant hRyR2-transfected HEK293 cells (see **Figure 3.8**). As anticipated, no differences were calculated in SERCa expression after treatment of hRyR2-transfected cells for 30 min with DcAMP, in comparison to untreated hRyR2-transfected cells (**Figure 4.17**). Given a HEK293 cell cycle takes ~24 hr, it would be implausible that pharmacological phosphorylation of transfected hRyR2 could cause subsequent adaptive remodelling to account for enhanced activity (Weber et al. 2014; Alberts et al. 2002; Brittsan et al. 2003). While SERCa expression is unaltered, SERCa activity may be modified by DcAMP, as well as various other Ca^{2+} cycling proteins within a HEK293 cell that may contribute to the altered store load. As discussed in **Section 3.4.3**, there is no evidence of PLB expression in HEK293 cells that would modify SERCa activity (Kurzydlowski 1996; Asahi et al. 2003; Toyofuku et al. 1994). The expression of Ca^{2+} handling proteins in HEK293 cells and the Ca^{2+} fluxes within this heterologous expression system are not yet fully elucidated so it remains difficult to speculate as to whether changes in ER load are due to hRyR2 mutation in this instance. It could be suggested that while S2808 phosphorylation doesn't seem to affect the spontaneous Ca^{2+} release, it may be affecting small quark/spark-type Ca2+ release that is not measurable in this system.

4.4.6 The suitability of DcAMP as an analogue to elicit endogenous PKA phosphorylation of hRyR2 in Ca^{2+} imaging experiments

Paavola et al. (2007) used DcAMP to simulate sympathetic stimulation in mutant RyR2-transfected HEK293 cells and these data in fact informed the choice of the cAMP analogue for experiments within this Chapter.

Western analysis concluded that treatment of hRyR2-transfected HEK293 cell homogenate sample with PKA increased phosphorylation at S2808 to levels similar to those observed after treatment with 100 µM or 1 mM DcAMP in DMSO (see **Figure 4.5**). It could therefore be assumed that cellular toxicity or osmolyte effects of DcAMP in DMSO were not to a level that could stop phosphorylation from occurring. However, as discussed in **Section 4.4.5**, it was apparent that less viable protein/cells may have been present after treatment with higher concentrations of DMSO, given a decreased signal for loading control vinculin.

In Ca^{2+} imaging experiments, DMSO affected Ca^{2+} imaging. DMSO was applied to HEK293 cells expressing WT hRyR2 and DMSO was applied in Ca^{2+} imaging experiments (1% (v/v) - equivalent to the volume added for 100 µM DcAMP in this solvent). It appeared that DMSO was stopping spontaneous Ca^{2+} release events and leading to a gradual increase in basal fluorescence of dye-loaded HEK293 cells (**Figure 4.8 A**). At 1% (v/v), this falls below the reported cytotoxicity of cells to the drug, at a level of 2-4 % (Galvao et al. 2013), suggestive that DMSO is not necessarily killing cells. It is well known that DMSO can affect the structure of lipid membranes because it is hydrophobic and is an osmolyte (Lang et al. 1998; Gordeliy et al. 1998; Cheng et al. 2015). A reduction or increase in osmolality of solution surrounding a cell *in vitro* can lead to cell swelling or cell shrinkage. These actions may be responsible for the ceasing of Ca^{2+} release events. While DMSO osmolality will eventually equilibrate (as DMSO can cross the cell membrane, osmolality will increase both inside and outside of the cell until both environments remain isotonic), this is not practical for Ca^{2+} imaging experiments, especially in obtaining data for a large number of different hRyR2-transfected HEK293 cells, from several fields of view for each type. Long periods to allow for equilibration were also not feasible given compartmentalization of Fluo-3 AM dye after ~45 min (see **Section 4.3.4**). DMSO has also been recently reported to affect Ca^{2+} fluorescent dye kinetics (Menorval et al. 2012). The maximum value of fluorescence of Fluo-4 AM was shown to be dependent on the DMSO

concentration in experiments with CHO cells. Authors also observed a plateau of the fluorescence value at higher volumes of DMSO (15 vol %).

The observation that methanol alone does not appear to stop or change Ca^{2+} release events of WT hRyR2-transfected HEK293 cells (**Figure 4.8 B**), suggests that it is DcAMP itself that is causing the increases in signal fluorescence seen in **Figure 4.8 D**. A cell viability assay revealed the toxic effect of 1mM DcAMP on hRyR2 transfected cells over a period of 30 minutes, whereas treatment with 100uM DcAMP or with methanol alone did not result in a decrease of cell viability. It is possible that the maximal dose of DcAMP causes a large release of Ca^{2+} (which could explain the increases in fluorescence seen) from maximally phosphorylated and therefore activated RyR2s. According to the mechanism put forward by Carter et al. (2006), an increase from three to four subunits being phosphorylated would cause this significant change in channel open duration, in other words a relatively small (25%) change in phosphorylation level between 100uM and 1mM DcAMP would result in a profound change in function. This small change in phosphorylation would not be deemed as significant in the data set presented in **Figure 4.5**. due to the variability therein. However, it is most likely that the effects of 1mM DcAMP on Ca^{2+} imaging are unlikely to be due to any effects on hRyR2 alone, especially considering the similarity to the effects produced by DMSO alone (which is not known to be an RyR2 agonist), signifying that this is more likely to be a general toxic/osmotic effect on the cells.

In the manuscript and supplemental material of Paavola et al. (2013), the solvent used to deliver DcAMP to cells is not described. However, authors applied lower concentrations of the drug to RyR2-transfected HEK293 cells (1, 10 and 50 µM) and this could explain why the addition of DcAMP did not prevent further Ca^{2+} release events. These concentrations did not elicit changes in S2808 phosphorylation levels as assessed by Western blot (**Figure 4.5**), nor in Ca^{2+} release events assessed by Ca^{2+} imaging within this Chapter. It should also be noted that experiments of the authors were very short (≤20 sec recordings), were not in any way quantified and authors did not assess cells that characteristically oscillated upon stimulation with either caffeine or DcAMP. It is interesting to note that RyR2-transfected cells in the work of Paavola et el. (2007) displayed an extremely low number of spontaneous Ca^{2+} transients, with no difference in occurrence of these events between WT and mutant RyR2 transfected cells, even at similar levels of extracellular Ca^{2+} as used in this thesis (1.8 mmol/l). While authors do report that RyR2

transfection was confirmed by the application of caffeine, they do not state the transfection efficiency. A low transfection efficiency may account for this finding.

While it is clear that dysfunction of S2246L and N4104K hRyR2 mutant channels may be attributed to the altered basal phosphorylation of PKA-specific sites, it remains that the influence of phosphorylation of other components within the HEK293 cell cannot be accounted for or easily eliminated in this system. Estimation of basal phosphorylation is this Chapter assesses phosphorylated RyR2 in a population of channels and does not account for varying phosphorylation status of each individual channel. The phosphorylation status of an individual channel can only be controlled by genetic phosphorylation or ablation. Homogeneous genetic phosphorylation may aid in revealing the functional relevance of a specific site on hRyR2 channel function individually and separated from the influence of other factors within a HEK293 cell.

Chapter 5

Cloning, expression and functional evaluation of phosphomimetic hRyR2 mutants - S2808D and S2031D

5.1 Introduction

5.1.1 Previous use of phosphomimetic amino acid substitutions to study RyR2 channel function

Phosphomimetic amino acid substitutions have been used to investigate the phosphorylation of various proteins implicated in EC coupling, including troponin C, phospholemman, PLB and cardiac voltage-gated sodium channel $Na_v1.5$ (T. Zhang et al. 2010; Guo et al. 2015; Glynn et al. 2015; Schlecht et al. 2014). The method has extensively been applied in the study of RyR2 phosphorylation by several groups in both recombinant RyR2 cDNA studies and the use of KI/KO mouse models (Marx et al. 2000; Stange et al. 2003; Xiao et al. 2007; Benkusky et al. 2007; Kushnir et al. 2010; Chelu et al. 2009) to mimic (S to D) or ablate (S to A) phosphorylation at the S2808, S2814 and S2031 sites.

It would be anticipated that KI/KO WT mouse models of the same phosphomimetic or ablative amino acid substitution would provide similar, independently corroborated results. However, as **Tables 5.1-3** outlines, this is not the case. Most notable is the stark contrast in results between the Marks and Valdivia/Houser S2808A RyR2 KI mouse (Benkusky et al. 2007; Shan, Kushnir, Betzenhauser, Reiken, Li, Lehnart, Lindegger, Mongillo, Mohler and Marks 2010b). The Marks group report blunted chronotropic responses to Iso and reduced exercise capacity in this mouse model (Shan et al. 2010) and the authors suggest these data support a key role for S2808 phosphorylation in the PKA-mediated β-adrenergic regulation of RyR2 (as well as a role for PKA phosphorylation in the progression of HF (Marx et al. 2000; Reiken et al. 2003; Marx et al. 2001; Antos et al. 2001). Conversely, Valdivia/Houser S2808A KI mice exhibit normal myocyte shortening and Ca^{2+} transients, normal responses to Iso and normal PKA-mediated incorporation of radioactive phosphate into RyR2, despite the elimination of the S2808 phosphorylation site (H. Zhang et al. 2012; Liu et al. 2014; Benkusky et al. 2007). These data suggest that the S2808 site is of little relevance, and that other site(s) (notably S2031) are more likely to be phosphorylated by and transduce the functional effects of PKA in this channel. These conflicting results, the Marks group argues, were due to the use of a different mouse strain in this study providing a change in genetic background which affected the authors' findings. However, even when using S2808A mice backcrossed with the same C57BI/6J strain

used by Marks, the Valdivia group found a normal cardiac adrenergic response and an unaltered progression towards HF in comparison to WT mice (Alvarado et al. 2017).

The relative importance of the S2031 site over S2808 is supported by single channel recordings of recombinant mouse S2031D RyR2, where channels exhibit an increased response to luminal Ca^{2+} compared to WT (Xiao et al. 2007). Work by Stange et al. (2003) also indicates little relevance of phosphorylation at the S2808 site, as recombinant rabbit S2808D RyR2 single channels show no subconductance states, an apparent feature of phosphorylation at this site (Marx et al. 2000) and no change in Ca^{2+} activation of the channels as assessed by [^{3}H] ryanodine binding in comparison to WT RyR2. No changes were observed in the caffeine-sensitive ER Ca^{2+}-stores of S2808D RyR2-transfected HEK293 cells in comparison to WT either.

While discrepancies between results remain, there is no doubt that precise control of phosphorylation at a specific site in RyR2 has advantages over other, less controlled methods of investigating phosphorylation (see **4.1.2.5**). In the main, it aids in determining the exact effect of phosphorylation of RyR2 at each individual site, away from the influence of other phosphorylatable targets. While many groups have investigated the effects of phosphomimetic mutations on WT RyR2 channel function, whether in recombinant cDNA or in mouse models, there is no published research to date that has investigated the effects of genetic phosphorylation or ablation on CPVT1 mutant hRyR2 function.

Work in the previous Chapter demonstrated that basal phosphorylation and the ability to be phosphorylated upon stimulation was different between WT and mutant hRyR2. This chapter will assess whether genetic phosphorylation at a given site (i.e. S2808 or S2031) emulates the functional effects of kinase phosphorylation with a view to being able to attribute the functional consequences seen to phosphorylation at one site or the other. This should be straightforward in the case of the WT, since the functional data collected in Chapter 4 (in the presence of 100uM DcAMP) were from a maximally phosphorylated population of channels and, if this maximal state represents full stoichiometry, should be comparable with that of cells expressing S2808D hRyR2, if this site is functionally relevant. One might expect to see that genetic phosphorylation at the S2808 site in S2246L hRyR2 does not elicit a response, given that it is already maximally phosphorylated under basal conditions. However, since the phosphorylation status of N4014K in the presence or absence of PKA activation via DcAMP is not so clearly

defined, it is difficult to predict whether genetic phosphorylation would likely bear any resemblance to that seen using kinase activating via DcAMP.

It is also difficult to comment on the likely effects of genetic phosphorylation at the S2031 site, as maximal phosphorylation levels were not investigated in experiments with DcAMP. However, mutants were dephosphorylated in comparison to WT hRyR2 in the absence of PKA activation, so it is reasonable to expect that genetic mimics of phosphorylation at S2031 in mutant hRyR2 may display different functional characteristics to their kinase equivalents. Given that the Badrilla anti-pSer2030 antibody was determined as too difficult to work with in subsequent experiments, utilizing phosphomimetic mutations in this Chapter also offers a further opportunity to investigate the functional relevance of phosphorylation at the S2031 site in hRyR2, which was not investigated using DcAMP in the previous Chapter.

	S2808A (Marks)	S2808A (Meissner)	S2808A (Valdivia#1)	S2808A (Valdivia#2)	S2808A (Chen)
References	(Ather et al. 2012; Marx et al. 2000; Wehrens et al. 2006; Sarma et al. 2010)	(Stange et al. 2003)	(H. Zhang et al. 2012; Liu et al. 2014; Benkusky et al. 2007)	Alvarado:2017wg}	(Xiao et al. 2007)
Species of RyR2 and model	Mouse: *S2808A*, *dmd*, also rRabbit, rHuman in HEK293 cells	rRabbit: HEK293 cells	Mouse: *S2808A* and triple model, (*S2808A, CSQ2$^{(-/-)}$, SERCa1a* overexpression)	Mouse: *S2808A* and *S2808A* with MI (different genetic background to Valdiva#1)	Mouse: *S2808A* and *S2808A* with MI
Phenotype of mouse model	Phospho-ablation at S2808A improved *dmd* phenotype, protecting against Iso induced HF.	N/A	Phospho-ablation doesn't impact HF remodelling. Triple mutant showed exacerbated cardiovascular disease.	Phospho-ablation didn't affect post-MI survival, no effect on basal or Iso stimulated functions or heart structure.	Phospho-ablation resulted in better cardiac function post-MI, reduced remodelling, cardioprotective effect.
Ca^{2+} release/ functional data	Phospho-ablation decreased the frequency of spontaneous Ca^{2+} release in dmd mice on application of Iso, in comparison to *dmd* mice.	No effect on caffeine-sensitive ER Ca^{2+} store, nor on Ca^{2+} activation (^{3}H-ryanodine binding) in the presence /absence of FKBP12.6.	No effect on SR Ca^{2+} load or kinetic parameters of Ca^{2+} release either before or after treatment with Iso, increased phosphorylation at the other sites. Western blots showed dephosphorylation of S2808 and phosphorylation of S2808 and S2031 by PKA.	Phospho-ablation has no effect on Ca^{2+} release in response to Iso and no effect on expression of other cardiac proteins involved in this process.	N/A
Single channel function	Po of S2808A channels from mouse hearts was comparable to that of WT channels under basal conditions, not affected by PKA phosphorylation.	S2808A channels did not exhibit subconductance states in the presence /absence of FKBP12.6.	PKA phosphorylated RyR2-S2808A channels displayed increased Po compared to WT.	N/A	S2808A channels increased in Po after PKA phosphorylation. No subconductance states were observed, even in channels from post-MI model.
Significance	Suggests that enhanced PKA-mediated phosphorylation at S2808 contributes to abnormal Ca^{2+} homeostasis that is associated with dystrophic cardiomyopathy.	Does not support significance of single site phosphorylation in RyR2 channel function, or the relevance of FKBP12.6 dissociation upon PKA phosphorylation.	Suggests S2808 hyperphosphorylation by PKA is not implicated in pathogenesis of cardiovascular disease, but implicates dephosphorylation and S2031 phosphorylation.	Given that preventing phosphorylation at S2808 does not alter adrenergic response or HF progression, suggests phosphorylation at this site is not functionally relevant.	Implicates PKA-specific phosphorylation site in RyR2 other than S2808.

Table 5.1 Summary of the effects of genetic ablation at the S2808 site of RyR2. Diverse interpretation of data from studies of S2808A mutation. Key for abbreviations in legend of Table 5.3 below.

	S2808D (Meissner)	S2808D (Chen)	S2808D (Marks)
References	(Stange et al. 2003)	(Xiao et al. 2007)	(Wehrens et al. 2006)
Species of RyR2 and model	rRabbit: HEK293 cells	rMouse: HEK293 cells	rHuman: HEK293 cells
Phenotype of mouse model	N/A	N/A	N/A
Ca^{2+} release/ functional data	No significant differences in caffeine-sensitive Ca^{2+} stores observed between mutant and WT rRabbit RyR2 expression HEK293 cells. S2808D did not alter Ca^{2+} activation in ryanodine binding experiments in comparison to WT, with or without co-expression of FKBP12.6.	N/A	N/A
Single channel function	No subconductance states observed in S2808D single RyR2 channel recordings in the presence/absence of FKBP12.6 co-expression.	S2808D RyR2 single channels exhibited a significantly increased Po after PKA treatment, in a manner similar to WT channels.	S2808D RyR2 single channels displayed the same activity as PKA-phosphorylated WT channels, in contrast to S2031D channels.
Significance	Results do not support the view that phosphorylation of one site in RyR2 substantially modulates channel function, or that dissociation of FKBP12.6 occurs upon PKA phosphorylation of the channel.	Suggests there is another PKA-specific RyR2 phosphorylation site and that the S2808 site may not be functionally relevant.	Suggests S2808 is the only PKA functional site.

Table 5.2 Summary of the effects of genetic phosphorylation at the S2808 site of RyR2. Diverse interpretation of data from studies of S2808D mutation. Key for abbreviations in legend of Table 5.3 below.

	S2031A (Marks)	S2031A (Chen)	S2031D (Chen)
References	(Wehrens et al. 2006)	(Xiao et al. 2007)	(Xiao et al. 2007)
Species of RyR2 and model	rHuman: HEK293 cells	rMouse: HEK293 cells	rMouse: HEK293 cells
Phenotype of mouse model	N/A	N/A	N/A
Ca^{2+} release/ functional data	N/A	N/A	N/A
Single channel function	S2031A RyR2 channels displayed an increased Po in response to PKA phosphorylation in comparison to S2808A channels.	PKA did not affect S2031A single channel activity in comparison to WT, with no increase in Po. In a double mutant construct (S2031A/S2808A), there was no alteration in response to PKA either.	S2031D mutation increased luminal Ca^{2+} response of single RyR2 channels, while PKA potentiated the luminal Ca^{2+} response, in comparison to WT single channels.
Significance	Suggests that S2031 is not a functionally relevant PKA phosphorylation site in RyR2.	Suggests that S2808 is not a functionally relevant PKA phosphorylation site in RyR2.	Suggests activation of RyR2 by PKA is largely mediated by phosphorylation at the S2031 site.

Table 5.3 Summary of the effects of genetic phosphorylation and ablation at the S2031 site of RyR2. Diverse interpretation of data from studies of S2808D mutation. Key: $^{(+/-)}$: heterozygous mutation, $^{(-/-)}$: homozygous mutation, CSQ2: cardiac calsequestrin, dmd: Duchenne muscular dystrophy, FKBP12.6: FK506 binding protein 12.6, Iso: isoproterenol, MI: myocardial infarction (induced by surgery), PKA: protein kinase A, rMouse/rRabbit/rHuman: recombinant mouse/rabbit/human RyR2, SERCa: sarco/endoplasmic reticulum Ca^{2+}-ATPase.

5.1.2 Chapter aims

In comparison to pharmacological phosphorylation, genetic phosphorylation will allow for complete control to elucidate the effects of this modification at the S2808 and S2031 PKA-specific RyR2 sites individually. While genetic phosphorylation and ablation have extensively been investigated in WT recombinant cDNA and KI/KO mouse studies, no publications to date have utilized the method of phosphomimetic amino acid substitutions to investigate the role of phosphorylation in the dysfunction of CPVT1 RyR2 mutant channels.

In order to assess the effects of site-specific phosphorylation on WT and mutant hRyR2 function, the aims were to:

- Engineer phosphomimetic substitutions (i.e. serine to aspartic acid to mimic complete phosphorylation) in WT, S2246L and N4104K plasmids at both the S2808 and S2031 sites
- Assess the expression of WT and mutant phosphomimetic hRyR2 in HEK293 cells by Western blotting to determine whether changes in function are attributable to changes in protein expression caused by 'genetic phosphorylation'
- Determine the intracellular localization of hRyR2 within HEK293 cells with immunofluorescence to confirm that molecular alterations of the constructs do not cause mislocalisation of recombinant mutant hRyR2
- Analyse the Ca^{2+} handling of HEK293 cells expressing these constructs to a) determine whether phosphomimetic mutations emulate the effects of phosphorylation and b) determine the functional effects of phosphorylation at the S2808 and S2031 sites

5.2 Materials and methods

5.2.1 Generation of eGFP-hRyR2 phosphomimetic constructs

The following six phosphomimetic hRyR2 constructs were first engineered using site directed mutagenesis and a cassette-based cloning strategy:

- WT with S2808D mutation (referred to in figures as **WT08**)
- WT with S2031D mutation (referred to in figures as **WT31**)
- S2246L with S2808D mutation (referred to in figures as **SL08**)
- S2246L with S2031D mutation (referred to in figures as **SL31**)
- N4104K with S2808D mutation (referred to in figures as **NK08**)
- N4104K with S2031D mutation (referred to in figures as **NK31**)

The method of cassette-based site-directed mutagenesis (SDM) was employed to generate full-length eGFP-hRyR2 WT and mutant phosphomimetic constructs. The protocol allows the introduction of nucleotide substitutions using *Pfu* DNA polymerase to amplify DNA. This process exploits the polymerase chain reaction (Mullis et al. 1986) to replicate mutagenic primer-directed plasmid strands and is limited to amplification of DNA sequences ~6-8 kb, which makes it unsuitable for mutagenesis of full length eGFP-hRyR2, a plasmid of >21 kb.

This was overcome by using the intermediate superlinker vector, pSL1180 (GE Healthcare). pSL1180 vectors altered to contain fragments of hRyR2 or 'cassettes' were obtained from Dr. CH George and Dr. NL Thomas. These cassettes are coding DNA fragments of hRyR2 bordered by specific restriction sites, meaning that a fragment can be digested from one vector and inserted into the other (**Figure 5.1**). Intermediate 'cassette' vectors used in SDM were as follows:

- KN1 cassette – plasmid size 7666 bp in length. This cassette contains the hRyR2 coding sequence 7553 bp (2518aa) to 11,857bp (3953aa) and contains the target amino acid S2808 (amino acids TCT beginning at nucleotide position T8422). Bordering the coding sequence are restriction sites *KpnI* and *NheI* (hence plasmid name KN1). Restriction site *FseI* is also present in this cassette and digesting with *KpnI* and *FseI* removes the correct fragment for insertion back into RyR2.

- SK1 cassette – plasmid size 5455 bp in length. This cassette contains the hRyR2 DNA coding sequence from 5421bp (1807aa) to 7553bp (2518aa) and contains the target amino acid S2031 (amino acids TCC beginning at nucleotide position T6091, derived from the ATG start codon). Bordering the coding sequence are restriction sites *SanDI* and *KpnI* (hence plasmid name SK1).

A schematic representation of pSL1180 cassettes and full-length mutagenized phosphomimetic constructs is found in **Figure 5.1.** After mutagenesis of the intermediate vector, the hRyR2-coding fragments were excised and ligated into the full-length hRyR2 sequence vector, using corresponding restriction enzymes (**Figure 5.2**).

5.2.1.1 Primer design for site-directed mutagenesis

Oligonucleotide primers for the purpose of site-directed mutagenesis were designed with the following considerations, sequences for which are in **Table 5.4**:

- Both mutagenic primers must contain the desired mutation, annealing to the same sequence on opposite strands of the DNA plasmid
- The desired mutation should be at the centre of the primer, with at least 10-15 bases of complementary sequence either side
- The melting temperature of primers (T_m) should be above 78 °C
- The primers should have a minimum GC content of 40 % and should terminate with one or more G or C bases
- Primers must be purified by High Performance Liquid Chromatography (HPLC) or polyacrylamide gel electrophoresis (PAGE)

Custom oligonucleotide primers were ordered and purified using reverse phase High Pressure Liquid Chromatography (HPLC) from Sigma Genosys, supplied as lyophilized pellets. Primers were complementary to the WT hRyR2 sequence, aside from two mismatched nucleotides that resulted in the desired amino acid substitution by site-directed mutagenesis. Pellets were resuspended in 250 µL dH_2O following manufacturer guidelines and stored at -20 °C. Primers were diluted to a concentration of 150 ng/mL for application in site-directed mutagenesis.

Name	Sequence	Nucleotide position	Amino acid substitution	Length (bp)	T_m (°C)	GC content (%)	Description
S2031DF	GAGGGCGTCTGCTA**GA**C CTGGTAGAAAAGGTGAC	G6077	S2031D	34	77.7	55	Forward primer for the mutagenesis of hRyR2 (S2031D)
S2031DR	GTCACCTTTTCTACCAGG **TC**TAGCAGACGCCCTC	C6077	S2031D	34	77.7	55	Reverse primer for the mutagenesis of hRyR2 (S2031D)
S2808DF	CCGGACTCGTCGTATT**GA** TCAGACAAGCCAGGTTTC	C8406	S2808D	36	81.3	53	Forward primer for the mutagenesis of hRyR2 (S2808D)
S2808DR	GAAACCTGGCTTGTCTGA **TC**AATACGACGAGTCCGG	C8406	S2808D	36	81.3	53	Reverse primer for the mutagenesis of hRyR2 (S2808D)

Table 5.4 Site-directed mutagenesis oligonucleotide primers. Mutagenesis primers used to insert the mutations S2031D and S2808D into mutagenesis cassettes (See **Figure 5.1** for cloning strategy). Sequences are given in the 5' to 3' direction, with nucleotides in red indicate those undergoing substitution. Positions of nucleotides are derived from the RyR2 ATG start codon.

5.2.1.2 Site-directed mutagenesis

The QuikChange II site-directed mutagenesis kit (Agilent) was utilized to introduce mutation into intermediate vectors. A schematic of the process is outlined in **Figure 5.1**.

Site-directed mutagenesis reaction mixtures were prepared as in **Table 5.5** and following thermal cycling as in **Table 5.6**, 1 µL *DpnI* enzyme was added and the reaction product incubated at 37°C for 90 minutes. This restriction endonuclease is specific for methylated and hemi methylated DNA and was used to digest the plasmid DNA pre-mutagenesis, taking advantage of the fact that DNA isolated from *E. coli* strains is methylated by deoxyadenosine methylase and susceptible to digestion. XL1 Blue cells were then transformed (according to manufacturer's instructions) with this *DpnI*-treated DNA for propagation of this plasmid. Mutagenesis of cassettes was confirmed by DNA sequencing (Cardiff Biotechnology Services), before progressing to construction of full-length eGFP-hRyR2 plasmids.

Reagent	**Volume**
10x reaction buffer	5 µL
dsDNA template	5-50 ng
Oligonucleotide primer (forward)	125 ng
Oligonucleotide primer (reverse)	125 ng
dNTP mix (proprietary)	1 µL
Deionized dH_2O	up to final volume of 50 µL

Table 5.5 Sample reaction for site-directed mutagenesis reaction.

Step	**Stage**	**Duration**	**Temperature**	**Number of cycles**
1	Denaturation	30 secs	95 °C	1
2	Denaturation	30 secs	95 °C	16
	Annealing	1 min	55 °C	
	Extension	1 min/kb of plasmid length	68 °C	

Table 5.6 Thermal cycling parameters for QuikChange II site-directed mutagenesis.

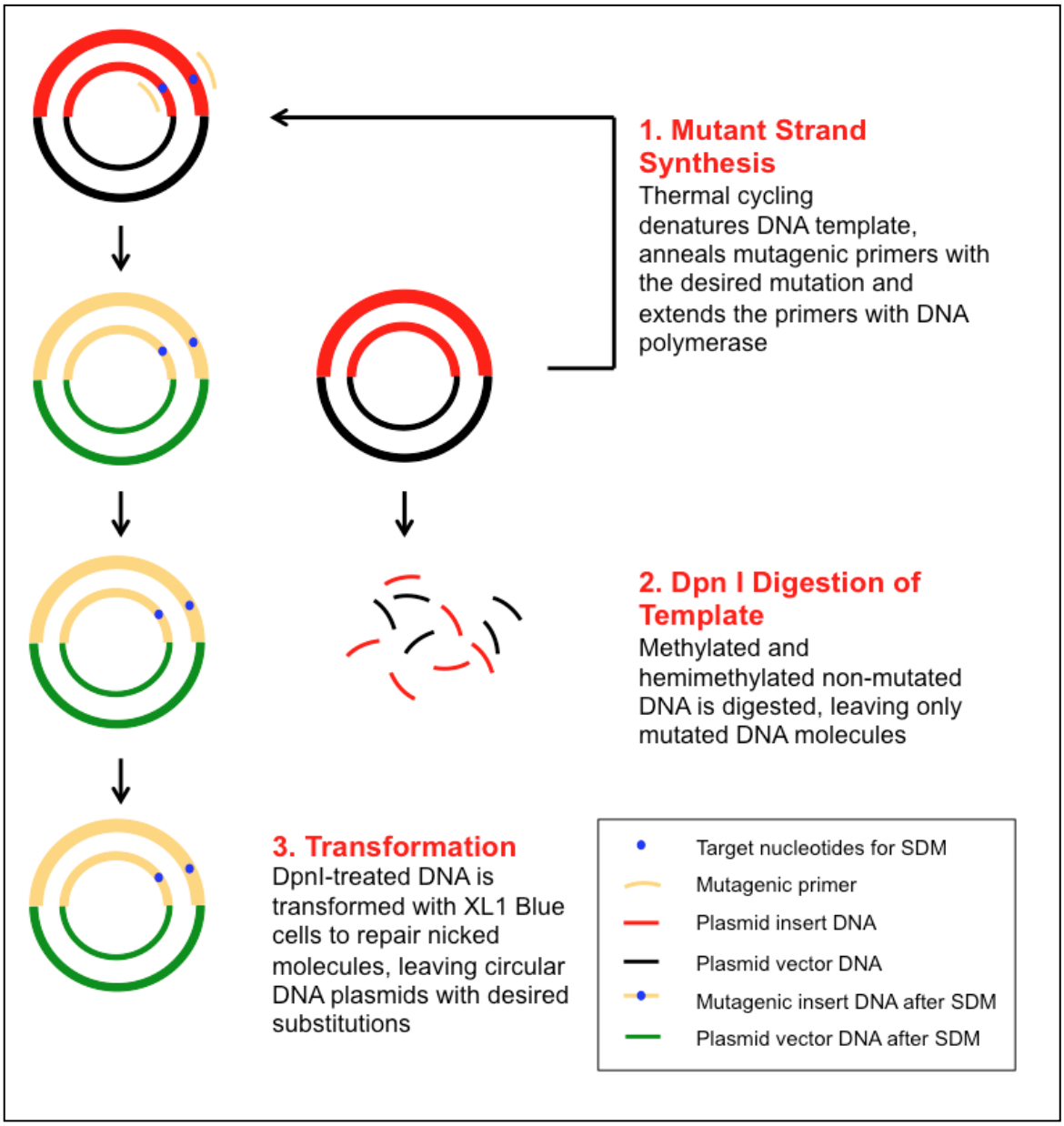

Figure 5.1 Schematic of the QuikChange II site-directed mutagenesis method. SDM was carried out to make nucleotide substitutions within RyR2 mutagenesis cassettes (plasmid insert DNA) in intermediate vectors (plasmid vector DNA). Adapted from the Agilent product manual.

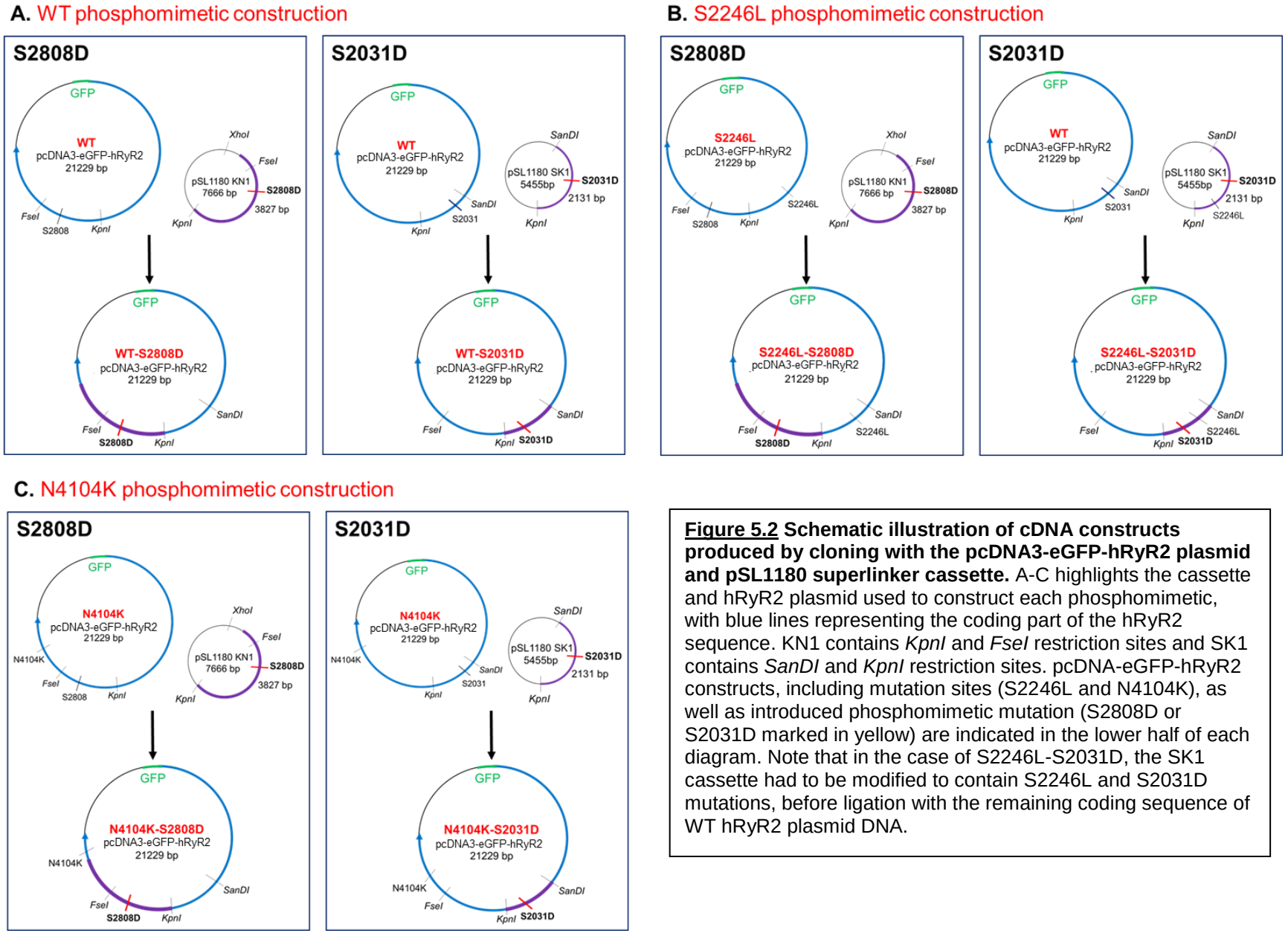

Figure 5.2 Schematic illustration of cDNA constructs produced by cloning with the pcDNA3-eGFP-hRyR2 plasmid and pSL1180 superlinker cassette. A-C highlights the cassette and hRyR2 plasmid used to construct each phosphomimetic, with blue lines representing the coding part of the hRyR2 sequence. KN1 contains *KpnI* and *FseI* restriction sites and SK1 contains *SanDI* and *KpnI* restriction sites. pcDNA-eGFP-hRyR2 constructs, including mutation sites (S2246L and N4104K), as well as introduced phosphomimetic mutation (S2808D or S2031D marked in yellow) are indicated in the lower half of each diagram. Note that in the case of S2246L-S2031D, the SK1 cassette had to be modified to contain S2246L and S2031D mutations, before ligation with the remaining coding sequence of WT hRyR2 plasmid DNA.

For the construction of S2031D phosphomimetics, the appropriate full length eGFP-hRyR2 plasmid DNA, together with the mutagenized SK1 shuttle vector (see **Figure 5.2**) underwent double-digest with *SanDI* and *KpnI* endonucleases (High Fidelity, New England Biolabs) for 30 minutes at 37°C. The resulting fragments were separated by agarose gel electrophoresis (see **Section 2.3.3**), shown in **Figure 5.3**.

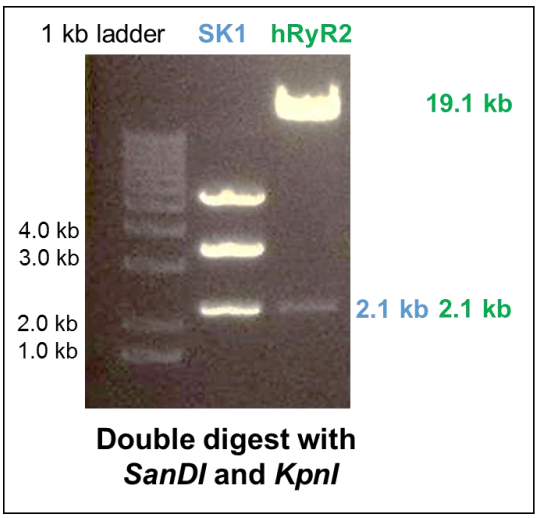

S2808D phosphomimetic construction		
	Vector: WT, SL, or NK pcDNA3-eGFP-hRyR2	**Insert:** Mutagenized KN1 cassette
cDNA	1 µg	1 µg
KpnI	10 U (1 µL)	10 U (1 µL)
FseI	3 U (1.5 µL)	3 U (1.5 µL)
XhoI	0	10 U (1 µL)
Buffer 1.1 (10x)	2 µL	3.5 µL
dH_20	up to 20 µL	up to 35 µL

Figure 5.3 Double digest of the S2031D mutagenized SK1 cassette and full length hRyR2 plasmid to obtain fragments for ligation. *SanDI* and *KpnI* are bordering restriction sites in the SK1 cassette. Upon a double digest of the cassette, 3326bp and 2129bp fragments are obtained as indicated in the gel electrophoresis image (left). The band at approximately 5400 bp is undigested/linearized SK1 plasmid. The table outlines the double digest reaction. Enzyme stock concentration: 20,000 U/ml. Both enzymes are compatible with Buffer 1.1 according to the New England Biolabs Double Digest Finder Tool. *SanDI* is now commercially known as *KflI* (ThermoFisher Scientific).

The process of fragment generation for ligation was not as straightforward for S2808D phosphomimetic constructs. While full-length eGFP-hRyR2 plasmid DNA was digested with restriction enzymes corresponding to the sites bordering the fragment for insertion (i.e. *KpnI* and *FseI*), the S2808D mutagenized KN1 plasmid was digested with an additional enzyme (i.e. a triple digest using *KpnI*, *FseI* and *XhoI*) in order that the fragment of interest could be effectively resolved by electrophoresis from that which remains (see **Figure 5.4**).

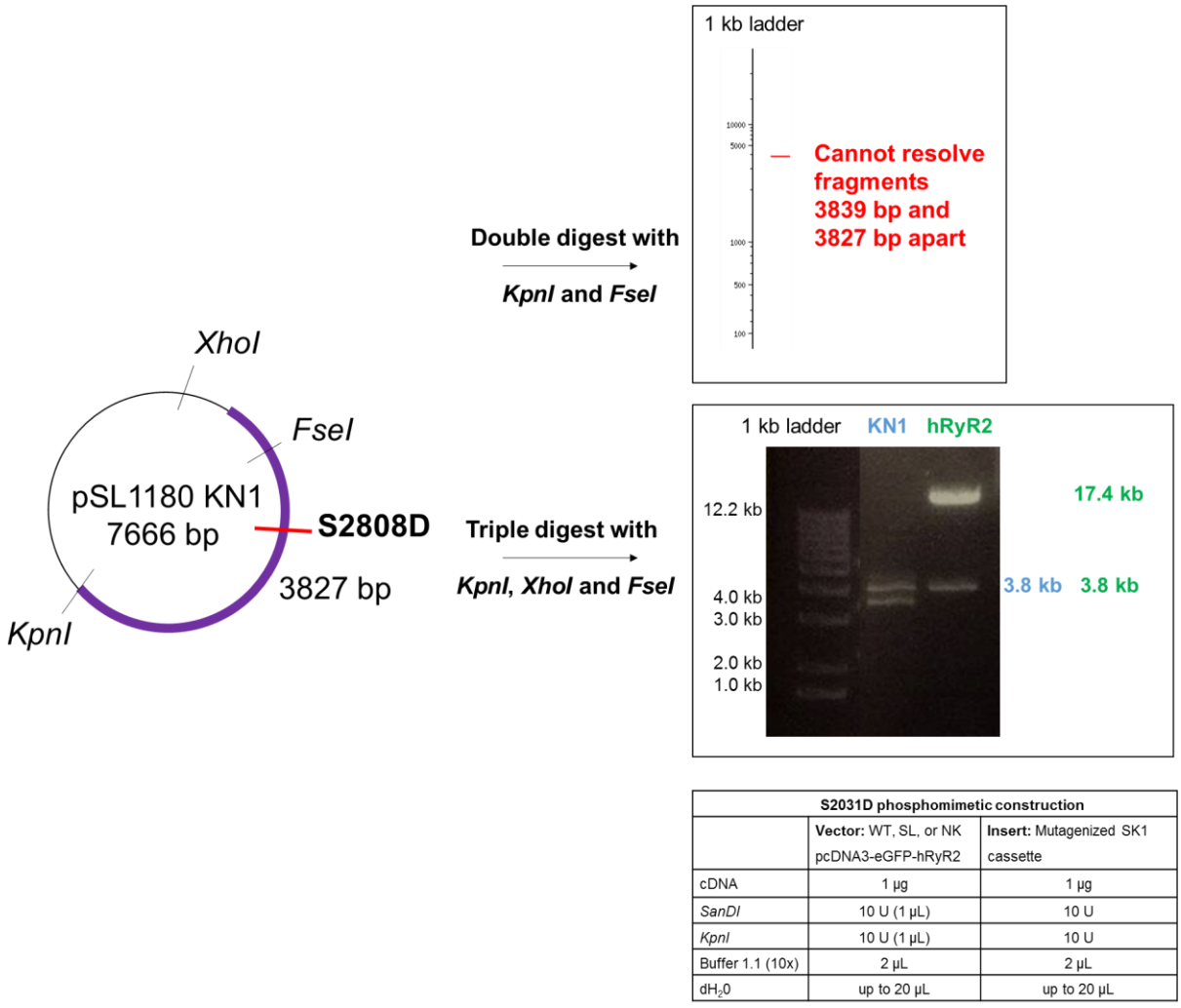

S2031D phosphomimetic construction		
	Vector: WT, SL, or NK pcDNA3-eGFP-hRyR2	**Insert:** Mutagenized SK1 cassette
cDNA	1 µg	1 µg
SanDI	10 U (1 µL)	10 U
KpnI	10 U (1 µL)	10 U
Buffer 1.1 (10x)	2 µL	2 µL
dH_20	up to 20 µL	up to 20 µL

Figure 5.4 Triple digest of the S2808D mutagenized KN1 cassette and full length hRyR2 plasmid to obtain fragments for ligation. Top left is a schematic of the KN1 cassette, with hRyR2 coding sequence (blue), showing *KpnI* and *FseI* bordering restriction sites and the XhoI site, outside of this coding sequence. Upon double digest with *Kpn*I and *FseI*, the resultant fragments, at 3839bp and 3827p, cannot be resolved using agarose gel electrophoresis (see illustration from NEB cutter v2.0, top right). Upon triple digest with *KpnI*, *FseI* and *XhoI*, fragments (3827 bp, 3291 bp and 548 bp) are obtained as indicated in the gel electrophoresis image. Enzyme stock concentration: *KpnI* and *XhoI* 20,000 U/ml, *FseI* 2,000 U/ml. Both enzymes are compatible with Buffer 1.1 according to the New England Biolabs Double Digest Finder Tool.

DNA fragments were purified using the QIAEX II kit (Qiagen). Briefly, resolved fragments were identified using UV trans illumination (very briefly to avoid DNA cross-linking), before removal using a scalpel. Gel slices were solubilized separately in the high salt QX1 buffer containing guanidium thiocyanate, at 3 volumes of buffer to 1 volume of gel. QIAEX II silica beads were resuspended by vortexing for 30 secs, before the addition of 30 µL to the sample. Samples were incubated at 50 ˚C in a waterbath for 10 minutes to allow agarose solubilisation and the binding of DNA to the silica beads. To keep the beads in suspension, the samples were gently inverted every 2 minutes of this incubation period. Samples were then centrifuged for 30 seconds at 13,000 rpm (5417R centrifuge, Eppendorf) and the supernatant carefully removed. Pellets were then washed with 500 µL QX1 wash buffer and centrifuged for a further 30 seconds to remove residual agarose contaminants. The pellets were then washed twice with 500 µL of ethanol-containing PE buffer, to remove residual salt contaminants. To elute DNA, 20 µL of dH_2O was added to pellets, which were resuspended by gentle inversion. After 30 seconds of centrifugation at 13,000 rpm the supernatant, containing the purified DNA was removed into a clean tube. The DNA Nanovue Plus (GE Lifesciences) was used to determine DNA concentration (see Section 2.3.5).

Ligation was carried out using the Roche Rapid DNA ligation kit (Roche), following manufacturer guidelines. Briefly, the digested insert was mixed with plasmid vector (50 ng) in a 3:1 molar ratio, with T4 DNA ligase (5 U/ µL) and ligase buffer (containing ATP) to join insert and vector 'sticky-ends' together. Ligation reaction mixtures were incubated at 4 ˚C for 16 hrs before being used to transform XL10-Gold competent bacterial cells (See **Section 2.3.1**) to begin the amplification process of full-length eGFP-hRyR2 plasmid DNA. LB_{AMP} broth and NZY broth (16 g/L NZ casein, 50 g/L yeast extract in dH_2O, autoclaved) were used as cell culture media in these experiments. For a sample ligation, see **Figure 5.5** below.

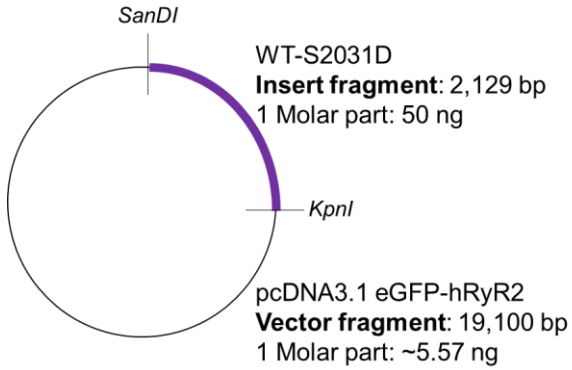

LIGATION (Vector:Insert, Molar ratio 3:1)	
Vector (50 ng)	6 µl
Insert (~20 ng)	2 µl
Buffer 2 (10x)	2 µl
Mix thoroughly	
Buffer 1 (2x)	10 µl
Mix thoroughly	
T4 DNA ligase	1 µl
Total	**21 µl**
Mix, incubate overnight at 4 ºC	

Figure 5.5 Sample ligation reaction to construct pcDNA3 eGFP-hRyR2-S2031D. In the ligation reaction, a ratio of 1 molar part of vector fragment to 3 parts insert fragment was used. Ligation was catalysed by T4 DNA ligase from the Roche Rapid DNA ligation kit (Roche).

5.2.1.3 Sequencing of the SDM site and restriction boundaries

After large scale plasmid preparation (see **Section 2.3.4**), mutated constructs were sequenced by Central Biotechnology Services, Cardiff University. Both the mutagenesis site and restriction boundaries were sequenced using appropriate primers (**See Table 5.7**). Data were compared to the hRyR2 sequence using the BLAST sequencing alignment tool. Electropherograms were visualized by 4peaks software.

Primer Name	Direction	Sequence	Start Nucleotide	Length (bp)	GC content (%)	Use
B23R1	Reverse	GGAAACTTTGGTGCTGCCTCAG	G5762	22	55	Verification of SanDI restriction site
B23F7	Forward	CTGCCAGAGCCAGTTAAATTGCAG	C5692	24	50	Verification of S2031D mutagenesis
B38R1	Reverse	GGATAGAAGCCATTGTAGCC	G7873	20	50	Verification of KpnI restriction site
SPFOR.8305-22	Forward	CCATGACAAATGGTCAAT	C8184	18	39	Verification of S2808D mutagenesis
B6/10(-)	Reverse	TTATGAACAAGAAATCAAGTTC	C8847	22	28	Verification of S2808D mutagenesis
24F	Forward	GGCACTAAGAGAGTTGATCCTC	G10969	22	50	Verification of FseI restriction site

Table 5.7 Sequencing oligonucleotide primers. 'In house' primers used in automated sequencing to verify correct mutagenesis and ligation of hRyR2 fragments at restriction boundaries. Sequences are given in the 5' to 3' direction. Start nucleotides are derived from the ATG start codon.

5.2.2 Evaluating the expression of phosphomimetic hRyR2 in HEK293 cells

Methods for the expression, preparation of cell homogenates and detection of hRyR2 proteins by Western Blot are detailed in Chapter 2. The expression of eGFP phosphomimetic hRyR2 constructs was assessed by methods described in **Section 3.2.3.**

5.2.3 Confocal microscopy and Ca^{2+} imaging

The kinetic parameters of Ca^{2+} release in HEK293 cells expressing phosphomimetic hRyR2 channels were assessed using the methods described in **Section 3.2.1**.

5.2.4 Immunofluorescence analysis of cells expressing eGFP-hRyR2

Localization of phosphomimetic hRyR2 channels, recombinantly expressed in HEK293 cells was assessed by IF as described in **Section 3.2.2.**

5.3 Results

5.3.1 Generation of phosphomimetic hRyR2 constructs

Cloning of hRyR2 cDNA plasmids is notoriously problematic (George *et al.* 2005) and construction of the six hRyR2 phosphomimetics described in **Section 5.2** was not straightforward. To engineer both S2031D and S2808D phosphomimetic mutations in each different hRyR2 construct (WT, S2246L and N4104K), 4-12 ligations were carried out in each case, with a total of 40 attempts made (see **Figure 5.6.C**). For each of these ligation attempts, 36-60 bacterial colonies were screened, with plasmids digested with restriction enzyme *EcoRI* to identify clones with the characteristic digest pattern (see **Figure 5.6 A and 2.3.1**). These are referred to as positive clones.

Average ligation efficiency did not surpass 50% for any of the full length hRyR2 phosphomimetic expression plasmids generated (with a range of 5.5-47.5% positive clones obtained). While ligation of the S2031D cassette fragment with either the WT or S2246L hRyR2 vector fragment led to the highest % of positive clones (42.5-47.5 %), and ligation success with the N4104K hRyR2 vector fragment was low at 19.8 %. Ligation of the S2808D cassette fragment with all the hRyR2 fragments (WT, S2246L or N4104K) led to a much lower % of positive clones in each case (5.5-23.3 %) in comparison to S2031D.

Yielding a positive clone from the ligation of either phosphomimetic fragment with the N4104K hRyR2 vector fragment was most difficult, with only 3 of 9 ligation attempts yielding any positive clones at the miniprep stage. The average % of positive clones in these cases was very low (5.5-19.8 %), with as few as three colonies out of a total of 60 identified with the characteristic *EcoRI* digest pattern.

While some of the positive clones that were sequenced at the mini-prep stage were verified as phosphomimetics, all efforts to culture these bacterial colonies at a larger scale in XL10 cells to yield usable quantities of DNA failed, with recombination of plasmids seen in all of 21 attempts (**Figure 5.6 B and C**).

To address the issue of recombination of positive clones when attempting to culture XL10 bacterial cells at a larger scale, multiple experimental conditions were tested (see **Table 5.8**).

Changing incubation conditions, including growing at a lower temperature of 27 ˚C and incubating for 15 hours as opposed to 18 hours, showed no success. Using a different culture media, NZY broth failed to yield any positive large-scale cultures, neither did using a smaller volume of media.

Number of maxi preparation attempt	Temperature	Growth media	Incubation time	Successful?
1	30 °C	LB_{AMP} broth	15 hours	X
2	27 °C	LB_{AMP} broth	18 hours	X
3	27 °C	LB_{AMP} broth	15 hours	X
4	30 °C	NZY broth	15 hours	X
5	27 °C	NZY broth	18 hours	X
6	27 °C	NZY broth	15 hours	X
7	30 °C	LB_{AMP} broth	15 hours	X

Table 5.8 Experimental conditions trialled in XL10 bacterial cell maxi preparation of phosphomimetic hRyR2 plasmid DNA. Changing experimental conditions of the large-scale culture of positive clones obtained from mini preparation of XL10 cells did not lead to the yield of any correctly digesting phosphomimetic plasmid DNA. The temperature, growth media and incubation time were all altered, with no success (indicated by a red X in the table).

All positive miniprep clones made in XL10 cells (verified by both digest and sequencing), scaled up under the careful culture conditions tabulated above, recombined and failed to show the correct digest pattern at the maxi prep stage (see **Figure 5.9** and **Table 5.8**). Verified miniprep cDNA was also re-transformed into XL10 cells an attempt to propagate further, but this was also unsuccessful, as plasmids again recombined at the large-scale culture stage.

A.

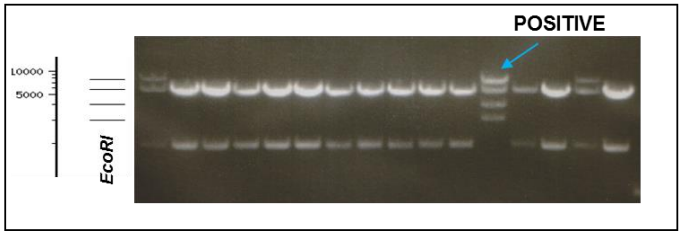

B.

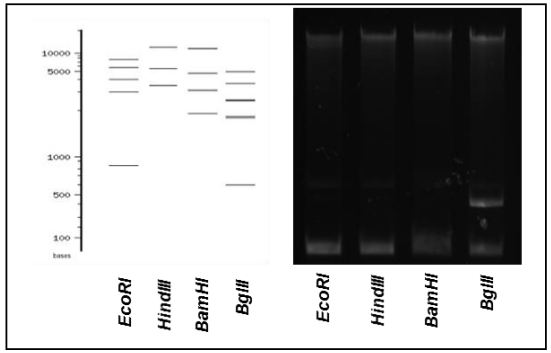

C.

Quantifiable criteria	Construct	WT S2031D	S2246L S2031D	N4104K S2031D	WT S2808D	S2246L S2808D	N4104K S2808D
1	Total number of ligations attempted	10	7	5	12	11	4
2	Ligations which yielded no positive RyR2 clones by digest	**4**	**1**	**5**	**7**	**3**	**4**
3	Ligations which yielded only re-ligated non-phosphomimetics	**2**	**2**	**3**	**1**	**2**	**2**
4	Ligations which yielded some positive RyR2 clones	4	4	2	4	6	1
5	The average % of positive clones from the ligations in 4	42.5 ±21.4	47.5 ±21.2	19.8 ±19.8	23.3 ±10.9	9.8 ±2.1	5.5 ±27.7
6	Ligations where positive RyR2 clones recombined during scale up from mini to maxi culture	**4**	**4**	**2**	**4**	**6**	**1**

Figure 5.6 Attempts to propagate phosphomimetic hRyR2 constructs in XL10 *E. coli* cells. *A.* A representative gel electrophoresis image of a mini preparation with XL10 cells digested with restriction enzyme *EcoRI*, with 15 picked colonies and 1 positive result (blue arrow). The illustration to the left shows expected positive digest result for the complete plasmid (simulation produced by NEB cutter). *B.* A representative gel electrophoresis image of digested plasmid DNA isolated following large-scale culture in XL10s after a positive sequencing result. *EcoRI*, *HindIII*, *BamHI* and *BgIII* were used to digest DNA and illustration to the left shows expected positive result. This shows failure to culture on the larger scale and recombination of clones. *C*. Table summarizing the cloning efficiency of phosphomimetics in XL10 cells. Data in row 5 are given as ± SEM.

In our laboratory's experience, XL10 *E. coli* cells are most suitable to culture more unstable hRyR2 constructs or introduce mutations by cloning. However, even after further optimisation of growing conditions, expansion of bacterial culture for large scale plasmid isolation was unsuccessful. As a result, it was decided to attempt retransformation of sequence-verified mini preparation plasmid DNA into Stbl2 *E. coli* cells. Stbl2 cells are not recommended for cloning by manufacturers, but have been routinely used in our laboratory to propagate WT hRyR2 DNA. Only one retransformation was attempted for each of the six phosphomimetic hRyR2 plasmids, with 7-24 bacterial colonies screened in each instance (**Figure 5.7 C**). Stbl2 cells showed a very high percentage of positive clones that displayed the correct *EcoRI* digest pattern at the miniprep stage (65-100 %, see **Figure 5.7 A and C**). After large scale culture of positive bacterial colonies, hRyR2 DNA displayed the correct restriction digest pattern (**Figure 5.7 B and C**) and were verified by sequencing. Alignment to the WT sequence confirmed that the correct nucleotide substitution had taken place and that no additional nucleotides were inserted. The primers described in **Table 5.8** were used to sequence over the mutation site and cassette insertion boundaries, with sequence chromatograms found in **Figure 5.8.** All six phosphomimetic constructs required for this project were successfully generated after retransformation of positive clones into Stbl2 cells.

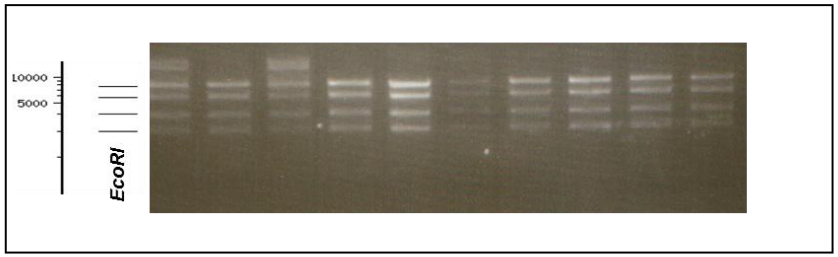

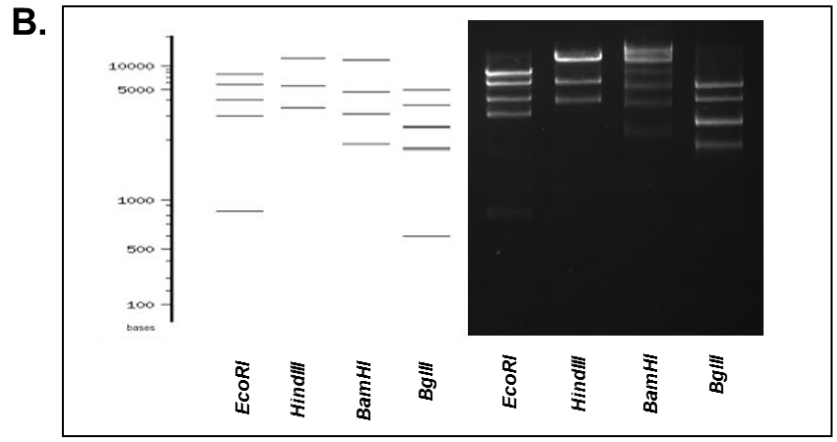

C.

Retransformation of clones in Stbl2 E. coli cells				
Attempt number [construct]	**Number of clones picked**	**Percentage of positive clones (%)**	**Number of maxipreps**	**Digest result at maxiprep**
1 [WTS2031D]	10	100%	2	Positive
2 [SLS2031D]	20	85%	2	Positive
3 [NKS2031D]	24	65%	1	Positive
4 [NKS2031D]	20	100%	2	Positive
6 [NKS2808D]	7	100%	2	Positive
7 [SLS2808D]	12	75%	2	Positive

Figure 5.7 Attempts to retransform and propagate phosphomimetic hRyR2 constructs in Stbl2 *E. coli* cells. *A.* A representative gel electrophoresis image of eGFP-hRyR2 WT-S2808D phosphomimetic mini prep clones obtained after the transformation of Stbl2 cells with verified phosphomimetic constructs made in XL10 cells (see **Figure 6** above), which all show the correct EcoRI digest pattern (two appear incompletely digested). Ladder shows expected positive digest result (simulation produced by NEB cutter: http://nc2.neb.com/NEBcutter2/). *B.* A representative gel electrophoresis image of eGFP-hRyR2 WT-S2808D phosphomimetic plasmid cDNA obtained by large scale culture in Stbl2 cells, showing the correct anticipated digest patterns using *EcoRI*, *HindIII*, *BamHI* and *BglII*. *C.* Table showing the number of attempts to generate positively sequenced phosphomimetic constructs using Stbl2 cells. All constructs were successfully generated and propagated by this method.

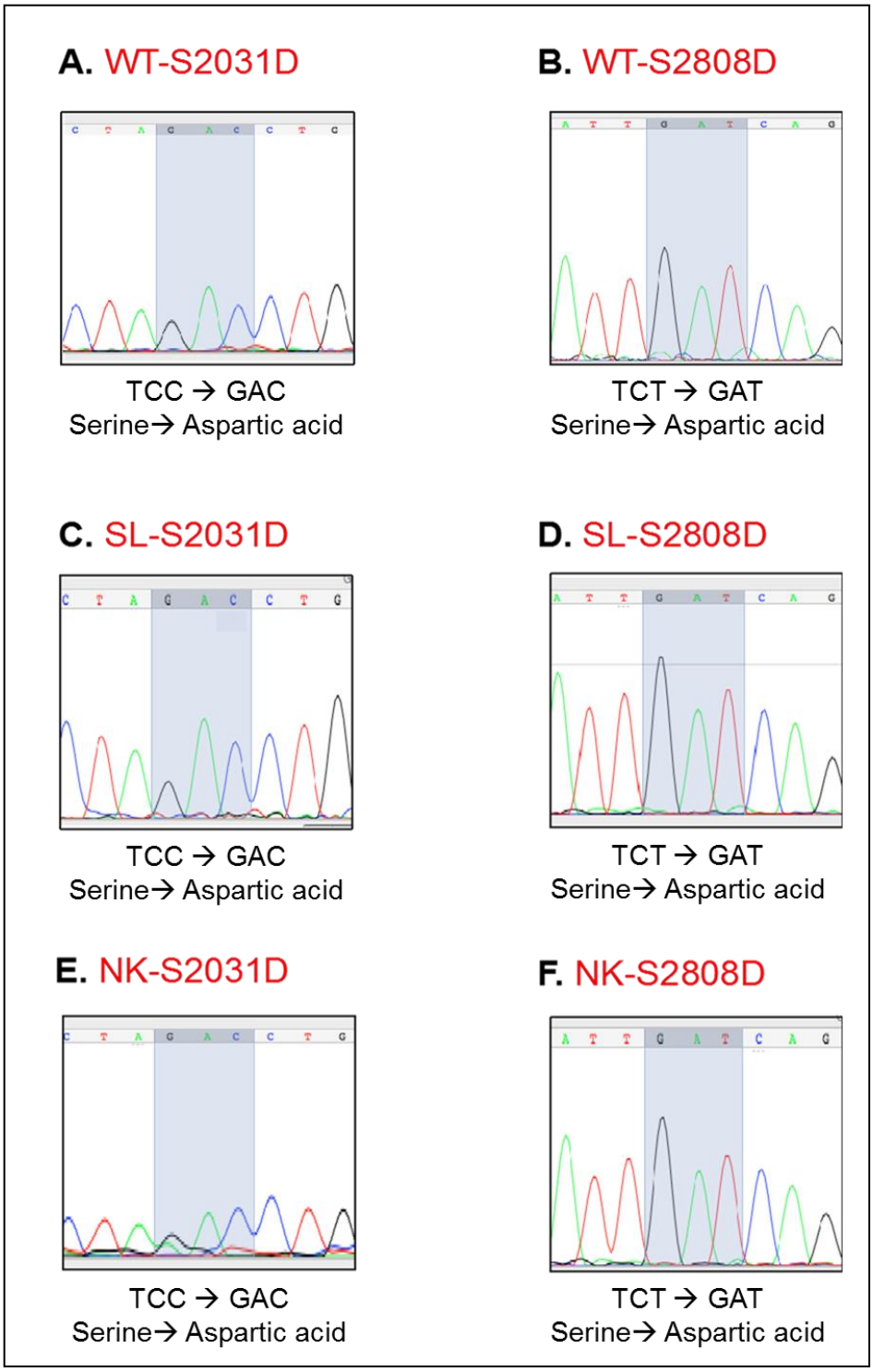

Figure 5.8 Phosphomimetic mutant pSL1180-cassette-hRyR2 chromatograms. A. WT-S2031D, B. WT-S2808D, C. S2246L-S2031D, D. S2246L-S2808D, E, N4104K-S2031D, and F. N4104K-S2808D. DNA sequencing was successful for all constructs, with desired point mutations verified. The codon substitution is highlighted in blue.

5.3.2 Do hRyR2 phosphomimetics traffic correctly in HEK293 cells?

Direct visualization of recombinant protein eGFP fluorescence or IF localization with an anti-RyR2 antibody (pAb-1093) with Alexa^{546}-conjugated secondary antibody suggests that the phosphomimetic RyR2 proteins target to the ER in HEK293 cells. The total co-incidence between eGFP fluorescence and immunolocalization was calculated by Manders overlap coefficient in ImageJ software as described previously in **Section 3.2.2** (Manders et al. 1993). WT phosphomimetic constructs all showed a high degree of colocalization (**Figure 5.9**). Analysis of green to red pixels gave coefficients between 0.79-0.96, and of red to green pixels between 0.75-0.93. No significant differences between WT and phosphomimetic constructs were found. S2246L constructs also displayed a high degree of colocalization (**Figure 5.10**), with Manders coefficients of green to red pixels between 0.85-0.92 and red to green pixels between 0.76-0.89 and no significant differences calculated between constructs. This indicates that the N-terminus and C-terminal end of the construct localize together in the ER, with little degradation.

However, one-way ANOVA found significant differences between N4104K and its S2808D and S2031D variants (**Figure 5.11**). N4104K phosphomimetics displayed a significantly lower degree of colocalization for green to red pixels (N4104K=0.9083 vs. NK4104K-S2808D=0.7447 and NK4104K-2031D=0.7048, $p<0.05$ by one way ANOVA with Bonferroni posthoc test). However, in the coefficient calculation of red to green pixels, no significant differences were calculated. Approximately one third (30 %, n=10) of HEK293 cells transfected with N4104K phosphomimetic constructs that were visualized did not have the characteristic reticular pattern of fluorescence and instead appeared ‘blobby’. Given the finding of lone red pixels in regions without green and the ‘blobby’ appearance of N4104K phosphomimetic hRyR2-transfected HEK293 cells, this indicates there may be some issue with protein integrity within the cell. However, all coefficients were calculated to have relatively strong cooccurrence, ranging between 0.683-0.9083, and this would indicate the expression of some intact, full-length recombinant hRyR2 within the ER.

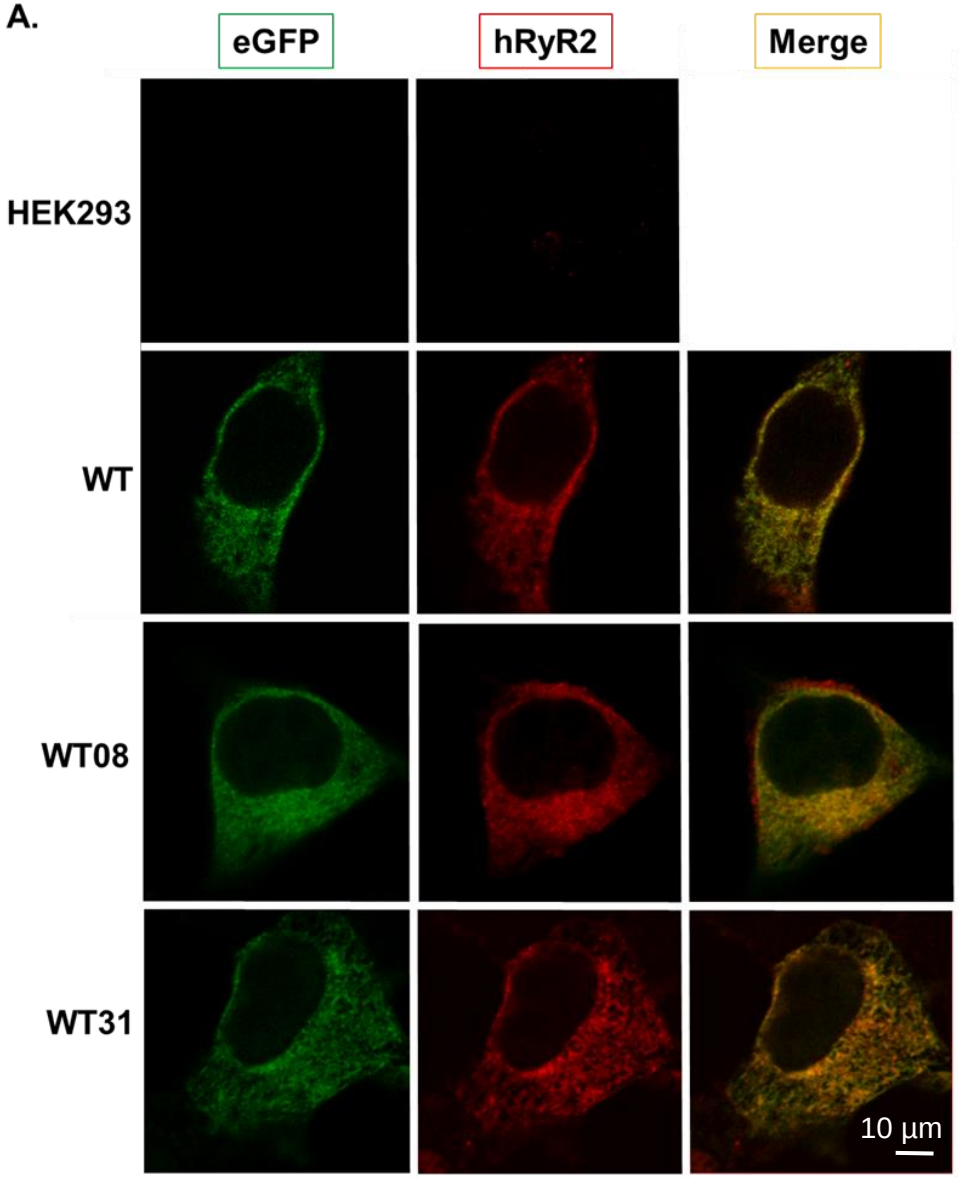

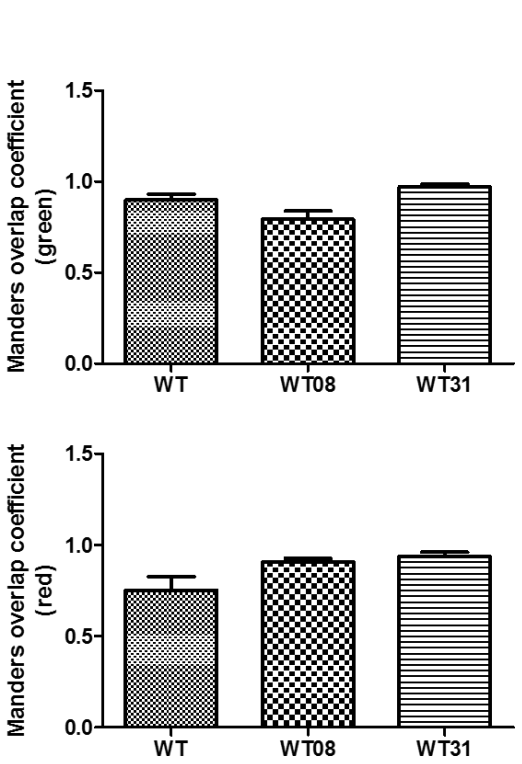

Figure 5.9 WT phosphomimetic hRyR2 constructs appear to exhibit correct intracellular trafficking. HEK293 cells transfected with hRyR2 constructs were examined for eGFP fluorescence (ex. 488 nm, em. 525±25 nm, left images) and immunofluorescence of Alexa546 secondary antibody targeted to hRyR2 primary antibody pAb-1093 (em. 546 nm, ex. 572±30 nm, centre images). Colocalization (of green to red and red to green) was calculated by Manders overlap coefficient (*B*), with no significant differences calculated by one way ANOVA with Bonferroni posthoc, n = 4-5 cells per construct. The scale bar represents 10 µm.

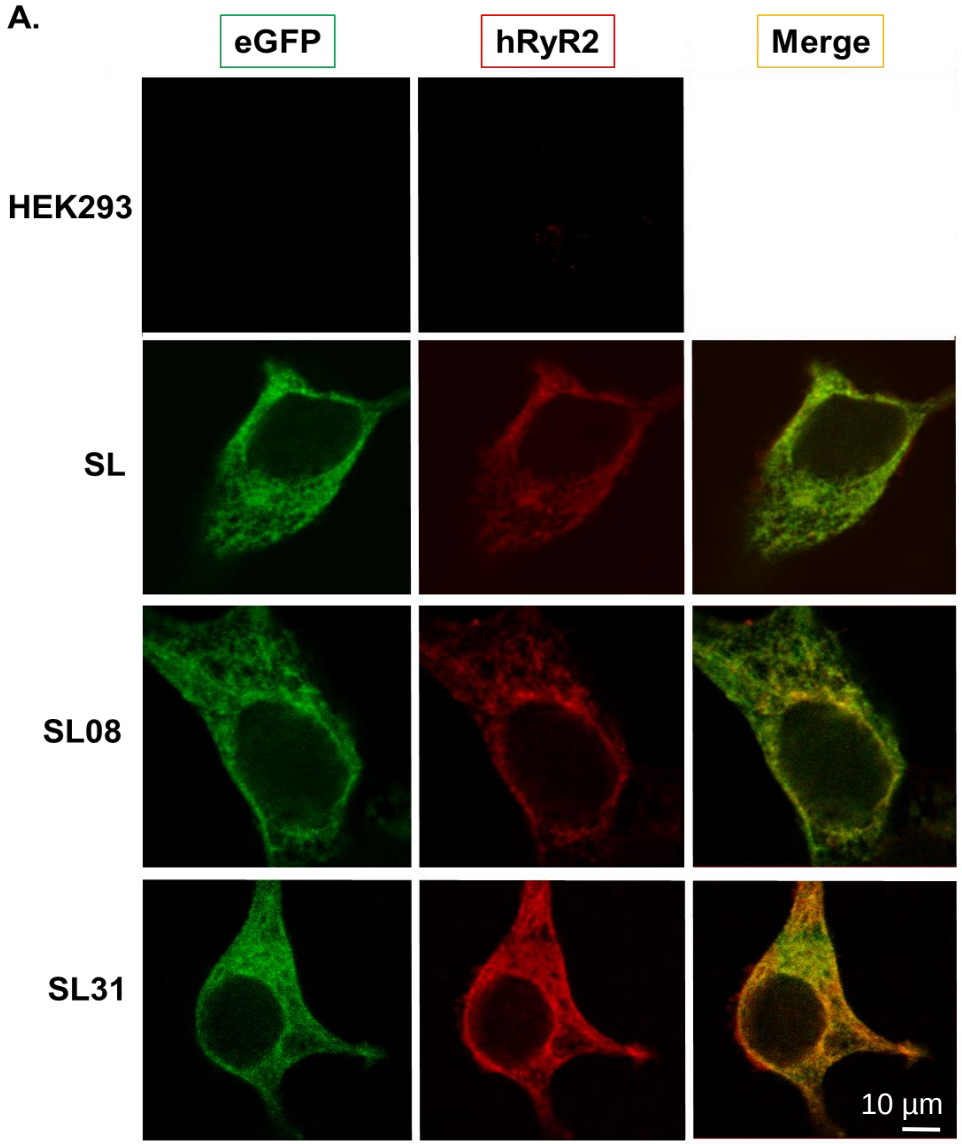

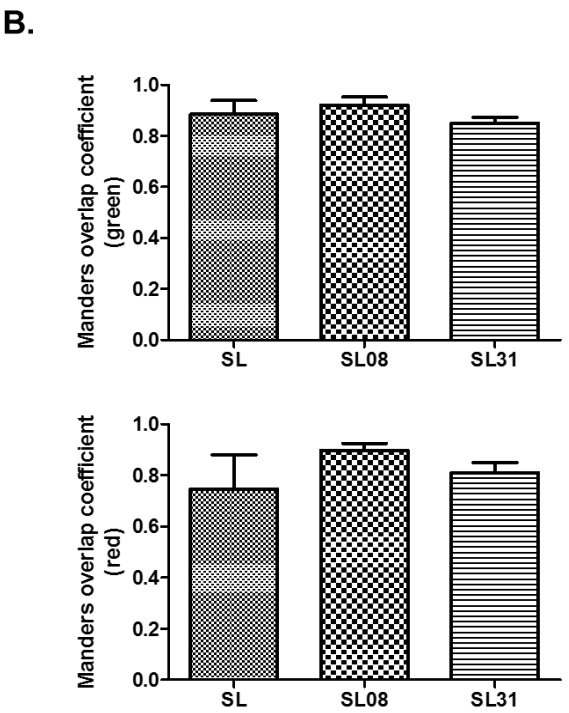

Figure 5.10 S2246L phosphomimetic hRyR2 constructs appear to exhibit correct intracellular trafficking. HEK293 cells transfected with hRyR2 constructs were examined for eGFP fluorescence (ex. 488 nm, em. 525±25 nm, left images) and immunofluorescence of Alexa546 secondary antibody targeted to hRyR2 primary antibody pAb-1093 (em. 546 nm, ex. 572±30 nm, centre images). Colocalization (of green to red and red to green) was calculated by Manders overlap coefficient (*B*), with no significant differences calculated by one way ANOVA with Bonferroni posthoc, n = 4-5 cells per construct. The scale bar represents 10 µm.

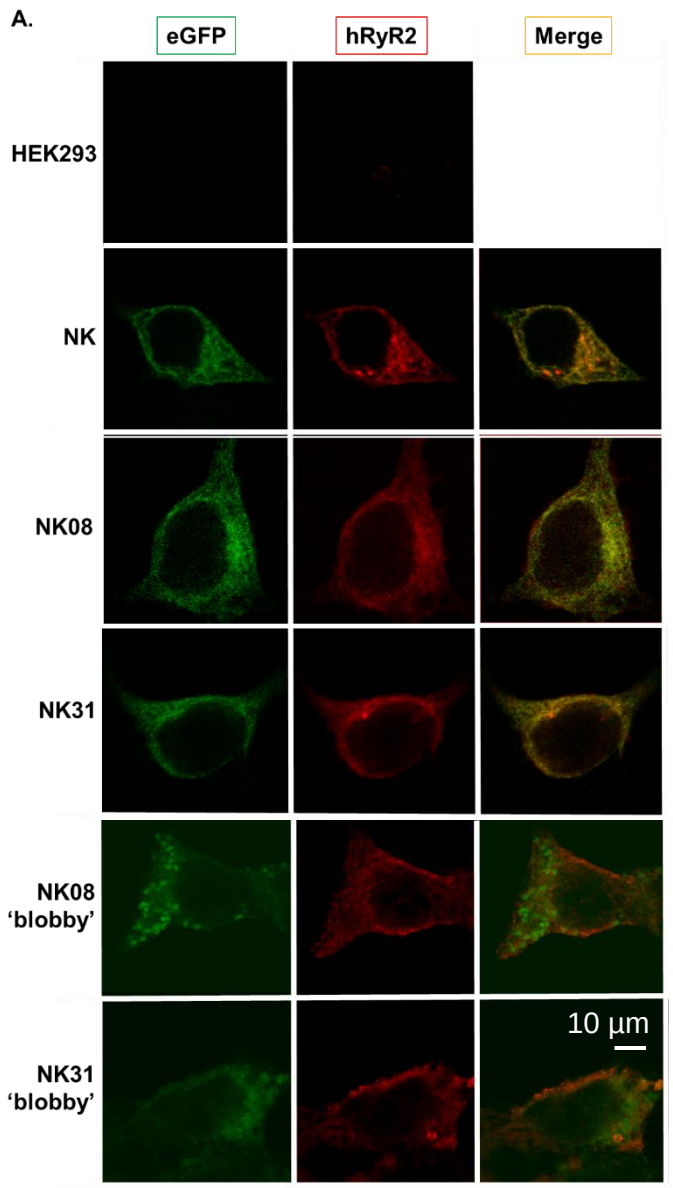

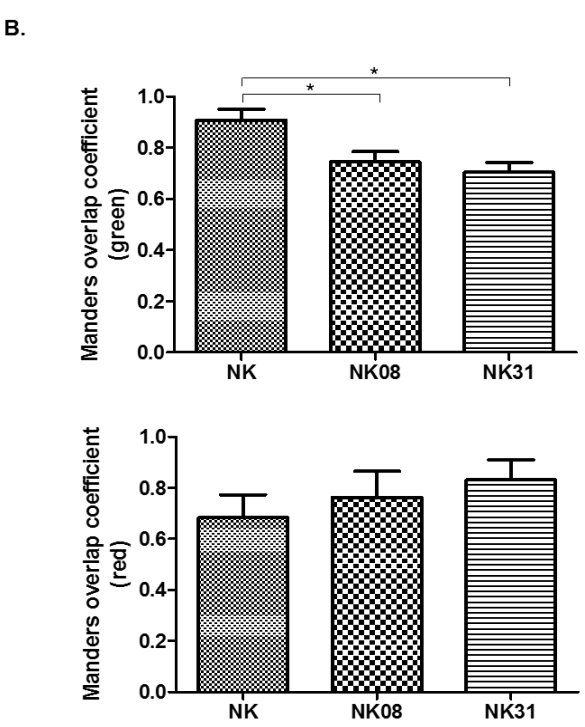

Figure 5.11 N4104K phosphomimetic hRyR2 constructs appear to exhibit mostly correct intracellular trafficking, although some cells appear unusual. HEK293 cells transfected with hRyR2 constructs were examined for eGFP fluorescence (ex. 488 nm, em. 525±25 nm, left images) and immunofluorescence of Alexa546 secondary antibody targeted to hRyR2 primary antibody pAb-1093 (ex. 546 nm, em. 572±30 nm, centre images). Colocalization (of green to red and red to green) was calculated by Manders overlap coefficient (*B*), with significant differences calculated by one way ANOVA with Bonferroni only in analysis of green to red pixels, not in red to green (n = 4-5 cells per construct). As indicated by images labelled 'blobby', some colocalization appears unusual in NK phosphomimetic constructs (~30 % of cells investigated). The scale bar represents 10 µm.

5.3.3 What is the transfection efficiency and Ca^{2+} release channel functionality of hRyR2 phosphomimetics in HEK293 cells?

HEK293 cells expressing WT or mutant phosphomimetic hRyR2 constructs were identifiable by their caffeine-induced Ca^{2+} release, with a sharp increase in fluo-3 signal amplitude after caffeine addition (10 mM) and no further spontaneous Ca^{2+} release events. This signified the expression of functional hRyR2 channels within the HEK293 cell as previously discussed (**Section 3.3.2**). Images used to assess the efficiency of transfection of HEK293 cells with each mutant and phosphomimetic hRyR2 DNA construct can be found in **Appendix XIX-XVI**.

Calculation of the percentage of cells exhibiting eGFP fluorescence following Effectene-mediated transfection did not demonstrate comparable efficiencies for all phosphomimetic hRyR2 DNA constructs (**Figure 5.12**). A significantly decreased mean transfection efficiency was calculated for WT08 hRyR2-transfected cells in comparison to WT (A). SL31 hRyR2-transfected cells also exhibited a significant decrease in comparison to S2246L, whereas SL08-transfected cells showed a similar transfection efficiency. Cells transfected with either N4104K phosphomimetic hRyR2 DNA construct (NK08 or NK31) showed a dramatic decrease in transfection efficiency in comparison to the parent mutant N4104K. However, low transfection efficiencies were reproducible with different DNA preparations for each construct, with 3 separate plasmid DNA preparations used in 3 transfections of each N4104K phosphomimetic hRyR2 DNA.

While every construct showed functional caffeine-induced Ca^{2+} release, indicative of the presence of functional hRyR2 channels, **Figure 5.13** shows that the ER Ca^{2+} content (calculated as described in **Section 3.2.3.4)** was significantly altered by the expression of some phosphomimetic hRyR2s. In comparison to WT, cells transfected with WT08 or WT31 were found to have a significantly increased ER Ca^{2+} load. Following a similar pattern, cells expressing SL08 also showed a significantly increased ER Ca^{2+} load in comparison to those expressing S2246L. The increase in load of cells expressing SL31, NK08 or NK31 was not significantly different to that of the parent mutant.

Heterogeneity in channel dysfunction (in particular the amplitude of a Ca^{2+} release transient) may result from an increased or reduced Ca^{2+} store and this therefore must be considered in data interpretation of these constructs. This is addressed in **Section 5.4.2**.

5.3.4 What is the expression level of hRyR2 phosphomimetics in HEK293 cells?

WT and mutant phosphomimetic hRyR2 cell homogenate preparations were generated and analysed by Western blotting as described in **Chapter 2**. Load was normalized to transfection efficiency as discussed in **Section 3.3.1,** such that expression level per hRyR2 expressing cell could be estimated. At loads of 100 µg (or equivalent after normalization), the signal detected for eGFP-hRyR2 (~565 kDa) for each lane was normalized to that for vinculin (~117 kDa) for each blot. An average was then taken for 3-9 separate blots (for WT, S2246L and N4104K expression, data were pooled from previous blots hence the higher n numbers). **Figure 5.14 A** shows an example of a Western blot for this assessment.

Densitometric analysis revealed comparable levels of expression in comparison to the equivalent parent hRyR2 (i.e. WT vs. WT08, WT vs. WT31) as assessed by one way ANOVA with Bonferroni posthoc ($p<0.05$, **Figure 5.14 B**).

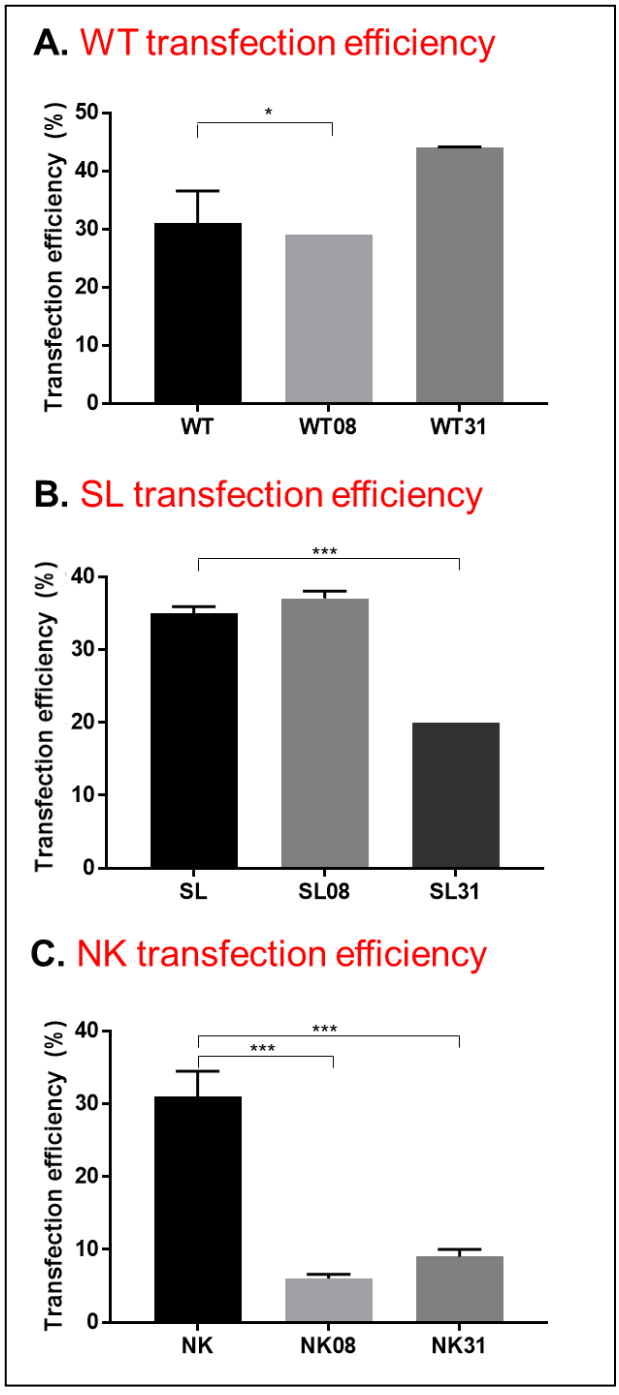

Figure 5.12 Most phosphomimetic hRyR2-expressing HEK293 cells do not have a comparable transfection efficiency to parent hRyR2. n transfection WT=6, WT08=2, WT31=2, SL=7, SL08=2, SL31=2, NK=4, NK08=3, NK31=3. Data are displayed as mean ± SEM and were analysed by Kruskal-Wallis with Dunn's posthoc or in GraphPad Prism, with $p<0.05$ indicated by *, $p<0.01$ by **, $p<0.001$ by ***. Where no error bars are shown, error was calculated as very small.

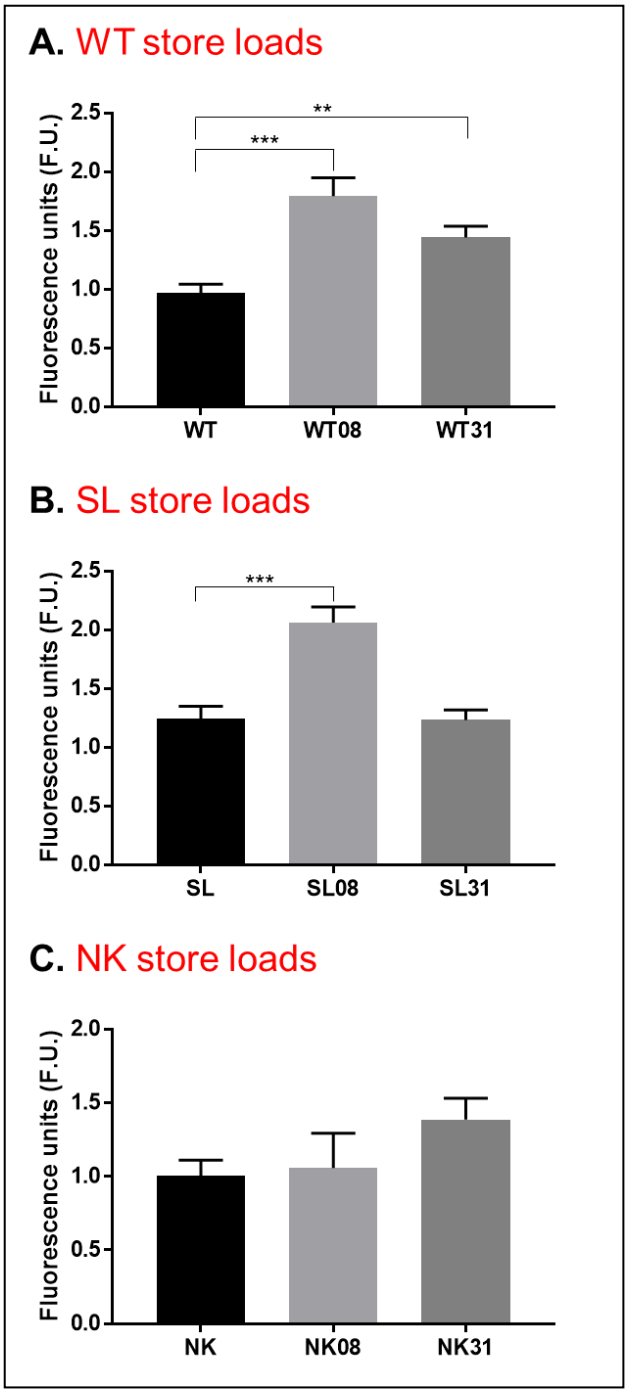

Figure 5.13 Mimic of phosphorylation at the S2808 site increases ER Ca^{2+} store load in cells expressing WT or S2246L but not N4104K hRyR2. n cells WT=41, WT08=44, WT31=63, SL=43, SL08=43, SL31=21, NK=25, NK08=7, NK31=34. Data are presented as mean ± SEM, $p<0.05$ is denoted by *, $p<0.01$ by ** and $p<0.001$ by *** as calculated by Kruskal-Wallis with Dunn's posthoc analysis with GraphPad Prism.

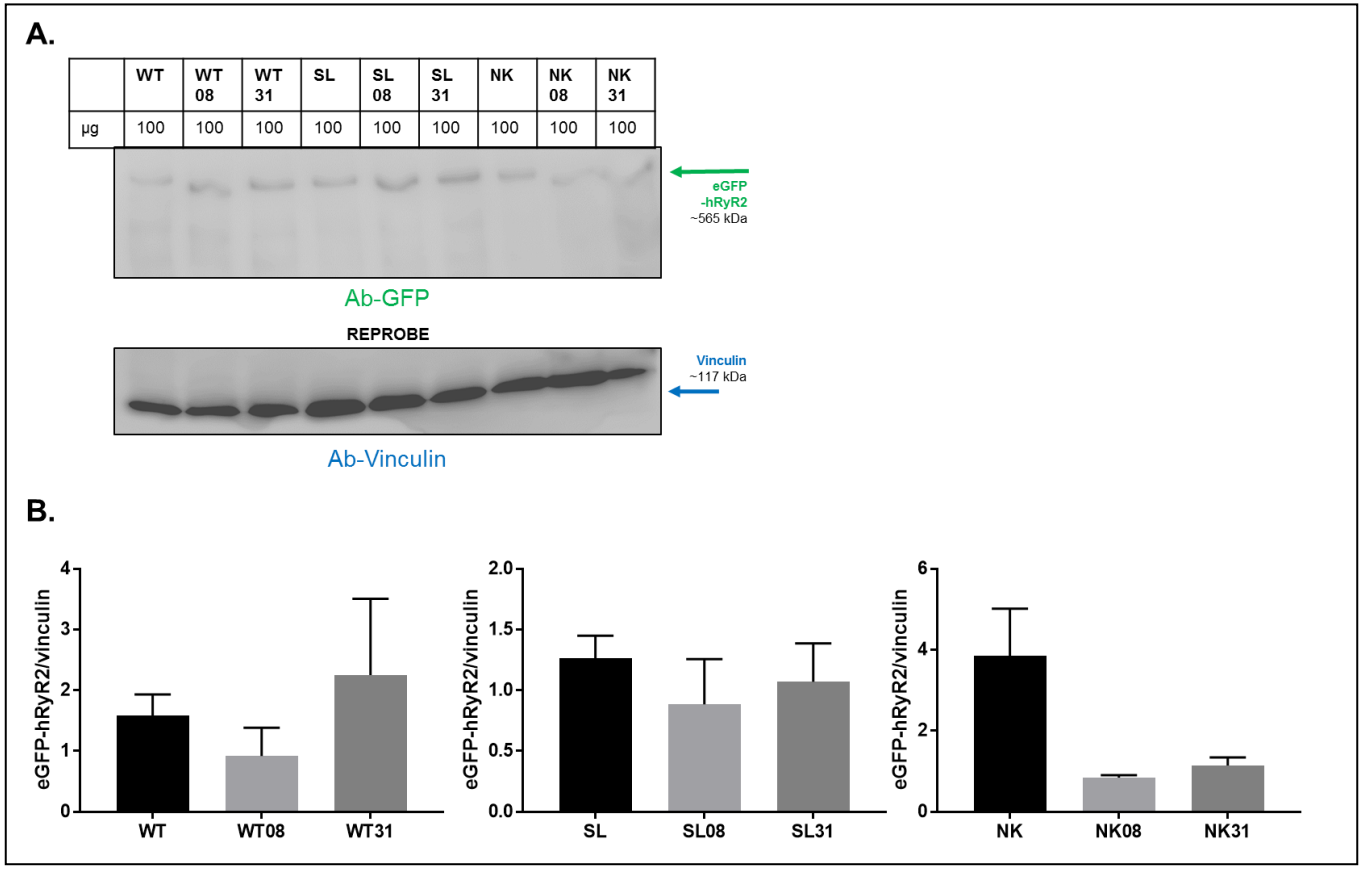

Figure 5.14 Assessment of WT, mutant and phosphomimetic hRyR2 protein in HEK293 cells reveals no significant differences in eGFP-hRyR2 expression. *A.* Representative protein bands achieved from Western blot analysis hRyR2 in HEK293 cells, detected in cell homogenate preparation. eGFP-hRyR2 band signals are 565 kDa in size. Vinculin was used as a loading control. Original and additional Western blots are found in **Appendix I** and **XXIII**. *B.* Densitometric analysis of the 100 µg signal of WT and mutant hRyR2 preparations revealed that N4104K levels were significantly higher, normalized to the vinculin signal. Data are displayed as mean ± SEM and were analysed by one way ANOVA with Bonferroni posthoc in GraphPad Prism. n=3-9 experiments (n WT, SL and NK=9, n WT08, WT31, SL08 and SL31=4, n NK08 and NK31=3).

5.3.5 What is the effect of hRyR2 phosphomimetics on the percentage of cells expected to respond to caffeine/show agonist-induced Ca^{2+} release, according to transfection efficiency?

The propensity for hRyR2-transfected HEK293 cells to undergo spontaneous Ca^{2+} oscillations was calculated as in **Section 3.3.4**. **Figure 5.15** compares the transfection efficiency of WT and mutant hRyR2 phosphomimetics (grey bars) with the number of cells responsive to caffeine (black bars), and therefore assumed to be expressing functional hRyR2 channels. It is important to compare these two parameters to determine whether changes in Ca^{2+} release propensity are attributed to altered transfection efficiency (see **Section 5.3.3**).

Compared to WT, WT31 hRyR2-transfected cells show an increased propensity for Ca^{2+} release (A). This is not due to an increased transfection efficiency – in fact, the number of oscillating cells is far higher than expected (significant by Mann-Whitney test, $p<0.001$). There is no significant difference in propensity for Ca^{2+} release between WT and WT08 hRyR2-transfected cells.

Compared to S2246L, SL31 hRyR2-transfected cells also show an increased propensity for Ca^{2+} release which cannot be attributed to an increased transfection efficiency (B). The number of oscillating cells is far higher than expected ($p<0.001$).

In comparison to N4104K, both NK08 and NK31 hRyR2-transfected cells exhibit a decreased propensity for Ca^{2+} release (C). This was anticipated, as transfection efficiencies cells expressing these DNA plasmids were calculated as very low (0.24 and 1.43 %, respectively), although the number of oscillating cells in both instances were significantly higher than expected when compared to the calculated transfection efficiency ($p<0.001$).

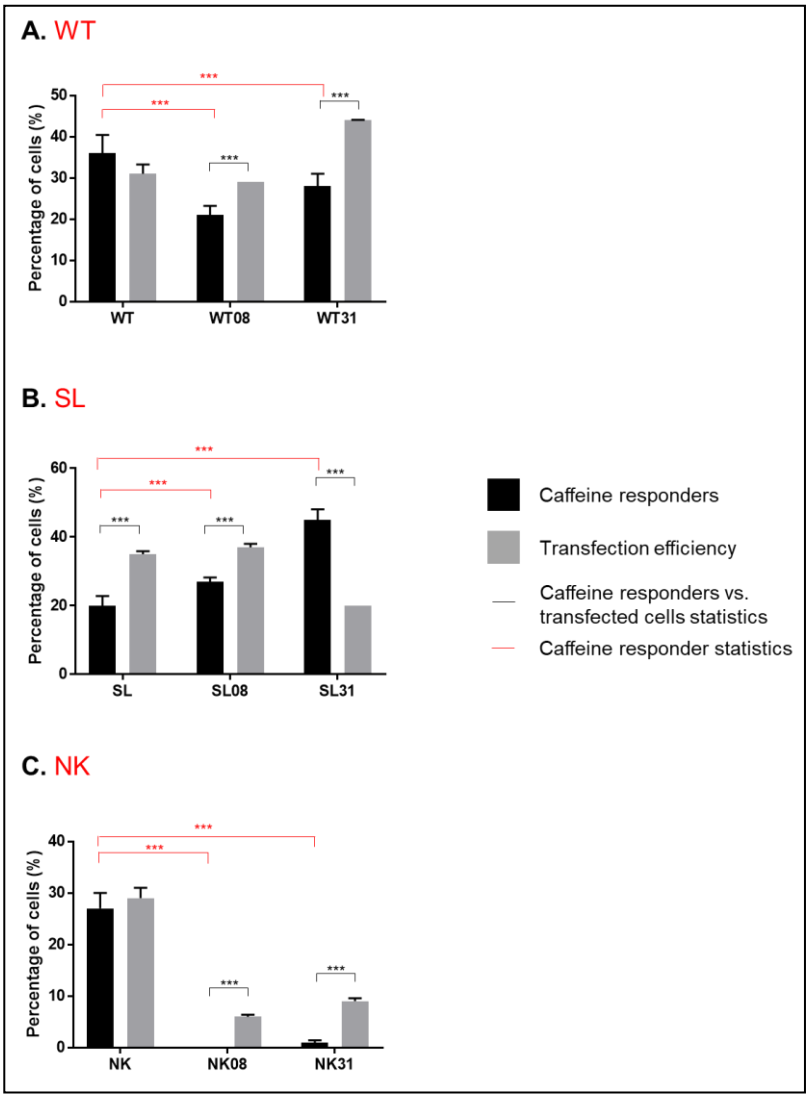

<u>Figure 5.15</u> Some mutant and phosphomimetic hRyR2-transfected HEK293 cells showed an altered percentage of cells displaying agonist-induced Ca^{2+} release in comparison to WT, but not as a result of altered transfection efficiency. Graphs show the propensity of hRyR2-transfected cells to respond to caffeine (black bars) in comparison to the calculated transfection efficiency (grey bars), as shown in **Figure 5.12**. Total number of cells recorded for caffeine response data WT=1003, WT08=439, WT31=514, SL=1274, SL08=1032, SL31=369, NK=1405, NK08=508, NK31=529. For transfection efficiency, n transfections WT=6, WT08=2, WT31=2, SL=7, SL08=2, SL31=2, NK=4, NK08=3, NK31=3. Data are displayed as mean ± SEM and where no error bar is present, error was very small. Data were analysed by Kruskal-Wallis with Dunn's posthoc (propensity of variants) or Mann-Whitney tests (responders vs. propensity for each variant) in GraphPad Prism, with $p<0.001$ indicated by ***. Black lines represent statistical differences in transfection efficiency compared to the proportion of caffeine responsive cells, while red lines represent statistically significant differences in caffeine response only.

5.3.6 How do phosphomimetic mutations modify the spontaneous Ca^{2+} release kinetics of hRyR2-transfected HEK293 cells?

A schematic representation of the Ca^{2+} release events from phosphomimetic hRyR2-transfected HEK293 cells is shown below.

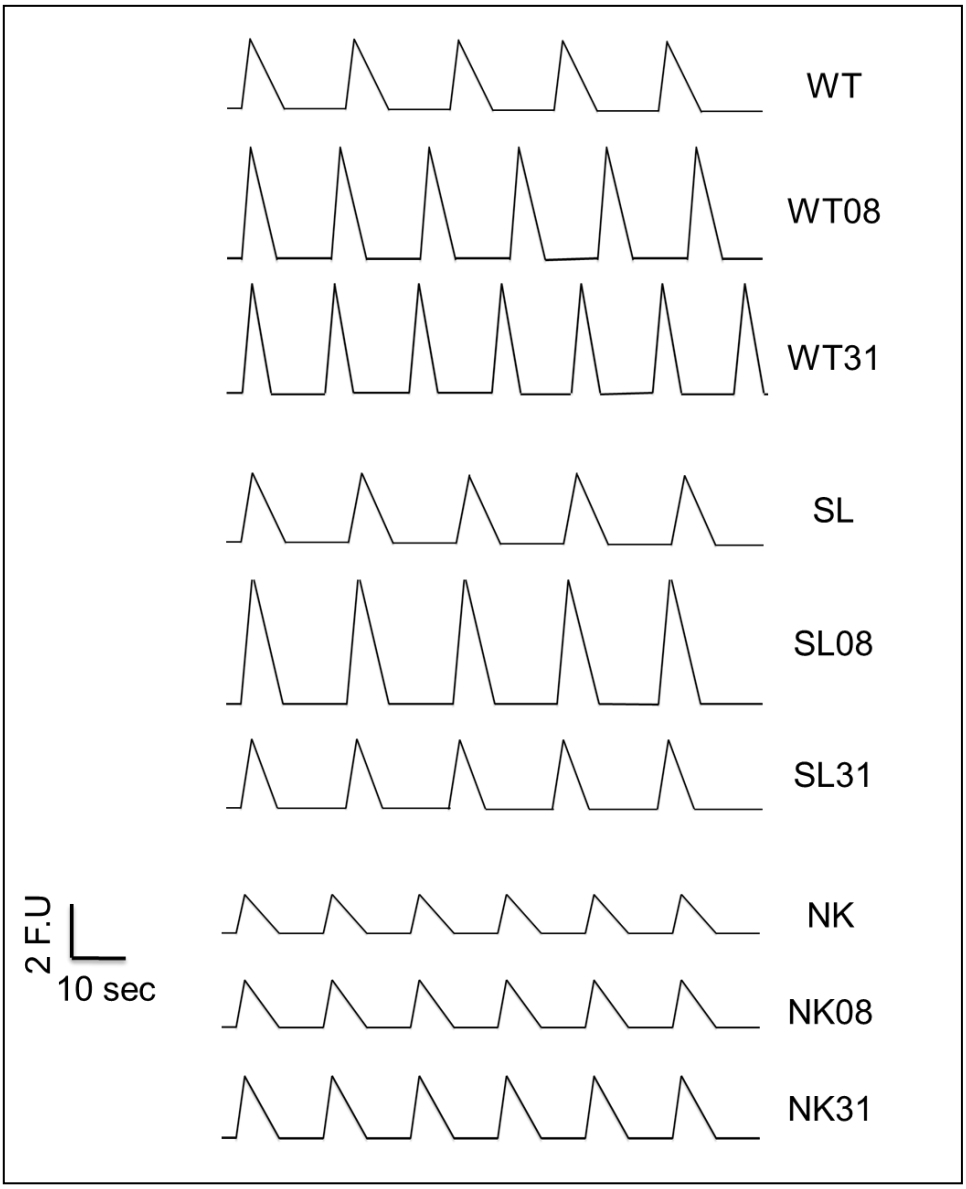

Figure 5.16 A schematic representation of spontaneous Ca^{2+} release events from WT, mutant and phosphomimetic hRyR2-transfected HEK293 cells. These are drawn, based on the mean values of the data sets (see **Table 5.9**).

An in-depth analysis of Ca^{2+} oscillation events is presented as a series of bar graphs in **Figures 5.17-19**, with Ca^{2+} handling kinetic parameters calculated as described in **Section 3.2.3.4** with SALVO analysis software. Scatter plots of imaging data can be found in **Appendix XXVIII-XXX**.

Amplitude, rate up and rate down are significantly increased in WT31 and WT08 expressing HEK293 cells in comparison to WT, resulting in a shorter duration of event while inter-event duration is significantly decreased. Frequency is only altered on introduction of the WT31 mutation in comparison to WT hRyR2-transfected cells (**Figure 5.17**).

Interestingly, the introduction of phosphomimetic mutations did not have quite such a profound effect on the function of S2246L channels expressed in HEK293 cells. SL08 expressing cells did however exhibit an increased amplitude and rate up of oscillation event with significantly decreased inter-event duration and rate down. On the other hand, the only change in Ca^{2+} release kinetics observed in SL31-expressing cells was a significant decrease in the duration of a release event (**Figure 5.18**).

Phosphomimetic mutation had even less of an effect on N4104K spontaneous Ca^{2+} release function with NK08 showing only an increased rate up and down and NK31 exhibiting an increased rate up and amplitude (**Figure 5.19**).

Table 5.9 summarizes the differences in Ca^{2+} handling parameters between phosphomimetic hRyR2-transfected cells in comparison to parent hRyR2-transfected cells.

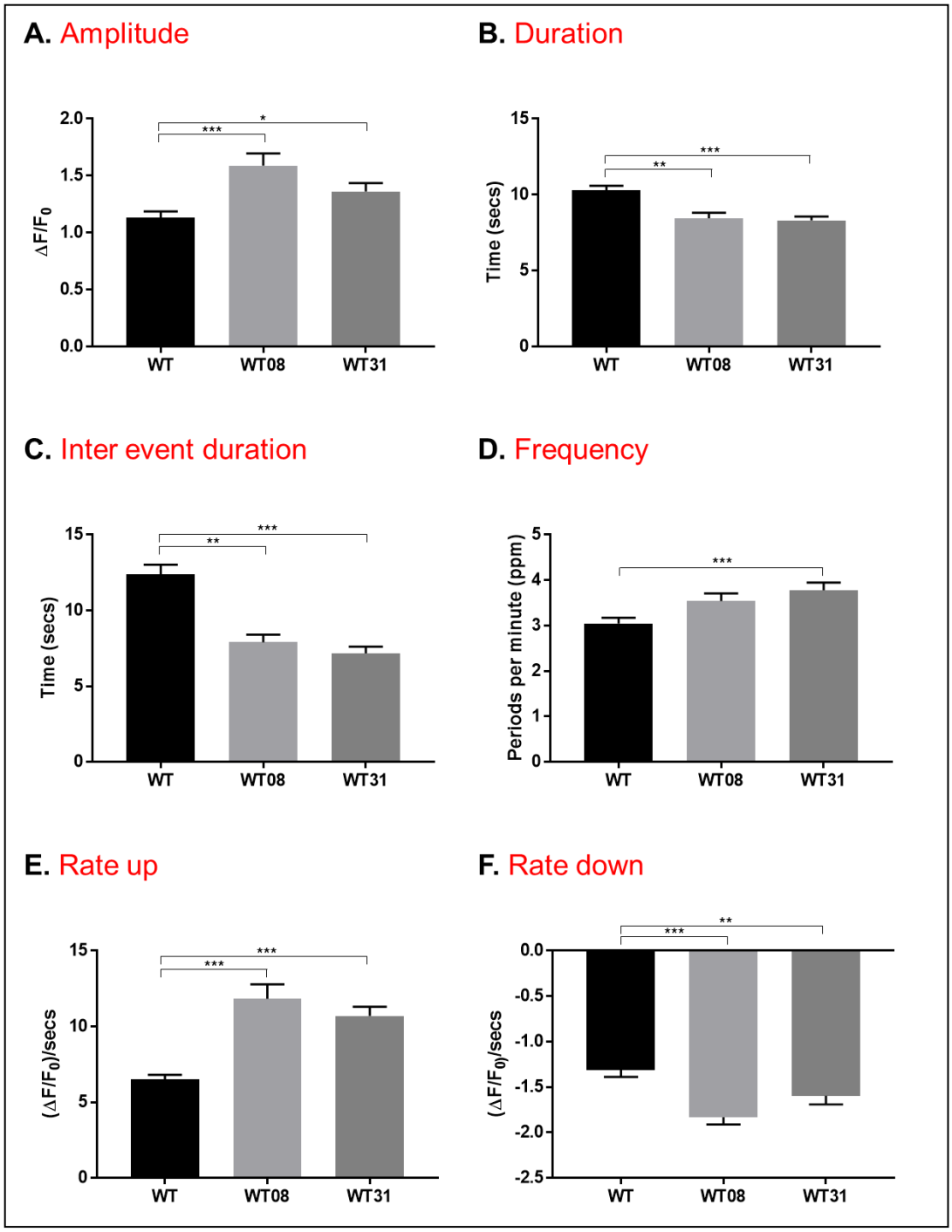

Figure 5.17 Assessment of spontaneous Ca^{2+} release events in HEK293 cells expressing WT phosphomimetic hRyR2. All parameters were calculated as described in **Section 3.2.1.4**. n WT=164, WT08=49, WT31=73. Data are presented as mean ± SEM, $p<0.05$ is denoted by *, $p<0.01$ by ** and $p<0.001$ by *** as calculated by Kruskal-Wallis with Dunn's posthoc analysis with GraphPad Prism.

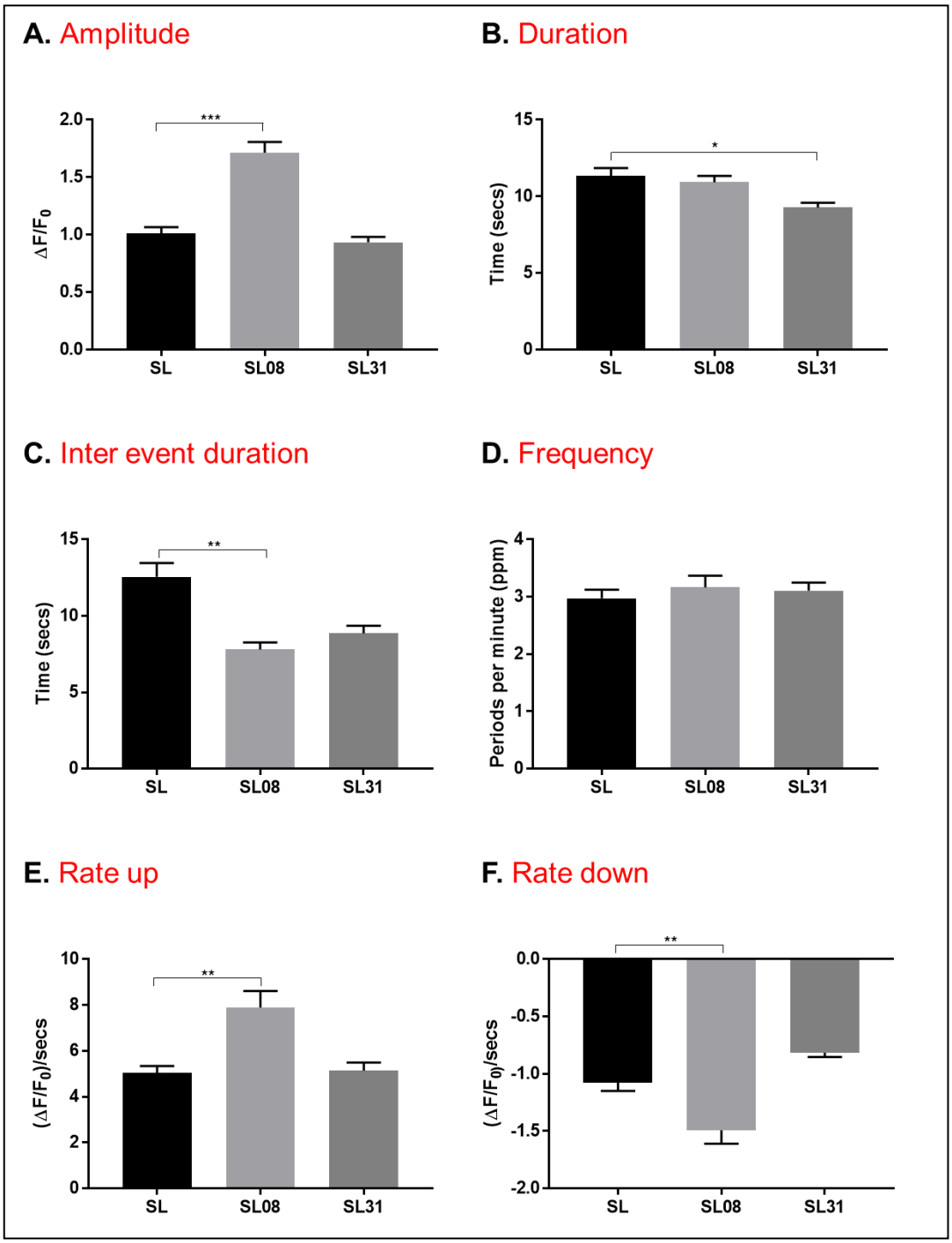

Figure 5.18 Assessment of spontaneous Ca^{2+} release events in HEK293 cells expressing S2246L phosphomimetic hRyR2. All parameters were calculated as described in **Section 3.2.1.4**. n SL=109, SL08=51, SL31=120. Data are presented as mean ± SEM, p<0.05 is denoted by *, p<0.01 by ** and p<0.001 by ***, as calculated by Kruskal-Wallis with Dunn's posthoc analysis with GraphPad Prism.

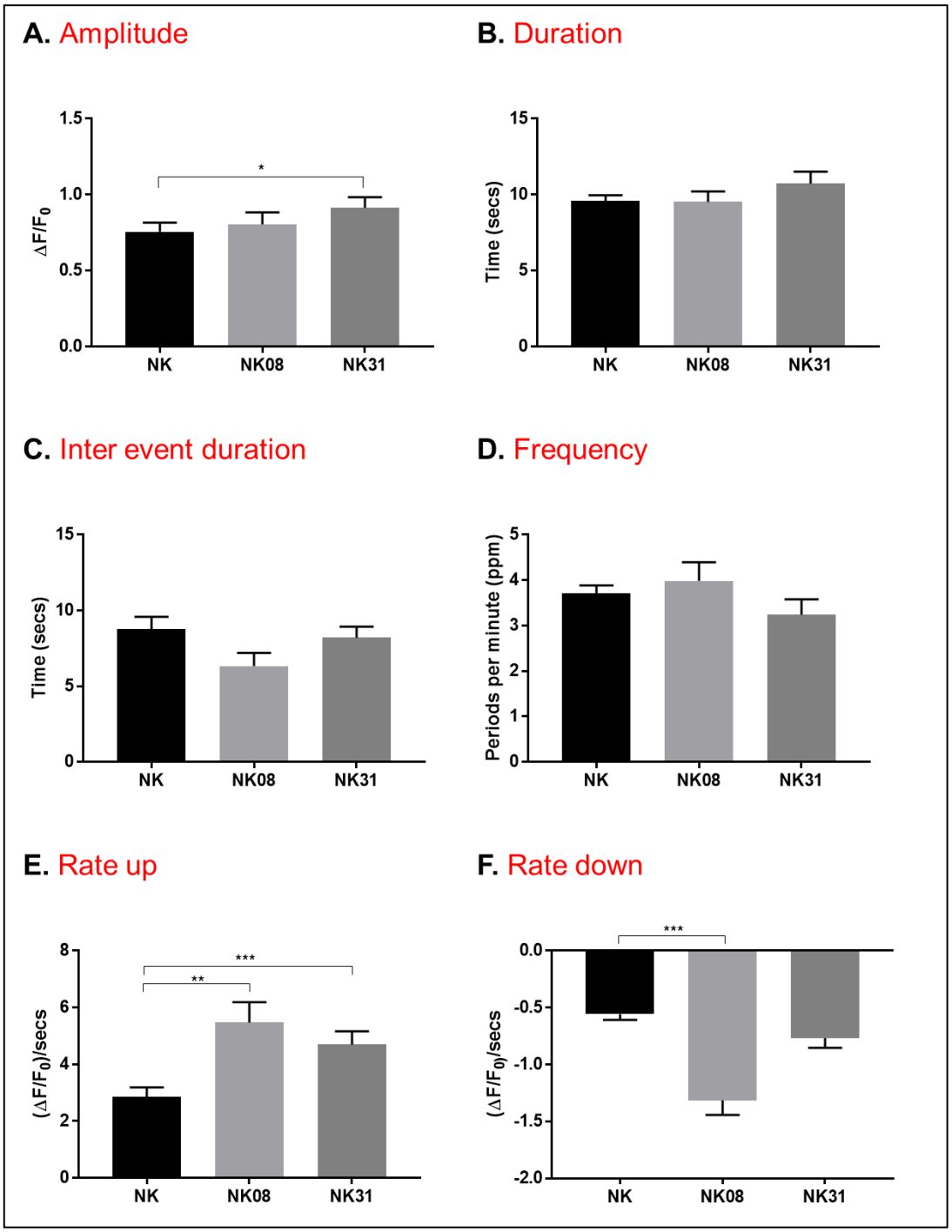

Figure 5.19 Assessment of spontaneous Ca^{2+} release events in HEK293 cells expressing N4104K phosphomimetic hRyR2. All parameters were calculated as described **in Section 3.2.1.4**. n NK=97, NK08=38, NK31=12 cells. Data are presented as mean ± SEM, p<0.05 is denoted by *, p<0.01 by ** and p<0.001 by *** as calculated by Kruskal-Wallis with Dunn's posthoc analysis with GraphPad Prism.

Ca^{2+} oscillation event parameters	WT	WT08	WT31
Amplitude	1.133 ± 0.05	1.590 ± 0.11	1.363 ± 0.07
Duration	10.29 ± 0.30	8.438 ± 0.36	8.305 ± 0.25
Inter-event duration	12.38 ± 0.64	7.901 ± 0.51	7.173 ± 0.44
Frequency	3.047 ± 0.13	3.538 ± 0.17	3.780 ± 0.17
Rate up	6.510 ± 0.29	11.83 ± 0.95	10.70 ± 0.61
Rate down	-1.313 ± 0.07	-1.832 ± 0.08	-1.594 ± 0.10

SL	SL08	SL31
1.011 ± 0.05	1.714 ± 0.09	0.935 ± 0.05
11.35 ± 0.50	10.94 ± 0.40	9.264 ± 0.32
12.56 ± 0.89	7.797 ± 0.48	8.861 ± 0.50
2.975 ± 0.15	3.166 ± 0.20	3.109 ± 0.14
5.042 ± 0.30	7.898 ± 0.71	5.14 ± 0.36
-1.076 ± 0.07	-1.492 ± 0.12	-0.817 ± 0.04

NK	NK08	NK31
0.756 ± 0.06	0.805 ± 0.08	0.913 ± 0.07
9.611 ± 0.35	9.528 ± 0.69	10.73 ± 0.78
8.773 ± 0.81	6.332 ± 0.86	8.208 ± 0.72
3.709 ± 0.18	3.984 ± 0.41	3.239 ± 0.34
2.861 ± 0.33	5.471 ± 0.72	4.694 ± 0.47
-0.5573 ± 0.05	-1.314 ± 0.13	-0.767 ± 0.08

Ca oscillation event parameters	WT08	SL08 vs WT08	NK08 vs WT08
Amplitude	1.590 ± 0.11	1.714 ± 0.09	0.935 ± 0.05
Duration	8.438 ± 0.36	10.94 ± 0.40	9.264 ± 0.32
Inter-event duration	7.901 ± 0.51	7.797 ± 0.48	8.861 ± 0.50
Frequency	3.538 ± 0.13	3.166 ± 0.20	3.109 ± 0.14
Rate up	11.83 ± 0.95	7.898 ± 0.71	5.14 ± 0.36
Rate down	-1.832 ± 0.08	-1.492 ± 0.12	-0.817 ± 0.04

WT31	SL31vs WT31	NK31 vs WT31
1.133 ± 0.05	0.935 ± 0.05	0.913 ± 0.07
10.29 ± 0.30	9.264 ± 0.32	10.73 ± 0.78
12.38 ± 0.64	8.861 ± 0.50	8.208 ± 0.72
3.047 ± 0.13	3.109 ± 0.141	3.239 ± 0.34
6.510 ± 0.29	5.14 ± 0.36	4.694 ± 0.47
-1.313 ± 0.07	-0.888 ± 0.04	-0.767 ± 0.08

Table 5.9 Summary of Ca^{2+} handling parameters in WT, mutant and phosphomimetic hRyR2-transfected HEK293 cells. Mean values for calcium handling parameters of WT and mutant hRyR2-expressing HEK cells, ± SEM. Differences are calculated compared to the equivalent parameter in parent hRyR2-expressing HEK293 cells i.e. WT08 and WT31 are compared to WT, SL08 and SL31 are compared to SL, NK08 and NK31 are compared to NK. Red indicates a statistically significant increase whereas blue indicates a statistically significant decrease as calculated by Mann Whitney or Kruskal-Wallis test with Dunn's post hoc test, $p<0.01$.

5.3.7 Is there an effect of hRyR2 phosphomimetic expression on that of the endogenous HEK293 SERCa?

Given that expression of some hRyR2 phosphomimetics altered ER Ca^{2+} store load (**Figure 5.13**) and increased Ca^{2+} release amplitude in Ca^{2+} imaging experiments (**Figure 5.17-19**), it was important to assess whether an alteration in the expression of SERCa could be contributing to these findings.

The expression of SERCa was determined for all hRyR2 homogenate preparations by Western blotting as described in **Section 3.3.1**. Loading was normalized by transfection efficiency as discussed in **Section 3.3.1** and β-tubulin (~50 kDa) was assessed as a loading control. Densitometric analysis of SERCa (~109 kDa) signals shows significant differences in expression for cells expressing WT or SL phosphomimetics and those expressing the parent construct (**Figure 5.20**). In particular introduction of the S2808D mutation into both WT and S2246L hRyR2s resulted in higher SERCa expression, going some way to explaining the increased store load observed in these cells (**Figure 5.13**). While introduction of S2031D into the S2246L hRyR2 also affected the expression of this pump in the absence of any measureable load change. As a result of a large variance, expression of SERCa in cells expressing N4104K phosphomimetics were comparable to that of the parent mutant.

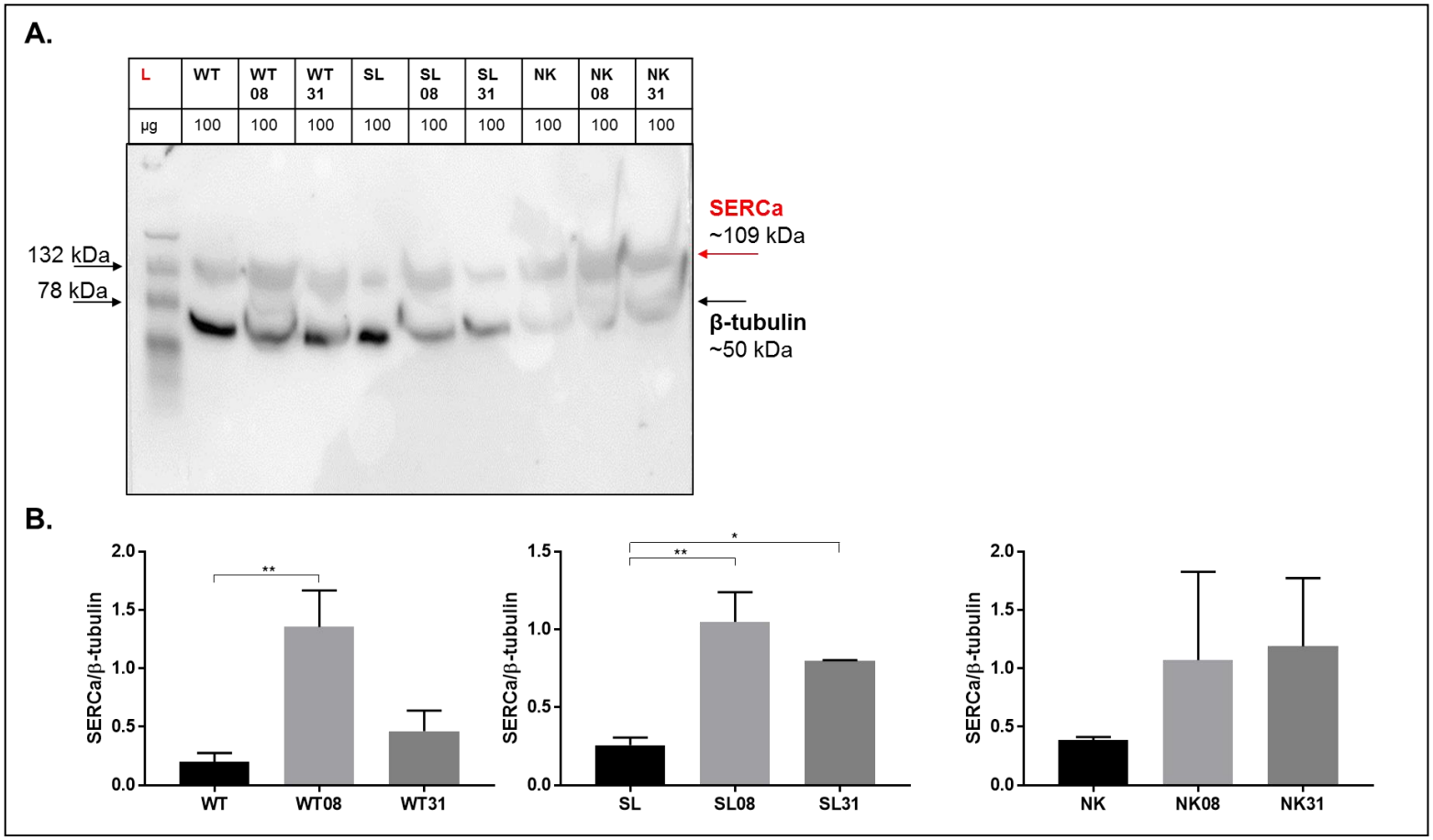

Figure 5.20 Assessment of cell homogenate from WT, mutant and phosphomimetic hRyR2-HEK293 reveals differences in SERCa expression. *A.* Representative bands of SERCa and β-tubulin signal of transfected HEK293 cells and of cells. L refers to protein ladder. Original and additional blots can be found in the Appendix *B.* Densitometric analysis of SERCa signal normalized to β-tubulin signal, n= 2-4 experiments (WT, SL and NK bands from 4 blots, phosphomimetic bands from 2 blots). Significant differences were detected by one way ANOVA with Bonferroni posthoc in GraphPad Prism, $p<0.05$ indicated by *, $p<0.01$ by **. Original and additional blots can be found in **Appendix XI** and **XX**.

5.4 Discussion

Major findings of this chapter include:

- Genetic phosphorylation affects N4104K channel expression and trafficking in HEK293 cells, highlighting that generating phosphomimetic mutations at S2808 and S2031 makes the N4104K hRyR2 channel unstable and likely causes it to break down
- Genetic phosphorylation profoundly alters the ER Ca^{2+} load, mainly by affecting SERCa expression even after transient transfection, highlighting the importance of understanding Ca^{2+} flux across a HEK293 cell
- Genetic phosphorylation does not have as profound an effect on CPVT hRyR2 mutant function as it does on that of the WT in HEK293 cells
- Effects of genetic phosphorylation are different to those of agonist-induced phosphorylation

5.4.1 Six phosphomimetic hRyR2 DNA plasmids were successfully generated via site-directed mutagenesis

After thorough optimization of the process, and use of supercompetent bacteria not normally used for hRyR2 cloning, all six phosphomimetic hRyR2 DNA plasmids were generated by SDM using the cassette-based strategy outlined in **Section 5.2.1**. and produced in sufficient quantity for transfection. This process was not straightforward and required many ligation attempts to produce a full-length hRyR2 plasmid in XL10 cells (**Figure 5.6**), following this, recombination was a major issue during large scale bacterial cell culture. This could not be overcome by changing incubation conditions or growth media (**Table 5.8**), nor by retransformation of XL10 cells with plasmid DNA generated during small scale plasmid isolation.

It is unclear why scaling up of hGFP-hRyR2 phosphomimetic plasmid cultures was possible in Stbl2 but not XL10 cells. Stbl2 competent *Escherichia coli* cells are described as high-efficiency chemically competent cells specifically designed for unstable inserts, with an efficiency of 1 $x10^9$ transformants/µg plasmid DNA for cloning rare sequences. XL10 Gold competent (*Epicurean coli)* cells are for 'extremely demanding cloning', with an average transformation efficiency of ≥5 $x10^9$ transformants/µg of plasmid DNA. The most notable difference between the two types of

cells (apart from being from a different genus) is that XL10 cells contain the F' episome, whereas Stbl2 cells do not. This F' fertility factor episome is a plasmid that can integrate itself into the bacterial chromosome by homologous recombination. Perhaps the presence of this episome in XL10 cells leads to recombination of plasmid DNA when large quantities of cells and DNA are present as in large scale culture. Stbl2 cells were specifically designed to reduce recombination in this setting.

5.4.2 Genetic phosphorylation affects N4104K channel expression and trafficking, while these fundamental properties remain unaltered for S2246L and WT phosphomimetics

Immunofluorescence was used to confirm that all six phosphomimetic hRyR2 channels localized to the ER of HEK293 cells, observing a reticular pattern of fluorescence as in **Chapter 3** (**Figures 5.9-11**). Manders overlap coefficient was calculated to indicate the overlap of green pixels (the inherent eGFP fluorescence of the recombinant protein) to red pixels (antibody raised to a portion of the hRyR2 C terminal), and vice versa. All values calculated indicated good cooccurrence of pixels (0.68-0.96), but of all WT and mutant phosphomimetic hRyR2 constructs, NK08 and NK31 hRyR2-transfected HEK293 cells were calculated to have the lowest coefficient values. In particular, red pixels (the C terminal of hRyR2) were found in regions alone and without green pixels (the eGFP tag). It could be suggested that with breakdown of protein, calpain cleavage would remove the N-terminal eGFP tag, leaving the C-terminal behind, visualized as lone red pixels in IF experiments. The staining pattern in 30 % of these cells also had a 'blobby' appearance, rather than the characteristic reticular pattern, a type of distribution more consistent with that of lysosomes within HEK293 cells. This suggests that N4104K phosphomimetic protein is more unstable and prone to degradation within the cell, with less ER targeting of intact protein and channels forming in an abnormal way. As well as this, N4104K hRyR2 phosphomimetic DNA plasmids were the most difficult to generate, requiring the highest number of ligation and transformation attempts. It can therefore be suggested that the combination of pathogenic and phosphomimetic amino acid mutation makes the hRyR2 protein unstable in this instance. This is reflected in significantly lower transfection efficiencies for NK08 and NK31 hRyR2 DNA in HEK293 cells in comparison to N4104K (0.24 % and 1.43 % vs. 31.14 % respectively, see **Figure 5.12**) and very low n numbers obtained for subsequent Ca^{2+} imaging experiments (see **Figure 5.19**).

For all constructs, a population of hRyR2-transfected cells displayed caffeine-induced Ca^{2+} release, indicative of the presence of functional hRyR2 channels (**Figure 5.13,** discussed further in **Section 5.4.4**). Western blot analysis also confirmed the expression of all WT and mutant eGFP-hRyR2 phosphomimetics at the correct molecular weight in HEK293 cell homogenates. No significant differences in expression level between phosphomimetics and their parent hRyR2 variant were found by one way ANOVA with Bonferroni posthoc test (**Figure 5.14**). Samples were assessed by Western blotting at least three times each. It is notable however that the

expression of NK08 and NK31 does appear to be lower than N4104K, albeit the differences were not calculated as significant. Lower expression may have been expected given cells transfected with these hRyR2 plasmids showed some protein degradation in the cell as evidenced by immunocolocalization (see above) and a lower transfection efficiency. Samples were loaded in a way that was normalized for transfection efficiency (i.e. more protein was loaded for N4104K phosphomimetics than N4104K in HEK293 cells). While this should mean that all lanes in the blot display equivalent signal, this would only be the case if the expression level of hRyR2 per cell was equivalent for each construct. As differences are not significant, this suggests that hRyR2 protein expression is not different between cells expressing N4104K and N4104K phosphomimetic hRyR2, although expression in this assay does not necessarily equate to functional channels in the cell. It should also be noted that N4104K hRyR2 expression in HEK293 cells was originally calculated as significantly increased in comparison to WT hRyR2 (see **Figure 3.3.7**). This likely means that expression of hRyR2 per cell is higher for N4104K but not for N4104K phosphomimetics, in comparison to WT, where there is suspected degradation. Changes in spontaneous Ca^{2+} release events caused by phosphomimetic mutations in both S2246L and N4104K hRyR2-transfected HEK293 cells is discussed in **Section 5.4.6**.

5.4.3 Genetic phosphorylation profoundly alters the ER Ca^{2+} load, mainly by affecting SERCa expression

ER Ca^{2+} load was estimated by the addition of a maximal dose of caffeine as described in **Section 3.2.3.3**. Both WT08 and WT31 hRyR2-transfected HEK293 cells exhibited an increased Ca^{2+} store load in comparison to WT-transfected cells (**Figure 5.20**). This is in contrast to work by Stange et al. (2003), who found that the caffeine-sensitive ER-Ca^{2+} store loads of S2808D mouse RyR2-transfected cells did not increase in comparison to WT. The effect of this genetic phosphorylation is in contrast to that of the pharmacological phosphorylation discussed in Chapter 4 (**Section 4.12)**, where the store load of cells expressing WT hRyR2 was decreased on application of DcAMP.

As the Ca^{2+} content of the ER is increased for WT phosphomimetic hRyR2-transfected HEK293 cells, it was important to assess SERCa expression levels given its role in sequestration of Ca^{2+} back into the store. Enhanced expression or activity of SERCa could account for the presence of more Ca^{2+} in the store. Introduction of plasmid vectors that are under the control of the CMV promoter (which is the promoter present in pcDNA3, the hRyR2 plasmid vector) forces the

translation of gene products in HEK293 cells by 'hijacking' the cell's protein machinery (Thomas and Smart 2005). An advantage of using transient transfection is that high levels of expression can be achieved without integrating the nucleic acid sequence within the host chromosome. The effects are therefore only temporary, and it would be reasonable to suggest that adaptive remodelling of other cellular components would not be observed within such a short period of expression (24-72 hr).

However, Western blot analysis of hRyR2-transfected HEK293 cell homogenate samples revealed that transfection with some phosphomimetic hRyR2 DNA plasmids (WT08, SL08, SL31) led to increased SERCa expression. This provides an explanation for the discrepancy seen between the effects of genetic vs pharmacological phosphorylation on the ER load for these phosphomimetics. In particular, phosphorylation of cells expressing S2246L hRyR2 exhibited a decreased Ca^{2+} store load (in **Section 4.12**), whereas genetic phosphorylation in this chapter resulted in increased ER load for SL08. SERCa expression/Ca^{2+} load was also increased in cells expressing WT08, suggesting that genetic phosphorylation at this site has resulted in an overall similar response in cells expressing these variants. N4104K phosphomimetic hRyR2-transfected HEK293 cells exhibited no change in ER Ca^{2+} store load in comparison to N4104K-transfected cells, but n numbers were very low (n: NK08=38, NK31=12).

In the majority of studies, phosphorylation at other sites is not assessed in tandem to the site of interest, nor is the expression of other Ca^{2+} cycling proteins such as SERCa or PLB. In terms of KI/KO mouse models and stable-transfected cell lines, adaptive remodelling may explain huge discrepancies between data (Brittsan et al. 2003). This is evident in S2808A cardiomyocytes of the Valdivia mouse model, where phosphorylation at S2031 and S2814 was increased in the presence of isoproterenol in comparison to WT as assessed by Western blotting (Benkusky et al. 2007).

In the assessment of Ca^{2+} release events from RyR2-transfected HEK293 cells, expression of SERCa or any alterations that transient expression of RyR2 may have on other proteins in the cell is not discussed in the literature, aside from Thomas et al. (2005), where no significant changes were seen in the store load or SERCa expression of WT, L433P, N2386I and R176Q/T2504M hRyR2-transfected HEK293 cells. Considering SERCa expression is revealed here as altered upon expression of certain hRyR2 phosphomimetics, future studies should consider that Ca^{2+} release events may also be influenced by enhanced Ca^{2+} sequestration into

the ER by SERCa in this setting. Given the length of a HEK293 cell cycle is approximately 24 hr (Bernard et al. 2007; Unsal-Kaçmaz et al. 2005), it is plausible that expression of hRyR2 for 48 hr (approximately the time at which Ca^{2+} imaging experiments take place after transfection) could lead to increased expression of SERCa in cells during this time. It is difficult to speculate as to how and why this occurs. Increased SERCa expression may be a process of adaptive remodelling, whereby the cell responds to increased influx of Ca^{2+} from the ER into the cytosol by increasing SERCa-mediated reuptake. Expression and phosphorylation levels of PLB should be also considered in cardiomyocytes when investigating RyR2 phosphorylation status, but this does not apply to HEK293 cells which are devoid of this protein (Kurzydlowski 1996; Asahi et al. 2003; Toyofuku et al. 1994).

While increased expression of SERCa may account for changes in Ca^{2+} release kinetics observed in WT08 hRyR2-transfected HEK293 cells (**Figure 5.17**, discussed in **Section 5.3.6**), this cannot account for changes observed on introduction of WT31 or SL31 mutation. An increased store load in this case could be indicative of an altered sensitivity of hRyR2 to luminal/cytosolic Ca^{2+}, since phosphorylation of RyR2 has previously been suggested to affect luminal Ca^{2+} sensing (Wehrens et al. 2004; Ullrich et al. 2012; Xiao et al. 2006).

5.4.4 eGFP fluorescence may misrepresent the proportion of cells expressing hRyR2 phosphomimetics

A proportion of all cell populations expressing WT or mutant phosphomimetic hRyR2 displayed caffeine-induced Ca^{2+} release, indicative of functional hRyR2. However, these experiments revealed a discrepancy between transfection efficiency (cells exhibiting eGFP fluorescence) and the proportion of cells showing spontaneous Ca^{2+} release.

While some phosphomimetic derivatives of S2246L and N4104K hRyR2 exhibited low transfection efficiency in HEK293 cells, compared to that of the parent hRyR2, this was not the case for WT hRyR2 phosphomimetics. While SL31-transfected HEK293 cells did have a lower transfection efficiency and a significantly increased proportion of caffeine responsive cells compared to S2246L, a disproportionately large number of caffeine responsive cells were recorded (see **Figure 5.12**, and **5.15**).

A discrepancy in the number of caffeine-responsive cells and calculated transfection efficiency may be due to detection limits. In cells where expression is at a low level, function can more easily be detected by caffeine-induced Ca^{2+} release, but there may not be enough protein to observe eGFP fluorescence.
This explanation does not follow for WT phosphomimetic mutations (**Figure 5.15**). Propensity was significantly decreased in WT08 hRyR2-transfected HEK293 cells and was not a result of an increased transfection efficiency (see **Figure 5.12** and **5.15**). This would suggest that transfection efficiency may have been overestimated in this instance.

The Chen group propose that enhanced propensity for spontaneous Ca^{2+} release events in this setting is a hallmark of dysfunction caused by CPVT1 mutation (Jiang et al. 2004; Jiang 2005). An enhanced propensity for caffeine-induced Ca^{2+} release is observed in HEK293 cells expressing SL31 in comparison to those expressing SL. Given the structure of the RyR2 channel with 4 subunits and 4 S2031 sites within the complex, genetically phosphorylated channels have phosphorylation mimicked at all 4 sites. In WT or mutant hRyR2-transfected HEK293 cells, channels may exist with 0-4 S2031 sites phosphorylated. Even the addition of DcAMP to activate PKA may not elicit phosphorylation at all four S2031 sites in these channels, therefore propensity does not increase. In contrast, no increase in propensity was observed on DcAMP-mediated phosphorylation in **Chapter 4**. While DcAMP-mediated phosphorylation will cause more channels in the population of a cell to be active, genetic phosphorylation at S2031 to full stoichiometry may cause all the hRyR2 channels in the population to have an increased P_o. These data may indicate functional relevance of PKA-mediated phosphorylation at the S2031 site in S2246L hRyR2 channels. However, functional relevance within a heterologous expression system does not necessarily equate to physiological relevance within a ventricular myocyte *in vivo*, given the artificial nature of the system.

Although differences have been observed in this instance when calculating caffeine-responsive cells as a percentage of the population, arguably propensity is generally not a good indicator of CPVT1 RyR2 channel dysfunction in HEK293 cells, given that others also have not observed a change in propensity for spontaneous Ca^{2+} release events when investigating disease-linked mutations (Loaiza et al. 2013). No differences in propensity for caffeine-induced Ca^{2+} release events between WT and mutant hRyR2-transfected HEK293 cells in previous experiments (**Figure 3.14** and **4.13**).

5.4.5 Genetic phosphorylation at S2808 and S2031 have similar effects on WT hRyR2 Ca^{2+} release

HEK293 cells were transfected with WT or mutant phosphomimetic hRyR2 for Ca^{2+} imaging experiments as in **Chapter 3**. Genetic phosphorylation at S2808 and S2031 resulted in similar changes to the Ca^{2+} release kinetics of HEK293 cells expressing hRyR2 i.e. an increased amplitude, a decreased inter-event duration, an increased rate up and an increased rate down (**Figure 5.17**).

Increased amplitude is indicative of phosphorylated hRyR2 channels releasing more Ca^{2+} from the store, however, rather than being due to any sensitization of the channel to agonist it is likely the result of the increased store loads observed in cells expressing WT08 and WT31 channels (**Figure 5.13**). Although the decreased inter-event duration would suggest that less Ca^{2+} can be sequestered into the cell during this shorter period, store load and amplitude of Ca^{2+} release events are also increased, likely because of an increase in SERCa expression observed in WT08 and WT31-transfected cells (**Figure 5.18**). In work of the Hajjar laboratory utilizing gene therapy to transduce SERCa2a into guinea pigs, isolated cardiomyocytes with overexpression of SERCa2a displayed accelerated reuptake of cytosolic Ca^{2+} as measured by τ, the Ca^{2+} transient decay time constant (Cutler et al. 2012). This also equates to a shortening of inter-event duration caused by SERCa.

While a change in propensity observed in WT phosphomimetics may be explained in the most part by changes in transfection efficiency and store load, density of hRyR2 clusters could also be affected, as mentioned in **Section 3.4.4** and **Section 4.1.1**.

Unlike WT08, expression of WT31 increases the frequency of Ca^{2+} release events in HEK293 cells compared to WT. An increased frequency of events may be an expected effect of phosphorylation, given that in a native cardiomyocyte, PKA-mediated phosphorylation of EC coupling proteins and enhanced Ca^{2+} cycling is a key response to increased metabolic demand. This was one of the effects of the N4104K mutation in the absence of PKA activation (see **Figure 3.16**). However, this was not due to phosphorylation at the S2031 site, as this was shown to be low (compared to that of the WT) in this mutant. It might be that this dephosphorylation of S2031 is responsible for higher channel Po, as similar conditions have

been shown to result from dephosphorylation at the S2808 site (Carter et al. 2011; Carter et al. 2006). Imaging data of N4104K phosphomimetic hRyR2 is discussed in the next section.

5.4.6 Genetic phosphorylation does not have as profound an effect on mutant function as it does on that of the WT

The Ca^{2+} release kinetics of phospho-CPVT1 mutants were compared to the parent mutant hRyR2 in order to assess the effects of genetic phosphorylation at each site e.g. Ca^{2+} release kinetics of SL08 and SL31 hRyR2-transfected cells were compared to SL rather than WT hRyR2.

SL31 hRyR2-transfected cells also display an increased propensity for caffeine-induced Ca^{2+} release in comparison to S2246L (**Figure 5.15**). This was also not because of increased transfection efficiency. Phosphorylation at the S2031 site must cause more channels to be active within a population of transfected cells. This suggests that enhanced channel activity caused by this CPVT1 mutation is exacerbated after PKA stimulation, (**Section 4.4.2**). As these changes in propensity follow that of WT upon phosphorylation at this site, it remains to be seen whether other changes will reveal S2246L channel dysfunction that has not been observed in previous experiments. No changes were identified in propensity of N4104K phosphomimetic hRyR2-transfected HEK293 cells, but n numbers were very low for these experiments.

In contrast to S2031D, introduction of S2808D to S2246L has a more marked effect on channel function – similar to the effects of this phosphomimetic on the WT i.e. increasing amplitude, rate up and down and decreasing inter-event duration (**Figure 5.18**). This could suggest that phosphorylation to full stoichiometry at this site could be instrumental in revealing S2246L dysfunction, however the changes seen are not in excess of those seen in WT08 (with WT and S2246L being largely comparable to begin with, see **Table 3.6**), suggesting that phosphorylation at this site has similar effects on WT and S2246L.

Analysis of Ca^{2+} release kinetics of N4104K phosphomimetic hRyR2-transfected HEK293 cells revealed very few changes in comparison to N4104K (**Figure 5.19**). NK08 hRyR2-transfected HEK293 cells (n=38) displayed an increased rate up and decreased rate down in comparison to N4104K-transfected cells, but no change in the overall Ca^{2+} release event duration. NK31 hRyR2-transfected cells displayed an increased rate up and an increase in amplitude (n=12)

that was not due to an alteration in ER Ca^{2+} store load (**Figure 5.13**). These alterations give rise to Ca^{2+} release kinetics which appear more analogous to those observed in WT hRyR2-transfected HEK293 cells.

On the basis of these results, we might conclude that phosphomimetic modification of either site in this mutant channel does not affect function in the same way as it does the WT. Given that cells expressing N4104K hRyR2 already exhibit altered Ca^{2+} release kinetics in comparison to WT before phosphorylation (**Figure 3.16**), phosphorylation of the mutant channel may not elicit the normal physiological response. The N4104K mutation is thought to cause disruptions to inter-domain interactions away from the phosphorylation domain that renders phosphorylation at this site irrelevant, or disrupts the phosphorylation domain (Tateishi et al. 2008). However, conclusions here are made on data with very low n numbers, given the very low transfection efficiencies obtained when using N4104K hRyR2 DNA plasmids.

5.4.7 Effects of genetic phosphorylation are different to those of agonist-induced phosphorylation

It is interesting that many of the observed changes caused by phosphomimetic amino acid substitution to hRyR2 are different to those caused by treatment of transfected cells with DcAMP. The discrepancy between results using DcAMP and genetic phosphorylation could be due to additional effects of the agonist used to promote phosphorylation. DcAMP may activate alternative endogenous kinases such as CaMKII and other cell signalling pathways given the role of cAMP as a ubiquitous secondary messenger (Hofer et al. 2007). Alterations in SERCa expression, occurring as a result of genetic phosphorylation (described in **Section 5.3.7),** may also account for differences.

An alternative explanation is that genetic phosphorylation can lead to an alteration of hRyR2 clustering. Transient treatment of WT hRyR2-transfected HEK293 cells with drug may not alter the clustering of RyR2 channels within the cells. However, the transfection of phosphomimetic hRyR2 DNA into cells over 48 hrs could lead to the expression of channels that are distributed more densely. As mentioned previously, work of Chen-Izu et al. (2007) highlighted that in the spontaneously hypertensive rat showing HF, RyR2 showed not only increased phosphorylation in this setting but also shortened spacing between RyR2 clusters in comparison to non-diseased controls. It should also be noted that in the work of Asghari et al. (2013) a change as fast and as transient as cytosolic Mg^{2+} concentration can modify the orientation of RyR2 tetramers relative to one another.

Genetic phosphorylation targets just one of the potential phosphorylation sites of RyR2. This method is very useful to elucidate the effects of phosphorylation on an individual site without modulation of other sites in the channel. Mimicked phosphorylation of one site however does not emulate phosphorylation in a physiological setting, therefore effects observed at one site alone may not be seen when other sites are phosphorylated. In an *in vitro* setting with the use of recombinant hRyR2 DNA plasmid, all four subunits of the RyR2 channel would be genetically phosphorylated, while physiologically, this may not happen.

While potentially more physiological, phosphorylation via treatment with an analogue of cAMP and activation of endogenous PKA could phosphorylate other sites in RyR2, in addition to the ones investigated. It cannot also be clarified exactly how many subunits of the RyR2 channel

are phosphorylated at each site, nor if all the channels in the population are phosphorylated to the same level. The phosphorylation level observed with 1mM DcAMP was the physiological maximum possible, as it wasn't significantly different from the PKA control included in these experiments. However, this may not equate to the assumed full stoichiometry of mimicked/genetic phosphorylation.

Given that in these experiments, a 48 hr window of hRyR2 expression was sufficient to alter the expression level of SERCa, it cannot be conclusively deduced that effects of genetic phosphorylation are solely due to a change in hRyR2 function. Any change in caffeine-sensitive ER Ca^{2+} load is likely not due to a change in hRyR2 Ca^{2+} sensitivity, but due to increased store filling by SERCa. The Chen group have previously utilized a stable, tetracycline-inducible HEK293 cell line expressing WT or mutant RyR2 to investigate spontaneous Ca^{2+} release events within this system (Jiang et al. 2004). In these stable cells a repressor of RyR2 expression is constantly expressed until the inducer, tetracycline, is added to the growth medium. If expression could be repressed until required such as in this system, reducing changes in the expression of other cellular proteins, the effects of genetic phosphorylation may be more similar to the effects of biochemical phosphorylation of DcAMP observed in **Chapter 4**.

Findings from this chapter reveal that genetic phosphorylation of hRyR2 has a different effect on spontaneous Ca^{2+} release than that induced by activating PKA. While changes in basal phosphorylation could explain why mutant channels displayed fewer changes in spontaneous Ca^{2+} release behaviour compared to WT following DcAMP-mediated PKA phosphorylation, adaptive changes in the expression of other ER resident proteins (namely SERCa) cloud our interpretation of any possible changes in function induced by genetic phosphorylation. However, both modes of phosphorylation have in common that their effects were diminished on mutant, compared to WT hRyR2 – even though basal function was profoundly different for each of these mutants.

Arguably, genetic phosphorylation of hRyR2 is a useful method to identify functional changes to channel activity caused by modification of one site, away from the influence of other modifications. In parallel with other methods, such as single channel analysis, this can allow the role of RyR2 phosphorylation at a single site to be untangled, while pharmacological phosphorylation allows investigation in a more physiological setting. Further experiments to expand on these findings are discussed in **Chapter 6**.

Chapter 6

General Discussion

6.1 General discussion and future work

The principal aim of this study was to investigate whether CPVT1 RyR2 mutations from different channel domains are functionally heterogeneous, as single channel preliminary data had suggested (**Section 3.1.2**). Investigations involved the biochemical and functional examination of two CPVT1-linked hRyR2 mutations - S2246L of the central domain and N4104K of the cytoplasmic portion of the I domain (see **Figure 1.15**).

Findings of this study are summarized in **Figure 6.1, 6.2** and **6.3,** and are described in the following sections.

6.1.1 N4104K hRyR2 exhibits more obvious dysfunction at the spontaneous Ca^{2+} release level than S2246L

Spontaneous Ca^{2+} release events in hRyR2-transfected HEK293 cells were assessed to determine whether a) this method could reveal differences between WT and mutant hRyR2 Ca^{2+} release kinetics and b) Ca^{2+} release between mutants was functionally heterogeneous. This method has previously been applied to study RyR2 (D. Jiang 2005; N. L. Thomas et al. 2004; N. L. Thomas et al. 2005), allowing interrogation of RyR2 channels away from other influencing proteins, a factor important for this study. HEK293 cells also appear to produce comparable functional data to that of RyR2 from native sources (Du 1998; Bhat et al. 1999; Li and Chen 2001; L. Xu and Meissner 1998). While the interaction of RyR2 with cytosolic and luminal cardiac proteins (not present in HEK293 cells) is known to modulate channel function, probing such interactions was not the goal of this study. Instead, transfected HEK293 cells permitted the investigation of fundamental hRyR2 channel defects caused by mutation alone. In the absence of any accessory proteins, preliminary single channel experiments with purified hRyR2 revealed that the N4104K mutation may cause fundamental functional defects, whereby channel gating occurred in the absence of activating ligand (**Section 3.1.2.2**). However, as a limitation to this method, it remains difficult to interpret changes in Ca^{2+} release kinetics while data on Ca^{2+} fluxes across the membrane in HEK293 cells are lacking.

As well as investigating the effects of mutation on the spontaneous Ca^{2+} release kinetics of hRyR2-transfected HEK293 cells (**Section 3.5**), expression level and intracellular trafficking were also assessed for any changes (**Section 3.3.1** and **3.3.3**, respectively). As a measure of functionality, the proportion of hRyR2 expressing cells exhibiting agonist-induced Ca^{2+} release was assessed (**Section 3.3.3**). This application of caffeine to hRyR2-transfected HEK293 cells also served to estimate the amount of Ca^{2+} within the ER Ca^{2+} store (**Section 3.3.3**).

The spontaneous Ca^{2+} release of cells expressing N4104K hRyR2 appeared dysfunctional in comparison to that of those expressing WT, with a smaller amplitude, slower rate of transient ascent/descent, shorter inter-event duration and an increased frequency of spontaneous Ca^{2+} release events (**Section 3.4.4**). The expression of N4104K was also increased compared to WT and S2246L (whose expression levels were comparable in HEK293 cells, **Section 3.3.1**). Western loading was normalised for batch transfection efficiency and so this increase in expression represented an increase in the protein production per cell and was not as a result of increased efficiency of transfection. More channels per cell could change the kinetics of spontaneous Ca^{2+} release from transfected HEK293 cells, but this may not account entirely for the result, given that preliminary single channel data indicated N4104K hRyR2 channels displayed a fundamental gating defect in comparison to WT. However, while normalisation for transfection efficiency was necessary for discovering changes in expression of hRyR2 per cell, this method may have exaggerated the expression levels observed. N4104K transfection efficiencies were often lower than that of the WT (though not significantly so on average, see **Figure 3.11**), meaning that an increased protein concentration was often loaded, which may have skewed the results slightly.

The increase in N4104K channel expression did not affect trafficking or have a significant downstream effect on SERCa expression or ER Ca^{2+} load (**Section 3.3.2** and **3.3.3**, respectively). The latter is somewhat surprising, given that more hRyR2 channels per cell that are 'leakier' than WT hRyR2 would suggest a decrease in total ER Ca^{2+}.

As evidenced in the work of MacLennan's group, the intracellular Ca^{2+} store of HEK293 cells is not entirely depleted by the addition of caffeine and there remains Ca^{2+} present that is caffeine-insensitive but thapsigargin-sensitive (Tong, McCarthy, et al. 1999; Tong, Du, et al. 1999). Thapsigargin increases the intracellular Ca^{2+} store by irreversible inhibition of SERCa, preventing Ca^{2+} reuptake. As an additional experiment, thapsigargin could be added to cells

after caffeine to ensure complete emptying of the ER Ca^{2+} store. However, caffeine-induced Ca^{2+} release remains a relevant measure to assess channel functionality (limitations and alternatives are discussed in **Section 3.4.3**) and is closely correlated to thapsigargin-induced Ca^{2+} release, indicating that it likely does reflect the size of the ER Ca^{2+} store (Tong, McCarthy, et al. 1999; Tong, Du, et al. 1999).

S2246L hRyR2 was different to the WT in a way that N4104K was not, in that with this mutant, a ~25 % discrepancy was evident between the transfection efficiency (percentage of green cells) and the percentage of cells showing channel functionality in the form of a caffeine-induced response (**Section 3.3.3**). This was also reflected in the effect of the S2246L on the propensity for cells expressing this hRyR2 mutant to undergo Ca^{2+} release, which was decreased in comparison to WT (**Section 3.3.3**). However, in the absence of exogenously stimulated phosphorylation, it was evident that S2246L hRyR2-transfected cells displayed similar Ca^{2+} release kinetics to those expressing WT, albeit with a slower rate up (**Section 3.3.5**). Even though experiments were calculated as adequately powered (**Section 3.3.4**) small magnitude changes for S2246L, which were not found to be statistically significant, could still possibly result in global dysfunction in a cardiac setting.

To summarise, data in **Chapter 3** pointed towards the 'gain-of-function' classification, often used as a blanket term for the dysfunction caused by CPVT1 RyR2 mutations that cause enhanced channel activity, as an oversimplification. While S2246L and N4104K may indeed both be gain-of-function mutations, hRyR2 channel dysfunction is manifested differently, as S2246L barely appeared dysfunctional when expressed in a heterologous system.

Given that S2246L and N4104K hRyR2 mutants appear to have different functional effects (see **Section 1.7.2**, **Figure 1.5**), the role of mutation location could be further explored. As discussed in **Section 1.7.3.2**, defective domain-domain interactions within RyR2 have previously been suggested to underlie channel dysfunction (Liu et al. 2013; Laver et al. 2007; Uchinoumi et al. 2016; Tateishi et al. 2008; Suetomi et al. 2011; Uchinoumi et al. 2010; Z. Xiao et al. 2016). Further mutations could be investigated from both the central domain and the C-terminal domain, to see if Ca^{2+} release kinetics are similar to those caused by mutations in the same domains. Cryo-EM structures of Yan et al. (2015), des Georges et al. (2016) and Zalk et al. (2015) could be utilized to determine whether mutations are in close vicinity or may interact with others in the overall RyR structure, interactions that may not be evident from the linear

polypeptide (as in **Figure 1.5**). This would further implicate the importance of domain interactions in RyR2 channel dysfunction and determine whether CPVT1 phenotype is locus dependent.

In recent work of Uehara et al. (2017), the functional effects of transmembrane (c-terminal) domain CPVT-linked mutation K4750Q were compared to those caused by central domain mutation R2474S. RyR2-K4750Q not only causes a more severe phenotype in patients, but mutant channels displayed more aberrant activity in comparison to both WT and R2474S channels in multiple experimental systems, including heterologous cells. HEK293 cells expressing RyR2-K4750Q displayed an increased frequency and a decreased amplitude of spontaneous Ca^{2+} release events in comparison to cells expressing WT. These parameters were also altered by RyR2-R2474S in the same manner, but to a significantly smaller extent. Modelling of single channel data revealed that K4750Q mutant recombinant mouse RyR2 single channels displayed not only more frequent closed state to open state transitions, but less frequent open state to closed state transitions, leading to prolonged channel openings. Essentially, the point mutation stabilizes the open state of the cytosolic and luminal Ca^{2+} activated RyR2 channel. K4750Q mutation also locked the channel in the open configuration at higher cytosolic Ca^{2+} concentrations, resulting in an increased P_o. Not only do these data support the kinetic scheme of Mukherjee et al. (2012), but highlight that a point mutation can simultaneously modify multiple control mechanisms of RyR2 – in this case, leading to increased luminal and cytosolic Ca^{2+} sensitivity, as well as a loss of Ca^{2+}/Mg^{2+} mediated inactivation (Uehara et al. 2017)

There is no evidence so far to suggest a locus-dependent effect on the severity of the clinical phenotype of CPVT1, however, it is possible that differences in mutant Ca^{2+} release dysfunction could be responsible for the different manifestations of clinical phenotype and responses to therapy seen with this arrhythmia syndrome. As discussed in **Chapter 1, Section 1.7.4**, ß-blocker treatment is often inadequate, with some patients suffering further arrhythmogenic events which are potentially fatal (Laitinen et al. 2001). It could be speculated that the identification of CPVT1-linked RyR2 mutations (and potentially mutation domains) that exhibit exaggerated dysfunction under basal conditions (as is the case for N4104K hRyR2 both in single channel experiments, **Section 3.1.2**, and in a heterologous cell system, **Section 3.3.5)** may aid in identifying more high-risk patients who require further interventions. Carvedilol analogues (such as VK-II-86) are β-blockers that display direct effects on RyR2 channel gating independent of their ability to inhibit β-adrenergic stimulation (Zhou et al. 2011). A combination

therapy of such an analogue with a standard β-blocker may improve the responses to therapy in patients with such a severe 'gain-of-function' mutation. However, data on disease penetrance and expression of inherited RyR2 mutations in families are scarce (van der Werf et al. 2012). Not all family members with a CPVT1-associated RyR2 mutation are symptomatic (Haugaa et al. 2010), so it remains that reduced penetrance, epigenetic and environmental factors also play a role in the severity of disease phenotype (van der Werf et al. 2012).

6.1.2 Basal phosphorylation levels at S2808 and S2031 are different for WT and mutant hRyR2 - but not necessarily in the way expected

Since the spontaneous Ca^{2+} release of S2246L-hRyR2 expressing cells was not very different from those expressing WT, it was concluded that an additional stimulus might be required to reveal channel dysfunction. Luminal Ca^{2+}, which is proposed to cause spontaneous Ca^{2+} release events (D. Jiang et al. 2004), did not reveal the dysfunction of S2246L hRyR2 in the heterologous system of HEK293 cells in this thesis and it was hypothesized that the additional stimulus of phosphorylation could be important for this. Posttranslational modification of RyR2, including phosphorylation, has been substantially investigated for over 30 years, yet remains a contentious subject, as discussed in detail in **Section 1.4**. In this study, the contribution of PKA-mediated phosphorylation to functional heterogeneity of mutant hRyR2 channels was explored, given that CPVT1 in patients occurs under periods of exercise or stress where the β-adrenergic signalling pathway is activated. In **Chapter 4**, this involved a) Western blot assessment of basal phosphorylation at both reported PKA-specific phosphorylation sites in RyR2-S2808 and S2031 and b) the investigation of Ca^{2+} release events under stimulated conditions, utilizing a cAMP analogue (DcAMP).

Basal phosphorylation of RyR2 is often assessed as an indicator of the functional relevance of phosphorylation at a particular site, where subsequent changes in phosphorylation level upon endogenous or exogenous stimulation may be linked to altered channel function {Terentyev:2016jf}. Investigation of basal phosphorylation at S2808 and S2031, via Western blotting using Badrilla phospho-RyR2 antibodies, found levels to be different in mutant compared to WT hRyR2s expressed in HEK293 cells (**Section 4.3.2** and **4.4.2**). Increased basal S2808 phosphorylation in mutant hRyR2 channels did not equate to Ca^{2+} release dysfunction in HEK293 cells. S2246L hRyR2 had a significantly higher basal phosphorylation at the S2808 site, yet displayed similar Ca^{2+} release events to WT (**Section 3.4** and **4.4.2.1**).

N4104K hRyR2 did not show significantly increased basal phosphorylation at S2808, but displayed dysfunction without further stimulation in the form of activated PKA phosphorylation (**Section 4.4.2.2**).

Both CPVT1 mutant hRyR2 channels exhibited a significantly decreased basal phosphorylation level at S2031 compared to WT-hRyR2 (see **Section 4.3.2 and 4.4.2**). Differences appeared robust, albeit levels were assessed with the unreliable Badrilla pS2030 antibody (see **Section 4.4.1**). Dephosphorylation by protein phosphatases may also elicit a change in activity in RyR2 and has been shown to be upregulated in many disease settings (Terentyev and Hamilton 2016). It also remains that a balance of phosphorylation levels at each of the PKA-specific sites may be important for RyR2 channel function, a possibility that was not feasible to investigate during the timeframe of laboratory work presented here.

The interaction of FKBP12.6 with RyR2 was originally proposed to be destabilized in disease settings such as HF, with arrhythmogenic Ca^{2+} release occurring through a hyperactive, 'hyperphosphorylated' RyR2 channel (Wehrens et al. 2003; Marx et al. 2000; Marx et al. 2001). The relevance of FKBP12.6 to channel dysfunction remains disputed (Barg et al. 1997; Timerman et al. 1996; Guo et al. 2010; Zissimopoulos et al. 2004; Xiao et al. 2004; Guo et al. 2006; Stange et al. 2003; Mukherjee et al. 2012). Rycal drugs (such as K201, see **Section 1.7.4**) are proposed to stabilize FKBP12.6 binding to RyR2, thereby normalizing channel dysfunction (Wehrens et al. 2004; Yano et al. 2003; Wehrens et al. 2005; Darcy et al. 2016). According to www.fda.gov, similar rycal derivatives targeting RyR1 in the treatment of Duchenne Muscular Dystrophy (Armgo Pharma, Inc.) were designated 'orphan drugs' by the United States Food and Drug Administration (FDA), allowing for a fast-track to Phase 2 clinical trials in humans after successful completion of Phase 1. However, there is currently no further information available on the outcome of the Phase 1 trial, nor any suggestion of recruitment for additional trials with rycals and their derivatives.

To explore the role of the FKBP12.6 accessory protein in CPVT1-linked hRyR2 channel phosphorylation and dysfunction, FKBP12.6 could be co-transfected with mutants in HEK293 cells. Coimmunoprecipitation experiments as described by Zissimopoulos et al. (2009) would elucidate the level of protein-protein interaction, while Ca^{2+} imaging experiments would reveal the effects (or lack of) of FKBP12.6 on spontaneous Ca^{2+} release kinetics through hRyR2 in this system. However, in the investigation of three CPVT-linked RyR2 mutations (R176Q, S2246L

and R4497C), FKBP12.6 binding affinity with mutant hRyR2 was unaltered or in fact increased in comparison to WT, when the proteins were coexpressed in HEK293 cells. These data provide evidence that CPVT-linked RyR2 mutations do not decrease the affinity of the channel for FKBP12.6.

Due to time restraints and difficulties encountered generating phosphomimetic mutations in hRyR2, the role and influence of CaMKII-dependent phosphorylation at S2814 was not investigated in this study.

6.1.3 Stimulation of PKA phosphorylation significantly increases WT, but not mutant, hRyR2 phosphorylation at S2808

Experiments to investigate changes in hRyR2 function after phosphorylation stimulated by PKA activation were carried out using DcAMP, a choice informed by experiments investigating RyR2 mutation by Paavola et. al (2007). Maximal phosphorylation was indicated by the inclusion of PKA-treated homogenate from WT hRyR2-transfected HEK293 cells, as per the methodology of Rodriguez et al. (2003) and homogenate from DMSO treated hRyR2-transfected cells was used as a vehicle control.

Concentrations of 100 µM and 1 mM elicited significant increases in S2808 phosphorylation level of WT hRyR2 in comparison to DMSO (control) treatment. A large increase in S2808 phosphorylation of WT hRyR2 from the basal level not only signified that PKA does in fact phosphorylate hRyR2 at this site, but that basal phosphorylation levels must be low to moderate in HEK293 cells to allow for this change.

In contrast to WT, treatment of S2246L and N4104K hRyR2-transfected HEK293 with increasing concentrations of DcAMP (**Section 4.3.3** and **4.4.5**) did not result in significantly increased phosphorylation at S2808 compared to basal levels. S2808 in S2246L hRyR2 may not have been phosphorylated any further by PKA given such high basal phosphorylation levels. However, in the case of N4104K hRyR2 this argument does not necessarily follow, as N4104K basal phosphorylation at S2808 was not calculated as significantly different to WT hRyR2, though low n numbers and normalization of expression levels may have influenced this result as discussed in **Section 4.3.2**. The data may therefore imply that N4104K hRyR2 channels were unable to undergo phosphorylation beyond the basal level at this site.

6.1.4 Phosphorylation at S2808 alters WT hRyR2 function - this is less straightforward for mutant hRyR2, but does not trigger dysfunction

Treatment of WT hRyR2-transfected HEK293 cells with DcAMP led to altered kinetics of Ca^{2+} release (**Section 4.4.3**). This would be anticipated as in the physiological setting, phosphorylation upregulates RyR2 channel function (**Section 1.4**). DcAMP treatment had limited effect on the S2808 phosphorylation status of mutant hRyR2 compared to WT, and this was reflected as a corresponding limited effect on spontaneous Ca^{2+} release (**Section 4.4.4**). Both S2246L and N4104K transfected cells displayed the same, minimal changes in Ca^{2+} release kinetics in response to DcAMP treatment. These changes may have been due to very minimal PKA phosphorylation at the S2808 site, or PKA-mediated phosphorylation at S2031 or other potential sites (see **Section 1.4.2** and **4.4.5**). However, toxicity-related side effects were observed with this reagent and Ca^{2+} signalling and expression of hRyR2 was altered in experiments (as discussed in **Section 4.4.6**).

In Ca^{2+} imaging experiments, it appeared that DMSO was stopping spontaneous Ca^{2+} release events (**Figure 4.8 A**), likely due to hydrophobic and osmotic properties of the chemical. Use of an alternative vehicle solvent (methanol) revealed a toxic effect of 1mM DcAMP on hRyR2 transfected cells over a period of 30 minutes, which was not observed with vehicle alone, indicating a toxic effect of the reagent itself at this high concentration. Future experiments could include trying other membrane-permeable cAMP analogues instead, including 8-bromo-cAMP (thought to be a less active version of DcAMP, according to manufacturers, Santa Cruz) which has previously been utilized in the study of transfected HEK293 cells (Shen et al. 2011).

6.1.5 Genetic phosphorylation induces compensatory changes in SERCa expression, making it difficult to interpret Ca^{2+} release data

As well as agonist (DcAMP) induced phosphorylation, genetic phosphorylation was also utilized as a technique to investigate the functional heterogeneity of these CPVT1 mutations (see **Section 5.1.1**). Introduction of phosphomimetic mutations to chemically mimic a phosphorylated site is a useful technique, as it allows the controlled investigation of the functional effects of that mutation, with the assumption that this prevents influences of other factors. Six phosphomimetic hRyR2 DNA plasmids were successfully generated by site-directed mutagenesis (**Section 5.4.1**), mimicking phosphorylation at PKA-specific sites: S2808 or S2031 (B. Xiao et al. 2006; Witcher et al. 1991).

The genetic phosphorylation technique was chosen to avoid the influence of other endogenous proteins to the cell that were likely modified upon stimulation with DcAMP, that may confound the interpretation of spontaneous Ca^{2+} release data. Surprisingly, the introduction of particular genetically phosphorylated hRyR2 mutants (WT08, SL08, SL31) induced changes in SERCa expression (**Section 5.3.7** and **5.4.3**). Adaptive remodelling is a characteristic of cardiac disease in a physiological setting, such as upregulation and increased expression of CaMKII, occurring in response to the increased demand to pump blood around the body through a failing heart (Anderson et al. 2011; Ai 2005). However, changes in endogenous protein expression after the introduction of hRyR2 were not expected in transiently transfected HEK293 cells, where hRyR2 was only expressed for ~48 hrs. Whether this was the result of the transfection of recombinant hRyR2, or the genetic phosphorylation of a specific site in hRyR2, is somewhat difficult to untangle. Further investigation (transfection of HEK293 cells with more hRyR2 CPVT1 mutants as well as phosphomimetics) would be necessary to elucidate how and why this may occur. In the literature, when using KI mice with a hRyR2 site genetically phosphorylated or ablated, very few studies assess the levels of phosphorylation at other sites in RyR2 (aside from Loiaza et al. (2013) and Terentyev et al. (2014) for example), let alone the expression of other key Ca^{2+} cycling proteins such as SERCa. Data presented in this thesis serve as a caution when interpreting data and highlights the importance of investigating changes of other endogenous Ca^{2+} handling proteins of a cell.

Genetic phosphorylation also affected the expression and trafficking of N4104K hRyR2 in HEK293 cells (**Section 5.3.2** and **5.4.2**). This indicated there was some issue with this mutant

protein's integrity, limiting the ability to obtain meaningful or well powered data from Ca^{2+} imaging experiments with N4104K phosphomimetics (**Section 5.3.6** and **5.4.6**). It could be suggested this may be a symptom of recombinant technology, whereby genetic phosphorylation prevents expression of functional channels. It could also be that fully phosphorylated N4104K channels may in fact be unstable or broken down and that this may potentially cause the CPVT phenotype in patients with this RyR2 mutation. CPVT-associated exon-3 deletion in RyR2 causes reduced protein expression and in this instance the lack of expression (because of reduced mutant allele) causes arrhythmia (Liu et al. 2014). In recent work of the Van Petegem and Chen groups, the CPVT-associated mutation G357S enhances arrhythmogenic SOICR activity in HEK293 cells and reduces total RyR2 expression (Liu et al. 2017). Alternatively, the combination of full stoichiometric phosphorylation (of all four phosphorylation sites within a tetramer) at S2808 or S2031 plus the N4104K mutation in hRyR2 may have caused the channel to be unstable and this phosphorylation to maximal stoichiometry would not be seen *in vivo*. Equally, working with homotetramers (four phosphorylated monomers) likely exacerbated this stability problem, which may not be equivalent in heterotetramers (a mixture of phosphorylated and unphosphorylated monomers).

Interestingly eGFP fluorescence, used as an indicator of transfection efficiency, was found to misrepresent the proportion of cells expressing hRyR2 phosphomimetics (**Section 5.3.3** and **5.4.4**). The discrepancy in the number of increased caffeine-responsive cells compared to calculated transfection efficiency may have been due to detection limits, whereby low-level expression of hRyR2 would have been more easily detected by caffeine-induced Ca^{2+} release. In the case where transfection efficiency was significantly higher than the number of caffeine-responsive cells, this may have been due to overestimation. While propensity in this thesis was calculated instead as the number of caffeine-responsive (as opposed to spontaneously Ca^{2+} responsive) cells as a percentage of the total, this finding also supported the suggestion that propensity (as described by D. Jiang et al. (2004)) is not a good indicator of CPVT1 RyR2 channel dysfunction in HEK293 cells, given that the number of transfected cells cannot be robustly calculated. Others also have not observed changes in propensity for spontaneous Ca^{2+} release events when investigating disease-linked mutations (Loaiza et al. 2013).

These additional changes and observations confounded the interpretation of spontaneous Ca^{2+} release events in hRyR2-transfected HEK293 cells in this study, and such occurrences must be considered for future experiments when utilizing a heterologous system.

6.1.6 S2808D and S2031D have similar functional effects in WT hRyR2, but different effects in S2246L and N4104K

Genetic phosphorylation at S2808 and S2031 had similar effects on the spontaneous Ca^{2+} release events of WT hRyR2-transfected HEK293 cells (**Section 5.4.6**), while genetic phosphorylation of mutant hRyR2 had less profound effects (**Section 5.4.7**).

For S2246L, genetic phosphorylation at S2808 influenced channel function with effects similar to those of S2808D on the WT i.e. increasing the amplitude of spontaneous Ca^{2+} release events and decreasing event duration and the time between them (**Figure 5.18**). Since these changes were not in excess of those seen upon introduction of the phosphomimetic to the WT (**Table 5.9**), this suggests that phosphorylation to full stoichiometry at S2808 is not key in revealing S2246L dysfunction. While introduction of S2031D affected WT Ca^{2+} release in a comparable way to S2808D, its introduction to the S2246L hRyR2 resulted only in a decreased duration of Ca^{2+} release event.

Notably, modification of either site in N4104K channels did not affect function as the same way in WT hRyR2 channels with few changes in Ca^{2+} release kinetics induced by introduction of phosphomimetic (**Figure 5.19**). N4104K hRyR2 already appears dysfunctional in Ca^{2+} imaging experiments in comparison to WT (**Figure 3.16**), so phosphorylation may not elicit the normal physiological response. However, phosphomimetic mutation of N4104K did have an effect on functionality, since it significantly decreased the number of caffeine-responsive cells (see **Section 5.4.2**).

As a future direction, single channel experiments could be used to verify findings of Ca^{2+} imaging studies with phosphomimetic hRyR2, given that HEK293 cells exhibited endogenous protein remodelling. This would eliminate any potential influence of the increased expression of SERCa on spontaneous Ca^{2+} release kinetics.

6.1.7 Genetic phosphorylation likely represents a vast oversimplification of the physiological state

The effects of genetic phosphorylation are different to those caused by the agonist-induced phosphorylation of hRyR2, as discussed in **Section 5.4.7**. This discrepancy may be due to additional effects of DcAMP, including activation of other endogenous kinases (Hofer et al. 2007). While genetic phosphorylation modified SERCa expression (see **Section 5.4.3**), this was almost certainly as a result of a change this mutation caused in RyR2 function, in line with an increase in channel activity. The mechanism for this cannot be deciphered from the data acquired here, but may include increased agonist sensitivity or changes to the dynamics of Ca^{2+} release through altered channel clustering.

It remains that genetic phosphorylation to full stoichiometry, as investigated in **Chapter 5**, is not necessarily representative of the physiological state. Important work of Carter et al. (2006) determined that RyR2 was phosphorylated to 75 % of maximum at the S2808 site under unstimulated conditions, meaning that only three available sites were phosphorylated, while one was not. Therefore, the co-expression of phosphomimetic hRyR2 with WT or mutant hRyR2 cDNA in HEK293 cells may give an insight into the consequences of phosphorylation on channel function under unstimulated conditions. Transfection in equal molar quantities will result in a mixed population of homo- and heterotetramers of different types (i.e. monomer ratios of 4 WT, 3 WT:1 S2808D, 2 WT: 2 S2808D, 1 WT: 1 S2808D) whose distribution, if assuming equal association can be calculated according to binomial theory (Loaiza et al. 2013). Skewing the ratio of molar quantities in the transfection will favour distribution towards a heterotetramer containing the required proportions of different monomers, but these will never constitute 100 % of the population. Furthermore, control of the phosphorylation status at S2808 would require genetic ablation of WT (introduction of S2808A) and these experiments were beyond the scope of this investigation.

It also remains that genetic phosphorylation of one site does not take into consideration that physiological phosphorylation at one site in hRyR2 alone is unlikely, with both S2808 and S2031 suggested as PKA-specific sites. A limitation to this investigation, as noted in **Figure 6.1**, is that upon genetic phosphorylation at one site, the phosphorylation status of others in hRyR2 were not assessed. It cannot be assumed that they would not change, especially given that alteration in basal phosphorylation levels was observed after introduction of a mutation (**Section 4.4.2**)

Generation of double phosphomimetics, with genetic phosphorylation of both the S2808 and S2031 sites, would be an interesting comparison to data presented in this thesis. However, N4104K hRyR2 phosphomimetics proved very difficult to work with, given low transfection efficiencies and the difficulty obtaining n numbers for Ca^{2+} imaging experiments (**Section 5.4.2**). It is reasonable to suggest that the addition of a further mutation to N4104K hRyR2 cDNA would only add to the plasmid fragility. Data presented in this thesis suggest that genetic phosphorylation may not be able to be applied to all CPVT1 mutant hRyR2 constructs. To instead utilize plasmids that have already been constructed, phosphomimetic hRyR2 transfected-HEK293 cells could also be treated with a cAMP analogue. As no changes would occur at the genetically phosphorylated site after treatment, this may highlight functional changes caused by phosphorylation at the other PKA-specific site(s) in hRyR2.

To explore and elucidate mechanisms of dysfunction caused by mutations and potentially phosphorylation of RyR2, it is important to apply multiple methods in the laboratory. Even so, it has been suggested that the use of so many different techniques to investigate RyR2 dysfunction contributes to disparity in findings (George 2007). As is particularly evident in the study of RyR2 phosphorylation, this is exacerbated by variation of methods between groups, such as transgenic mouse background, mode of recombinant expression and choice of antibody (Bers 2008; Respress et al. 2012; Jiang et al. 2004, Benkusky et al. 2007; Wehrens et al. 2014; Mukherjee et al. 2012). This thesis reinforces that these differences must be taken into account when applying other complimentary systems to study RyR2 dysfunction.

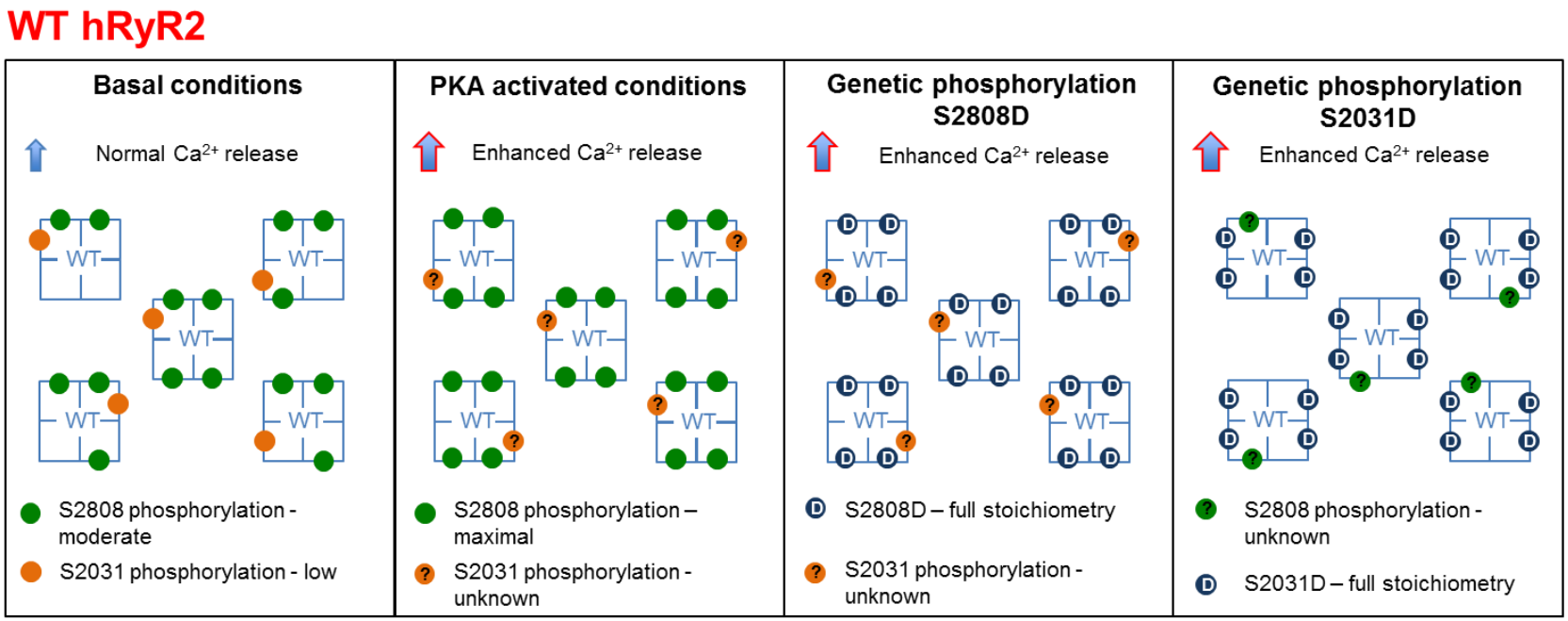

Figure 6.1 Schematic of the major findings in this study for WT hRyR2. Each larger square indicates an individual hRyR2 channel tetramer, with the four smaller squares indicating each monomer. Basal conditions are defined as being in the absence of PKA activation (by DcAMP) or genetic phosphorylation (by introduction of a phosphomimetic mutation at S2808 or S2031). Under basal conditions, HEK293 cells expressing WT hRyR2 displayed spontaneous Ca^{2+} release events, considered 'normal' in these figures. S2808 hRyR2 phosphorylation was moderate, similar to that of WT, but S2031 phosphorylation was low (although this was inferred only by comparison to mutant hRyR2 basal phosphorylation levels). Under PKA activating conditions, Ca^{2+} release was enhanced and the level of S2808 phosphorylation was maximal (as inferred by comparison to a PKA-treated control). S2031 phosphorylation was not investigated further due to difficulties with the antibody. Genetic phosphorylation at either site (S2808D or S2031D) enhanced spontaneous Ca^{2+} release kinetics of transfected cells.

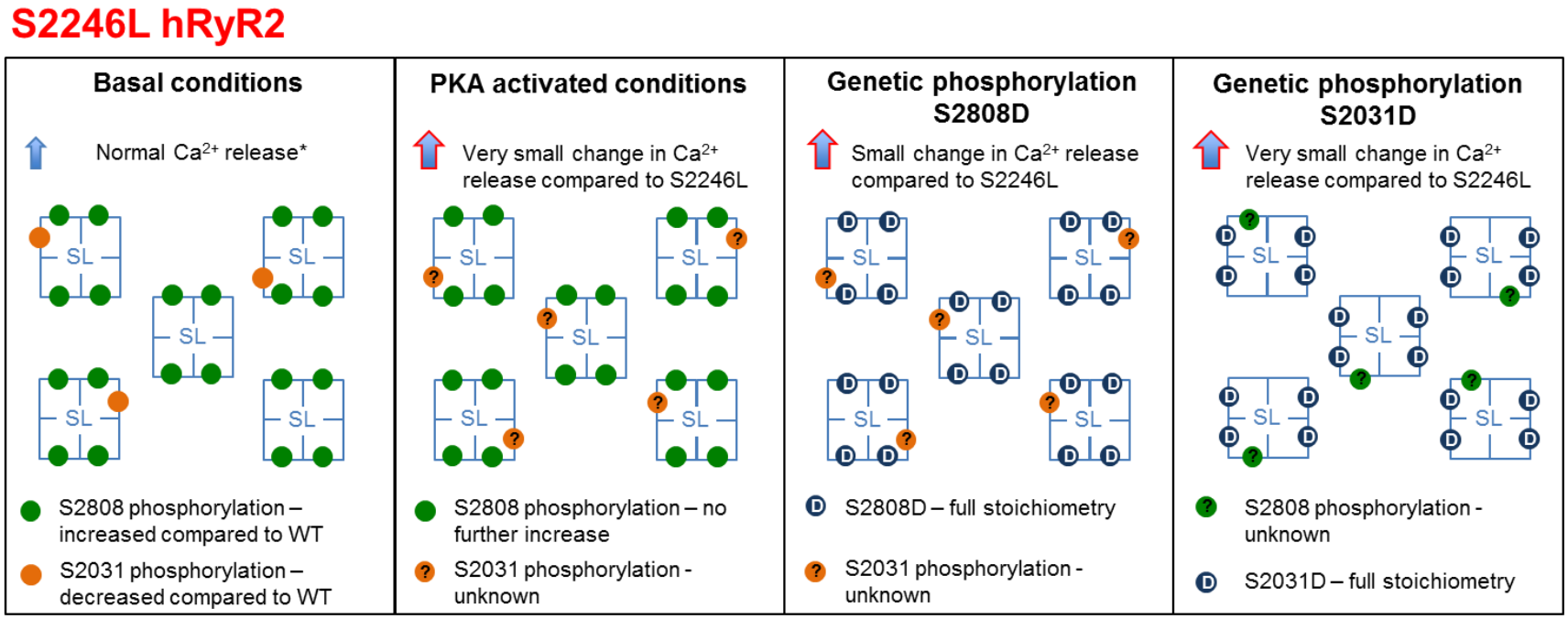

Figure 6.2 Schematic of the major findings in this study for S2246L hRyR2. Basal conditions are defined as being in the absence of PKA activation (by DcAMP) or genetic phosphorylation (by introduction of a phosphomimetic mutation at S2808 or S2031). Each larger square indicates an individual hRyR2 channel tetramer, with the four smaller squares indicating each monomer. Under basal conditions, HEK293 cells expressing S2246L hRyR2 displayed normal spontaneous Ca^{2+} release events, similar to those of WT. However, as indicated by the *, the propensity of cells for caffeine-induced Ca^{2+} release was significantly decreased compared to that of WT, but was not as a result of altered expression. S2808 hRyR2 phosphorylation was increased in comparison to WT, while S2031 phosphorylation was decreased. Under PKA activating conditions, there were no significant changes in the level of S2808 phosphorylation, and only a very small change in the Ca^{2+} release events in comparison to release events under basal conditions. Genetic phosphorylation (S2808D) similarly only induced a small change in spontaneous Ca^{2+} release kinetics of transfected cells, while the change induced by S2031D was very small.

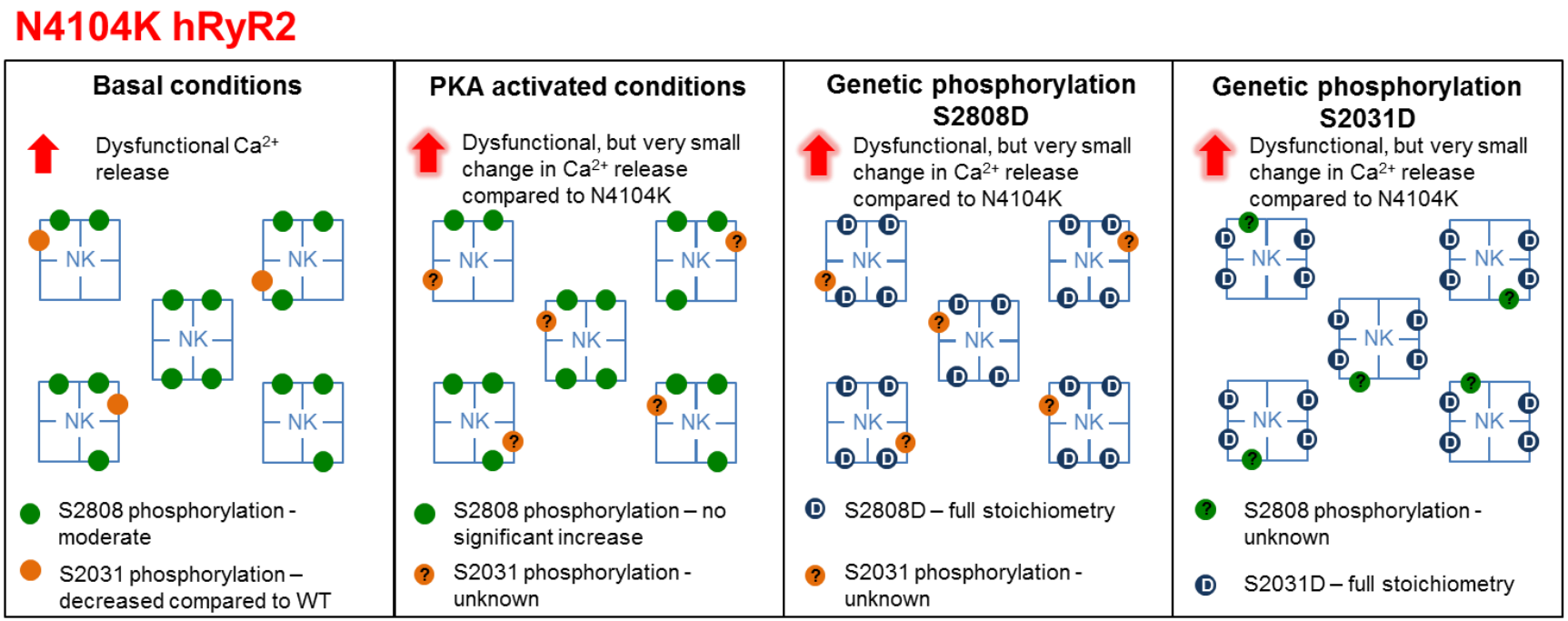

Figure 6.3 Schematic of the major findings in this study for N4104K hRyR2 Basal conditions are defined as being in the absence of PKA activation (by DcAMP) or genetic phosphorylation (by introduction of a phosphomimetic mutation at S2808 or S2031). Each larger square indicates an individual hRyR2 channel tetramer, with the four smaller squares indicating each monomer. Under basal conditions, HEK293 cells expressing N4104K hRyR2 displayed dysfunctional spontaneous Ca^{2+} release events in comparison to WT, as well as an increased expression of channels per cell. S2808 hRyR2 phosphorylation was moderate, similar to that of WT, but S2031 phosphorylation was decreased. Under PKA activating conditions, there were no significant changes in the level of S2808 phosphorylation, and only a small change in the already dysfunctional Ca^{2+} release. Genetic phosphorylation (S2808D or S2031D) similarly only induced a small change in spontaneous Ca^{2+} release kinetics of transfected cells. N numbers for cells transfected with phosphomimetic N4104K hRyR2 were very low, given that the protein seemed to degrade in IF experiments.

6.1.8 Study limitations and future experiments

While limitations of this study and future works have been integrated throughout this Chapter when pertaining to experimental design, major points to be highlighted include:

The lack of assessment of CaMKII phosphorylation

There is substantial evidence for a major role of CaMKII-dependent phosphorylation of RyR2 in modulating channel function, in both physiological and disease settings (Bers, 2006; Uchinoumi et al. 2010; 2016), as discussed in **Section 1.4.1.2** and **1.4.2.3**. Due to difficulties encountered generating phosphomimetic hRyR2 constructs, CaMKII-dependent phosphorylation of RyR2 and the potential influence on functional heterogeneity of CPVT hRyR2 mutants was not assessed here, nor were the phosphorylation levels of S2814-hRyR2 via Western blotting. In future works, these investigations would be high priority to strengthen this thesis.

The need to assess membrane Ca^{2+} fluxes in the heterologous HEK293 expression system

The Ca^{2+} flux balance of cardiomyocytes has been long investigated in multiple species and it is well established that in the steady state, the amount of Ca^{2+} entering the cell must equal the amount of Ca^{2+} that leaves in (Eisner et al. 2017). While using HEK293 cells as a heterologous cell system to investigate changes in hRyR2 function induced by mutation has its advantages as discussed in **Section 3.1.1.3**, it also remains that the Ca^{2+} fluxes of this cell type remain poorly characterized. In future works, investigation of Ca^{2+} influx and efflux systems and the expression level and activity of Ca^{2+} handling proteins would be paramount to properly interpreting changes in Ca^{2+} release kinetics after transfection with hRyR2.

The limitations of ER Ca^{2+} content with caffeine

The amplitude of Ca^{2+} transient amplitude is steeply dependent on the Ca^{2+} content of the SR (ER in HEK293 cells). While application of high-dose caffeine is frequently used to determine the store content (D. Jiang et al. 2007; Loaiza et al. 2013; George et al. 2006; D. Jiang 2005), as discussed in **Section 3.4.3**, it is an indirect measurement dependent on the timing of Ca2+ release events prior to application. Genetically encoded biosensors are now more commonly used to monitor Ca^{2+} and would be utilized in future experiments for more accurate measurements (Palmer et al. 2004).

Appendix

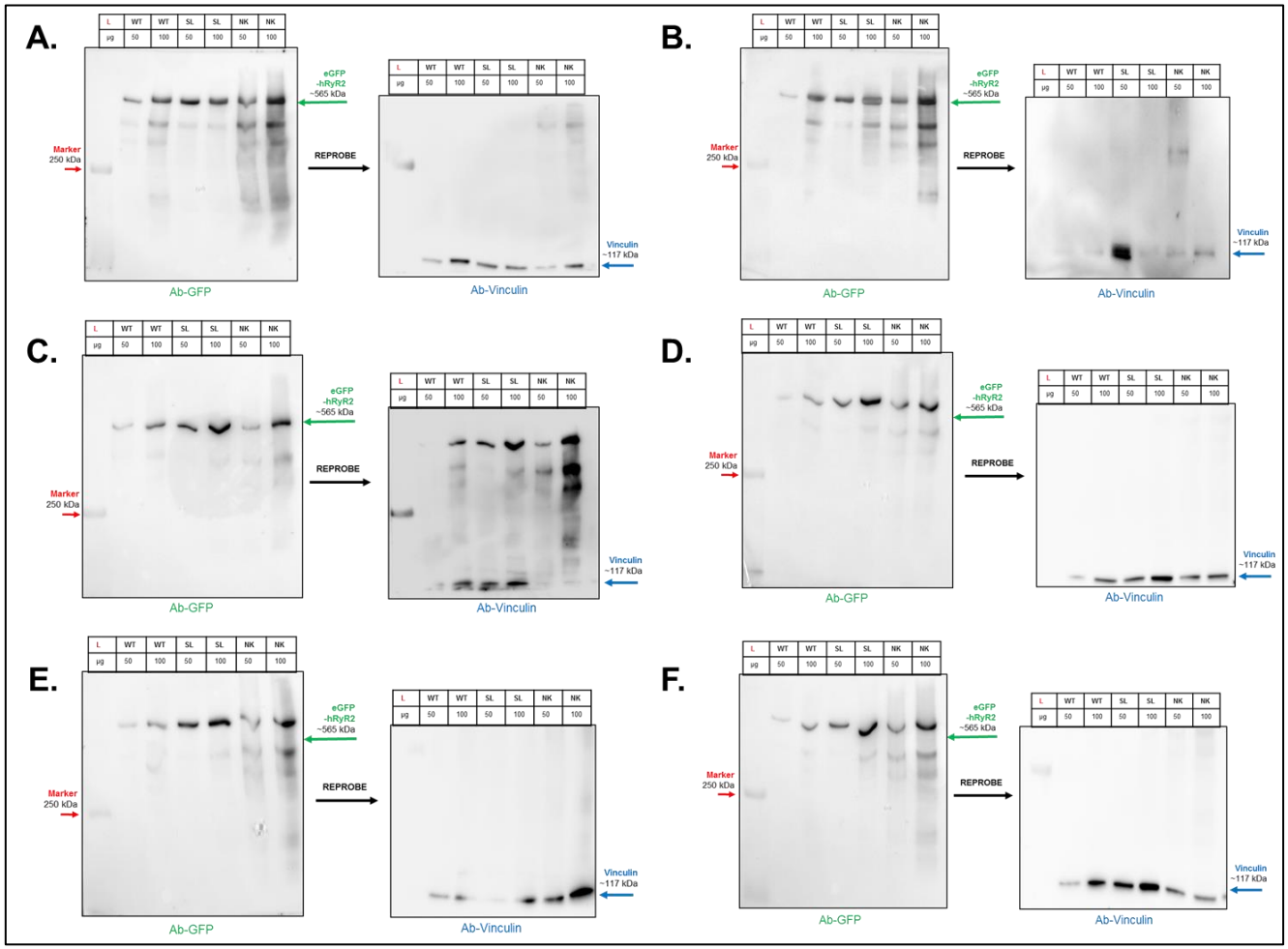

<u>Appendix I</u> Western blotting of WT and mutant eGFP-hRyR2 expression in HEK293 cells. Following SDS PAGE of cell homogenate preparations, blots A-F were assessed for GFP-hRyR2 expression (left image) and vinculin expression as a loading control (right image) at loads of 50 µg and 100 µg for each construct. Molecular weight of bands was estimated against the prestained Kaleidoscope ladder (Biorad, lane marked L). For clarity, these images were obtained after stripping of a phospho-antibody in experiments described in **Chapter 4**, see **Appendix VIII** *A* and *B*, **Appendix VIV** *A-D*. Membrane stripping does not appear to degrade the sample, see **Figure 3.7**.

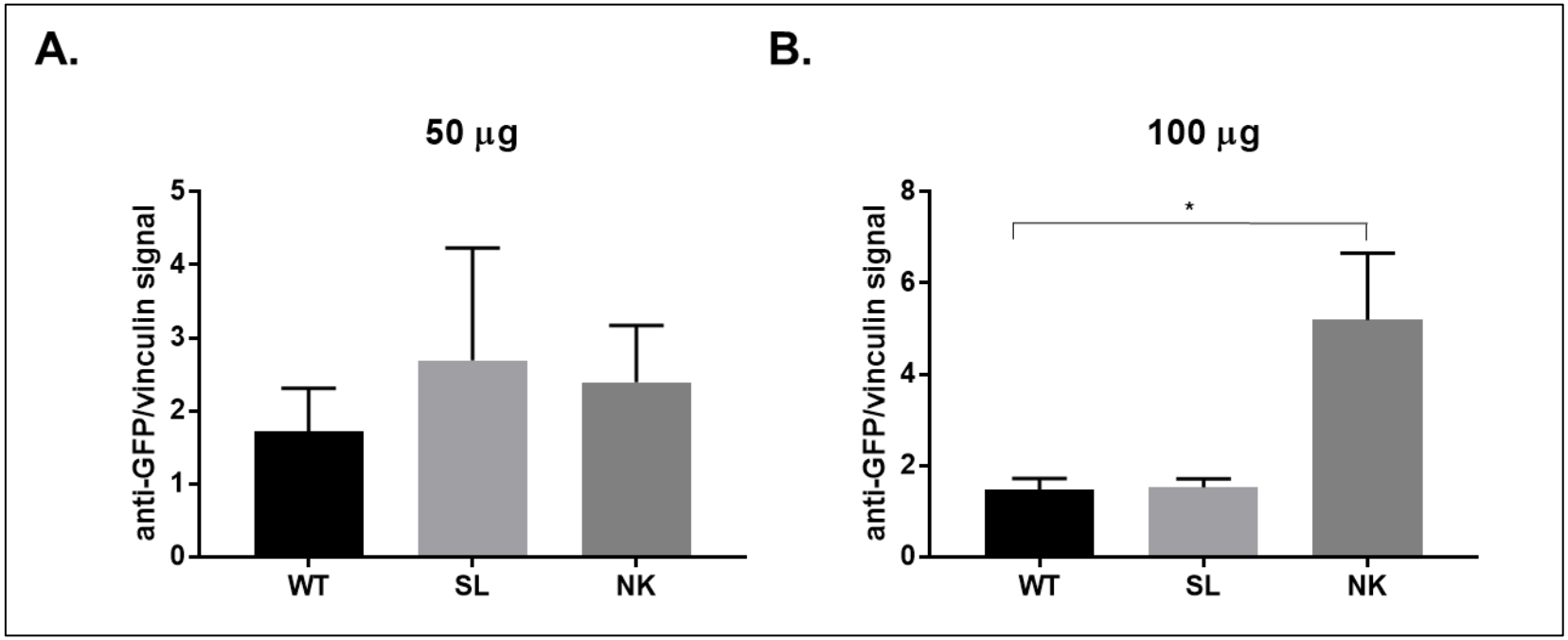

<u>Appendix II</u> Densitometric analysis of WT and mutant eGFP-hRyR2 expression in HEK293 cells at 50 µg and 100 µg of loading reveals larger error at lower sample loads. Densitometric analysis of Western blots found in **Appendix III**, by normalization of anti-GFP signal to vinculin signal as described in **Section 3.2.1**, reveals significant differences between results at 50 µg and 100 µg of sample loading. Data are presented as mean ± SEM, with $p<0.05$ indicated by * as calculated by one way ANOVA with Bonferroni posthoc test

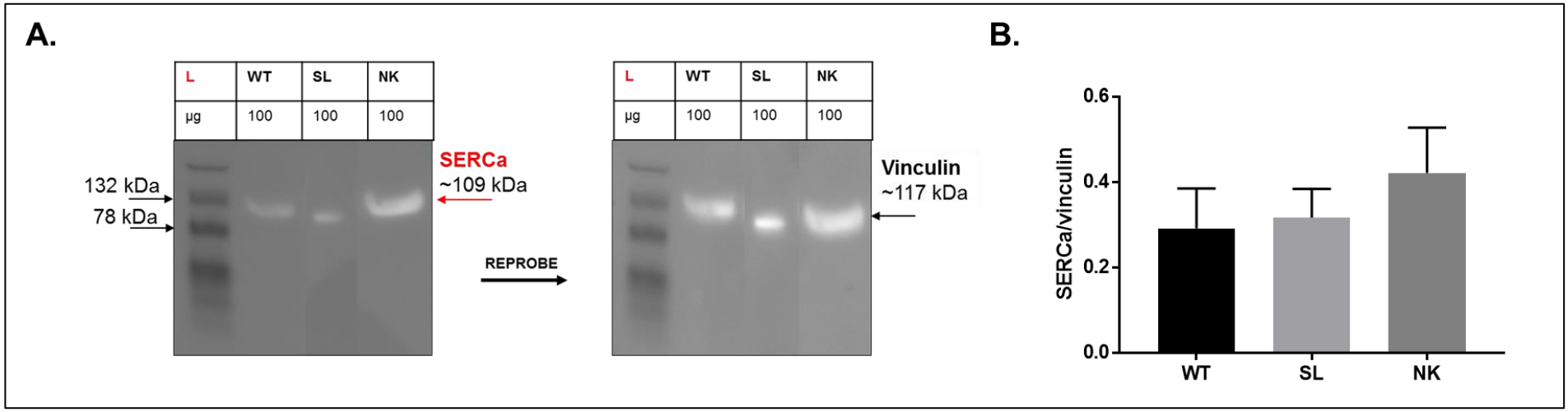

<u>Appendix III</u> SERCa expression cannot be normalized to vinculin in Western blot experiments. *A.* Representative bands of SERCa and vinculin protein. Bands appear very close together. Bands are spliced together from the same blot – original blots can be found in **Appendix XVII and XXIX**. *B.* Densitometric analysis of SERCa expression normalized to vinculin expression, n=4 experiments. Data are presented as mean ± SEM, with $p<0.05$ indicated by * as calculated by one way ANOVA with Bonferroni posthoc test.

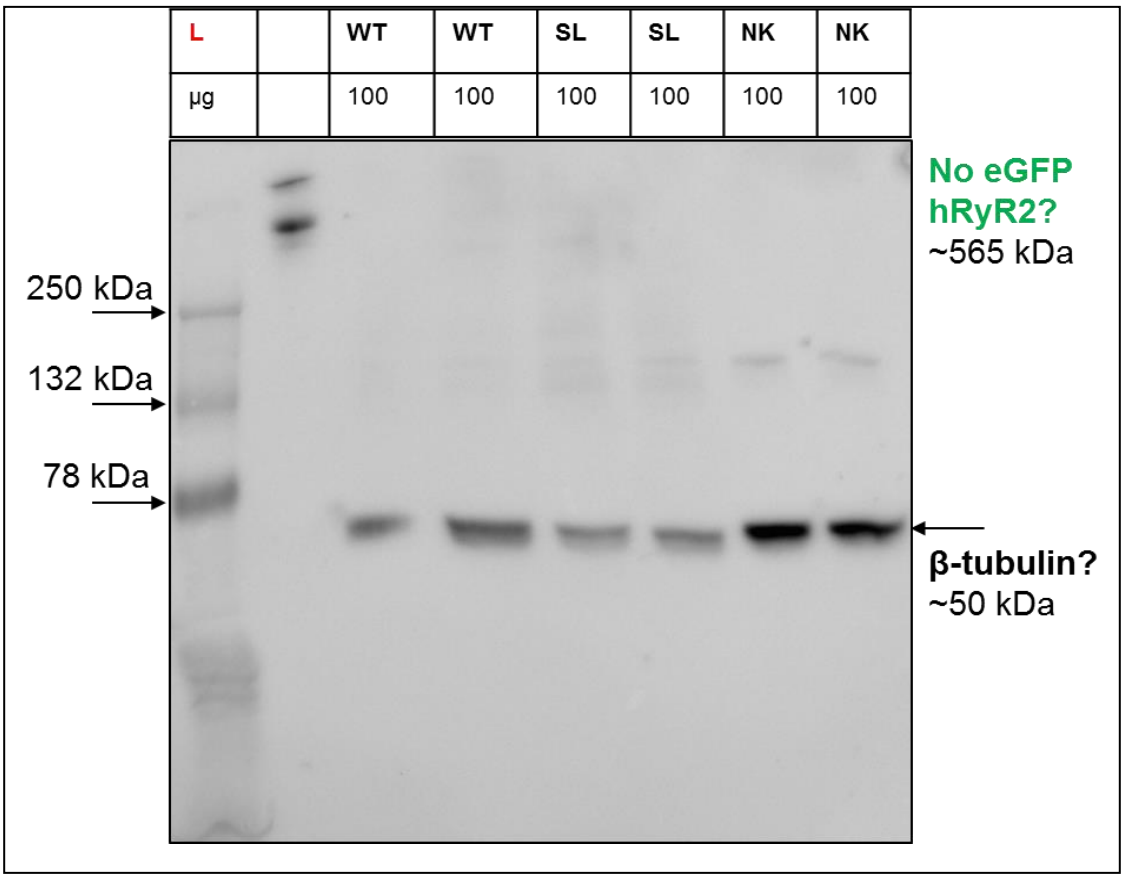

<u>Appendix IV</u> Attempts to assess both eGFP-hRyR2 and β-tubulin protein expression on a gradient gel were unsuccessful.

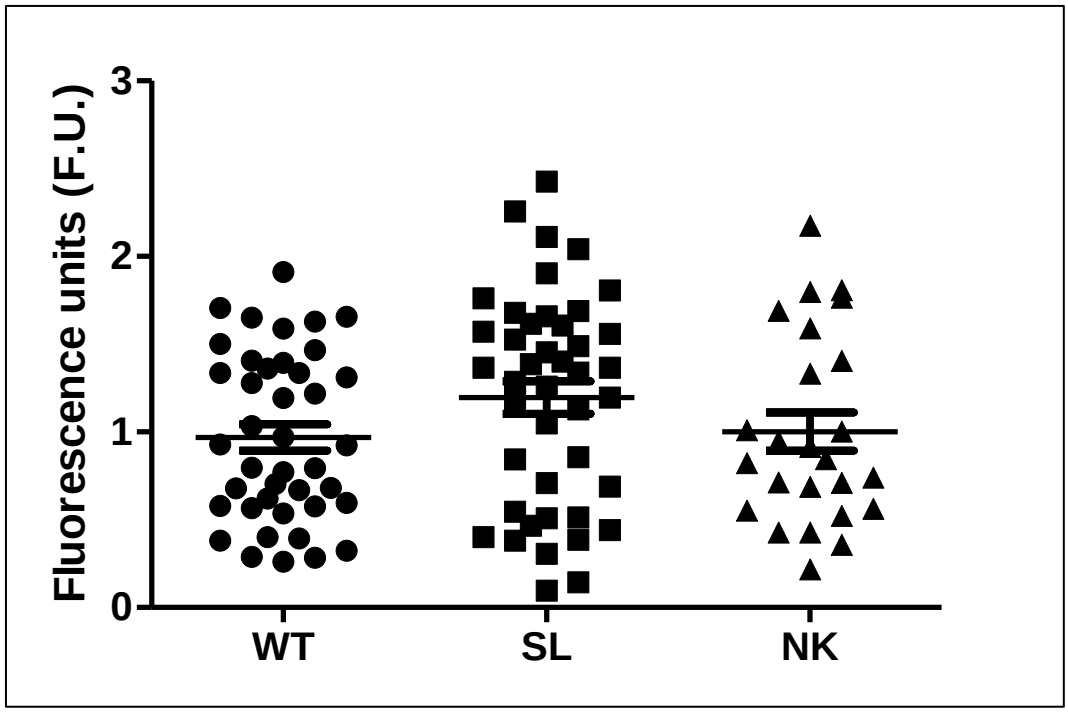

<u>Appendix V</u> Scatter plots of ER Ca^{2+} store load of WT and mutant hRyR2-transfected HEK293 cells. Equivalent bar graphs are found in **Figure 3.6**.

	hRyR2 construct vs. WT	PARAMETRIC One way ANOVA with Bonferroni posthoc test	NON-PARAMETRIC Kruskal-Wallis with Dunn's posthoc test
Amplitude	S2246L	ns	ns
	N4104K	p<0.001	p<0.001
Duration	S2246L	ns	ns
	N4104K	ns	ns
Inter-event duration	S2246L	ns	ns
	N4104K	p<0.01	p<0.001
Frequency	S2246L	ns	ns
	N4104K	p<0.01	p<0.01
Rate up	S2246L	p<0.01	p<0.01
	N4104K	p<0.001	p<0.001
Rate down	S2246L	ns	ns
	N4104K	p<0.001	p<0.001

Appendix VI Table of comparison of parametric and non-parametric test results from Ca^{2+} imaging data discussed in Chapter 3. Imaging data was analyzed with GraphPad Prism, either by parametric one way ANOVA with Bonferroni posthoc, or by nonparametric Kruskal-Wallis with Dunn's posthoc test. The are no differences in results, aside from inter-event duration significance when a comparison of WT and N4104K data is made. This difference is only by a matter of one degree – the result remains significant with both parametric and non-parametric tests.

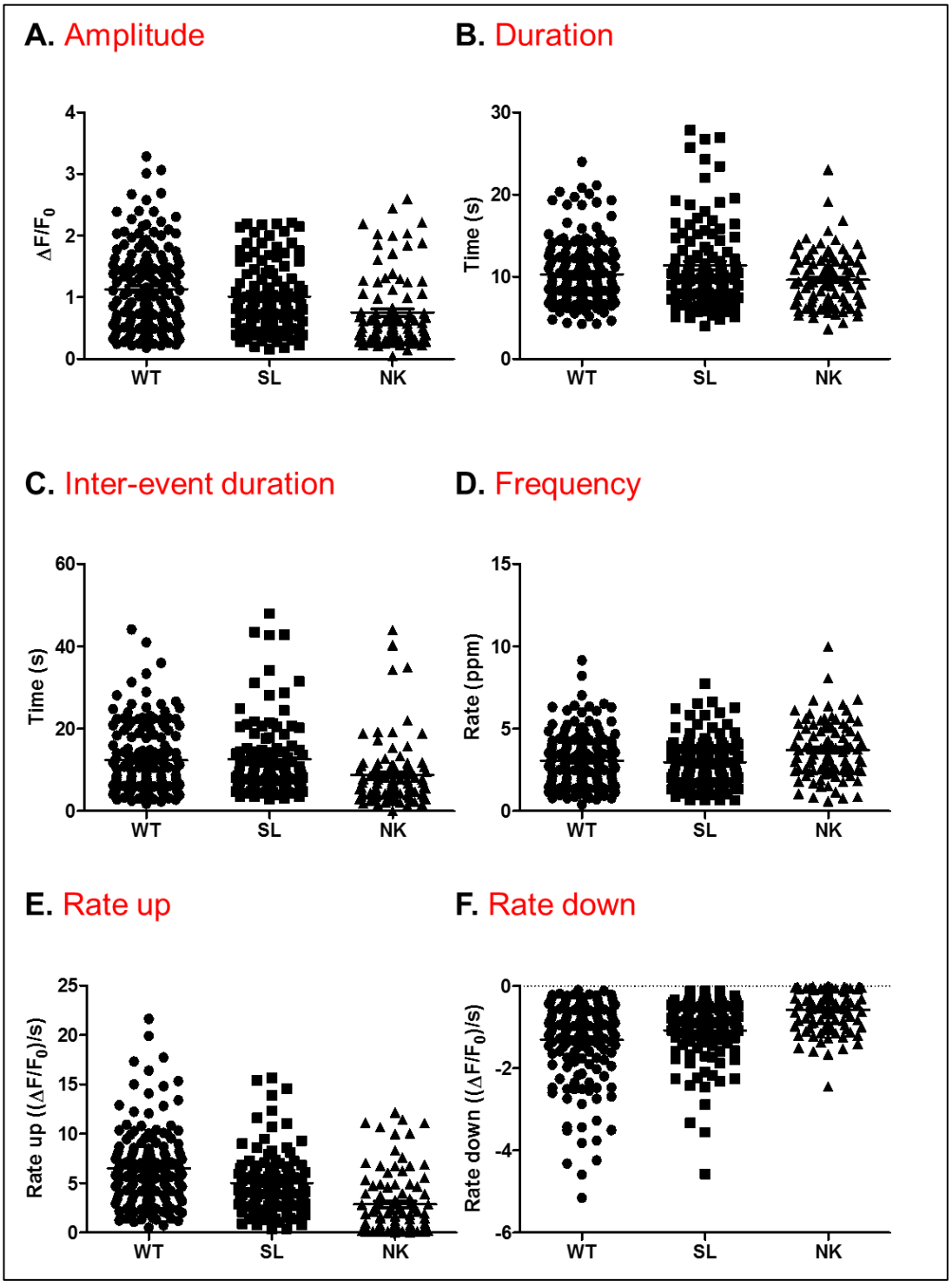

<u>Appendix VII</u> Scatter plots of Ca^{2+} release kinetics of WT, S2246L and N4104K hRyR2-transfected HEK293 cells. Equivalent bar graphs and statistics are found in **Figure 3.1.**

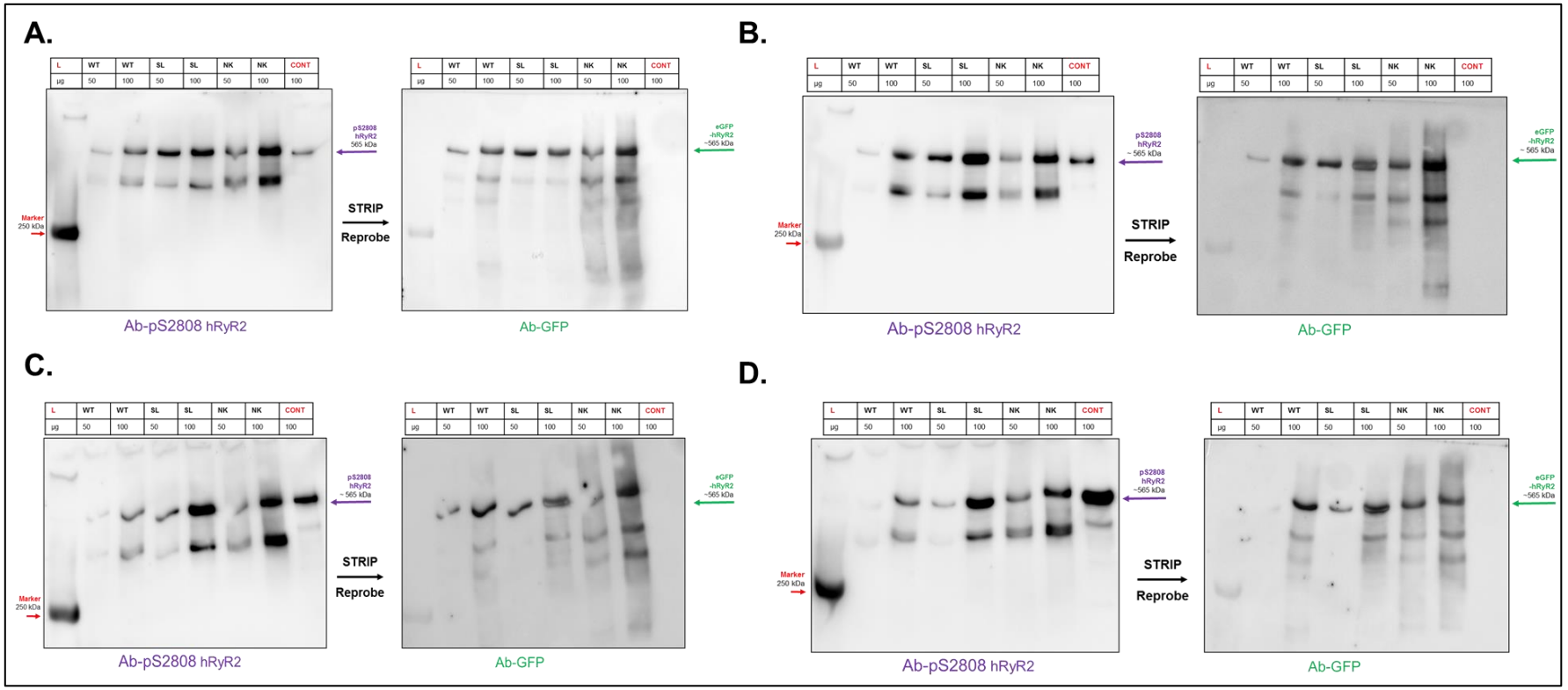

<u>Appendix VIII</u> Western blotting of the basal phosphorylation at the S2808 hRyR2 site. Following SDS PAGE of cell homogenate preparations, blots *A-D* were assessed for pSer-2808 hRyR2 expression (left image), before membrane stripping and the assessment of GFP-hRyR2 expression (right image). Molecular weight of bands was estimated against the prestained Kaleidoscope ladder (Biorad, lane marked L). CONT refers to 100 µg of a mouse cardiac homogenate preparation. Densitometric analysis in **Figure 4.4** was of 100 µg loads only.

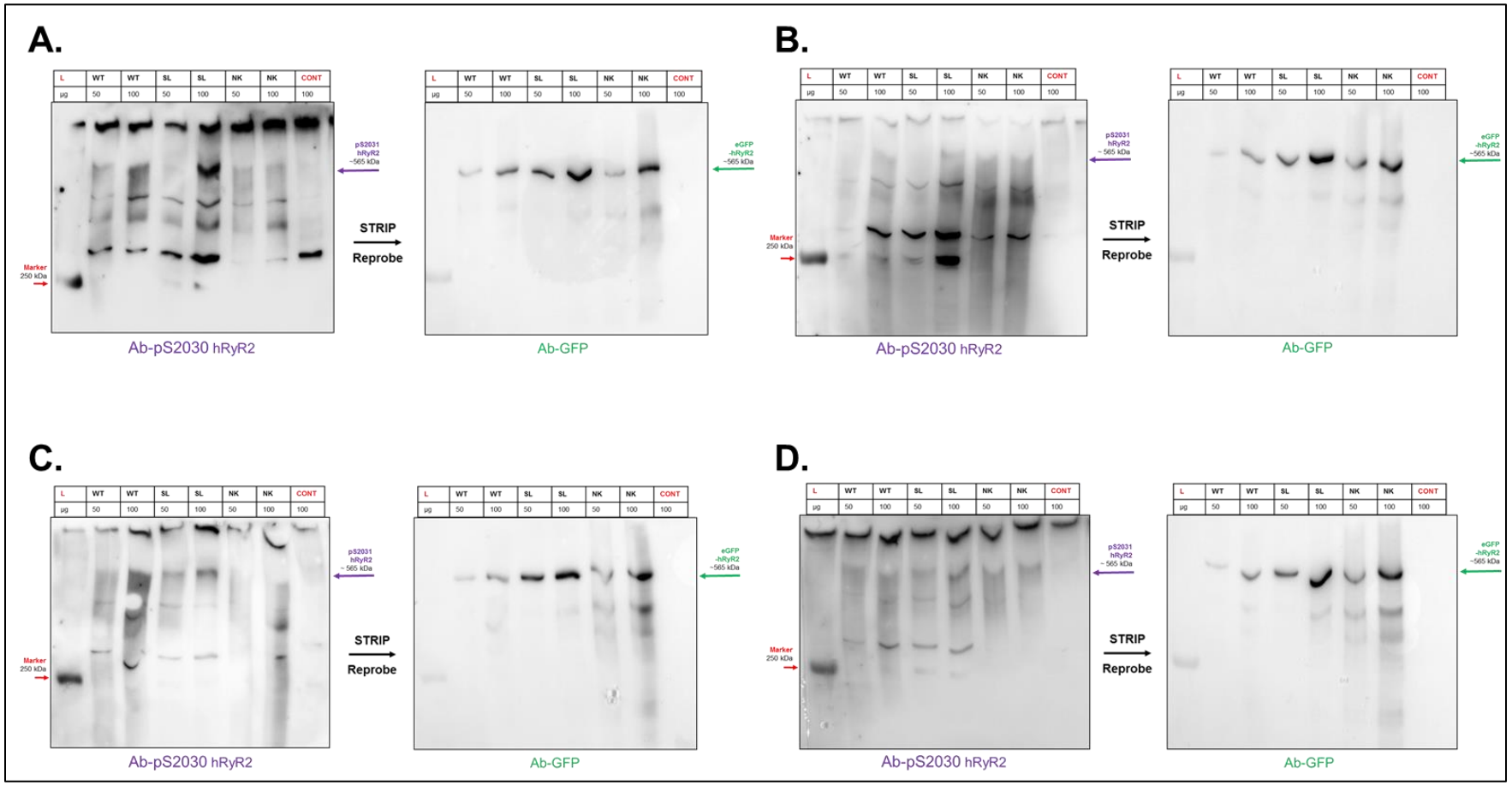

Appendix IX Western blotting of the basal phosphorylation at the S2031 hRyR2 site. Following SDS PAGE of cell homogenate preparations, blots A-D were assessed for pS2031-hRyR2 expression (left image), before membrane stripping and the assessment of eGFP-hRyR2 expression (right image). Molecular weight of bands was estimated against the prestained Kaleidoscope ladder (Biorad, lane marked L). CONT refers to 100 µg of a mouse cardiac homogenate preparation. Densitometric analysis in **Figure 4.5** was of 100 µg loads only.

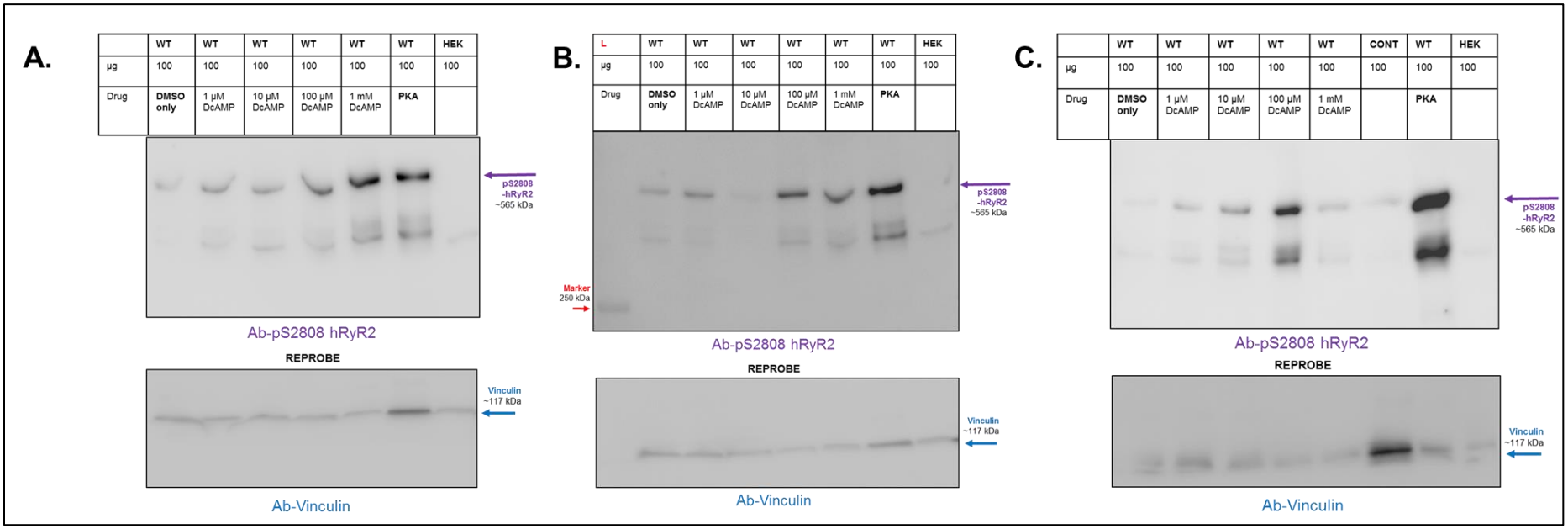

<u>Appendix X</u> Western blotting of WT hRyR2-transfected HEK293 cells treated with dioctanoyl-cAMP, investigating phosphorylation at the S2808 site. Transfected HEK293 cells were treated with various concentrations of dioctanoyl-cAMP in DMSO, as described in **Section 4.2.2.2**. Following SDS PAGE of cell homogenate preparations, blots *A-C* were assessed for pS2808-hRyR2 expression (top image), and reprobed for vinculin expression (lower image) as a loading control, at loads of 100 µg. No strip was necessary since antibodies were raised in different animals and proteins were far apart on the blot. Where ladder was visible, molecular weight of bands was estimated against the prestained Kaleidoscope ladder (Biorad, marked L). CONT refers to 100 µg of a mouse cardiac homogenate preparation – this was only included in one blot since a control for strip was not necessary. Where ladder was not visible, blots were using GBOX system to match equivalent bands. HEK refers to 100 µg of a preparation of untransfected HEK293 cells. WT PKA refers to a PKA-treated sample which should indicate total phosphorylation levels.

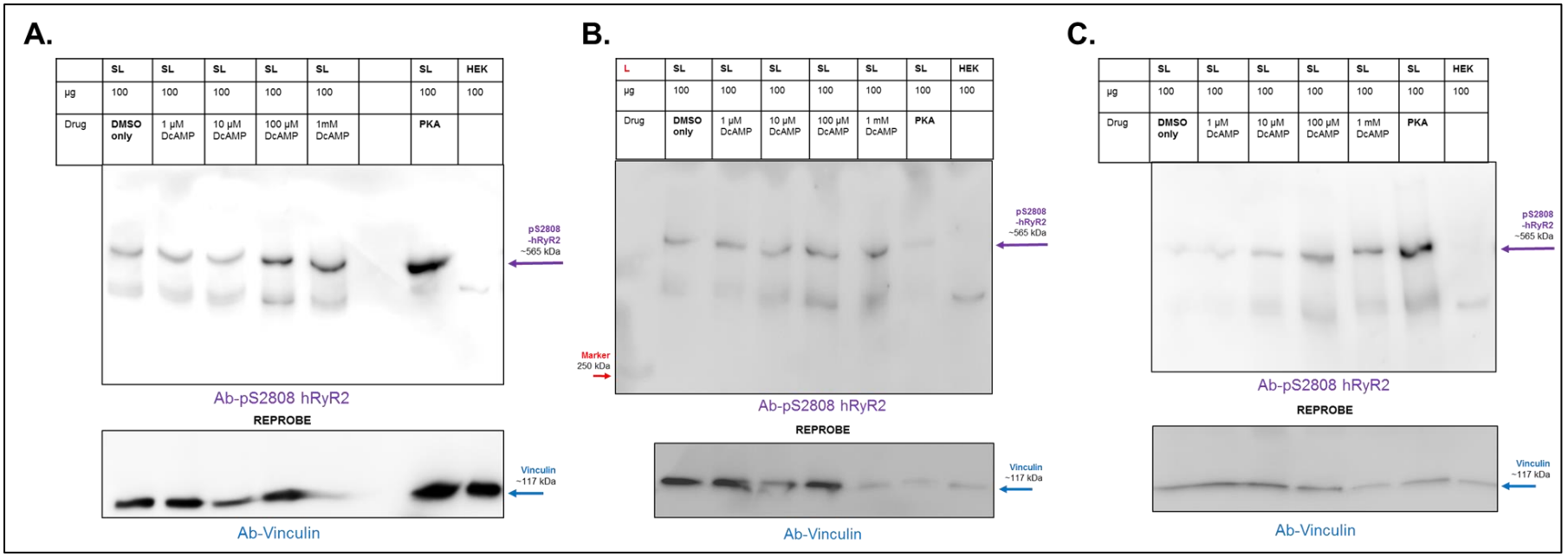

<u>Appendix XI</u> Western blotting of S2246L hRyR2-transfected HEK293 cells treated with dioctanoyl-cAMP, investigating the phosphorylation at the S2808 site. Transfected HEK293 cells were treated with various concentrations of dioctanoyl-cAMP in DMSO, as described in **Section 4.2.2.2**. Following SDS PAGE of cell homogenate preparations, *A-C* were assessed for pS2808-hRyR2 expression (top image), and reprobed for vinculin expression (lower image) as a loading control, at loads of 100 µg. No strip was necessary since antibodies were raised in different animals and proteins were far apart on the blot. Where ladder was visible, molecular weight of bands was estimated against the prestained Kaleidoscope ladder (Biorad, marked L). Where ladder was not visible, blots were using GBOX system to match equivalent bands. HEK refers to 100 µg of a preparation of untransfected HEK293 cells. WT PKA refers to a PKA-treated sample which should indicate total phosphorylation levels.

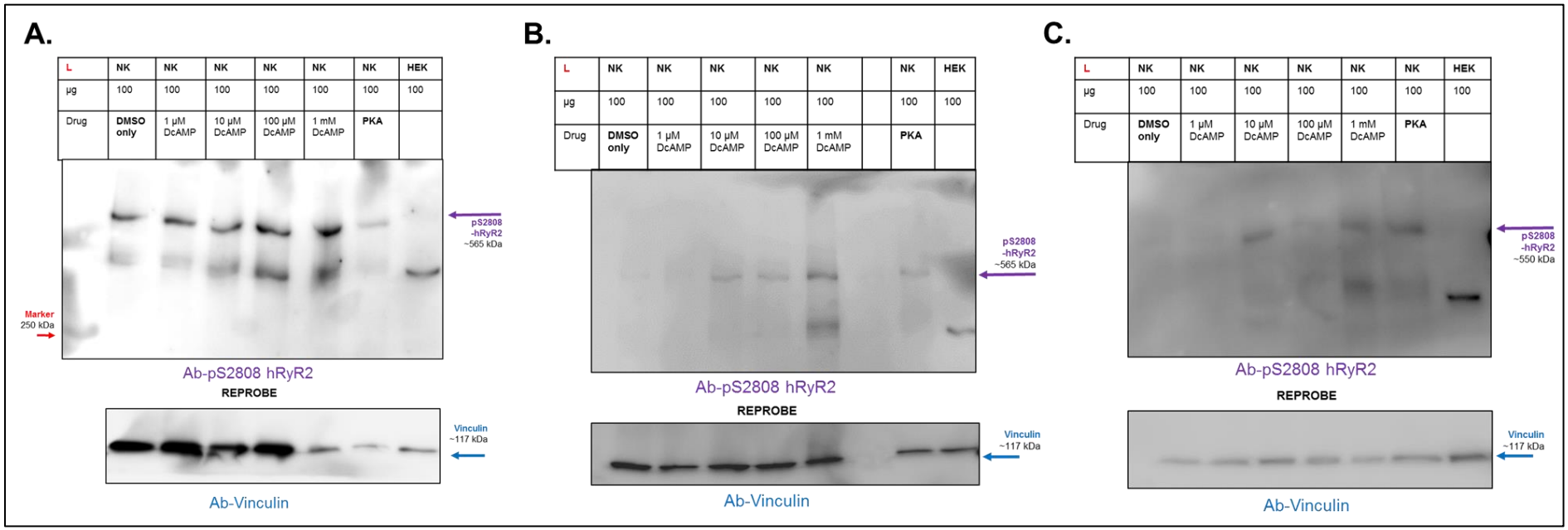

<u>Appendix XII</u> Western blotting of N4104K hRyR2-transfected HEK293 cells treated with dioctanoyl-AMP, investigating phosphorylation at the S2808 site. Transfected HEK293 cells were treated with various concentrations of dioctanoyl-cAMP in DMSO, as described in **Section 4.2.2.2**. Following SDS PAGE of cell homogenate preparations, blots *A-C* were assessed for pS2808-hRyR2 expression (top image), and reprobed for vinculin expression (lower image) as a loading control, at loads of 100 µg. No strip was necessary since antibodies were raised in different animals and proteins were far apart on the blot. Molecular weight of bands was estimated against the prestained Kaleidoscope ladder (Biorad, marked L). HEK refers to 100 µg of a preparation of untransfected HEK293 cells.

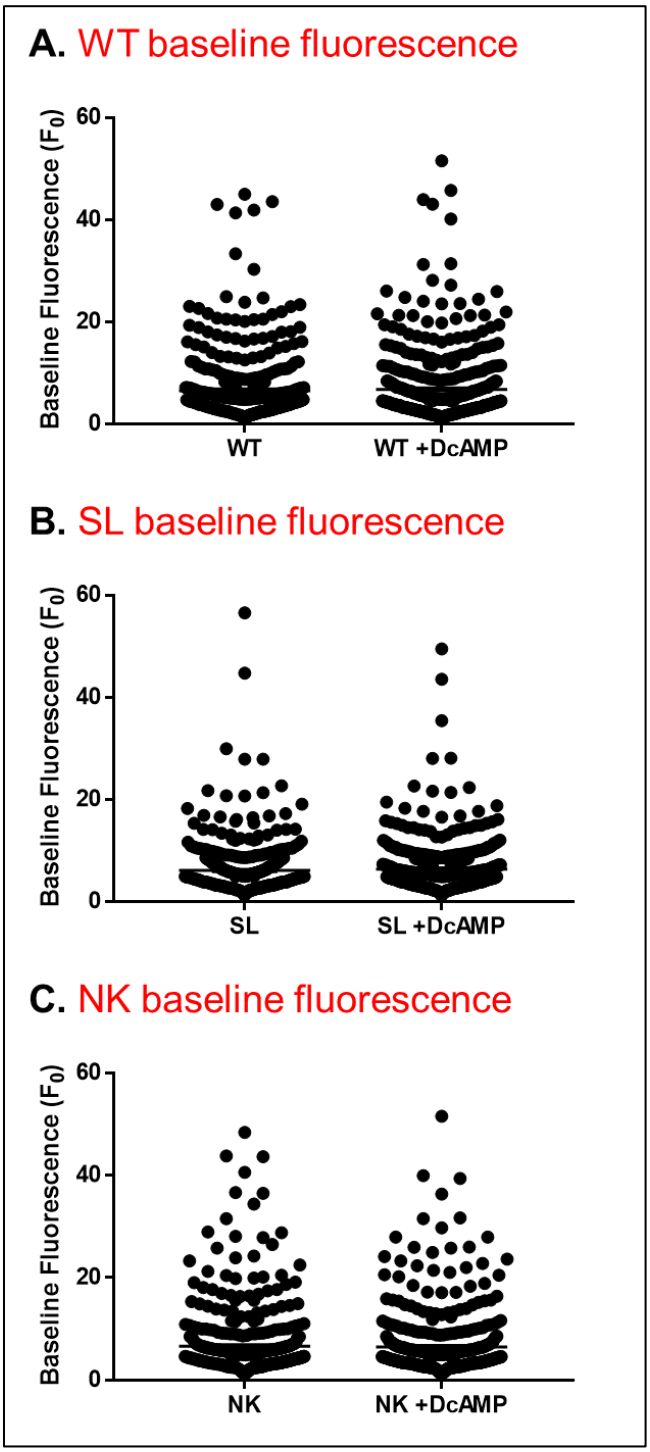

<u>Appendix XIII</u> Scatter plots of baseline fluorescence of WT and mutant hRyR2-transfected HEK293 cells, before and after treatment with dioctanoyl-cAMP. Corresponding graphs can be found in Figure 4.15. DcAMP refers to treatment with 100 µM DcAMP in methanol.

Ca^{2+} oscillation event parameters	WT	WT + DcAMP
Amplitude	0.0080	0.0001
Duration	0.0023	0.0007
Inter-event duration	<0.0001	<0.0001
Frequency	<0.0001	0.0062
Rate up	<0.0001	0.0314
Rate down	0.0005	<0.0001

Ca^{2+} oscillation event parameters	SL	SL + DcAMP
Amplitude	0.0012	0.0002
Duration	<0.0001	0.0022
Inter-event duration	<0.0001	<0.0001
Frequency	0.2262	0.0273
Rate up	0.0165	0.0002
Rate down	0.0790	<0.0001

Ca^{2+} oscillation event parameters	NK	NK + DcAMP
Amplitude	<0.0001	<0.0001
Duration	0.1458	0.0012
Inter-event duration	0.0002	0.0021
Frequency	0.0176	0.3318
Rate up	0.1396	0.0216
Rate down	0.1196	0.0019

Appendix XIV Normality testing of WT and mutant hRyR2-transfected HEK293 cells reveals data is not normally distributed. Equivalent bar graphs are displayed in **Figure 4.15**, **4.16** and **4.17**. Analyzed by D'Agnosti-Pearson omnibus for normality test in GraphPad Prism, with red font indicating data is not normal. Gaussian distribution cannot be assumed at $p<0.05$

Ca^{2+} oscillation event parameters	WT+ 100μM DcAMP vs WT	S2246L+ 100 μM DcAMP vs SL	N4104K+ 100 μM DcAMP vs NK
Amplitude	98%	>99%	>99%
Duration	>99%	>99%	>99%
Inter-event duration	>99%	>99%	>99%
Frequency	82%	99%	>99%
Rate up	>99%	>99%	>99%
Rate down	99%	99%	99%

Appendix XV Posthoc power analysis of imaging data indicates that data is highly-powered for experiments with dioctanoyl-cAMP in Ca^{2+} imaging analysis. DcAMP refers to treatment with 100 μM dioctanoyl-cAMP in methanol. All experimental groups have power of >80% are in black font calculated with G*Power*3.19.2 software (Faul *et al.* 2009). n WT=164, WT+ DcAMP=49, S2246L=109, S2246L+ DcAMP=51, N4104K=97, N4104K+ DcAMP=38.

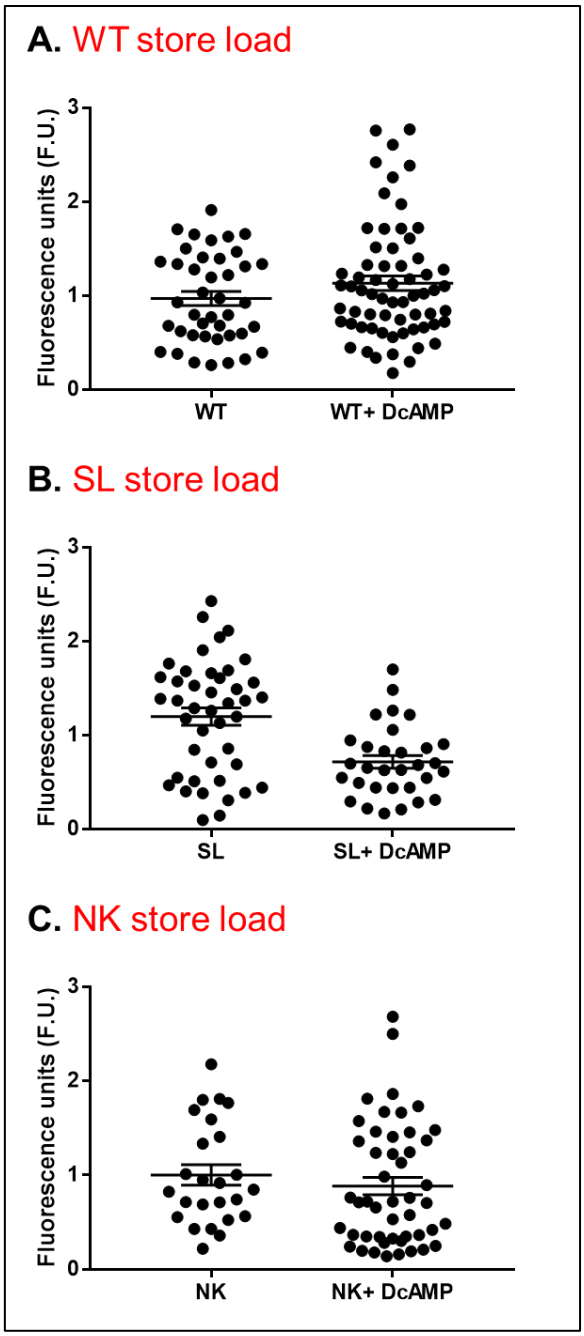

<u>Appendix XVI</u> Scatter plots of ER Ca^{2+} store load of WT and mutant hRyR2-transfected HEK293 cells, before and after treatment with dioctanoyl-cAMP. DcAMP refers to the addition of 100 μM dioctanoyl-cAMP in methanol. Equivalent bar graphs are found in **Figure 4.12.**

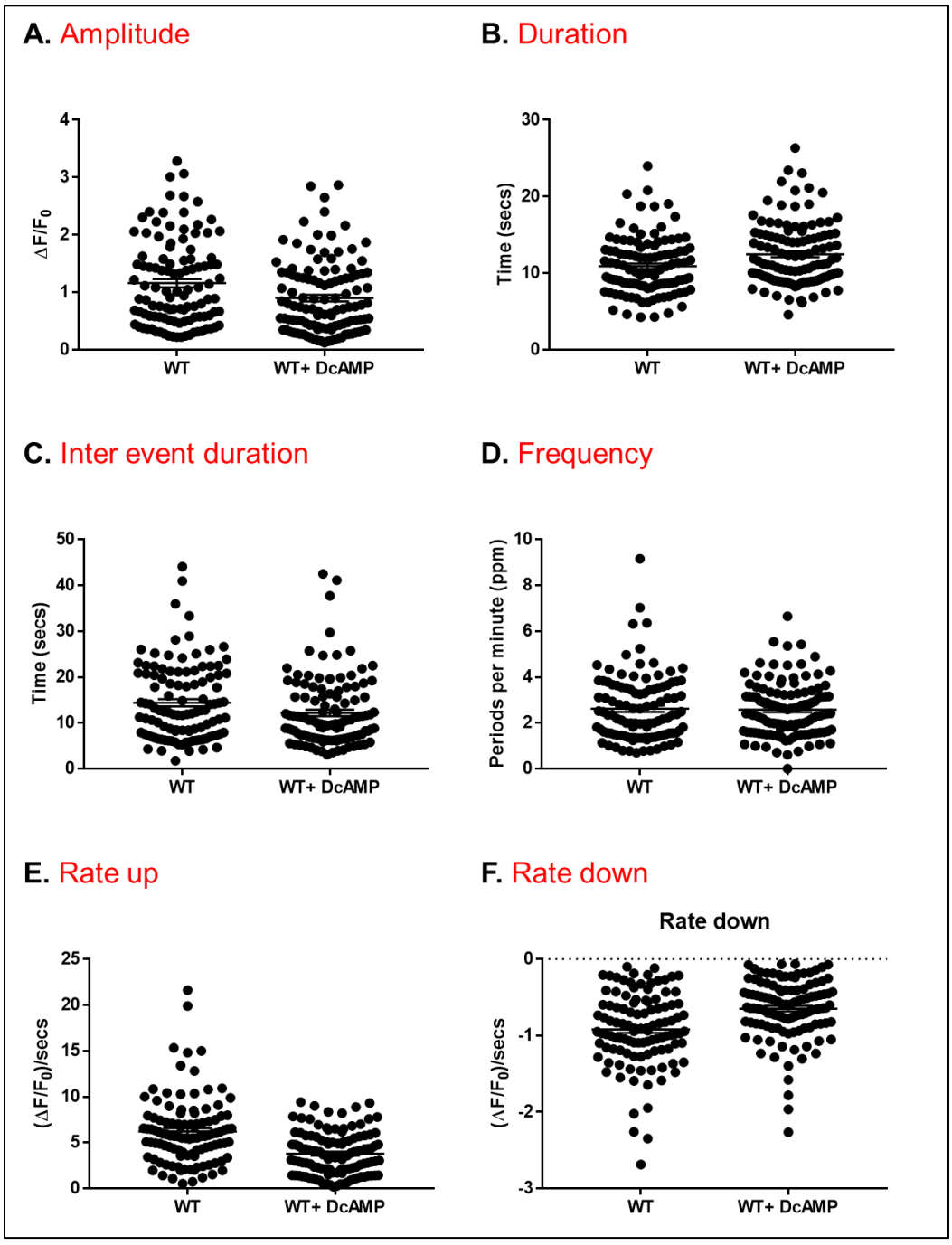

<u>Appendix XVII</u> Scatter plots of Ca^{2+} release kinetics of WT hRyR2-transfected HEK293 cells, before and after treatment with dioctanoyl-cAMP. DcAMP refers to treatment with 100 μM dioctanoyl-cAMP in methanol. Equivalent bar graphs and statistics are found in **Figure 4.15**.

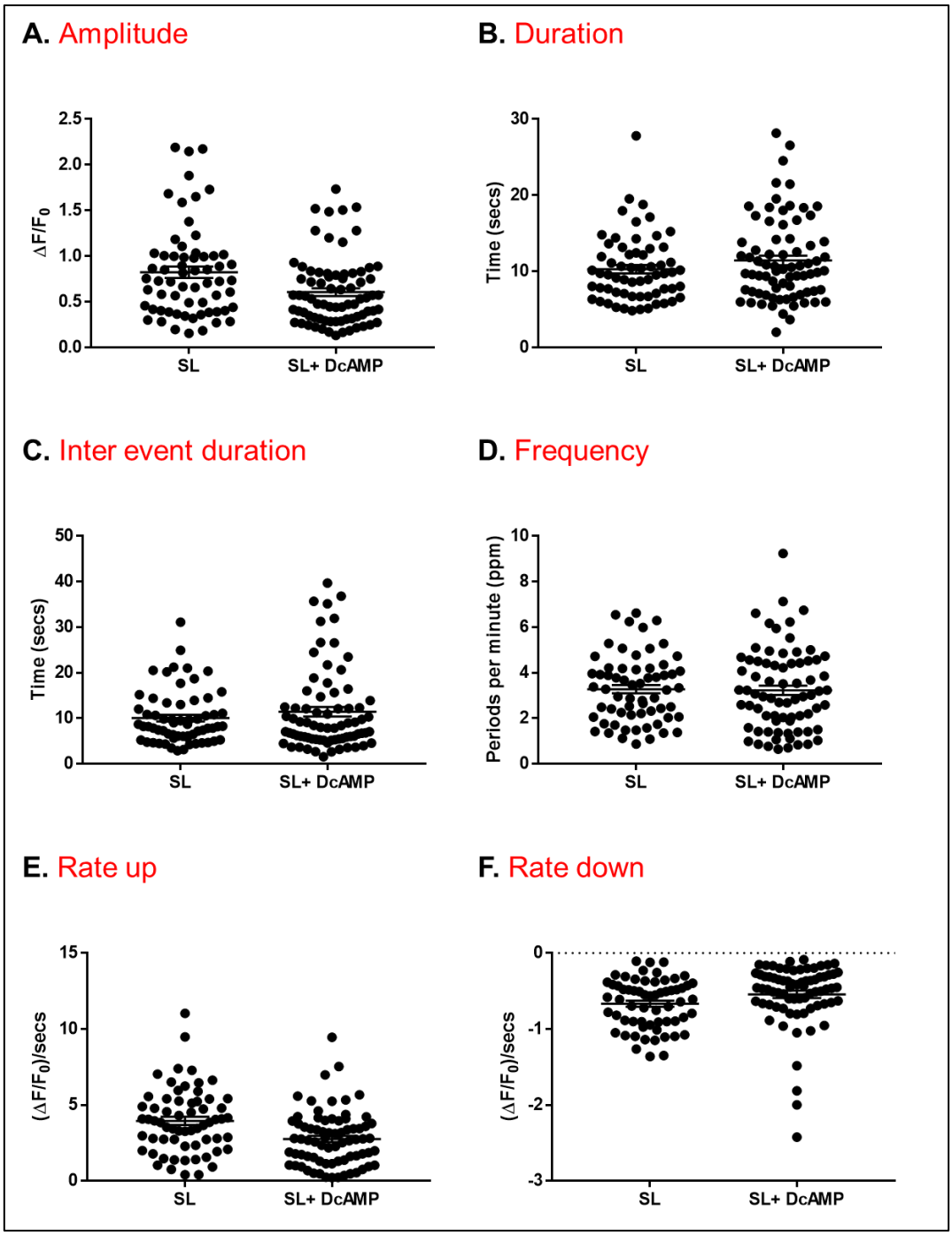

<u>Appendix XVIII</u> Scatter plots of Ca^{2+} release kinetics of S2246L hRyR2-transfected HEK293 cells, before and after treatment with dioctanoyl-cAMP. DcAMP refers to treatment with 100 μM dioctanoyl-cAMP in methanol. Equivalent bar graphs and statistics are found in **Figure 4.16**.

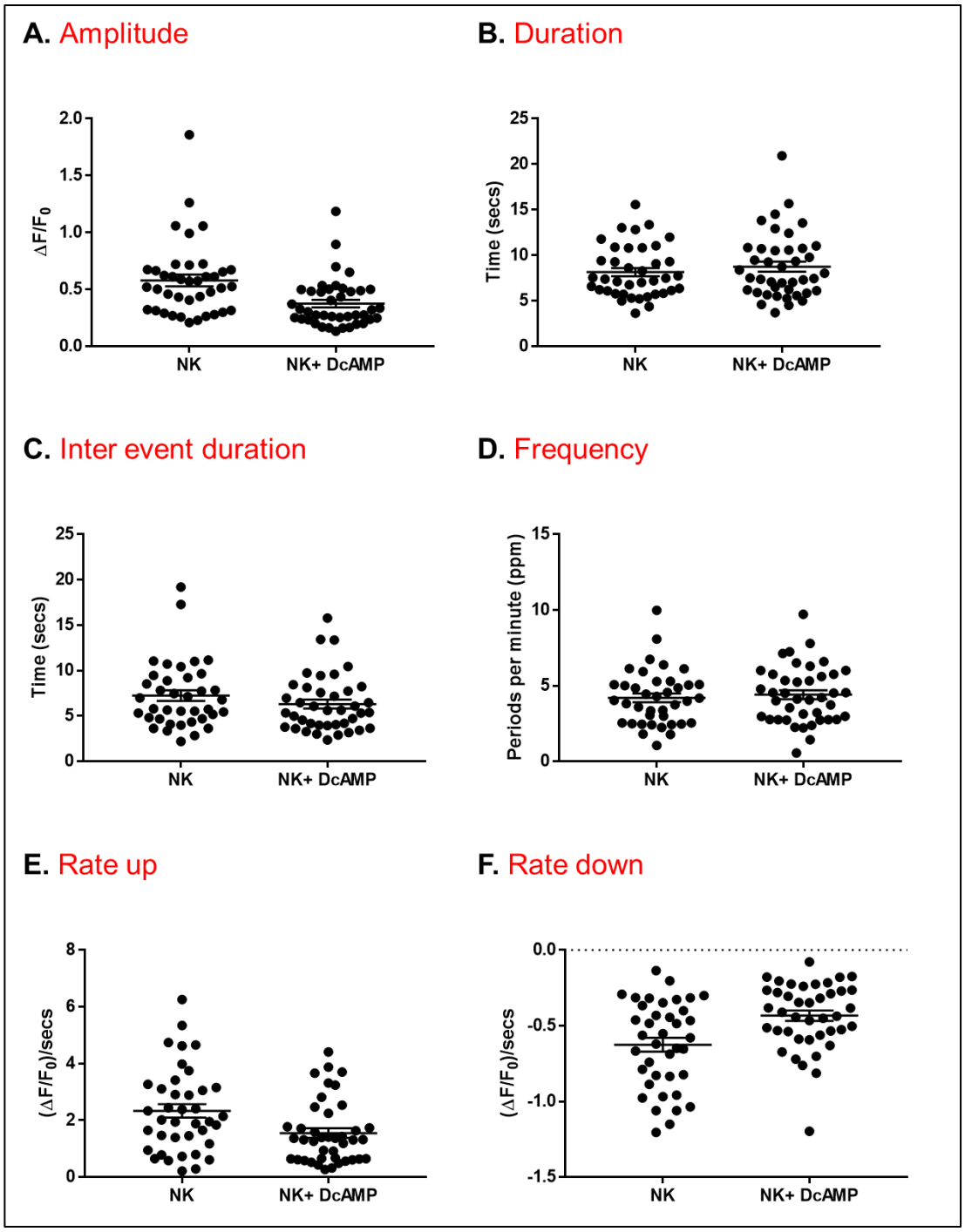

<u>Appendix XIX</u> Scatter plots of Ca^{2+} release kinetics of N4104K hRyR2-transfected HEK293 cells, before and after treatment with dioctanoyl-cAMP. DcAMP refers to treatment with 100 μM dioctanoyl-cAMP in methanol. Equivalent bar graphs and statistics are found in **Figure 4.17**.

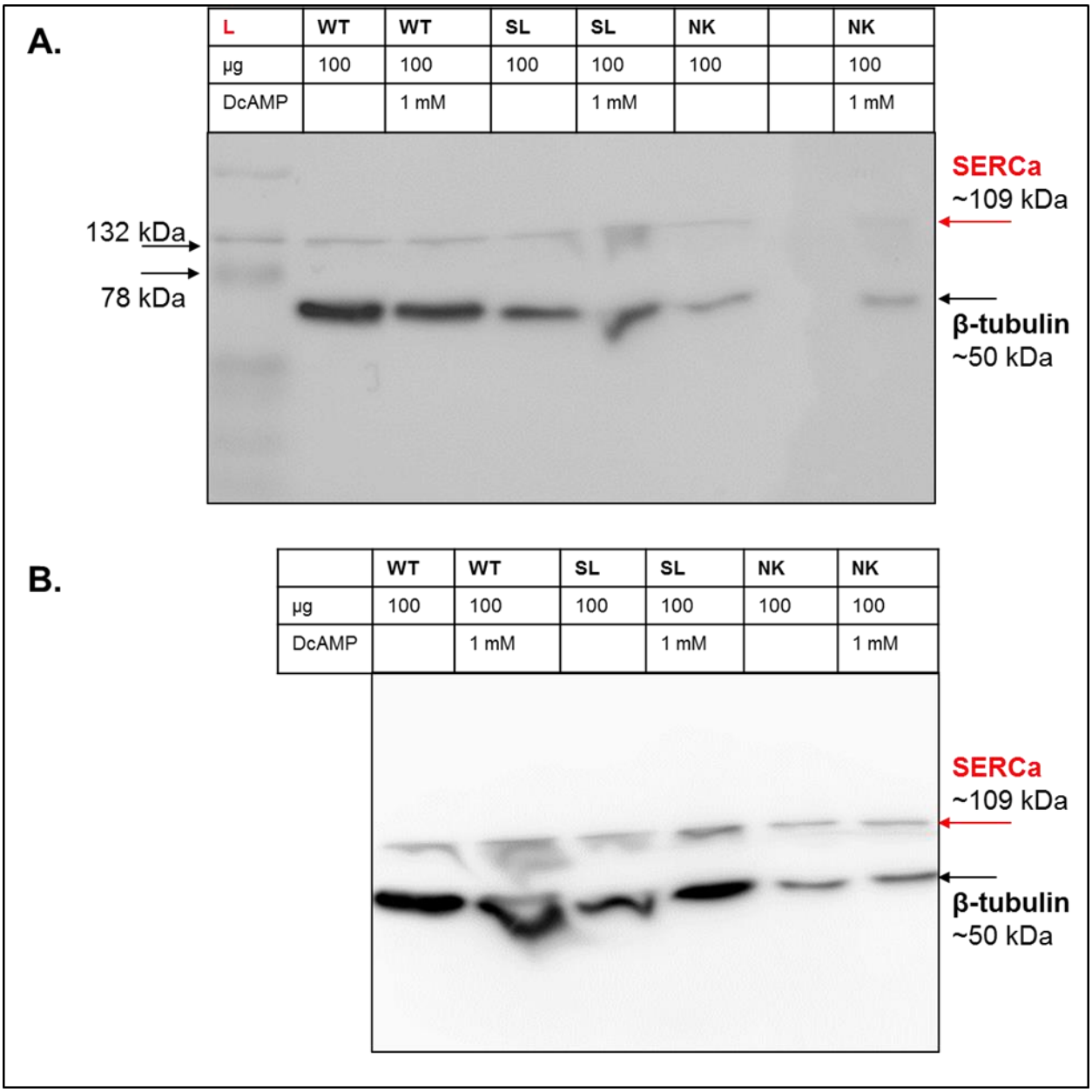

Appendix XX Western blotting of WT and mutant hRyR2-transfected HEK293 cells, treated with 1 mM dioctanoyl-cAMP, for SERCa expression. Transfected HEK293 cells were treated with 1 mM dioctanoyl-cAMP in DMSO (+DcAMP), as described in **Section 4.2.2.2**. Following SDS PAGE of cell homogenate preparations, blots *A* and *B* were assessed for SERCa signal (higher band) and for β-tubulin signal (lower band) as a loading control. Molecular weight of bands was estimated against the prestained Kaleidoscope ladder (Biorad, marked L). Where ladder was not visible, blots were overlaid using GBOX system to match equivalent bands.

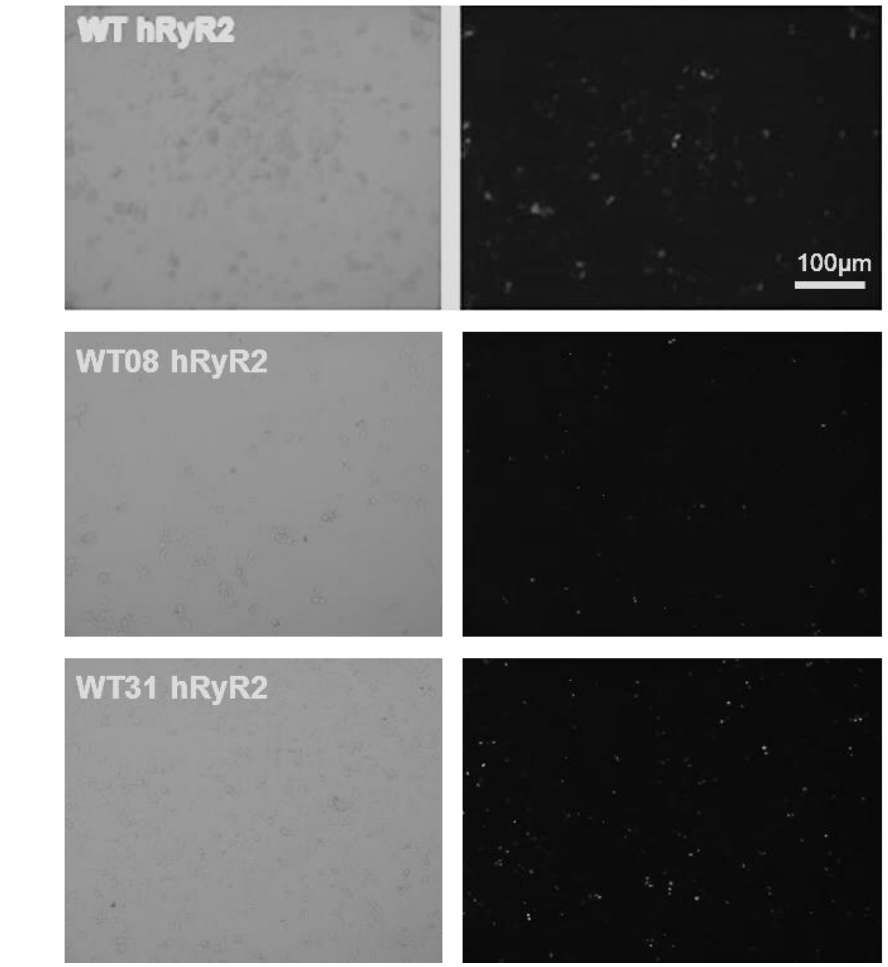

Appendix XXI Expression of recombinant eGFP-tagged WT phosphomimetic hRyR2 in HEK293 cells following Effectene-mediated transfection. A. Left images were taken in phase, right images were taken under fluorescence. B. Transfection efficiencies of each hRyR2 construct were not comparable, with phosphomimetic WT31 hRyR2 transfection efficiencies significantly increased in comparison to WT (Kruskal-Wallis with Dunn's posthoc, $p<0.05$ indicated by *. The total number of transfections for each hRyR2 construct n WT=8, WT08=2 WT31=2. The implications of this data are discussed in **Section 5.3.4**.

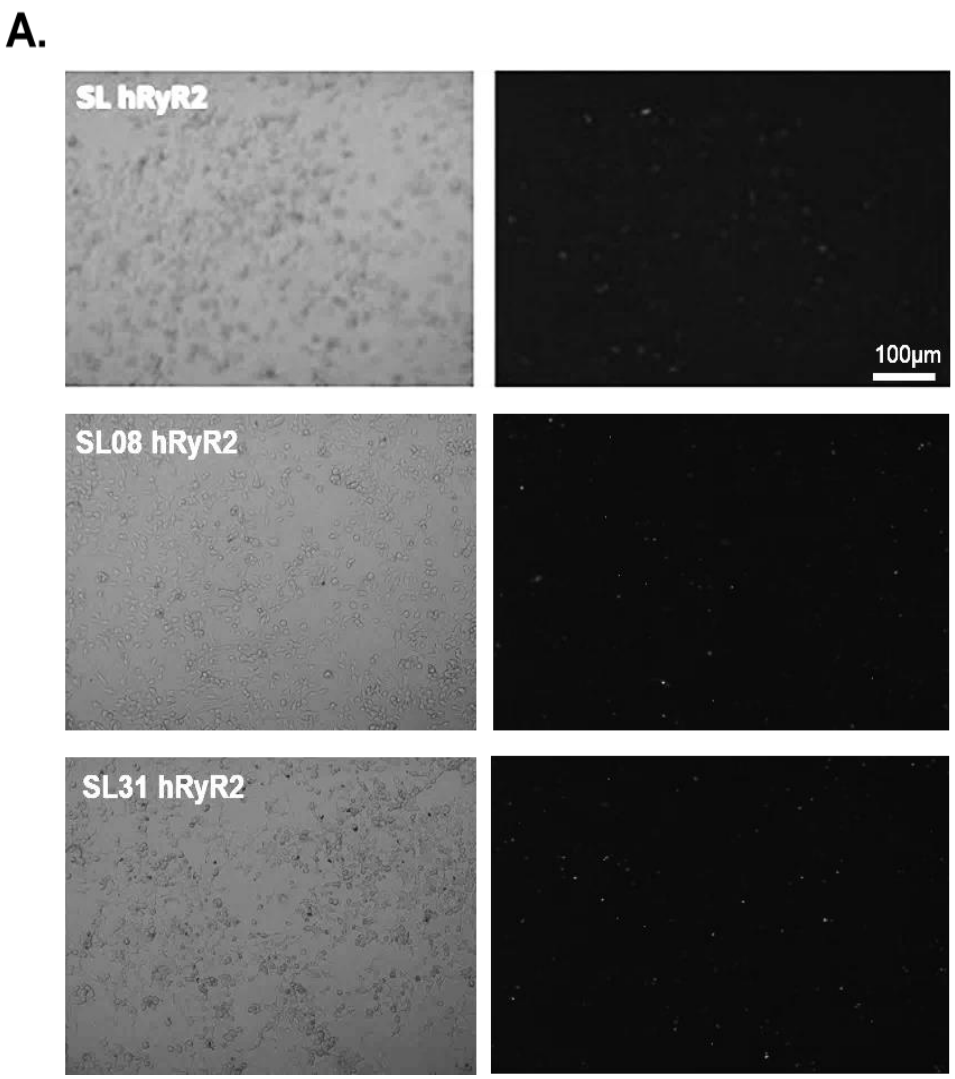

Appendix XXII Expression of recombinant eGFP-tagged S2246L phosphomimetic hRyR2 in HEK293 cells following Effectene-mediated transfection. A. Left images were taken in phase, right images were taken under fluorescence. B. Transfection efficiencies of each hRyR2 construct were not comparable, with phosphomimetic SL08 hRyR2 transfection efficiencies significantly reduced in comparison to S2246L (Kruskal-Wallis with Dunn's posthoc, $p<0.001$ by ***. The total number of transfections for each hRyR2 construct n SL=7, SL08=2, SL31=2. The implications of this data are discussed in **Section 5.3.4**.

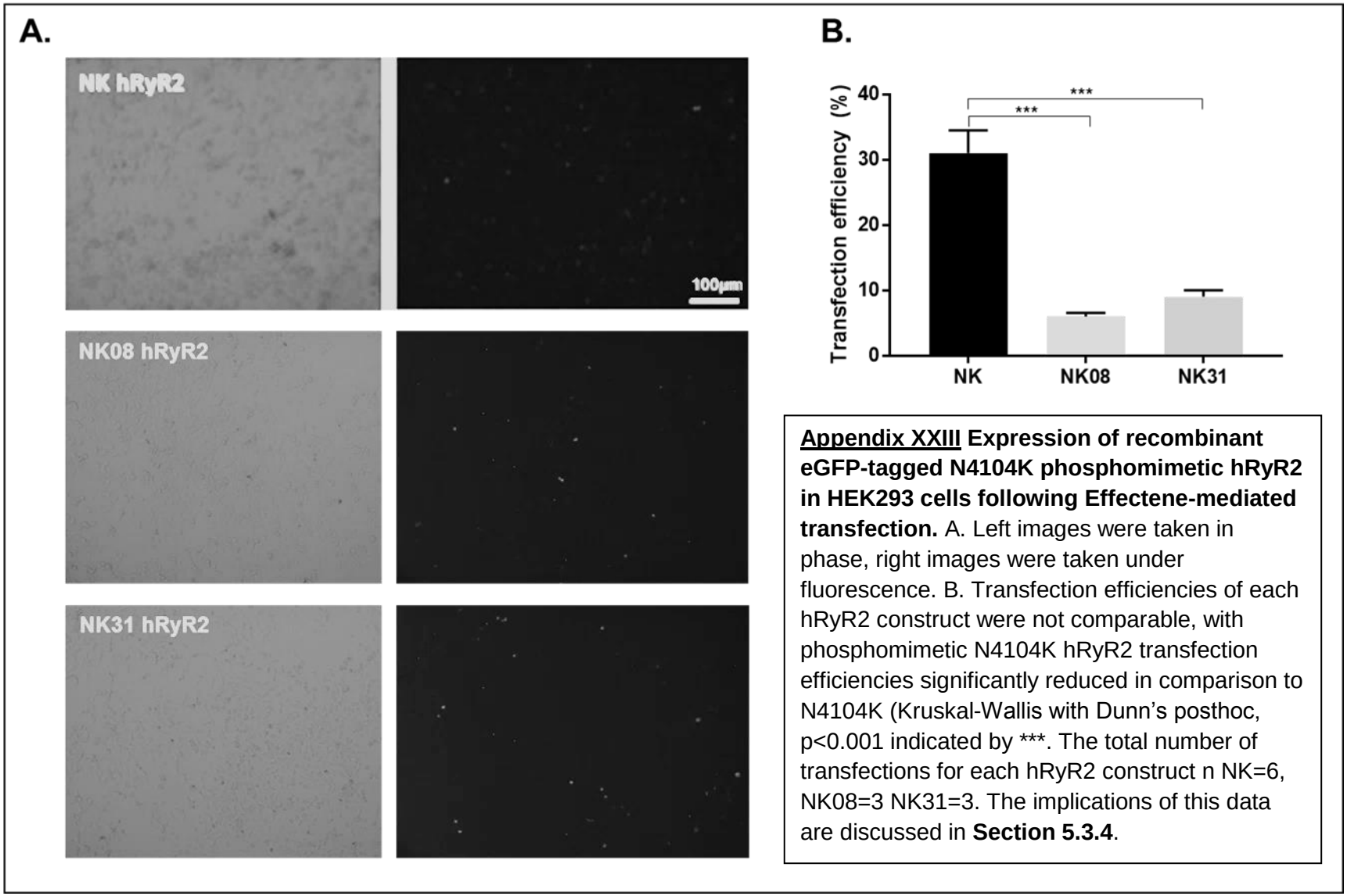

Appendix XXIII Expression of recombinant eGFP-tagged N4104K phosphomimetic hRyR2 in HEK293 cells following Effectene-mediated transfection. A. Left images were taken in phase, right images were taken under fluorescence. B. Transfection efficiencies of each hRyR2 construct were not comparable, with phosphomimetic N4104K hRyR2 transfection efficiencies significantly reduced in comparison to N4104K (Kruskal-Wallis with Dunn's posthoc, $p<0.001$ indicated by ***. The total number of transfections for each hRyR2 construct n NK=6, NK08=3 NK31=3. The implications of this data are discussed in **Section 5.3.4**.

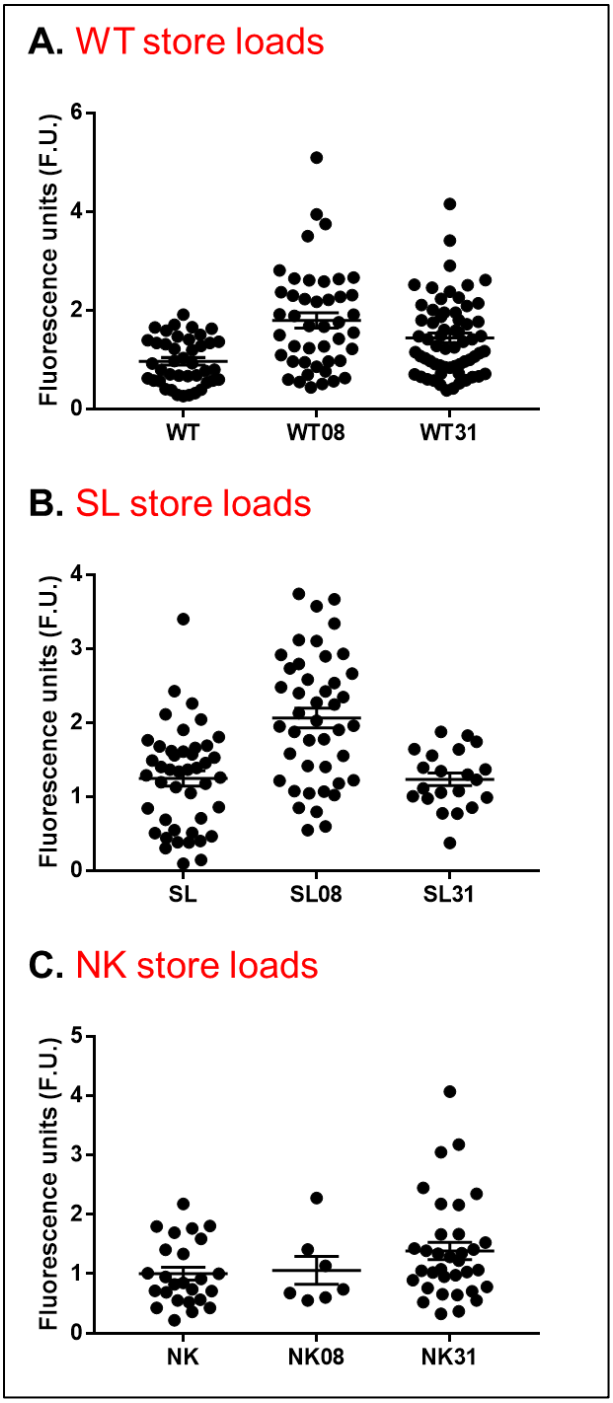

<u>Appendix XXIV</u> Scatter plots of ER Ca^{2+} store load of WT, mutant and phosphomimetic hRyR2-transfected HEK293 cells. Equivalent bar graphs are found in **Figure 5.13**.

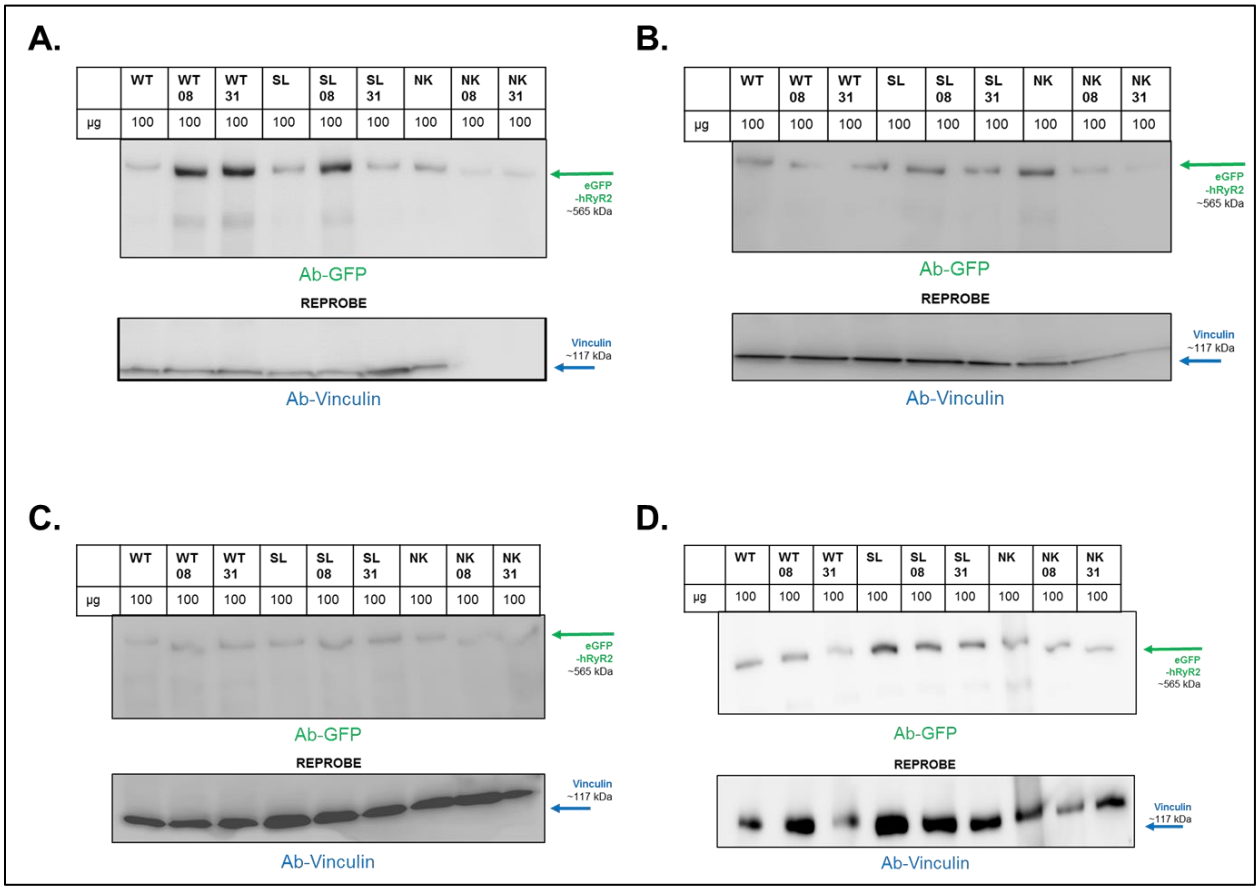

<u>Appendix XXV</u> Western blotting of WT and mutant phosphomimetic eGFP-hRyR2 expression in HEK293 cells. Following SDS PAGE of cell homogenate preparations, blots *A-C* were assessed for GFP-hRyR2 expression (top image), and reprobed for vinculin expression (lower image) as a loading control, at loads of 100 µg. Where protein ladder was not visible, blots were overlaid using the GBOX system to Where ladder was not visible, blots were using GBOX system to match equivalent bands. For clarity, WT, SL and NK data was also combined with expression data in **Appendix I** for analysis in **Figure 3.11** and **5.14**.

Ca^{2+} oscillation event parameters	**WT**	**WT08**	**WT31**
Amplitude	0.0015	0.4289	0.0401
Duration	<0.0001	<0.0001	0.1638
Inter-event duration	<0.0001	<0.0001	<0.0001
Frequency	0.0002	0.0240	0.0005
Rate up	<0.0001	0.0103	0.0380
Rate down	<0.0001	0.3063	0.0004

Ca^{2+} oscillation event parameters	**SL**	**SL08**	**SL31**
Amplitude	0.0086	0.2449	0.4181
Duration	<0.0001	0.7199	0.0395
Inter-event duration	<0.0001	0.0651	0.0038
Frequency	0.0267	<0.0001	0.0721
Rate up	<0.0001	0.2487	0.0003
Rate down	<0.0001	0.1653	0.1647

Ca^{2+} oscillation event parameters	**NK**	**NK08**	**NK31**
Amplitude	0.0015	0.0086	<0.0001
Duration	<0.0001	<0.0001	0.0001
Inter-event duration	<0.0001	<0.0001	<0.0001
Frequency	0.0002	0.0267	0.0113
Rate up	<0.0001	<0.0001	<0.0001
Rate down	<0.0001	<0.0001	0.0063

Appendix XXVI Normality testing of WT and mutant phosphomimetic hRyR2-transfected HEK293 cells reveals data is not normally distributed. Equivalent bar graphs are displayed in **Figure 5.17**, **5.18** and **5.19**. Analysed by D'Agnosti-Pearson omnibus for normality test in GraphPad Prism, with red font indicating data is not normal. Gaussian distribution cannot be assumed at $p<0.05$.

Ca^{2+} oscillation event parameters	WT-S2808D vs WT	WT-S2031D vs WT	S2246L-S2808D vs SL	S2246L-S2031D vs SL	N4104K-S2808D vs NK	N4104K-S2031D vs NK
Amplitude	99%	90%	>99%	91%	95%	**31%**
Duration	>99%	>99%	>99%	>99%	>99%	83%
Inter-event duration	>99%	>99%	>99%	>99%	>99%	>99%
Frequency	>99%	>99%	**40%**	**30%**	>99%	**25%**
Rate up	>99%	>99%	>99%	>99%	>99%	>99%
Rate down	>99%	98%	**71%**	>99%	**15%**	95%

Appendix XXVII Posthoc power analysis of imaging data indicates that some phosphomimetic hRyR2-transfected HEK293 cell data is low powered in some parameters of Ca^{2+} imaging analysis. All experimental groups have power of >80% are in black font, those with power <80% are highlighted in red font, calculated with G*Power*3.19.2 software (Faul *et al.* 2009). n WT=164, WT-S2808D=49, WT-S2031D=73, S2246L=109, S2246L-S2808D=51, S2246L-S2031D=120, N4104K=97, N4104K-S2808D=38, N4104K-S2031D=12. Although SL08, SL31, NK08 and NK31 appear to have low power in some parameters, they are very highly powered in others.

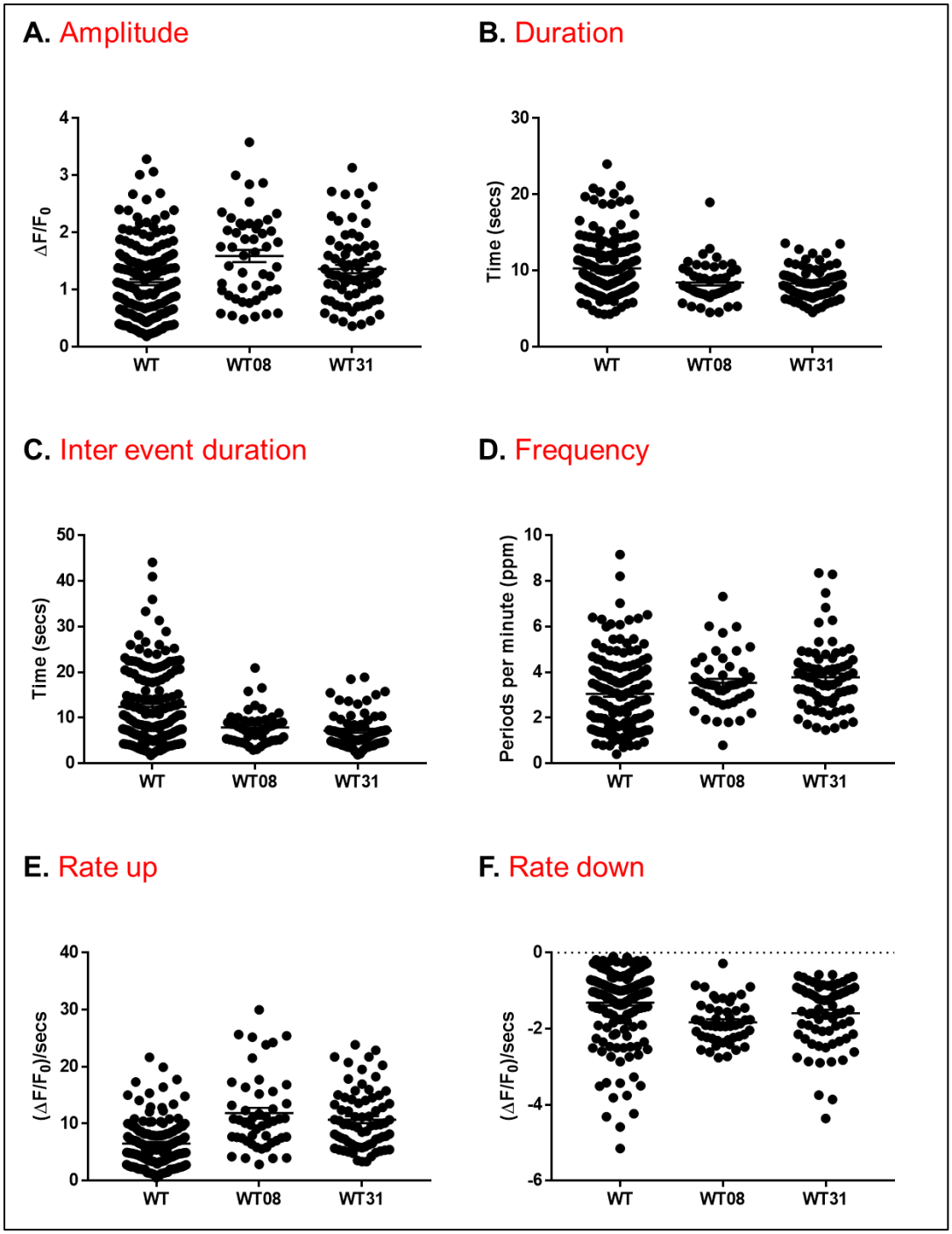

<u>Appendix XXVIII</u> Scatter plots of Ca^{2+} release kinetics of WT and phosphomimetic WT hRyR2-transfected HEK293 cells. Equivalent bar graphs and statistics are found in **Figure 5.17**.

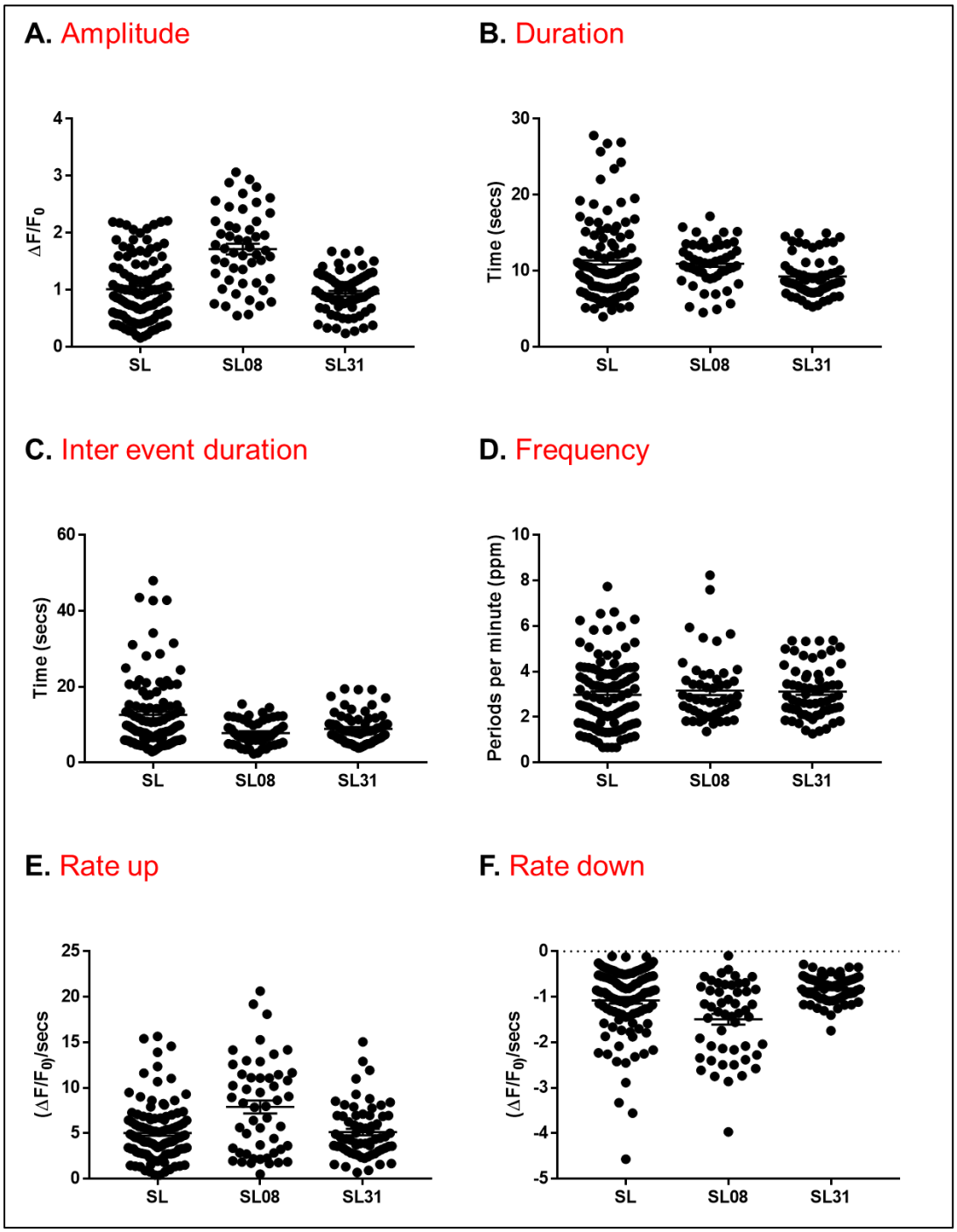

<u>Appendix XXIX</u> Scatter plots of Ca^{2+} release kinetics of S2246L and phosphomimetic S2246L hRyR2-transfected HEK293 cells. Equivalent bar graphs and statistics are found in **Figure 5.18**.

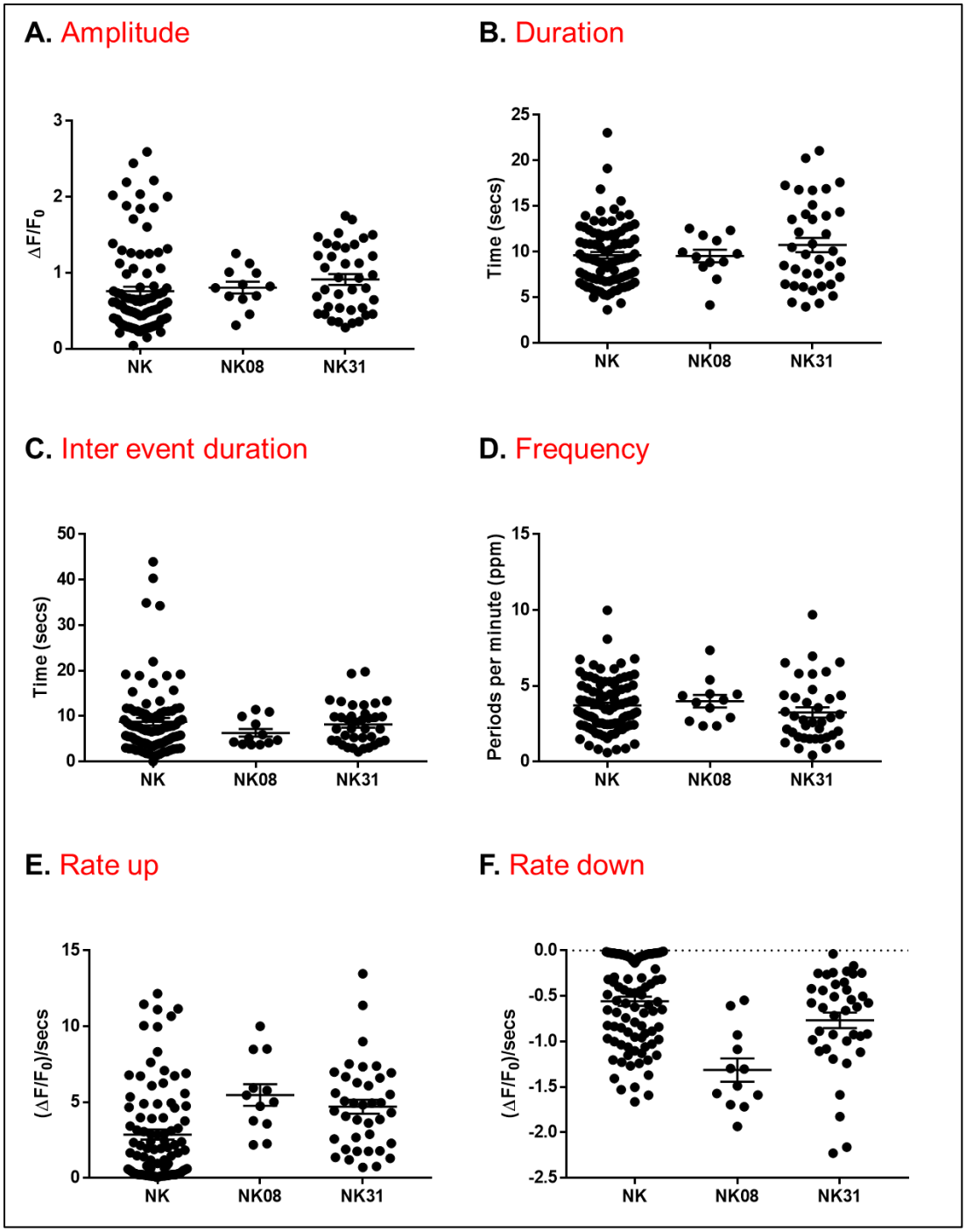

<u>Appendix XXX</u> Scatter plots of Ca^{2+} release kinetic of N4104K and phosphomimetic hRyR2-transfected HEK293 cells. Equivalent bar graphs and statistics are found in **Figure 5.19.**

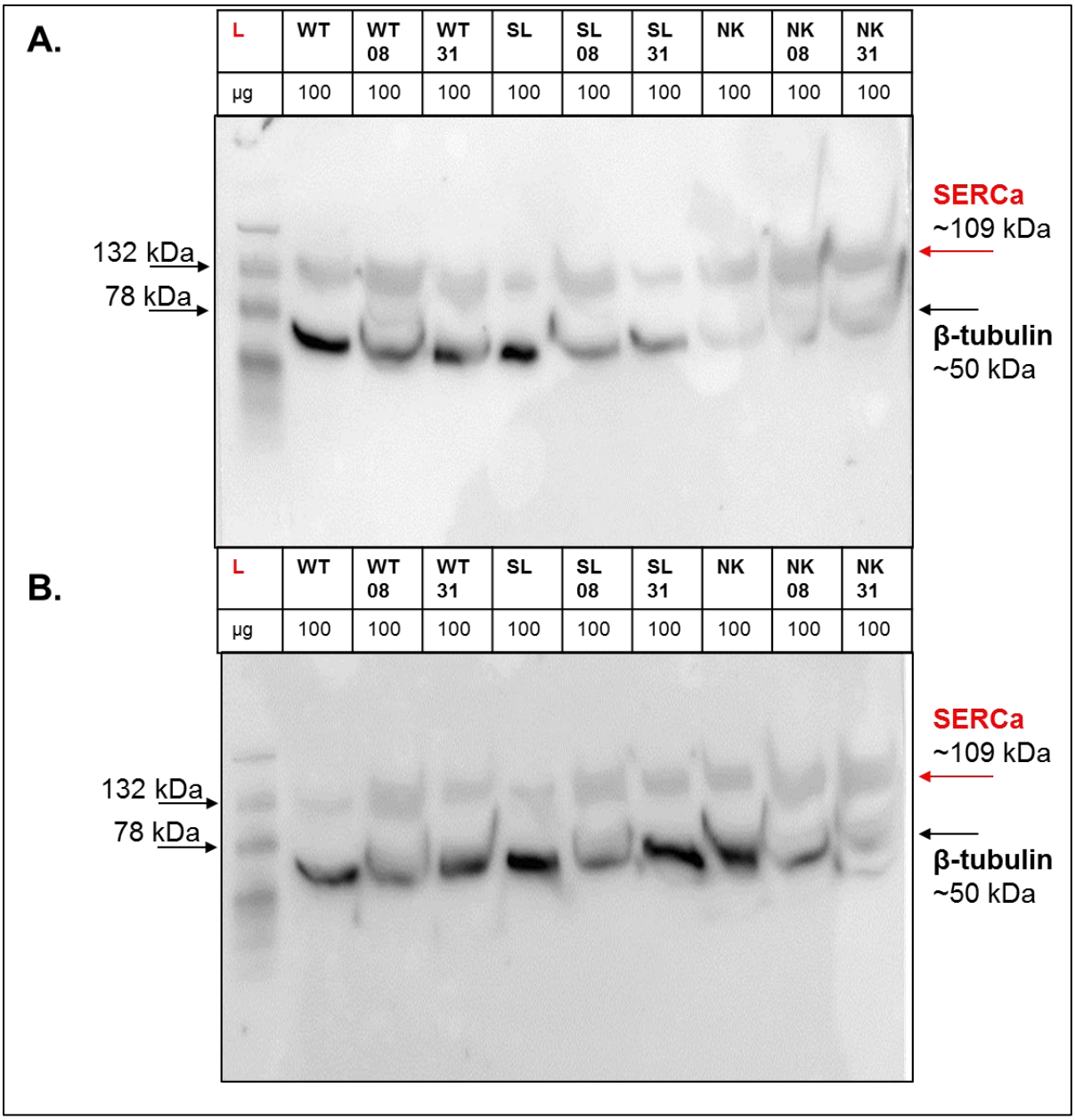

Appendix XXXI Western blotting of WT and mutant and phosphomimetic hRyR2-transfected HEK293 cells, for SERCa expression. Following SDS PAGE of cell homogenate preparations, blots *A* and *B* were assessed for SERCa signal (higher band) and for β-tubulin signal (lower band) as a loading control. Molecular weight of bands was estimated against the prestained Kaleidoscope ladder (Biorad, marked L).

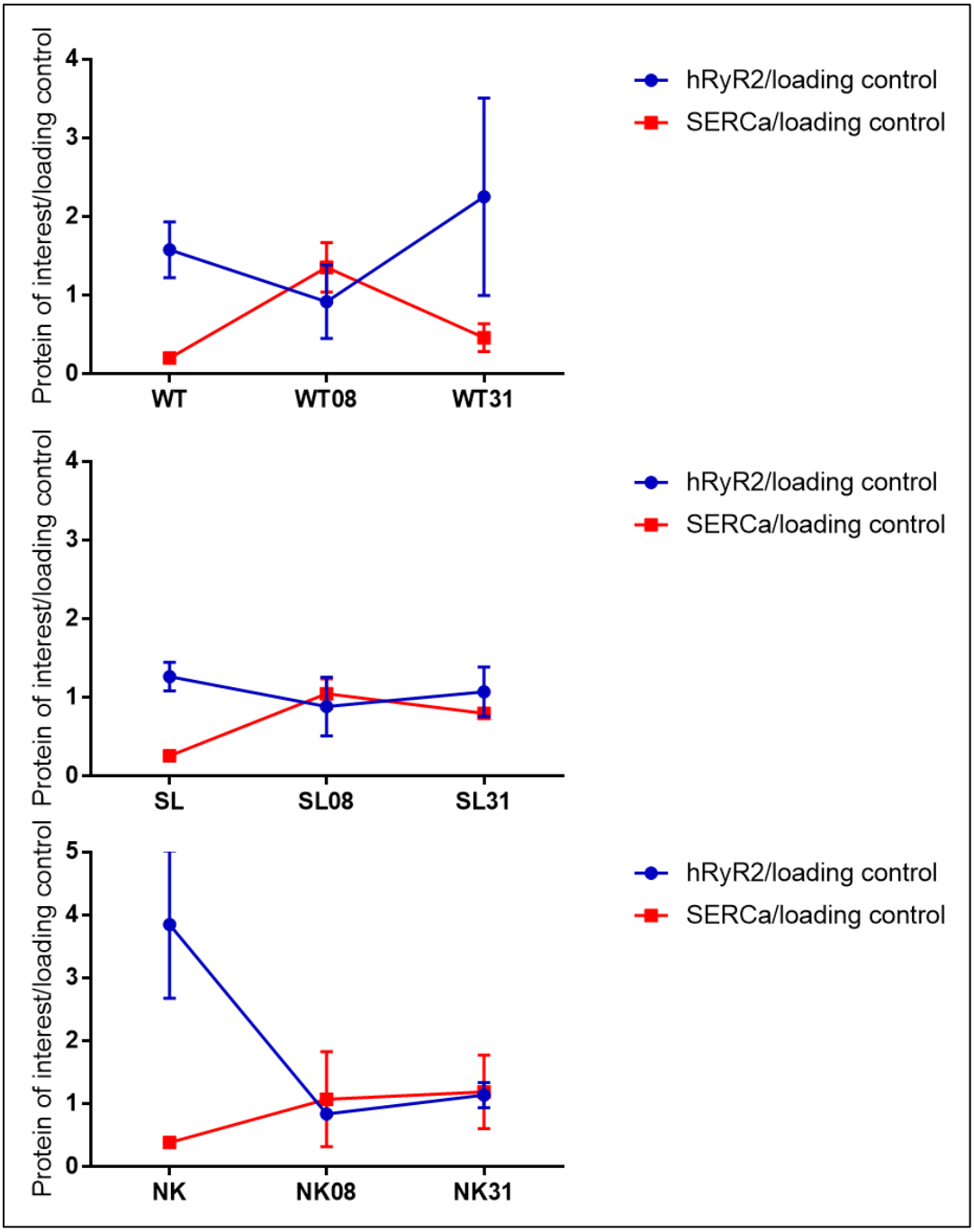

<u>Appendix XXXII</u> A comparison of changes in hRyR2 and SERCa expression in transfected HEK293 cells. Data are protein expression level of interest, normalized to a loading control, presented as mean ± SEM. hRyR2 protein expression was normalized to vinculin expression, while SERCa protein expression was normalized to β-tubulin expression. See Chapter 5 for blots and discussion pertaining to this data

REFERENCES

Adler, J. and Parmryd, I. 2012. *Colocalization Analysis in Fluorescence Microscopy*.

Ai, X. et al. 2005. Ca^{2+}/Calmodulin-Dependent Protein Kinase Modulates Cardiac Ryanodine Receptor Phosphorylation and Sarcoplasmic Reticulum Ca^{2+} Leak in Heart Failure. *Circulation Research* 97(12), pp. 1314–1322.

Aizawa, Y. et al. 2007. Human cardiac ryanodine receptor mutations in ion channel disorders in Japan. *International Journal of Cardiology* 116(2), p. 263.

Alberts, B. et al. 2002. An overview of the cell cycle. *Springer Reference*.

Alvarado, F.J. et al. 2017. Ablation of the cardiac ryanodine receptor phospho-site Ser2808 does not alter the adrenergic response or the progression to heart failure in mice. Elimination of the genetic background as critical variable. *Journal of Molecular and Cellular Cardiology* 103(2), pp. 40-47.

Al-Zaiti, S.S. and Magdic, K.S. 2016. Paroxysmal Supraventricular Tachycardia: Pathophysiology, Diagnosis, and Management. *Critical Care Nursing Clinics of North America* 28(3), pp. 309–316.

Alcalai, R. et al. 2010. Prevention of Ventricular Arrhythmia and Calcium Dysregulation in a Catecholaminergic Polymorphic Ventricular Tachycardia Mouse Model Carrying Calsequestrin-2 Mutation. *Journal of Cardiovascular Electrophysiology* 22(3), p. 316.

Allen, P.D. 2003. Not all sudden death is the same. *Circulation Research* 93(6), pp. 484–486.

Allouis, M. et al. 2005. Unusual clinical presentation in a family with catecholaminergic polymorphic ventricular tachycardia due to a G14876A ryanodine receptor gene mutation. *The American Journal of Cardiology* 95(5), pp. 700–702.

Altschafl, B.A. et al. 2011. Dual role of junctin in the regulation of ryanodine receptors and calcium release in cardiac ventricular myocytes. *The Journal of Physiology* 589(Pt 24), pp. 6063–6080.

Anderson, M.E. et al. 2011. CaMKII in myocardial hypertrophy and heart failure. *Journal of Molecular and Cellular Cardiology* 51(4), p. 468.

Anthony, D.F. et al. 2007. Interaction of calcium/calmodulin-dependent protein kinase II deltaC with sorcin indirectly modulates ryanodine receptor function in cardiac myocytes. *Journal of Molecular and Cellular Cardiology* 43(4), pp. 492–503.

Antos, C.L. et al. 2001. Dilated cardiomyopathy and sudden death resulting from constitutive activation of protein kinase A. *Circulation Research* 89(11), pp. 997–1004.

Asahi, M. et al. 2003. Sarcolipin regulates sarco(endo)plasmic reticulum Ca^{2+}-ATPase (SERCA) by binding to transmembrane helices alone or in association with phospholamban. *Proceedings of the National Academy of Sciences* 100(9), p. 5040.

Asghari, P. et al. 2014. Nonuniform and variable arrangements of ryanodine receptors within mammalian ventricular couplons. *Circulation Research* 115(2), pp. 252–262.

Ashpole, N.M. et al. 2012. Ca^{2+}/calmodulin-dependent protein kinase II (CaMKII) regulates cardiac sodium channel NaV1.5 gating by multiple phosphorylation sites. *Journal of Biological Chemistry* 287(24), pp. 19856–19869.

Ather, S. et al. 2012. Inhibition of CaMKII phosphorylation of RyR2 prevents inducible ventricular arrhythmias in mice with Duchenne muscular dystrophy. *Heart Rhythm* 10(4), pp. 592–599.

Ather, S. et al. 2013. Inhibition of CaMKII phosphorylation of RyR2 prevents inducible ventricular arrhythmias in mice with Duchenne muscular dystrophy. *Heart Rhythm* 10(4), pp. 592–599.

Bai, X.-C. et al. 2016. The Central domain of RyR1 is the transducer for long-range allosteric gating of channel opening. *Cell Research* 26(9), pp. 995–1006.

Balshaw, D.M. et al. 2002. Modulation of intracellular calcium-release channels by calmodulin. *Journal of Membrane Biology* 185(1), pp. 1–8.

Bannister, M.L. et al. 2015. The mechanism of flecainide action in CPVT does not involve a direct effect on RyR2. *Circulation Research* 116(8), pp. 1324–1335.

Bannister, M.L. et al. 2016. Effect of flecainide derivatives on sarcoplasmic reticulum calcium release suggests a lack of direct action on the cardiac ryanodine receptor. *British Journal of Pharmacology* 173(15), pp. 2446–2459.

Barg, S. et al. 1997. Different interactions of cardiac and skeletal muscle ryanodine receptors with FK-506 binding protein isoforms. *Journal of Biological Chemistry* 272(5 Pt 1), pp. C1726–33.

Baroudi, G. et al. 2002. Expression and intracellular localization of an SCN5A double mutant R1232W/T1620M implicated in Brugada syndrome. *Circulation Research* 90(1), pp. E11–6.

Bauce, B. et al. 2002. Screening for ryanodine receptor type 2 mutations in families with effort-induced polymorphic ventricular arrhythmias and sudden death. *Journal of the American College of Cardiology* 40(2), p. 341.

Beard, N.A. et al. 2005. Regulation of ryanodine receptors by calsequestrin: effect of high luminal Ca^{2+} and phosphorylation. *Biophysical Journal* 88(5), pp. 3444–3454.

Beard, N.A. et al. 2009. $Ca^{(2+)}$ signaling in striated muscle: the elusive roles of triadin, junctin, and calsequestrin. *European Biophysics Journal* 39(1), pp. 27–36.

Beca, S. et al. 2012. Phosphodiesterase type 3A regulates basal myocardial contractility through interacting with sarcoplasmic reticulum calcium ATPase type 2a signaling complexes in mouse heart. *Circulation Research* 112(2), pp. 289–297.

Belevych, A.E. et al. 2009. Redox modification of ryanodine receptors underlies calcium alternans in a canine model of sudden cardiac death. *Cardiovascular Research* 84(3), pp. 387–395.

Belevych, A.E. et al. 2013. 'Ryanopathy': causes and manifestations of RyR2 dysfunction in heart failure. *Cardiovascular Research* 98(2), pp. 240–247.

Belevych, A.E., Sansom, S.E., et al. 2011. MicroRNA-1 and -133 increase arrhythmogenesis in heart failure by dissociating phosphatase activity from RyR2 complex. Rota, M. ed. *PloS ONE* 6(12), p. e28324.

Belevych, A.E. et al. 2012. Shortened Ca^{2+} signaling refractoriness underlies cellular arrhythmogenesis in a postinfarction model of sudden cardiac death. *Circulation Research* 110(4), pp. 569–577.

Belevych, A.E., Terentyev, D., et al. 2011. The relationship between arrhythmogenesis and impaired contractility in heart failure: role of altered ryanodine receptor function. *Cardiovascular Research* 90(3), pp. 493–502.

Bellinger, A.M. et al. 2008. Remodeling of ryanodine receptor complex causes 'leaky' channels: a molecular mechanism for decreased exercise capacity. *Proceedings of the National Academy of Sciences* 105(6), pp. 2198–2202.

Bendall, J.K. et al. 2004. Role of myocardial neuronal nitric oxide synthase-derived nitric oxide in beta-adrenergic hyporesponsiveness after myocardial infarction-induced heart failure in rat. *Circulation* 110(16), pp. 2368–2375.

Benkusky, N.A. et al. 2007. Intact β-Adrenergic Response and Unmodified Progression Toward Heart Failure in Mice With Genetic Ablation of a Major Protein Kinase A Phosphorylation Site in the Cardiac Ryanodine Receptor. *Circulation Research* 101(8), pp. 819–829.

Berridge, M.J. et al. 2000. The versatility and universality of calcium signalling. *Nature Reviews Molecular Cell Biology.* 1(1), pp. 11-21.

Berridge, M.J. et al. 2003. Calcium signalling: dynamics, homeostasis and remodelling. *Nature Reviews Molecular Cell Biology* 4(7), pp. 517–529.

Bers, D.M. 2001. *Excitation-Contraction Coupling and Cardiac Contractile Force*. Dordrecht: Springer Netherlands.

Bers, D.M. 2002a. Cardiac excitation-contraction coupling. *Nature* 415(6868), pp. 198–205.

Bers, D.M. 2004. Macromolecular complexes regulating cardiac ryanodine receptor function. *Journal of Molecular and Cellular Cardiology* 37(2), pp. 417–429.

Bers, D.M. 2006. Cardiac ryanodine receptor phosphorylation: target sites and functional consequences. *The Biochemical Journal* 396(1), pp. e1–3.

Bers, D.M. 2007. Going to cAMP just got more complicated. *The Journal of Physiology* 583(Pt 2), pp. 415–416.

Bers, D.M. 2008. Calcium Cycling and Signaling in Cardiac Myocytes. *Annual Review of Physiology* 70(1), p. 23.

Bers, D.M. 2012. Ryanodine receptor S2808 phosphorylation in heart failure: smoking gun or red herring. *Circulation Research* 110(6), pp. 796–799.

Bers, D.M. 2014. Cardiac sarcoplasmic reticulum calcium leak: basis and roles in cardiac dysfunction. *Annual Review of Physiology* 76(1), pp. 107–127.

Bers, D.M. et al. 2006. Regulation of Ca^{2+} and Na^{+} in normal and failing cardiac myocytes. *Annals of the New York Academy of Sciences* 1080(1), pp. 165–177.

Bhat, M.B. et al. 1999. Expression and functional characterization of the cardiac muscle ryanodine receptor $Ca^{(2+)}$ release channel in Chinese hamster ovary cells. *Biophysical Journal* 77(2), pp. 808–816.

Bhatnagar, P. et al. 2016. Trends in the epidemiology of cardiovascular disease in the UK. *Heart* 102(24), pp. 1945–1952.

Bidasee, K.R. et al. 2003. Streptozotocin-induced diabetes increases disulfide bond formation on cardiac ryanodine receptor (RyR2). *Journal of Pharmacology and Experimental Therapeutics* 305(3), pp. 989–998.

Bovo, E. et al. 2011. Regulation of sarcoplasmic reticulum Ca^{2+} leak by cytosolic Ca^{2+} in rabbit ventricular myocytes. *The Journal of Physiology* 589(Pt 24), pp. 6039–6050.

Bridge, J.H. 1986. Relationships between the sarcoplasmic reticulum and sarcolemmal calcium transport revealed by rapidly cooling rabbit ventricular muscle. *The Journal of General Physiology* 88, pp. 437-473.

Brill, L.M. et al. 2009. Phosphoproteomic analysis of human embryonic stem cells. *Cell Stem Cell* 5(2), pp. 204–213.

Brittsan, A.G. et al. 2003. Chronic SR Ca^{2+}-ATPase inhibition causes adaptive changes in cellular Ca^{2+} transport. *Circulation Research* 92(7), pp. 769–776.

Brochet, D.X.P. et al. 2005. Ca^{2+} blinks: rapid nanoscopic store calcium signaling. *Proceedings of the National Academy of Sciences* 102(8), pp. 3099–3104.

Cabra, V. et al. 2016. Ultrastructural Analysis of Self-Associated RyR2s. *Biophysical Journal* 110(12), pp. 2651–2662.

Camors, E. et al. 2014. CaMKII regulation of cardiac ryanodine receptors and inositol triphosphate receptors. *Frontiers in Pharmacology* 5, p. 101.

Campbell, K.P. et al. 1987. Identification and characterization of the high affinity [3H] ryanodine receptor of the junctional sarcoplasmic reticulum Ca^{2+} release channel. *Journal of Biological Chemistry* 262(14), pp. 6460–6463.

Cannell, M.B. et al. 1985. Ryanodine block of calcium oscillations in heart muscle and the sodium-tension relationship. *Federation Proceedings* 44(15), pp. 2964-9.

Cappola, T.P. et al. 2001. Allopurinol improves myocardial efficiency in patients with idiopathic dilated cardiomyopathy. *Inpharma Weekly* 104(20), pp. 2407–2411.

Carnes, C. et al. 2008. Dysregulated sarcoplasmic reticulum calcium release: Potential pharmacological target in cardiac disease. *Pharmacology & Therapeutics* 119(3), pp. 340–354.

Carter, S. et al. 2006. Maximum phosphorylation of the cardiac ryanodine receptor at serine-2809 by protein kinase a produces unique modifications to channel gating and conductance not observed at lower levels of phosphorylation. *Circulation Research* 98(12), pp. 1506–1513.

Carter, S. et al. 2011. Ca^{2}+-dependent phosphorylation of RyR2 can uncouple channel gating from direct cytosolic Ca^{2}+ regulation. *The Journal of Membrane Biology* 240(1), pp. 21–33.

Ceconi, C. et al. 1988. The role of glutathione status in the protection against ischaemic and reperfusion damage: effects of N-acetyl cysteine. *Journal of Molecular and Cellular Cardiology* 20(1), pp. 5–13.

Ceulemans, H. and Bollen, M. 2004. Functional diversity of protein phosphatase-1, a cellular economizer and reset button. *Physiological Reviews* 84(1), pp. 1–39.

Chakraborty, A. et al. 2014. Inhibition of CaMKII does not attenuate cardiac hypertrophy in mice with dysfunctional ryanodine receptor. *PLoS ONE* 9(8), p. e104338.

Chelu, M.G. et al. 2009. Calmodulin kinase II–mediated sarcoplasmic reticulum Ca^{2+} leak promotes atrial fibrillation in mice. *The Journal of Clinical Investigation* 119(7), pp. 1940–1951.

Chen, C. and Okayama, H. 1987. High-efficiency transformation of mammalian cells by plasmid DNA. *Molecular and Cellular Biology* 7(8), pp. 2745–2752.

Chen, J. et al. 1992. Regulation of protein serine-threonine phosphatase type-2A by tyrosine phosphorylation. *Science (New York, N.Y.)* 257(5074), pp. 1261–1264.

Chen, Wei et al. 2011. A mathematical model of spontaneous calcium release in cardiac myocytes. *American Journal of Physiology. Heart and circulatory physiology* 300(5), pp. H1794–805.

Chen, Wenqian et al. 2014. The ryanodine receptor store-sensing gate controls Ca^{2+} waves and Ca^{2+}-triggered arrhythmias. *Nature Medicine* 20(2), pp. 184–192.

Chen, X. et al. 2002. L-type Ca^{2+} channel density and regulation are altered in failing human ventricular myocytes and recover after support with mechanical assist devices. *Circulation Research* 91(6), pp. 517–524.

Chen, Y. et al. 2014. Myoplasmic resting Ca^{2+} regulation by ryanodine receptors is under the control of a novel Ca^{2+}-binding region of the receptor. *Biochemical Journal* 460(2), pp. 261–271.

Chen-Izu, Y. et al. 2007. Phosphorylation of RyR2 and shortening of RyR2 cluster spacing in spontaneously hypertensive rat with heart failure. *American Journal of Physiology. Heart and Circulatory Physiology* 293(4), pp. H2409–17.

Cheng, H. et al. 1994. Calcium sparks: elementary events underlying excitation-contraction coupling in heart muscle. *Science (New York, N.Y.)* 262(5134), p. 740.

Cheng, X. et al. 2008. Epac and PKA: a tale of two intracellular cAMP receptors. *Acta Biochimica et Biophysica Sinica* 40(7), p. 651.

Cheng, Y. et al. 2015. A primer to single-particle cryo-electron microscopy. *Cell* 161(3), pp. 438–449.

Cheng, Y.-S. et al. 2011. Sildenafil and FDP-Sr attenuate diabetic cardiomyopathy by suppressing abnormal expression of myocardial CASQ2, FKBP12.6, and SERCA2a in rats. *Acta Pharmacologica Sinica* 32(4), p. 441.

Cheung, J.W. et al. 2015. Short-coupled polymorphic ventricular tachycardia at rest linked to a novel ryanodine receptor (RyR2) mutation: Leaky RyR2 channels under non-stress conditions. *International Journal of Cardiology* 180, pp. 228–236.

Chin, D. and Means, A.R. 2000. Calmodulin: a prototypical calcium sensor. *Trends in Cell Biology* 10(8), pp. 322–328.

Ching, L.L. et al. 2000. Evidence for $Ca^{(2+)}$ activation and inactivation sites on the luminal side of the cardiac ryanodine receptor complex. *Circulation Research* 87(3), pp. 201–206.

Cho, Y. 2015. Left cardiac sympathetic denervation: An important treatment option for patients with hereditary ventricular arrhythmias. *Journal of Arrhythmia* 32(5), pp. 340–343.

Chugun, A. et al. 2006. Mg^{2+} activates the ryanodine receptor type 2 (RyR2) at intermediate Ca^{2+} concentrations. *AJP: Cell Physiology* 292(1), pp. C535–44.

Claycomb, W.C. et al. 1998. HL-1 cells: A cardiac muscle cell line that contracts and retains phenotypic characteristics of the adult cardiomyocyte. *Proceedings of the National Academy of Sciences* 95(6), pp. 2979–2984.

Cohen, P.T. and Cohen, P. 1989. Discovery of a protein phosphatase activity encoded in the genome of bacteriophage lambda. Probable identity with open reading frame 221. *The Biochemical Journal* 260(3), pp. 931–934.

Cohen, P.T.W. 2002. Protein phosphatase 1--targeted in many directions. *Journal of Cell Science* 115(Pt 2), pp. 241–256.

Collier, M.L. et al. 1999. Relationship between L-type Ca^{2+} current and unitary sarcoplasmic reticulum Ca^{2+} release events in rat ventricular myocytes. *The Journal of Physiology* 516(1), p. 117.

Cooper, L.L. et al. 2013. Redox modification of ryanodine receptors by mitochondria-derived reactive oxygen species contributes to aberrant Ca^{2+} handling in ageing rabbit hearts. *The Journal of Physiology* 591(23), pp. 5895–5911.

Coronado, R. et al. 1992. Planar bilayer recording of ryanodine receptors of sarcoplasmic reticulum. *Methods in Enzymology* 207, pp. 699–707.

Coumel, P. 1978. *Catecholamine-induced severe ventricular arrhythmias with Adams-Stokes syndrome in children: report of four cases*.

Curran, J. et al. 2007. Beta-adrenergic enhancement of sarcoplasmic reticulum calcium leak in cardiac myocytes is mediated by calcium/calmodulin-dependent protein kinase. *Circulation Research* 100(3), pp. 391–398.

Curran, J. et al. 2010. Spontaneous Ca waves in ventricular myocytes from failing hearts depend on Ca^{2+}-calmodulin-dependent protein kinase II. *Journal of Molecular and Cellular Cardiology* 49(1), pp. 25–32.

Currie, S. et al. 2004. Calcium/calmodulin-dependent protein kinase II delta associates with the ryanodine receptor complex and regulates channel function in rabbit heart. *The Biochemical Journal* 377(Pt 2), pp. 357–366.

Cutler, M.J. et al. 2012. Aberrant S-nitrosylation mediates calcium-triggered ventricular arrhythmia in the intact heart. *Proceedings of the National Academy of Sciences of the United States of America* 109(44), pp. 18186–18191.

D'Agostino, R.B., Sr 2005. *Normality, Tests of*. Chichester, UK: John Wiley & Sons, Ltd.

D'Cruz, A.A. et al. 2013. Crystal structure of the TRIM25 B30.2 (PRYSPRY) domain: a key component of antiviral signalling. *Biochemical Journal* 456(2), pp. 231–240.

Darcy, Y.L. et al. 2016. K201 (JTV519) is a Ca^{2+}-Dependent Blocker of SERCA and a Partial Agonist of Ryanodine Receptors in Striated Muscle. *Molecular Pharmacology* 90(2), pp. 106–115.

De Ferrari, G.M. et al. 2015. Clinical Management of Catecholaminergic Polymorphic Ventricular Tachycardia: The Role of Left Cardiac Sympathetic Denervation. *Circulation* 131(25), p. 2185.

Degasperi, A. et al. 2014. Evaluating strategies to normalise biological replicates of Western blot data. Vrana, K. E. ed. *PloS ONE* 9(1), p. e87293.

DeGrande, S.T. et al. 2013. Molecular mechanisms underlying cardiac protein phosphatase 2A regulation in heart. *The Journal of Biological Bhemistry* 288(2), pp. 1032–1046.

Dephoure, N. et al. 2013. Mapping and analysis of phosphorylation sites: a quick guide for cell biologists. *Molecular Biology of the Cell* 24(5), pp. 535–542.

Dhein, S. et al. 2001. Muscarinic receptors in the Mammalian Heart. *Pharmacological Research* 44(3), p. 161.

Dipla, K. et al. 1999. The sarcoplasmic reticulum and the Na^{+}/Ca^{2+} exchanger both contribute to the Ca^{2+} transient of failing human ventricular myocytes. *Circulation Research* 84(4), pp. 435–444.

Dobrev, D. 2014. Role of RyR2 phosphorylation in heart failure and arrhythmias: Controversies around ryanodine receptor phosphorylation in cardiac disease. *Circulation Research* 114(8), pp. 1311–9– discussion 1319.

Dobrev, D. and Wehrens, X.H.T. 2014. Role of RyR2 phosphorylation in heart failure and arrhythmias: Controversies around ryanodine receptor phosphorylation in cardiac disease. *Circulation Research* 114(8), p. 1311.

Dodge-Kafka, K.L. et al. 2010. cAMP-stimulated protein phosphatase 2A activity associated with muscle A kinase-anchoring protein (mAKAP) signaling complexes inhibits the phosphorylation

and activity of the cAMP-specific phosphodiesterase PDE4D3. *The Journal of Biological Chemistry* 285(15), pp. 11078–11086.

Domingo, D. et al. 2015. Non-ventricular, Clinical, and Functional Features of the RyR2(R420Q) Mutation Causing Catecholaminergic Polymorphic Ventricular Tachycardia. *Revista Española de Cardiología (English ed.)* 68(5), pp. 398–407.

Du, G.G. et al. 2001. Functional characterization of mutants in the predicted pore region of the rabbit cardiac muscle $Ca^{(2+)}$ release channel (ryanodine receptor isoform 2). *Journal of Biological Chemistry* 276(34), pp. 31760–31771.

Dulhunty, A. et al. 2009. Junctin - the quiet achiever. *The Journal of Physiology* 587(Pt 13), pp. 3135–3137.

Dulhunty, A.F. et al. 2012. Proteins within the intracellular calcium store determine cardiac RyR channel activity and cardiac output. *Clinical and Experimental Pharmacology & Physiology* 39(5), p. 477.

Dunn, K.W. et al. 2011. A practical guide to evaluating colocalization in biological microscopy. *AJP: Cell Physiology* 300(4), p. C723.

Eager, K.R. et al. 1997. Actions of sulfhydryl reagents on single ryanodine receptor $Ca^{(2+)}$-release channels from sheep myocardium. *Handbook of Membrane Channels* 272(6 Pt 1), pp. C1908–18.

Efremov, R.G. et al. 2014. Architecture and conformational switch mechanism of the ryanodine receptor. *Nature* 517(7532), pp. 39–43.

Eisner, D. 1998. The control of Ca release from the cardiac sarcoplasmic reticulum: regulation versus autoregulation. *Cardiovascular Research* 38(3), pp. 589–604.

Eisner, D.A. et al. 2009. What role does modulation of the ryanodine receptor play in cardiac inotropy and arrhythmogenesis? *Journal of Molecular and Cellular Cardiology* 46(4), p. 474.

Eisner, D.A. et al. 2017. Calcium and Excitation-Contraction Coupling in the Heart. *Circulation Research* 121, pp. 181-195.

El-Armouche, A. 2006. Molecular Determinants of Altered Ca^{2+} Handling in Human Chronic Atrial Fibrillation. *Circulation* 114(7), pp. 670–680.

El-Armouche, A. et al. 2003. Evidence for protein phosphatase inhibitor-1 playing an amplifier role in beta-adrenergic signaling in cardiac myocytes. *FASEB Journal* 17(3), pp. 437–439.

Elison, C. and Jenden, D.J. 1967. The effects of ryanodine on model systems derived from muscle—II: Myofibrils and natural actomyosin. *Biochemical Pharmacology* 16(7), p. 1347.

England, P.J. 1976. Studies on the phosphorylation of the inhibitory subunit of troponin during modification of contraction in perfused rat heart. *Biochemical Journal* 160(2), pp. 295–304.

Eschenhagen, T. 2010. Is ryanodine receptor phosphorylation key to the fight or flight response and heart failure? *The Journal of clinical investigation* 120(12), pp. 4197–4203.

Fabiato, A. 1985a. Effects of ryanodine in skinned cardiac cells. *Federation Proceedings* 44(15), pp. 2970–2976.

Fabiato, A. 1985b. Time and calcium dependence of activation and inactivation of calcium-induced release of calcium from the sarcoplasmic reticulum of a skinned canine cardiac Purkinje cell. *The Journal of General Physiology* 85(2), pp. 247–289.

Fabiato, A. 1992. Two Kinds of Calcium-Induced Release of Calcium from the Sarcoplasmic Reticulum of Skinned Cardiac Cells. *Calcium Signaling*. Advances in Experimental Medicine and Biology. Boston, MA: Springer US, pp. 245–262.

Fairhurst, A.S. 1973. Effect of ryanodine on skeletal muscle reticulum calcium adenosine triphosphatase (CaATPase). *Biochemical Pharmacology* 22(22), p. 2815.

Fan, G.-C. et al. 2008. Regulatory roles of junctin in sarcoplasmic reticulum calcium cycling and myocardial function. *Trends in Cardiovascular Medicine* 18(1), pp. 1–5.

Farrell, E.F. and Antaramian, A. 2003. Sorcin inhibits calcium release and modulates excitation-contraction coupling in the heart. *Journal of Biological Chemistry* 278(36), pp. 34660–34666.

Fauconnier, J. et al. 2010. Leaky RyR2 trigger ventricular arrhythmias in Duchenne muscular dystrophy. *Proceedings of the National Academy of Sciences* 107(4), pp. 1559–1564.

Faul, F. et al. 2009. Statistical power analyses using G*Power 3.1: Tests for correlation and regression analyses. *Behavior Research Methods* 41(4), pp. 1149–1160.

Favre, I. et al. 1999. Reconstitution of native and cloned channels into planar bilayers. *Methods in Enzymology* 294, pp. 287–304.

Ferguson, D.G. et al. 1984. Subunit structure of junctional feet in triads of skeletal muscle: a freeze-drying, rotary-shadowing study. *The Journal of Cell Biology* 99(5), pp. 1735–1742.

Fernández-Velasco, M. et al. 2009. Increased Ca^{2+} sensitivity of the ryanodine receptor mutant RyR2R4496C underlies catecholaminergic polymorphic ventricular tachycardia. *Circulation Research* 104(2), pp. 201–9– 12p following 209.

Ferrier, G.R. et al 1973. A cellular mechanism for the generation of ventricular arrhythmias by acetylstrophanthidin. *Circulation Research* 32, pp. 600-609.

Fessenden, J.D. et al. 2004. Mutational analysis of putative calcium binding motifs within the skeletal ryanodine receptor isoform, RyR1. *Journal of Biological Chemistry* 279(51), pp. 53028–53035.

Fill, M. and Copello, J.A. 2002. Ryanodine receptor calcium release channels. *Physiological Reviews* 82(4), pp. 893–922.

Fischer, T.H. et al. 2012. The ryanodine receptor leak: how a tattered receptor plunges the failing heart into crisis. *Heart Failure Reviews* 18(4), pp. 475–483.

Fischer, T.H. et al. 2014. $Ca^{(2+)}$ /calmodulin-dependent protein kinase II equally induces sarcoplasmic reticulum $Ca^{(2+)}$ leak in human ischaemic and dilated cardiomyopathy. *European Journal of Heart Failure* 16(12), pp. 1292–1300.

Fischer, T.H., Herting, J., Tirilomis, T., Renner, A., Neef, S., Toischer, K., Ellenberger, D., Förster, A., Schmitto, J.D., Gummert, J., Schöndube, F.A., Hasenfuss, G., Maier, L.S. and Sossalla, S. 2013a. Ca^{2+}/calmodulin-dependent protein kinase II and protein kinase A differentially regulate sarcoplasmic reticulum Ca^{2+} leak in human cardiac pathology. *Circulation* 128(9), pp. 970–981.

Frank, J. 2009. Single-particle reconstruction of biological macromolecules in electron microscopy--30 years. *Quarterly Reviews of Biophysics* 42(3), pp. 139–158.

Franzini-Armstrong, C. 2016. Can the Arrangement of RyR2 in Cardiac Muscle Be Predicted? *Biophysical Journal* 110(12), pp. 2563–2565.

Franzini-Armstrong, C. et al. 1998. Comparative Ultrastructure of Ca^{2+} Release Units in Skeletal and Cardiac Muscle. *Annals of the New York Academy of Sciences* 853, p. 20.

Froemming, G.R. et al. 2000. Comparative analysis of the isoform expression pattern of $Ca^{(2+)}$-regulatory membrane proteins in fast-twitch, slow-twitch, cardiac, neonatal and chronic low-frequency stimulated muscle fibers. *Biochimica et Biophysica Acta* 1466(1-2), pp. 151–168.

Fruen, B.R. et al. 2000. Differential $Ca^{(2+)}$ sensitivity of skeletal and cardiac muscle ryanodine receptors in the presence of calmodulin. *Skeletal Muscle* 279(3), pp. C724–33.

Forn, J. and Greengard, P. 1978. Depolarizing agents and cyclic nucleotides regulate the phosphorylation of specific neuronal proteins in rat cerebral cortex slices. *Proceedings of the National Academy of Sciences* 75(10), pp. 5195–5199.

Fujii, J. et al. 1991. Identification of a mutation in porcine ryanodine receptor associated with malignant hyperthermia. *Survey of Anesthesiology* 253(5018), pp. 448–451.

Fujita, T. et al. 2016. The role of Epac in the heart. *Cellular and Molecular Life Sciences*.

Gaburjakova, J. and Gaburjakova, M. 2008. Effect of luminal Ca^{2+} on the stability of coupled gating between ryanodine receptors from the rat heart. *Acta Physiologica* 193(3), p. 219.

Gaburjakova, J. and Gaburjakova, M. 2010. Identification of changes in the functional profile of the cardiac ryanodine receptor caused by the coupled gating phenomenon. *Journal of Membrane Biology* 234(3), p. 159.

Gaburjakova, J. and Gaburjakova, M. 2014. Coupled gating modifies the regulation of cardiac ryanodine receptors by luminal Ca^{2+}. *Biochimica et Biophysica Acta* 1838(3):867-73.

Gaburjakova, J. and Gaburjakova, M. 2016. Cardiac ryanodine receptor: Selectivity for alkaline earth metal cations points to the EF-hand nature of luminal binding sites. *Bioelectrochemistry (Amsterdam, Netherlands)* 109, pp. 49–56.

Gaburjakova, M. et al. 2012. Functional interaction between calsequestrin and ryanodine receptor in the heart. *Cellular and Molecular Life Sciences* 70(16), pp. 2935–2945.

Gaertner, T.R. et al. 2004. Comparative Analyses of the Three-dimensional Structures and Enzymatic Properties of alpha, beta, gamma, and delta Isoforms of Ca^{2+}-Calmodulin-dependent Protein Kinase II. *Journal of Biological Chemistry* 279(13), p. 12484.

Galvao, J. et al. 2013. Unexpected low-dose toxicity of the universal solvent DMSO. *The FASEB Journal* 28(3), pp. 1317–1330.

Gaughan, J.P. et al. 1999. Sodium/calcium exchange contributes to contraction and relaxation in failed human ventricular myocytes. *Cardiovascular Research* 277(2 Pt 2), pp. H714–24.

Gautel, M. and Djinović-Carugo, K. 2016. The sarcomeric cytoskeleton: from molecules to motion. *Journal of Experimental Biology* 219(Pt 2), pp. 135–145.

Gellen, B. et al. 2008. Conditional FKBP12.6 overexpression in mouse cardiac myocytes prevents triggered ventricular tachycardia through specific alterations in excitation-contraction coupling. *Circulation* 117(14), pp. 1778–1786.

George, C.H. 2007a. Sarcoplasmic reticulum Ca^{2+} leak in heart failure: mere observation or functional relevance? *Cardiovascular Research* 77(2), pp. 302–314.

George, C.H. et al. 2004. Ryanodine receptor regulation by intramolecular interaction between cytoplasmic and transmembrane domains. *Molecular Biology of the Cell* 15(6), pp. 2627–2638.

George, C.H. et al. 2006. Arrhythmogenic mutation-linked defects in ryanodine receptor autoregulation reveal a novel mechanism of Ca^{2+} release channel dysfunction. *Circulation Research* 98(1), pp. 88–97.

George, C.H. et al. 2007. Ryanodine receptors and ventricular arrhythmias: Emerging trends in mutations, mechanisms and therapies. *Journal of Molecular and Cellular Cardiology* 42(1), pp. 34–50.

George, C.H., Higgs, G.V., et al. 2003. Ryanodine receptor mutations associated with stress-induced ventricular tachycardia mediate increased calcium release in stimulated cardiomyocytes. *Circulation Research* 93(6), pp. 531–540.

George, C.H. et al. 2005. Toward a molecular understanding of the structure-function of ryanodine receptor Ca^{2+} release channels: perspectives from recombinant expression systems. *Cell Biochemistry and Biophysics* 42(2), pp. 197–222.

George, C.H., Sorathia, R., et al. 2003. In situ modulation of the human cardiac ryanodine receptor (hRyR2) by FKBP12.6. *The Biochemical Journal* 370(Pt 2), pp. 579–589.

Georges, des, A. et al. 2016. Structural Basis for Gating and Activation of RyR1. *Cell* 167(1), p. 145.

Giles, G.I. and Jacob, C. 2002. Reactive sulfur species: an emerging concept in oxidative stress. *Biological Chemistry* 383(3-4), pp. 375–388.

Gillard, E.F. et al. 1991. A substitution of cysteine for arginine 614 in the ryanodine receptor is potentially causative of human malignant hyperthermia. *Genomics* 11(3), pp. 751–755.

Glass, G.V. et al. 1972. Consequences of Failure to Meet Assumptions Underlying the Fixed Effects Analyses of Variance and Covariance. *Review of Educational Research* 42(3), pp. 237–288.

Glynn, P. et al. 2015. Voltage-Gated Sodium Channel Phosphorylation at Ser571 Regulates Late Current, Arrhythmia, and Cardiac Function In Vivo. *Circulation* 132(7), pp. 567–577.

Gomez, N. et al. 2016. Novel CPVT-associated calmodulin mutation in CALM3 (CALM3-A103V) activates arrhythmogenic Ca waves and sparks. *Circulation: Arrhythmia and Electrophysiology* 9(8), p. e004161.

Gonzalez, D.R. et al. 2007. Deficient ryanodine receptor S-nitrosylation increases sarcoplasmic reticulum calcium leak and arrhythmogenesis in cardiomyocytes. *Proceedings of the National Academy of Sciences* 104(51), pp. 20612–20617.

Gonzalez, D.R. et al. 2010. Impaired S-nitrosylation of the ryanodine receptor caused by xanthine oxidase activity contributes to calcium leak in heart failure. *Journal of Biological Chemistry* 285(37), pp. 28938–28945.

Goonasekera, S.A. et al. 2005. Reconstitution of local Ca^{2+} signaling between cardiac L-type Ca^{2+} channels and ryanodine receptors: insights into regulation by FKBP12.6. *AJP: Cell Physiology* 289(6), pp. C1476–84.

Gordeliy, V.I. et al. 1998. Lipid membrane structure and interactions in dimethyl sulfoxide/water mixtures. *Biophysical Journal* 75(5), pp. 2343–2351.

Gorman, C.M. et al. 1983. Expression of recombinant plasmids in mammalian cells is enhanced by sodium butyrate. *Nucleic Acids Research* 11(21), pp. 7631–7648.

Graham, F.L. and van der Eb, A.J. 1973. A new technique for the assay of infectivity of human adenovirus 5 DNA. *Virology* 52(2), pp. 456–467.

Greiser, M. et al. 2009. Distinct contractile and molecular differences between two goat models of atrial dysfunction: AV block-induced atrial dilatation and atrial fibrillation. *Journal of Molecular and Cellular Cardiology* 46(3), pp. 385–394.

Grosman, C. and Auerbach, A. 2000. Kinetic, mechanistic, and structural aspects of unliganded gating of acetylcholine receptor channels: a single-channel study of second transmembrane segment 12' mutants. *The Journal of General Physiology* 115(5), pp. 621–635.

Guo, K. et al. 2015. Impact of phosphomimetic and non-phosphorylatable mutations of phospholemman on L-type calcium channels gating in HEK 293T cells. *Journal of Cellular and Molecular Medicine* 19(3), pp. 642–650.

Guo, T. et al. 2006. Ca^{2+}/Calmodulin-dependent protein kinase II phosphorylation of ryanodine receptor does affect calcium sparks in mouse ventricular myocytes. *Circulation Research* 99(4), pp. 398–406.

Guo, T. et al. 2010. Kinetics of FKBP12.6 binding to ryanodine receptors in permeabilized cardiac myocytes and effects on Ca sparks. *Circulation Research* 106(11), pp. 1743–1752.

Guo, T. et al. 2012. Ryanodine receptor current amplitude controls Ca^{2+} sparks in cardiac muscle. *Circulation Research* 111(1), pp. 28–36.

Guo, W. and Campbell, K.P. 1995. Association of triadin with the ryanodine receptor and calsequestrin in the lumen of the sarcoplasmic reticulum. *Journal of Biological Chemistry* 270(16), pp. 9027–9030.

Guo, W. et al. 2016. The EF-hand Ca^{2+} Binding Domain Is Not Required for Cytosolic Ca^{2+} Activation of the Cardiac Ryanodine Receptor. *Journal of Biological Chemistry* 291(5), pp. 2150–2160.

Gupta, R.C. et al. 2003. Cardiac SR-coupled PP1 activity and expression are increased and inhibitor 1 protein expression is decreased in failing hearts. *American Journal of Physiology. Heart and circulatory physiology* 285(6), pp. H2373–81.

Gustavsson, M. et al. 2013. Allosteric regulation of SERCA by phosphorylation-mediated conformational shift of phospholamban. *Proceedings of the National Academy of Sciences* 110(43), pp. 17338–17343.

Gyorke, I. 1998. Regulation of the Cardiac Ryanodine Receptor Channel by Luminal Ca^{2+} Involves Luminal Ca^{2+} Sensing Sites. *Biophysical Journal* 75(6), pp. 2801–2810.

Györke, S. 1999. Ca^{2+} spark termination: inactivation and adaptation may be manifestations of the same mechanism. *The Journal of General Physiology* 114(1), pp. 163–166.

Györke, S. and Fill, M. 1993a. Ryanodine receptor adaptation: control mechanism of $Ca^{(2+)}$-induced Ca^{2+} release in heart. *Science (New York, N.Y.)* 260(5109), pp. 807–809.

Gómez, A.M. and Richard, S. 2004. Mutant cardiac ryanodine receptors and ventricular arrhythmias: is 'gain-of-function' obligatory? *Cardiovascular Research* 64(1), pp. 3–5.

Hagemann, D. et al. 2001. Expression of Ca^{2+}/calmodulin-dependent protein kinase II delta-subunit isoforms in rats with hypertensive cardiac hypertrophy. *Molecular and Cellular Biochemistry* 220(1-2), pp. 69–76.

Hakamata, Y. et al. 1992. Primary structure and distribution of a novel ryanodine receptor/calcium release channel from rabbit brain. *FEBS letters* 312(2-3), p. 229.

Hamilton, S.L. et al. 2001. Calmodulin and Excitation-Contraction Coupling. *Circulation Research* 15(6), pp. 281–284.

Handhle, A. et al. 2016. Calsequestrin interacts directly with the cardiac ryanodine receptor luminal domain. *Journal of Cell Science* 129(21), pp. 3983–3988.

Hare, J.M. and Stamler, J.S. 2005. NO/redox disequilibrium in the failing heart and cardiovascular system. *Journal of Clinical Investigation* 115(3), pp. 509–517.

Harvey, R.D. and Belevych, A.E. 2003. Muscarinic regulation of cardiac ion channels. *British Journal of Pharmacology* 139(6), p. 1074.

Harwell, M.R. et al. 1992. Summarizing Monte Carlo Results in Methodological Research: The One- and Two-Factor Fixed Effects ANOVA Cases. *Journal of Educational and Behavioral Statistics* 17(4), pp. 315–339.

Haugaa, K.H. et al. 2010. High prevalence of exercise-induced arrhythmias in catecholaminergic polymorphic ventricular tachycardia mutation-positive family members diagnosed by cascade genetic screening. *Europace* 12(3), p. 417.

Hayashi, M. et al. 2009. Incidence and risk factors of arrhythmic events in catecholaminergic polymorphic ventricular tachycardia. *Circulation* 119(18), pp. 2426–2434.

Heijman, J. et al. 2012. Dominant-negative control of cAMP-dependent IKs upregulation in human long-QT syndrome type 1. *Circulation Research* 110(2), pp. 211–219.

Heijman, J. et al. 2013. Function and regulation of serine/threonine phosphatases in the healthy and diseased heart. *Journal of Molecular and Cellular Cardiology* 64, pp. 90–98.

Heijman, J. et al. 2016. The value of basic research insights into atrial fibrillation mechanisms as a guide to therapeutic innovation: a critical analysis. *Cardiovascular Research* 109(4), pp. 467–479.

Heineke, J. and Ritter, O. 2012. Cardiomyocyte calcineurin signaling in subcellular domains: from the sarcolemma to the nucleus and beyond. *Journal of Molecular and Cellular Cardiology* 52(1), pp. 62–73.

Henkel, D.M. et al. 2009. Death in heart failure: a community perspective. *Circulation: Heart Failure* 1(2), pp. 91–97.

Heroes, E. et al. 2013. The PP1 binding code: a molecular-lego strategy that governs specificity. *The FEBS journal* 280(2), pp. 584–595.

Herzig, S. and Neumann, J. 2000. Effects of serine/threonine protein phosphatases on ion channels in excitable membranes. *Physiological Reviews* 80(1), pp. 173–210.

Hester, N. et al. 2004. The role of calsequestrin, triadin, and junctin in conferring cardiac ryanodine receptor responsiveness to luminal calcium. *Biophysical Journal* 86(4), pp. 2121–2128.

Hidalgo, C. et al. 2009. PKC Phosphorylation of Titin's PEVK Element: A Novel and Conserved Pathway for Modulating Myocardial Stiffness. *Circulation Research* 105(7), p. 631.

Hiess, F. et al. 2015. Distribution and Function of Cardiac Ryanodine Receptor Clusters in Live Ventricular Myocytes. *The Journal of Biological Chemistry* 290(33), pp. 20477–20487.

Hilliard, F.A. et al. 2009. Flecainide inhibits arrhythmogenic Ca^{2+} waves by open state block of ryanodine receptor Ca^{2+} release channels and reduction of Ca^{2+} spark mass. *Journal of Molecular and Cellular Cardiology* 48(2), pp. 293–301.

Ho, H.-T. et al. 2014. Genetic ablation of ryanodine receptor 2 phosphorylation at Ser-2808 aggravates $Ca^{(2+)}$-dependent cardiomyopathy by exacerbating diastolic Ca^{2+} release. *The Journal of Physiology* 592(9), pp. 1957–1973.

Ho, H.-T. et al. 2016. Muscarinic Stimulation Facilitates Sarcoplasmic Reticulum Ca Release by Modulating Ryanodine Receptor 2 Phosphorylation Through Protein Kinase G and Ca/Calmodulin-Dependent Protein Kinase II Novelty and Significance. *Hypertension* 68(5), p. 1171.

Hoch, B. et al. 1999. Identification and Expression of alpha-Isoforms of the Multifunctional Ca^{2+}/Calmodulin-Dependent Protein Kinase in Failing and Nonfailing Human Myocardium. *Circulation Research* 84(6), p. 713.

Hofer, A.M. and Lefkimmiatis, K. 2007. Extracellular calcium and cAMP: second messengers as 'third messengers'? *Physiology* 22(5), p. 320.

Hohenegger, M. and Suko, J. 1993. Phosphorylation of the purified cardiac ryanodine receptor by exogenous and endogenous protein kinases. *The Biochemical Journal* 296(Pt 2), pp. 303–308.

Holmberg, S.R. and Williams, A.J. 1989. Single channel recordings from human cardiac sarcoplasmic reticulum. *Circulation Research* 65(5), pp. 1445–1449.

Hong, T. and Shaw, R.M. 2016. Cardiac T-Tubule Microanatomy and Function. *Physiological Reviews* 97(1), p. 227.

Hothi, S.S. et al. 2008. Epac activation, altered calcium homeostasis and ventricular arrhythmogenesis in the murine heart. *Pflügers Archiv - European Journal of Physiology* 457(2), pp. 253–270.

Houser, S.R. 2014. Role of RyR2 phosphorylation in heart failure and arrhythmias: protein kinase A-mediated hyperphosphorylation of the ryanodine receptor at serine 2808 does not alter cardiac contractility or cause heart failure and arrhythmias. *Circulation Research* 114(8), pp. 1320–7– discussion 1327.

Houser, S.R. and Margulies, K.B. 2003. Is depressed myocyte contractility centrally involved in heart failure? *Circulation Research* 92(4), pp. 350–358.

Houser, S.R. et al. 2001. Functional properties of failing human ventricular myocytes. *Trends in Cardiovascular Medicine* 10(3), pp. 101–107.

Hove-Madsen, L. et al. 2004. Atrial fibrillation is associated with increased spontaneous calcium release from the sarcoplasmic reticulum in human atrial myocytes. *Circulation* 110(11), pp. 1358–1363.

Hu, S.-T. et al. 2009. Altered intracellular Ca^{2+} regulation in chronic rat heart failure. *The Journal of Physiological Sciences* 60(2), p. 85.

Huang, F. et al. 2006. Analysis of calstabin2 (FKBP12.6)-ryanodine receptor interactions: rescue of heart failure by calstabin2 in mice. *Proceedings of the National Academy of Sciences* 103(9), pp. 3456–3461.

Huang, L.J. et al. 1997. Identification of a novel protein kinase A anchoring protein that binds both type I and type II regulatory subunits. *Journal of Biological Chemistry* 272(12), pp. 8057–8064.

Huke, S. and Bers, D.M. 2007. Temporal dissociation of frequency-dependent acceleration of relaxation and protein phosphorylation by CaMKII. *Journal of Molecular and Cellular Cardiology* 42(3), pp. 590–599.

Huke, S. and Bers, D.M. 2008. Ryanodine receptor phosphorylation at Serine 2030, 2808 and 2814 in rat cardiomyocytes. *Biochemical and Biophysical Research Communications* 376(1), pp. 80–85.

Hulme, E. 1990. Muscarinic Receptor Subtypes. *Annual Review of Pharmacology and Toxicology* 30(1), p. 633.

Hunt, D.J. et al. 2007. K201 (JTV519) suppresses spontaneous Ca $^{2+}$ release and [^{3H}]ryanodine binding to RyR2 irrespective of FKBP12.6 association. *Biochemical Journal* 404(3), p. 431.

Huttlin, E.L. et al. 2010. A tissue-specific atlas of mouse protein phosphorylation and expression. *Cell* 143(7), pp. 1174–1189.

Hwang, H.S. et al. 2011. Inhibition of cardiac Ca^{2+} release channels (RyR2) determines efficacy of class I antiarrhythmic drugs in catecholaminergic polymorphic ventricular tachycardia. *Circulation: Arrhythmia and Electrophysiology* 4(2), pp. 128–135.

Hymel, L. et al. 1988. Reconstitution of purified cardiac muscle calcium release channel (ryanodine receptor) in planar bilayers. *Biochemical and Biophysical Research Communications* 152(1), pp. 308–314.

Inoue, M. and Bridge, J. 2003. Ca^{2+} Sparks in Rabbit Ventricular Myocytes Evoked by Action Potentials Involvement of Clusters of L-Type Ca^{2+} Channels. *Circulation Research* 92(5), p. 532.

Inui, M. et al. 1987. Isolation of the ryanodine receptor from cardiac sarcoplasmic reticulum and identity with the feet structures. *Journal of Biological Chemistry* 262(32), pp. 15637–15642.

Jabbari, J. et al. 2013. New exome data question the pathogenicity of genetic variants previously associated with catecholaminergic polymorphic ventricular tachycardia. *Circulation: Cardiovascular Genetics* 6(5), pp. 481–489.

Janse, M. et al. 2004. Electrophysiological changes in heart failure and their relationship to arrhythmogenesis. *Cardiovascular Research* 61(2), pp. 208–217.

Jenden, D.J. and Fairhurst, A.S. 1969. The pharmacology of ryanodine. *Pharmacological Reviews* 21(1), pp. 1–25.

Jeyakumar, L.H. et al. 2001. FKBP binding characteristics of cardiac microsomes from diverse vertebrates. *Biochemical and Biophysical Research Communications* 281(4), pp. 979–986.

Jiang, D. et al. 2005. Enhanced Store Overload-Induced Ca^{2+} Release and Channel Sensitivity to Luminal Ca^{2+} Activation Are Common Defects of RyR2 Mutations Linked to Ventricular Tachycardia and Sudden Death. *Circulation Research* 97(11), pp. 1173–1181.

Jiang, D. et al. 2002. Enhanced basal activity of a cardiac Ca^{2+} release channel (ryanodine receptor) mutant associated with ventricular tachycardia and sudden death. *Circulation Research* 91(3), pp. 218–225.

Jiang, D. et al. 2004. RyR2 mutations linked to ventricular tachycardia and sudden death reduce the threshold for store-overload-induced Ca^{2+} release (SOICR). *Proceedings of the National Academy of Sciences* 101(35), pp. 13062–13067.

Jiang, D. et al. 2007. Loss of luminal Ca^{2+} activation in the cardiac ryanodine receptor is associated with ventricular fibrillation and sudden death. *Proceedings of the National Academy of Sciences of the United States of America* 104(46), pp. 18309–18314.

Jiang, M.T. et al. 2002. Abnormal Ca^{2+} release, but normal ryanodine receptors, in canine and human heart failure. *Circulation Research* 91(11), pp. 1015–1022.

Jones, L.R. et al. 1995. Purification, Primary Structure, and Immunological Characterization of the 26-kDa Calsequestrin Binding Protein (Junctin) from Cardiac Junctional Sarcoplasmic Reticulum. *Journal of Biological Chemistry* 270(51), p. 30787.

Jones, P.P. et al. 2008. Endoplasmic reticulum Ca^{2+} measurements reveal that the cardiac ryanodine receptor mutations linked to cardiac arrhythmia and sudden death alter the threshold for store-overload-induced Ca^{2+} release. *The Biochemical Journal* 412(1), pp. 171–178.

Jones, P.P. et al. 2008. Localization of PKA phosphorylation site, Ser(2030), in the three-dimensional structure of cardiac ryanodine receptor. *The Biochemical Journal* 410(2), pp. 261–270.

Jones, T.A. et al. 1993. Localization of the genes encoding the catalytic subunits of protein phosphatase 2A to human chromosome bands 5q23→q31 and 8p12→p11.2, respectively. *Cytogenetic and Genome Research* 63(1), pp. 35–41.

Jung, C. et al. 2007. Dystrophic cardiomyopathy: amplification of cellular damage by Ca^{2+} signalling and reactive oxygen species-generating pathways. *Cardiovascular Research* 77(4), pp. 766–773.

Jung, C.B. et al. 2012. Dantrolene rescues arrhythmogenic RYR2 defect in a patient-specific stem cell model of catecholaminergic polymorphic ventricular tachycardia. *EMBO Molecular Medicine* 4(3), pp. 180–191.

Jungbluth, H. et al. 2005. Minicore myopathy with ophthalmoplegia caused by mutations in the ryanodine receptor type 1 gene. *Neurology* 65(12), pp. 1930–1935.

Kalyanasundaram, A. et al. 2013. Up-regulation of sarcoplasmic reticulum Ca^{2+} uptake leads to cardiac hypertrophy, contractile dysfunction and early mortality in mice deficient in CASQ2. *Cardiovascular Research* 98(2), p. 297.

Kaneko, N. et al. 1994. New 1,4-benzothiazepine derivative, K201, demonstrates cardioprotective effects against sudden cardiac cell death and intracellular calcium blocking action. *Drug Development Research* 33(4), p. 429.

Kannankeril, P.J. et al. 2006. Mice with the R176Q cardiac ryanodine receptor mutation exhibit catecholamine-induced ventricular tachycardia and cardiomyopathy. *Proceedings of the National Academy of Sciences* 103(32), pp. 12179–12184.

Karczewski, P. 1991. Back-Phosphorylation — A Sensitive Technique to Study Protein Phosphorylation in the Intact Heart. In: *Cellular Regulation by Protein Phosphorylation*. Berlin, Heidelberg: Springer Berlin Heidelberg, pp. 51–65.

Kashimura, T. et al. 2010. In the RyR2(R4496C) mouse model of CPVT, β-adrenergic stimulation induces Ca waves by increasing SR Ca content and not by decreasing the threshold for Ca waves. *Circulation Research* 107(12), pp. 1483–1489.

Keurs, ter, H.E.D.J. and Boyden, P.A. 2007. Calcium and Arrhythmogenesis. *Physiological reviews* 87(2), pp. 457–506.

Khan, S.A. et al. 2004. Neuronal nitric oxide synthase negatively regulates xanthine oxidoreductase inhibition of cardiac excitation-contraction coupling. *Proceedings of the National Academy of Sciences* 101(45), pp. 15944–15948.

Kim, E. et al. 2007. Characterization of human cardiac calsequestrin and its deleterious mutants. *Journal of Molecular Biology* 373(4), pp. 1047–1057.

Kim, Y.M. et al. 2005. A myocardial Nox2 containing NAD(P)H oxidase contributes to oxidative stress in human atrial fibrillation. *Circulation Research* 97(7), pp. 629–636.

Knollmann, B.C. 2010. A 'rough' journey to the sarcoplasmic reticulum—implications of altered calsequestrin trafficking for cardiac arrhythmia. *Journal of Molecular and Cellular Cardiology* 49(4), pp. 554–555.

Kobayashi, S. et al. 2009. Dantrolene, a Therapeutic Agent for Malignant Hyperthermia, Markedly Improves the Function of Failing Cardiomyocytes by Stabilizing Interdomain Interactions Within the Ryanodine Receptor. *Journal of the American College of Cardiology* 53(21), p. 1993.

Kobayashi, S. et al. 2010. Dantrolene, a Therapeutic Agent for Malignant Hyperthermia, Inhibits Catecholaminergic Polymorphic Ventricular Tachycardia in a RyR2R2474S/+ Knock-In Mouse Model. *Circulation journal : official journal of the Japanese Circulation Society* 74(12), pp. 2579–2584.

Kobayashi, Y.M. and Jones, L.R. 1999. Identification of Triadin 1 as the Predominant Triadin Isoform Expressed in Mammalian Myocardium. *Journal of Biological Chemistry* 274(40), p. 28660.

Kobayashi, Y.M. et al. 2000. Localization and characterization of the calsequestrin-binding domain of triadin 1. Evidence for a charged beta-strand in mediating the protein-protein interaction. *Journal of Biological Chemistry* 275(23), pp. 17639–17646.

Kong, H. et al. 2008. Caffeine induces Ca^{2+} release by reducing the threshold for luminal Ca^{2+} activation of the ryanodine receptor. *The Biochemical Journal* 414(3), pp. 441–452.

Kooij, V. et al. 2013. PKCÎ±-Specific Phosphorylation of the Troponin Complex in Human Myocardium: A Functional and Proteomics Analysis. *PLoS ONE* 8(10), p. e74847.

Kubalova, Z. et al. 2005. Abnormal intrastore calcium signaling in chronic heart failure. *Proceedings of the National Academy of Sciences* 102(39), pp. 14104–14109.

Kunitomo, Y. and Terentyev, D. 2011. How to stop the fire? Control of Ca^{2+}-induced Ca^{2+} release in cardiac muscle. *The Journal of Physiology* 589(24), pp. 5899–5900.

Kurzydlowski, K. 1996. Phospholamban Regulates the Ca^{2+}-ATPase through Intramembrane Interactions. *Journal of Biological Chemistry* 271(36), p. 21726.

Kushnir, A. et al. 2010. Role of CaMKIIdelta phosphorylation of the cardiac ryanodine receptor in the force frequency relationship and heart failure. *Proceedings of the National Academy of Sciences of the United States of America* 107(22), pp. 10274–10279.

Kučerová, D. et al. 2012. Modulation of SR Ca^{2+} release by the triadin-to-calsequestrin ratio in ventricular myocytes. *AJP: Heart and Circulatory Physiology* 302(10), pp. H2008–17.

Kyrychenko, S. et al. 2012. Hierarchical accumulation of RyR post-translational modifications drives disease progression in dystrophic cardiomyopathy. *Cardiovascular Research* 97(4), pp. 666–675.

Laemmli, U.K. 1970. Cleavage of structural proteins during the assembly of the head of bacteriophage T4. *Nature* 227(5259), pp. 680–685.

Lahat, H. et al. 2001. A missense mutation in a highly conserved region of CASQ2 is associated with autosomal recessive catecholamine-induced polymorphic ventricular tachycardia in Bedouin families from Israel. *American Journal of Human Genetics* 69(9), pp. 1378-84.

Lahat, H. et al. 2002. Autosomal recessive catecholamine-induced polymorphic ventricular tachycardia. *Trends in Cardiovascular Medicine* 13(4), p. 148.

Lai, F.A. et al. 1988. Purification and reconstitution of the calcium release channel from skeletal muscle. *Nature* 331(6154), pp. 315–319.

Lai, F.A. et al. 1989. The ryanodine receptor-Ca^{2+} release channel complex of skeletal muscle sarcoplasmic reticulum. Evidence for a cooperatively coupled, negatively charged homotetramer. *Journal of Biological Chemistry* 264(28), pp. 16776–16785.

Lai, F.A. and Meissner, G. 1989. The muscle ryanodine receptor and its intrinsic Ca^{2+} channel activity. *Journal of Bioenergetics and Biomembranes* 21(2), pp. 227–246.

Laitinen, P.J. et al. 2001. Mutations of the cardiac ryanodine receptor (RyR2) gene in familial polymorphic ventricular tachycardia. *ACC Current Journal Review* 103(4), pp. 485–490.

Lakatta, E.G. 1992. Functional implications of spontaneous sarcoplasmic reticulum Ca^{2+} release in the heart. *Cardiovascular Research* 26(3), pp. 193–214.

Lamb, G.D. and Stephenson, D.G. 1995. Activation of ryanodine receptors by flash photolysis of caged Ca^{2+}. *Biophysical Journal* 68(3), pp. 946–948.

Lamb, G.D. et al. 2000. Questions about adaptation in ryanodine receptors. *The Journal of General Physiology* 116(6), pp. 883–890.

Lang, F. et al. 1998. Functional significance of cell volume regulatory mechanisms. *Contributions to Nephrology* 78(1), pp. 247–306.

Laver, D. 2001. The power of single channel recording and analysis: its application to ryanodine receptors in lipid bilayers. *Clinical and Experimental Pharmacology & Physiology* 28(8), pp. 675–686.

Laver, D.R. 2007. Ca^{2+} stores regulate ryanodine receptor Ca^{2+} release channels via luminal and cytosolic Ca^{2+} sites. *Biophysical Journal* 92(10), pp. 3541–3555.

Laver, D.R. et al. 1995. Cytoplasmic Ca^{2+} inhibits the ryanodine receptor from cardiac muscle. *The Journal of Membrane Biology* 147(1), pp. 7–22.

Laver, D.R. et al. 2007. A domain peptide of the cardiac ryanodine receptor regulates channel sensitivity to luminal Ca^{2+} via cytoplasmic Ca^{2+} sites. *European Biophysics Journal* 37(4), pp. 455–467.

Laver, D.R. et al. 2012. Termination of calcium-induced calcium release by induction decay: an emergent property of stochastic channel gating and molecular scale architecture. *Journal of Molecular and Cellular Cardiology* 54, pp. 98–100.

Lehnart, S.E. et al. 2004. Cardiac ryanodine receptor function and regulation in heart disease. *Annals of the New York Academy of Sciences* 1015(1), pp. 144–159.

Lehnart, S.E. et al. 2004. Sudden death in familial polymorphic ventricular tachycardia associated with calcium release channel (ryanodine receptor) leak. *Circulation* 109(25), pp. 3208–3214.

Lehnart, S.E. et al. 2006. Stabilization of cardiac ryanodine receptor prevents intracellular calcium leak and arrhythmias. *Proceedings of the National Academy of Sciences* 103(20), pp. 7906–7910.

Lehnart, S.E. et al. 2008. Leaky Ca^{2+} release channel/ryanodine receptor 2 causes seizures and sudden cardiac death in mice. *The Journal of Clinical Investigation* 118(6), pp. 2230–2245.

Lei, M. et al. 2015. Regulation of $Ca^{(2+)}$ transient by PP2A in normal and failing heart. *Frontiers in Physiology* 6, p. 13.

Leong, P. and MacLennan, D.H. 1998. The cytoplasmic loops between domains II and III and domains III and IV in the skeletal muscle dihydropyridine receptor bind to a contiguous site in the skeletal muscle ryanodine receptor. *Journal of Biological Chemistry* 273(45), pp. 29958–29964.

Li, L. et al. 2015. A new cytoplasmic interaction between junctin and ryanodine receptor Ca^{2+} release channels. *Journal of Cell Science* 128(5), p. 951.

Li, N. et al. 2012. Inhibition of CaMKII Phosphorylation of RyR2 Prevents Induction of Atrial Fibrillation in FKBP12.6 Knockout Mice. *Circulation Research* 110(3), pp. 465–470.

Li, N. et al. 2014. Ryanodine receptor-mediated calcium leak drives progressive development of an atrial fibrillation substrate in a transgenic mouse model. *Circulation* 129(12), pp. 1276–1285.

Li, P. and Chen, S.R. 2001. Molecular basis of $Ca^{(2)+}$ activation of the mouse cardiac $Ca^{(2)+}$ release channel (ryanodine receptor). *The Journal of General Physiology* 118(1), pp. 33–44.

Li, Y. et al. 2002. Protein kinase A phosphorylation of the ryanodine receptor does not affect calcium sparks in mouse ventricular myocytes. *Circulation Research* 90(3), pp. 309–316.

Lim, G. et al. 2007. Does nitric oxide modulate cardiac ryanodine receptor function? Implications for excitation-contraction coupling. *Cardiovascular Research* 77(2), pp. 256–264.

Lim, H.W. and Molkentin, J.D. 1999. Calcineurin and human heart failure. *Nature Medicine* 5(3), pp. 246–247.

Lindemann, J.P. et al. 1983. beta-Adrenergic stimulation of phospholamban phosphorylation and Ca^{2+}-ATPase activity in guinea pig ventricles. *Journal of Biological Chemistry* 258(1), pp. 464–471.

Lindsay, A.R. et al. 1994. How does ryanodine modify ion handling in the sheep cardiac sarcoplasmic reticulum $Ca^{(2+)}$-release channel? *The Journal of General Physiology* 104(3), pp. 425–447.

Ling, H. et al. 2009. Requirement for Ca^{2+}/calmodulin–dependent kinase II in the transition from pressure overload–induced cardiac hypertrophy to heart failure in mice. *The Journal of Clinical Investigation* 119(5), pp. 1230–1240.

Lipp, P. and Niggli, E. 1996. Submicroscopic calcium signals as fundamental events of excitation--contraction coupling in guinea-pig cardiac myocytes. *The Journal of Physiology* 492(1), p. 31.

Liu, B. et al. 2014. Genetic ablation of ryanodine receptor 2 phosphorylation at Ser-2808 aggravates $Ca^{(2+)}$-dependent cardiomyopathy by exacerbating diastolic Ca^{2+} release. *The Journal of Physiology* 592(9), pp. 1957–1973.

Liu, G. and Pessah, I.N. 1994. Molecular interaction between ryanodine receptor and glycoprotein triadin involves redox cycling of functionally important hyperreactive sulfhydryls. *PLoS ONE* 269(52), pp. 33028–33034.

Liu, N. et al. 2006. Arrhythmogenesis in catecholaminergic polymorphic ventricular tachycardia: insights from a RyR2 R4496C knock-in mouse model. *Circulation Research* 99(3), pp. 292–298.

Liu, N. et al. 2010. Calmodulin kinase II inhibition prevents arrhythmias in RyR2($R4496C^{+/-}$) mice with catecholaminergic polymorphic ventricular tachycardia. *Journal of Molecular and Cellular Cardiology* 50(1), pp. 214–222.

Liu, N. et al. 2011. Short communication: flecainide exerts an antiarrhythmic effect in a mouse model of catecholaminergic polymorphic ventricular tachycardia by increasing the threshold for triggered activity. *Circulation Research* 109(3), pp. 291–295.

Liu, R. et al. 2015. Cardiac-specific deletion of protein phosphatase 1β promotes increased myofilament protein phosphorylation and contractile alterations. *Journal of Molecular and Cellular Cardiology* 87, pp. 204–213.

Liu, Y. et al. 2014. Generation and characterization of a mouse model harboring the exon-3 deletion in the cardiac ryanodine receptor. *PLoS ONE* 9(4), p. e95615.

Liu, Y. et al. 2013. The CPVT-Associated RyR2 Mutation G230C reduces the Threshold for Store Overload-Induced Ca Release (SOICR). *Biophysical Journal* 104(2), p. 442a.

Liu, Z. et al. 2001. Three-dimensional reconstruction of the recombinant type 3 ryanodine receptor and localization of its amino terminus. *Proceedings of the National Academy of Sciences* 98(11), p. 6104.

Liu, Z. et al. 2005. Localization of a Disease-associated Mutation Site in the Three-dimensional Structure of the Cardiac Muscle Ryanodine Receptor. *Journal of Biological Chemistry* 280(45), pp. 37941–37947.

Liu, Z. et al. 2010. Dynamic, inter-subunit interactions between the N-terminal and central mutation regions of cardiac ryanodine receptor. *Journal of Cell Science* 123(Pt 10), pp. 1775–1784.

Lix, L.M. et al. 1996. Consequences of Assumption Violations Revisited: A Quantitative Review of Alternatives to the One-Way Analysis of Variance F Test. *Review of Educational Research* 66(4), pp. 579–619.

Loaiza, R. et al. 2013. Heterogeneity of ryanodine receptor dysfunction in a mouse model of catecholaminergic polymorphic ventricular tachycardia. *Circulation Research* 112(2), pp. 298–308.

Lokuta, A.J. et al. 1997. Modulation of cardiac ryanodine receptors by sorcin. *Journal of Biological Chemistry* 272(40), pp. 25333–25338.

Loughrey, C.M. et al. 2007. K201 modulates excitation-contraction coupling and spontaneous Ca^{2+} release in normal adult rabbit ventricular cardiomyocytes. *Cardiovascular Research* 76(2), pp. 236–246.

Lukyanenko, V. and Wiesner, T.F. 1998. Termination of Ca^{2+} release during Ca^{2+} sparks in rat ventricular myocytes. *The Journal of Physiology* 507(3), pp. 667–677.

Luo, M. and Anderson, M.E. 2013. Mechanisms of Altered Ca^{2+} Handling in Heart Failure. *Circulation Research* 113(6), p. 690.

MacDonnell, S.M. et al. 2008. Adrenergic regulation of cardiac contractility does not involve phosphorylation of the cardiac ryanodine receptor at serine 2808. *Circulation Research* 102(8), pp. e65–72.

MacDougall, L.K. et al. 1991. Identification of the major protein phosphatases in mammalian cardiac muscle which dephosphorylate phospholamban. *European Journal of Biochemistry / FEBS* 196(3), pp. 725–734.

MacLennan, D.H. and Kranias, E.G. 2003. Phospholamban: a crucial regulator of cardiac contractility. *Nature Reviews Molecular Cell Biology* 4(7), pp. 566–577.

MacLennan, D.H. and Zvaritch, E. 2011. Mechanistic models for muscle diseases and disorders originating in the sarcoplasmic reticulum. *Biochimica et Biophysica Acta (BBA) - Molecular Cell Research* 1813(5), pp. 948–964.

Macquaide, N. et al. 2015. Ryanodine receptor cluster fragmentation and redistribution in persistent atrial fibrillation enhance calcium release. *Cardiovascular Research* 108(3), pp. 387–398.

Malhotra, R. et al. 2010. Gα q -mediated Activation of GRK2 by Mechanical Stretch in Cardiac Myocytes. *Journal of Biological Chemistry* 285(18), p. 13748.

Manders, E.M.M. et al. 1993. Measurement of co-localization of objects in dual-colour confocal images. *Journal of Microscopy* 169(3), p. 375.

Manning, D.R. et al. 1980. Protein phosphorylation: quantitative analysis in vivo and in intact cell systems. *Molecular and Cellular Endocrinology* 19(1), pp. 1–19.

Manotheepan, R. et al. 2016. Exercise training prevents ventricular tachycardia in CPVT1 due to reduced CaMKII-dependent arrhythmogenic Ca^{2+} release. *Cardiovascular Research* 111(3), pp. 295–306.

Marbán, E. 2002. Cardiac channelopathies. *Nature* 415(6868), pp. 213–218.

Marcus, F.I. et al. 1982. Right ventricular dysplasia: a report of 24 adult cases. *Circulation* 65(2), pp. 384–398.

Marcus, F.I. et al. 2010. Diagnosis of arrhythmogenic right ventricular cardiomyopathy/dysplasia: proposed modification of the task force criteria. *Circulation* 121(13), pp. 1533–1541.

Marengo, J.J. et al. 1998. Sulfhydryl oxidation modifies the calcium dependence of ryanodine-sensitive calcium channels of excitable cells. *Biophysical Journal* 74(3), pp. 1263–1277.

Marjamaa, A. et al. 2009. Search for cardiac calcium cycling gene mutations in familial ventricular arrhythmias resembling catecholaminergic polymorphic ventricular tachycardia. *BMC Medical Genetics* 10(1), p. 2035.

Marks, A.R. et al. 1989. Molecular cloning and characterization of the ryanodine receptor/junctional channel complex cDNA from skeletal muscle sarcoplasmic reticulum. *Proceedings of the National Academy of Sciences* 86(22), pp. 8683–8687.

Marks, A.R. et al. 2002. Regulation of ryanodine receptors via macromolecular complexes: a novel role for leucine/isoleucine zippers. *Trends in Cardiovascular Medicine* 12(4), pp. 166–170.

Marty, I. 2014. Triadin regulation of the ryanodine receptor complex. *The Journal of Physiology* 593(15), p. 3261.

Marx, S.O. and Marks, A.R. 2013. Dysfunctional ryanodine receptors in the heart: New insights into complex cardiovascular diseases. *Journal of Molecular and Cellular Cardiology* 58, pp. 225–231.

Marx, S.O. et al. 1998. Coupled gating between individual skeletal muscle Ca^{2+} release channels (ryanodine receptors). *Science (New York, N.Y.)* 281(5378), p. 818.

Marx, S.O. et al. 2000. PKA Phosphorylation Dissociates FKBP12.6 from the Calcium Release Channel (Ryanodine Receptor). *Cell* 101(4), pp. 365–376.

Marx, S.O., Gaburjakova, J., et al. 2001. Coupled gating between cardiac calcium release channels (ryanodine receptors). *Circulation Research* 88(11), p. 1151.

Marx, S.O., Reiken, S., et al. 2001. Phosphorylation-dependent regulation of ryanodine receptors: a novel role for leucine/isoleucine zippers. *The Journal of Cell Cardiology* 153(4), pp. 699–708.

Massion, P.B. 2003. Nitric Oxide and Cardiac Function: Ten Years After, and Continuing. *Circulation Research* 93(5), p. 388.

Mattiazzi, A. et al. 2015. Chasing cardiac physiology and pathology down the CaMKII cascade. *American Journal of Physiology, Heart Circulation Physiology* 308(10) pp. H1177-1191.

Medeiros-Domingo, A. et al. 2009. The RYR2-Encoded Ryanodine Receptor/Calcium Release Channel in Patients Diagnosed Previously With Either Catecholaminergic Polymorphic Ventricular Tachycardia or Genotype Negative, Exercise-Induced Long QT Syndrome. *Journal of the American College of Cardiology* 54(22), pp. 2065–2074.

Meisenhelder, J. et al. 2008. Phosphopeptide mapping and identification of phosphorylation sites. *Current Protocols in Molecular Biology* Chapter 18, pp. Unit–18.9.

Meissner, G. and El-Hashem, A. 1992. Ryanodine as a functional probe of the skeletal muscle sarcoplasmic reticulum Ca^{2+} release channel. *Molecular and Cellular Biochemistry* 114(1-2), pp. 119–123.

Meli, A.C. et al. 2011. A novel ryanodine receptor mutation linked to sudden death increases sensitivity to cytosolic calcium. *Circulation Research* 109(3), pp. 281–290.

Meng, X. et al. 2007. Three-dimensional localization of serine 2808, a phosphorylation site in cardiac ryanodine receptor. *Journal of Biological Chemistry* 282(35), pp. 25929–25939.

Meyers, M.B. et al. 1998. Sorcin associates with the pore-forming subunit of voltage-dependent L-type Ca^{2+} channels. *Journal of Biological Chemistry* 273(30), pp. 18930–18935.

Milone, M. et al. 1997. Slow-channel myasthenic syndrome caused by enhanced activation, desensitization, and agonist binding affinity attributable to mutation in the M2 domain of the acetylcholine receptor alpha subunit. *The Journal of Neuroscience* 17(15), pp. 5651–5665.

Miyake, C.Y. et al. 2013. Efficacy of implantable cardioverter defibrillators in young patients with catecholaminergic polymorphic ventricular tachycardia: success depends on substrate. *Circulation: Arrhythmia and Electrophysiology* 6(3), pp. 579–587.

Miyazaki, Y. et al. 2012. Heart failure-inducible gene therapy targeting protein phosphatase 1 prevents progressive left ventricular remodeling. *PLoS ONE* 7(4), p. e35875.

Mohler, P.J. and Hund, T.J. 2011. Role for CaMKII in cardiovascular health, disease and arrhythmia. *Heart Rhythm* 8(1), pp. 142-144.

Mojzisova, A. 2002. Coupled gating between individual cardiac ryanodine calcium release channels. *General Physiology and Biophysics*.

Monsuez, J.J. et al. 1995. Sudden cardiac death in heart failure: the role of abnormal repolarization. *Circulation* 91(6), pp. 1899–1900.

Mortensen, M. and Smart, T.G. 2007. Single-channel recording of ligand-gated ion channels. *Nature Protocols* 2(11), pp. 2826–2841.

Moss, A.J. et al. 2000. Effectiveness and Limitations of beta-Blocker Therapy in Congenital Long-QT Syndrome. *Circulation* 101(6), p. 616.

Muijsers, R.B.R. et al. 2002. Fixed combination trandolapril/verapamil sustained-release: a review of its use in essential hypertension. *Drugs* 62(17), pp. 2539–2567.

Mukherjee, S. et al. 2012. A mechanistic description of gating of the human cardiac ryanodine receptor in a regulated minimal environment. *The Journal of General Physiology* 140(2), pp. 139–158.

Mulley, J.C. et al. 1993. Refined genetic localization for central core disease. *American journal of Human Genetics* 52(2), pp. 398–405.

Mullis, K. et al. 1986. Specific enzymatic amplification of DNA in vitro: the polymerase chain reaction. *Cold Spring Harbor Symposia on Quantitative Biology* 51 Pt 1, pp. 263–273.

Nakai, J. et al. 1990. Primary structure and functional expression from cDNA of the cardiac ryanodine receptor/calcium release channel. *FEBS letters* 271(1-2), pp. 169–177.

Nayler, W.G. et al. 1970. Effect of ryanodine on calcium in cardiac muscle. *American Journal of Physiology -- Legacy Content* 219(6), pp. 1620–1626.

Negretti, N. et al. 1995. Estimate of net calcium fluxes and sarcoplasmic reticulum calcium content during systole in rat ventricular myocytes. *The Journal of Physiology* 486(pt 3), pp. 581-591.

Neumann, J. et al. 1997. Increased Expression of Cardiac Phosphatases in Patients with End-stage Heart Failure. *Journal of Molecular and Cellular Cardiology* 29(1), pp. 265–272.

Newlon, M.G. et al. 1999. The molecular basis for protein kinase A anchoring revealed by solution NMR. *Nature Structural Biology* 6(3), pp. 222–227.

Niggli, E. 2016. Real-time intra-store confocal $Ca^{(2+)}$ imaging in isolated mouse cardiomyocytes. *Cell Calcium* 60(5), pp. 331-340.

Niggli, E. and Shirokova, N. 2007. A guide to sparkology: the taxonomy of elementary cellular Ca^{2+} signaling events. *Cell Calcium* 42(4-5), pp. 379–387.

Niggli, E. et al. 2012. Posttranslational modifications of cardiac ryanodine receptors: $Ca^{(2+)}$ signaling and EC-coupling. *Biochimica et Biophysica Acta* 1833(4), pp. 866–875.

Nishimura, S. et al. 2015. Abstract 13816: Dantrolene Enhances Binding of Calmodulin to RyR2 in CPVT Which Mutation Located at Central Domain but Does Not Enhance That in CPVT With Mutation at CaM-like Domain. *Circulation* 132(Suppl 3), p. A13816.

Orn, S. and Dickstein, K. 2002. How do heart failure patients die? *European Heart Journal* 4, pp. D59–D65.

Oda, T. et al. 2005. Defective regulation of interdomain interactions within the ryanodine receptor plays a key role in the pathogenesis of heart failure. *Circulation* 111(25), pp. 3400–3410.

Oda, T. et al. 2015. Oxidation of ryanodine receptor (RyR) and calmodulin enhance Ca release and pathologically alter, RyR structure and calmodulin affinity. *Journal of Molecular and Cellular Cardiology* 85, p. 240.

Ogawa, Y. 1994. Role of ryanodine receptors. *Critical Reviews in Biochemistry and Molecular Biology* 29(4), pp. 229–274.

Ohkura, M. et al. 1998. Dual Regulation of the Skeletal Muscle Ryanodine Receptor by Triadin and Calsequestrin. *Biochemistry* 37(37), p. 12987.

Ohno, S. 2016. The genetic background of arrhythmogenic right ventricular cardiomyopathy. *Journal of Arrhythmia* 32(5), pp. 398–403.

Okeyo, G. et al. 2013. Converting nonhydrolyzable nucleotides to strong cystic fibrosis transmembrane conductance regulator (CFTR) agonists by gain of function (GOF) mutations. *The Journal of Biological Chemistry* 288(24), pp. 17122–17133.

Olsen, J.V. et al. 2010. Quantitative phosphoproteomics reveals widespread full phosphorylation site occupancy during mitosis. *Science Signaling* 3(104), p. ra3.

O'Neill, S.C., Eisner, D.A. 1990 A mechanism for the effects of caffeine on Ca^{2+} release during diastole and systole in isolated rat ventricular myocytes. *Journal of Physiology* 430, pp. 519-536.

Oo, Y.W. et al. 2015. Essential Role of Calmodulin in RyR Inhibition by Dantrolene. *Molecular Pharmacology* 88(1), pp. 57–63.

Orchard, C.H. et al. 1983. Oscillations of intracellular Ca^{2+} in mammalian cardiac muscle. *Nature* 304(5928), pp. 735–738.

Otsu, K. et al. 1990. Molecular cloning of cDNA encoding the Ca^{2+} release channel (ryanodine receptor) of rabbit cardiac muscle sarcoplasmic reticulum. *The Journal of Biological Chemistry* 265(23), pp. 13472–13483.

Paavola, J. et al. 2007. Mutant ryanodine receptors in catecholaminergic polymorphic ventricular tachycardia generate delayed afterdepolarizations due to increased propensity to Ca^{2+} waves. *European Heart Journal* 28(9), pp. 1135–1142.

Palmer, A.E. et al. 2004. Bcl-2-mediated alterations in endoplasmic reticulum Ca^{2+} analyzed with an improved genetically encoded fluorescent sensor. *Proceedings of the National Academy of Sciences* 101(50), pp. 17404–17409.

Paul-Pletzer, K. et al. 2005. Probing a putative dantrolene-binding site on the cardiac ryanodine receptor. *The Biochemical Journal* 387(Pt 3), pp. 905–909.

Pedrozo, Z. et al. 2010. Calpains and proteasomes mediate degradation of ryanodine receptors in a model of cardiac ischemic reperfusion. *Biochimica et Biophysica Acta - Molecular Basis of Disease* 1802(3), p. 356.

Percival, A.L. et al. 1994. Chicken skeletal muscle ryanodine receptor isoforms: ion channel properties. *Biophysical Journal* 67(5), pp. 1834–1850.

Pereira, L. et al. 2007. The cAMP binding protein Epac modulates Ca^{2+} sparks by a Ca^{2+}/calmodulin kinase signalling pathway in rat cardiac myocytes. *The Journal of Physiology* 583(2), pp. 685–694.

Pereira, L. et al. 2013. Epac2 mediates cardiac β1-adrenergic-dependent sarcoplasmic reticulum Ca^{2+} leak and arrhythmia. *Circulation* 127(8), pp. 913–922.

Pessah, I.N. et al. 1985. The calcium-ryanodine receptor complex of skeletal and cardiac muscle. *Biochemical and Biophysical Research Communications* 128(1), pp. 449–456.

Pessah, I.N. et al. 1986. Calcium-ryanodine receptor complex. Solubilization and partial characterization from skeletal muscle junctional sarcoplasmic reticulum vesicles. *Journal of Biological Chemistry* 261(19), pp. 8643–8648.

Petroff, M.G. et al. 2001. Endogenous nitric oxide mechanisms mediate the stretch dependence of Ca^{2+} release in cardiomyocytes. *Nature Cell Biology* 3(10), pp. 867–873.

Piacentino, V. et al. 2003. Cellular Basis of Abnormal Calcium Transients of Failing Human Ventricular Myocytes. *Circulation Research* 92(6), pp. 651–658.

Pizzale, S. et al. 2008. Sudden death in a young man with catecholaminergic polymorphic ventricular tachycardia and paroxysmal atrial fibrillation. *Journal of Cardiovascular Electrophysiology* 19(12), pp. 1319–1321.

Pogwizd, S. 2004. Cellular Basis of Triggered Arrhythmias in Heart Failure. *Trends in Cardiovascular Medicine* 14(2), pp. 61–66.

Ponting, C. et al. 1997. SPRY domains in ryanodine receptors ($Ca^{(2+)}$-release channels). *Trends in Biochemical Sciences* 22(6), pp. 193–194.

Porta, M. et al. 2011. Single Ryanodine Receptor Channel Basis of Caffeine's Action on Ca^{2+} Sparks. *Biophysical Journal* 100(4), p. 931.

Porta, M. et al. 2012. Coupled gating of skeletal muscle ryanodine receptors is modulated by Ca^{2+}, Mg^{2+}, and ATP. *AJP: Cell Physiology* 303(6), pp. C682–97.

Porter, K.R. et al. 1945. A study of tissue culture cells by electron microscopy: methods and preliminary observations. *Journal of Experimental Medicine* 81(3), pp. 233–246.

Postma, A.V. 2005. Catecholaminergic polymorphic ventricular tachycardia: RYR2 mutations, bradycardia, and follow up of the patients. *Journal of Medical Genetics* 42(11), pp. 863–870.

Pott, C. et al. 2006. Regulation of cardiac L-type Ca^{2+} current in Na^{+}-Ca^{2+} exchanger knockout mice: functional coupling of the Ca^{2+} channel and the Na^{+}-Ca^{2+} exchanger. *Biophysical Journal* 92(4), pp. 1431–1437.

Prestle, J. et al. 2001. Overexpression of FK506-binding protein FKBP12.6 in cardiomyocytes reduces ryanodine receptor-mediated $Ca^{(2+)}$ leak from the sarcoplasmic reticulum and increases contractility. *Circulation Research* 88(2), pp. 188–194.

Priori, S.G et al. 2002. Clinical and Molecular Characterization of Patients With Catecholaminergic Polymorphic Ventricular Tachycardia. *Circulation* 106(1), pp. 69–74.

Priori, S.G. and Chen, S.R.W. 2011. Inherited dysfunction of sarcoplasmic reticulum Ca^{2+} handling and arrhythmogenesis. *Circulation Research* 108(7), pp. 871–883.

Priori, S.G. et al. 2001. Mutations in the cardiac ryanodine receptor gene (hRyR2) underlie catecholaminergic polymorphic ventricular tachycardia. *Circulation* 103(2), pp. 196–200.

Priori, S.G. et al. 2013. HRS/EHRA/APHRS expert consensus statement on the diagnosis and management of patients with inherited primary arrhythmia syndromes: document endorsed by

HRS, EHRA, and APHRS in May 2013 and by ACCF, AHA, PACES, and AEPC in June 2013. *Heart Rhythm* 10(12), pp. 1932–1963.

Prosser, B.L. et al. 2011. S100A1 and calmodulin regulation of ryanodine receptor in striated muscle. *Cell Calcium* 50(4), pp. 323–331.

Purohit, P. and Auerbach, A. 2009. Unliganded gating of acetylcholine receptor channels. *Proceedings of the National Academy of Sciences of the United States of America* 106(1), pp. 115–120.

Quane, K.A. et al. 1993. Mutations in the ryanodine receptor gene in central core disease and malignant hyperthermia. *Nature Genetics* 5(1), pp. 51–55.

Radwański, P.B. et al. 2012. Store-dependent deactivation: cooling the chain-reaction of myocardial calcium signaling. *Journal of Molecular and Cellular Cardiology* 58, pp. 77–83.

Rampazzo, A. et al. 1995. A new locus for arrhythmogenic right ventricular cardiomyopathy (ARVD2) maps to chromosome 1q42-q43. *Human Molecular Genetics* 4(11), pp. 2151–2154.

Rebbeck, R.T. et al. 2016. S100A1 Protein Does Not Compete with Calmodulin for Ryanodine Receptor Binding but Structurally Alters the Ryanodine Receptor·Calmodulin Complex. *Journal of Biological Chemistry* 291(30), pp. 15896–15907.

Reiken, S. et al. 2001. -Adrenergic Receptor Blockers Restore Cardiac Calcium Release Channel (Ryanodine Receptor) Structure and Function in Heart Failure. *Circulation* 104(23), pp. 2843–2848.

Reiken, S. et al. 2003. Beta-blockers restore calcium release channel function and improve cardiac muscle performance in human heart failure. *Circulation* 107(19), pp. 2459–2466.

Reiken, S. et al. 2003. Protein kinase A phosphorylation of the cardiac calcium release channel (ryanodine receptor) in normal and failing hearts. Role of phosphatases and response to isoproterenol. *Journal of Biological Chemistry* 278(1), pp. 444–453.

Reppel, M. et al. 2007. Regulation of Na^+/Ca^{2+} exchange current in the normal and failing heart. *Annals of the New York Academy of Sciences* 1099(1), pp. 361–372.

Respress, J.L. et al. 2012. Role of RyR2 phosphorylation at S2814 during heart failure progression. *Circulation Research* 110(11), pp. 1474–1483.

Respress, J.L. et al. 2014. Long-term simulated microgravity causes cardiac RyR2 phosphorylation and arrhythmias in mice. *International Journal of Cardiology* 176(3), pp. 994–1000.

Reuter, H. 1974 Localization of beta adrenergic receptors, and effects of noradrenaline and cyclic nucleotides on action potentials, ionic currents and tension in mammalian cardiac muscle. *Journal of Physiology* 242, pp. 429-451.

Rodriguez, P. et al. 2003. Stoichiometric phosphorylation of cardiac ryanodine receptor on serine 2809 by calmodulin-dependent kinase II and protein kinase A. *Journal of Biological Chemistry* 278(40), pp. 38593–38600.

Rooryck, C. et al. 2015. New family with catecholaminergic polymorphic ventricular tachycardia linked to the Triadin gene. *Journal of Cardiovascular Electrophysiology* 26(10), p. 1146.

Rosenberg, O.S. et al. 2006. Oligomerization states of the association domain and the holoenyzme of Ca^{2+}/CaM kinase II. *FEBS Journal* 273(4), p. 682.

Rousseau, E. et al. 1986. Single channel and Ca^{2+} flux measurements of the cardiac sarcoplasmic reticulum calcium channel. *Biophysical Journal* 50(5), pp. 1009–1014.

Rostas, J.A.P. and Dunkley, P.R. 1992. Multiple Forms and Distribution of Calcium/Calmodulin-Stimulated Protein Kinase II in Brain. *Journal of Neurochemistry* 59(4), p. 1191.

Roston, T.M. et al. 2015. Catecholaminergic polymorphic ventricular tachycardia in children: analysis of therapeutic strategies and outcomes from an international multicenter registry. *Circulation: Arrhythmia and Electrophysiology* 8(3), pp. 633–642.

Rousseau, E. and Meissner, G. 1989. Single cardiac sarcoplasmic reticulum Ca^{2+}-release channel: activation by caffeine. *Anesthesiology* 256(2 Pt 2), pp. H328–33.

Rousseau, E. et al. 1987. Ryanodine modifies conductance and gating behavior of single Ca^{2+} release channel. *Molecular Pharmacology* 253(3 Pt 1), pp. C364–8.

Rovetti, R. et al. 2010. Spark-Induced Sparks as a Mechanism of Intracellular Calcium Alternans in Cardiac Myocytes. *Circulation Research* 106(10), pp. 1582–1591.

Ruder, M.A. et al. 1985. Arrhythmogenic right ventricular dysplasia in a family. *Practical ECG Interpretation* 56(12), pp. 799–800.

Ruiz-Hurtado, G. et al. 2012. Epac in cardiac calcium signaling. *Journal of Molecular and Cellular Cardiology* 58, pp. 162–171.

Russell, W.C. et al. 1977. Characteristics of a Human Cell Line Transformed by DNA from Human Adenovirus Type 5. *Journal of General Virology* 36(1), pp. 59–72.

Salama, G. et al. 2001. Molecular interaction between nitric oxide and ryanodine receptors of skeletal and cardiac sarcoplasmic reticulum. *Antioxidants & Redox Signaling* 2(1), pp. 5–16.

Samsó, M. 2016. A guide to the 3D structure of the ryanodine receptor type 1 by cryoEM. *Protein Science* 26(1), pp. 52-68.

Samsó, M. and Wagenknecht, T. 2001. Apocalmodulin and Ca^{2+}-calmodulin bind to neighboring locations on the ryanodine receptor. *Journal of Biological Chemistry* 277(2), pp. 1349–1353.

Samsó, M. et al. 2009. Coordinated movement of cytoplasmic and transmembrane domains of RyR1 upon gating. *PLoS Biology* 7(4), p. e85.

Sankaranarayanan, R. et al. 2016. Biphasic decay of the Ca transient results from increased sarcoplasmic reticulum Ca leak. *The Journal of Physiology* 594(3), p. 611.

Sarma, S. et al. 2010. Genetic inhibition of PKA phosphorylation of RyR2 prevents dystrophic cardiomyopathy. *Proceedings of the National Academy of Sciences of the United States of America* 107(29), pp. 13165–13170.

Sato, D. and Bers, D.M. 2011. How does stochastic ryanodine receptor-mediated Ca leak fail to initiate a Ca spark? *Biophysical Journal* 101(10), pp. 2370–2379.

Schlecht, W. et al. 2014. FRET study of the structural and kinetic effects of PKC phosphomimetic cardiac troponin T mutants on thin filament regulation. *Archives of Biochemistry and Biophysics* 550-551, pp. 1–11.

Schwartz, P.J. 2004. Left Cardiac Sympathetic Denervation in the Management of High-Risk Patients Affected by the Long-QT Syndrome. *Circulation* 109(15), p. 1826.

Schwartz, P.J. et al. 1991. Left cardiac sympathetic denervation in the therapy of congenital long QT syndrome. A worldwide report. *Circulation* 84(2), p. 503.

Scoote, M. and Williams, A.J. 2002. The cardiac ryanodine receptor (calcium release channel): emerging role in heart failure and arrhythmia pathogenesis. *Cardiovascular Research* 56(3), pp. 359–372.

Scott, J.D. and McCartney, S. 1994. Localization of A-kinase through anchoring proteins. *Molecular Endocrinology* 8(1), pp. 5–11.

Sedej, S. et al. 2010. Na+-dependent SR Ca^{2+} overload induces arrhythmogenic events in mouse cardiomyocytes with a human CPVT mutation. *Cardiovascular Research* 87(1), pp. 50–59.

Seidel, M. et al. 2014. Dantrolene rescues aberrant N-terminus intersubunit interactions in mutant pro-arrhythmic cardiac ryanodine receptors. *Cardiovascular Research* 105(1), pp. 118–128.

Seiler, S. et al. 1984. High molecular weight proteins in cardiac and skeletal muscle junctional sarcoplasmic reticulum vesicles bind calmodulin, are phosphorylated, and are degraded by Ca^{2+}-activated protease. *The Journal of Biological Chemistry* 259(13), pp. 8550–8557.

Sham, J.S. et al. 1998. Termination of Ca^{2+} release by a local inactivation of ryanodine receptors in cardiac myocytes. *Proceedings of the National Academy of Sciences* 95(25), pp. 15096–15101.

Shan, J. et al. 2012. Calcium leak through ryanodine receptors leads to atrial fibrillation in 3 mouse models of catecholaminergic polymorphic ventricular tachycardia. *Circulation Research* 111(6), pp. 708–717.

Shan, J., Betzenhauser, M.J., et al. 2010. Role of chronic ryanodine receptor phosphorylation in heart failure and β-adrenergic receptor blockade in mice. *The Journal of Clinical Investigation* 120(12), pp. 4375–4387.

Shan, J. et al. 2010a. Phosphorylation of the ryanodine receptor mediates the cardiac fight or flight response in mice. *Journal of Clinical Investigation* 120(12), p. 4388.

Shannon, T.R. et al. 2000. Potentiation of Fractional Sarcoplasmic Reticulum Calcium Release by Total and Free Intra-Sarcoplasmic Reticulum Calcium Concentration. *Biophysical Journal* 78(1), pp. 334–343.

Shannon, T.R. et al. 2003. Ca^{2+} scraps: local depletions of free [Ca^{2+}] in cardiac sarcoplasmic reticulum during contractions leave substantial Ca^{2+} reserve. *Circulation Research* 93(1), pp. 40–45.

Shen, B. et al. 2011. cAMP activates TRPC6 channels via the phosphatidylinositol 3-kinase (PI3K)-protein kinase B (PKB)-mitogen-activated protein kinase kinase (MEK)-ERK1/2 signaling pathway. *Journal of Biological Chemistry* 286(22), pp. 19439–19445.

Shirai, N. et al. 2002. A mutant cardiac sodium channel with multiple biophysical defects associated with overlapping clinical features of Brugada syndrome and cardiac conduction disease. *Cardiovascular Research* 53(2), pp. 348–354.

Sikkel, M.B. et al. 2013. Flecainide reduces $Ca^{(2+)}$ spark and wave frequency via inhibition of the sarcolemmal sodium current. *Cardiovascular Research* 98(2), pp. 286–296.

Sitsapesan, R. and Williams, A.J. 1990a. Inactivation of the cardiac sarcoplasmic reticulum calcium-release channel by high calcium concentrations. *Journal of Molecular and Cellular Cardiology* 22, p. S21.

Sitsapesan, R. and Williams, A.J. 1990b. Mechanisms of caffeine activation of single calcium-release channels of sheep cardiac sarcoplasmic reticulum. *The Journal of Physiology* 423(1), pp. 425–439.

Sitsapesan, R. and Williams, A.J. 1994. Gating of the native and purified cardiac SR $Ca^{(2+)}$-release channel with monovalent cations as permeant species. *Biophysical Journal* 67(4), pp. 1484–1494.

Sitsapesan, R. and Williams, A.J. 1994a. Gating of the native and purified cardiac SR $Ca^{(2+)}$-release channel with monovalent cations as permeant species. *Biophysical Journal* 67(4), pp. 1484–1494.

Sitsapesan, R. and Williams, A.J. 1994b. Regulation of the gating of the sheep cardiac sarcoplasmic reticulum $Ca^{(2+)}$-release channel by luminal Ca^{2+}. *The Journal of Membrane Biology* 137(3), pp. 215–226.

Skiniotis, G. and Southworth, D.R. 2015. Single-particle cryo-electron microscopy of macromolecular complexes. *Microscopy* 65(1), pp. 9–22.

Sobie, E.A. et al. 2005. The Ca^{2+} leak paradox and rogue ryanodine receptors: SR Ca^{2+} efflux theory and practice. *Progress in Biophysics and Molecular Biology* 90(1-3), pp. 172–185.

Somekawa, S. 2005. Enhanced Functional Gap Junction Neoformation by Protein Kinase A-Dependent and Epac-Dependent Signals Downstream of cAMP in Cardiac Myocytes. *Circulation Research* 97(7), p. 655.

Song, L.-S. et al. 2005. Calcium Biology of the Transverse Tubules in Heart. *Annals of the New York Academy of Sciences* 1047(1), p. 99.

Song, Q. et al. 2011. Phosphomimetic mutations enhance oligomerization of phospholemman and modulate its interaction with the Na/K-ATPase. *Journal of Biological Chemistry* 286(11), pp. 9120–9126.

Sorrentino, V. and Volpe, P. 1993. Ryanodine receptors: how many, where and why? *Trends in Pharmacological Sciences* 14(3), pp. 98–103.

Sossalla, S. et al. 2010. Inhibition of elevated Ca^{2+}/calmodulin-dependent protein kinase II improves contractility in human failing myocardium. *Circulation Research* 107(9), pp. 1150–1161.

Stange, M. et al. 2003. Characterization of Recombinant Skeletal Muscle (Ser-2843) and Cardiac Muscle (Ser-2809) Ryanodine Receptor Phosphorylation Mutants. *The Journal of Biological Chemistry* 278(51), pp. 51693–51702.

Stern, M.D. 1992. Theory of excitation-contraction coupling in cardiac muscle. *Biophysical Journal* 63(2), pp. 497–517.

Stern, M.D. and Cheng, H. 2004. Putting out the fire: what terminates calcium-induced calcium release in cardiac muscle? *Cell Calcium* 35(6), pp. 591–601.

Suetomi, T. et al. 2011. Mutation-Linked Defective Interdomain Interactions Within Ryanodine Receptor Cause Aberrant Ca^{2+} Release Leading to Catecholaminergic Polymorphic Ventricular Tachycardia. *Circulation* 124(6), pp. 682–694.

Sumandea, M.P. 2003. Identification of a Functionally Critical Protein Kinase C Phosphorylation Residue of Cardiac Troponin T. *Journal of Biological Chemistry* 278(37), p. 35135.

Sumitomo, N. et al. 2002. Catecholaminergic polymorphic ventricular tachycardia: electrocardiographic characteristics and optimal therapeutic strategies to prevent sudden death. *Heart* 89(1), pp. 66–70.

Sun, B. et al. 2016. The Cytoplasmic Region of Inner Helix S6 Is an Important Determinant of Cardiac Ryanodine Receptor Channel Gating. *Journal of Biological Chemistry* 291(50), pp. 26024–26034.

Sun, J. et al. 2008. Regulation of the cardiac muscle ryanodine receptor by O(2) tension and S-nitrosoglutathione. *Biochemistry* 47(52), pp. 13985–13990.

Sutko, J.L. 1991. Foot protein isoforms are expressed at different times during embryonic chick skeletal muscle development. *The Journal of Cell Biology* 113(4), p. 793.

Sutko, J.L. and Kenyon, J.L. 1983. Ryanodine modification of cardiac muscle responses to potassium-free solutions. Evidence for inhibition of sarcoplasmic reticulum calcium release. *The Journal of General Physiology* 82(3), pp. 385–404.

Swan, H. et al. 1999a. Arrhythmic disorder mapped to chromosome 1q42-q43 causes malignant polymorphic ventricular tachycardia in structurally normal hearts. *Journal of the American College of Cardiology* 34(7), pp. 2035–2042.

Tada, M. et al. 1975. Phosphorylation of a 22,000-dalton component of the cardiac sarcoplasmic reticulum by adenosine 3':5'-monophosphate-dependent protein kinase. *Journal of Biological Chemistry* 250, pp. 2640-2647.

Takasago, T. et al. 1989. Phosphorylation of the cardiac ryanodine receptor by cAMP-dependent protein kinase. *Journal of Biochemistry* 106(5), pp. 872–877.

Takasago, T. et al. 1991. Regulation of the cardiac ryanodine receptor by protein kinase-dependent phosphorylation. *Journal of Biochemistry* 109(1), pp. 163–170.

Takeshima, H. et al. 1989. Primary structure and expression from complementary DNA of skeletal muscle ryanodine receptor. *Nature* 339(6224), pp. 439–445.

Tang, H. et al. 2011. Ca(v)1.2 calcium channel is glutathionylated during oxidative stress in guinea pig and ischemic human heart. *Free Radical Biology & Medicine* 51(8), pp. 1501–1511.

Tateishi, H. et al. 2008. Defective domain-domain interactions within the ryanodine receptor as a critical cause of diastolic Ca^{2+} leak in failing hearts. *Cardiovascular Research* 81(3), pp. 536–545.

Terentyev, D. 2008. Modulation of ryanodine receptor by luminal calcium and accessory proteins in health and cardiac disease. *Cardiovascular Research* 77(2), pp. 245–255.

Terentyev, D. and Hamilton, S. 2016. Regulation of sarcoplasmic reticulum $Ca^{(2+)}$ release by serine-threonine phosphatases in the heart. *Journal of Molecular and Cellular Cardiology* 101, pp. 156–164.

Terentyev, D. et al. 2002. Luminal Ca^{2+} controls termination and refractory behavior of Ca^{2+}-induced Ca^{2+} release in cardiac myocytes. *Circulation Research* 91(5), pp. 414–420.

Terentyev, D. et al. 2003. Protein phosphatases decrease sarcoplasmic reticulum calcium content by stimulating calcium release in cardiac myocytes. *The Journal of Physiology* 552(Pt 1), pp. 109–118.

Terentyev, D. et al. 2007. Protein protein interactions between triadin and calsequestrin are involved in modulation of sarcoplasmic reticulum calcium release in cardiac myocytes. *The Journal of Physiology* 583(Pt 1), pp. 71–80.

Terentyev, D. et al. 2009. miR-1 overexpression enhances $Ca^{(2+)}$ release and promotes cardiac arrhythmogenesis by targeting PP2A regulatory subunit B56alpha and causing CaMKII-dependent hyperphosphorylation of RyR2. *Circulation Research* 104(4), pp. 514–521.

Terentyev, D., Belevych, A.E., et al. 2008. Redox modification of ryanodine receptors contributes to sarcoplasmic reticulum Ca^{2+} leak in chronic heart failure. *Circulation Research* 103(12), pp. 1466–1472.

Terentyev, D., Kubalova, Z., et al. 2008. Modulation of SR Ca release by luminal Ca and calsequestrin in cardiac myocytes: effects of CASQ2 mutations linked to sudden cardiac death. *Biophysical Journal* 95(4), pp. 2037–2048.

Terentyev, D. et al. 2014a. Hyperphosphorylation of RyRs underlies triggered activity in transgenic rabbit model of LQT2 syndrome. *Circulation Research* 115(11), pp. 919–928.

Tester, D.J. et al. 2004. Targeted mutational analysis of the RyR2-encoded cardiac ryanodine receptor in sudden unexplained death: a molecular autopsy of 49 medical examiner/coroner's cases. *Mayo Clinic Proceedings* 79(11), pp. 1380–1384.

Tester, D.J. et al. 2006. Genotypic heterogeneity and phenotypic mimicry among unrelated patients referred for catecholaminergic polymorphic ventricular tachycardia genetic testing. *Heart Rhythm* 3(7), p. 800.

Tester, D.J. et al. 2007. A mechanism for sudden infant death syndrome (SIDS): Stress-induced leak via ryanodine receptors. *Heart Rhythm* 4(6), pp. 733–739.

Thevenon, D. et al. 2003. Human skeletal muscle triadin: gene organization and cloning of the major isoform, Trisk 51. *Biochemical and Biophysical Research Communications* 303(2), p. 669.

Thomas, D. et al. 2000. A comparison of fluorescent Ca^{2+} indicator properties and their use in measuring elementary and global Ca^{2+} signals. *Cell calcium* 28(4), pp. 213–223.

Thomas, G.D. 2011. Neural control of the circulation. *AJP: Advances in Physiology Education* 35(1), p. 28.

Thomas, N.L. et al. 2004. Functional heterogeneity of ryanodine receptor mutations associated with sudden cardiac death. *Cardiovascular Research* 64(1), pp. 52–60.

Thomas, N.L. et al. 2006. Role of ryanodine receptor mutations in cardiac pathology: more questions than answers? *Biochemical Society Transactions* 34(5), pp. 913–918.

Tian, L. et al. 2002. Leucine zipper domain targets cAMP-dependent protein kinase to mammalian BK channels. *Journal of Biological Chemistry* 278(10), pp. 8669–8677.

Timerman, A.P. et al. 1996. Selective binding of FKBP12.6 by the cardiac ryanodine receptor. *Journal of Biological Chemistry* 271(34), pp. 20385–20391.

Tjio, J.H. 1958. Genetics of somatic mammalian cells: II. Chromosomal constitution of cells in tissue culture. *Journal of Experimental Medicine* 108(2), pp. 259–268.

Tiso, N. et al. 2001. Identification of mutations in the cardiac ryanodine receptor gene in families affected with arrhythmogenic right ventricular cardiomyopathy type 2 (ARVD2). *Human Molecular Genetics* 10(3), pp. 189–194.

Tong, J., Du, G.G., et al. 1999. HEK-293 cells possess a carbachol- and thapsigargin-sensitive intracellular Ca^{2+} store that is responsive to stop-flow medium changes and insensitive to caffeine and ryanodine. *Biochemical Journal* 343 Pt 1(1), pp. 39–44.

Tong, J., McCarthy, T.V., et al. 1999. Measurement of Resting Cytosolic Ca^{2+} Concentrations and Ca^{2+} Store Size in HEK-293 Cells Transfected with Malignant Hyperthermia or Central Core Disease Mutant Ca^{2+} Release Channels. *Journal of Biological Chemistry* 274(2), pp. 693–702.

Townsend, D.M. 2008. S-glutathionylation: indicator of cell stress and regulator of the unfolded protein response. *Molecular Interventions* 7(6), pp. 313–324.

Toyofuku, T. et al. 1994. Amino acids Glu2 to Ile18 in the cytoplasmic domain of phospholamban are essential for functional association with the $Ca^{(2+)}$-ATPase of sarcoplasmic reticulum. *Journal of Biological Chemistry* 269(4), pp. 3088–3094.

Trafford, A.W. et al. 2000. Modulation of CICR has no maintained effect of systolic Ca2+: simultaneous measurements of sarcoplasmic reticulum and sarcolemmal Ca2+ fluxes in rat ventricular myocytes. *Journal of Physiology* 522(2), pp. 259-270.

Tripathy, A. and Meissner, G. 1996. Sarcoplasmic reticulum lumenal Ca^{2+} has access to cytosolic activation and inactivation sites of skeletal muscle Ca^{2+} release channel. *Biophysical Journal* 70(6), pp. 2600–2615.

Tripathy, A. et al. 1995. Calmodulin activation and inhibition of skeletal muscle Ca^{2+} release channel (ryanodine receptor). *Biophysical Journal* 69(1), pp. 106–119.

Tulloch, L.B. et al. 2011. The inhibitory effect of phospholemman on the sodium pump requires its palmitoylation. *Journal of Biological Chemistry* 286(41), pp. 36020–36031.

Tunwell, R.E. et al. 1996. The human cardiac muscle ryanodine receptor-calcium release channel: identification, primary structure and topological analysis. *The Biochemical Journal* 318 (Pt 2)(Pt 2), pp. 477–487.

Uchinoumi, H. et al. 2010. Catecholaminergic polymorphic ventricular tachycardia is caused by mutation-linked defective conformational regulation of the ryanodine receptor. *Circulation Research* 106(8), pp. 1413–1424.

Uchinoumi, H. et al. 2016. CaMKII and Heart Failure Promote a Pathological Ryanodine Receptor Conformation that Reduces Calmodulin Binding and Enhances SR Ca^{2+} Leak. *Biophysical Journal* 110(3), p. 599a.

Uehara, A. et al. 2017. Extensive Ca^{2+} leak through K4750Q cardiac ryanodine receptors caused by cytosolic and luminal Ca^{2+} hypersensitivity. *The Journal of General Physiology* 149(2), pp. 199–218.

Ullrich, N.D. et al. 2012. PKA phosphorylation of cardiac ryanodine receptor modulates SR luminal Ca^{2+} sensitivity. *Journal of Molecular and Cellular Cardiology* 53(1), pp. 33–42.

Valdivia, H.H. 2012. Ryanodine receptor phosphorylation and heart failure: phasing out S2808 and ‘criminalizing’ S2814. *Circulation Research* 110(11), pp. 1398–1402.

Valdivia, H.H. et al. 1995. Rapid adaptation of cardiac ryanodine receptors: modulation by Mg^{2+} and phosphorylation. *Science (New York, N.Y.)* 267(5206), pp. 1997–2000.

van der Werf, C. et al. 2012. Familial evaluation in catecholaminergic polymorphic ventricular tachycardia: disease penetrance and expression in cardiac ryanodine receptor mutation-carrying relatives. *Circulation: Arrhythmia and Electrophysiology* 5(4), pp. 748–756

Van Petegem, F. 2012. Ryanodine Receptors: Structure and Function. *Journal of Biological Chemistry* 287(38), pp. 31624–31632.

van Oort, R.J. et al. 2010. Ryanodine Receptor Phosphorylation by Calcium/Calmodulin-Dependent Protein Kinase II Promotes Life-Threatening Ventricular Arrhythmias in Mice With Heart Failure. *Circulation* 122(25), pp. 2669–2679.

Venetucci, L.A. et al. 2008. The sarcoplasmic reticulum and arrhythmogenic calcium release. *Cardiovascular Research* 77(2), pp. 285–292.

Vest, J.A. et al. 2005. Defective cardiac ryanodine receptor regulation during atrial fibrillation. *Circulation* 111(16), pp. 2025–2032.

Viero, C. et al. 2012. Techniques and Methodologies to Study the Ryanodine Receptor at the Molecular, Subcellular and Cellular Level. *Calcium Signaling*. Advances in Experimental Medicine and Biology. Dordrecht: Springer Netherlands, pp. 183–215.

Wagenknecht, T. and Radermacher, M. 1997. Ryanodine receptors: structure and macromolecular interactions. *Current Opinion in Structural Biology* 7(2), pp. 258–265.

Wayne Chen, S.R. et al. 2002. Role of the Proposed Pore-Forming Segment of the Ca^{2+} Release Channel (Ryanodine Receptor) in Ryanodine Interaction. *Biophysical Journal* 82(5), pp. 2436–2447.

Walsh, D.A. et al. 1968. An adenosine 3‘,5’-monophosphate-dependant protein kinase from rabbit skeletal muscle. *Journal of Biological Chemistry* 243(13), pp. 3763–3765.

Walsh, M.A. et al. 2016. Compound Heterozygous Triadin Mutation Causing Cardiac Arrest in Two Siblings. *Pacing and Clinical Electrophysiology* 39(5), p. 497.

Walweel, K. et al. 2014. Differences in the regulation of RyR2 from human, sheep, and rat by Ca^{2+} and Mg^{2+} in the cytoplasm and in the lumen of the sarcoplasmic reticulum. *The Journal of General Physiology* 144(3), pp. 263–271.

Walweel, K. et al. 2016. The emerging role of calmodulin regulation of RyR2 in controlling heart rhythm, the progression of heart failure and the antiarrhythmic action of dantrolene. *Clinical and Experimental Pharmacology & Physiology* 44(1), pp. 135-142.

Wang, Q. et al. 2015. Crosstalk between RyR2 oxidation and phosphorylation contributes to cardiac dysfunction in mice with Duchenne muscular dystrophy. *Journal of Molecular and Cellular Cardiology* 89(Pt B), pp. 177–184.

Wang, Y. et al. 2014. Calcineurin-dependent ion channel regulation in heart. *Trends in Cardiovascular Medicine* 24(1), pp. 14–22.

Wang, Z.-W. 2008. Regulation of Synaptic Transmission by Presynaptic CaMKII and BK Channels. *Molecular Neurobiology* 38(2), p. 153.

Watanabe, H. et al. 2009. Flecainide prevents catecholaminergic polymorphic ventricular tachycardia in mice and humans. *Nature Medicine* 15(4), pp. 380–383.

Wayne Chen, S.R. et al. 2002. Role of the Proposed Pore-Forming Segment of the Ca^{2+} Release Channel (Ryanodine Receptor) in Ryanodine Interaction. *Biophysical Journal* 82(5), pp. 2436–2447.

Weber, S. et al. 2015. Counteracting Protein Kinase Activity in the Heart: The Multiple Roles of Protein Phosphatases. *Frontiers in Pharmacology* 6(Suppl. 1), p. 270.

Weber, T.S. et al. 2014. Quantifying the length and variance of the eukaryotic cell cycle phases by a stochastic model and dual nucleoside pulse labelling. *PLoS Computational Biology* 10(7), p. e1003616.

Wehrens, X. 2003. Altered function and regulation of cardiac ryanodine receptors in cardiac disease. *Trends in Biochemical Sciences* 28(12), pp. 671–678.

Wehrens, X.H.T. et al. 2003. FKBP12.6 deficiency and defective calcium release channel (ryanodine receptor) function linked to exercise-induced sudden cardiac death. *Cell* 113(7), pp. 829–840.

Wehrens, X.H.T. et al. 2005. Enhancing calstabin binding to ryanodine receptors improves cardiac and skeletal muscle function in heart failure. *Proceedings of the National Academy of Sciences* 102(27), pp. 9607–9612.

Wehrens, X.H.T. et al. 2006. Ryanodine receptor/calcium release channel PKA phosphorylation: A critical mediator of heart failure progression. *Proceedings of the National Academy of Sciences* 103(3), pp. 511–518.

Wehrens, X.H.T., Lehnart, S.E., Reiken, S.R. and Marks, A.R. 2004. Ca^{2+}/calmodulin-dependent protein kinase II phosphorylation regulates the cardiac ryanodine receptor. *Circulation Research* 94(6), pp. e61–70.

Wehrens, X.H.T., Lehnart, S.E., Reiken, S.R., Deng, S.-X., et al. 2004. Protection from cardiac arrhythmia through ryanodine receptor-stabilizing protein calstabin2. *Science (New York, N.Y.)* 304(5668), pp. 292–296.

Wei, R. et al. 2016. Structural insights into Ca^{2+}-activated long-range allosteric channel gating of RyR1. *Cell Research* 26(9), p. 977.

Werns, S.W. et al. 1992. Myocardial glutathione depletion impairs recovery of isolated blood-perfused hearts after global ischaemia. *Journal of Molecular and Cellular Cardiology* 24(11), pp. 1215–1220.

White, S.H. 1986. The Physical Nature of Planar Bilayer Membranes. In: *Ion Channel Reconstitution*. Boston, MA: Springer US, pp. 3–35.

Wijnker, P.J.M. et al. 2011. Protein phosphatase 2A affects myofilament contractility in non-failing but not in failing human myocardium. *Journal of Muscle Research and Cell Motility* 32(3), pp. 221–233.

Williams, A.J. et al. 2001. Light at the end of the $Ca^{(2+)}$-release channel tunnel: structures and mechanisms involved in ion translocation in ryanodine receptor channels. *Quarterly Reviews of Biophysics* 34(1), pp. 61–104.

Witcher, D.R. et al. 1991. Unique phosphorylation site on the cardiac ryanodine receptor regulates calcium channel activity. *The Journal of Biological Chemistry* 266(17), pp. 11144–11152.

Wolska, B.M. 2009. Calcineurin and cardiac function: is more or less better for the heart? *American journal of physiology. Heart and Circulatory Physiology* 297(5), pp. H1576–7.

Wu, Y. et al. 2016. A Single Protein Kinase A or Calmodulin Kinase II Site Does Not Control the Cardiac Pacemaker Ca^{2+} Clock. *Circulation: Arrhythmia and Electrophysiology* 9(2), p. e003180.

Xiao, B. et al. 2004. Protein Kinase A Phosphorylation at Serine-2808 of the Cardiac Ca^{2+}-Release Channel (Ryanodine Receptor) Does Not Dissociate 12.6-kDa FK506-Binding Protein (FKBP12.6). *Circulation Research* 94(4), p. 487.

Xiao, B. et al. 2005. Characterization of a novel PKA phosphorylation site, serine-2030, reveals no PKA hyperphosphorylation of the cardiac ryanodine receptor in canine heart failure. *Circulation Research* 96(8), pp. 847–855.

Xiao, B. et al. 2006. Ser-2030, but not Ser-2808, is the major phosphorylation site in cardiac ryanodine receptors responding to protein kinase A activation upon β-adrenergic stimulation in normal and failing hearts. *The Biochemical Journal* 396(1), pp. 7–16.

Xiao, B. et al. 2007. Functional consequence of protein kinase A-dependent phosphorylation of the cardiac ryanodine receptor: sensitization of store overload-induced Ca^{2+} release. *Journal of Biological Chemistry* 282(41), pp. 30256–30264.

Xiao, J. et al. 2007. Removal of FKBP12.6 Does Not Alter the Conductance and Activation of the Cardiac Ryanodine Receptor or the Susceptibility to Stress-induced Ventricular Arrhythmias. *Journal of Biological Chemistry* 282(48), p. 34828.

Xiao, Z. et al. 2016. Enhanced Cytosolic Ca^{2+} Activation Underlies a Common Defect of Central Domain Cardiac Ryanodine Receptor Mutations Linked to Arrhythmias. *Journal of Biological Chemistry* 291(47), p. 24528.

Xie, L.H. and Weiss, J.N. 2009. Arrhythmogenic consequences of intracellular calcium waves. *American journal of physiology. Heart and Circulatory Physiology* 297(3), pp. H997–H1002.

Xu, L. and Meissner, G. 1998. Regulation of Cardiac Muscle Ca^{2+} Release Channel by Sarcoplasmic Reticulum Lumenal Ca^{2+}. *Biophysical Journal* 75(5), pp. 2302–2312.

Xu, L. et al. 1998. Activation of the cardiac calcium release channel (ryanodine receptor) by poly-S-nitrosylation. *Science (New York, N.Y.)* 279(5348), pp. 234–237.

Xu, X. et al. 2010. Defective calmodulin binding to the cardiac ryanodine receptor plays a key role in CPVT-associated channel dysfunction. *Biochemical and Biophysical Research Communications* 394(3), pp. 660–666.

Yamazoe, M. and Furukawa, T. 2016. Long-Term Prognosis of Catecholaminergic Polymorphic Ventricular Tachycardia Patients With Ryanodine Receptor (RYR2) Mutations. *Circulation Journal: official journal of the Japanese Circulation Society* 80(9), pp. 1892–1894.

Yan, Z. et al. 2014. Structure of the rabbit ryanodine receptor RyR1 at near-atomic resolution. *Nature* 517(7532), p. 50.

Yang, D. et al. 2007. Ca^{2+}/calmodulin kinase II-dependent phosphorylation of ryanodine receptors suppresses Ca^{2+} sparks and Ca^{2+} waves in cardiac myocytes. *Circulation Research* 100(3), pp. 399–407.

Yang, L. et al. 2004. Ser1928 is a common site for Cav1.2 phosphorylation by protein kinase C isoforms. *Journal of Biological Chemistry* 280(1), pp. 207–214.

Yang, Z. et al. 2006. The RyR2 central domain peptide DPc10 lowers the threshold for spontaneous Ca^{2+} release in permeabilized cardiomyocytes. *Cardiovascular Research* 70(3), pp. 475–485.

Yamamoto, T. and Ikemoto, N. 2002. Peptide Probe Study of the Critical Regulatory Domain of the Cardiac Ryanodine Receptor. *Biochemical and Biophysical Research Communications* 291(4), pp. 1102–1108.

Yano, M. et al. 2003. FKBP12.6-mediated stabilization of calcium-release channel (ryanodine receptor) as a novel therapeutic strategy against heart failure. *Circulation* 107(3), pp. 477–484.

Yano, M. et al. 2009. Role of ryanodine receptor as a Ca^{2+} regulatory center in normal and failing hearts. *Journal of Cardiology* 53(1), p. 1.

Ylänen, K. et al. 2010. Catecholaminergic polymorphic ventricular tachycardia. *European Journal of Pediatrics* 169(5), pp. 535–542.

Yuchi, Z. et al. 2012. Disease mutations in the ryanodine receptor central region: crystal structures of a phosphorylation hot spot domain. *Structure (London, England: 1993)* 20(7), pp. 1201–1211.

Yuchi, Z. et al. 2013. Structural Insight into the Phosphorylation Domain in Ryanodine Receptors. *Biophysical Journal* 104(2), p. 444a.

Yuchi, Z. et al. 2015. Crystal structures of ryanodine receptor SPRY1 and tandem-repeat domains reveal a critical FKBP12 binding determinant. *Nature Communications* 6, p. 7947.

Zahradník, I. et al. 2005. Calcium activation of ryanodine receptor channels--reconciling RyR gating models with tetrameric channel structure. *The Journal of General Physiology* 126(5), pp. 515–527.

Zalk, R. et al. 2014. Structure of a mammalian ryanodine receptor. *Nature* 517(7532), pp. 44–49.

Zamparelli, C. et al. 2000. Structure-function relationships in sorcin, a member of the penta EF-hand family. Interaction of sorcin fragments with the ryanodine receptor and an Escherichia coli model system. *Biochemistry* 39(4), pp. 658–666.

Zhabyeyev, P. et al. 2013. S4153R is a gain-of-function mutation in the cardiac $Ca^{(2+)}$ release channel ryanodine receptor associated with catecholaminergic polymorphic ventricular tachycardia and paroxysmal atrial fibrillation. *The Canadian Journal of Cardiology* 29(8), pp. 993–996.

Zhang, H. et al. 2012. Hyperphosphorylation of the cardiac ryanodine receptor at serine 2808 is not involved in cardiac dysfunction after myocardial infarction. *Circulation Research* 110(6), pp. 831–840.

Zhang, J. et al. 2003. Three-dimensional Localization of Divergent Region 3 of the Ryanodine Receptor to the Clamp-shaped Structures Adjacent to the FKBP Binding Sites. *Journal of Biological Chemistry* 278(16), pp. 14211–14218.

Zhang, L. et al. 1997. Complex formation between junctin, triadin, calsequestrin, and the ryanodine receptor. Proteins of the cardiac junctional sarcoplasmic reticulum membrane. *Journal of Biological Chemistry* 272(37), pp. 23389–23397.

Zhang, R. et al. 2005. Calmodulin kinase II inhibition protects against structural heart disease. *Nature Medicine* 11(4), pp. 409–417.

Zhang, T. et al. 2010. Phospholamban ablation rescues sarcoplasmic reticulum $Ca^{(2+)}$ handling but exacerbates cardiac dysfunction in CaMKII delta(C) transgenic mice. *Circulation Research* 106(2), pp. 354-362.

Zhang, Y. et al. 2008. Downregulated FKBP12.6 expression and upregulated endothelin signaling contribute to elevated diastolic calcium and arrhythmogenesis in rat cardiomyopathy produced by l-thyroxin. *International Journal of Cardiology* 130(3), p. 463.

Zhao, M. et al. 1999. Molecular identification of the ryanodine receptor pore-forming segment. *Journal of Biological Chemistry* 274(37), pp. 25971-15974.

Zhao, Y.-T. et al. 2015. Arrhythmogenesis in a catecholaminergic polymorphic ventricular tachycardia mutation that depresses ryanodine receptor function. *Proceedings of the National Academy of Sciences of the United States of America* 112(13), pp. E1669–77.

Zhou, Q. et al. 2011. Carvedilol and its new analogs suppress arrhythmogenic store overload-induced Ca^{2+} release. *Nature Medicine* 17(8), pp. 1003–1009.

Zima, A.V. et al. 2010. Ca^{2+} spark-dependent and -independent sarcoplasmic reticulum Ca^{2+} leak in normal and failing rabbit ventricular myocytes. *Journal of Physiology* 588, pp. 4743-4757.

Zima, A.V. and Mazurek, S.R. 2016. Functional Impact of Ryanodine Receptor Oxidation on Intracellular Calcium Regulation in the Heart. *Reviews of Physiology, Biochemistry and Pharmacology* 171, pp. 39–62.

Zima, A.V. et al. 2008. Termination of cardiac Ca^{2+} sparks: role of intra-SR $[Ca^{2+}]$, release flux, and intra-SR Ca^{2+} diffusion. *Circulation Research* 103(8), pp. e105–15.

Zima, A.V. et al. 2014. Ca handling during excitation-contraction coupling in heart failure. *Pflügers Archiv - European Journal of Physiology* 466(6), pp. 1129–1137.

Zissimopoulos, S. and Lai, F.A. 2004. Interaction of FKBP12.6 with the cardiac ryanodine receptor C-terminal domain. *Journal of Biological Chemistry* 280(7), pp. 5475–5485.

Zissimopoulos, S. and Lai, F.A. 2005. Central domain of the human cardiac muscle ryanodine receptor does not mediate interaction with FKBP12.6. *Cell Biochemistry and Biophysics* 43(2), pp. 203–219.

Zissimopoulos, S. et al. 2012. Disparities in the association of the ryanodine receptor and the FK506-binding proteins in mammalian heart. *Journal of Cell Science* 125(Pt 7), pp. 1759–1769.

Zissimopoulos, S. et al. 2013. N-terminus oligomerization regulates the function of cardiac ryanodine receptors. *Journal of Cell Science* 126(21), p. 5042.

Zorzato, F. et al. 1990. Molecular cloning of cDNA encoding human and rabbit forms of the Ca^{2+} release channel (ryanodine receptor) of skeletal muscle sarcoplasmic reticulum. *Journal of Biological Chemistry* 265(4), pp. 2244–2256.